COMPARISON OF SIMPLIFIED PHYSICS-BASED BUILDING ENERGY MODEL TO AN ADVANCED NEURAL NETWORK FOR AUTOMATIC FAULT DETECTION

A Thesis
Presented to
The Academic Faculty

by

Christopher Fernandez

In Partial Fulfillment
of the Requirements for the Degree
Ph.D. in the
George W. Woodruff School of Mechanical Engineering

Georgia Institute of Technology
December 2021

COMPARISON OF SIMPLIFIED PHYSICS-BASED BUILDING ENERGY MODEL TO AN ADVANCED NEURAL NETWORK FOR AUTOMATIC FAULT DETECTION

Approved by:

Dr. Sheldon M. Jeter, Advisor
George W. Woodruff School of
Mechanical Engineering
Georgia Institute of Technology

Dr. William J. Wepfer
George W. Woodruff School of
Mechanical Engineering
Georgia Institute of Technology

Dr. Said Abdel-Khalik
George W. Woodruff School of
Mechanical Engineering
Georgia Institute of Technology

Dr. Zhuomin Zhang
George W. Woodruff School of
Mechanical Engineering
Georgia Institute of Technology

Dr. Thomas Lawrence
UGA College of Engineering
University of Georgia

Dedicated to my family and friends for always being there to support me.

Thanks to Dr. Godfried Augenbroe for challenging me to meet higher expectations.

To Dr. Sheldon M Jeter, for all the help and encouragement he bestowed upon me these many years.

For Dr. Said Abdel-Khalik, Dr. Thomas Lawrence, Dr. William J. Wepfer, and Dr. Zhuomin Zhang, I express my deepest gratitude for their recommendations and guidance.

Special acknowledgement of Greg Spiro, Federico Del Risco, and Donald Alexander in appreciation of their training.

TABLE OF CONTENTS

LIST OF TABLES

LIST OF FIGURES

LIST OF SYMBOLS

A	Area
C	Thermal capacitance
C_p	Specific heat
F	View factor
$\mathrm{F_o}$	Fourier number
$\dot{\mathrm{G}}$	Radiation energy transfer
H	Convection heat transfer coefficient
I	Irritation
P	Pressure
P_W	Perimeter of surface
$\dot{Q}$	Heat transfer rate
$Q_{e,\tau}$	Conduction load from ASHRAE time series
R	Thermal resistance
R_C	Gas constant
R_f	Roughness of surface
R_Ω	Ground reflectance
T	Temperature
T_{rc}	Constant interior temperature for ASHRAE time series

$T_{\mathrm{sol-air}}$	Temperature adjusted to include solar loading
$T_{e,\tau-n\delta}$	Sol-air temperatures for ASHRAE time series
U	Internal energy
V	Volume
V_w	Wind velocity
W	Humidity ratio
W_f	Wayward factor (1 if wind strikes surface within 100 degrees, 0 otherwise)
b_n	B coefficient for ASHRAE time series conduction equation
c_n	C coefficient for ASHRAE time series conduction equation
d_n	D coefficient for ASHRAE time series conduction equation
h	Enthalpy
l	Length
$\dot{m}$	Mass flow rate
$\dot{q}$	Heat transfer rate per area
$q_{e,\tau-n\delta}$	Previous values for conduction load for ASHRAE time series
t	Timestep
u	Specific internal energy
α	Absorptivity
α_{Fo}	Thermal diffusivity
α_S	Solar altitude angle
ϵ	Emissivity

θ	Angle
σ	Stefan–Boltzmann constant

List of symbols continued: subscripts

E	Exfiltration
G	Generated
I	Infiltration
O	Outdoor air
R	Return
S	supply
Z	Zone
f	Forced convection
n	Natural convection
rad	radiation

List of symbols continued: superscripts

D	Dry air
M	Moist air
V	Water vapor

SUMMARY

Buildings are complex structures with dynamic loading and ever-changing usage. Additionally, the need to reduce unnecessary energy consumption in buildings is increasing. As a result, buildings and building energy systems should be designed to conserve energy, and buildings should be monitored and evaluated to ensure that the designs are executed properly and that the buildings are operated correctly. Most building designers now use very adequate energy modeling software such as EnergyPlus, IES, EQUEST, and others to support the design task. However, the problem with the current lineup of programs is that they require extensive inputs for material properties and usage loads; this results in spending extensive amounts of time performing model calibration or having to adjust multiple values (sometimes hundreds) to bring a model in alignment with actual building use. As a consequence, the existing software is complex and awkward for efficient monitoring and evaluation, especially for fault detection and diagnosis. Due to the limitations of current modeling programs, development has begun on rule-based and component-based fault detection by a number of companies. However, a suitable rigorous physics-based model has not been developed for the purpose of fault detection. Consequently, this thesis research will discuss the design, development, evaluation, and testing of a model-based fault detection program and procedure as well as comparisons to state-of-the-art neural networks.

Considering how complex some buildings have become, it has become important to make sure the building systems are operating as intended. Some current progress is being done by the large energy service companies in the form of logic-based fault

detection for individual components. While component-based fault detection is effective, it relies on accurate sensor readings and does not account for actual building performance. This research herein is the result of the development, testing, and refinement of a simplified but rigorous and complete physics-based model for buildings and building energy systems that is purposely designed and implemented to support fault detection and similar applications. The usefulness and effectiveness of this simplified physics-based model (SPBM) is demonstrated by comparison with the obvious currently available alternative, a state of the art purely data driven neural network black-box model. The models, a simplified physics-based energy model and a neural network, will evaluated total building performance using weather and minimal load data that is common to most buildings to determine, identify, and measure the impact of building faults. Evaluation of performance and accuracy of such a system to a state-of-the-art machine learning model provides substantial insight to current and future fault detection methods.

CHAPTER 1. INTRODUCTION

Most modern buildings and their HVAC building energy systems (BES) are reasonably well designed and executed considering the constraints faced by developers. Nevertheless, buildings are likely to perform worse than expected because of improper or changed construction (especially including errors in the control or building automation system), loads or usage that are different from expected, and unavoidable degradation with age. For example, one highly regarded study found that out of 22 LEED Gold and Platinum certified buildings 12 used, on average, 60% more energy than modeled. With such a high percentage of new high-efficiency building performing noticeably worse than expected, it is important to have some means of fault detection to understand when and why the excessive or ineffective energy use is occurring. Even in existing buildings, materials degrade, and it is important to make sure faults are not occurring in buildings both to maintain occupant comfort and to avoid wasting energy. Consequently, fault detection (FD) methods are needed, and currently, independent fault simulation programs are largely in development stages. Being able to accurately fit faults in addition to detecting abnormalities can allow for higher accuracy diagnostics as well as prediction of fault energy impact. This document discusses the development of the first of its kind rigorous physics-based fault simulation model and the comparison of this model with a model based on a neural network to identify specific faults. This chapter introduces the proposed FD candidates and outlines the supporting technology.

Efficient FD methods and software are highly desirable to prevent energy waste, occupant discomfort, or unhealthy environments. At least two very general FD

categories can be identified as either rule-based systems or model-based systems. While this approach is promising, it has limitations because it requires human experts to define the rules based on their personal experience and is also mostly limited to detecting faults in individual sensors and HVAC components. The number of rules needed to usefully detect faults in a major system or subsystem, such as the overall HVAC system or an entire building, increases with the product of the number of rules needed for each component and may quickly become excessive. The obvious alternative is a model-based FD system, and two approaches for model-based systems are presented in this proposal: one being a statistically based neural network (NN) model and the other being a simplified but fundamentally rigorous physics-based model. A detailed physics-based model may be another FD approach, but at present the available detailed models are complex and understandably design-oriented, not diagnostics-oriented. Consequently, it is believed that the high number of parameters in models such as EnergyPlus unnecessarily increase the complexity of FD attempts; therefore, it is appropriate at this time to consider and compare the two reasonable alternatives, a simplified physics-based model (SPBM) and a neural network (NN) model. This paper discusses the development, testing, results, and comparisons of a physics-based building energy model and neural networks. Both of these simplified modeling techniques have different strengths and will be compared by how accurately they match metered loads, reliability of fault detection, and training data. Fault detection is of course not new, but in-person fault detection is costly and probably only appropriate for obviously high-cost or high-value buildings. The causes for differences in performance can include excessive infiltration, economizer dampers being stuck at one position, malfunctioning occupancy sensors, and unnecessary

preheat. While other faults are possible, these four faults test different parts of building dynamics while being common and having significant impact on building loads. This proposal will investigate the initial process for testing different methods of fault detection and describe future plans for determining the best procedure and tools to answer the proposed questions stated at the end of this chapter.

Test buildings are needed for the proposed research, and the availability of numerous buildings on the campus of the Georgia Institute of Technology provides an opportunity to explore different types of buildings with different loads, constructions, and levels of building metering. Since most of the buildings are served by centralized chilled water and steam as well as being well-instrumented and networked, our campus provides an excellent test environment. These advantages are enhanced by previous experience in a campus-wide process called Continuous Monitoring, Modeling, And Evaluation (CMME), which is a developing, but different method, of FD. CMME has been useful, but it needs to be computerized to be convenient and fully cost effective. Currently, this method of fault detection is being performed by spending several months evaluating building energy patterns and comparing results with detailed models. Experience has shown that manual CMME is costly and time consuming. This was as expected, and it was recognized that CMME should eventually be automated. Consequently, the automation of CMME is a perfectly suitable application for a SPBM or NN based fault detection. Due to the large number of building options, two representative buildings were chosen: Whitehead and Old Civil Engineering (Old CE). Whitehead is a modern building with high internal loads while Old CE is a historic building that is primarily low in occupant count and internal load.

Most currently available thermodynamically rigorous energy modeling programs were developed primarily for detailed design and research, are very complex, and are not easily calibrated or adjustable to the performance of an actual building. Building models have however become sufficiently realistic to use in the development and testing of FD models. As described herein and further to be elaborated on in the proposed thesis, the first and second generation of building models approximated the conditioned space with a "heat balance" model rather than thermodynamically rigorous and realistic transient energy and moisture models. Consequently, these models were not well suited to support FD research, but the extensive development of the rigorous energy and moisture simulation inherent in state of the art models such as EnergyPlus has made the development of the FD methods described herein more feasible and practical, and EnergyPlus in particular will be a useful tool for the development and testing of the proposed SPBM and NN.

Within the framework of general modeling theory, three diverse approaches can be recognized : (1) Black Box modeling where the internal workings of the system are unknown, and the model is evaluated based on input/output data alone (e.g. a neural network), (2) White Box modeling is possible where a priori of information is available (e.g. an extensively detailed EnergyPlus model), finally, (3) Grey Box modeling which is a combination of white and black modeling (e.g. a SPBM) . The SPBM is a grey box model, while the NN model is a black box model; consequently, the thesis will demonstrate and utilize all three levels of modeling.

This thesis will (1) fully explore the conceptualization, development, and testing of a SPBM-based procedure to demonstrate the feasibility of modeling a building with

automatic calibration, (2) demonstrate the development of a neural network to model the same buildings, and finally, (3) compare the methods for automatic fault detection to determine which method is superior when minimal information about a building is known. A SPBM has certain advantages in that it has the basic capability to account for all loading within a building, with some acceptable uncertainty, and to respond to changes of use or environment in a realistic manner. In contrast, while a well-trained NN may be more accurate in some cases, there is a disadvantage because NNs may not reliably extrapolate data and may need to be trained in 'normal' and 'faulty' operation. In addition to programming and electronic errors, building materials degrade over time or may be unknown. Consequently, a SPBM may have advantages over both a NN model and a complex model because of its inherent adaptability. The nature of a SPBM allows for convenient estimation of unknown properties or the automated estimation of changed thermal properties. The exact materials used may not be provided in construction documents, so it may be more convenient and accurate to initially estimate the bulk resistance and heat capacity of one or two hypothetical layers rather than defining a minimum of four properties for each of several building layers as required in a complex model such as EnergyPlus. If properties change, or are unknown, inferring a few bulk properties from observational data will be much easier than trying to evaluate upwards of nine properties per material layer.

This thesis also shows that the research is feasible and useful. Research began by (1) developing a suitable rigorous thermodynamic model in EnergyPlus of Whitehead and Old CE buildings, (2) testing various resistance-capacitance (R-C) configurations for opaque surface modeling, (3) conducting preliminary investigation of opaque surface

parameter estimation to determine if the SPBM could produce realistic variables, (4) implementing, testing, and evaluating various fenestration simplification methods, (5) simulating realistic HVAC system performance in the SPBM with the introduction of humidity and temperature control, (6) generating suitable internal load models for the SPBM, (7) conducting baseline parameter value estimation of surface properties and internal loads, (8) developing and testing of NN algorithms and parameters against simulated and real building data, (9) testing the fault detection capabilities of the SPBM. , (10) Refine indoor air, moisture, and contaminant simulation, (11) Evaluate performance of SPBM for fault detection and sensitivity analysis, (12) Test the NN with different training and input/output conditions and data (13) Introduce multiple faults and evaluate if either the SPBM or NN can accurately determine multiple simultaneous faults. The proposed faults are: 1) Excessive infiltration, 2) Malfunctioning occupancy sensors, 3) Malfunctioning outdoor air control system, such as a stuck outdoor air damper, and 4) Unnecessary/excessive preheat. These faults were chosen in part because of how common they are and partly because they provide various kinds of loads on the building. Together, the completed thesis will compare a SPBM, which represents all the transport and thermodynamic processes in a building with adequate detail, to a neural network and determine the optimum approach for automatic fault detection with various amounts of building information.

CHAPTER 2. LITERATURE AND TECHNOLOGY REVIEW

A fundamental understanding of previous works is vital to innovation. This section will cover developmental history of building energy models (rigorous, simplified, and neural network systems), calibration of models, and fault detection in buildings. Reviewing what has previously been accomplished and what programs are available led to the decision to develop a SPBM for automatic fault detection. Automatic fault detection of building energy systems is developing in both technology and demand. Using as few inputs as possible (basic weather and building energy meters) provided the most benefit by allowing for minimal information and avoided the new practice of rule-based automatic fault detection. As machine learning advances, determining what modeling system (SPBM or NN) best identifies difficult to notice faults, using only basic building data, is vital to success in improving building health, occupant comfort, and energy conservation.

2.1 Overview of Popular Energy Analysis and Simulation Software

The desire to understand building dynamics is not new. Transient building heat flow calculations were published as early the 1920s. Building energy analysis and design methods have existed for many years as exemplified by various heat balance estimations and the popular Cooling Load Temperature Difference (CLTD) building system sizing method[10]. These early load estimation methods were a useful basic energy demand and peak load calculation tool; but such models are not especially useful or intended for seasonal or annual simulations. CLTD specifically relies on profiles that disperse thermal loads across time to replicate physical processes that are modeled in modern high-fidelity

building energy simulations as well as the SPBM. However, contemporary high-fidelity building energy models and the SPBM are capable of incorporating more specifications and perform load prediction for any time period.

The energy crisis of the 1970s sparked a desire for buildings to use less energy, and methods for calculating hourly loads for an entire season or year such as the National Bureau of Standards Loads Determination (NBSLD) were developed. A first generation of annual modeling programs such as BLAST and DOE-2 (later repackaged as eQUEST), expanded on the NBSLD approach to facilitate annual energy simulations of buildings and HVACs system through heat balance modeling. These programs were designed to be used with the limited computing power available and operated as hourly heat balance programs rather than full-featured energy simulation tools. Early energy modeling or hourly load calculation models finally developed into more robust programs such as EnergyPlus, a rigorous thermodynamic and conservation of energy and mass (air, moisture, CO_2, and contaminant) model and the similar commercially-available IES program. However, these programs require a high degree of information about the building including occupancy schedules, number of people, lighting loads, electrical loads, material properties, detailed HVAC systems, and many other parameters. For instance, to model wall construction in EnergyPlus it is necessary to manually specify the thickness, density, specific heat, and conductivity for every layer within a surface . From a design perspective, increasing available specifications can increase model accuracy as BIM data use becomes more common. However, an abundance of parameters can also lead to lowered sensitivity and reduce automatic parameter estimation accuracy. Overall, models have become more advanced over time, which while excellent when parameters

are known, are prohibitively awkward when attempting to calibrate a model to an existing building. In contrast, a comprehensive SPBM or NN may provide benefits the complex models cannot allow while delivering comparable results.

Internal loads have the same issue where an hourly schedule is needed to calculate loads for lighting, electric equipment, and occupancy. While it is possible to use a tabulated hourly schedule generated with building occupancy sensors and electric meters, many buildings do not have accurate meters, and even fewer buildings subdivide meters to different areas and functions throughout the building. All the limitations make tuning a model to match an existing building extremely difficult (an accuracy of 10% is often considered excellent) and determining the optimal selection of model inputs is challenging. Nonetheless, both methods of simplified building energy modeling (SPBM and NN) were capable of a faithful reproduction of heating demand and cooling demand.

The level of detail allowed in existing programs is beneficial if a reasonably accurate estimation of real-world parameters can be made, but increasing complexity can make fitting limited data difficult. All modern buildings are not monitored to the same degree. To give an example, some have occupancy counters, others have motion sensors, and others have no occupancy sensing at all. Additionally, some buildings only provide total electrical power used, total heating water load, and total cooling water load. In addition, complex simulation programs require a plethora of inputs. As an example, EnergyPlus requires at least four variables, but usually seven variables for most cases, for each wall layer, numerous settings for each internal load, and specifications for the HVAC system. Calibration with so many variables would be difficult and time consuming compared to the SPBM method which only may require as few as two

variables per layer.

Currently a HVAC design engineer must adapt or tune the control system to a building; although, refinements such as lighting control based off people occupancy and natural lighting have been implemented for years. Additionally, interior zone climate control based primarily on temperature may also monitor CO_2 concentration in an effort to reduce outdoor air and energy demand by controlling ventilation based on actual occupancy as opposed to theoretical occupancy. Therefore, physical models must be able to account for different control strategies in order to better represent the physical world.

Modern simulation programs offer unmatched tools for building evaluation and design, but the parameters that allow for fine detail hinder calibration when there are many unknown parameter values. Simplified building models very greatly in complexity and method of energy simulation but potentially offer overall similar results to detailed models but require fewer parameters.

2.2 Implementation of Simplified Models

An appreciation for uncertainty in design and construction is important for understanding building energy models. Analysis of existing elaborate, or high-fidelity, building energy models revels that they tend to difficult to quickly implement due to the need for extensive information about the building being modeled. For example, without electrical and occupancy metering for every room, it is impossible to fully replicate such an environment. When lack of knowledge compounds, it can lead to inaccurate building energy simulations.

The SPBM being developed herein is designed to automatically adjust for the

actual performance of the building with minimal reprocessing . Some detailed calibrations have been done, but require extensive data gathering, including individual room temperatures which is not practical in most applications. An objective of the research is to be able to retroactively implement the program where not all the design data is known or available.

An error minimization tool was needed to help identify the parameters involved. There are many options for calibration: linear, least squares, cost, and Monte Carlo to name a few. Least squares had many tools available and was pre-programmed into Engineering Equation Solver (EES), an equation-based modeling program, and MATLAB. Both were also able to use Nelder-Mead method of error minimization, which is an efficient and effective tool for the proposed parameter estimation. The calibration of the model plays a crucial part in the effectiveness of automatic fault detection; therefore, investigating, selecting, and using the proper error minimization technique and algorithm is vital to success.

2.3 Simulation of Wall Construction

There are many earlier and some current articles on simulating walls with thermal mass such as: solving for second-order Fourier series, developing thermal resistance-capacitance networks, using measured inputs and output optimization, lumped slab simplifications, and lumped parameter constructions. Additionally, there are some parameter models that aim to match an EnergyPlus simulation to the performance of a real building using numerous parameters or pre-defined conditions. These detailed models are useful for design, especially when modern energy saving designs are used, such as phase change materials.

While it is possible to use a fine mesh to simulate wall conduction, estimating wall thermal properties is difficult even under controlled and high temperature difference conditions. However, it is important to be able to model envelope transient temperature change as different materials affect how quickly the interior surface heats up and cools down in relation to external loading. Building thermal mass can have a significant impact on energy demand throughout the day and accurately representing transient building responses is a goal of this model. After thorough comparison presented below it was determined that a simple R-C circuit equivalent provides the most flexibility and accuracy for this model.

2.4 In-Field Experiences

Preliminary work on fault detection instilled knowledge of the requirements of monitoring and modeling a variety of buildings throughout Georgia Tech's campus; and as such, first-hand experience with HVAC systems and modeling industry standards was obtained. For several years work has been done monitoring and modeling buildings such as: Clough Undergraduate Learning Commons, Engineered Biosystems Building, Carbon Neutral Energy Solutions Laboratory, J. Erskine Love Building, and the Biotech Quad and Old Civil Engineering . Additionally, models and optimization has been conducted for future projects including the Price Gilbert renewal project, known locally as Library Next, and ongoing modeling of the first net-zero college building in Georgia Tech. Being exposed to a wide diversity of building constructions, systems, and faults allows for an appreciation of the subtlety of automatic fault detection.

Current work is being done on developing rule-based fault detection. The idea is

to have individual components (VAV, fans, CO_2 sensors, etc.) send fault alerts when operating outside specified rules. Rule-based fault detection is limited because currently only individual component faults are reported, different sensors are required in each component, and only instantaneous readings are used . Building-wide fault detection allows for analysis of energy use and changes within the building without needing to reprogram flags for faults. SPBM and NN based fault detection relies on minimal sensing equipment and changes in loading, providing different benefits to fault detection.

2.5 Benefits of Building Model Simplification

The physical structure of buildings is incredibly complex and would be impossible to perfectly model every feature. Even constructions and material properties are not perfectly uniform . Consequently, even under experimental conditions where everything is known, building simulations can get only within a few percentages of actual values ; but accurately calibrating and modeling every window, frame, wall, etc. for a real building would be impractical if not essentially impossible. Radiation transfer is another common point of simplifying real behaviors - EnergyPlus has an option to have the floor absorb all transmitted solar energy instead of calculating radiation exchange for every surface .

A common simplification for some overly simplified models is to not account for thermal capacity within the mass of a building. Research later in this paper demonstrates that the thermal-flywheel effect will delay the impact of all envelope loads and many internal loads; therefore, the thermal mass is important in any hour-by-hour (or shorter) simulation. The choice to include thermal capacity is especially important when needed for predictive control simulations with peak shifting . Peak shifting of thermal loads

requires storing heat or “coolth” (actually the exergy of warm or cool material) within the mass of the building, or in a dedicated thermal storage medium, to be released later in the day when cooling or heating is demanded and electrical prices are high . Additionally, predictive control can be used by a building model to accommodate occupant comfort and reduce energy consumption. The SPBM is uniquely suited for this type of implementation as a cost-effective and simple method of predicting impact on heating and cooling loads is desired.

One method being explored for simplifying the modeling of a number of buildings is to create a detailed model of one building, calibrate that model, then adjust the initial model to reflect the performance of nearby buildings . Popular with urban building modeling, this approach allows multiple, similar buildings to be evaluated with minimal effort. This method is useful for determining if some buildings are operating outside the average performance of buildings without having to create detailed and calibrated models .

Another way to model thermal storage with a simplified model is to evaluate heat transfer analogous to current through a resistance-capacitance electrical circuit. These models tend to have nodes representing zone air temperatures with a resistor and capacitor linking nodes together and to external stimulus such as outdoor air temperature and solar loads . Research explored later in this proposal considered thermal capacity in walls and discovered that even one thermal capacitance value in a surface is beneficial, but some constructions require more R-C nodes to accurately simulate the lag between external surface loads entering a zone. Testing also showed the importance of accounting for thermal capacitance and wall construction as distributing material properties

differently (while keeping overall capacitance and resistance consistent) lead to a decrease of 25% in cooling demand over occupied hours . One paper of special interest analyzed the order required to accurately represent a building subject to cyclic loading with a RC model. It was discovered that lower number of nodes (one and two nodes) were capable of a close approximation, higher order was more accurate. Surprisingly, as the frequency of the cyclic loading increased only the three-node RC model remained close to the detailed model's phase angle as the four-node (highest order tested) diverged . An RC model was even tested and proved to be successful in controlling an AHU supply temperature setpoint with weather and occupancy prediction to use less energy while maintaining thermal comfort. Given the success of RC models, it will be interesting to see how one compares to a neural network in fault detection with minimal input information.

Additionally, it is possible to simulate only one day that represents the average loading for a month then weight the load for that day to represent a month's load . This approach is computationally efficient and excellent for use with specific applications such as statistical analysis of future loads and building degradation. However, automatic fault detection devices usually operate continuously in order to model components in real time and compare predicted performance to actual building data. This kind of analysis is susceptible to changes in solar loading, internal loads, outdoor air temperature, and humidity that a monthly average load may miss. Success with various simplified building models gives confidence that either SPBM or NN modeling may be useful for automatic fault detection.

2.6 Neural Network

Neural networks are a series of nodes that are linked together to generate input/output responses . some networks can account for time delay between inputs and output response. A benefit of neural networks is that no model needs to be created; the system is created purely through the real data provided when training. However, neural networks perform poorly when extrapolating data, so faulty data or modeled faulty data needs to be provided during training if fault identification is desired . Additionally, it is difficult to analyze a network once it is created to allow for direct modification, and it is possible that the same input/output data can create a different network every time it is trained . Due to the above limitations, neural network fault detection can be achieved by noticing deviations between predicted and metered data on a network trained only with non-faulty data. Fault identification requires extensive data training using sets of data that contain both normal and faulty input/output information.

Work has been done on neural networks for building models for performance evaluation and fault detection. Due to the unknown inputs to a building in the future, some previous works have had difficulty getting a Coefficient of Determination, or R^2, above 0.7 which may be unacceptable in this application. Some methods involved a hybrid approach of two or more models working together and comparing the results between the two . However, a study by Alberto Hernandez Neto and Flavio Augusto Sanzovo Fiorelli found that a neural network was able to achieve higher accuracy when compared to an EnergyPlus model with a minimal amount of internal load specifications . Some attempt training with a calibrated model while adding faults to the model, one at a time, to get extensive input/output data of different faults . Using a calibrated model to train a network may work, but adds additional steps, including the time-intensive task of

creating a detailed model that is properly calibrated, and possibility for errors when the trained network is used with actual building information.

In terms of fault detection for buildings using neural networks, there are generally two kinds of fault detection. One approach is data driven-based methods that rely on large amounts of training and faulty data. While these data driven neural networks can obtain high fault detection accuracy, they cannot extrapolate fault conditions beyond the levels of training, according to Zhao, et. al.. Zhao's artificial intelligence fault detection review continues to discuss knowledge-based methods, the other kind of artificial intelligence fault detection. It is stated that while knowledge-based methods are capable of reasoning with different kinds of diagnostic information, they rely too heavily on expert knowledge . Given the drawbacks presented for fault detection, it is of no surprise that a separate neural network review discovered that HVAC and analysis of heating and cooling loads had the fewest attention by researchers while electrical energy use prediction for industrial work was the most researched .

To explore the two main kinds of neural network fault detection two separate approaches are explored: time series and decision trees. Time series neural networks take training data and constructs a network that, ideally, can be used to predict outputs. Diverse fields from economics to hydrology have seen successful implementation and time series data is present in almost all human processes. However, most network specifications and results still need to be created and analyzed by a trained modeler . While it is true that time series networks do automatically generate a prediction model, it is not an effortless task to have said model be effective.

Decision trees are different from time series neural networks in that trees classify

data, rather than predict values. Pattern recognition and feature discovery from large data sets while maintaining an intuitive nature have contributed to their use for over two decades. Another benefit to decision trees is their relatively short construction time when compared to other neural network methods. A potential shortcoming of decision trees is that they require data for normal and faulty operation to effectively classify data. Additionally, training algorithms tend towards overfitting data when the number of data points is fewer than the algorithm, while more data points tend towards generalization. Despite the inherent difficulties of neural network decision trees, the successful implementation of these types of systems, along with their straightforward methodology, provides a perfect candidate for fault identification comparison for the SPBM.

Given the amount of potential promise discussed thus far, it may raise questions as to why neural networks are not the standard modeling technique used for energy modeling. While it is true that neural networks have a lot of promise, they also have unique drawbacks that put them at a disadvantage in some circumstances when compared to traditional modeling techniques. One potential problem of neural networks is overfitting, or when input/output relations become fitted to noise instead of underlying data . However, the most prominent problem with neural networks is systematic to their operation: parts of the model cannot be tweaked, but rather tricks and parameter tuning need to be performed by an experienced person to generate a useable model. Model tuning is further set back by the recommended method for simulation optimization being to try the maximum number of potential configurations, compare results using various metrics, to try and discern a pattern, and pick the ‘best’ result. The need for large sets of data for accurate training also means that either a building needs to operate in a faulty

condition over long periods of time or a high-fidelity model of a building needs to be constructed in order to provide enough data to train a neural network. Given the nuance and data requirements that are necessary for neural networks, it is obvious that machine learning is not a simple and self-generating modeling technique.

2.7 Uncertainty Analysis and Model Calibration

Models that represent reality have uncertainty in their results. It is usually important to understand how different inputs to a model will affect the output values. For automatic fault detection devices, knowing the range of outputs based on reasonable changes to inputs may help avoid false positives in detection. Additionally, uncertainty analysis could be used after automatic calibration to test parameters and identify what could be the cause of a possible fault. Uncertainty analysis is also used to determine which parameters have the largest effect on building loads .

There are usually several parameters that are common across different models when testing uncertainty in calibration. These typically include wall and window unit conductance values, lighting power, plug load power, and occupant count . Physical parameters will often be estimated through construction documents or in conjunction with on-site measurements. Initial work on the SPBM has utilized Nelder-Mead in conjunction with a sum squared error to find parameter values. The equation-based modeling system used for SPBM calibration has built-in sensitivity analysis, so parameter values can be found and tested for sensitivity using the same program. Additionally, uncertainty analysis of load prediction during faulty building operation allows for a numerical comparison between parameters and model results.

Probably the most simplistic way to calibrate a model is to compare outputs of a

simulation to metered data. While automated methods for calibration have been explored , manual calibration of detailed simulations is possible, although rely heavily on the experience of the modeler. The process of calibrating detailed models often involved gathering construction plans and HVAC information from drawing data and using standard input values for internal loads based on what activities zones would be used. Metered data and simulated data are compared, and manual tweaking of parameters would be made until the model was in sufficient agreement. Because of this need for a skilled person to manually construct a detailed model, simplified building modeling for automatic fault identification has been investigated.

2.8 Fault Detection

There are numerous methods for fault detection in buildings: rule based, logic trees, complex modeling, group modeling, and manual inspection to name a few. Automatic fault detection devices are primarily focusing on individual component faults . Most of the current AFDDs focus specifically on AHU or component faults.

While automatic fault detection in HVAC components has been explored, fault detection usually requires extensive use of sensors coupled with simulations of a specific component . Currently some research and actual applications are done based on creating rules for a program along with sensor data to determine if components are not behaving properly ; some methods rely on pattern recognition of existing sensors to determine faults . Additionally, some model the HVAC system or individual component to see if overall performance, and component performance, is similar to actual energy use . Practical applications of automatic fault detection are not perfect but are a useful tool for building evaluations.

There is some work using building models and incorporating the data and weather files into EnergyPlus to compare the results between the simulated results and actual performance . This method requires a detailed model and knowledge of the existing building to effectively compare a model with real building results. While this method is effective for determining if a building is operating as planned, it still requires making an accurate model that is calibrated to the building. This type of building evaluation is being done through Continuous Monitoring, Metering, and Evaluation (CMME). The process involved making a detailed model (such as with EnergyPlus) that replicated the desired building as closely as possible. Any available metering was fed into the complex model to be used as internal load data and custom weather files were generated so that the model operated in the same conditions as the real building . Then, modeled and metered data was compared to try and determine if there was a problem. If modeled and metered data did not align, individual components were examined to attempt to find the cause of energy divergence. While effective, CMME is a time intensive method to detect faults because someone needs to create a detailed model, evaluate multiple points of comparison, and check performance of a real building.

NNs are another method for AFDD. This method requires a NN be trained to understand input/output dynamics of a building. The issue with this method is that NNs are susceptible to dramatic changes in output if the inputs are not the same as the training conditions . For fault detection, this may be a desired trait such as output deviation from normal or may be undesirable because outputs may be artificially amplified but because NN structure is unknown and poorly extrapolates. However, if deviation as such, NNs may be good programs for alarms but are not easily adapted to changing conditions

without retraining.

2.9 Patent Investigation

Due to the industrial nature of HVAC, an extensive look into patents was conducted. Both predictive control and automatic fault detection were investigated. The majority of patents appeared to be in the area of predictive control, specifically adjusting temperature setpoints to either take advantage of “free” cooling at night , predict how HVAC settings will change zone temperatures before switching modes , and identify if areas are occupied to change setpoints . These patents reflect the academic papers investigated earlier and together give insight to the current work on predictive control.

Fault detection patents were fewer in number but also matched the ideas discussed in the academic paper reviews: mainly with modeling individual components and comparing real performance data or using detailed on-site information in conjunction with a model to estimate load or temperature in a room . None of the patents revealed a way in which a model or method would be used to identify faults, only that a model of a room could be used to identify faults. Considering the vagueness of patents, and how recently they were posted, using an automatically calibrated SPBM in conjunction with limited building metered data, and comparing the performance to neural networks, is a novel and useful area of research.

2.10 Overview

After evaluating the history of fault detection and building modeling techniques, there does not appear to be a thorough investigation on what type of procedure for automatic fault detection is the most accurate for limited building information. Recent

developments show that automatic fault detection is an increasing priority for different researchers and private companies. Understanding what sensors are necessary, and how limited information can be used for fault detection, would have far reaching benefits. The scope of this research will be limited to physics-based modeling and neural networks as they are at opposite ends of computer-based modeling techniques.

CHAPTER 3. ENVELOPE REPRESENTATIONS

Heat transfer into a building is inherently transient. Consequently, the thermal resistance and capacity of the various layers in the opaque building envelope determine the amount and timing of a large fraction of the heat gain or loss, and these features are determined in a non-trivial way by the properties, thickness, and placement of the structural and insulating materials. Obviously, envelope construction greatly affects how much and when a building will experience heating and cooling demand; therefore, adequately modeling the opaque walls of a building from design data or by inferring the parameters from observed data is necessary for effective fault detection and similar applications. Opaque wall models in the SPBM for fault detection must be simple enough for efficient computer implementation and parameter estimation while being sophisticated enough to realistically model a multiple layer thermally massive wall without introducing so many adjustable parameters that implementation of automatic calibration will be difficult or impossible. Generally, there are three types of opaque wall constructions: one when most of the mass is on the exterior with insulation on the interior, another where a majority of mass on the interior with insulation on the exterior, and walls with distributed mass and insulation. The model must be compatible with all three kinds of constructions and be able to automatically estimate parameters when given minimal information. The purpose of this chapter is to demonstrate the process of identifying possible envelope heat transfer representations, evaluating and comparing these models, and finally selecting an adequate but not overly complex opaque envelope

model for the SPBM. Ultimately, a suitable relatively simple model is successfully identified and demonstrated.

3.1 History of Envelope Conduction Modeling

Transient envelope conduction modeling was utilized for over fifty years of building energy modeling . However, accounting for transient envelope heat conduction relied on manual calculation methods such as CLTD, Radiant Time series Cooling Load Calculation Procedure (RTS), or a thermal time constant . These methods often relied on extensive calculations to be able to simplify the conduction equation for the period being investigated. However, for when the material properties are unknown, or many hundreds of wall configurations are being tested, this approach requires a lot of work in order to set up each wall representation.

A transfer function heat transfer model, such as the one used for CLTD, was explored for the sake of completeness. The equations to determine the constants of the material are not excessively difficult to compute but do require knowledge of the wall structure and materials to process the equations . If the construction and wall properties are known, then a time series method of evaluating conduction loads is an attractive choice. However, due to the assumption that wall construction and material properties are unknown, the time series method, and others like it, have significant disadvantages. The primary disadvantage of time series type methods is having to estimate the number of wall materials, and the properties of each material. While an R-C wall representation can assume bulk wall properties, a time series method would need to calculate the number of different materials, material thickness, density, conductivity, and specific heat. These additional properties would add significantly more challenge to the process of automatic

calibration and any computational speed benefit is lost from the additional steps in determining wall properties.

Modern programs have different options for calculating conduction heat transfer. A common method is finite difference and finite element estimation which is reliable for most cases and produce accurate results. The main drawback to these methods is the limitation of the program timestep and how it relates to stability . For very thin or conductive materials, the stability of the finite estimation often requires a short timestep which can dramatically increase simulation time. The short timestep is due to the dependence of material Fourier number as shown in Equation (1).

$$\text{Fo} = \frac{\alpha t}{l^2} \quad \text{where Fo} < 0.5 \text{ for 2D finite difference} \tag{1}$$

However, iterative solving as utilized by the SPBM has been found to be more stable than typical forward difference calculations. Nevertheless, the finite difference method has many similarities to the R-C method used by the SPBM and discussed in depth in this chapter.

3.2 Initial Testing

A primary objective of the SPBM is to model a complex wall, or any wall, with a minimum number of independent nodes and inputs. This model was tested numerically by comparing the results from different constructions in EnergyPlus, a complex, highly developed, and well-verified model, which can be assumed to generate accurate wall conduction loads , to the results gathered from various simplified wall models implemented in the equation-based modeling system. EnergyPlus was chosen for its high level of accuracy and its open-source nature . Additionally, testing wall constructions and

conduction performance with real-world data was not feasible for the scope of the investigation.

To test the model the conductive load through the wall was represented by calculating the heat transferred to the interior zone through convection and comparing values generated by EnergyPlus. The convective heat load was compared to both EnergyPlus and Time series method solutions at first to validate both external models . The transfer function uses a set of constant values with previous hour sol-air temperature and conduction load and is explained in greater detail after Equation (2). While EnergyPlus is a dynamic simulation, ASHRAE uses a time series solution that assumes a constant interior temperature, external heat transfer coefficient, and internal heat transfer coefficient. The interior temperature was held constant for comparing the SPBM to the time series method, however, the complete SPBM normally operates with a full interior air and moisture model with internal air temperature fluctuations.

Generally, the models were compared using TMY3 Atlanta weather for a week in January and a week in July. TMY data is a typical meteorological year derived from National Solar Radiation Data Base . This weather data was chosen for its typical performance and consistent data; while on-site weather is available, it has inconsistencies and missing information associated with a small weather station. Equation (2), which gives an hourly heat gain through a surface, requires previous values for $T_{e,\tau-n\Delta}$ (external sol-air temperature) and heat through the wall ($\dot{Q}_{e,\tau}$) at time $\tau - n\Delta$ where the time is n hours behind the current time. For reference, the sol-air temperature is an adjusted outdoor air temperature to account for thermal radiation and solar radiation on external surfaces.

$$\dot{Q}_{e,\tau} = A\left(\sum_{n=0} b_n T_{e,\tau-n\Delta} - \sum_{n=1} \frac{d_n \dot{Q}_{e,\tau-n\Delta}}{A} - T_{rc}\sum_{n=0} c_n\right) \quad (2)$$

The sol-air temperature, Equation (3), takes the outdoor air temperature, adds the solar irradiation, and subtracts the total emitted thermal radiation and divides the sum of radiation by the external convection heat transfer coefficient.

$$\mathrm{T}_{\mathrm{sol-air}} = \mathrm{T}_{\mathrm{OA}} + (\alpha I - \dot{Q}_{emission})/h_O \quad (3)$$

The transfer function equation relies on previous values of $\dot{Q}_{e,\tau}$ and therefore the evaluated day must be repeated several times until a periodic steady-state solution is found as initial conditions have a high impact on starting results. The amount of thermal mass and the placement of thermal mass in conjunction with thermal resistance increases the number of repeated days until a periodic response forms. Likewise, the value of *n*, or the number of previous inputs that impact the current heat flux also increases for walls with more thermal delay. For example, ASHRAE wall 102, a relatively massive wall with brick on the exterior, concrete block with foam interior, and insulation interior , Equation (1) requires six values for the summation and five days of analysis to generate a periodic function; walls with less extreme thermal flywheel effects require fewer values. While a time series solution is computationally efficient once the constants are known, determining the number of previous values needed and the constant for those previous values is a non-trivial task. Because wall material properties are unknown, trying to determine not only the value of *n*, but the values for the transfer function coefficients *b*, *c*, and *d* for each value of *n* was deemed unreasonable for an automatic calibration method. However, other methods for numerical modeling that are thermodynamically rigorous may be explored to decrease computational time.

The initial design for simplification of wall and roof models was to have one outer layer of high-resistance, low-thermal-capacitance material and one inner layer with low thermal resistance but high thermal capacity. This simplification is based on the 1985 ASHRAE 32 wall construction and was desirable as there would only be two variables: the insulation thickness and thermal mass thickness. However, it failed when evaluating more massive walls such as those in Figure 1. The material properties of the 1985 ASHRAE 32 wall were used, and the thickness of each layer was changed to match the performance. Early problems arose with using thickness because while each of the two layers had different kinds of materials, increasing the resistive layer would also increase thermal capacity and vice versa. This method leads to low accuracy and an inability to use materials other than the ones specified as each layer contained both thermal resistance and thermal capacitance.

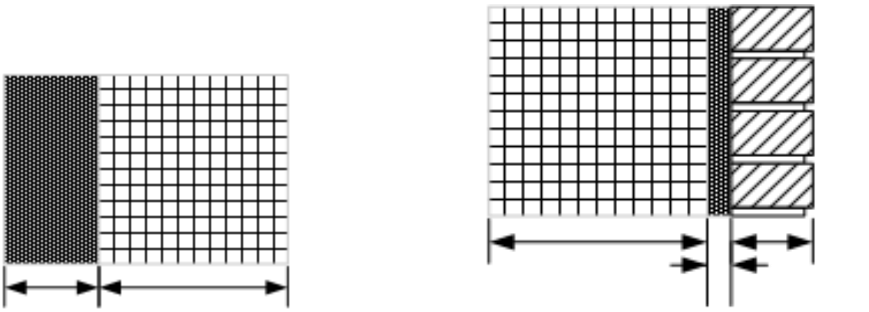

Figure 1: Cross section of ASHRAE 32 type layer wall and a heavy wall such as ASHRAE 102

The SPBM was changed so that each layer has a resistance, or R value, and capacitance, or C value, which is adjusted independently. A diagram of the new design can be seen in Figure 2. The new model removed the unnecessary dependence on thickness and allows for an equivalent resistance or capacitance using any material

desired. This design has an additional benefit of requiring fewer inputs while allowing for simulation of any material combination and allowing for any number of nodes or "layers". Different wall constructions require different number of nodes to accurately model conduction loads; the paper covers different wall constructions and required number of nodes later in this section.

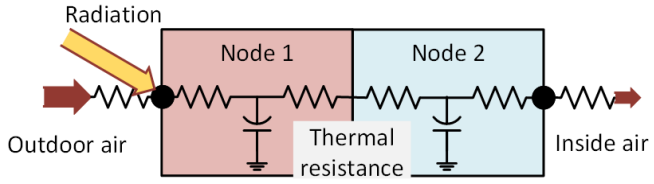

Figure 2: Simplified model node network for SPBM showing 2 layers, where each layer has independent properties.

It was discovered that the internal and external air heat transfer coefficient being used in the simplified model, and time series method, was much higher than the calculated heat transfer coefficient generated by EnergyPlus. ASHRAE reference provides an external heat transfer coefficient of 17 [W/m^2k] and internal heat transfer coefficient of 8.5 [W/m^2k] ; while EnergyPlus calculates a heat transfer coefficient that averages 5 [W/m^2k] for the exterior and 1.7 [W/m^2k] for the interior. However, EnergyPlus convection heat transfer coefficient values do not appear to change dramatically for vertical surfaces while horizontal surfaces appear to have two primary values depending on the surface temperature and the air temperature. The model was tested to see if one interior and one exterior heat transfer coefficient could be used for an accurate model. The roof was used as a benchmark as that surface goes through the largest change in level of energy gain, energy loss, and surface temperature in a day. The test resulted in a constant heat transfer coefficient that had less than 1% error when compared to the imported heat transfer coefficient version. One value could be given for

vertical surfaces and two for horizontal (one with surface hotter than air and one with surface colder than air). However, calculating convection heat transfer coefficients improves accuracy while reducing unknown parameters at the expense of computation time. To summarize, a constant convection heat transfer coefficient can be used but requires calibration; a calculated coefficient is more computationally intensive but does not require calibration.

3.3 Development of Weather Correlations

A critical objective of the SPBM is to only require widely available weather information: solar intensity, temperature, humidity ratio, wind speed, and wind direction. This data is often available for many locations and provides all necessary information for external envelope loading required for any practical building energy model. Correlations for solar, and convection heat transfer coefficients were used to estimate the load on the different surfaces.

3.3.1 Radiation Load

Testing revealed that one of the most influential loads on a building comes from the heat gained from the sun and lost to long wave infrared radiation. However, those loads are often easy to estimate with a few basic equations. Solar loading is affected by the beam normal radiation rate, diffuse solar radiation, cosine angle0 the surface makes with the sun, and the absorptivity of the outer most material. It is important to find reference information for the absorptivity of the exterior material as different materials have varying radiation properties depending on wavelength. Equation (4) relates the direct radiation ($\dot{G}_{\text{direct}}$), the diffuse radiation ($\dot{G}_{\text{diffuse}}$), the cosine angle the sun makes

with a surface ($\cos(\theta)$), solar altitude ($\sin(\alpha_{Sol})$), the ground reflectance (R_Ω), the view factor a surface has to the sky (F_{sky}), solar absorptivity(α) to determine the total solar load on any particular surface. While determining the absorptivity of a surface can be difficult, most building surfaces have an estimate of solar absorptivity.

$$\dot{Q}_{\text{solar}} = \alpha A \left(\dot{G}_{\text{direct}} \left(\cos(\theta) + R_\Omega \sin(\alpha_{Sol})\right) + \dot{G}_{\text{diffuse}} \left(F_{\text{sky}} + R_\Omega\right) \right) \quad (4)$$

Solar radiation is not the only kind of substantial radiation load on external surfaces, long wave infrared radiation emitted by surfaces provides a not insignificant level of cooling. As with solar absorptivity, longwave radiation emissivity values for common construction equipment are similar to each other and have established estimated values that produce respectable levels of accuracy . Due to infrared radiation heat transfer rate being a function of two different surface temperatures, Equation (5) for calculating the emission rate is slightly more complicated. It is important to note that the equation below assumes that the ground surface temperature and the air temperature are similar enough to be combined into one view factor and temperature.

$$\dot{Q}_{rad} = \epsilon \sigma A \left(F_{sky} \left(T_{surface}^4 - T_{sky}^4\right) + F_{ground} \left(T_{surface}^4 - T_{ground}^4\right) \right) \quad (5)$$

Internal radiation has been grouped into exchange between fenestration and the floor, which absorbs all solar radiation transmitted through fenestration and emits that thermal energy through convection into the zone air or through radiation exchange with fenestration. Results show that incorporating the internal heat capacity into a generalized and directly irradiated “floor” is an adequate model as simple physical reasoning would indicate.

Radiation exchange between the floor and windows is calculated using the same basic equation as for external radiation exchange although there is the added calculation of

determining the view factor of the window to the floor. Luckily, there are a number of built-in view factor calculators for different geometries.

3.3.2 Convection Heat Transfer Coefficients

There are a number of different external convection heat transfer coefficient correlations available for building energy modeling. The most simplistic being a fixed heat transfer coefficient for all weather and surface temperature conditions. Conversely, there are many computationally intensive calculations that attempt to account for complex fluid dynamics. More advanced convection heat transfer coefficient correlations can provide a higher level of accuracy at the cost of increased computation time, but at a point diminishing returns needs to be evaluated. Meters on the buildings that measure heating and cooling load are not very precise, nor is the weather instrumentation. As such, it was deemed unnecessary to attempt to match high precision convection heat transfer coefficient calculations as later testing revealed a constant term could be sufficient.

It was decided to test BLAST (Building Loads Analysis and System Thermodynamics) heat transfer coefficient correlation for its simple correlation yet relatively high accuracy . BLAST was selected for the relatively simple set of equations, shown below, and high accuracy. For example, a study found that for a multi-story building error averaged less than 5% for total daily load.

BLAST uses two distinct calculations, one for forced convection (Equation (6)), and one for natural convection (Equation (7)), then combines the two (Equation (8)). Neither equation is dimensionally consistent, require SI units, and produce a value with units of w/m^2-C. h is the convection heat transfer coefficient with units of W/m^2-C. W is a

dimensionless factor that is 1 if the angle of wind is within 55 degrees of the surface and 0.5 if the wind is leeward. *R* is a dimensionless roughness constant. *P* and *A* represent wall perimeter in meters and area in square meters respectively. *V* is air velocity is m/s.

$$H_f = 2.537 W_f R_f \sqrt{P_W V_W / A} \quad (6)$$

For natural convection, the temperature difference between the interior zone air temperature and the interior wall surface temperature is used to get an approximate value.

$$H_n = 1.31 |\Delta T|^{1/3} \quad (7)$$

Forced and natural convection heat transfer coefficients are added together for a reasonably accurate total coefficient value.

$$H = H_f + H_n \quad (8)$$

Upon further development of the SPBM, it was discovered that the wind speed modifier to account for the ground boundary layer became more significant. The value V in Equation (6) refers to the wind at the surface height and not necessarily the wind speed at the height measured. Obviously, as wind speed increases, the convection heat transfer coefficient also increases . For walls with less thermal resistance the convection heat transfer coefficient plays a more significant factor in conduction loss. The difference in energy transmission due to the convection heat transfer coefficient can be significant if a significant wind speed difference exists. However, for moderate walls, such as those tested in the example buildings in this thesis, the difference between purely natural convection and extremely high forced convection heat transfer coefficient could be as little as 10% difference. Therefore, both natural and forced convection terms are calculated for the SPBM.

For the purpose of further simplification, an investigation was conducted to see if part, or all, of the external heat transfer coefficient correlation could be set to a constant value. Computational time is spent calculating the different coefficients and if an insignificant loss in accuracy can be exchanged for a significant time savings, then the SPBM could proceed without detailed convection calculations. The test first compared six months of convection load from the south wall from BLAST, calculating the forced natural convection but having a fixed natural convection term, and a completely fixed heat transfer coefficient. The results were promising showing at most 2.5% loss in average accuracy and at most 0.16% loss in accuracy over the six-month test period – as shown in Table 1. Which could potentially lead to a reduction in simulation time while maintaining sufficient accuracy for all weather conditions.

Table 1: Numerical comparison between the three tested convection heat transfer coefficient correlation methods

	BLAST [MJ]	Fixed heat transfer coefficient	Fixed natural convection
Sum of conduction load	-494	-572	-608
Average % difference from BLAST	-	0.72%	2.52%
% difference for total load	-	0.16%	0.06%

Next, the results from convection load for the south wall, as calculated by EnergyPlus, was compared with the SPBM convection load, BLAST with a fixed natural convection heat transfer coefficient term, and a completely fixed convection heat transfer coefficient term. Figure 3 shows the monthly sum of convection loads through the south wall. All the methods of calculating the convection heat transfer coefficient were reasonably close to each other; while the SPBM/BLAST equation is closest to EnergyPlus.

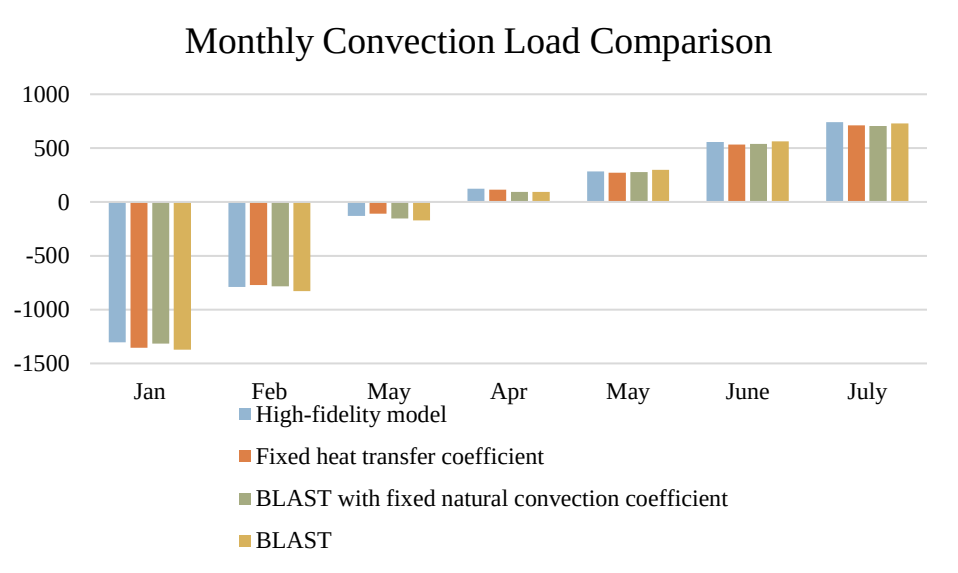

Figure 3: Comparison of the four different convection heat transfer coefficient correlation monthly convection load from the south wall

For every case, there is a small gain in accuracy for total convection load (R^2 greater than 0.99 for all cases) for the computational cost associated with the correlations. However, a decrease in computational time and complexity comes at the cost of calibrating these convection coefficient constants. While constant values showed promise, reducing the number of parameters was given a greater priority so as not hinder automatic calibration.

Fenestration has a slightly more complex relation between radiation exchange and convection because windows are assumed to not have significant thermal mass. Neglecting thermal mass means that fenestration acts like a heat balance between absorbed radiation from external and internal sources as well as internal and external convection. Due to the heat balance like performance of fenestration, the interior surface can get much hotter or colder than an opaque surface with the same external weather conditions. As a result of the greater temperature difference between surfaces and air, the convection heat transfer coefficient has more impact on the accuracy of fenestration load

into the zone than opaque surfaces. For double and triple pane glass there is a simple resistive element between the internal and external surface temperatures. Also, fenestration convection heat transfer coefficients are estimated using ISO 15099.

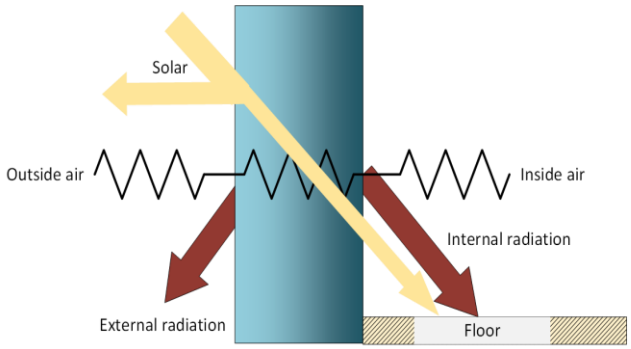

Figure 4: Representation of radiation and conduction load modeling for fenestration

Instead of calculating the convection heat transfer coefficient for every floor of a building, a study was performed on the relative difference between the loads on the first and second floor of a simple building. This investigation would see if the computational time for calculating convection heat transfer coefficients was necessary or if each cardinal direction could be calculated once and used multiple times. For more than one level buildings, the convection load was examined to see how different floor temperatures affected the convection load from the fenestration. There was less than a 5% difference in annual convection load between the two windows over a year, the results can be seen below in Figure 5.

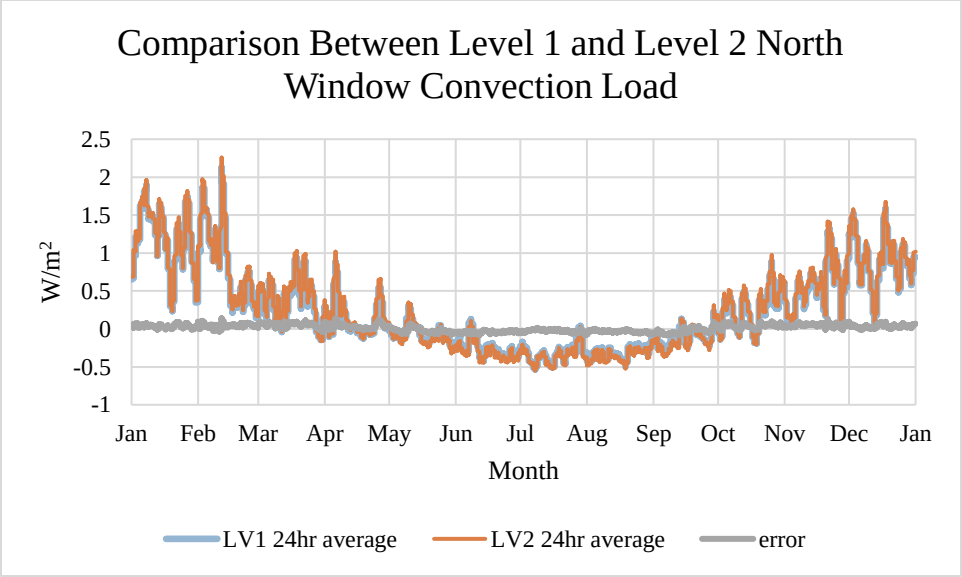

Figure 5: Comparison between north window convection load difference on level 1 and level 2

For the above and all subsequent comparisons between loads in this chapter the absolute error was plotted as to give a better representation of the divergence between the compared data sets. Other methods of comparison were investigated such as percent error and weighted percent error. These methods were deemed impractical due to the data having averages near zero as well as substantial portion of the data having values near zero. Division by zero, and other problems associated with values close to zero lead to the choice to stay in a dimensional, yet normalized comparison between data. As such, an XY scatter plot to show correlation, as in Figure 6, is also included when comparing different methods.

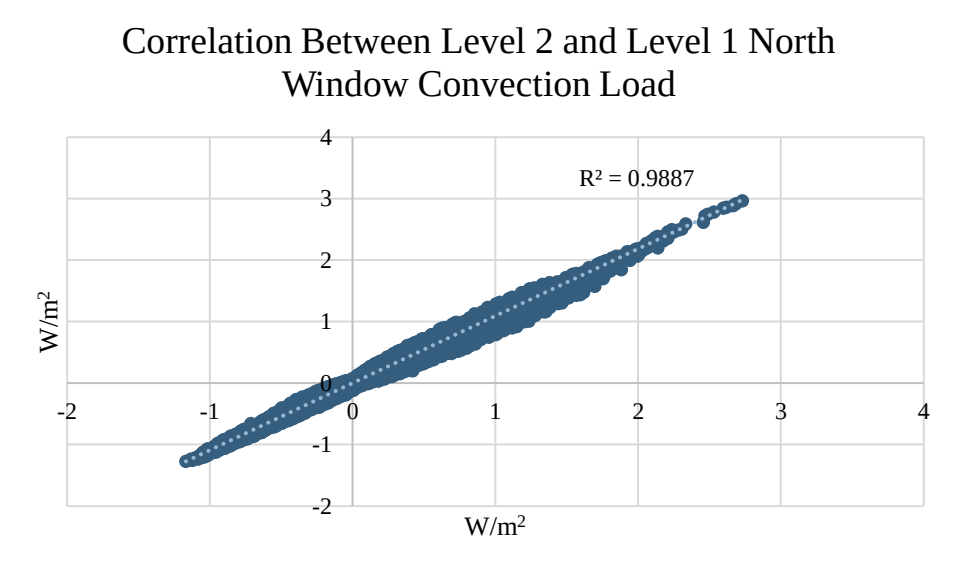

Figure 6: Scatter plot showing the correlation between the north window convection load from level 1 and level 2

The divergence in Figure 7 for the south wall appears to have a similar level of agreement as the fenestration convection load. While the scatter plot of Figure 8 shows divergence, it is around the zero-load value, which has minimal impact on building performance, meaning a fixed convection coefficient may be suitable.

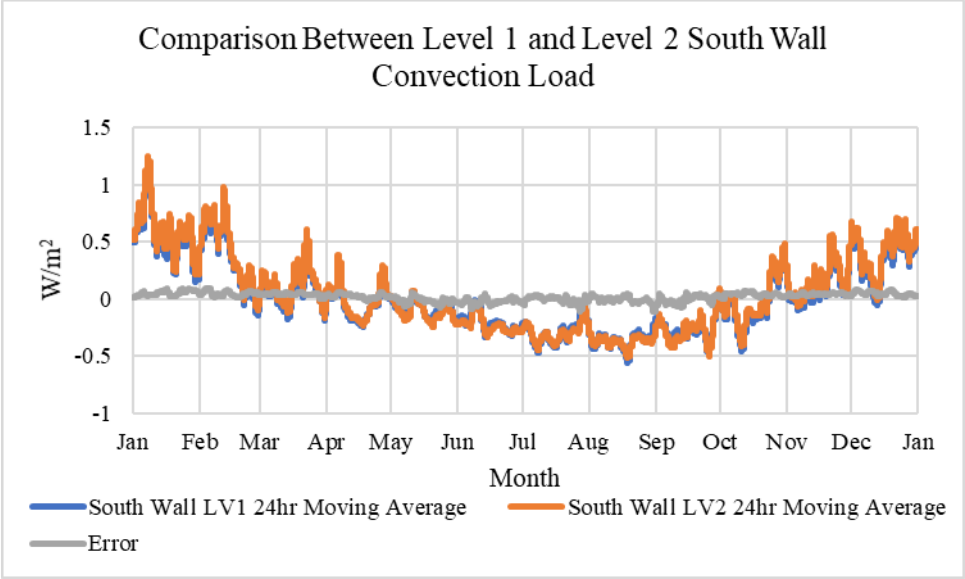

Figure 7: Comparison between south wall convection load difference on level 1 and level 2

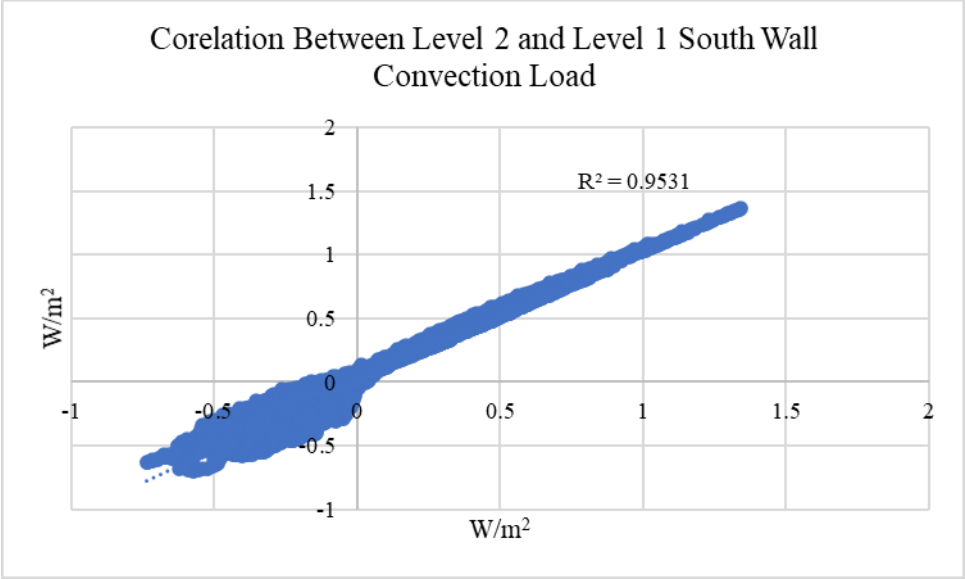

Figure 8: Scatter plot showing the correlation between the south wall convection load from level 2 and level 1

To reduce differences in internal temperature, both zones were specified to maintain a 0.25C° deadband about 22.5C and the results for the fenestration and wall convection were compared again in Figure 9 through Figure 12. Wall and fenestration divergences were significantly reduced by keeping zones the same temperature. This

experiment was only to see how different indoor air temperatures affect conduction load and if modeling one floor for the entire building would be possible. However, results were not promising and the complete SPBM will include independent air temperatures with a deadband.

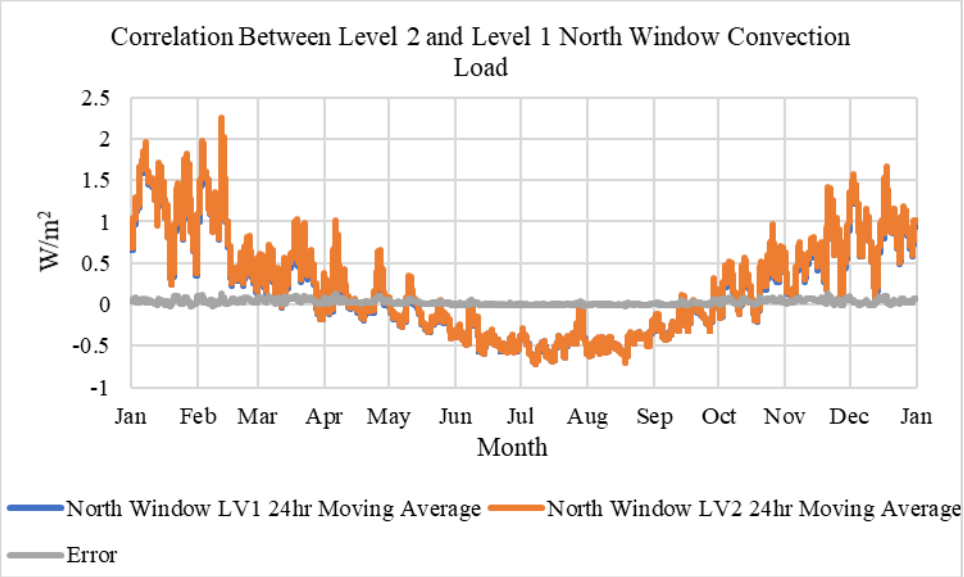

Figure 9: Comparison between north window convection load difference on level 1 and level 2

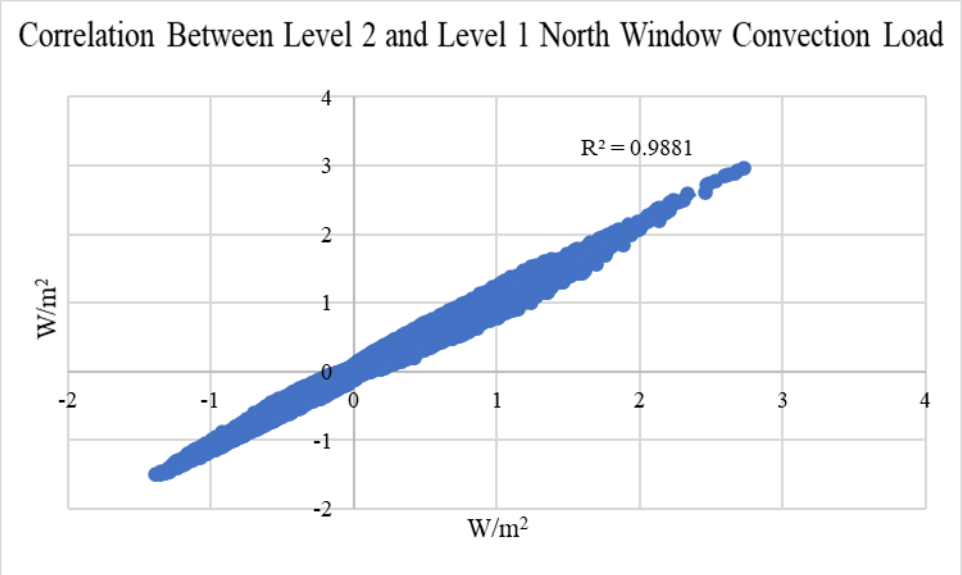

Figure 10: Scatter plot showing the correlation between the north window convection load from level 2 and level 1 when zone temperature is held constant

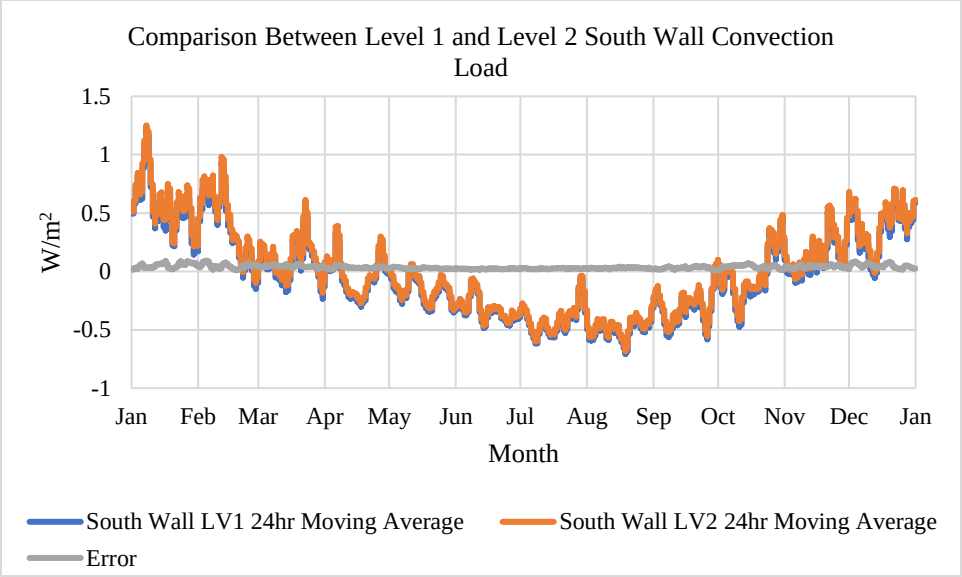

Figure 11: Comparison between south wall convection load difference on level 1 and level 2

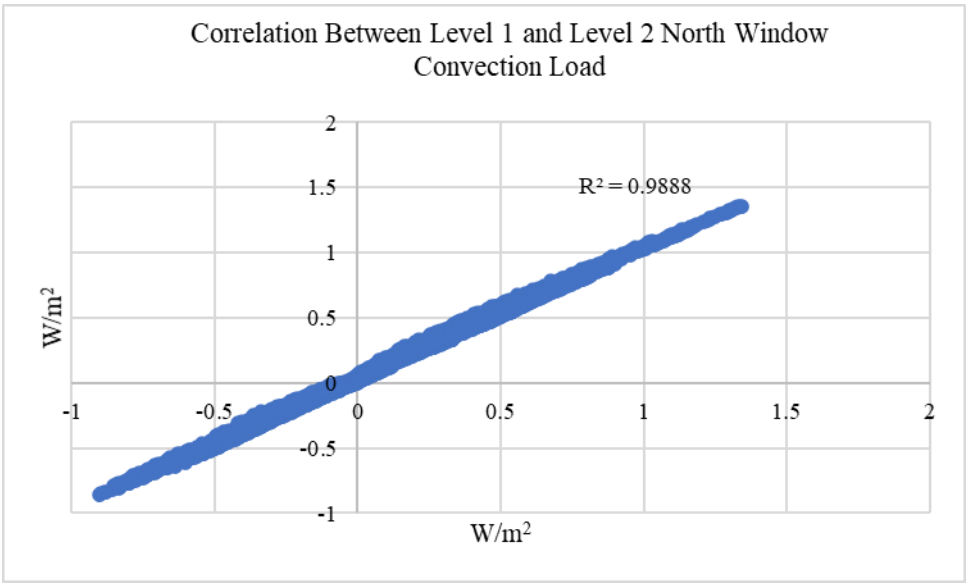

Figure 12: Scatter plot showing the correlation between the south wall convection load from level 2 and level 1 when zone temperature is held constant

As another point of comparison, the floor temperature was analyzed to see how it may impact loading. The surface of the LV2 floor was approximately 2C° colder than the ground floor surface temperature due to it being able to conduct heat to the LV1 zone air. However, the test floor used was simply a thin slab of concrete with no insulation, so a

real-world floor with insulation would not be as susceptible to heat dissipation through the bottom. Additionally, the LV1 floor has an adiabatic outside surface boundary condition which confines all absorbed thermal energy to LV1 unlike the LV2 floor.

The second level floor was replaced with a floor comprised of an outer layer of concrete and 6 inches of insulation. This was done to thermally isolate the two zones to better understand how the conduction load between floors behaves with less coupling. Conduction load for the south wall was analyzed to see if a multiplication factor could be applied to minimize the error between floor convection loads. A multiplication factor of 1.05 was able to bring the two convection loads in close agreement for the part of the year with the biggest load. The multiplication factor was found by minimizing the sum squared error between a correlation using the convection load for lv1, the zone temperatures, and a constant. The constant "a" settled around 1.05 while b and c went to 0. While there is some difference during the summer months, the difference is relatively small in Figure 13 as the convection load is small. Again, the majority of the divergence in Figure 14 is around small convection values that doesn't greatly impact the building load.

$$\dot{Q}_2 = \dot{Q}_1 a \left(\frac{T_2}{T_1}\right)^b + c \tag{9}$$

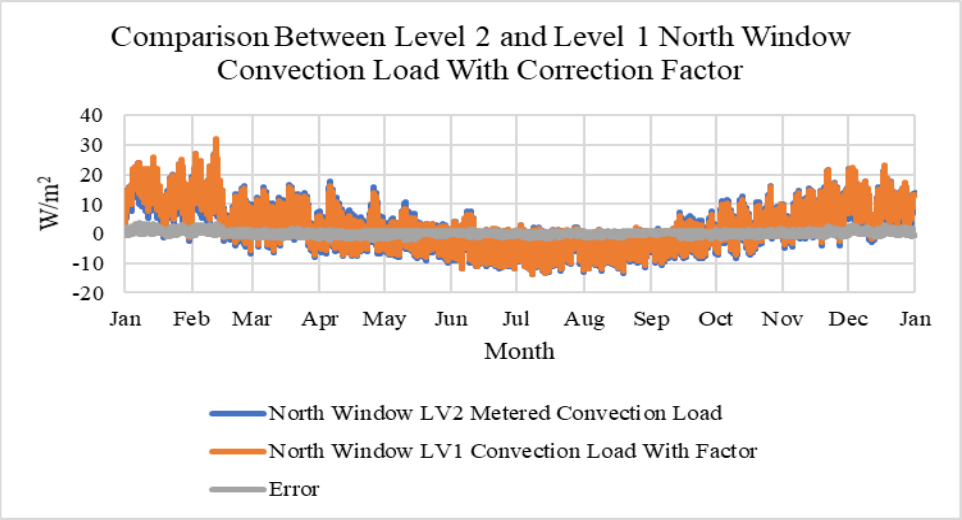

Figure 13: Comparison between south wall convection load difference on level 2 and level 1 when using a correction factor

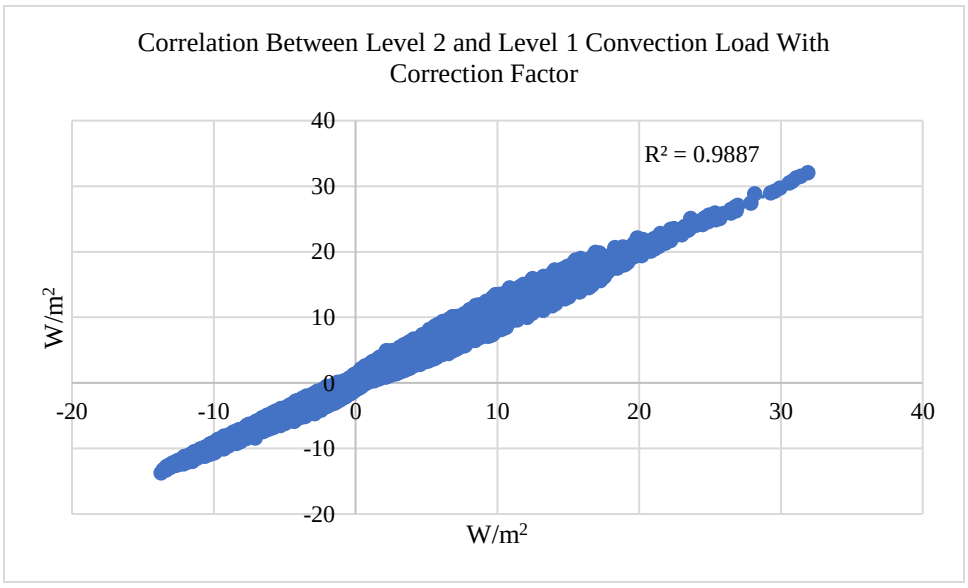

Figure 14: Scatter plot showing the correlation between the south wall convection load from level 2 and level 1 when adjusting the load using a correction factor

The use of a correction factor for different floors is a substantial decrease in computational time. The difference is small enough that the accuracy gained from simulating all the floors is outweighed by the associated decrease in computational time .

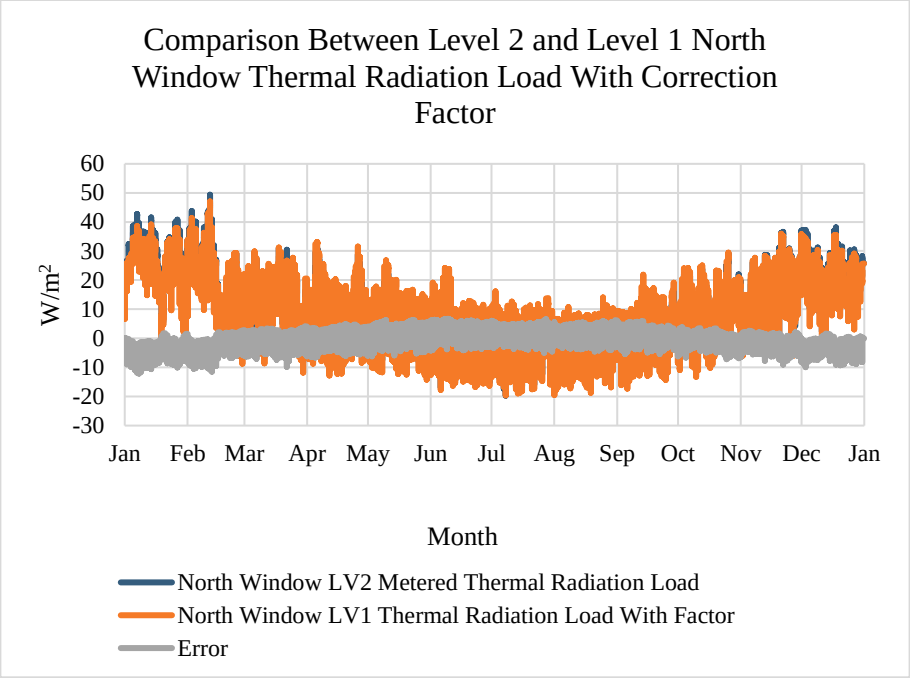

Figure 15: Comparison between north window internal radiation load difference on level 2 and level 1

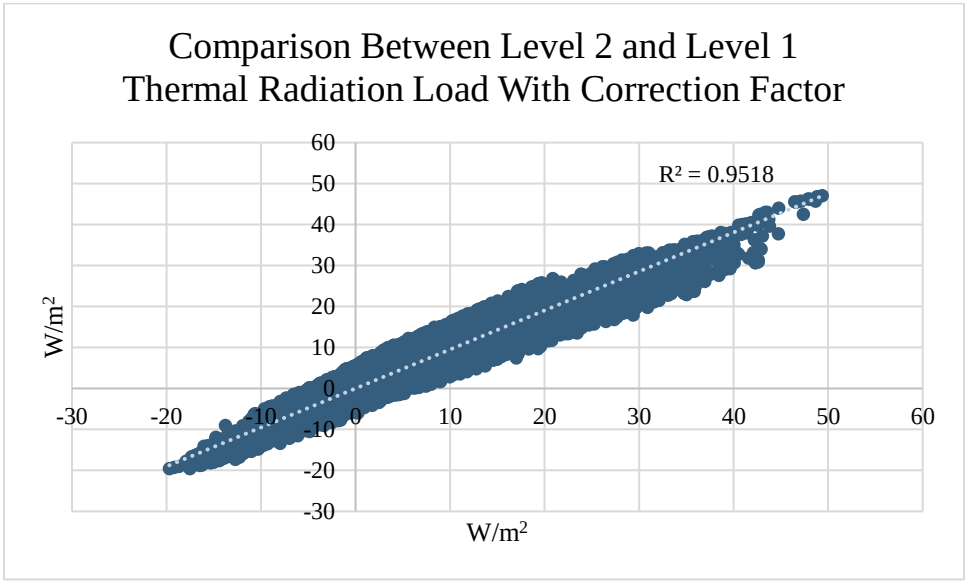

Figure 16: Scatter plot showing the correlation between the north window internal radiation exchange load from level 2 and level 1

In addition to the correlation presented above, other correlations between floor loads were investigated. These ranged from using the surface sol-air temperature, internal air temperature, and just the outdoor air temperature. These attempts did not lend

themselves to any greater level of agreement and often lead to issues when the factor would approach zero values and often required arbitrary constraints. The only real difference between floors is the internal air temperature and the slight change of forced convection heat transfer due to different distances from the ground (and higher floors being less susceptible to the ground boundary layer effect).

Lastly, the heat transfer coefficient was plotted against the delta between a wall surface temperature and the zone temperature. The profile is exponential, as expected, and would make a fixed value for HTC difficult to estimate. This profile does fit the complex HTC estimation correlation used. The profile of the convection heat transfer coefficient means that it would be possible to calculate the conduction load through all the surfaces without needing to recalculate external or internal heat transfer coefficients.

To conclude this section, it has been demonstrated that a simple multiplication factor for higher floors is sufficient. The greatest level of accuracy for the conduction load was when the load was most extreme in the heating season. This method of adapting the load from one level to multiple levels will dramatically reduce the computational time of the model, as every level can be expected to add the same amount of time. However, if desired, every surface could calculate its own convection heat transfer coefficient terms, but this section demonstrated that for most cases this is an unnecessary process.

3.4 Internal Loads

Internal loads and accurate associated use schedules are vital to model accuracy yet also are significant sources of uncertainty . These kinds of loads are often difficult to analyze on a level necessary to account for natural variations throughout the days. To combat the irregular nature of internal loads, the electrical meter data, shown below in

Figure 17, for Whitehead was used. The meter does not distinguish between different internal loads (such as HVAC, lighting, or plug) so a factor is applied to the total energy consumption to estimate what fraction of the real load is internal and what part is HVAC electricity consumption. In addition to providing the internal load information, the nature of the electrical data provides a useful metric to determine if the building is occupied. The other building being analyzed, Old Civil Engineering, also displays a similar pattern of a steady baseline load and peaks during occupied hours in Figure 18. A simple if-then command was implemented to say that if electrical load was a significant portion over baseline/night use then the building is occupied and allowed for automatic workday detection.

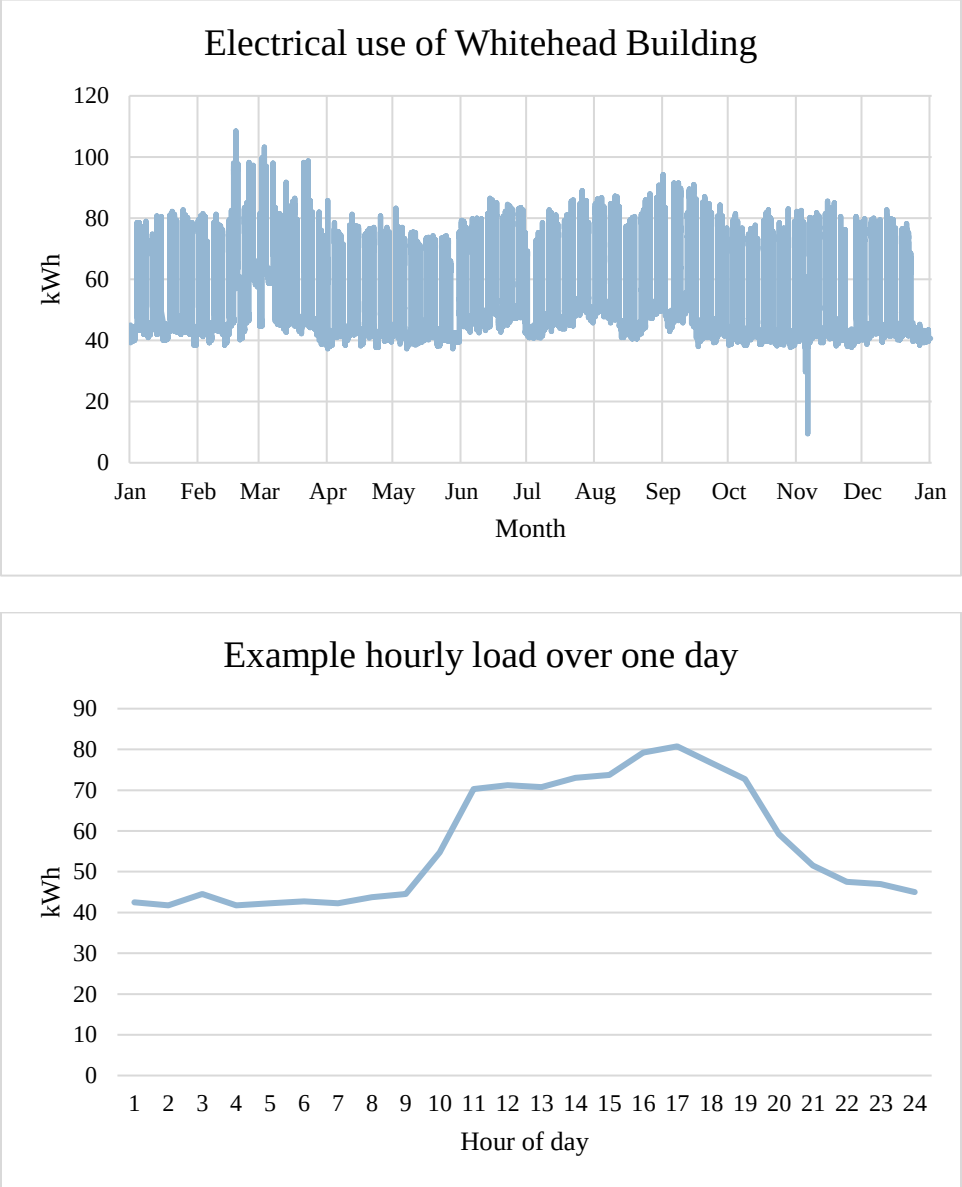

Figure 17: Annual hourly electrical load for Whitehead Building (top) and for one day (bottom)

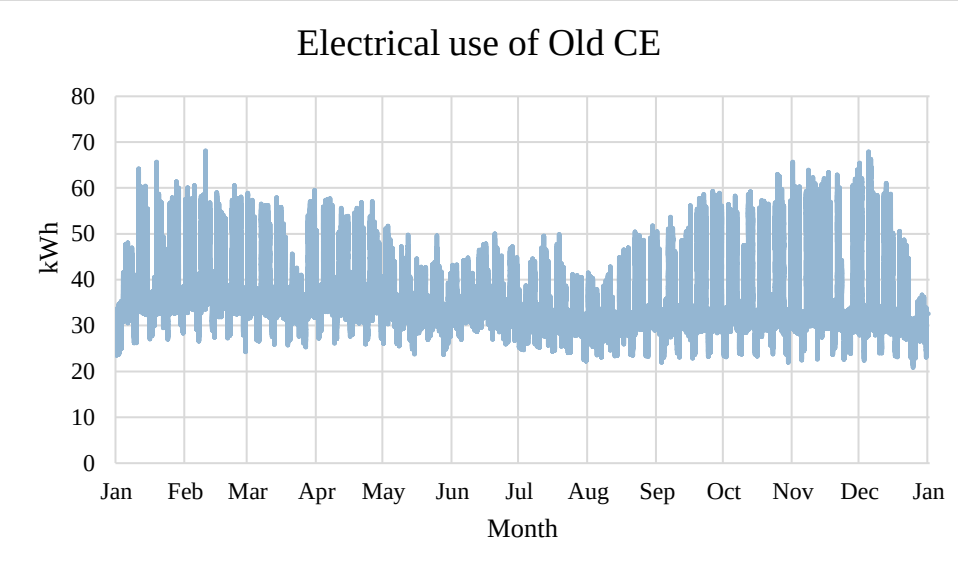

Figure 18: Annual hourly electrical load for Old CE

Electrical data gathered from the building can also serve as a way to distinguish between occupied and unoccupied times. Rather than implementing a strict schedule, any time building electrical use is a significant percent more than the base/night load then the building can be assumed to be occupied. Using electrical load to predict occupancy has been studied and deemed to be an accurate way of estimating occupancy levels . Not relying on a strict schedule for occupancy also has benefits in buildings with variable occupancy such as institutional, government, and commercial locations as there are many days where a building may be closed that are not official holidays or that change on a year-to-year basis as these changes appear as a reduced electrical demand for that day.

Occupants present a unique load to a building when compared to electric loads. While electric loads are purely sensible, people both heat their environment, and produce water vapor and CO2. Both water vapor and CO2 need to be removed from internal zones to satisfy occupant comfort and safety. Removing internal contaminates is often done by

supplying enough outdoor air to the building to ventilate spaces; details of HVAC and air handling will be discussed in a later section.

3.5 Testing Property Estimation of Simplified Walls

Once the model of the wall construction was operational, testing of property estimation was done before trying to analyze complex walls. 1985 ASHRAE 32 wall material properties was used as a baseline and the conductive load through the south wall was gathered. Both the R and C values for the two layers were decreased by 20% and the new conductive load was recorded. Error minimization through Nelder-Mead minimization of sum squared error (SSE) was utilized to determine if overall conductive load could be used to regain the initial material properties. Figure 19 showcases how different parameter values alter conductive load through surfaces and also how SSE-based minimization can be utilized by the SPBM to arrive at a unique solution.

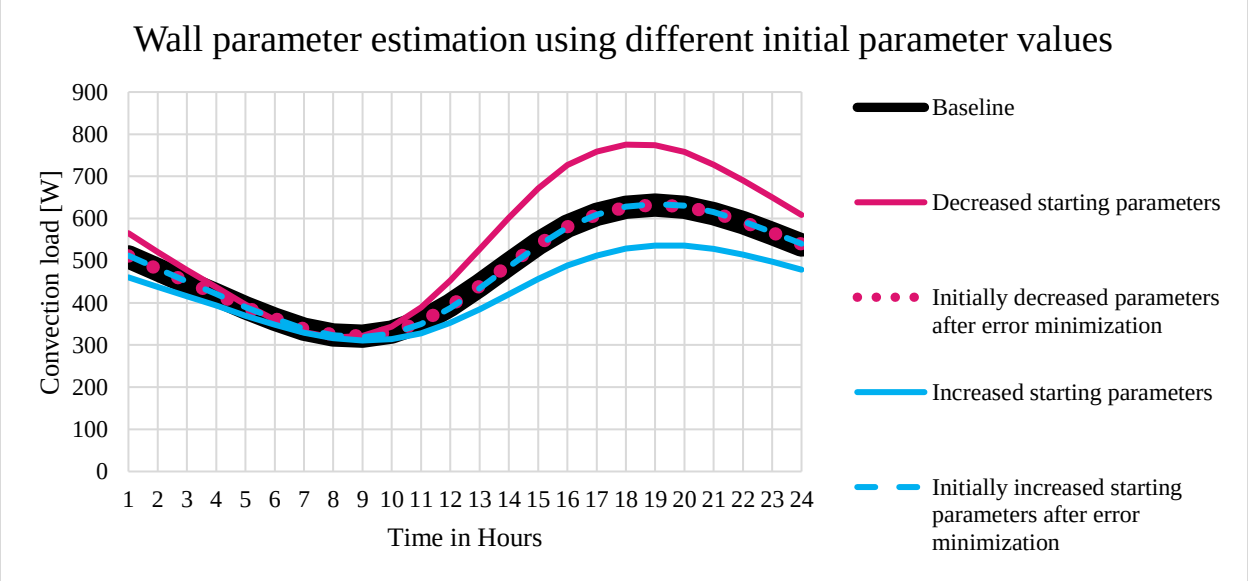

Figure 19: Results of wall parameter estimation showcasing unique solutions with convergence towards the same parameter values despite different initial conditions

The results converged on the original values and are displayed in Table 2; the first layer was within 5%, the second layer had less than 1% difference. The total conductive load error dropped seven orders of magnitude from the 20% material difference to a negligible difference in total conductive load. The test was performed again with a 20% increase in material properties and the results were even better with a maximum material property difference of -0.12% from baseline values.

Table 2: Analysis of how parameter values are improved through sum squared error minimization to regain original values after initially being lowered by 20% from control.

	Layer 1 R [C/W]	**Layer 1 C [J/C]**	**Layer 2 R [C/W]**	**Layer 2 C [J/C]**	**SSE [W^2]**
Control	12.6	361	0.631	17700	0.00E+00
20% decrease	10.1	285	0.504	14200	1.92E+07
Post analysis	13.1	380	0.571	18200	5.24+E00
Percent off control	3.30%	2.74%	-9.61%	2.85%	0.00%

Given the high level of accuracy parameter estimation with simple constructions, testing of the model with complex walls was the next step. While the objective of the SPBM is not to get exact property values, the accuracy of the estimated values gives some confidence in the method of calibration.

3.6 Complex Wall Modeling

Initial comparisons of modeling a two-layer-two-parameter wall were met with success, but problems began to arise when trying to fit heavy or distributed mass walls. To test the SPBM with a variety of constructions, several ASHRAE standard walls were examined including 1991 ASHRAE wall 01 (steel siding with four inches of insulation), wall 13 (face brick, four inches of heavyweight concrete, and 0.61 inches of insulation, and wall 34 (face brick, twelve inches of heavyweight concrete and 1.36 inches

insulation. These walls were chosen as a representation of different kinds of wall constructions available. To demonstrate the amount of thermal load delay that is available, below in Figure 20 are the time series method solution and corresponding R-C results for those three different walls. The model shows how construction can drastically change peak load time and daily loading. The lightweight wall (Wall 01) has the load coincide with the external sol-air temperature. The medium wall (Wall 13) has a peak approximately eight hours after external sol-air peak. The heavy wall (Wall 34) has a peak approximately 12 hours after external peak load (Figure 20 shows that Wall 34 has the minimum load when the external load has the highest load, showing the 12-hour phase shift). Figure 20 also demonstrates how different constructions require different number of nodes for R-C analysis: a lightweight wall only needs one node, a medium weight wall provides better agreement with two nodes, and heavyweight walls generally require three nodes to achieve sufficient accuracy.

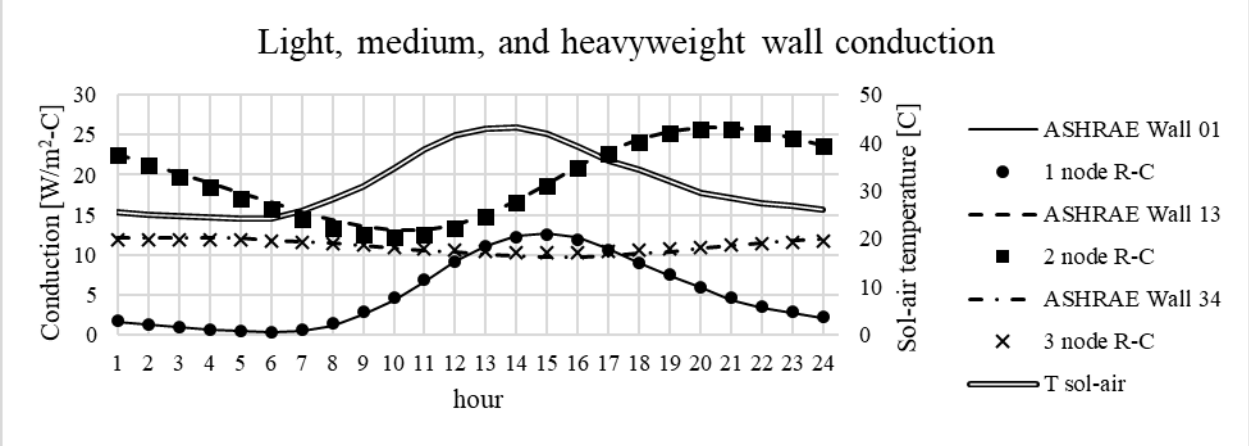

Figure 20: Comparison between the accuracy of a R-C conduction model to Time series method. Three different weights of walls were used to demonstrate the effect of material property placement and scale

To further explore the importance of placement of thermal mass and thermal resistance a simple study was conducted. The same 1985 ASHRAE 32 test wall (wall

with two inches of exterior foam insulation and four inches of heavyweight concrete) was analyzed in ‘standard’ configuration (when the concrete was on the interior and the foam on the exterior) in a ‘flipped’ configuration (where the foam was on the interior and concrete on the exterior), and when the concrete and foam was ‘mixed’ together to create a homogenized material (illustrations of the different construction are in Figure 21). All the walls have identical thickness, U-value (thermal resistance), mass, and thermal capacity. EnergyPlus was used for model validation because of its accuracy and internal air temperature control.

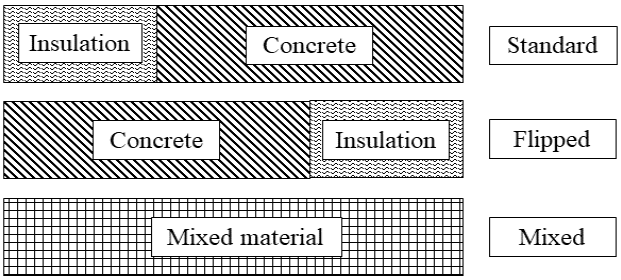

Figure 21: Illustrations of the three different constructions used to demonstrate importance of material placement

The R-C model was able to match the performance of EnergyPlus with two or three nodes. ‘R-C standard’ and ‘R-C flipped’ are both modeled with two nodes while ‘R-C distributed’ is modeled with three nodes, as demonstrated in Figure 22. While each wall has the same overall bulk properties, all three R-C models have differing values to create an optimum fit. In addition to different total conduction loads, the test wall demonstrates the importance of proper construction properties and that, generally, more nodes are required when a wall has substantial thermal delay.

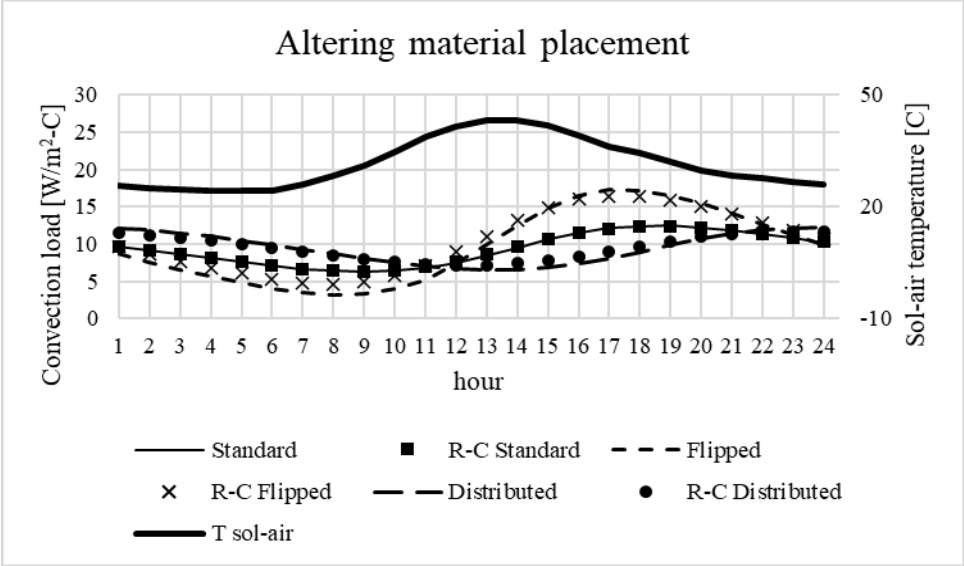

Figure 22: Comparison between how material placement in a wall changes conduction load while bulk wall properties remain constant. EnergyPlus and r-c models are used to demonstrate accuracy of two-node R-C system.

The test wall demonstrates the importance of accurate construction properties and material placement in models. All wall constructions have the same total weight, thermal capacitance, thermal resistance, and thickness; all that was changed is the placement of thermal mass and thermal capacitance. Properly accounting for different constructions is difficult and cannot be determined only by bulk properties, but the R-C model can replicate any reasonable conduction load profile. Identifying and accurately modeling the energy use associated with different construction materials and material placement is vital for any kind of building model, and something the R-C model can do.

3.7 Fenestration

Fenestration is more complicated than opaque surfaces in some ways but simpler than others. For instance, a common simplification of fenestration is to ignores the thermal mass of glass which makes conduction heat transfer simpler to calculate. However, fenestration is transparent to solar radiation yet opaque to long wave radiation;

meaning there are more parameters to account for both visible and long wave radiation. Using ISO 15099 specifications, the window does not contain thermal mass. While the importance of thermal mass is demonstrated to be important with most opaque surfaces, the thinness, high thermal conductivity, and small mass of glass means it cannot store a substantial amount of thermal energy to be released later.

The fenestration has the option to model panes of glass by treating the window as a solid piece with an effective resistance. The "center" of the glass is where the visible light is absorbed (shown in white in Figure 23, with hotter temperatures to the left and colder temperatures to the right, as the case would be during the day in summer). Convection and long wave radiation exchange is calculated from the two surface temperatures. There is assumed to be a linear temperature gradient between the two surface temperatures with the slope determined by the overall R value. All temperature and energy calculations are assumed to be instantaneous which greatly simplifies the process.

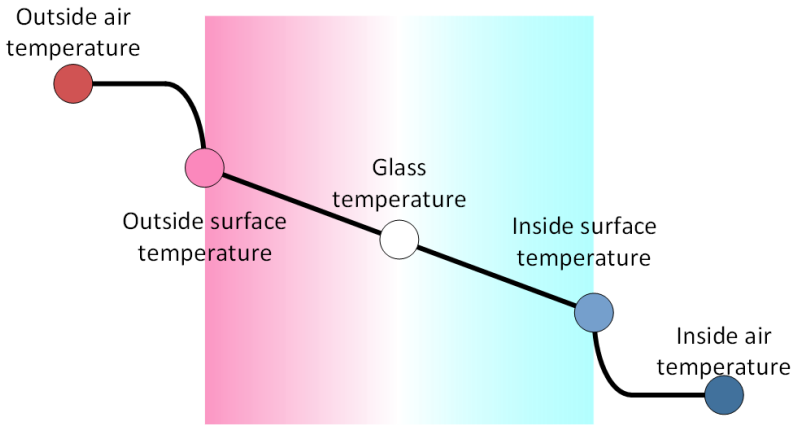

Figure 23: Representation of the temperature gradient from the outdoor air temperature, through the fenestration, to the indoor air temperature

Fenestration presents a challenge by transmitting solar energy to the interior. Solar transmittance is not a constant, but rather changes depending on the angle in which

solar energy arrives at the surface of glass, optical properties of the glass, and how many panels are present . Keeping with the simplification desired, the SPBM utilizes a lookup table for transmissivity; absorptivity is roughly constant for all but extreme angles, and reflectivity is simply one minus transmissivity and absorptivity . Additionally, multiple pieces of glass are accounted for by approximating changes in overall transmissivity, such as decreased transmittance due to multiple reflections. Combining the above strategies results in a fenestration model that is within 40[w/m^2], or 8%, in the most extreme solar loading.

3.8 Conclusion

Envelope dynamics is a complicated and critical portion of building simulation and vital to accurate fault detection. The SPBM showed the ability to match complex wall conduction loads with similar accuracy to EnergyPlus and Time series method. In addition to matching the results of complex simulation tools the SPBM can automatically estimate property values, a task complex modeling procedures have difficulty performing. This chapter has demonstrated that a R-C model is able to replicate wall and fenestration dynamics accurately and efficiently with a minimal number of variables and complexity. Faithful reproductions of building envelope thermal energy transfer lay a foundation in which internal loads can be reliably estimated and fault identification can be performed.

CHAPTER 4. FURTHER DEVELOPMENT OF SPBM AND NN FOR ENTIRE BUILDING

Having established a method for modeling opaque surfaces, the next step for creating a fully functioning SPBM would be to account for internal loads. Modeling the internal workings of a building presents new challenges because precise information about internal loads is often unknown. Few buildings have occupant counting or sufficient submetering to know where in a building electricity is being used. The buildings that use extensive metering present another problem in the form of malfunctioning systems, such as occupant sensors reading false positives; a fault that usually is only detected at night when the building is unoccupied. Consequently, some assumptions on occupancy, lighting, and plug load need to be made in the form of presumed schedules and peak values. Because of the uncertain nature of internal loads, machine learning may recognize patterns and more accurately predict loads than the SPBM, but that is explored in Chapter 7 and 8. This section explores the process in which the components necessary to model a building are created in a SPBM and NN. Additionally, the benefits and disadvantages of both model types will be discussed for which system may perform better for fault detection.

4.1 Weather Information

To make a clear comparison of model performance, it was decided to run a high temperature and clear sky solar load summer design day. The use of tables was unavoidable for some properties such as exterior dry bulb temperature, humidity ratio,

and solar load as the inputs for weather conditions. Interior air temperature was held constant for testing wall convection loading instead of the HVAC system at this point. However, the SPBM normally models interior temperature drift.

Local weather information is available for this test, including temperature, humidity, multiple solar meters, rain, wind speed and direction. While most locations do not have a weather station on site, local weather can usually be gathered from a nearby airport or university agriculture department weather station. Even weather websites often have enough information for the SPBM or NN training. For example, hourly temperature and humidity are typically available and solar load can be estimated through cloud cover and rain percent.

4.2 Rigorous Zone Temperature Equation Derivation

Beginning from first principles guarantees thermodynamic completeness in terms of conservation of mass and energy. Only by starting with a rigorous equation and working through the derivation can the final zone temperature equation be used with confidence. For reference, superscripts denote dry air (D), moist air (M), and water vapor (V). Subscripts denote location or source of the variable i.e., zone (Z), supply (S), infiltration (I), exfiltration (E), return (R), and generated (G).

Beginning with the energy and mass balance for the zone (control volume) leads to equation (10).

$$\frac{dU_Z^M}{dt} = \dot{Q}_S + \dot{m}_S^D h_S^M + \dot{m}_I^D h_I^M - \dot{m}_E^D h_Z^M - \dot{m}_R^D h_Z^M + \dot{m}_G^V h_G^G \tag{10}$$

Internal energy is then broken into its discrete variables of specific internal energy and mass. Note that the moist air internal energy is also broken into dry air and water vapor in equation (11).

$$m_Z^D \frac{du_Z^D}{dt} + m_Z^V \frac{du_Z^V}{dt} + u_Z^D \frac{dm_Z^D}{dt} + u_Z^V \frac{dm_Z^V}{dt} = \dot{Q}_S + \dot{m}_S^D h_S^M + \dot{m}_I^D h_I^M - \dot{m}_E^D h_Z^M - \dot{m}_R^D h_Z^M + \dot{m}_G^V h_G^G \quad (11)$$

Some simplifications are necessary to generate an equation that has a solvable closed form solution. This comes from the realistic assumption that the mass flow rate of infiltration is roughly equal to the mass flow rate of exfiltration. However, the mass flow rate of dry air entering through the HVAC may not be identical to the amount of dry air leaving. Therefore, equation (12) shows the supply dry air mass flow rate being equal to the return dry air mass flow rate in addition to any change in mass of dry air in the zone.

$$m_Z^D \frac{du_Z^D}{dt} + m_Z^V \frac{du_Z^V}{dt} + u_Z^D \frac{dm_Z^D}{dt} + u_Z^V \frac{dm_Z^V}{dt} = \dot{Q}_S + \dot{m}_S^D (h_S^M - h_Z^M) + \dot{m}_I^D (h_I^M - h_Z^M) + \frac{dm_Z^D}{dt} h_Z^M + \dot{m}_G^V h_G^G \quad (12)$$

Realizing that moist air enthalpy is comprised of dry air enthalpy and water vapor components, it is possible to replace h_Z^M on the right side of equation (12) and combine that term with u_Z^D to give equation (13).

$$m_Z^D \frac{du_Z^D}{dt} + m_Z^V \frac{du_Z^V}{dt} + \left(u_Z^D - h_Z^D - W_Z h_Z^V\right) \frac{dm_Z^D}{dt} + u_Z^V \frac{dm_Z^V}{dt} - = \dot{Q}_S + \dot{m}_S^D \left(h_S^M - h_Z^M\right) + \dot{m}_I^D \left(h_I^M - h_Z^M\right) + \dot{m}_G^V h_G^G \quad (13)$$

Next, the ideal gas law relating pressure and volume to mass, density, and temperature is used to rewrite some of the rate of change of mass terms. Additionally, relating specific internal energy with enthalpy, gas constant (R), and temperature allows for additional substitutions leading to equation (14):

$$m_{\mathrm{Z}}^{D}\frac{du_{\mathrm{Z}}^{\mathrm{D}}}{dt}+m_{\mathrm{Z}}^{\mathrm{V}}\frac{du_{\mathrm{Z}}^{\mathrm{V}}}{dt}-\left(R_{C}^{D}T_{\mathrm{Z}}-W_{\mathrm{Z}}h_{\mathrm{Z}}^{\mathrm{V}}\right)\left(\frac{m_{\mathrm{Z}}^{\mathrm{D}}}{P_{\mathrm{Z}}}\frac{dP_{\mathrm{Z}}^{\mathrm{D}}}{dt}-\frac{m_{\mathrm{Z}}^{\mathrm{D}}}{T_{\mathrm{Z}}}\frac{dT_{\mathrm{Z}}}{dt}\right)$$

$$+\left(h_{\mathrm{Z}}^{\mathrm{V}}-R_{C}^{\mathrm{V}}T_{\mathrm{Z}}\right)\left(\frac{m_{\mathrm{Z}}^{V}}{P_{\mathrm{Z}}}\frac{dP_{\mathrm{Z}}^{V}}{dt}-\frac{m_{\mathrm{Z}}^{\mathrm{V}}}{T_{\mathrm{Z}}}\frac{dT_{\mathrm{Z}}}{dt}\right) \tag{14}$$

$$=\dot{Q}_{\mathrm{S}}+\dot{m}_{\mathrm{S}}^{\mathrm{D}}\left(h_{\mathrm{S}}^{\mathrm{M}}-h_{\mathrm{Z}}^{\mathrm{M}}\right)+\dot{m}_{\mathrm{I}}^{\mathrm{D}}\left(h_{\mathrm{I}}^{\mathrm{M}}-h_{\mathrm{Z}}^{\mathrm{M}}\right)+\dot{m}_{\mathrm{G}}^{\mathrm{V}}h_{\mathrm{G}}^{\mathrm{G}}$$

Note that the right side of equation (14) will be represented as "RHS" in the below equations. Some additional assumptions are applied at this point, namely that the zone pressure does not change substantially. Keeping a constant total zone pressure allows the relation between the partial pressure of dry air and water vapor; namely that the rate at which one partial pressure increases is the same rate at which the other decreases. The other assumption being that the specific heat at constant pressure and volume do not substantially change. This assumption is made due to the limited temperature and pressure changes that a building zone will experience; typically, less than 10°C swing in a year. Applying the above assumptions in addition to the ideal gas law results in equation (15).

$$\left(m_{\mathrm{Z}}^{D}C_{v}^{\mathrm{D}}+m_{\mathrm{Z}}^{\mathrm{V}}C_{v}^{V}+m_{\mathrm{Z}}^{\mathrm{D}}R^{\mathrm{D}}+m_{\mathrm{Z}}^{\mathrm{V}}R^{\mathrm{V}}\right)\frac{dT_{\mathrm{Z}}}{dt}-\left(\frac{R_{C}^{\mathrm{D}}T_{\mathrm{Z}}m_{\mathrm{Z}}^{\mathrm{D}}}{P_{\mathrm{Z}}}-\frac{R_{C}^{\mathrm{V}}T_{\mathrm{Z}}m_{\mathrm{Z}}^{V}}{P_{\mathrm{Z}}}\right)\frac{dP_{\mathrm{Z}}^{\mathrm{D}}}{dt}-W_{\mathrm{Z}}h_{\mathrm{Z}}^{\mathrm{V}}\frac{dm_{\mathrm{Z}}^{\mathrm{D}}}{dt}+h_{\mathrm{Z}}^{\mathrm{V}}\frac{dm_{\mathrm{Z}}^{\mathrm{V}}}{dt} \tag{15}$$
$$=\mathrm{RHS}$$

Applying the ideal gas laws and relation between the specific heats of a gas allows for the following rearrangement within equation (16).

$$\left(m_{\mathrm{Z}}^{D}C_{p}^{\mathrm{D}}+m_{\mathrm{Z}}^{\mathrm{V}}C_{p}^{V}\right)\frac{dT_{\mathrm{Z}}}{dt}-\left(\cancel{V_{\mathrm{Z}}-V_{\mathrm{Z}}}\right)\frac{dP_{\mathrm{Z}}^{\mathrm{D}}}{dt}-W_{\mathrm{Z}}h_{\mathrm{Z}}^{\mathrm{V}}\frac{dm_{\mathrm{Z}}^{\mathrm{D}}}{dt}+h_{\mathrm{Z}}^{\mathrm{V}}\frac{dm_{\mathrm{Z}}^{\mathrm{V}}}{dt}=\mathrm{RHS} \tag{16}$$

Equation (17) has the rate of change of the mass of water vapor in the zone is adjusted and rearranged.

$$\frac{dm_{\mathrm{Z}}^{\mathrm{V}}}{dt}-W_{\mathrm{Z}}^{\mathrm{D}}\frac{dm_{\mathrm{Z}}^{\mathrm{D}}}{dt}=\dot{m}_{\mathrm{S}}^{\mathrm{D}}(W_{\mathrm{S}}-W_{\mathrm{Z}})+\dot{m}_{\mathrm{I}}^{\mathrm{D}}(W_{\mathrm{I}}-W_{\mathrm{Z}})+\dot{m}_{\mathrm{G}}^{\mathrm{V}} \tag{17}$$

Substituting the above equation in to the into the previous total energy equation and adding in the unchanged right-hand side of the equation results in:

$$(m_{\mathrm{Z}}^{D} C_{p}^{\mathrm{D}} + m_{\mathrm{Z}}^{\mathrm{V}} C_{p}^{V}) \frac{dT_{\mathrm{Z}}}{dt} + h_{\mathrm{Z}}^{\mathrm{V}} (\dot{m}_{\mathrm{S}}^{\mathrm{D}} (W_{\mathrm{S}} - W_{\mathrm{Z}}) + \dot{m}_{\mathrm{I}}^{\mathrm{D}} (W_{\mathrm{I}} - W_{\mathrm{Z}}) + \dot{m}_{\mathrm{G}}^{\mathrm{V}}) \quad (18)$$
$$= \dot{Q}_{\mathrm{S}} + \dot{m}_{\mathrm{S}}^{\mathrm{D}} \left(h_{\mathrm{S}}^{\mathrm{M}} - h_{\mathrm{Z}}^{\mathrm{M}}\right) + \dot{m}_{\mathrm{I}}^{\mathrm{D}} \left(h_{\mathrm{I}}^{\mathrm{M}} - h_{\mathrm{Z}}^{\mathrm{M}}\right) + \dot{m}_{\mathrm{G}}^{\mathrm{V}} h_{\mathrm{G}}^{\mathrm{G}}$$

Finally, after rearranging and removing the terms that cancel out, we are left with the complete zone temperature equation (19). It is important to note that room sources term include thermal energy exchange from water either as a liquid or vapor.

$$m_{\mathrm{Z}}^{\mathrm{D}} C_{p}^{D} \frac{dT_{\mathrm{Z}}}{dt} = \dot{Q}_{\mathrm{S}} + \dot{m}_{\mathrm{S}}^{\mathrm{D}} \left(h_{\mathrm{S}}^{\mathrm{D}} - h_{\mathrm{Z}}^{D} + h_{\mathrm{Z}}^{\mathrm{V}} (W_{\mathrm{S}} - W_{\mathrm{Z}})\right) + \dot{m}_{\mathrm{I}}^{\mathrm{D}} \left(h_{\mathrm{I}}^{\mathrm{D}} - h_{\mathrm{Z}}^{\mathrm{D}} + h_{\mathrm{Z}}^{\mathrm{V}} (W_{\mathrm{I}} - W_{\mathrm{Z}})\right) \quad (19)$$

Comparisons between the EnergyPlus and SPBM zone air temperature equation. A subtle difference exists between the two models; how external and inter-zone infiltration energy transfer is calculated. Equation (20) is used for calculating zone temperature change that is used by EnergyPlus . EnergyPlus and SPBM zone temperature change calculations differ in how thermal energy of air entering or leaving a zone is calculated. Below, zone air specific heat and a temperature difference between the zone and the source of infiltrating or exfiltrating air is used to determine energy transfer. Conversely, Equation (19), used by the SCBM, calculates enthalpy values for zone air and infiltration/exfiltration air as well as humidity ratio differences. Inclusion of humidity differences increases accuracy as differences in humidity can have a significant influence on thermal energy exchange. Nevertheless, these zone energy equations are very similar

$$C_{Z}^{M} \frac{dT_{\mathrm{Z}}}{dt} = \dot{Q}_{\mathrm{S}} + \dot{m}_{I} C_{p}^{M} (T_{OA} - T_{Z}) + \sum_{i=1}^{N\_Zones} \dot{m}_{i} C_{p}^{M} (T_{zi} - T_{Z}) \quad (20)$$

The above derivation demonstrates the thermodynamic completeness of the SPBM model. By starting from first principles, it is possible to ensure conservation of mass and energy is maintained. Additionally, a thermodynamically consistent model

allows for humidity and other contaminant analysis through conservation of mass and energy. The rigor and complete thermodynamic modeling of a building while maintaining minimal parameters allows for this simplified model to be uniquely suited for model-based fault detection.

4.3 Assumptions and Justifications

Due to the emphasis on simplicity, it was decided to have as few zones as possible. This resulted in having one zone per floor and averaging loads out throughout the zone. This assumption was done on the idea that in most buildings there would not be one occupied area with an extensively high loading when compared to the rest of the floor and that averaging loading throughout the zone would not greatly impact the overall accuracy of the model especially with respect to overall energy use. Additionally, fewer zones obviously lead to fewer difficult to estimate or infer zone-dependent parameters such as occupant count and electrical use.

In keeping with the theme of simplicity, the floor is a single layer constructed from the same concrete as the walls and roof and the outside boundary condition of the floor is assumed to be adiabatic, which is a common simplification and shown to be reasonably accurate in other R-C models .

Because the SPBM was being directly compared to EnergyPlus, some variables were imported from the EnergyPlus results into equation-based modeling system in the form of a lookup table. These variables were those that did not have an explicit closed

form solution, such as turbulent natural convection coefficient. These values are normally calculated within the SPBM using reliable approximation equations, but the goal of this testing was to determine maximum accuracy to the EnergyPlus model. The SPBM was attempting to replicate EnergyPlus, using the same independent variables as EnergyPlus allowed for easier direct comparison with less ambiguity as to what was causing the differences between the SPBM and EnergyPlus.

Fenestration is unique to other surface types as it absorbs and radiates far infrared energy quite well while being transparent to visible light. Modern buildings have two or more layers of glass with a gas gap between panes. EnergyPlus uses two different methods: for advanced simulations it uses WINDOW 5 algorithm and for simple simulations it uses an effective U-value (or measure of effective conductivity, usually energy transmission rate per unit area) and solar heat gain coefficient . Due to the complexity of fenestration the SPBM shares many properties with WINDOW 5 such as isothermal surfaces, no thermal capacity, opacity to long wave radiation, and absorptance and transmittance dependence on incidence angle. The simplifications used are: one layer of glass with an equivalent U-value that can represent air gaps present in multi-layer fenestrations, transmittance depending on the number of panes of glass in the actual building, transmitted solar energy is only absorbed by the floor (which is the same assumption as in EnergyPlus when using ‘Full Exterior’ model), and negligible conduction to the surrounding wall. This simple model could represent the complex

model within a reasonable degree of accuracy. Preliminary investigations show good agreement between the SPBM and WINDOW 5 values.

For multiple windows facing the same direction, the total surface area of the glass is combined to create one surface window. In the case where different wall directions (e.g., south and north walls have fenestration) the fenestration interacts with the floor but not directly with each window. The justification for not having windows directly interacting with each other is derived from buildings often having significant distances between windows of different directions and the presence of obstructions between windows. If windows are unable to see each other or have such a great distance between them such that the view factor is extremely small, then the interactions can safely be assumed to be insignificant.

To justify the above simplifications, a north and east window was placed on the test building; the fenestration takes up 80% of the north and east wall surface area. The load from the two windows were compared with a baseline high-fidelity model. Over a week period the total load difference was less than two percent, acceptable for a simplified model. Considering the normal level of deviation between the SPBM and high-fidelity model, and the lack of circumstances in which two large windows would have an unobstructed view of each other, the agreement presented in the test is deemed sufficient.

While internal radiation exchange calculations may be important for detailed accuracy or for radiative zone conditioning, at this time its inclusion only serves to slow down calculation time for overall energy analysis. For the SPBM the floor is assumed to be the only surface that absorbs solar energy (this assumption mimics the EnergyPlus

method for dealing with transmitted solar energy), and the other surfaces are assumed to have no significant energy gain or loss through longwave internal radiation transfer. This assumption was justified by numerical simulation by running EnergyPlus with walls as black, completely absorbing, surfaces and again as completely reflective surfaces. The total difference in cooling demand over a summer design day for the simple one floor model was 79.5[MJ], a change of 4.5%. The difficulty of determining view factors for complex geometries and the small gain in accuracy lead to the decision to remove internal reradiation from the SPBM.

4.4 Internal Load Analysis

Most buildings have internal energy loading sources; these range from lights, electric equipment, people, infiltration, and more. To keep in line with the minimal parameter approach, internal loads were grouped into two groups: electric equipment, and occupant loads. Aside from very few buildings, most internal loads operate on a similar pattern, especially commercial and institutional buildings. The simplest, and most often used method for analyzing internal loads is to create an hourly schedule for weekdays and another for vacation days as there are broad patterns for everyday life. The most convenient method for implementing a schedule is to create a fractional hourly schedule; this means that each hour has a value between 0 and 1 which represents the fraction of the maximum value for that load. For instance, if the maximum possible occupancy is 100 and from 1200 to 1500 hours and the fractional value was 0.9, that would mean 90 people were in that zone from 1200 to 1500 hours; this approach gives a convenient single factor to identify.

A fractional schedule was gathered from NREL and reflects an average trend in what is described as a medium office building. In addition to simply adding heating loads to the interior space, some interior loads effect other parameters other than cooling demand. ASHRAE specifies 0.21 cubic meters of outdoor air per minute per person and additional 0.0187 cubic meters per minute outside air per square meter of floor area. Additionally, people generate a latent load and carbon dioxide through breathing, so the HVAC system needs to be able to cope with removing water vapor, thermal energy, and contaminates from the air and zone.

Initial parameter identification testing for interior loads began with an EnergyPlus model containing people and lights on a fractional schedule. The same fractional schedule was imported into equation-based modeling system but the multiplier for the schedule was left as an unknown parameter. Because only cooling load would be known for the actual building calibration, error minimization was based on cooling demand. The SPBM was able to estimate the multiplier for internal loads with reasonable accuracy and was also able to identify internal load and material parameters at the same time.

While a fractional schedule of the different internal loads of a real building will probably not be available, it may be possible to combine different fractional schedules each with a separate multiplier. For instance, there could be a constant baseline load, additional load during working hours, and a smaller increase above baseline load in the evening or weekend. Another method would be to evaluate building electrical load and investigate if power levels correspond to occupancy hours. Evaluation of building use and corresponding load data can provide insight to minute details that may otherwise go unnoticed.

4.5 Results of Investigations

A SPBM can represent the overall performance of a reasonably complex building accurately and can be used as shown in Chapter 5 to correctly independently identify constructions and internal loads. The success of the simplified model matching so well to a rigorous EnergyPlus model gives confidence that a SPBM could be used for overall energy evaluation on a realistic building. Additionally, the accuracy would possibly allow a SPBM to be used in the development stage of a new building to aid in optimizing constructions early in the design phase resulting in the most efficient building through controlling thermal lag.

4.6 Modeling an Example Test Case Building (Whitehead Building)

Real representative buildings were needed to compare the SPBM and NN model and see if faults can be detected with real data. Initial comparisons were done with the Whitehead Building because it has limited metered information, has state of the art construction, and has a repeatable and constant weekly schedule for occupancy and other internal loads. Old CE is also examined later and is the opposite of Whitehead with legacy construction, has multiple AHUs with energy recovery, and fluctuating internal loads. Both buildings are tested to see how different buildings work with automatic fault detection and also to increase testing rigor.

4.6.1 Example Building Analysis

For the analysis of the Whitehead Building, a substantial amount of data was collected including shape, layout, environmental factors, HVAC setpoints, operational schedules, wall and roof materials, and construction. The goal of obtaining this much

information is to see how well a SPBM can compare to an actual building. The Whitehead Building was picked for its relatively simple construction, standard use, and having easy access to all information about the building. Most institutional buildings are mixed-use and often have large lecture halls, labs, or classrooms. These factors help in constructing a building model and demonstrating a proof-of-concept simulation. In person inspections of the Whitehead building were conducted on the exterior and interior. The building experiences a similar occupancy pattern every weekday and has minimal to no staff on weekends and holidays. Surrounding buildings and structures were analyzed to determine the magnitude of the shadows cast on the Whitehead building. It was determined that most of the shade would be very early in the morning and late at night when solar energy is at the weakest. This level of analysis can easily be done to any building and is representative of the baseline evaluation done when creating any model of a building.

Both example buildings are located in Atlanta, which has a climate with a mean air temperature above 10°C for at least 8 months of the year and a substantial humidity load. High relative humidity inside buildings has numerous impacts on a building including decreased occupant comfort, accelerated mold growth, and is a violation of ASHRAE 2016b. To combat humidity levels inside buildings, the tactic used by many engineers is to cool supply air to 13°C to dehumidify supply air. This makes the relative humidity at 13°C between 90 and 100% on humid days; but when the air gets to the zone and warms up to room temperature, 24°C, the relative humidity will be 55%.

Inspecting the metered data from the Whitehead building revealed that direct cooling data, total electrical use, and steam condensate flow was available. Initially,

matching the cooling load was the initial focus because it is the higher energy consumer in Atlanta when compared to heating load. Additionally, the cooling load data has a much higher resolution than the heating data. The heating data appeared relatively constant with a slight increase in winter. Likewise, the electrical data appears relatively constant throughout the year. The low resolution of some of the data, and the erratic loading patterns may prove to benefit SPBM or NN-based FD.

4.6.2 Neural Network

MATLAB was used for neural network training due to the program's ease of use and reliability. The main options available for creating a NN are the number of neurons in the hidden layer and the 'number of delays' or how far in the past inputs can affect outputs. Training data was January through July of 2016 and the whole year was used to test the network. Different combinations of neurons and delays were investigated although some combinations resulted in unreasonably long computational time. The 15-minute interval was changed to an hourly interval and for cooling data, 10 nodes and 2 delays was sufficient to achieve a R^2 of 0.986 in testing. Two different kinds of time-series neural networks were evaluated: non-linear and non-linear autoregressive network with exogenous inputs (NARX). The difference in these models is feedback, or if output data of the system the network is being trained to replicate will be available when the NN is deployed . Analysis of these different kinds of time-series neural networks in relation to fault detection performance is explored later.

Both methods of time series neural networks agreed well with the training data (less than 5% deviation in average difference and annual load), but the NARX method appeared cleaner and more tightly fit when comparing the percent difference charts. This

is to be expected as NARX is a more accurate model and is recommended when output data is available . It is important to point out that the large percent deviations are mostly from inaccurate real data values rather than a failure of the NN. The overall agreement of both methods instill confidence that either method should be able to be used to identify faults via simulation deviations.

Heating data for the building is based on steam condensate while cooling load information is gathered from campus supply chilled water temperature difference and flow rate. Heating data is somewhat unreliable as condensate is measured in roughly 4L increments. Measurement occurs when a holding container for condensate is full, tips over, and sends a signal that 4L of liquid water has been condensed. In periods of low demand, sparse “ticks” of heating occur which making fine-tuning a model difficult. Cooling load is more precise as a 10°C temperature change in liquid water has significantly less thermal energy that 4L of latent energy.

Due to the problems with metered data discussed above, creating a network for heating data was met with less success than cooling information. The data itself was noisy and does not appear to corollate well with outdoor conditions. A different training method was used to try and compensate for the poor quality of the data, the Bayesian Regularization. Bayesian training requires more time but is better for noisy/difficult data sets . A training set similar to the cooling data was established (50 node, 36 delay) and took over 24 hours to train on an I7-6700 CPU at 3.4GHz. An attempt to train at 200 nodes and 12 delay values was made but was only 10% of the way through training at 24 hours. If it is discovered that a more accurate network is needed for fault detection, then a request will be made to use a computing cluster.

4.6.3 Simplified physics-based model

Unlike neural networks that uses data for training, the SPBM uses data for calibration. As such, SPBM accuracy is not as dependent on data resolution because only a limited number of parameter values are adjusted for calibration. Reasonably accurate data is still required for both SPBM and NN models as building faults need to cause enough of a change to energy meters to be detected and so that fault identification can be performed. Model sensitivity of the SPBM has already been demonstrated and fault detection sensitivity for both the SPBM and NN are discussed later.

Overall, both the SPBM and NN models of real-world whitehead data was able to be performed. Evaluating performance of real data was done to determine the viability of both models to be calibrated to data not artificially generated. However, calibrated high-fidelity model data will still be used for fault detection and identification tests as that is the only financially viable method for testing different faults over long periods of time on a complex structure.

4.7 HVAC System:

The most vital component to keeping a building comfortable is the heating, ventilation, and air conditioning (HVAC) system, which uses 44% of energy in commercial buildings in the US . While the designs are numerous, a popular system is having a large air processing area somewhere in the building that sends air to the rest of the zones. Some reasonable assumptions were made to remove unnecessary computation and simplify the parameters. Return air was assumed to have the same thermal properties and be at the same temperature and humidity as the zone. Additionally, zone air was

assumed to be relatively well mixed, and mass was increased by several times to account for various lightweight objects in the zone that maintain equilibrium with the zone air temperature. Increasing air mass allows for a more controlled temperature oscillation as more energy is required to change the zone temperature. Increasing mass does not diminish from rigor, in fact, slower temperature changes reduce small errors brought about by the temperature control procedure. These assumptions were justified based on the layout not having areas of excessively hot or humid loads when compared to the rest of the floor, and load averaging being common assumptions in other energy modeling programs.

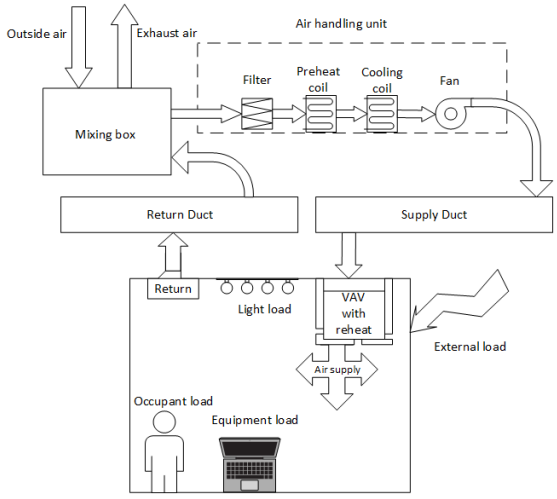

Figure 24: HVAC system and internal load diagram to demonstrate how air flow and air cooling and heating is performed before entering a zone as well as how air is circulated

To quickly review the basics of air handling units, the outdoor air is first brought into a mixing box with return air from the building. This mixed air is first passed over heating coils to prevent freezing of the cooling coils later in the HVAC system. Cooling coils chill the air to 13°C, and in the process, lowers the humidity ratio to a maximum of 0.08 [kg water/kg air]. Air then enters the supply fan and is distributed to different floors.

If a zone does not need cooling but requires air to meet the outside air flow requirement or to remove CO_2 and humidity, then heating coils in the zone air supply unit heats air entering the zone (a process called reheat). As CO_2 monitoring becomes more common, concentration levels and patterns can be used to more accurately determine occupant count and air flow rate faults. Other zone conditioning approaches are similar or may have small changes such as dedicated heating and cooling in individual zones, but the SPBM is flexible and can easily accommodate these demands while the NN can be trained using the basic data from any building.

Usually, the minimum amount of outdoor air needed to meet ventilation requirements is used because outdoor air typically requires more energy to condition than return air . However, sometimes outdoor air is used exclusively when the outdoor air is within the right temperature and humidity conditions are met . A SPBM accounts for outdoor air control depending on the type of control used in the real building. The model can also include heat recovery or economizers such as with the Old CE model.

Two different methods for indoor temperature control were evaluated: a fixed, average internal temperature for the entire run period, and a complex system based on maximum and minimum temperature setpoints that can be adjusted based on time of day. The simplified method achieved success in initial calibration with the high-fidelity model reference. Addition of setpoint based systems allows for time-of-day based temperature ranges so that cooling or heating energy is not needlessly being used during unoccupied hours. The complex system is also able to more accurately calculate convection loads as the inside air temperature fluctuates and which would reduce additional load into the space. However, the setpoint-based system introduces up to six parameters per zone:

maximum occupied temperature, minimum occupied temperature, maximum unoccupied temperature, minimum unoccupied temperature, time where system switches from unoccupied to occupied, and time when system switches back to unoccupied setpoints. OSHA recommends a temperature band of 20-24°C with humidity between 20-60% ; so, if the building occupancy schedule is unknown the detailed control system may add unnecessary complexity. Therefore, it is only necessary to use the complex settings if the building is known to use setback setpoints or has a wide temperature deadband. Either way, the SPBM can accommodate any zone temperature setting schedule while the NN can use a 'time of day' variable to predict high and low energy demand periods.

Implementation of building AHUs has many significant benefits in addition to differentiating the SPBM from other simplified models. As discussed throughout the above sections, modeling zone loads and AHU components concurrently allows for accurate representation of building load dynamics. Additionally, zone contamination in the forms of water vapor and CO2 can be modeled for accurate loads, demand control ventilation, occupancy prediction, and fault detection. The following section covers the implementation and benefits of simplified dynamic physics-based building energy modeling.

4.8 Advanced HVAC Development

Implementing advanced features such as CO2 control or drifting interior air temperature is possible for buildings with modern metering and sensor technology. Additionally, these features proved useful when faults produced a small change in energy demand.

4.8.1 CO2 Control

Being able to model CO2 based outdoor air control is vital for fault detection in buildings that implement such technology. The process used is quite eloquent as the SPBM assigns a value of CO2 production per person and accounts for activity level. By roughly accounting for activities in the building, CO2 metering leads to a more precise level of air flow control and contamination monitoring. It has been demonstrated that simplified transient models are more than sufficient for modeling CO2 within the errors of CO2 sensors .

Demand control ventilation is one potential benefit of CO2 monitoring in buildings, which can provide electrical savings of almost 30% to conventional air delivery methods . Considering the cost of monitoring air flow and CO2 of return and supply HVAC components can be done for less than $1000 per AHU, the potential energy and economic savings would appear to easily justify the prevalence of demand control ventilation . Additionally, this technology is already implemented in some net-zero/living buildings .

The use of a simultaneous equation solver did bring a few challenges for implementing CO2 levels. A CO2 level that is dependent on current-value air flow rates that also affects air flow rates causes two potentially correct values for the simulation (a high CO2 value where air flow rate remains low and a low CO2 value when air flow has increased to lower CO2 levels). As such, Equation (21) demonstrates the differential approach was taken to determine the change in CO2 that would have been experienced over the previous timestep.

$$\frac{dCO2}{dt} = ((CO2_S - CO2_R)\dot{m}_S + CO2_G)|^{t-1} \quad (21)$$

The above equation shows how the level of CO2 will change from the previous hour to the current time value. This can easily be rearranged into Equation (22) that a computer program can use.

$$CO2|^t = \left(\frac{(CO2_S - CO2_R)\dot{m}_S + CO2_G)|^{t-1}}{\mathrm{m}_Z}\right)\Delta\mathrm{t} \quad (22)$$

While Equation (22) is stable for large zone air mass, or low supply air mass flow rate, it becomes unstable when either of those conditions are not met. Artificially raising the zone air mass would work but would eventually dampen out the changes and make detecting changes in CO2 or humidity difficult. As a result, the Taylor Series was used to dampen the rate of change without altering zone properties. A third order Taylor series representation of a first derivative is more stable and more accurate without increasing computational time, the form of the Taylor series is represented in equation (23). Using more than one term in calculating the derivative increases stability in the overall humidity calculation .

$$F'(x) \approx \left(\frac{11F(x)}{6} - 3F(t-\delta t) + \frac{3}{2}F(t-2\delta t) - \frac{F(t-3\delta t)}{3}\right)/\delta t \quad (23)$$

Implementing the Taylor series with infiltration results in Equation (24).

$$CO2_z^t = \frac{\left(-3CO2_z^{t-1} + \frac{3}{2}CO2_Z^{t-2} - \frac{1}{3}CO2_z^{t-3} - \frac{CO2_G}{m_Z} - \frac{\dot{m}_{SA}CO2_S}{m_Z} - \frac{\dot{m}_I CO2_O}{m_z}\right)}{-\frac{\dot{m}_S}{m_Z} - \frac{\dot{m}_I}{m_z} - \frac{11}{6}} \quad (24)$$

By using previous timestep values and predicting the CO2 level for current timestep allows for simultaneous equation solving within the limitations of two possible

correct values. This technique can also be applied to other control logic such as zone temperature control.

4.8.2 Humidity Modeling

Humidity is a significant variable for modeling HVAC systems as the cooling coil not only cools air but removes water vapor. In the cooling season, removing water vapor from supply air it consumes a considerable amount of energy. For example, to cool air from 21°C at 90% relative humidity to 13°C at 90% relative humidity takes three times as much energy to cool than dry air for the same temperature change. Because of this increased energy cost, it was deemed necessary to include zone humidity modeling to the SPBM.

Humidity modeling was approached with the same simplistic numerical derivative based approach as CO2. While the below equation was stable in low air mass flow rates it became unstable as the air flow rate increased. An option for increasing the stability of this kind of finite difference equation would be to increase the mass of the zone. However, increasing the mass of the zone would effectively dampen out changes from humidity. To increase stability, a new method of calculating the derivative was used.

$$m_z \frac{dW_z}{dt}|^t = ((W_S - W_z)\dot{m}_S + W_G)|^{t-1} \quad (25)$$

Using the above approximation for the derivative, a new equation could be crafted to represent the humidity per level. Equation (26) represents the humidity level per floor and could be used to represent the humidity for the entire building. By using a mathematical derivative representation that is only dependent on previous values means that the simulation time is not greatly affected with increased iterations. Additionally, this

same approach can be applied to any situation that uses a finite difference method for derivatives to increase stability should the need arise.

$$W_z^t = \frac{\left(-3W_z^{t-1} + \frac{3}{2}W_Z^{t-2} - \frac{1}{3}W_z^{t-3} - \frac{\dot{m}_G^V}{m_Z} - \frac{\dot{m}_S W_S}{m_Z} - \frac{\dot{m}_I W_O}{m_z}\right)}{-\frac{\dot{m}_S}{m_Z} - \frac{\dot{m}_I}{m_z} - \frac{11}{6}} \quad (26)$$

4.8.3 Deadband Zone Temperature Control

Zone temperature control for variable air valve (VAV) systems is very similar to CO2 based demand control ventilation. The main difference is that temperature is bounded with a maximum and minimum temperature rather than just a maximum. Additionally, the HVAC unit behaves differently depending on if the zone requires heating or cooling. In most non-residential buildings, when heating is required the air flow rate is kept at a minimum value, but the zone supply duct uses some form of mechanism to heat the air (usually electrical resistance or hot water coils). Conversely, when a zone requires cooling, the air flow is increased as there is usually not a way to further cool supply air in the supply duct. Lastly, the duct has three possible modes: 1) minimum air flow rate at AHU supply conditions, 2) minimum air flow rate with the duct increasing supply temperature, and 3) greater than minimum air flow rate at AHU supply conditions. This section will explore the logic for how deadband temperature control was achieved.

The default operation for VAVs is to supply a minimum air flow at the AHU supply conditions. For the modeled buildings in this paper the AHU supply condition is supposed to be 13C. It is important to account for this minimum air flow rate because it means there is a constant supply of cold air into the zone. This cold air may need to be

heated to maintain the minimum zone temperature setpoint, but not so much that the supply temperature exceeds the minimum zone temperature setpoint; e.g., VAV warms supply air to 17C to keep the zone at 21C due to the small heating load on the space not being sufficient to overcome the cooling effect from 13C air.

In a zone heating operation, the VAV supplies air above the AHU supply air temperature while keeping air flow rate at the minimum flow setting. To vary the amount of heating, the VAV increases heating energy supplied until 100% heating capacity is met.

The final mode of operation is cooling mode which involves increasing the air flow rate into the zone. When accounting for zone humidity or CO2 increasing the cooling rate can also affect the supply rates into the zone. Depending on how the AHU is configured, increased cooling air flow can lead to an increase in outdoor air flow if the AHU is running a fixed percentage of outdoor air. Conversely, if the AHU supplies a fixed amount of outdoor air, then recirculation would increase instead. Figure 25 demonstrates the ability to maintain temperatures within the deadband for a simple proof of concept test.

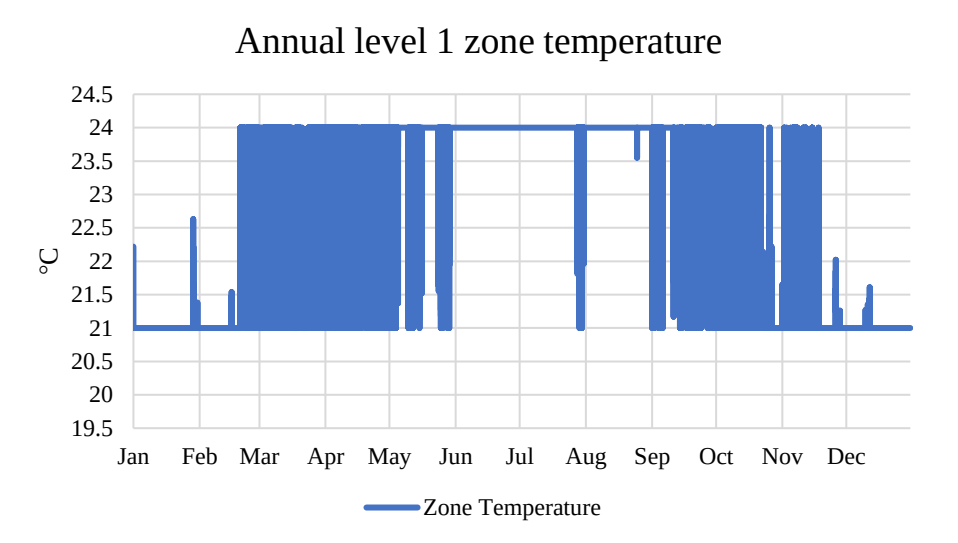

Figure 25: Plot of annual zone temperature while maintaining temperature between 21 and 24C. Winter has zone temperatures near minimum while summer zone temperatures remain at the maximum; spring and fall demonstrate that zone temperatures fluctuate between maximum and minimum temperature depending on external load.

Implementation of a deadband required some clever optimization to get this kind of control in a simultaneous equation solver. However, given the prevalence of deadband control and temperature setback design it was deemed necessary to include. Due to using previous timestep values in calculations the program did not see a large increase in computation time and greatly increased the potential accuracy. Additionally, a non-functioning temperature setback is a common fault for buildings on the test campus and being able to evaluate such a common and energy saving fault is invaluable.

4.9 Calibration of SPBM

Due to the nature of a SPBM, both heating and cooling loads were calibrated at the same time. This is because the SPBM is attempting to represent an actual building and having two different sets of parameter values for heating and cooling (and subsequently having two different output sets). The primary condition that would lead to

a cooling and heating load at the same time would be a large amount of reheat - or cooling outside air and then heating the air as it enters the zone. Some buildings need to have a large amount of reheat if they have high air change rate demand, but excessive reheat can also be an indicator of faulty control logic or system performance. The dynamic nature of the model compares loads on an hourly basis with cooling load during the day, and heating loads during unoccupied times.

4.10 SPBM Improvements

As the SPBM grew in complexity, so too did the computational time to perform a simulation. Initially, all the procedure-based calculations were put into one procedure. Additionally, some correlations and AHU specifications were calculated in real time. To see if program optimization could be performed, different arrangements of program layout was tested.

Engineering Equation Solver (EES) is a simultaneous equation solver, not a traditional program script. As such, EES attempts to solve for all the variables at the same time through iteration. Iterative solving is normally acceptable but slowed as calculations that rely on the same variable were added. For instance, the external surface convection heat transfer coefficient affects the heat into the wall nodes, internal surface temperature, and load into the zone, among others. The load into the zone has significant coupling as all surfaces simultaneously contribute to it; and the zone load affects the HVAC controls which determines the air into the zone, outdoor air flow rate, and all related calculations. Coupling of all these variables dramatically slows computations as EES attempts to iterate values that satisfy all the equations simultaneously. Because of this coupling, reducing parameters that are linked together substantially decreases run time.

Before beginning the optimization, a simple, one level, model was simulated to get a run time. A 72hr simulation took 22.03 seconds to complete for a one level model with all calculations and correlations. Changing the external convection heat transfer coefficient correlation for one wall to use the external wall temperature of the previous hour saw a decrease in time to 20.84 seconds (5% improvement). Changing all the walls to use the previous hour external surface for external convection heat transfer coefficient calculations had a reduction to 13.95 seconds (37% improvement). The difference for moving all interior walls to the previous hour value only saw a reduction to 12.69 seconds (42% total improvement). Using the previous value for convection heat transfer coefficients did not have an appreciable effect on total zone loading (less than 5% change in total load just from convection). As such, a 42% decrease in computation time for an insignificant loss in accuracy is well worth the compromise.

At this point all the calculations that are run in a traditional programming method are all clustered in to one procedure. It was hypothesized that EES runs the entire procedure for each time it calls a variable. The south wall was placed into its own procedure to see how the number of calls changed with further reduction. Having outside and inside air convection heat transfer coefficient correlations and the solar load calculations in their own procedures lead to a total of 1722 calls for the south wall. Total number of calls was reduced to 1068 by isolating the inside convection heat transfer coefficient, external convection heat transfer coefficient, and solar loading. Separating all wall correlations into their own procedure led to a total reduction in time to 0.89 seconds (96% reduction in computation time). While these improvements are substantial, there are still some model improvements that could be done by moving the code to a more

streamlined program. However, the simultaneous equation solving of the current program allows for more flexibility while providing a reasonably fast simulation.

4.11 Conclusion

Evaluation of the Whitehead and Old CE buildings reveal ideal buildings to test the SPBM and comparison to a NN. Both buildings have different internal uses but have a repeating daily use pattern, removing unnecessary early-stage complexity. Preliminary evaluation of both modeling methods shows a capacity for reasonable accuracy for building modeling and promising results for use in fault detection with successful fault identification occurring with as little as 1% change in demand.

CHAPTER 5. UNCERTAINTY

Before final evaluation of the models presented in this paper, it is important to remember that models are a representation of a complex system. As such, modeling real-world systems is inherently flawed and results should not be expected to be identical. Due to the complex nature of buildings, uncertainty is approximated by comparing metered energy use to modeled energy use. Conducting analysis of variance about the linear regression line between metered and modeled energy results in an approximate normal distribution and therefore, approximate confidence intervals can be drawn from this analysis.

In any useful model it is important to carefully calibrate parameters using available observations. Parameter estimation can be seen as constrained optimization where the constraints are placed based on easily obtainable information gathered from building drawings or in-person inspections. Based on the listed information it is reasonable to approach parameter estimation as an inverse problem with values limited by known quantities; while the goal is to generate unique parameter values that result in model output to match that of data not used for calibration. That being said, it is important to remember that parameter estimation is attempting to find parameter values that are approximations which result in the desired model performance, not the exact real world parameter value – a task that is impossible.

Due to the nature of the systems being modeled and that the SPBM is using thermodynamically consistent modeling equations, it is reasonable to constrain parameters to reasonable values and also undergo optimization for different parameters

separately. Additionally, it is important to remember it is not possible to quantify a "best model" when it comes to inverse problems for parameter estimation. As such, best practice for evaluating complex models is by breaking down complex systems into individual components and individually compare a high-fidelity model or system with the proposed model to reveal the discrepancies between the two models.

Due to a lack of a definitive method for determining if the model is "best" and that the objective of the model is to be used as a tool for fault detection and not determining real world property values, model-to-model comparisons, model alignment factor, and analysis of result differences due to different parameter values are used to determine "goodness of fit". To add some degree of qualitative measure to the model uncertainty, sum squared error-based model result analysis will be performed on parameters after being fit.

X.1 Uncertainty analysis of building envelope

As stated earlier, it is recommended to start at broad model analysis and work towards the complete system. As such, this section will describe the process used to calibrate the SPBM to the Whitehead Building. As before, the analysis began by determining the affect wall parameters played on heating and cooling load. Heating data for two weeks in January for Whitehead while unoccupied and running 100% recirculated air was used for model calibration. Being winter, the cooling load is near 0 and therefore is not plotted. Figure 26 visually shows the high level of agreement between the baseline heating rate and SPBM rate while Figure 27 shows the alignment factor for the two heating rates as well as the R^2 of the SPBM.

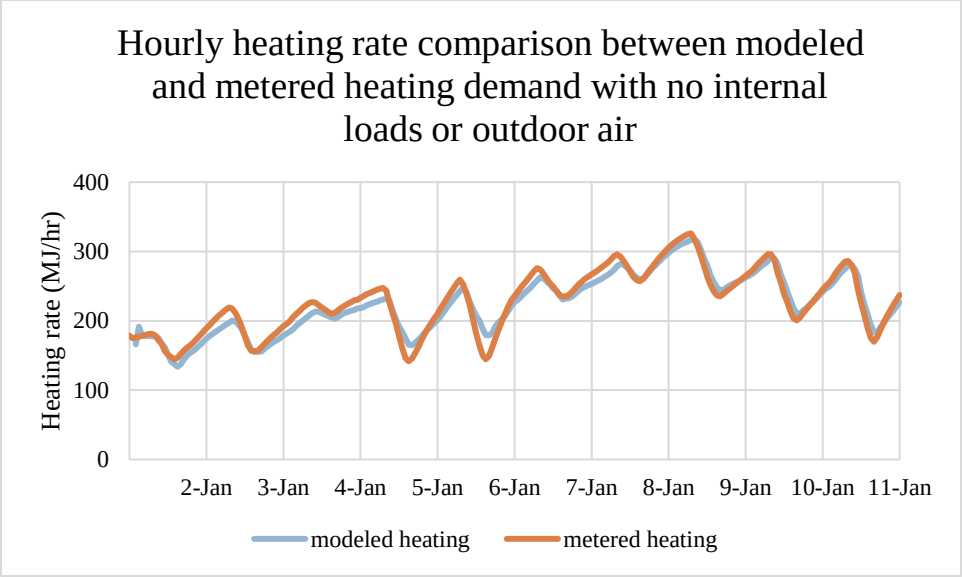

Figure 26: Comparison between baseline and calibrated SPBM heating rate

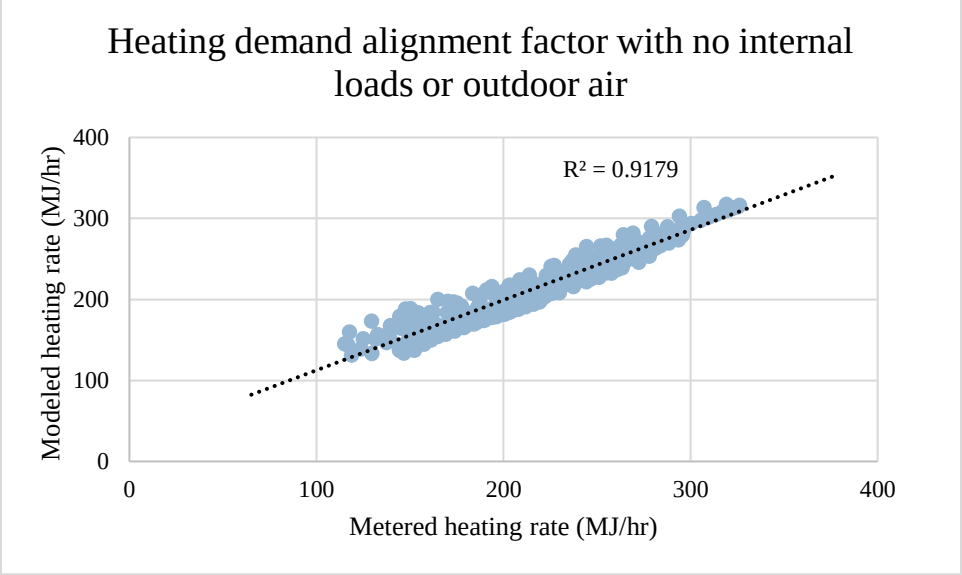

Figure 27: Alignment factor for calibrated SPBM with baseline heating rate

For the purpose of fault detection, uncertainty analysis was performed on the four parameters for wall construction: external node resistance and capacitance values (R1 and C1) as well as the interior node resistance and capacitance values (R2 and C2). The uncertainty of the system the envelope parameters are defined by Equation (27) but represent a general process for any number of parameters.

$$U_A = \sqrt{\left(\frac{\delta Q}{\delta R_1} U_{R1}\right)^2 + \left(\frac{\delta Q}{\delta R_2} U_{R2}\right)^2 + \left(\frac{\delta Q}{\delta C_1} U_{C1}\right)^2 + \left(\frac{\delta Q}{\delta C_2} U_{C2}\right)^2} \quad (27)$$

The change of total heat (Q) was, unsurprisingly, more affected by the resistance than the capacitance by several orders of magnitude. Total heat energy being strongly coupled with the resistance is not surprising as the resistance affects the amount of thermal transfer while the capacitance affects the amplitude of thermal transfer. To determine $U_A$the capacitance terms were dropped as their contribution was statistically insignificant. Additionally, the uncertainty of the resistance was combined due to having a statistically similar change in heat per change in resistance. Therefore, U_A for cooling and heating was approximated using equations (28) and (29).

$$U_{A,cooling} \approx \sqrt{\left(\frac{\delta Q_{cool}}{\delta R} U_R\right)^2} \quad (28)$$

$$U_{A,heating} \approx \sqrt{\left(\frac{\delta Q_{heat}}{\delta R} U_R\right)^2} \quad (29)$$

Equation (30) details the process for determining U_A and SSE is simply the sum squared error between the baseline and modeled heat rate; h_c is considered to be 2 due to the large number or points (336). The resulting plot demonstrating the heating rate with the associated uncertainty is shown in Figure 28 and demonstrates an acceptable level of uncertainty.

$$U_A = h_c\left(\frac{SSE}{N - N_P}\right) \quad (30)$$

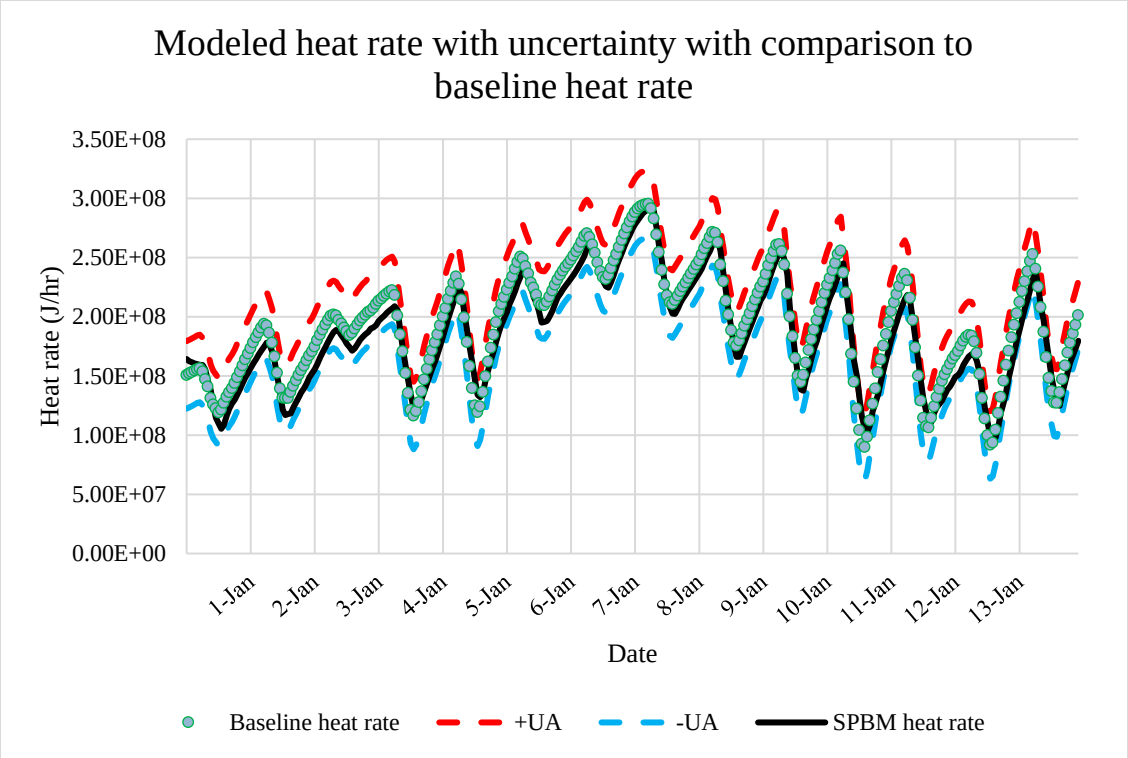

Figure 28: Plot of SPBM heat rate with uncertainty along with baseline heat rate

Initial uncertainty analysis for this simplest-case model reveals that fundamentals of SPBM development allow for unique solutions. Further uncertainty and uniqueness analysis for fault identification and identification are presented later in the paper.

5.1 Envelope Uncertainty with Internal Loads

The above demonstration was done with no internal loads or infiltration. The same envelope uncertainty procedure was repeated while the building was subjected to realistic internal loads and infiltration to see if the inclusion of these variables would decrease or increase the uncertainty of the envelope parameter estimation. Additionally, the time of the year was moved to June to have both a heating and cooling load.

A problem with using one zone per floor is the loss of per-room granularity. Even in real buildings not every room has a thermostat and, as a result, individual rooms can

experience different temperatures from the room with the thermostat. Figure 29 through Figure 32 demonstrate the high level of agreement possible with the SPBM when accounting for lighting load, plug load, occupancy, infiltration, outside air, and humidity.

As demonstrated in the following set of figures, the SPBM cooling rate is more aligned with baseline data than the heating rate from the SPBM is aligned with the baseline heating rate. Greater agreement with cooling load as opposed to heating load is expected because June in Atlanta is a cooling load dominated time of the year and only loads with minimal internal load will have heat demand. Heating rate does not necessarily mean that the output temperature from the VAV is above room temperature, but rather the temperature of air into the zone is required to be higher than the temperature of air from the cooling coil in order to maintain a zone temperature within the temperature deadband (21°C to 24°C in this example).

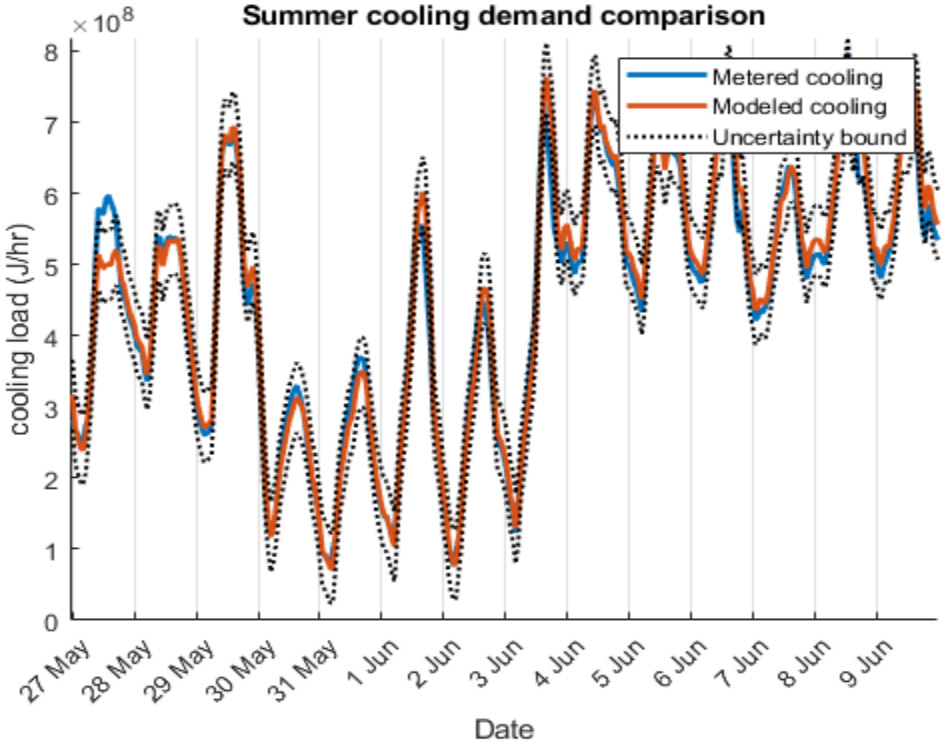

Figure 29: July cooling rate data from baseline and SPBM, uncertainty remains reasonable even when internal loads are incorporated

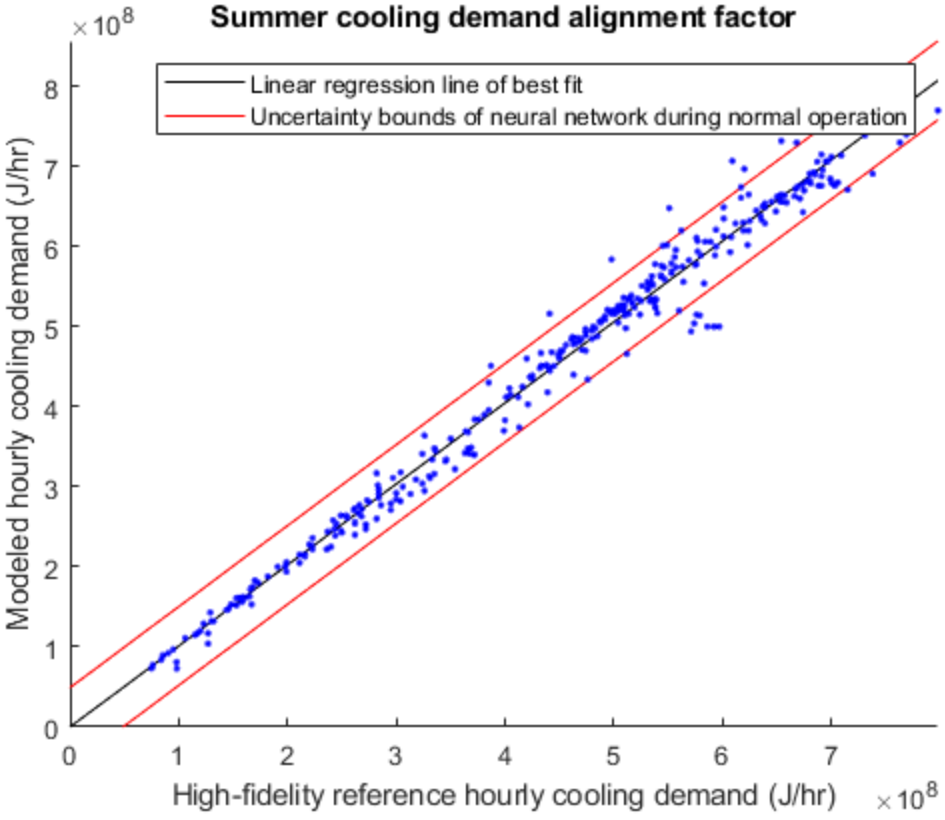

Figure 30: Alignment factor between SPBM and baseline cooling rate demonstrating high degree of agreement and low uncertainty

The heating rate has a similar profile and overall agreement and has a strong linear relationship when looking at the alignment factor between SPBM and baseline heating rates. The primary differentiator between the SPBM and baseline information is the low heating rate (<100MJ/hr) in the baseline model while the SPBM reads 0MJ/hr. This is due to the SPBM being slower to react and not having small rooms, such as conference or break rooms, which may require some level of heating all the time and cannot be faithfully represented in a one zone per floor physics-based model.

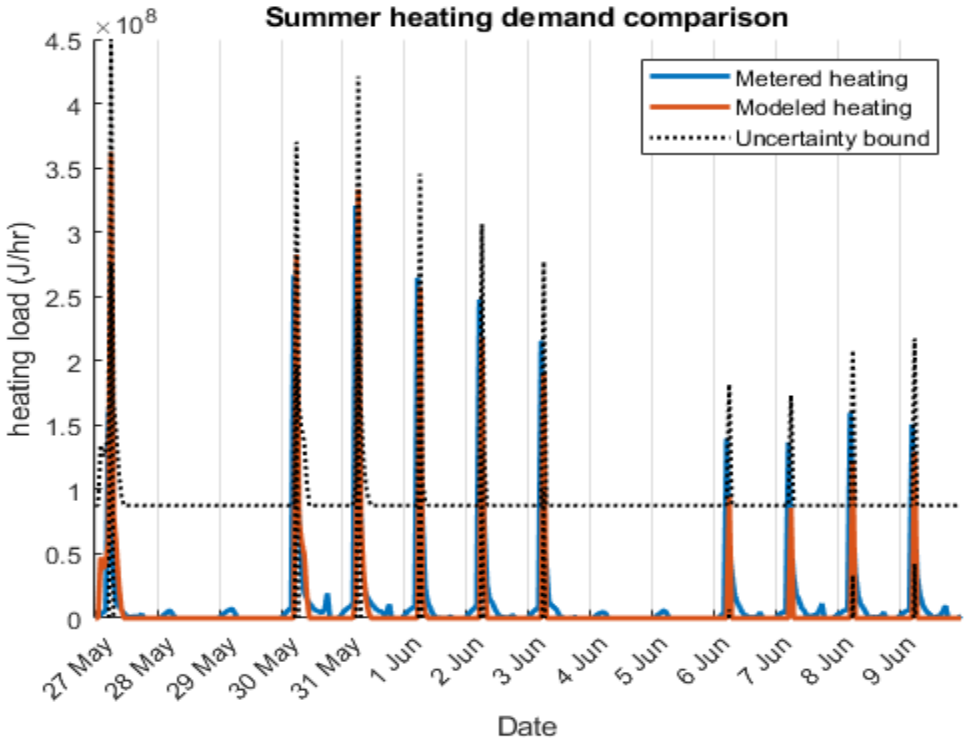

Figure 31: July heating rate data from baseline and SPBM with slightly higher uncertainty due to low load and abrupt change in demand

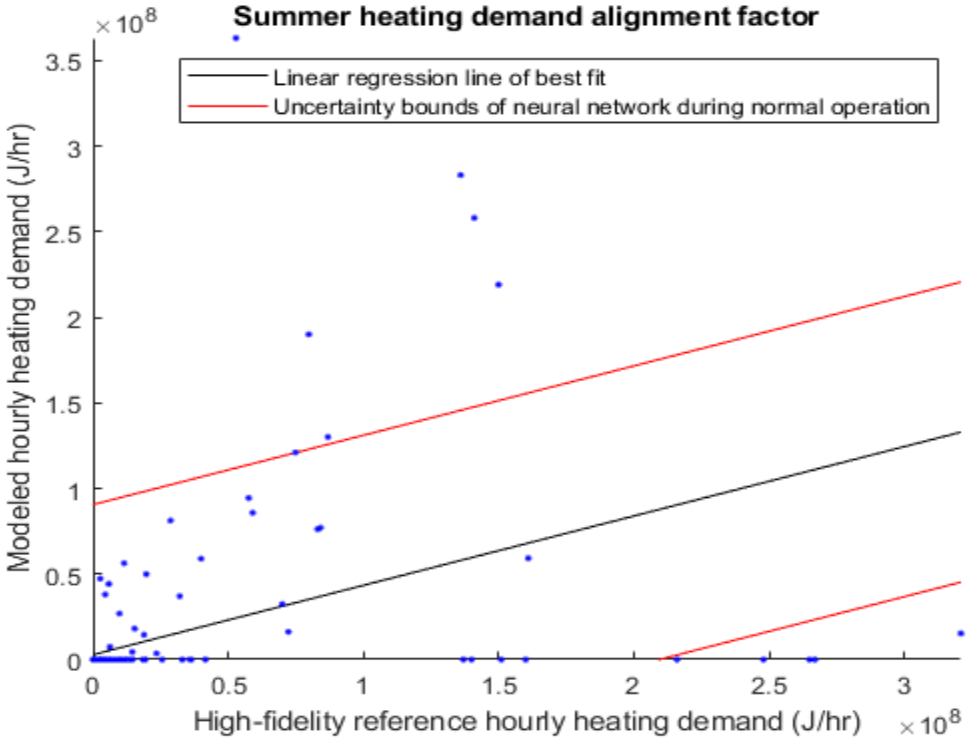

Figure 32: Alignment factor between SPBM and baseline heating rate

While summer heating demand may initially appear to have an unacceptable level of uncertainty, it is important to note how relatively small heating demand is when compared to cooling. For instance, a majority of testing does not have any heating demand at all and there is only a short window when zone temperature setpoints are adjusted at the beginning of the day when heating demand spikes. As such, a relatively high uncertainty is still capable of detecting faults due to any increase in demand being noticeable.

5.2 Sensitivity of Envelope for Heating and Cooling Load

Given the relative uncertainty of the heating and cooling load when analyzing the envelope, a brief investigation on how changing the envelope properties results in changing of heating and cooling loads was conducted. Envelope properties were adjusted by +/-10% and +100%/-50%. Analyzing these scenarios provides useful insight for when parameter estimation-based fault detection occurs in a later section.

Beginning with bulk wall resistance, an increase in bulk wall thermal resistance resulted in an increase in heating demand and decrease in cooling demand as shown in Figure 33. Such a tradeoff is expected as the total load from the interior is constant and less external thermal energy can make it into the zone. Likewise, with a decrease in bulk wall thermal resistance the cooling load increased, and heating load decreased. Given the relatively low thermal resistance of the baseline wall, a 10% change in resistance is a relatively minor adjustment and well within error of construction.

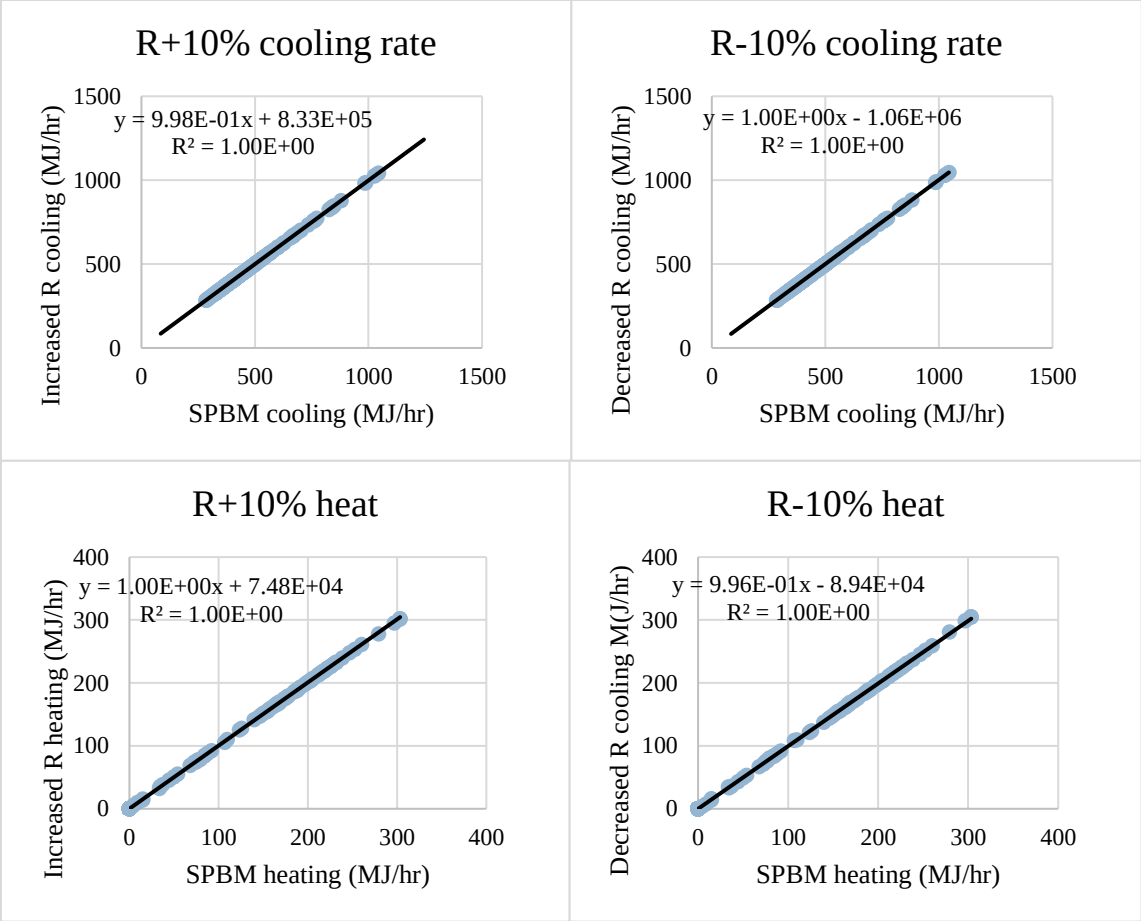

Figure 33: Results of bulk wall resistance alteration to demonstrate relative change in heating and cooling rates

For bulk wall heat capacity, a similar trend was experienced. Although similar, there was less of a divergence than for resistance. While the change on total heating and cooling load was statistically insignificant when compared to thermal resistance, the change in thermal capacity has a similar change on the alignment factor. This is because heat capacity changes the peak and amplitude of conducted thermal energy and not the total thermal energy entering or leaving a building.

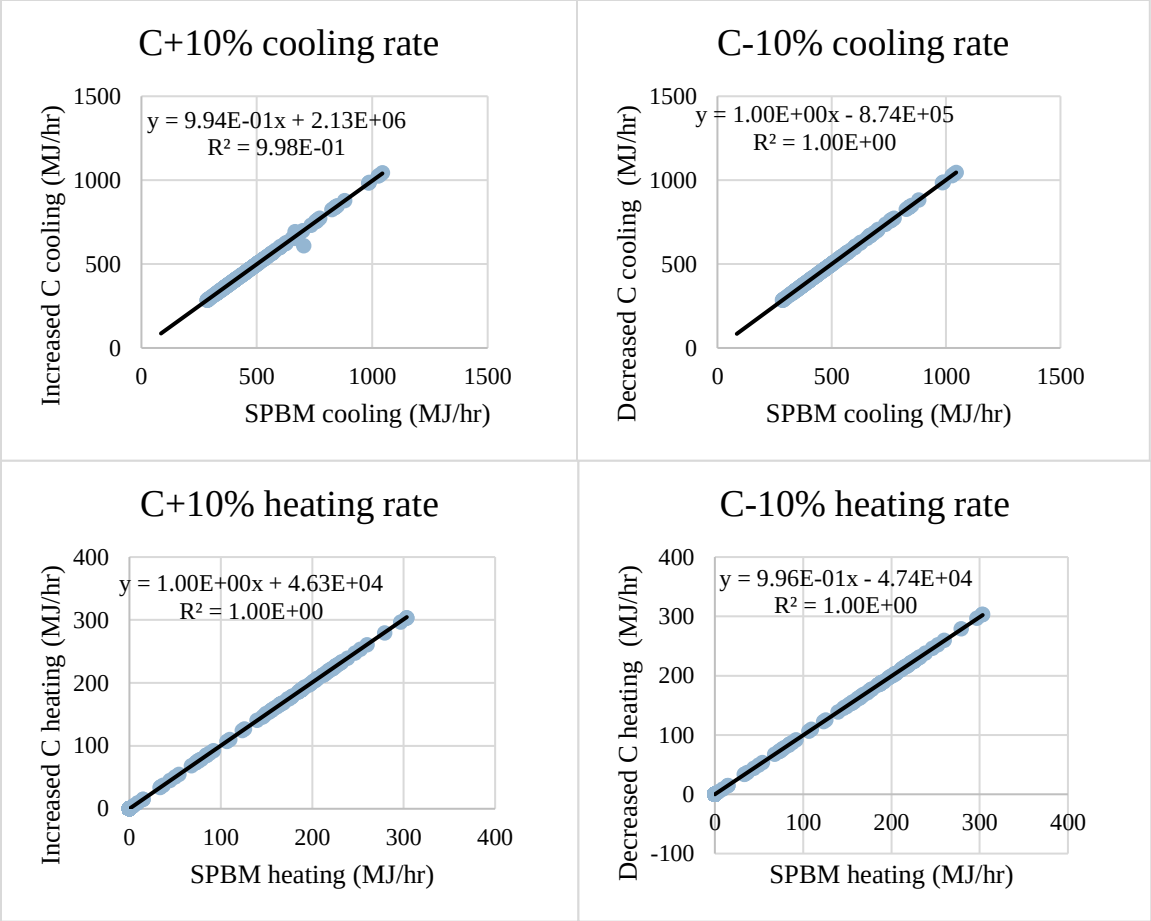

Figure 34: Alignment factor of SPBM and SPBM with altered bulk wall heat capacity

A severe alteration to the bulk wall properties was conducted to show how the envelope would behave if parameter estimation was severely off calibration. The bulk wall resistance was tested by doubling and halving total thermal resistance to evaluate sensitivity of energy demand. The overprediction was more noticeable than the 10% change but not nearly as much as Figure 35 demonstrates with the loss of thermal resistance. When a building has internal loads and a relatively high air flow rate, there is only so much the wall thermal resistance can do to lower cooling load; as demonstrated in the alignment factor in the following figure. However, underprediction of bulk wall thermal resistance shows how thermal bridging would cause significant deviation in both heating and cooling loads.

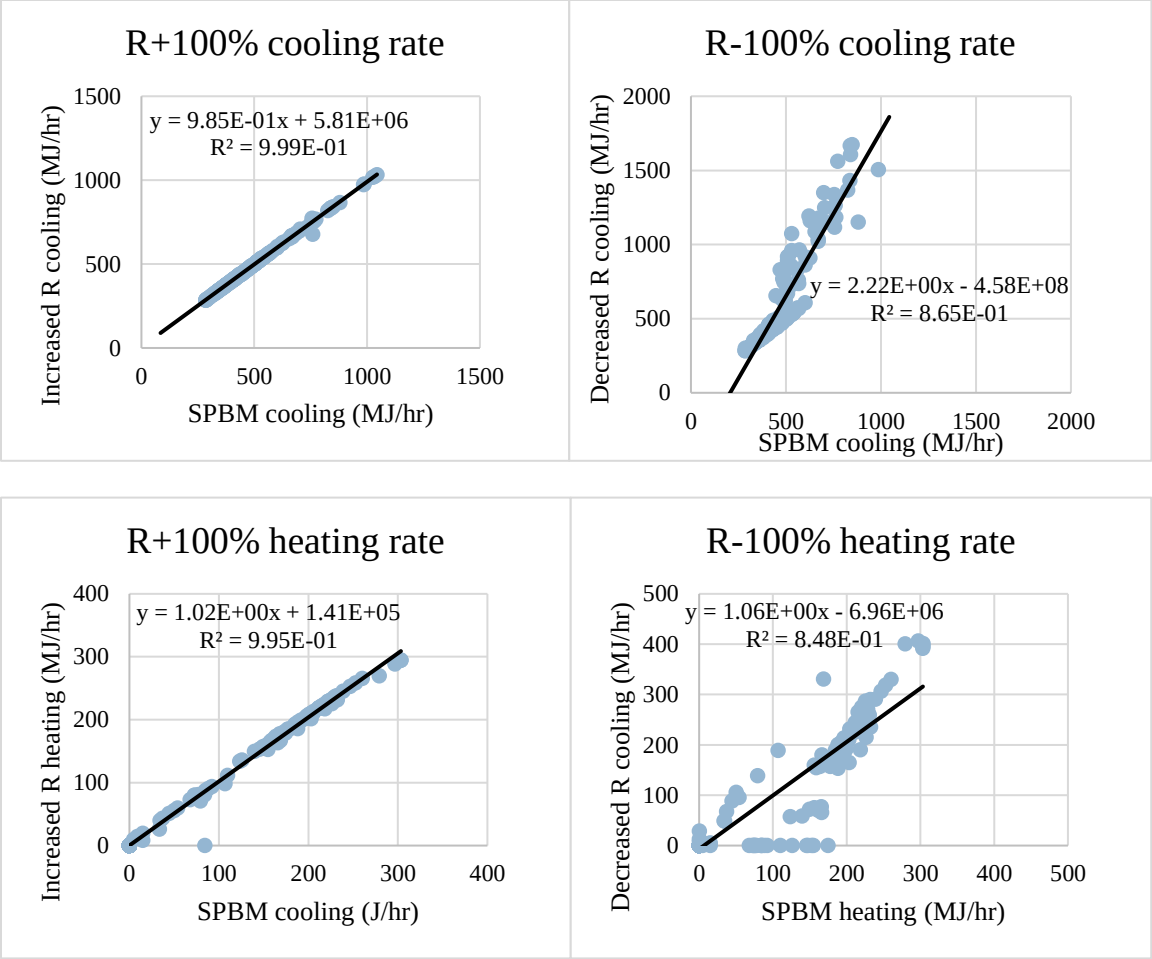

Figure 35: Alignment factor of SPBM and SPBM with bulk wall thermal resistance

Altering the wall bulk thermal capacitance had the expected effect of either damping the cooling rate by increasing capacitance or exaggerating the cooling rate by lowering capacitance. Again, thermal capacitance influences the profile of conducted thermal energy, not the average thermal energy that is transmitted. The linear regression trendline equations in Figure 36 show that increasing the capacitance increased the baseline cooling rate (*b* in Equation (31)) while lowering the impact dynamic changes had (*m* in Equation (31)).

	$y = mx + b$	(31)

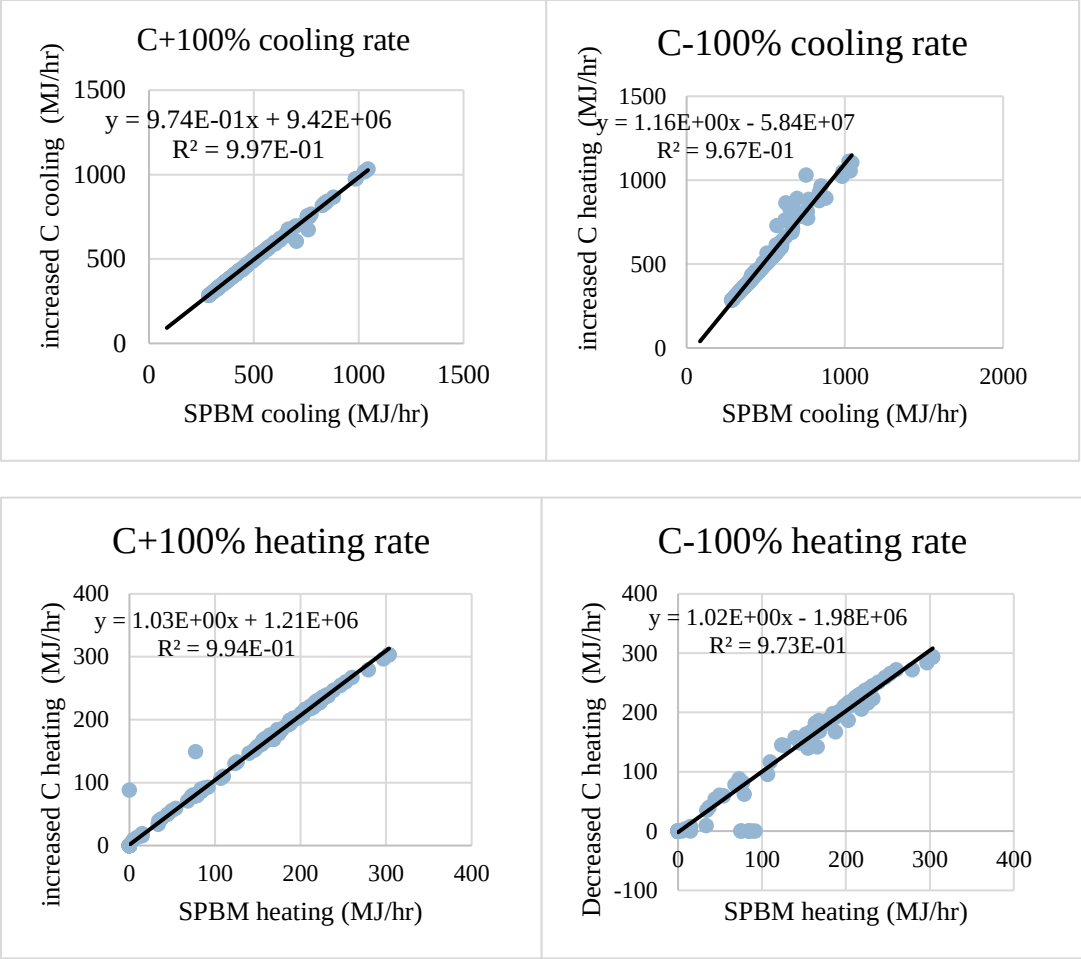

Figure 36: Alignment factors of SPBM and SPBM with altered bulk wall thermal capacitance

In conclusion of envelope uncertainty, analysis of bulk wall material values produced the expected results of needing to be broadly accurate but extreme precision is not vital to model integrity. Large deviations from baseline values have distinct results but only until a certain point; diminishing returns dictates that by increasing thermal resistance or capacitance from 2x over to 3x would produce a significantly smaller change in cooling load than a change from 1x values to 2x over. However, underprediction of bulk wall properties has noticeable and distinct effects on cooling and heating rate alignment. As such, the interior loads will also be examined to see how the

SPBM reacts to alterations within the building and if the model is more sensitive to interior load sources.

5.3 Sensitivity and Uncertainty of Outdoor Air

Determining the amount of outdoor air is vital to properly estimating the heating and cooling demand of a building. Even if outdoor and return air temperatures are the same, an increase of relative humidity from 20% to 40% can increase the enthalpy of the air by almost 30%. Whitehead operates at a fixed outdoor air flow rate and excessive outdoor air is a significant source of wasted energy, and therefore is a fault desired to be detected .

Excessive outdoor air affects the load on a building in different ways depending on the season. In winter, excessive outdoor air increases the amount of preheat required while in summer it increases the amount of cooling. The outdoor air sensitivity analysis took place in June, just as the envelope sensitivity analysis, to see how different aspects of unknown variables affect model sensitivity. As expected, altering the outdoor air percentage did not change the heating requirements but increased the cooling load in a typical fashion, as shown in Figure 37.

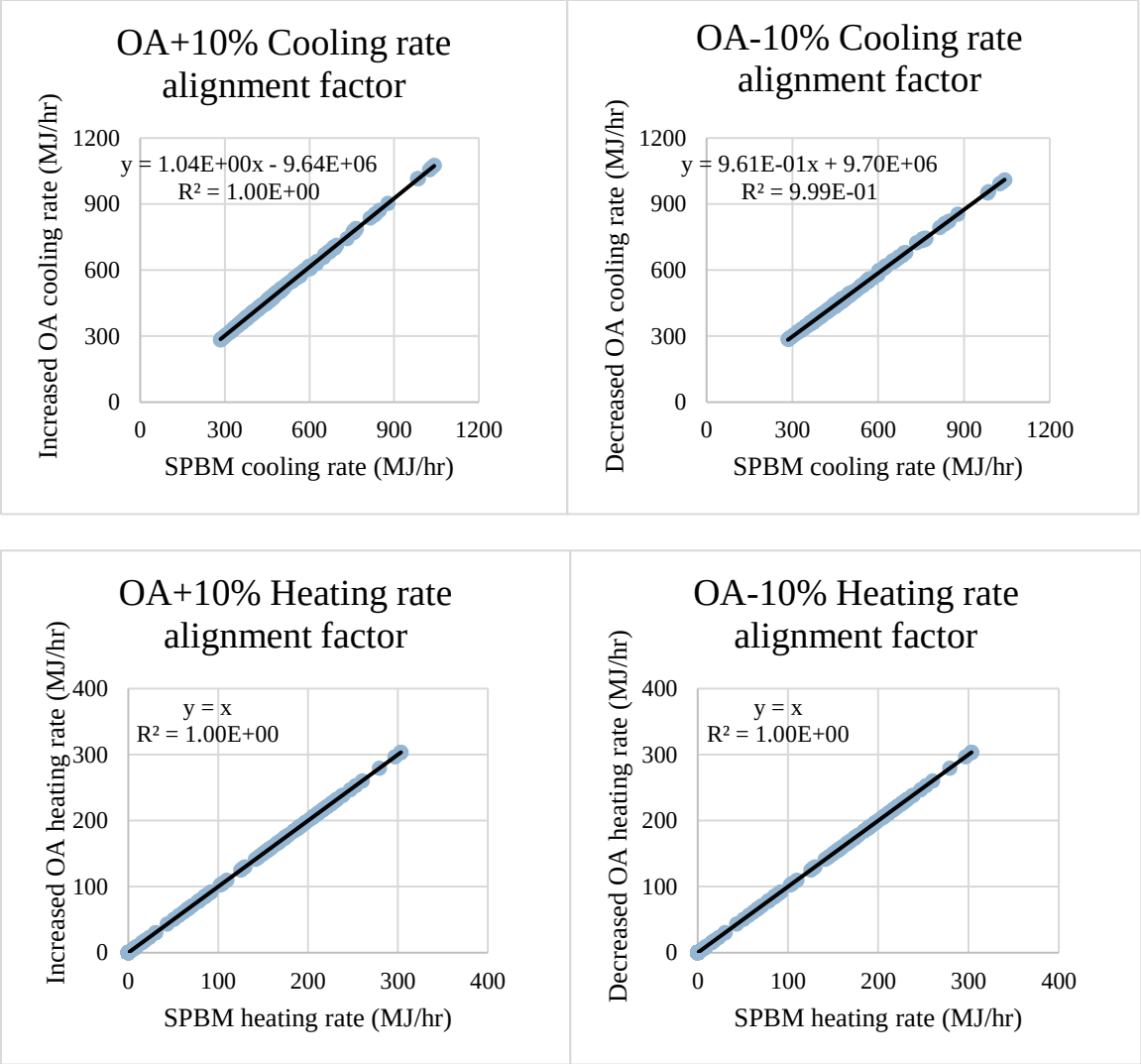

Figure 37: Alignment factors of SPBM and SPBM with altered outdoor air percentage

Increasing outdoor air in summer increased the cooling load as return air was, on average, hotter and more humid. Conversely, lowering outdoor air lowered return air temperature and humidity. Behavior such as this where only one of two metrics are affected is useful to know when performing outdoor air fault detection. Additionally, CO2 monitoring can also be used for outdoor air fault detection and will be explored in the fault detection portion of the paper.

5.4 Evaluations of Interior Loads

The interior loads placed by people and electric equipment affect the heating and cooling demand on a building's HVAC system. Internal loads can create a cooling demand even when outdoor conditions are cool. Considering one of the faults for automatic detection is malfunctioning occupancy sensors, being confidant on the internal loads in a building is vital for fault detection.

Three metrics were evaluated for interior loads: 1) unoccupied, or base, fraction of metered electricity used inside the building for lighting and other electric equipment. 2) fraction of metered electricity used inside the building when occupied. And 3) the number of occupants in the building. Unoccupied electrical use is the electricity used by the buildings overnight when the building is mostly vacant. This value dictates heating load during winter and should not affect cooling load as the building should be at minimum air temperature setpoint. Figure 38 demonstrates this expectation with a minimal change to cooling load and increase in heating load when electrical use is decreased and vice versa.

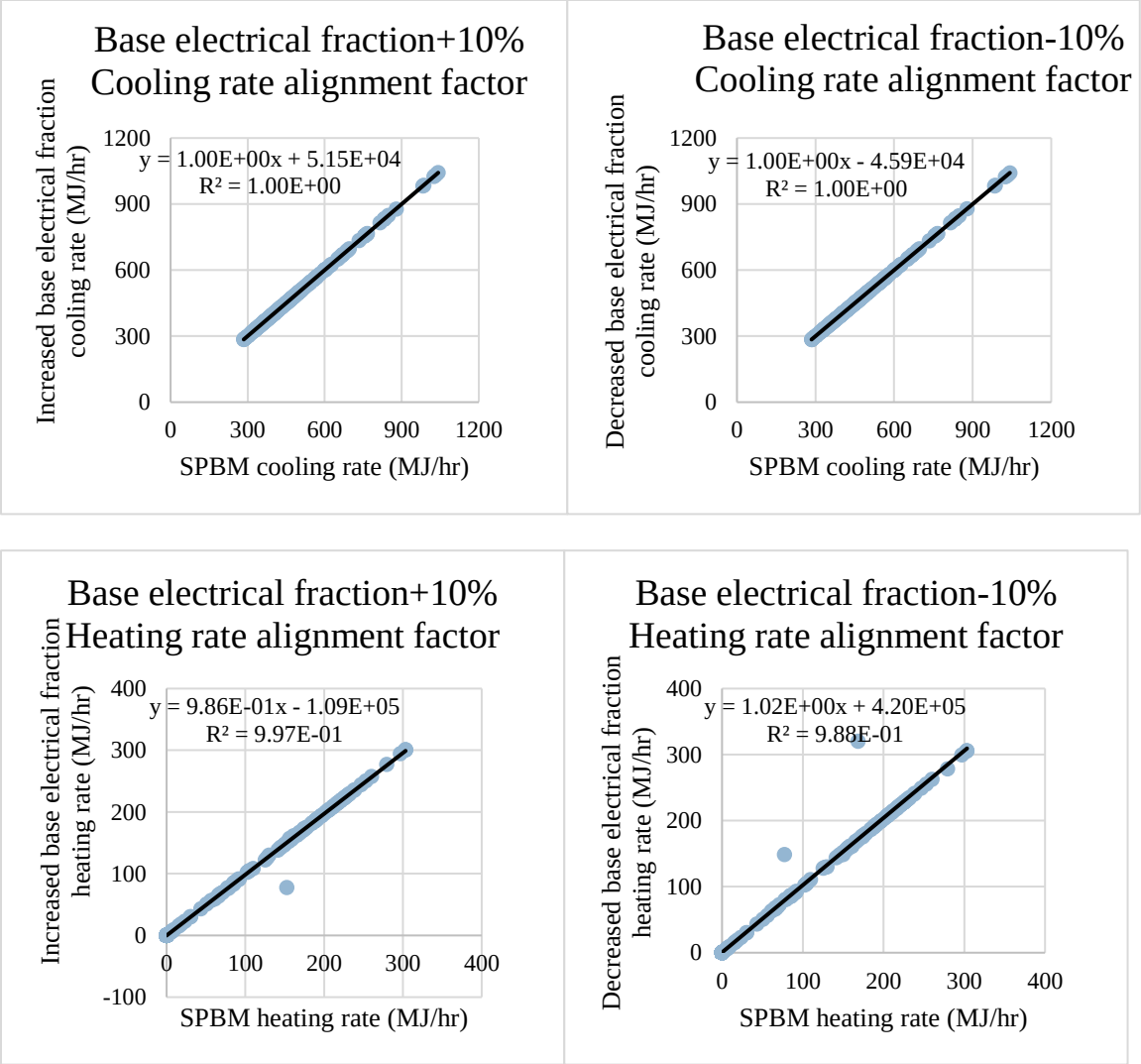

Figure 38: Alignment factors of SPBM and SPBM with altered base electrical use

Peak electrical use refers to the amount of electricity that is used while the building is occupied as this is when lights and equipment such as computers are used. Altering occupied electrical use should reduce heating demand and increase cooling demand. As expected, Figure 39 demonstrates the expected change in loading associated with the alteration of occupied electrical use.

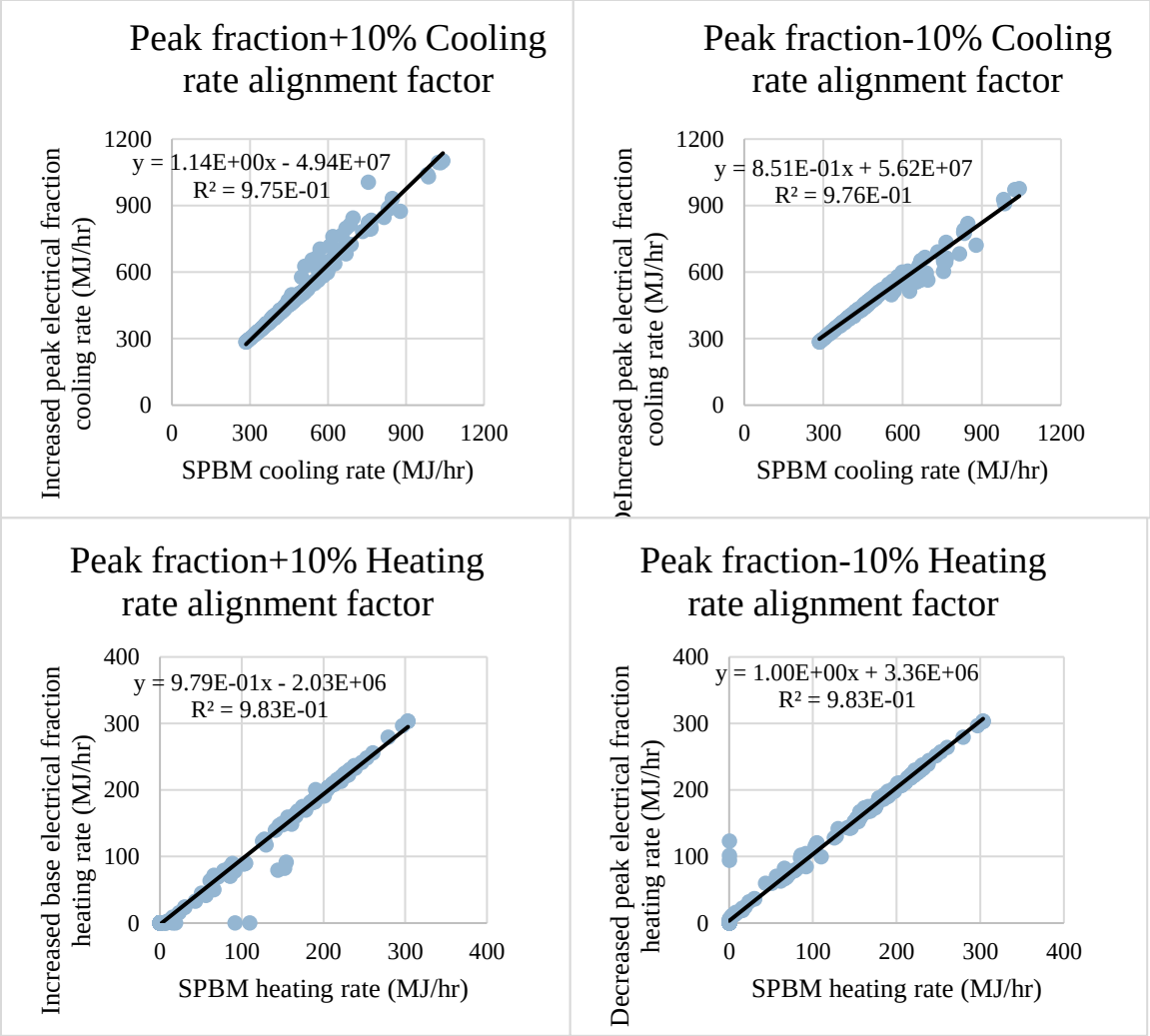

Figure 39: Alignment factor of SPBM compared to SPBM with altered peak electrical use

Lastly, the number of occupied people was examined to determine its characteristic impact on building dynamics. Both occupancy and occupied electrical use take place over the same timeframe but unlike electrical use, occupants produce both CO2 and latent energy (water vapor). While CO2 will be explored in another section, the latent impact of occupants produces an increase in cooling load at all times of the year by increasing the humidity of air going through the cooling coils. However, this latent fraction of heating load does not lower heating demand as it does not increase the temperature inside a room. Therefore, occupants should increase cooling load while not

increasing the air flow demand as much as a pure sensible load would; this result is shown in Figure 40 with the R^2 change for cooling load being significantly more than the change for heating load. Additionally, during winter the same results are expected where an increase in cooling coil load would occur even if the zones remained in heating mode.

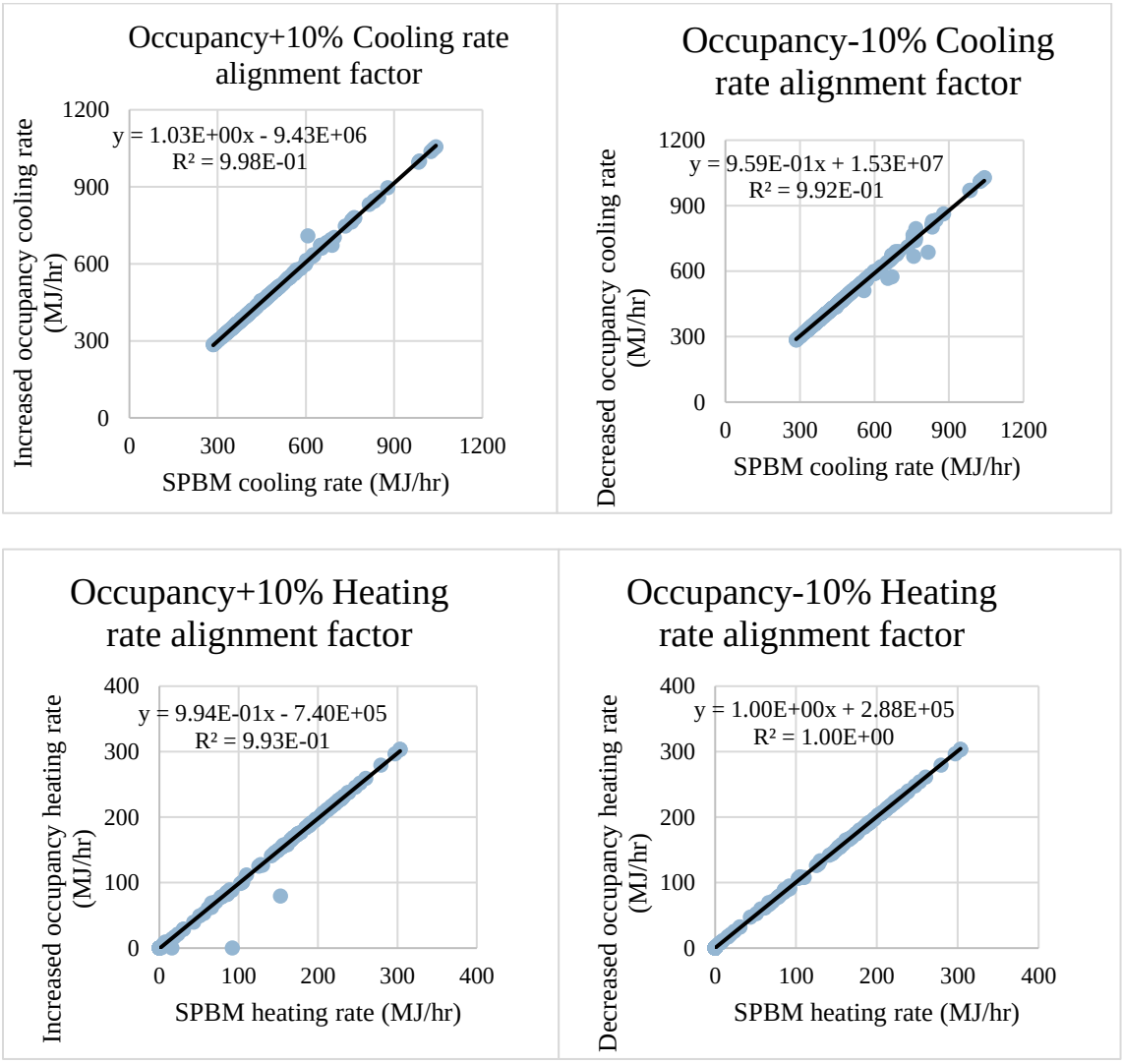

Figure 40: Alignment factors of SPBM compared to SPBM with altered occupancy levels

Overall, sensitivity for a number of different parameters was tested and results suggest that the SPBM is more sensitive to some parameters over others. If automatic fault detection and identification was to be conducted, these results suggest that total load

would need to be altered by a non-insignificant amount to be detected. However, if a fault does not noticeably alter energy demand, then it is possible that building operators would choose not to fix a fault that is not causing problems.

X.4 Discussion of results

The SPBM was able to demonstrate a high level of convergence with a highly detailed model. For all examined parameters the resulting variable uncertainty was less than 1%. While this uncertainty value does not mean that variable values are within 1% of real-world representations, it does mean the overall process and system representing building dynamics is not overly sensitive to small parameter adjustments but that small changes are still noticed. In addition, alterations in parameter values produced an expected and realistic response associated with each variable. The following section will examine how uncertainty and the system effect of individual components can be used for automatic fault detection.

CHAPTER 6. PARAMETER ESTIMATION

Parameter estimation is the cornerstone of the SPBM's fault detection method. However, it is important to note that the goal of parameter value estimation is not to determine the true value of parameters in the real world but rather to determine how changes in parameter values over time corollate to different building faults. Afterall, a model is considered calibrated when it has an acceptable fit and fits within data parameter values . So once the SPBM is calibrated with parameter values within a reasonable window then any real-world deviation from the model could potentially be seen as a system fault; and any significant change in parameter value could shine a light on the real-world cause of the error.

6.1 High-Fidelity Test Models

Given the extensive number of different faults that were desired to be induced, and the inability to induce faults in occupied buildings, a high-fidelity building model was constructed in EnergyPlus, a leading open-source building energy simulation program. Using detailed building blueprints and design specifications a calibrated high-fidelity EnergyPlus model was able to accurately replicate energy use based on building metered data.

6.1.1 Whitehead

Use of building blueprints allowed for detailed envelope, zoning, and HVAC specifications. Based on Figure 41, the wall is constructed with an exterior brick surface, small air gap, insulation, water barrier, and drywall. The roof has an impermeable top

followed by 9mm of insulation and a drop ceiling. AHU specifications are relatively simple with no energy saving measures, providing a unique structure to Old CE.

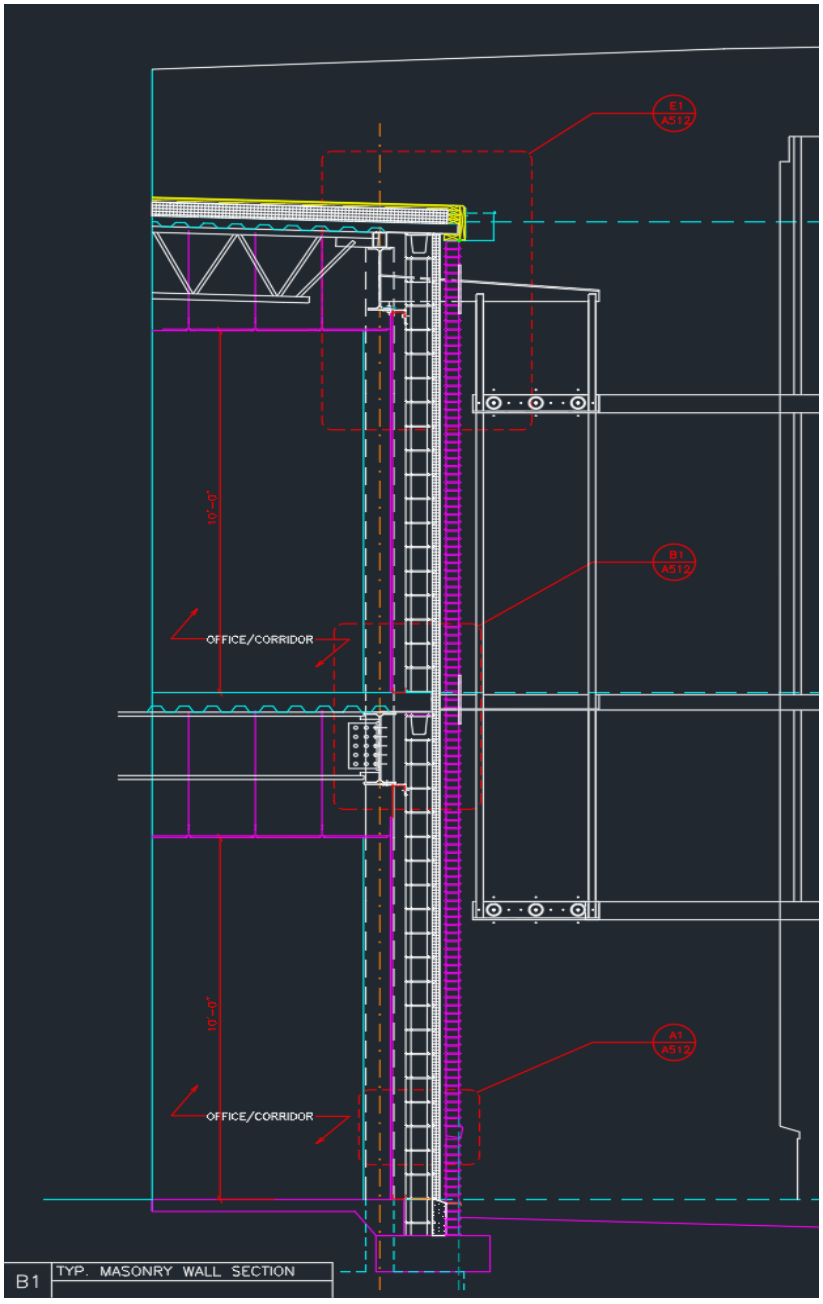

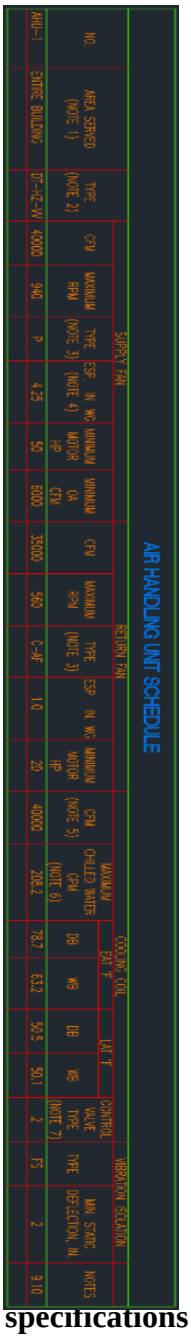

Figure 41: Building drawings of exterior wall and roof (left) AHU specifications (right)

Below are figures demonstrating the HVAC layout for Whitehead level 1 and 2 for illustration and reference. The information was used to construct an identical layout in EnergyPlus and assign the proper interior loads based on the specifications for each zone.

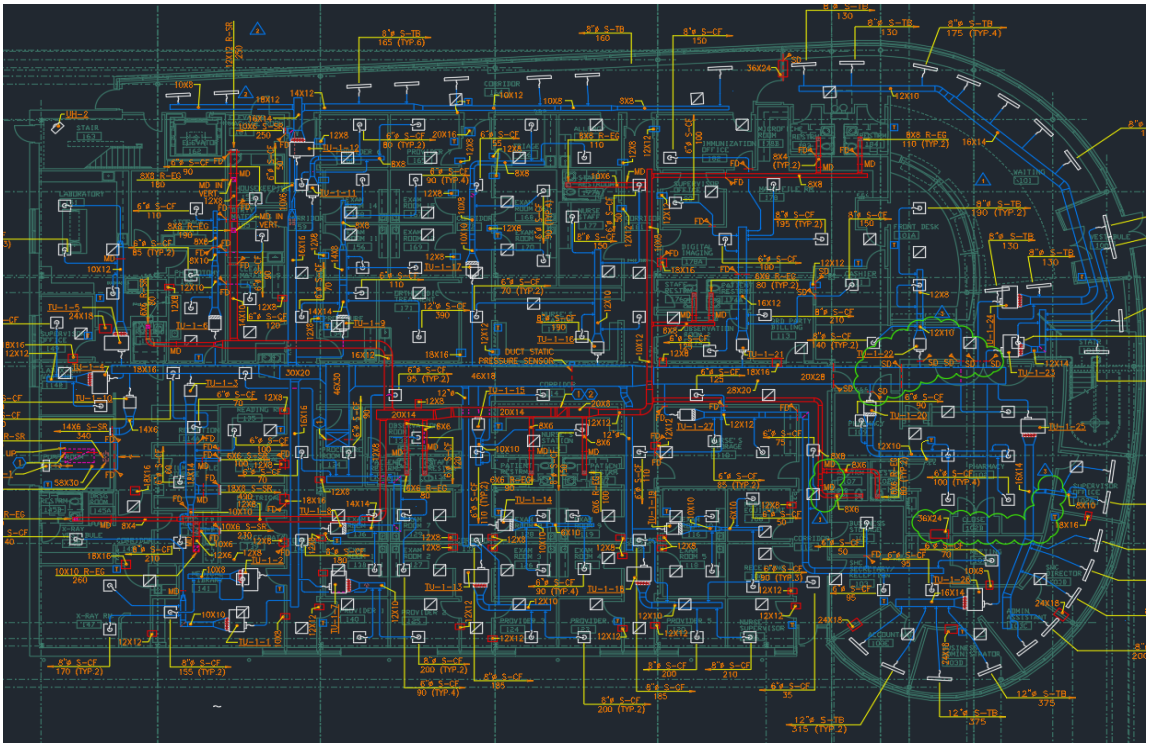

Figure 42: Design drawings of Whitehead level 1

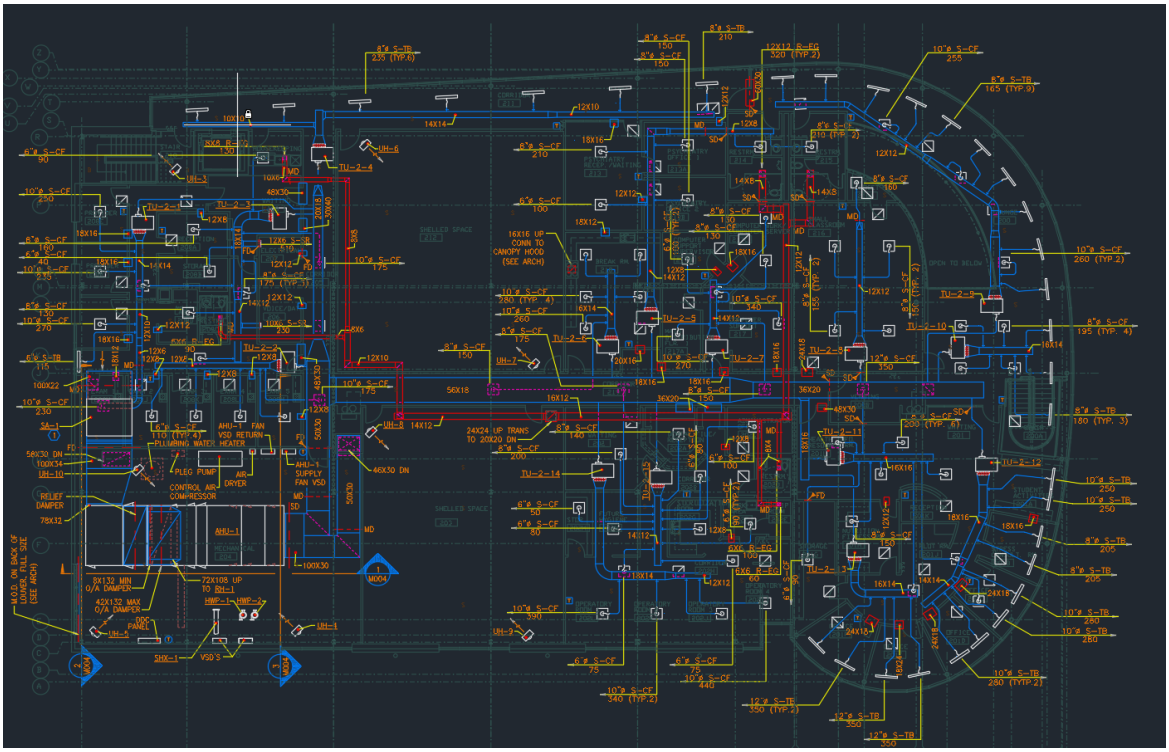

Figure 43: Drawing documents of Whitehead level 2

Beginning with such a high level of resemblance to the real building resulted in initial performance of the high-fidelity model to not be significantly off of from metered

data. However, it is important to note that a high-fidelity model will not be an exact match as it is impossible to catch every small detail that affects a building's load.

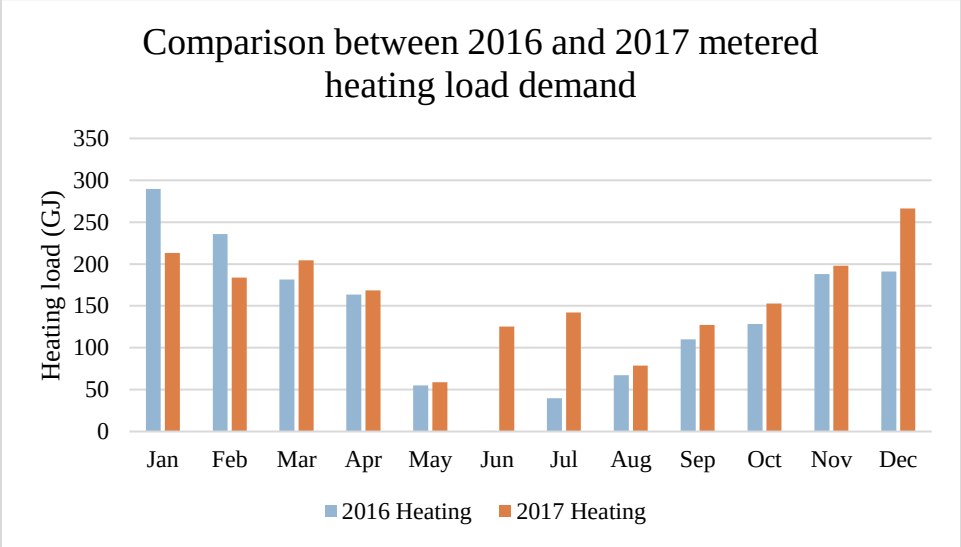

Figure 44: Monthly heating load demand for Whitehead metered from 2016 and 2017

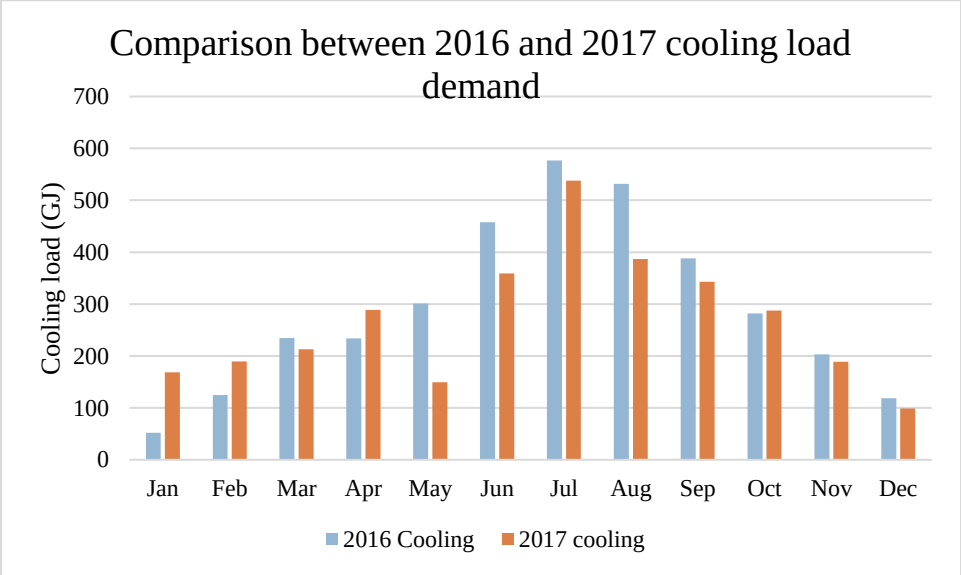

Figure 45: Monthly cooling load demand for Whitehead metered from 2016 and 2017

While the monthly loads displayed in Figure 44 and Figure 45 are similar, the hourly loads displayed below demonstrate how volatile small changes in exterior environmental and interior loads can have a dramatic change in specific demand.

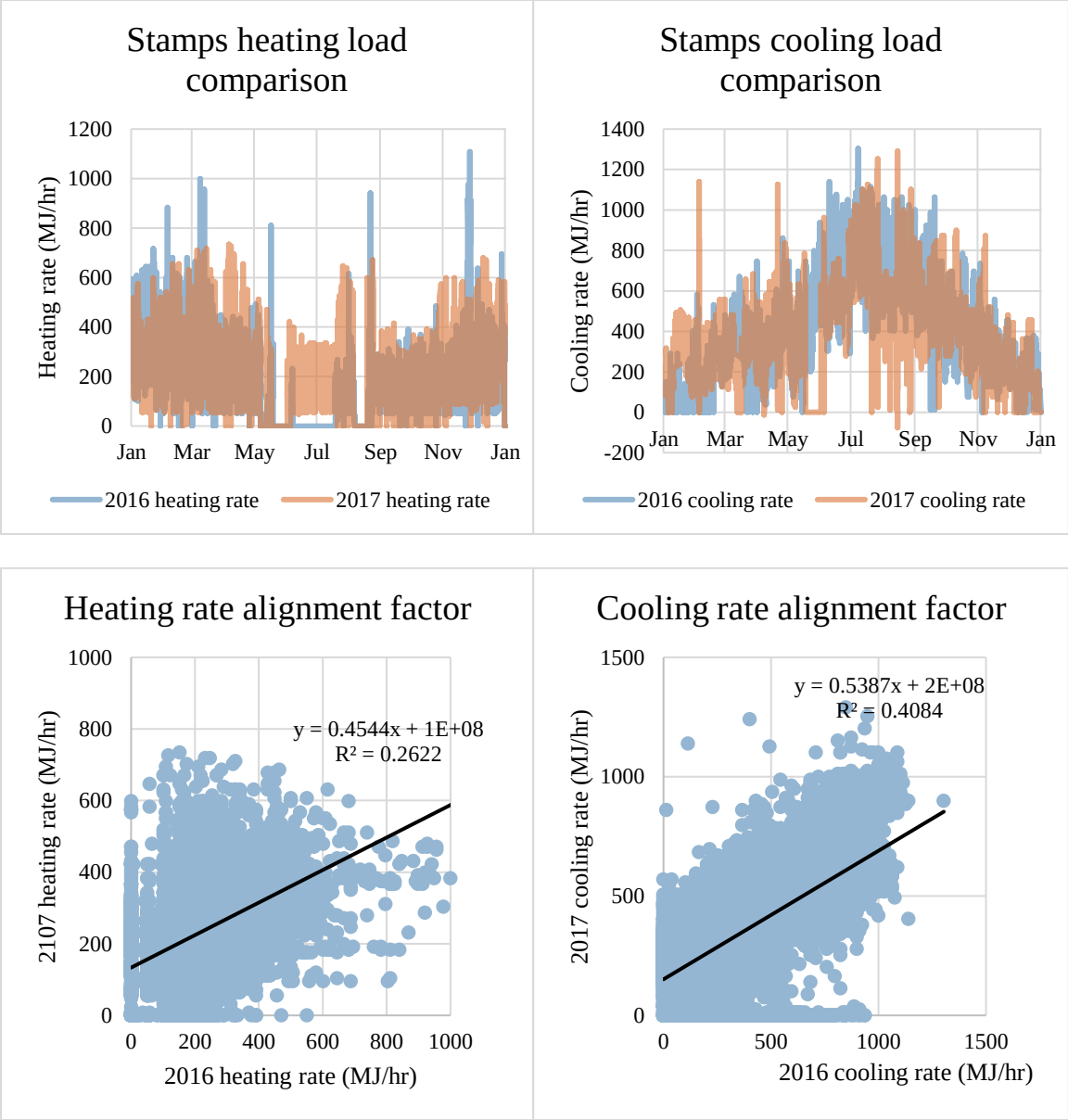

Figure 46: Plots and alignment factor of metered heating and cooling rates from Whitehead over 2016 and 2017

While the heating meter not reporting for the summer months is a factor in the low alignment factor between the two years, there was a noticeable difference in outdoor air temperature between 2016 and 2017 as shown in Figure 47.

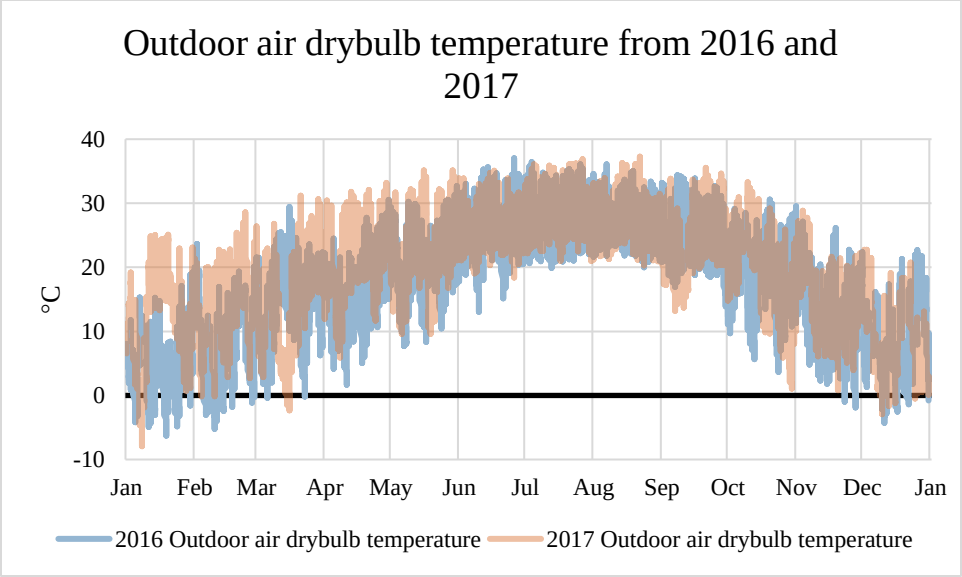

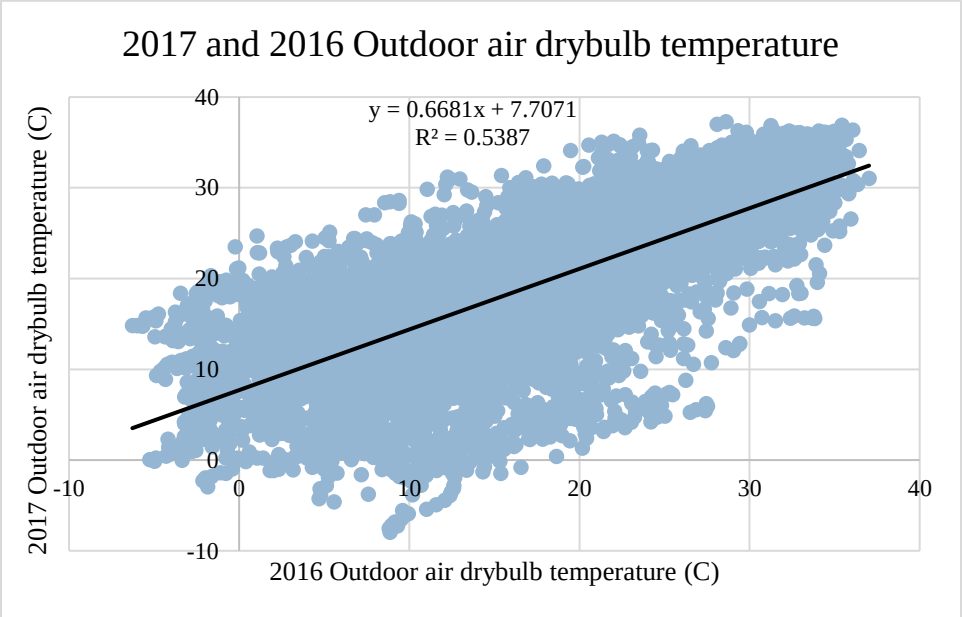

Figure 47: Plot and alignment factor of outdoor air drybulb temperature for 2016 and 2017, demonstrating low year-to-year consistently and importance of weather information

Like any model, the high-fidelity model required calibration. For model calibration, 2016 weather data was used because it had the highest level of accuracy as it came from an official source while interior load profiles were gathered from UK NCM, the same source as DesignBuilder. While building metered data for heating rate is

missing over the summer, it is generally a low demand time of the year and would not deviate much from the data that is there.

At this point, interior loads are still based on schedules but were replaced with electricity meter data fed in to EnergyPlus. Figure 17 shows the electrical use for the year of 2016 and was fed in to EnergyPlus as the fractional load for the interior lighting and equipment. As stated by Yang-Seon Kim, using electrical metered data to estimate occupancy leads to increased accuracy over a strict schedule . It is simple to see when building energy is used, and due to the relatively steady occupancy of Whitehead, can be used as a method for providing occupancy fractional schedule different from the schedule used by lighting and plug loads.

Based on interviews with Georgia Tech Facilities staff and intuition, the following changes were made to reflect real problems in Whitehead or see if similar problems across Georgia Tech campus also occurred at Whitehead. 1) Excessive heating in winter 2) increased air flow 3) increased outdoor air flow 4) not entering temperature setback. Electrical and occupancy data was not changed because metered electrical data was fed in to EnergyPlus to use as the fractional schedule for interior plug loads and occupancy data was based on specifications from DesignBuilder.

A common fault is when the preheat coil temperature setpoint is overridden in winter months as a quick fix to prevent AHU automatic shutdown to prevent cooling coils to freeze. Overriding the preheat coil temperature to be higher than13°C is usually due to improper air temperature sensor placement and calibration that results in the sensors reading an artificially low temperature; this fault causes a complete system shutdown to prevent freezing the cooling coils that follow the preheat coils . As such, to

prevent system shutdown the preheat coils are set to a higher temperature; but this is wasteful as air is heated for no reason and then immediately cooled by the cooling coils. Excessive preheat is easy to spot by looking at the cooling load and seeing if the cooling demand follows a similar profile as the heating demand. Additionally, there will be a non-zero minimum cooling load. None of the usual symptoms of an elevated preheat coil temperature setpoint were noticed, so this was ruled out for calibration.

Whitehead drawings specifies a minimum of 2.3 m^3/s and maximum of 18.9 m^3/s for outdoor air, however, as expected, the actual flow rate was higher than the minimum designed. Although the minimum air flow applies to unoccupied minimum air flow setting and the model uses 3.5 m^3/s outdoor air and 8.3m^3/s of total air flow as a minimum. This airflow is well within normal operating flow rates and was determined to be a major contributor to the difference in calibration; especially once evening temperature setback was removed.

Lastly, not entering unoccupied temperature setback is a common problem on campus . Temperature setback results in a more spread out minimum and maximum load and also a sharp increase in demand when temperature setpoints change to occupied settings. This too was not present in the calibration data and the EnergyPlus model had a noticeable increase in minimum and maximum load.

Below, there are figures showing the monthly heating and cooling loads for the building meter, high-fidelity model before calibration, and model results post calibration. Additionally, there are plots detailing the hourly heating and cooling rates of the building meter and calibrated model as well as the alignment factor of the model. Note that for the

hourly data the modeled rates are semi-transparent which allows one to view both the metered and modeled rates simulations.

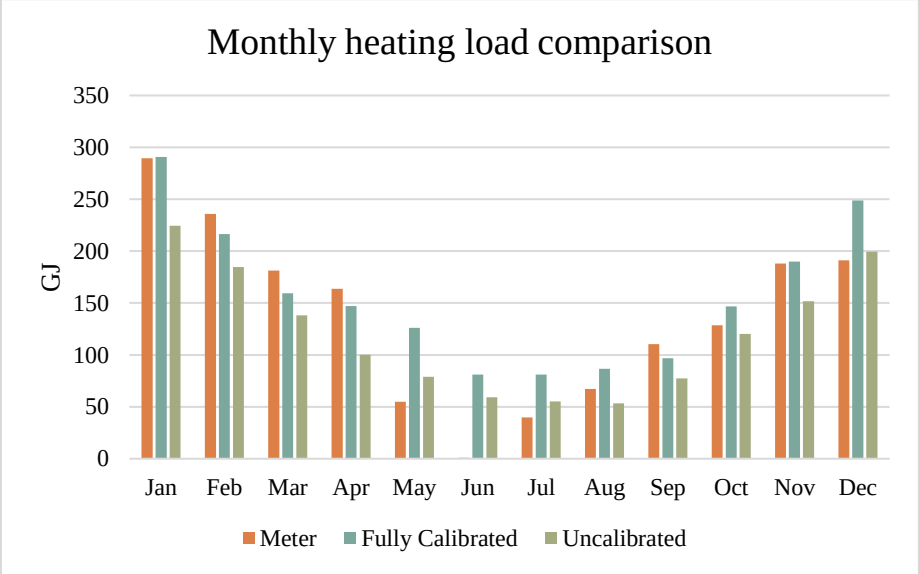

Figure 48: Monthly heating load for Whitehead as well as the calibrated and uncalibrated EnergyPlus model

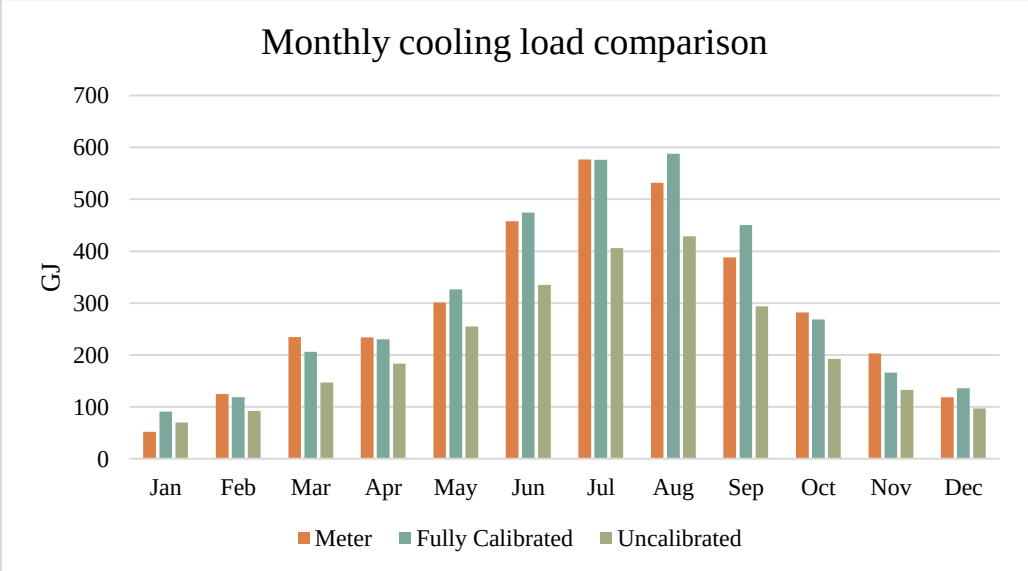

Figure 49: Monthly heating load for Whitehead as well as the calibrated and uncalibrated EnergyPlus model

As shown, a calibrated model dramatically improves the accuracy of a building energy model while learning about current problems with building operations. However,

this process takes considerable time and skill on the part of the person doing the calibration. Also, note that the difference in heating load over the summer months is due to a meter malfunction resulting in a loss of data.

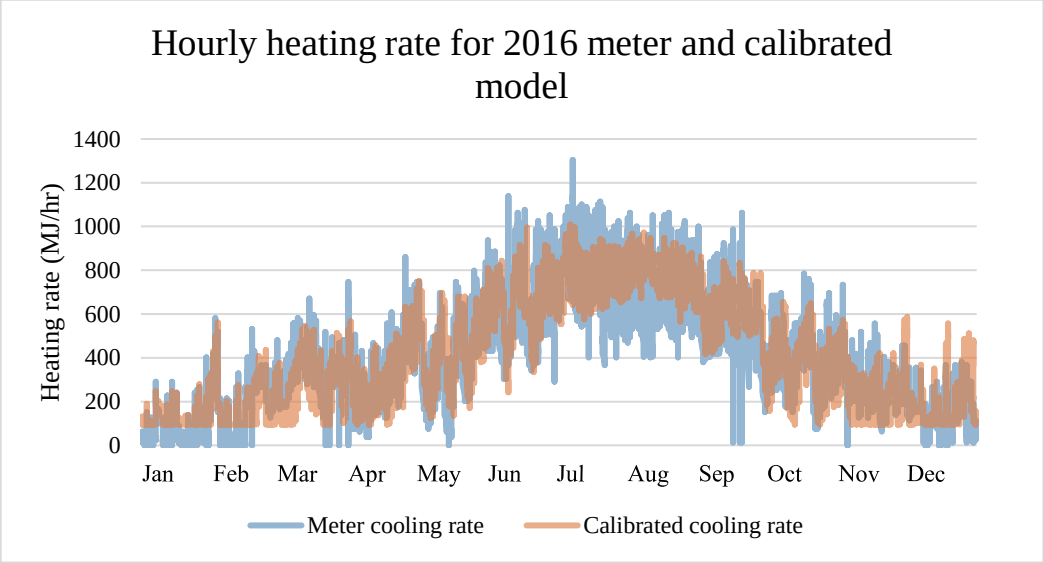

Figure 50: Hourly heating rate comparison between meter and calibrated heating rate

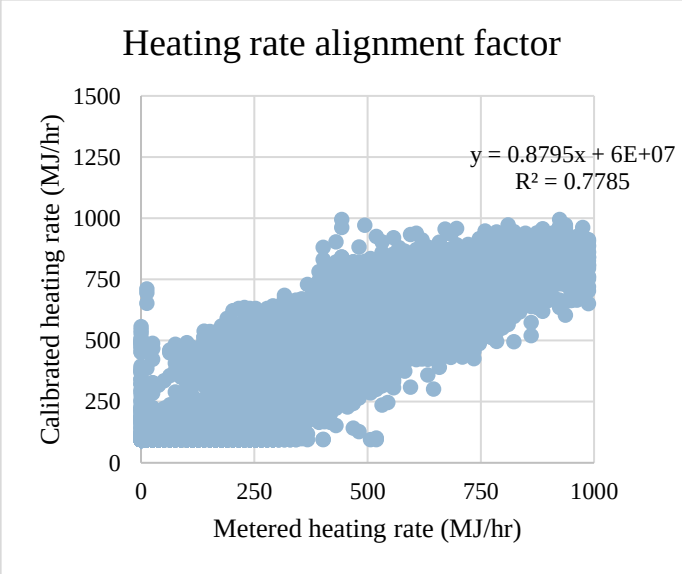

Figure 51: Alignment factor of calibrated and metered heating rates

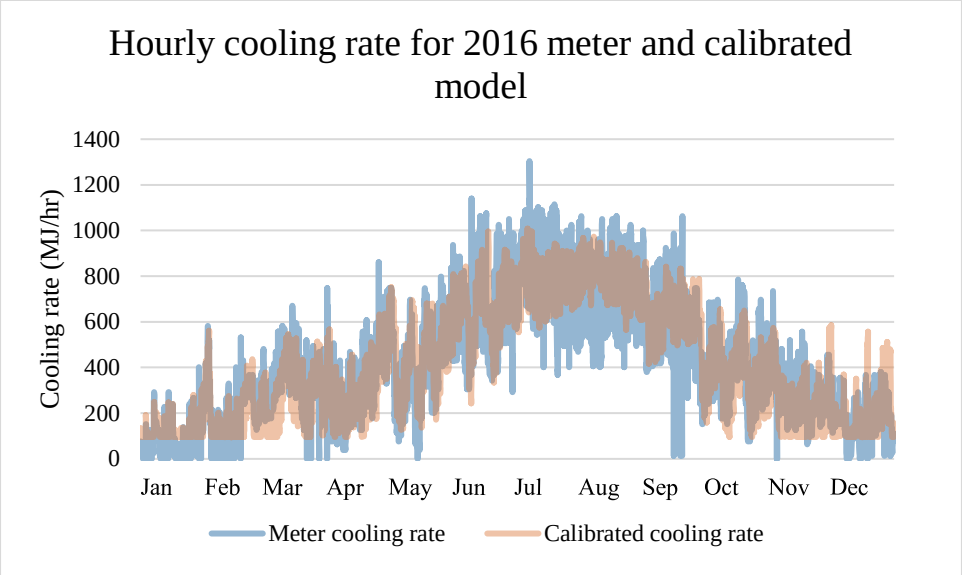

Figure 52: Hourly heating rate comparison between meter and calibrated cooling rate

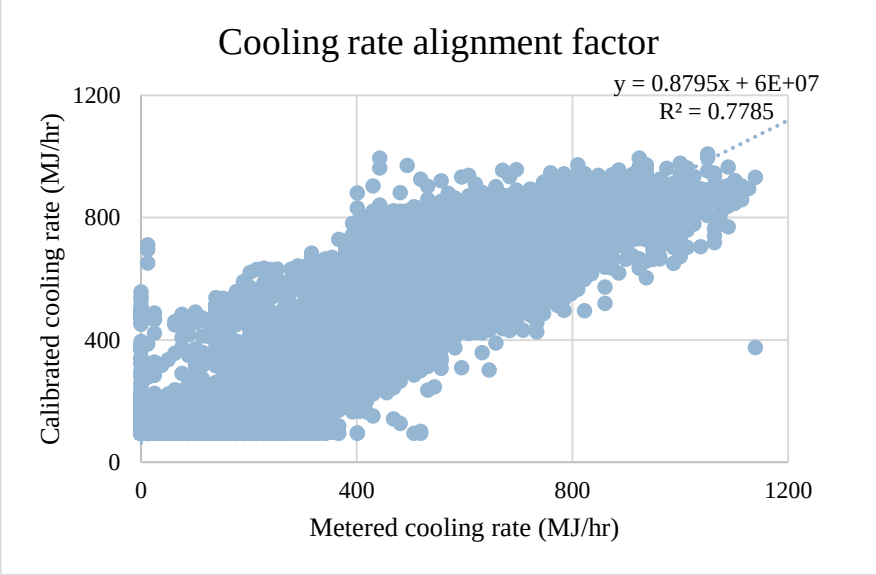

Figure 53: Alignment factor of calibrated and metered cooling rates

Overall, the alignment of the model with metered data is acceptable for this level of analysis based on the information that was available. Considering the variation in loads between just one year of use, the model's alignment and representation of a system as complex as a building is acceptable.

6.1.2 SPBM Calibration for Whitehead

The SPBM is able to replicate the same level of accuracy as a high-fidelity model while using far fewer inputs and greatly simplifying the design of the modeled layout. Additionally, this level of accuracy will be shown to be sufficient for auto-calibration of model parameters in addition to being able to detect faults within the building. Reliability and processes of automatic fault detection of the SPBM is discussed as it compares to machine learning is also discussed. Accuracy predicted heating and cooling loads from the SPBM were in agreement with metered data as well as the calibrated high-fidelity EnergyPlus model (henceforth referred to as 'high-fidelity reference data'). For the sake of readable data, results have been separated into winter (January and February) and summer (June and July); no parameter values were changed between runs. Winter and summer demonstrations were chosen because that is when building energy losses due to faults are most severe.

Calibration was first performed on Whitehead during winter weather. As shown in Figure 54 and Figure 55, heating is the primary demand but there is also a non-negligible cooling load as well. The SPBM is capable of replicating both heating and cooling demand with a high level of precision and accuracy. Both hourly plot and alignment factor figures are provided as hourly plots convey system dynamics and the alignment factor is often used as a quick visual aid to demonstrate the "goodness of fit" of a model.

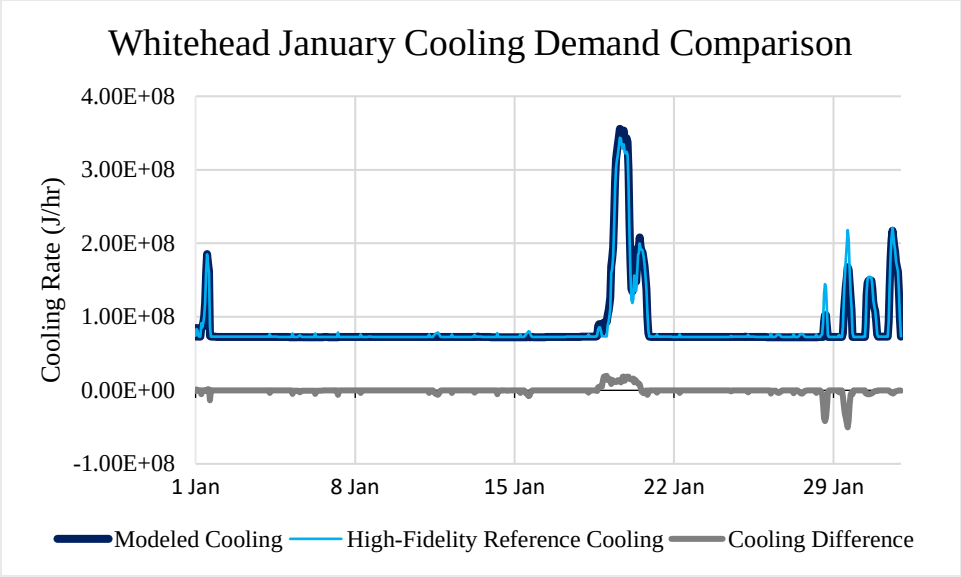

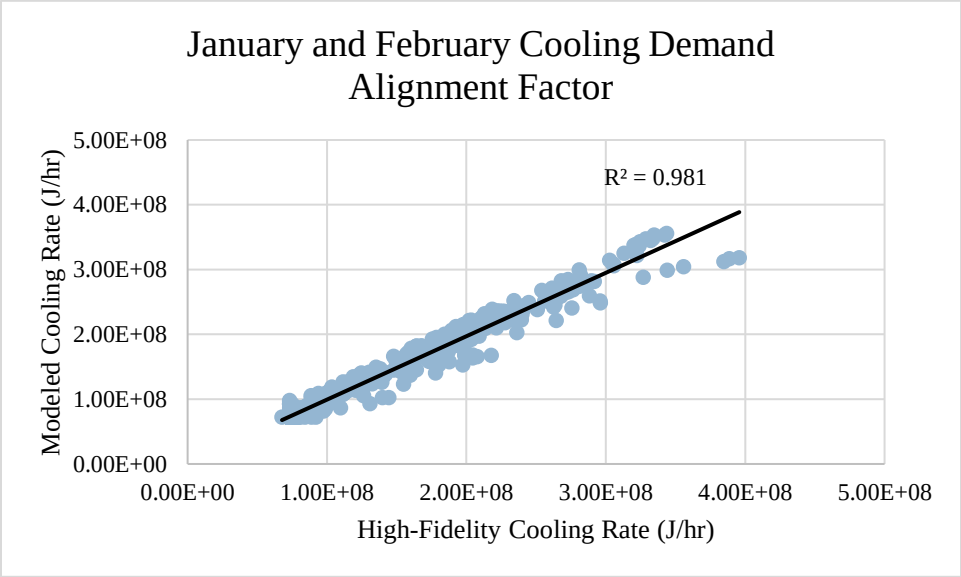

Figure 54: Whitehead winter cooling load comparison and alignment factor, demonstrating excellent initial calibration

Figure 55 shows the overall dynamic accuracy of the SPBM and its ability to respond accordingly to internal and external loading during high cooling demand periods. Heating demand for Whitehead building also includes brief peaks of demand as temperature setpoints move from the lower unoccupied value to occupied settings.

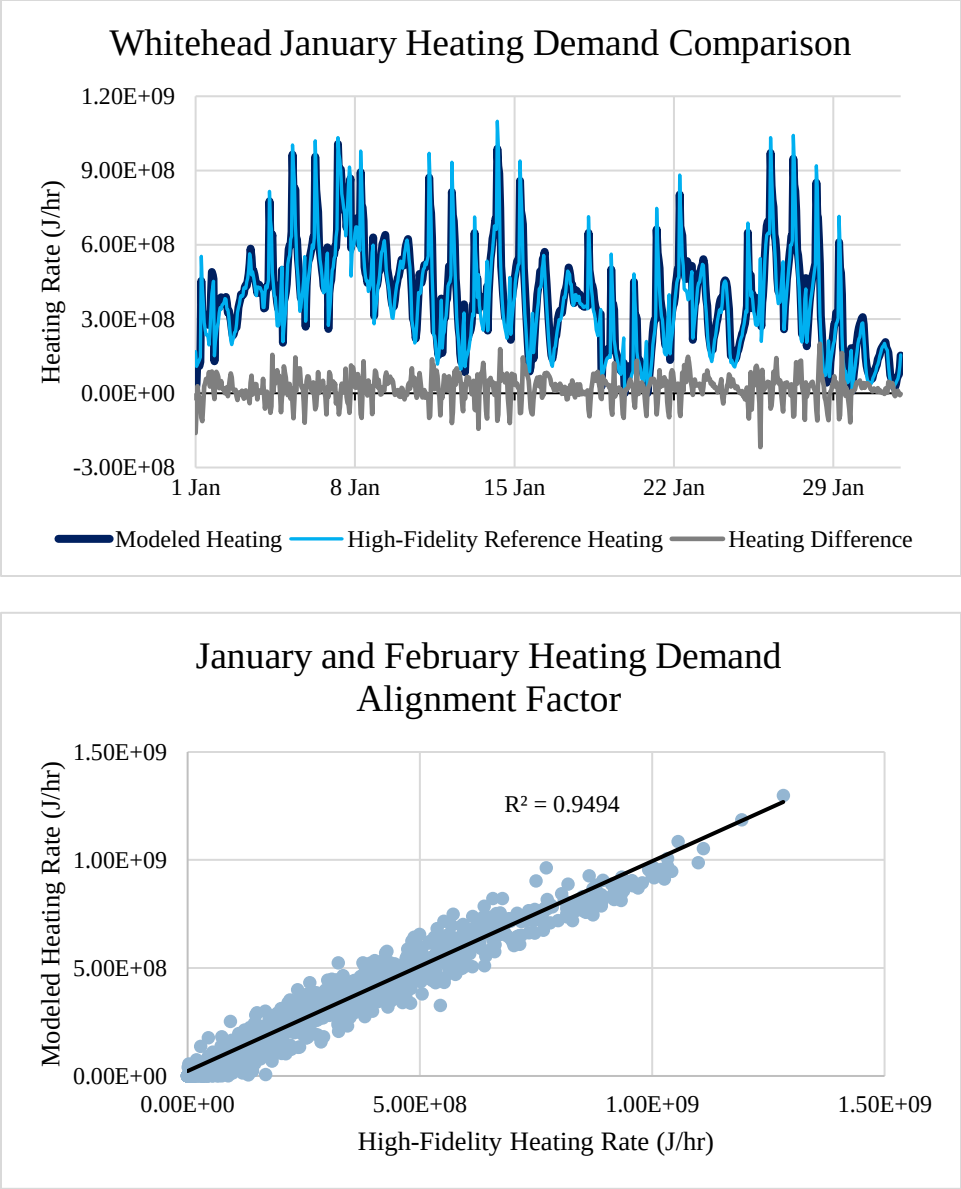

Figure 55: Whitehead winter heating load comparison and alignment factor

During June and July, cooling demand becomes the dominate load for the AHU. As such, Figure 56 demonstrates that the SPBM is able to replicate this change in demand as well as the increased humidity from outside air as well as heightened air flow requirements brought by increased cooling load.

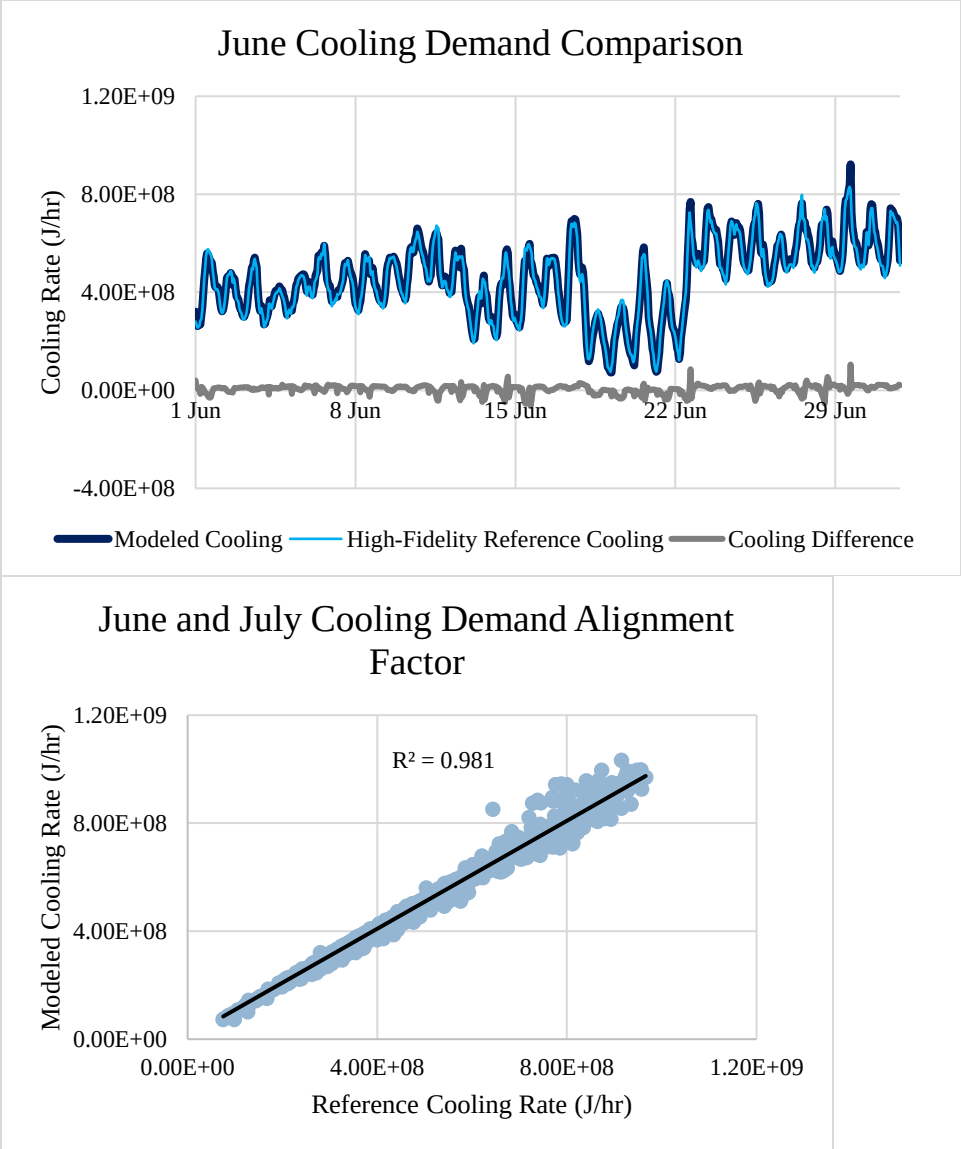

Figure 56: Whitehead summer cooling load comparison and alignment factor

Conversely, heating demand in summer in Georgia is sparse. While the time comparison plot from Figure 57 appears to demonstrate a failure to model heating loads in summer, the alignment factor shows that the SPBM does respond with heat demand as the AHU switches from a low temperature zone setpoint to a higher occupied zone setpoint temperature, the heating demand only lasts for an hour. Given that the SPBM models an entire building floor as one zone, heating loads from the internal, small zones of a building are not always able to be represented. In any regard, the level of accuracy

demonstrated has proven to be more than sufficient in automatic fault detection; the purpose of the SPBM's creation.

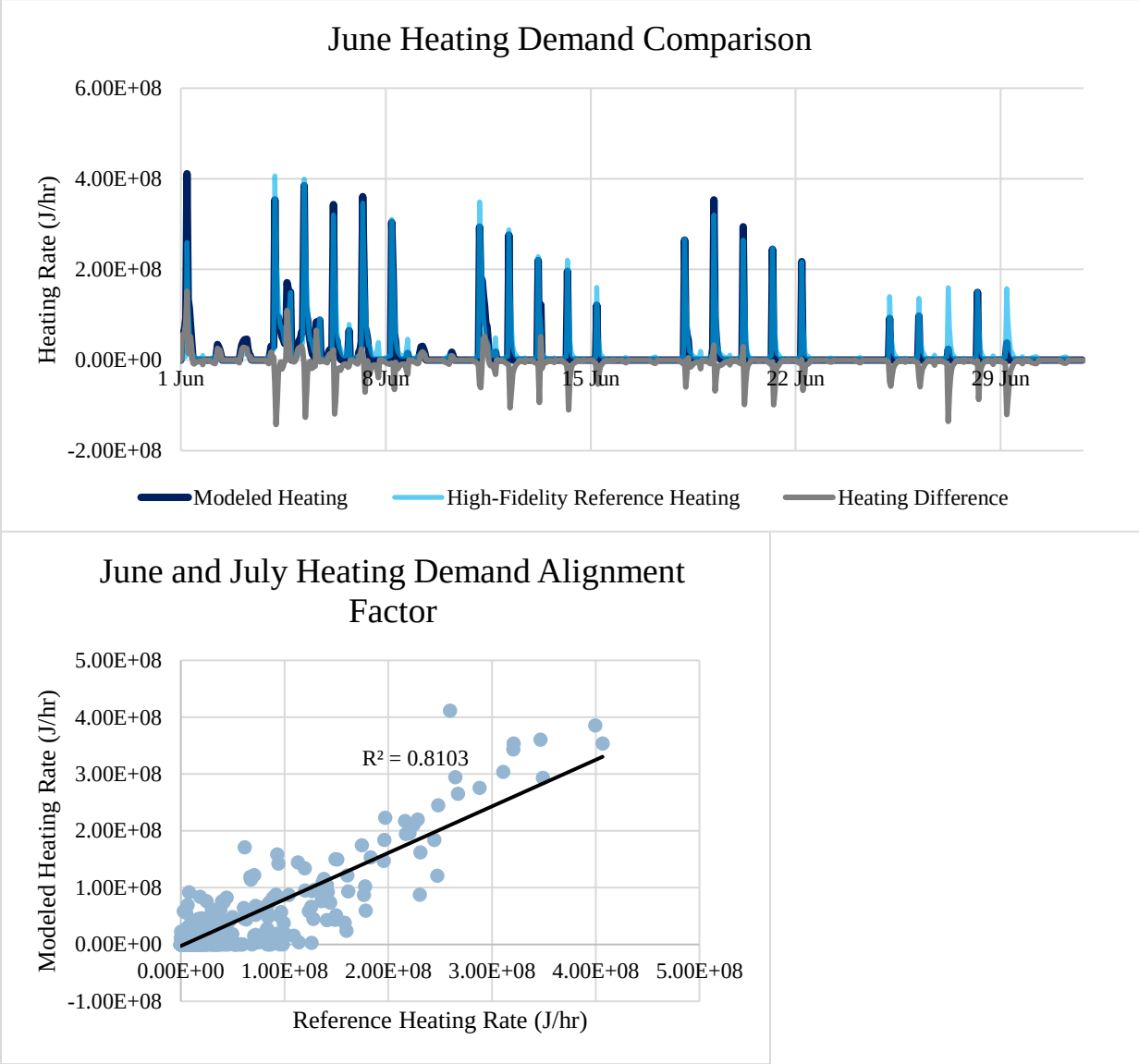

Figure 57: Whitehead summer heating load comparison and alignment factor

Again, it is important to note that while the alignment factor of heating in Summer appears to not be in line with reference data, the heating demand is so low and so brief that it does not represent a sizeable impact on building energy demand. However, the demonstrated level of accuracy and precision will prove to be sufficient for automatic fault detection and identification discussed later.

6.1.3 Old CE

A similar level of calibration was applied to Old CE, which resulted in often under 15% error for cooling and electrical data (heating load data was nonsensical). For this building, an in-person walkthrough of the entire building was conducted which allowed a room-by-room analysis of lighting fixture makes, high-load electrical items such as computers or personal heaters, occupants per zone, and VAV occupied and unoccupied flow rates. Recorded information was used in EnergyPlus, along with model tuning based on observed and theorized faults.

Old CE has more outdoor air control systems available than Whitehead and therefore required some additional tuning of the SPBM. Most notably, Old CE has a heat recovery system, economizer, and scheduled air flow rates. Heat recovery was not implemented at Whitehead due to the possibility of contamination from exhaust carrying contaminates from the medical rooms . Implementing these energy conservation features was not difficult and demonstrates the ease of use with the SPBM.

Heat recovery is a process of exchanging sensible and latent heat between exhaust and incoming outdoor air, often through a heat exchanger in the form of a heat wheel or runaround pipe. By transferring latent and sensible heat between exhaust and incoming outdoor air, the incoming air can either increase in humidity and temperature (as is the case in winter) or decrease in humidity and temperature (as is the case in summer). Exchanging energy in Old CE occurs with a rotating large metal wheel that is coated in desiccant; heat and humidity from whatever air stream is higher will be absorbed by the wheel and be absorbed when the wheel spins to the other air stream. This presents a low-cost system to reduce energy consumption on outdoor air and a vital component to model

correctly to ensure accuracy.

HVAC Economizer mode is when a higher proportion of outdoor air than is necessary for minimum ventilation requirements . Typically, outdoor air requires more conditioning than return air because the temperature of outdoor air is hotter than room temperature in summer and colder than room temperature in winter. However, cold outdoor air can be used advantageously if it is closer to supply air specifications than return air. Old CE has a supply temperature setting of 12.8°C and when the outdoor air temperature is between 18.3°C and 7.2°C outdoor air is used so reduce the cooling load .

Lastly, Old CE has scheduled minimum air flow rates that lower during unoccupied times. Reducing air flow rates decreases the amount of energy required to condition supply air by lowering the amount of air that is cycled. Coupling the lower air flow with a zone temperature setback would alleviate problems with an insufficient air flow being unable to keep a zone within occupied temperature setpoints as well as further lowering energy demand.

The heating load, shown in Figure 58, shows four dramatically different and implausible loads. For instance, 2018 shows peak load from March through July and then a demand in December that is 2.5x the load in January, typically the highest demand load in Atlanta. Another anomaly is that all four years have identical loads for January which should not happen, especially considering the difference shown in Figure 46 for Whitehead between 2016 and 2017. Due to the lack of reliable heating data, accurate heating demand calibration was impossible.

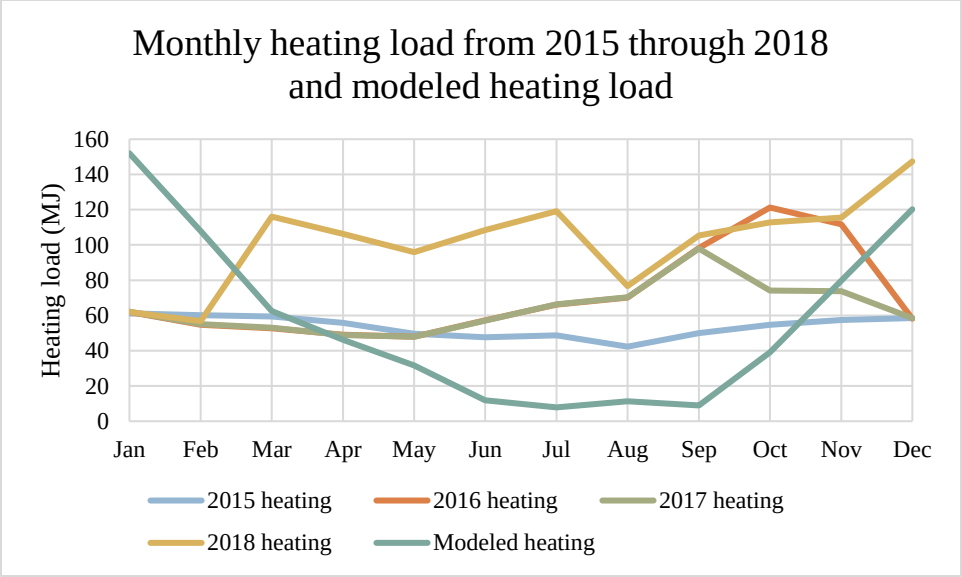

Figure 58: Monthly heating load of Old CE from 2015 through 2018 as well as the modeled heating load showcasing the poor metered data for heating load demand

Unlike the heating loads, the cooling load is more in line with what is typical for a building in Atlanta. Additionally, all four years are similar to each other in profile and demand.

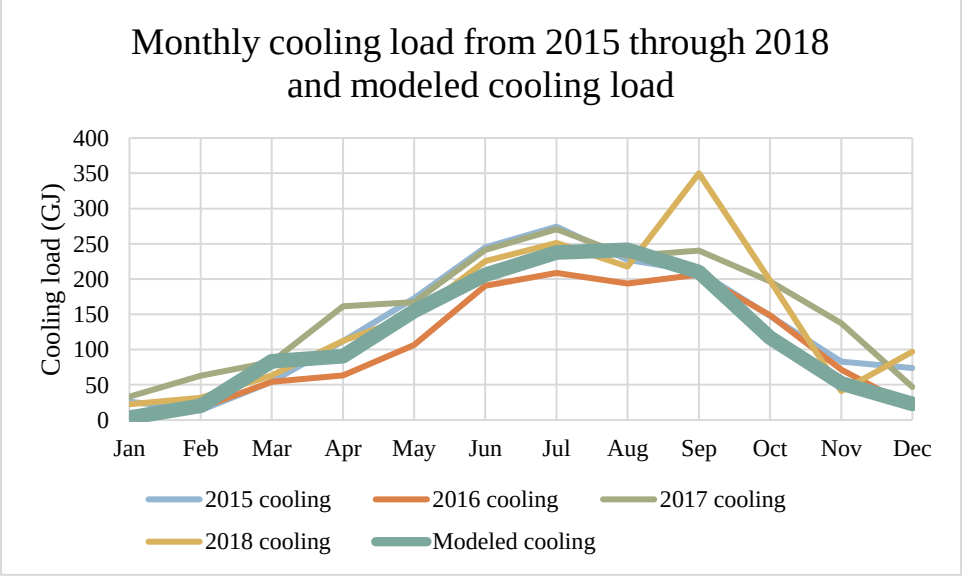

Figure 59: Monthly cooling load of Old CE from 2015 through 2018 as well as the modeled cooling load displaying high year to year agreement in cooling load

Electrical use is the most consistent across the four years with all years overlapping with no major divergence. Figure 60 has a subtle but important dip in load during summer months when there are fewer students on campus but also when the building would have an increased electrical load due to the increase in HVAC cooling demand. The dip in electrical load coupled with the increased cooling demand means that there is actually less interior load than there appears by just observing the figure as the AHU would be using more electricity to cool the building.

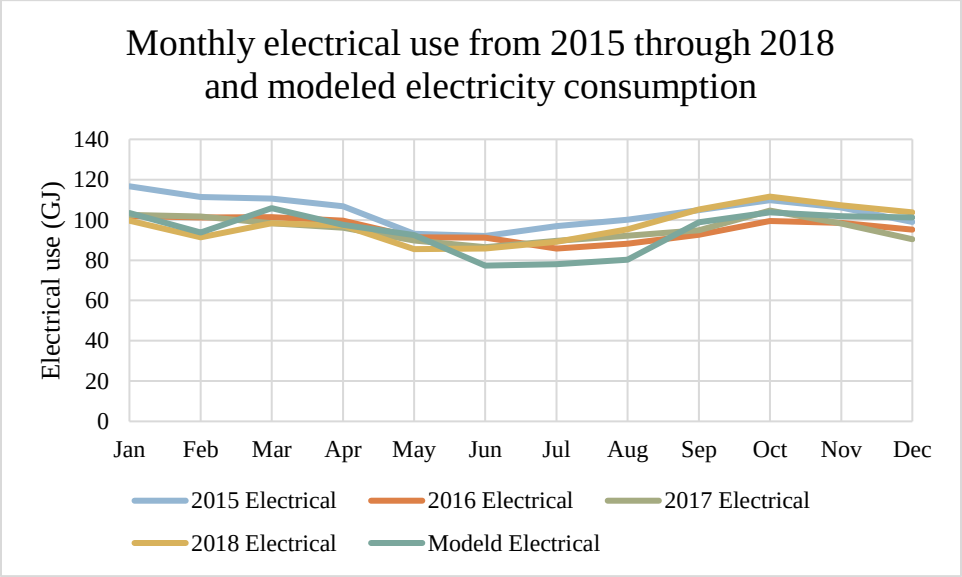

Figure 60: Monthly electricity consumption of Old CE from 2015 through 2018 as well as the modeled heating load

Lastly, a pie chart in Figure 61 was made to show an estimated breakdown of interior cooling demand based on the calibrated model. Envelope heat gain only accounts for thermal energy transferred into the building, not thermal energy leaving the building. Occupant, light, and plug loads all are a direct load on the system and the loads are easily calculated by EnergyPlus. Lastly, ventilation requirement cooling represents excessive cooling on the building in addition to necessary demand for dehumidification.

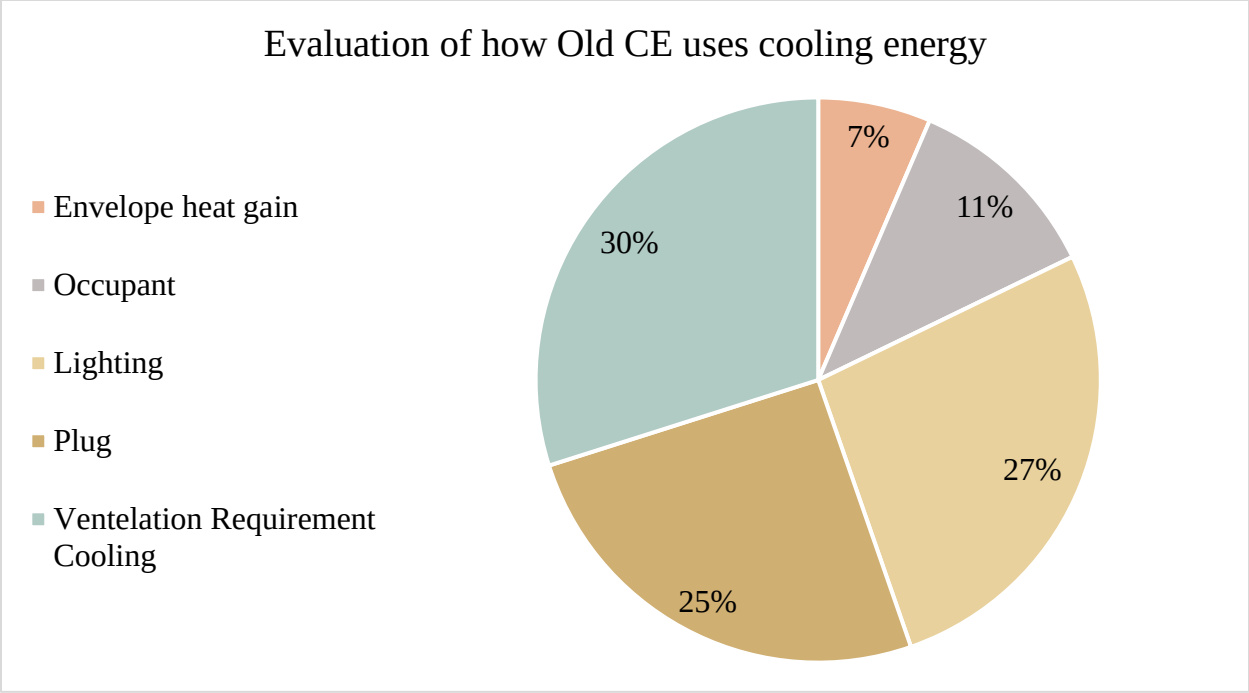

Figure 61: Estimated percentage of cooling load based on demand subcategory

Given the agreement of electrical and cooling loads for four years of metered results, it is safe to say that Old CE has a repeatable and steady use. Additionally, EnergyPlus was able to recreate the typical energy profile when using real weather and internal load data from 2016.

Both Old CE and Whitehead went through the same development process, but systems were developed and tested with Whitehead then adapted for Old CE. Using Whitehead as the development basis is due to the simpler operation, size, and layout. However, each system was verified with Old CE data before continuing and a resulting model comparison between Whitehead high-fidelity and SPBM will be included.

6.1.4 SPBM Calibration for Old CE

Having demonstrated the proficiency of the SPBM with Whitehead building, the focus turns to Old CE. Unlike Whitehead, Old CE is a legacy building that experiences

different loading characteristics and has a more complex AHU system and design. Also of note is envelope properties are unknown because of the age of the building. Despite the increased challenges of Old CE, the cooling load as represented in Figure 62 demonstrates high accuracy and the ability to model heat recovery, schedule-based air flow demand, and complex internal loading.

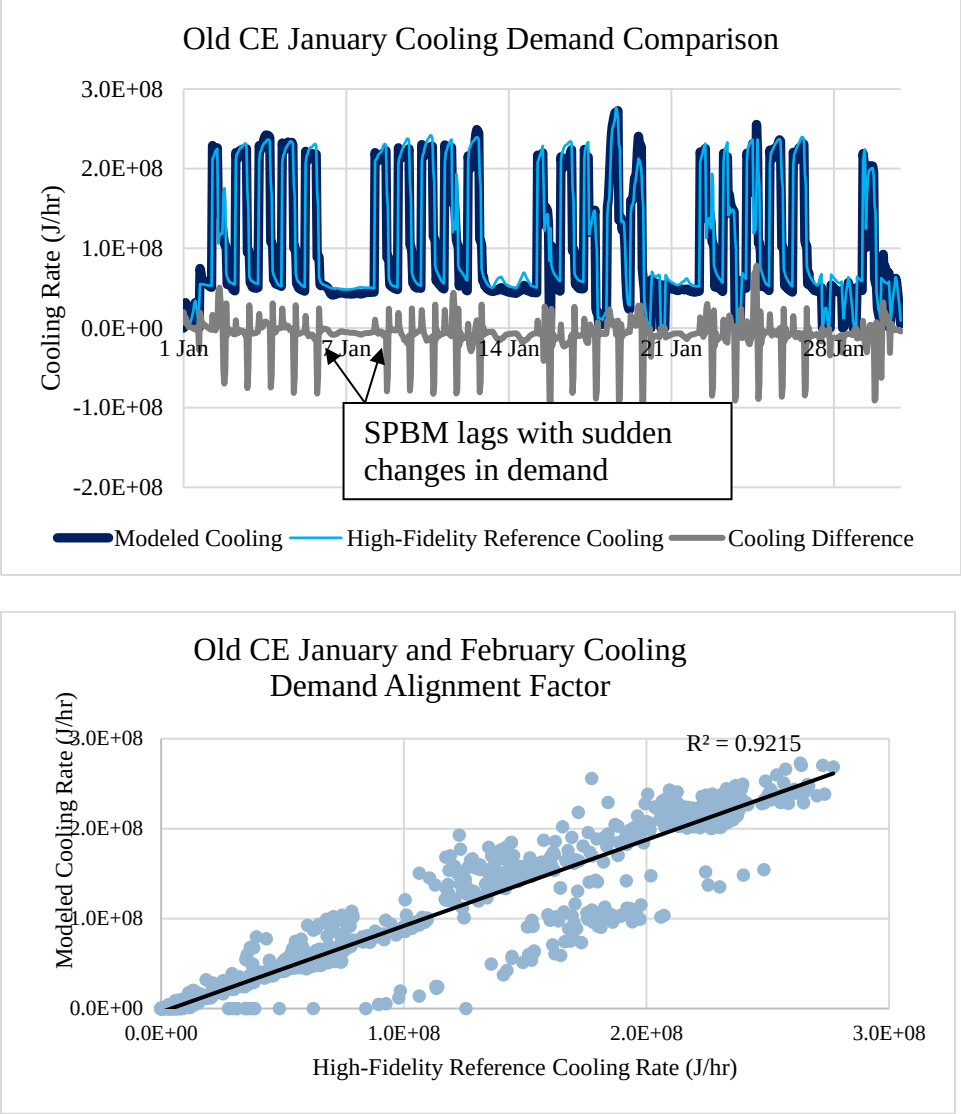

Figure 62: Old CE winter cooling load comparison and alignment factor displays the slight lag associated with sudden changes in demand

Similar to Whitehead, heating is the primary demand in winter. Additionally, the SPBM demonstrates similar levels of proficiency in representing heating demand, as shown in Figure 63, that has been demonstrated before.

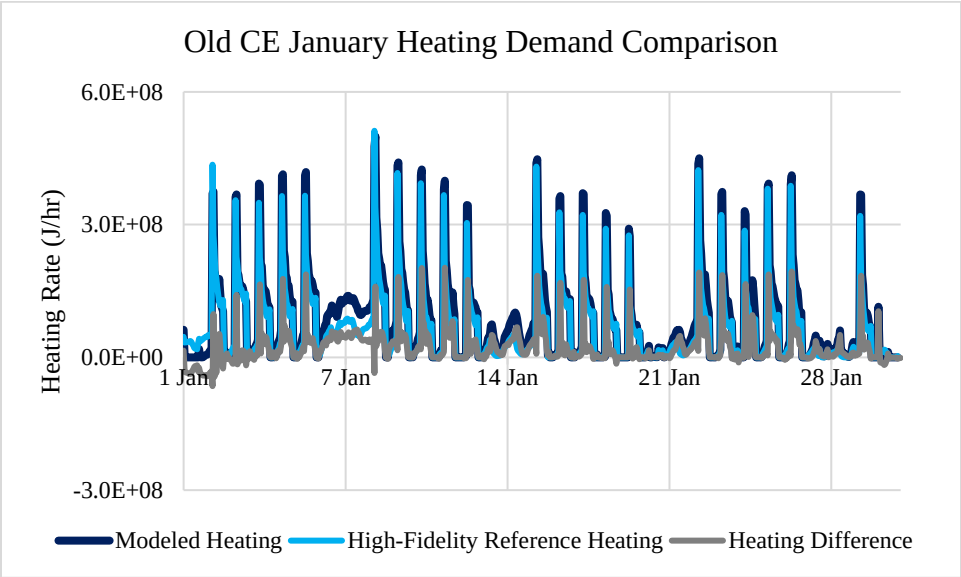

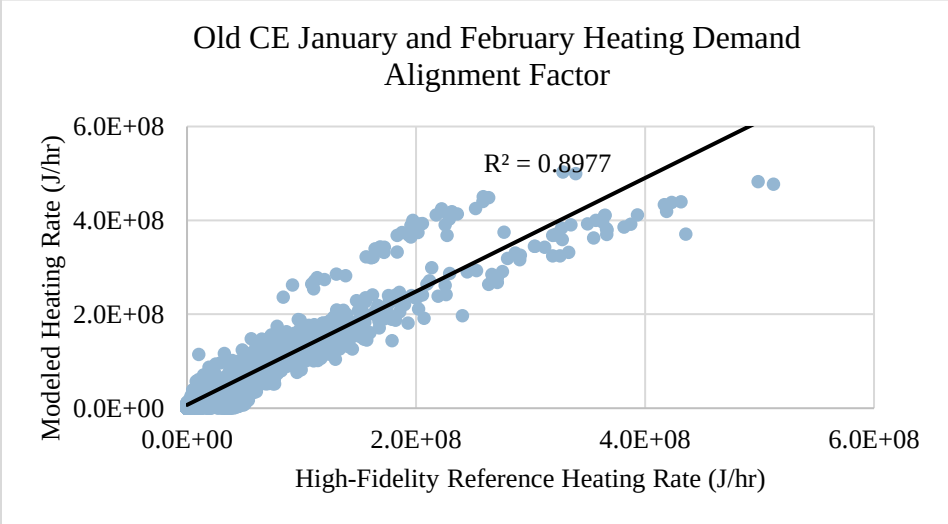

Figure 63: Old CE winter heating load comparison and alignment factor

Summer for Old CE again demonstrates high levels of accuracy for a simplified modeling program. Figure 64 shows a slight underprediction of cooling load at peak time as well as deviation when setpoints change from occupied to unoccupied.

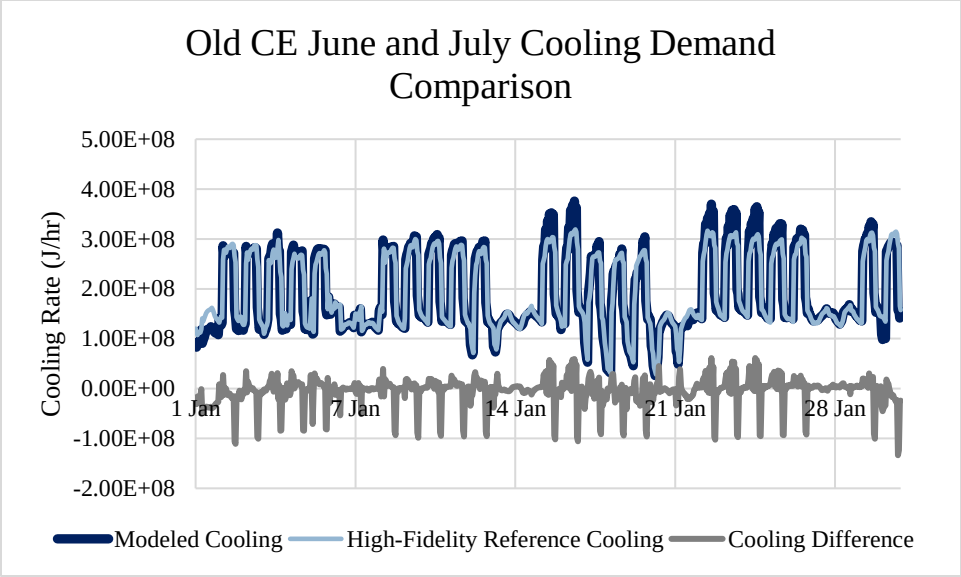

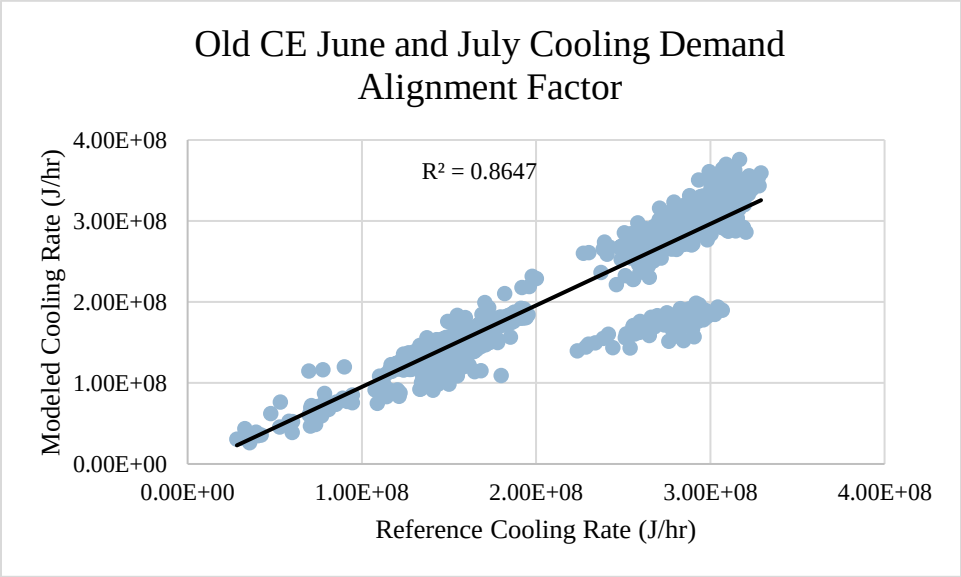

Figure 64: Old CE summer cooling load comparison and alignment factor

As with Whitehead heating demand in summer, Figure 65 demonstrates the inability of the SPBM to capture small, brief periods of demand as temperature setpoints change.

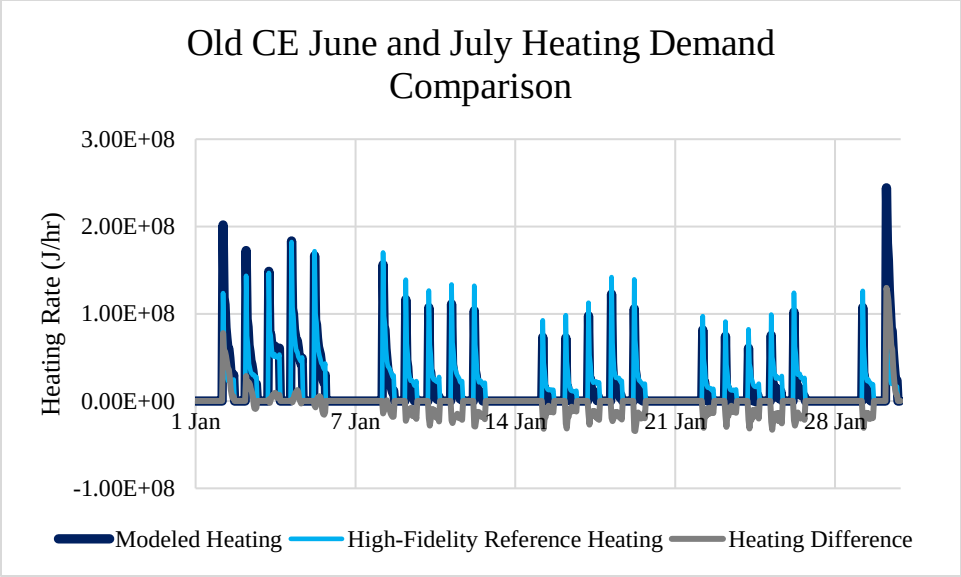

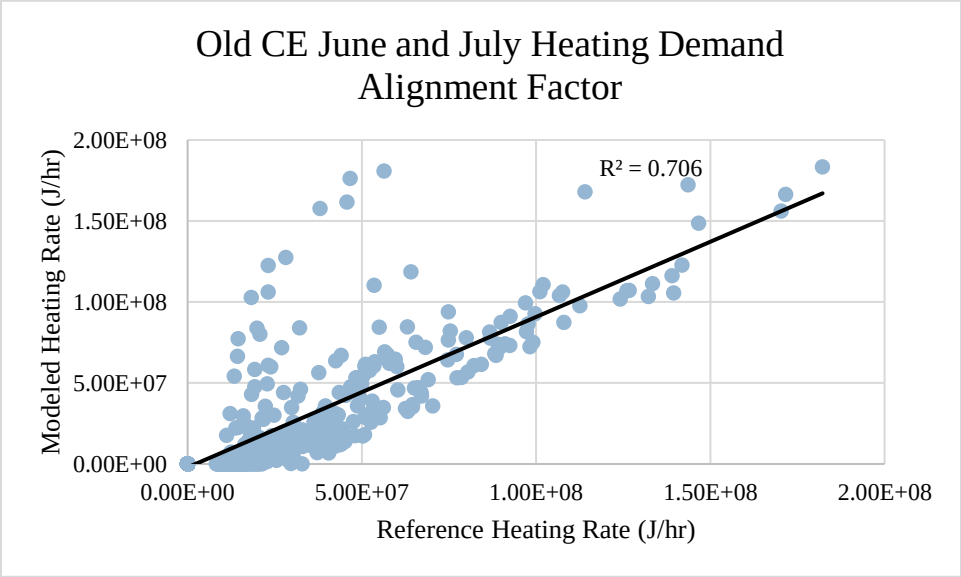

Figure 65: Old CE summer heating load comparison and alignment factor

Overall performance of the SPBM to capture building load profile for all weather and for significantly different buildings and loading conditions has been proven to be more than adequate. More importantly, the ability to be sensitive enough to building faults makes the SPBM sufficient for automatic building model calibration and fault detection.

6.2 Outdoor Air

Controlling the amount of outdoor air in a building is critical to occupant comfort and health, as well as minimizing energy consumption. Some of the more popular options for outdoor air control is a fixed minimum flow rate of outdoor air or a fixed outdoor air fraction of total supply air. The primary method of controlling outdoor air flow percentage is done with a system of dampers and fans ; however, building modeling programs tend to specify the amount or fraction of outdoor air explicitly. These two methods for controlling outdoor air in a building were implemented in the building model.

In general, most HVAC systems have a minimum flow rate that is higher than the minimum amount of outdoor air. Due to dampers not being precision instruments and errors that accumulate over time, determining the actual amount of outdoor air entering the system is difficult to pinpoint and a common point for a fault. However, by inspecting the heating, cooling, and electrical demand, it may be possible to determine if the amount of outdoor air being used by the building is within a reasonable level of control.

For practical purposes, a sample model was made in EnergyPlus. Initial tests of the outdoor air system showed consistent results comparable to those from EnergyPlus. For fault detection via parameter estimation, the envelope properties were adjusted while the air handling unit remained unchanged. Six variables were assigned as “unknown”, and a minimum finding technique was used to attempt to detect changes in envelope properties while finding no change in HVAC specifications. The six variables were: layer 1 thermal resistance, layer 1 thermal capacity, layer 2 thermal resistance, layer 2 thermal capacity, outdoor air fraction, and minimum outdoor air flow rate. The thermal resistance,

outdoor air fraction, and outdoor air flow rate were all within 10% error of the metered variable values. Thermal capacitance had a slightly higher percent error at about 25% but this is mostly due to the way thermal capacitance alters when thermal energy is transmitted rather than how much energy is transferred.

For testing the outdoor air system, multi-variable parameter estimation was not as successful. The proposed variables were outdoor air flow rate, additional air outdoor air percentage, level 1 minimum supply air flow rate, and level 2 minimum supply air flow rate. These variables are all coupled together, and lead to some cases in automatic minimum finding where the values would exceed bounds and cause an error. More sophisticated techniques were developed to add AHU specifications while removing conflicting variables.

One variable at a time resulted in near perfect (>99%) accuracy but is somewhat limited as changes elsewhere in the building may falsely alter parameter values through error minimization. However, Chapter 7 Automatic Fault Detection shows that an overall global minimum can be found through careful analysis and testing of error minimization. Additionally, the section shows that the SPBM can detect changes in error from minimal changes in outdoor air flow and differentiate between AHU outdoor air and infiltration.

With the more sophisticated multi-parameter estimation such as inclusion of CO2, the outdoor air fault detection methods were able to be more reliable. Understanding the outdoor air system and changes in energy consumption that accompany critical parameters is vital for successful fault detection.

6.3 Developmental Stages for Whitehead Parameter Estimation

Having established the fundamentals of SPBM development and modeling, this section will explore how the model was developed to accurately depict a complex building such as Whitehead. Due to the complexity and layout of the Whitehead building, and for diligent testing of the SPBM, it was decided to test parameter estimation in stages. As before, initial testing was conducted to see if a rectangular shape could represent curved surfaces, especially curved windows. Once the model was calibrated for the envelope, the interior zones were added to the detailed baseline to see how the loading on the building would change. Lastly, interior loads were added to see to what degree the SPBM can calibrate to a highly detailed baseline.

The exterior of Whitehead has full windows on the north with shaded windows on the east; the west and south faces have minimal windows as represented by Figure 66. Due to complex geometry and resulting solar load through the windows, it was theorized that perhaps the cooling or heating load would be substantially different with a four-sided rectangle due to how wind and solar loads interact with faces at varying angles. However, no significant difference in envelope loading due to shape was found during testing.

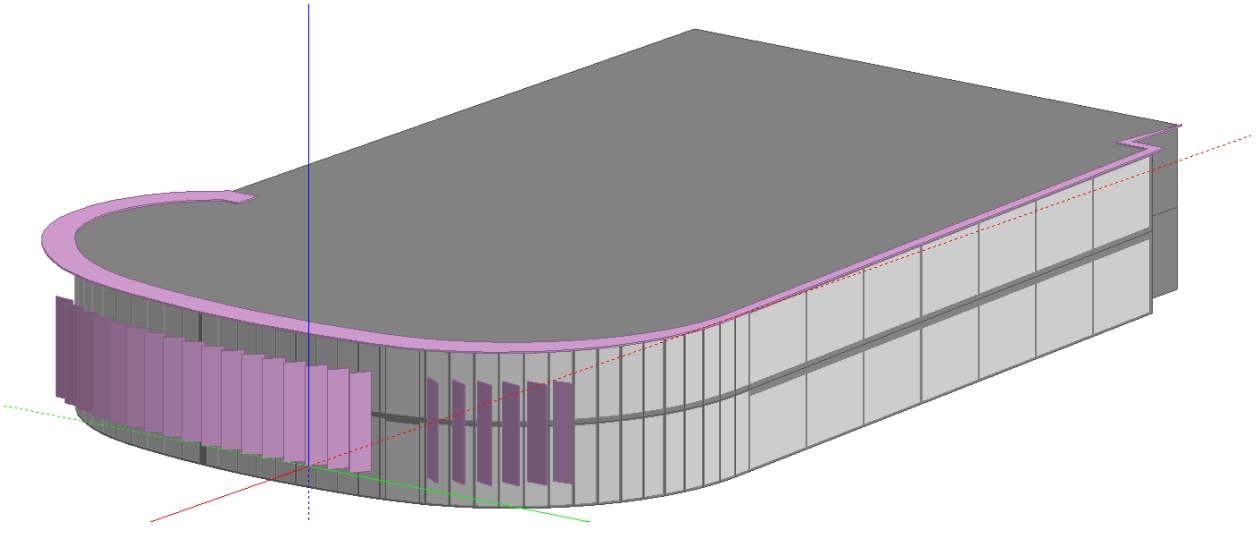

Figure 66: High-fidelity model render of Whitehead looking at the north windows

and shaded east windows

An unexpected difference in loads was initially found due to how the external convection heat transfer coefficient is calculated. The high-fidelity model uses an equation which employs a correction factor to account for differences in wind speed between the height of the surface and the height of the station where the wind speed reading was recorded. This value is not difficult to determine, but very important in generating accurate convection heat transfer coefficient values.

After accounting for the difference in surface heigh, the heating load was used to automatically calibrate the SPBM to the baseline. The heating load during January was chosen because the cooling load depends only on the air flow rate as increases in heating demand results in increased zone supply air temperature rather than increased air flow rate. During the heating season, air flow tends to be at the minimum air flow rate because heating occurs at the minimum air flow rate for the AHU design within this building. As such, without a cooling demand the cooling coil load is simply the minimum air flow rate and the difference in enthalpy between the return and the setpoint for air temperature after the cooling coil. Additionally, the heating season was chosen because there is typically a greater temperature difference between indoor air temperatures and the external air temperature which increases model sensitivity to conduction.

After giving the SPBM time to settle from the initial conditions, the match between the SPBM and the baseline is in excess of 95%. The below figures were generated by comparing the total heating load and total cooling load from the baseline, much like the heating and cooling load data would be gathered from a building's meter. Both the baseline and SPBM used a fraction of outdoor air, so the AHU portion of the SPBM is working as desired.

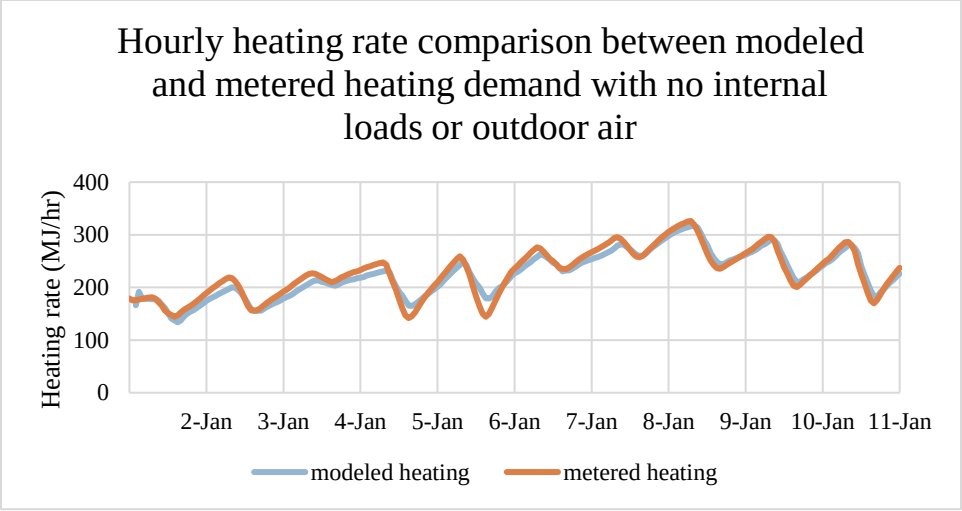

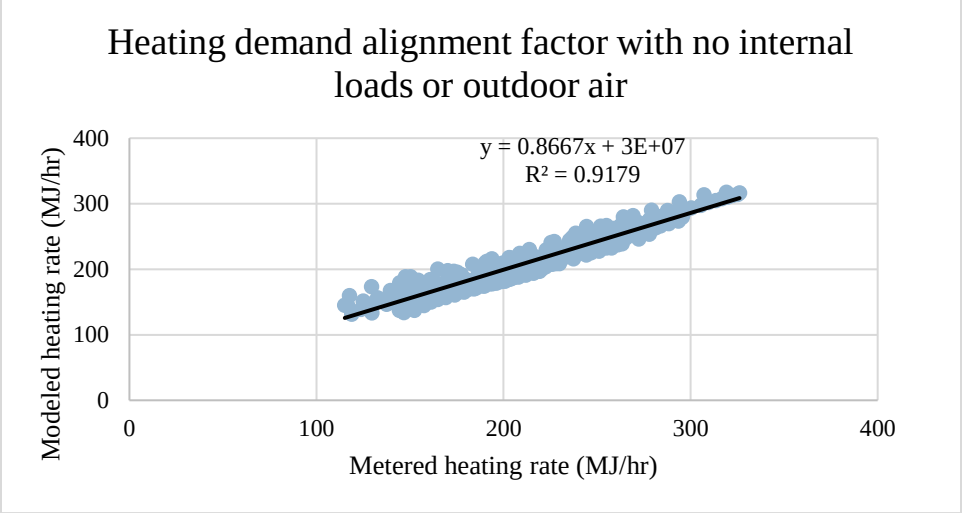

Figure 67: Hourly heating demand for Whitehead without internal loads or outdoor air time series (above) and alignment factor (below)

Accurate envelope representation was considered important in order to maintain a desirable level of predicted energy load validity for reasons already mentioned. The following sections examines how minimum error finding works and how such a process is useful both for calibration and for fault detection.

6.3.1 Minimization Finding

Having established the validity of the SPBM, the problem became one of data driven model calibration. The SPBM relies on parameter values to model input/output relations and does require calibration based on data to operate effectively – this chapter will briefly cover the process used for the SPBM calibration.

The initial test of the simplified system was one where the parameter values of an existing building are unknown, and a reasonably accurate model of an existing building is required. Due to the nature of the system, data driven error minimization was introduced to test how well the simulation would be able to converge when specifics of the building materials and interior loads were unknown. Sum squared error minimization was used to quantify error between modeled and metered heating and cooling demand. Fault identification and detection for the SPBM works by automatically adjusting parameter values until predicted loads result in a minimum sum squared error when compared to metered data. Then, a fault is considered detected either if parameter values or expected building loads fall outside a specified range.

While being able to identify real-world parameters may not be possible, having a rough value that makes sense in context helps in understanding if the SPBM is calibrating properly or if the building is behaving correctly. The most evident drawback to Nelder-Mead is that is loses effectiveness with more variables . Preliminary research has shown that around 10 parameters might be sufficient to calibrate the SPBM. These parameters include four unknowns for walls, two for fenestration, three for internal loads, and two or more for the HVAC system. If it turns out more parameters are needed, other search algorithms, such as genetic method, may be used that are slower but are more robust.

While other methods exist for minimizing error in calibration, a trusted method is sum squared error minimization. Comparing final total sum squared error or root mean square error is a proven method for building model tuning . Sum squared error allows for the use of any desired granularity in available data and the desired result. This is useful for people who may not have hourly performance data of their building. A daily, weekly, monthly, or annual data points can possibly be used with sum squared data error minimization. The more granular the data being evaluated, the more accurate the calibration may become; but the program should still be able to provide useful information about the building with equivalent clarity to the data being analyzed.

There are numerous minimization algorithms available but one of the most common and effective is Nelder-Mead simplex algorithm, even if the function is in multiple dimensions or contains multiple parameters. Nelder-Mead is a useful tool as a minimum finding program did not need to be constructed while providing a system that allows for a number of parameters to be minimized. Additional methods for minimum error finding were used, such as bootstrapping for comparing error sensitivity, but Nelder-Mead allows for the most simplistic automatic minimum finding tool that was available. The number of points of the simplex is n+1 where n is the number of dimensions being minimized. The algorithm works by analyzing a simplex and flipping the highest point of the simplex to the other side of the shape created by linking points of the simplex: The process of flipping the highest point is also referred to as a downhill method and is useful when gradients are not available. The algorithm can find the minimum by adjusting the distance of the changed point based on how the new point compares to the pre-flip point. If the new point (x_r) is closer to the solution than the old

point (x_h) the distance from the line connecting the points upon the flip occurred (x_s, x_l) then the distance of x_r increases to that of x_e. Conversely, the opposite happens and the distance of the flip decreases if x_r is further away from the solution than x_h but still closer than x_s or x_l.

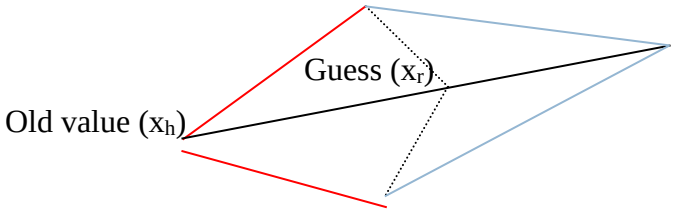

Figure 68: Visual representation of how Nelder-Mead algorithm flips the point that is furthest away from the minimum while increasing distance if change leads to a greater decrease in value

Updated new value as error decreased (x_h)

Nelder-Mead algorithms can calibrate the SPBM with reliability for limited number of variables. For equation-based modeling system initial guesses have a chance to impact parameter values if a local minimum is far enough away from the absolute minimum. However, realistic initial guesses resulted in finding correct values when testing parameter identification. If more variables are needed, or a more accurate calibration is desired, a genetic search method may be used; the downside to this search method is that it typically takes substantially longer to solve due to a significant increase in iterations. However, unlike Nelder-Mead algorithms, genetic algorithm results are not constrained to local minima and often produce results close to the global minimum error.

To test the automatic calibration, simple changes were made to the building model such as flipping building constructions, having different lighting and occupancy schedules, and outdoor air changes. Then, error minimization was conducted with the original model to see if the differences could be spotted. By using error minimization, the SPBM was able to calibrate to original data even with multiple unknown variables. Reliability and accuracy achieved during these preliminary investigations will be explored in later sections when evaluating complex parameter estimation.

6.3.2 Fault Detection Test Case Evaluation

A test of the SPBM to detect thermal bridging was conducted to evaluate the performance of fault detection in the simplest form. The south and west walls, along with the roof, were constructed with an external four inches of concrete followed by two inches of insulation (ASHRAE standard wall 32). To simulate thermal bridging the insulation was reduced by half to one inch. Initial surface properties resulted in a total resistance of 1.23[m^2-°C/W] and thermal capacitance of 194[kJ/m-°C] while the reduced insulation resulted in a total resistance of 0.62 [m^2-°C/W] and total thermal capacitance of 192[kJ/m-°C]. Testing was conducted from January 1 through July 31 to capture both a heating and cooling season. Figure 69 demonstrates how thermal bridging increases both heating and cooling demand and how primary demand changes over time. The objective was to see if the SPBM could automatically calibrate wall property parameters to match the desired heating and cooling output of the EnergyPlus models. Internal loads (plug, lighting, and occupancy) remained constant between the two models. Additionally, the HVAC heat and moisture system (including outdoor air mixing with return air) was modeled to get heating and cooling coil loads for comparison.

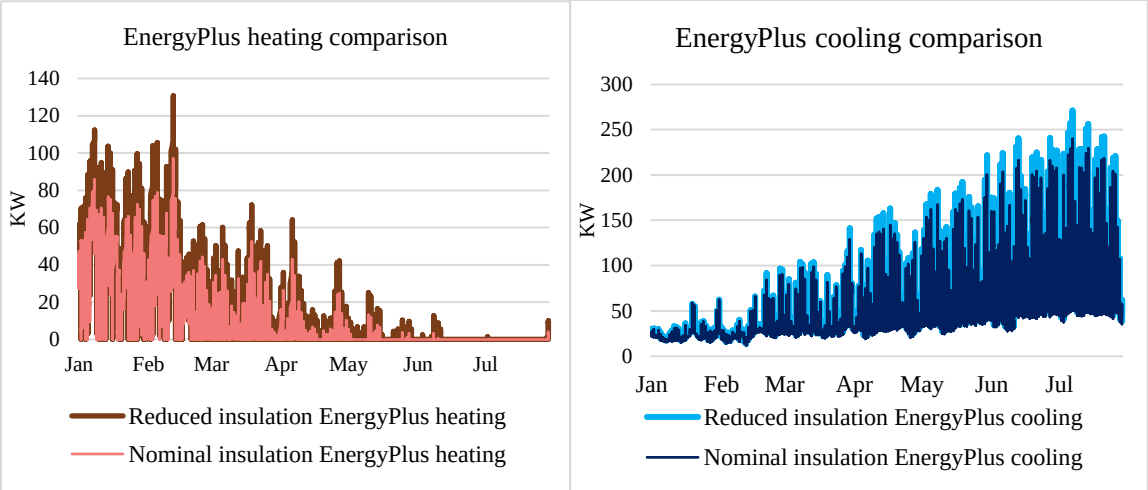

Figure 69: Nominal and reduced insulation heating and cooling loads. Reduced insulation results in both increased heating and cooling demand when compared to nominal insulation loads.

The SPBM was first calibrated to the nominal heating and cooling values. The parameters that were being calibrated were: layer 1 thermal resistance, layer 1 thermal capacitance, layer 2 thermal resistance, and layer 2 thermal capacitance. The exclusion of other parameters is due, in part, to demonstrate the sensitivity of the model and because different days will be gathered to test parameters independently. For example, a Saturday with high outdoor temperature and solar load would be ideal for testing envelope faults while a workday in winter could be used for outdoor air analysis.

Determining values for the SPBM was done by minimizing the sum squared error between heating and cooling loads. On the standard insulation, the SPBM had an overall resistance of 1.20[m^2-°C/W] and thermal capacitance of 147[kJ/m-°C] (2.9% error on insulation and 24% error on capacitance). Capacitance error is to be expected as that value is more of a way for the SPBM to delay heat entering a zone rather limiting the total amount of transmitted thermal energy. However, Figure 70 reveals how thermal capacitance has a much smaller impact on overall model demand accuracy when

compared to thermal resistance but influences timing of conducted load.

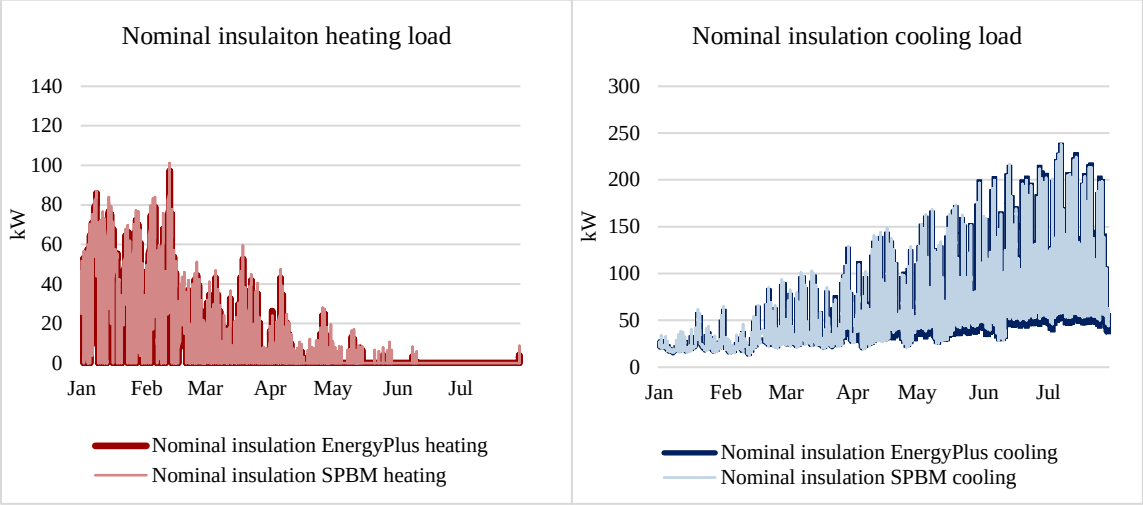

Figure 70: SPBM after automatic parameter calibration to nominal heating and cooling data. SPBM has great agreement with nominal EnergyPlus loads aside from slight underprediction of cooling demand lower bounds.

Optimization was again performed with the data from the reduced insulation EnergyPlus model. Resilience and accuracy of the SPBM thermal energy transport modeling can be tested by adjusting metered data to be from the same reference model but only with alternative envelope insulation. By only changing metered and modeled envelope parameters and arriving at a similar result for all test cases verified that thermal energy transport was adequately represented by the SPBM.

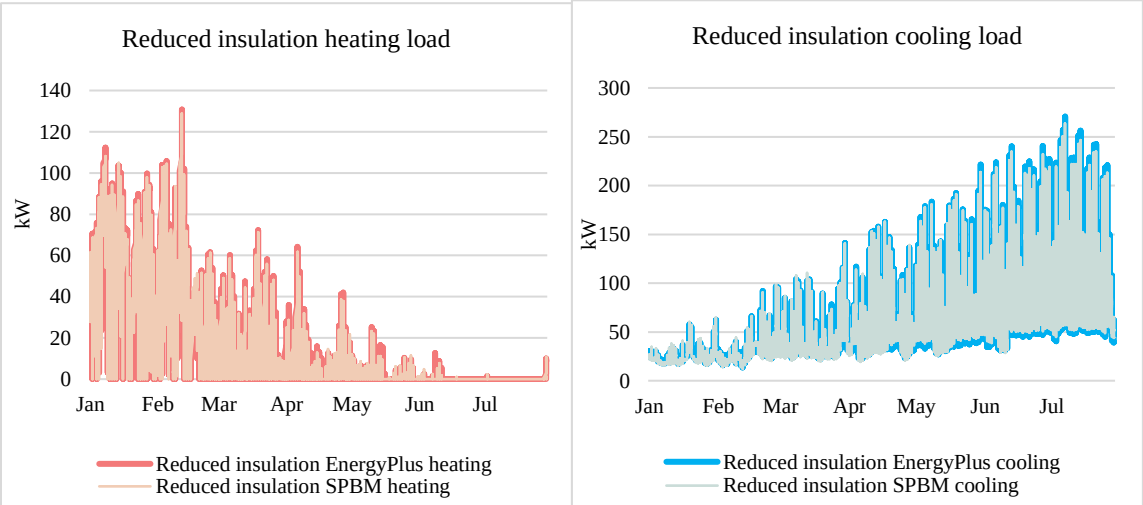

Figure 71: SPBM after automatic parameter calibration to simulated thermal bridging heating and cooling data

This preliminary test demonstrates the ability of the SPBM to detect faulty insulation successfully. Additional testing of the other important components of a physics-based building energy model will be tested in the following sections.

6.3.3. Advanced Whitehead SPBM Development

Now that it has been demonstrated that envelope thermal energy transfer can be reliably represented by the SPBM, the interior zones were added to see how subdividing zones would change load requirements. The primary concern is that many of the interior zones do not have exposure to the sun, so there may be a significant change in demand due to the high number of interior areas, a layout of level one can be seen in the figure below. Additionally, the solar load is primarily in the lobby area, so possibly having a smaller floor area to absorb the transmitted solar energy would have a dramatic effect on the overall load profile. However, SPBM results were all within a desired range.

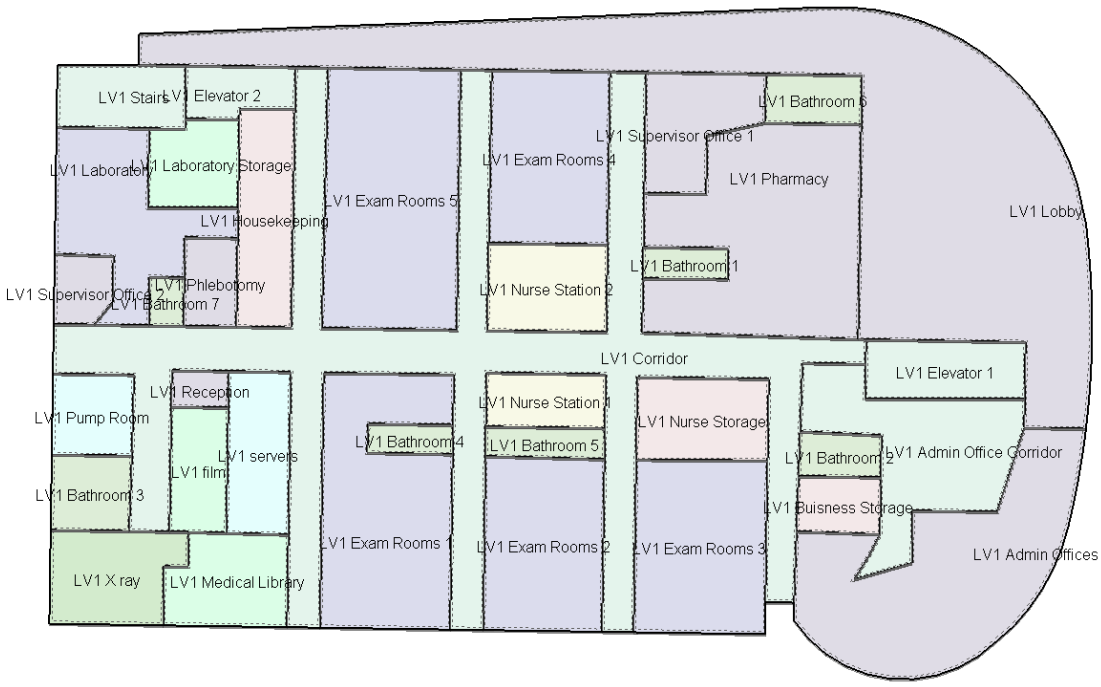

Figure 72: Layout of Whitehead LV1 zones for high-fidelity model

Representing multiple small zones with a single zone per floor induces changes to zone temperature dynamics. A zone will have less thermal capacitance when compared to the entirety of a building level and therefore will react different to loads. Discrete zones also allow for discrete zone temperature controls and air flow demand, meaning a single zone representation may be less sensitive to discrete loads. These concerns were addressed through analysis of zone temperature, AHU loading, and return air properties which resulted in results sufficient for fault detection and identification.

6.3.4 Internal Loads

Once the envelope has been shown to be easily automatically calibrated, the focus turned to interior loads. Automatic calibration for the interior loads was first tested with a more complicated method to see if the SPBM can specify loading per floor. For simplicity and ease of calibration, metered electrical data from the building will be fed

into the SPBM to determine occupancy and internal loads. Using metered electrical data will only require two variables for calibration: unoccupied hours HVAC electrical fraction, and occupied hours HVAC electrical fraction. As there is no submeter for lighting, plug, or HVAC loads, there is an average fraction of the electrical load that is used during unoccupied hours and a different average fraction for occupied hours. However, for initial testing there were four variables: level 1 unoccupied hours load, level 1 occupied hours load, level 2 unoccupied hours load, and level 2 occupied hours load. These variables were chosen to see what chance there was of being able to pinpoint level-specific use problems.

Lighting load inherently tends to be a more consistent power draw with a minimal load for weekends and a higher constant value for occupied hours. Lighting is sometimes automated with timers or motion sensors. While automating lighting systems have the potential to save energy, it is possible for sensors to fail and negate any potential energy savings. Unoccupied lighting is a fault that can present itself and may be difficult to detect due to the problem occurring when nobody is in the building to observe the fault. As such, being able to calibrate to lighting load is an important test for the SPBM.

Once lighting was able to be successfully calibrated, the logical progression would be to include equipment, or plug load. The same kind of calibration was conducted by attempting to specify an unoccupied and occupied load value. With the addition of plug load, there were zones in the baseline model that required cooling while other zones required heating. The SPBM was able to successfully calibrate to the interior loads while accounting for the heating and cooling demands of different zones.

Lastly, building electrical meter was used as an input for internal load. This reduced the number of variables to occupied hours electrical HVAC fraction, unoccupied hours electrical HVAC fraction, and level 1 power fraction. For each level, the fractional load reduces the number of variables by one. Additionally, using actual building electrical load leads to a more accurate plug, and by extension, occupancy schedule. The following figure shows the total interior load from both the high-fidelity model and the SPBM when the models use Whitehead's true electrical meter as inputs.

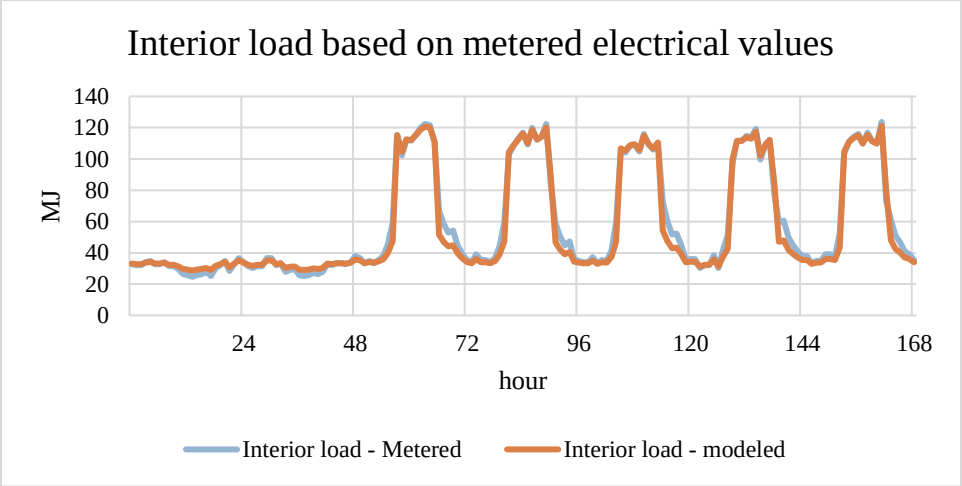

Figure 73: Hourly interior load from high-fidelity model and SPBM when using Whitehead's electrical meter for load input

Being able to use commonly available real-world metered data as inputs significantly reduces guesswork required during calibration. Unfortunately, not all inputs are as easily implemented. Determining the number of occupants in a building when no occupant counter is available requires estimation of both occupant number and activity level as discussed in the following section with favorable results.

6.3.5 Occupancy

Occupants are unique to interior loading as they produce both latent, sensible, and CO2 loads. Due to the latent and sensible load produced by occupants, it was discovered

that cooling load calibration was more reliable than heating load calibration. Using results from the previous envelope and internal sensible load calibrations, a calibration of occupancy count and occupancy level split was attempted.

Occupancy calibration was conducted during two weeks in March for the purpose of seeing how a less intense envelope load and higher humidity ratio would play into occupancy calibration. The values being calibrated were total building occupancy and occupancy level split (number of occupants on LV1 and LV2). Building occupancy for the high-fidelity model begins at 08:00 with 80 occupants and reaches a peak of 320 at 11:00 where an hour-long lunch break occurs; the peak of 320 occupants continues until 17:00 where the number of people dwindles to 0 at 24:00. For this test, the SPBM only has one value for occupancy and assumes the building is occupied when the electrical load is higher than the evening level, although an occupancy schedule similar to plug or lighting demand can easily be implemented. Calibration resulted in an occupied value of 300 people with a 50/50 split for level occupancy, similar to those from the high-fidelity model. While the baseline value averaged 225 during all occupied hours, a peak of 320 for five hours makes the calibration value more accurate. Below are figures for cooling load as well as return air humidity ratio and CO2 concentration to show that the SPBM is capable of accurately modeling humidity and contamination.

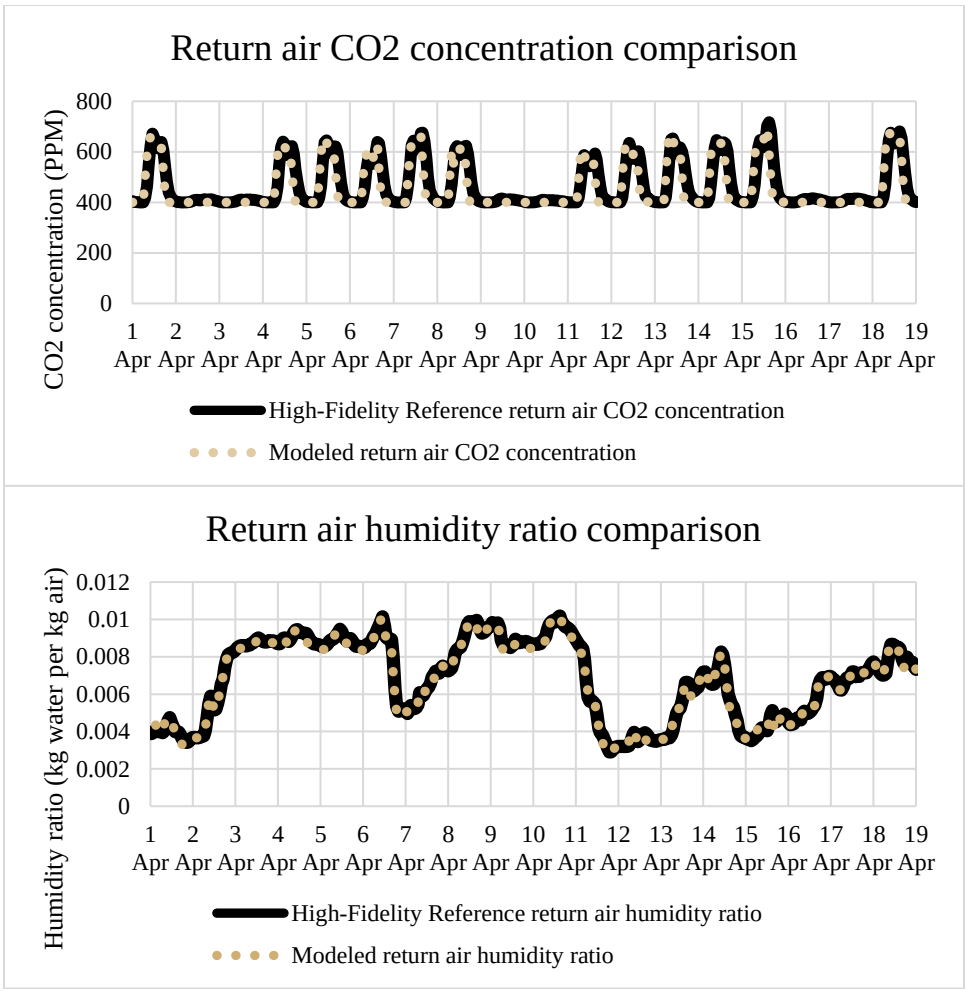

Figure 74: Whitehead SPBM occupancy test showing return air humidity and CO2 concentration

The preceding tests have all demonstrated the competency of the SPBM in regard to individual component parameter estimation. However, multiple parameters need to be calibrated to be sure that a model is in agreement with metered data. The next section reviews how multiple parameter calibration is implemented.

6.3.6 Combined Internal Load Testing

After demonstrating the success of individual component calibration, the SPBM was tested to see how it performed when attempting to calibrate multiple variables at the same time. Occupancy level and occupied electrical use was used as the first test to

determine what methods were best for distinguishing between purely sensible and loads with sensible and latent components.

Two weeks in March was used to calibrate internal loads. As stated above, March provides less external envelope loading on the structure due to the temperate climate environment. At first, considering cooling load alone did not lead to a high level of success, however, minimizing both heating and cooling load error proved to be a more fruitful venture. Being able to accurately match and detect the difference between occupants and plug load demonstrates the resolution of the SPBM.

With minimum finding, it is often a concern that the solution is not unique. Figure 75 helps to demonstrate how some bulk building values only have one minimum error associated with its value. Additionally, several minimum finding sessions were conducted, all with random initial values, and they converged on a similar value. Due to the complexity of the data fit, cooling rate and heating rate data was also provided by Figure 76 through Figure 77 for a visualization on the level of fit achieved by the SPBM.

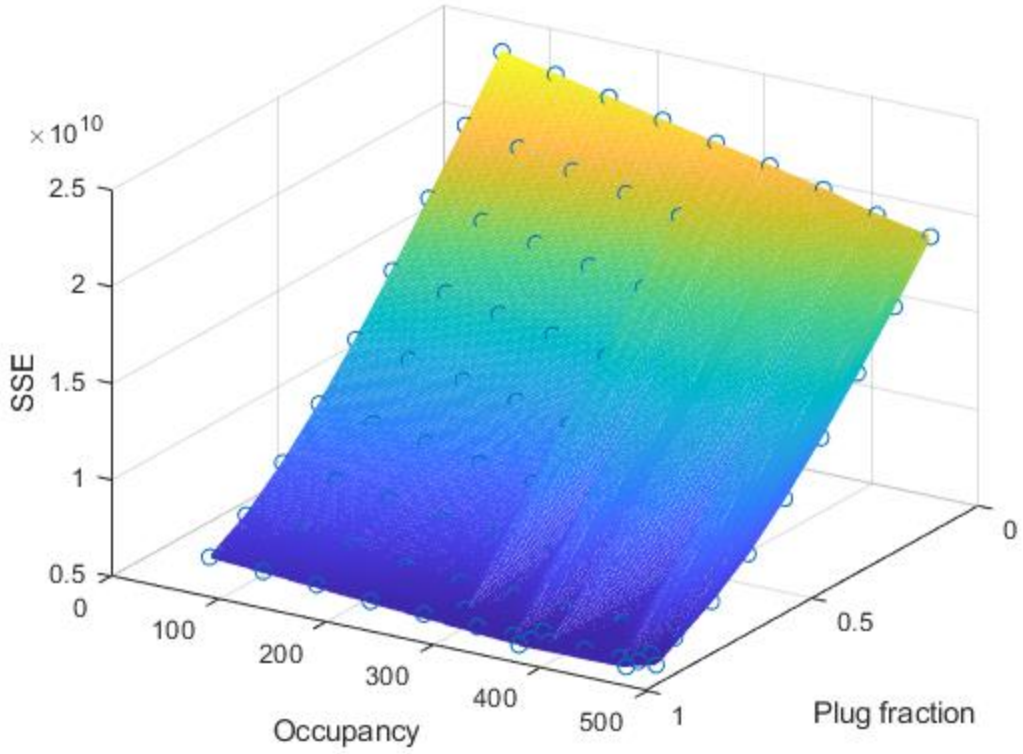

Figure 75: Plot showing relation between error (SSE), plug load occupied fraction, and occupancy level and how error reduces towards a unique solution at the expected parameter values

In addition to finding the minimum error associated with calibrating a group of parameters, it is also vital that the resulting heating and cooling demand are representative of metered demand. Cooling demand hourly results and alignment factor are plotted in Figure 76 and again show the slightly slower response of the SPBM but also the overall great agreement.

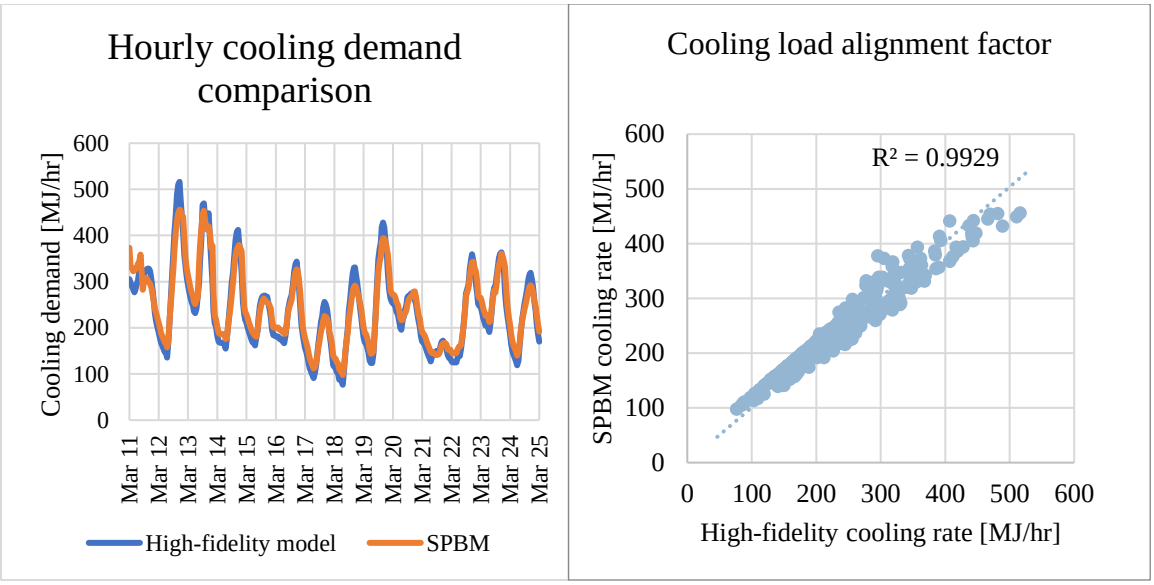

Figure 76: Comparison between high-fidelity model and SPBM cooling demand with time plot and alignment factor

Figure 77 shows how heating demand disappears during occupied hours when internal loads are sufficient for maintaining zone temperature. However, the heating demand alignment factor reveals more deviation than from the cooling load as sudden changes in demand are difficult to model with a single-zone system. However, later discussions on fault detection and identification results are unhindered by these small differentiation between predicted and metered energy consumption.

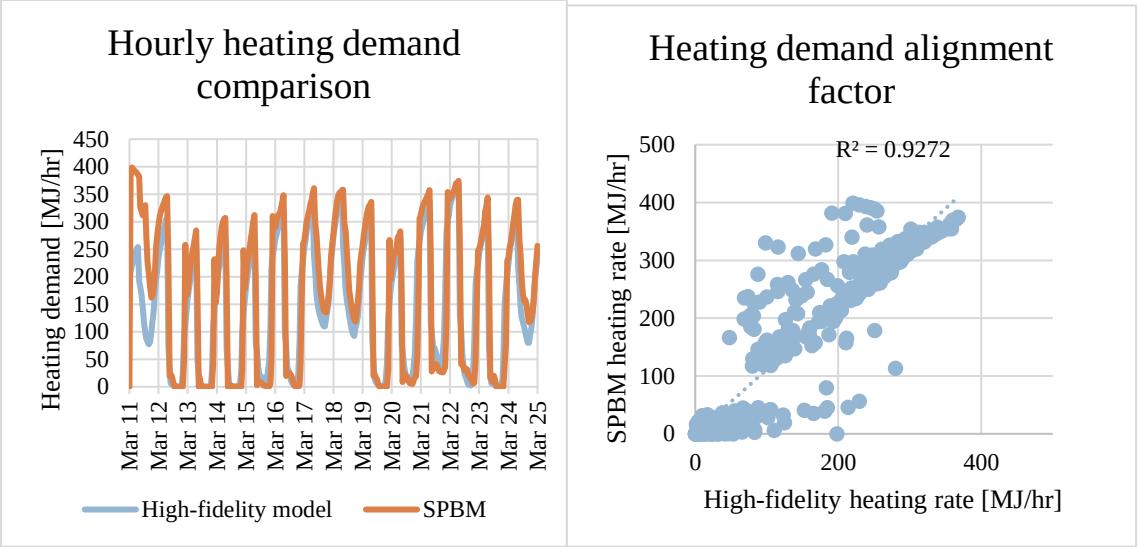

Figure 77: Comparison between high-fidelity model and SPBM heating demand with time plot and alignment factor. Alignment factor has some points far removed from 1:1 alignment, but those are points of sudden demand change as hourly load comparison demonstrates agreement.

Overall, this section has shown that the SPBM is able to automatically and simultaneously find the minimum error associated with multiple parameters. More in depth analysis of multiple parameter error minimization will be extensively detailed in the fault detection and identification sections.

6.3.7 Infiltration

The last variable for parameter estimation, and the one where no real-world value can easily be assessed, is air infiltration. Infiltration is often measured by determining the amount of air flow required to uniformly pressurize a building or by measuring trace gas and even after this measurement, model prediction was found to be at most 60% accurate . There are many different methods for accounting for infiltration in buildings, including, constant air change rate, velocity dependent, terrain and building dependent, and CFD models. However, many advanced infiltration modeling techniques, while potentially more accurate, require an abundance of difficulty to obtain data and are computationally

taxing . As keeping with the minimalist approach of the SPBM, a proportional wind speed-based infiltration simulation technique was used that is in accordance with DOE2, a proven and simple method.

While both infiltration and occupancy affect internal humidity, and subsequently, zone air enthalpy, infiltration has a direct correlation to wind speed. The coupling of infiltration to wind speed and occupants to electricity usage allows for a separation of these two parameters.

When testing infiltration calibration, there was originally a wide trough of similar infiltration values that resulted in a relatively low minimum, as seen in Figure 78. Seeing how infiltration values affect the sensitivity of the model, a wide range of values can be used for fault detection; meaning fault identification tests would only declare a suspected detected fault if infiltration parameter values were outside of an allowable range. By providing an acceptable width of possible parameter values for a high infiltration building fault, a reasonable deviation could be allowed considering how rapidly the error diverges. While the overall error minimization was successful, a wind speed-based error minimization approach was desired.

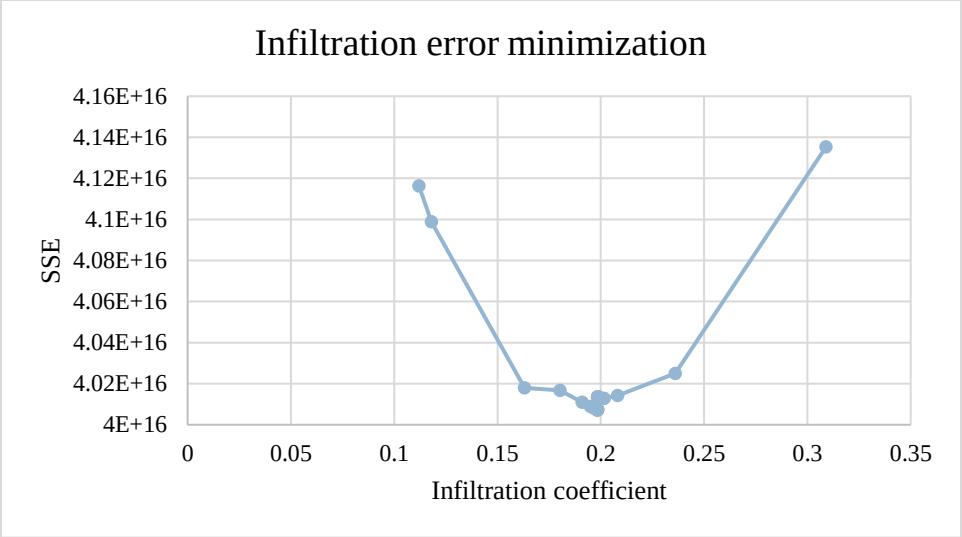

Figure 78: Infiltration parameter identification based on cooling load reveals significant convergence towards singular unique solution

Because infiltration is dependent on wind speed, error minimization was attempted over a longer period of time and where error was only added when wind speed was above a significant threshold. In addition to using heating, cooling, and wind data, a longer period of three months was used. The longer period was necessary to get a substantial set of time with high wind speed and to make sure outdoor air was cold enough to increase heating load and also hot enough to increase cooling load. Figure 79 shows the dramatic improvement in parameter estimation from simply using cooling load over a two-week period. It is important to note that both Figure 78 and Figure 79 converge to the same unique infiltration parameter value; meaning that changes in error are being affected by changes in predicted load due to infiltration while increasing fault sensitivity. In addition to a more defined minimum error value, the percent change in error went from 3% from minimum to maximum error to 700% difference in minimum to maximum. While this weather and time dependent error minimization will be discussed more in the following section on fault detection, a brief introduction was included here to demonstrate the promise of this kind of approach.

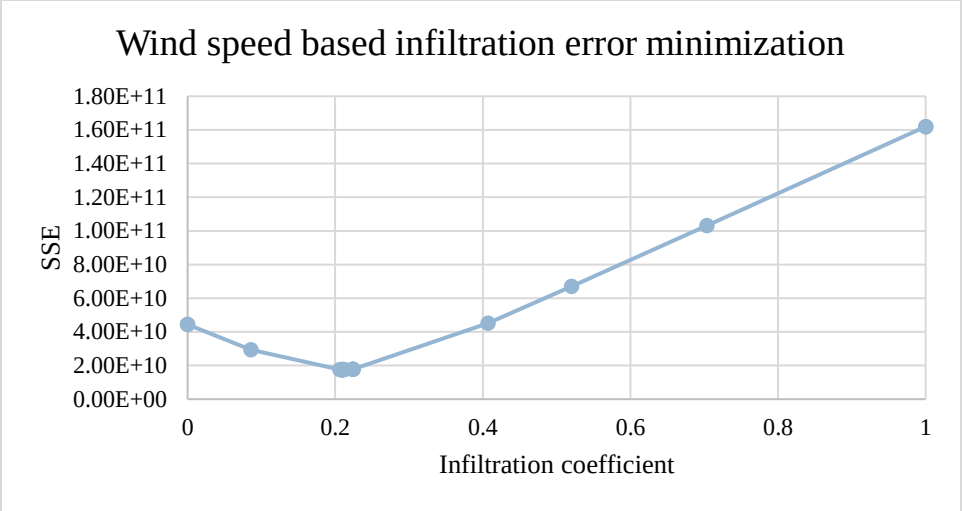

Figure 79: Infiltration parameter estimation based on both heating and cooling error when wind speed is used to limit error collection to periods of significant wind speed displays even more significant convergence to a solution.

Infiltration demonstrates how different approaches to parameter estimation can result in increased model sensitivity while maintaining accuracy.

6.3.8 Occupancy and Infiltration

Automatic calibration on infiltration and occupancy at the same time was tested due to the similar increase in humidity that comes from both sources. When just calibrating on the cooling load in March, a false solution was found, even though the solution was the global minimum, as shown in Figure 80. While the cooling load was similar to the baseline data, the heating load had significant deviation; sometimes over 100% error. As such, automatic calibration of both data sets using combined heating and cooling error as well as calibrating infiltration alone only when wind speeds were significant was attempted but did not lead to a change of a minimum error at 500 occupants (200 more than baseline model). With the success of high wind speed-based calibration of infiltration, a single optimization of occupancy when wind speed was low was attempted.

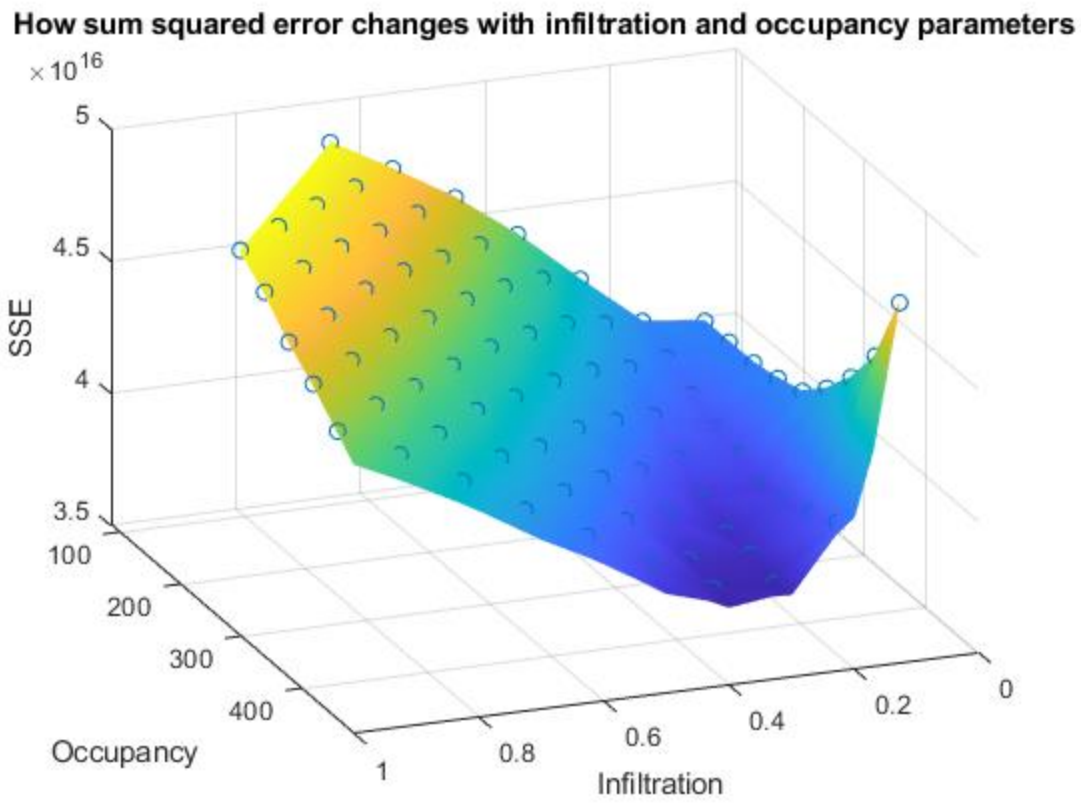

Figure 80: Sum squared error of cooling load based on infiltration and occupancy level displayed in 3D with low point aligning with unique solution

Limiting error minimization of occupancy to periods of low wind would limit the infiltration component of altered zone humidity. However, this was not sufficient to reliably detect occupancy values within a satisfactory error percentage. Additional limiting factors were added, such as using cooler months to decrease indoor humidity and only searching for error during occupied hours. Both of these factors lead to a much more distinct error minimum for parameter estimation as shown in Figure 81.

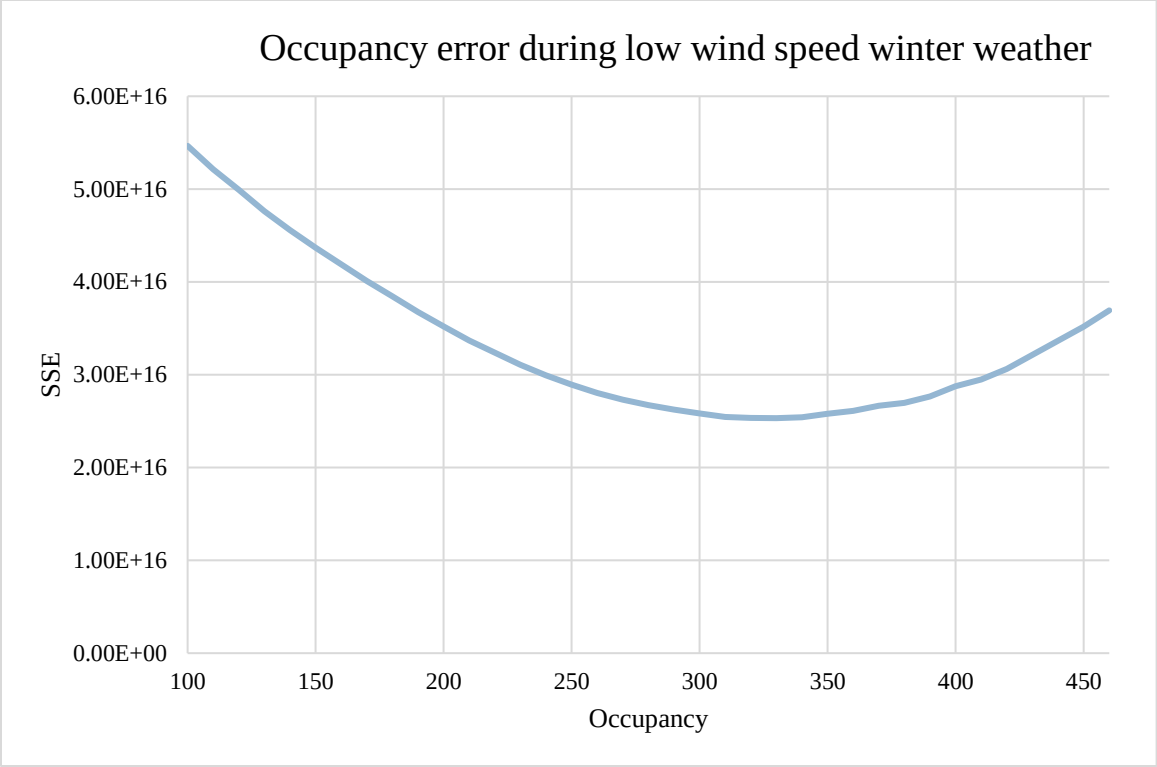

Figure 81: Occupancy parameter estimation with both increased air flow based on return air temperature and normal operation

Evaluating occupancy with infiltration shows that the importance of specifying conditions for error minimization. While this test shows that multiple low-sensitivity parameters are able to be calibrated, the sensitivity of each parameter must be high enough to produce a noticeable change in heating or cooling demand.

6.3.9 CO2 Occupancy Estimation

Using CO2 levels for estimating occupancy levels have been shown to be broadly accurate . With the dramatic potential for energy savings with CO2-based demand control ventilation, potentially up to 45% in savings, it is not difficult to imagine that CO2 sensors will become more prevalent in future buildings and renovations . As such,

exploring the effectiveness of CO2-based occupancy estimation provides several benefits while not hampering the SPBM or requiring excessive metering from buildings.

As with internal loads, the building is assumed to be either occupied or unoccupied when modeling CO2 generation with the SPBM. However, the number of people within the building follows a more natural progression throughout the day, is based on UK NCM, and can be seen in Figure 82. Using an occupancy profile that is designed to replicate typical use could increase accuracy while not impacting simulation time.

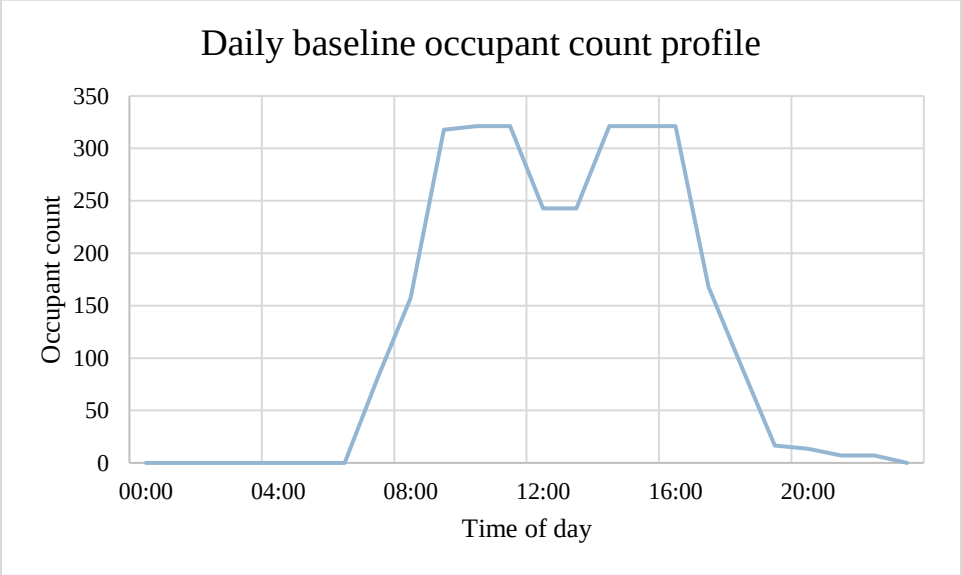

Figure 82: hourly occupant count profile used by EnergyPlus

By using return air CO2 levels, occupant level was estimated to the same level as using low wind speed cooling load, but the percent difference between maximum and minimum error went from 110% for cooling load-based error to 320% for return air CO2-based error. Figure 83 clearly demonstrates how using CO2 for error minimization directly correlates with occupancy. Given the cheap cost of instillation along with a

potential for significant reduction in energy costs, modeling CO2 and using it for parameter estimation and fault detection is an obvious choice.

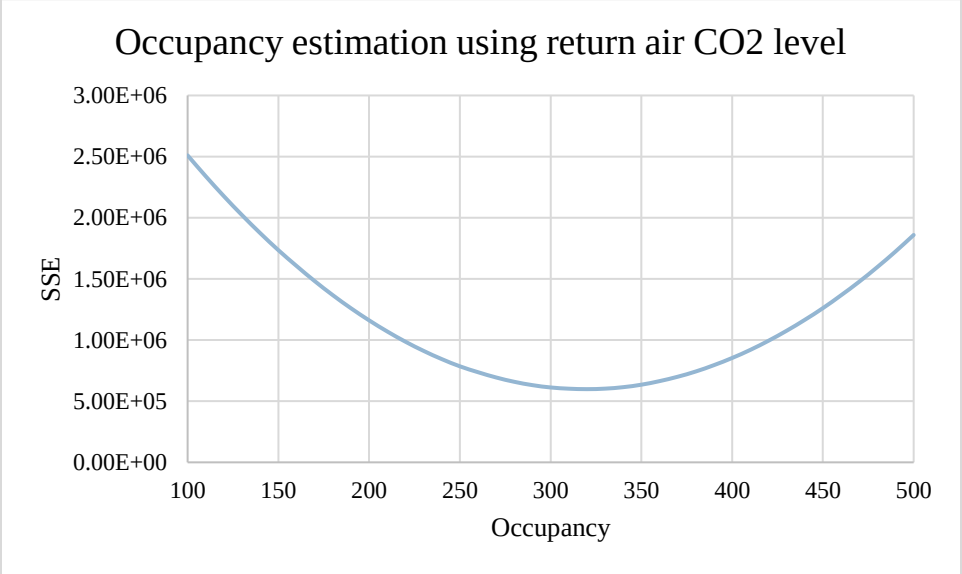

Figure 83: return air CO2 based occupancy estimation demonstrates how multiple meters can be used for calibration of same parameter

CO2 for occupancy parameter estimation showcases how adaptability and interconnectivity of model components can be utilized to cross-calibrate this SPBM. Because occupants produce latent heat, sensible heat, and CO2, all three loads can be used for error minimization and calibration.

6.4 Unexpected Results of Building Calibration

A test was done to see how zones with different zone temperature setpoints behave. Some zones that are not normally occupied, such as storage, were given a wider zone temperature deadband. While these kinds of low use zones are often unconditioned, it was tested to see how these zones would affect heating and cooling demand if conditioned. While the SPBM generated similar heating and cooling demand profiles when compared to metered data, they were often not able to exactly match the metered

performance. That being said, the model was still able to calibrate performance to this kind of zone layout. More advanced buildings and interior setpoint configuration could lend itself well to postdoc work or further research opportunities.

Having a mix of zone loads and temperatures naturally results in different heating and cooling demands throughout the building. Varying air flow demands across zones was attempted to be solved via an increase in air flow rate depending on how much higher the return air temperature was above the minimum air flow rate. While not perfect, and somewhat dependent on an arbitrary factor, it does appear to solve the issue of accounting for increased air flow in parts of the building with increased demand.

6.5 Conclusion

With the impressive abilities shown by the SPBM with parameter estimation it is important to remember that parameter estimation is not attempting to find the exact value that perfectly replicates the real world; but rather is using parameter estimation to detect possible changes. For instance, if the occupancy value changed from 300 to 100, that may not directly correlate with an exact drop in occupancy of exactly 200 people, but rather that a building change occurred that resulted in a change of 200 people with parameter estimation. The change of estimated parameter values is what can be used for fault detection.

CHAPTER 7. AUTOMATIC FAULT DETECTION

Implementation of automatic fault detection is not a trivial task; for rigor, variable sensitivity and percent confidence will be assessed to determine the quality of the SPBM and NN for determining faults. Faults for observation are 1) Excessive infiltration, 2) Unnecessary/excessive preheat, 3) Malfunctioning occupancy sensors and, 4) Malfunctioning outdoor air control system. The above system faults were chosen due to their high associated energy cost, likelihood of occurring, prevalence in NREL's list of common energy faults, experience detecting these faults using alternative methods, or potential impact on occupant health .

To determine what (if any) fault is occurring, parameter values were adjusted and the corresponding change in error was analyzed. By observing how error values change in relation to parameter values, it is possible to arrive at a conclusive minimum error value. The minimum error value is then used as justification for detecting that fault. For neural networks, fault detection and classification are handled with time series neural networks and decision trees. Time series neural networks are unable to classify a fault but have the advantage of not needing data of faulty operation. Decision trees can both detect and identify a fault but require information of all building states (faulty and normal operation) in order to classify data.

7.1 Automatic Fault Detection and Classification for One Degree of Freedom Tests

Evaluating the sensitivity and percent confidence of the variables that are being evaluated for fault detection can aid in the fault detection process. There is no perfect tool

for evaluating model performance, even deep neural networks can display high (greater than 70% confidence) for the wrong image when only a pixel is changed . Regardless, some quantitative value for parameter estimation and fault detection is necessary. For the purpose of this thesis, variable sensitivity and overall evaluation of error with estimated variables are provided and a fault will be considered “identified” when error values are at a minimum. This decision was made because practical results were considered sufficient and due to complex computer science quantitative data evaluation is beyond the scope of a mechanical engineering topic.

A multi-pronged approach was used when analyzing the potential fault in relation to model performance and detection First, individual faults were evaluated to determine if the SPBM was sensitive enough to estimate a parameter value associated with each fault. One at a time, four fault conditions were evaluated by adjusting parameter values for the four potential faults to see if a unique global minimum error exists for all faulty states. Multiple simultaneous faults were tested by altering the four fault parameter values in search of a global minimum where both fault parameter values aligned with test values. The described approach allows for a step-by-step verification of model and testing results.

7.1.1 Excessive Infiltration

Infiltration is a building fault that does not have an associated system component such as fan speed or a setpoint. Infiltration is typically modeled through estimation of cracks which also depend on wind direction and speed, or a set number of air changes per hour . The SPBM approaches infiltration with an air change rate that is dependent on wind speed to mimic the approach used by DOE2. As such, deviations in load are

expected to strongly correlate with wind speed and the difference between indoor and outdoor air temperature. With one zone per floor, a wind speed dependence does not affect different locations in the building separately like it would in the baseline model.

Testing occurred by increasing the infiltration coefficient in the baseline high-fidelity model and exporting the heating, cooling, and building electrical use information. Only using the updated metered information, the SPBM used that information to first automatically calibrate to the new infiltration coefficient using the wind speed-based sum squared error minimization method as discussed in 6.3.7 Infiltration. Results as displayed in Figure 85 and Figure 86 show the automatic calibration of the SPBM; cooling information is not displayed as it is a flat line (constant cooling).

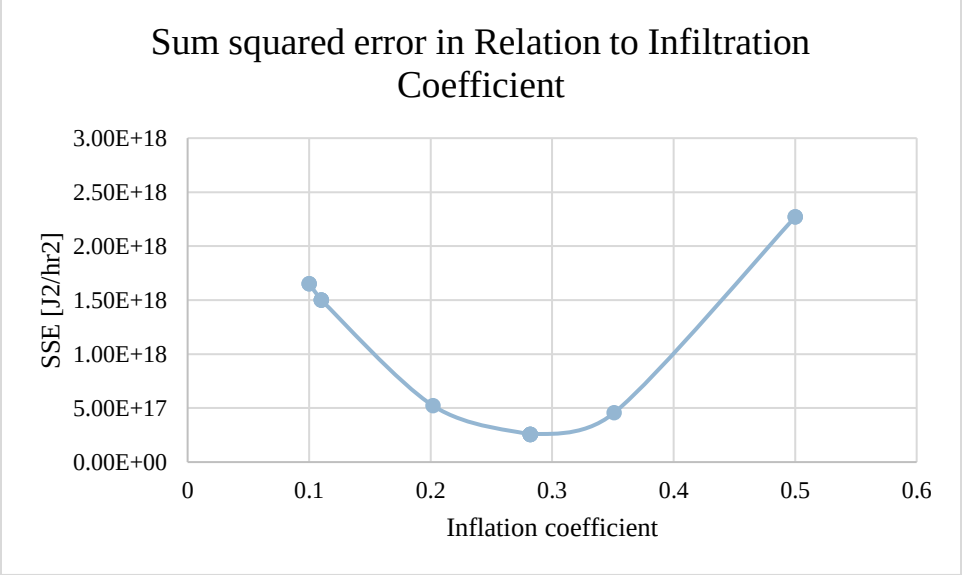

Figure 84: Error minimization results for 1DOF excessive infiltration, fit converges towards same value while demonstrating significant error reduction

Heating and cooling results from infiltration fault identification in Figure 85 and Figure 86 showcase how adaptable the SPBM is to data outside nominal calibration settings.

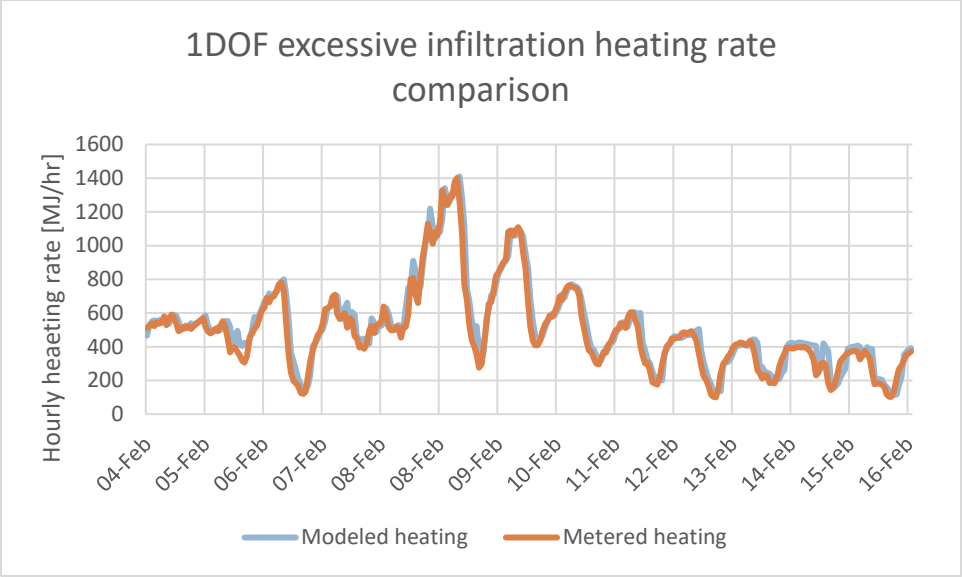

Figure 85: hourly heating rate of SPBM and metered data with excessive infiltration fault occurring, Modeled results follow metered demand almost exactly

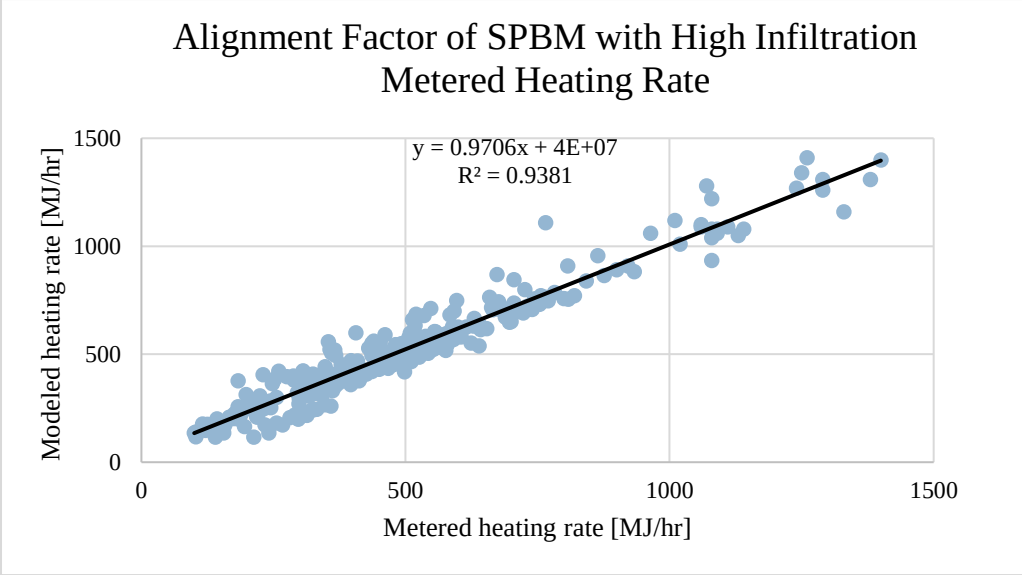

Figure 86: Alignment factor of SPBM and metered heating rate with high infiltration, again demonstrating the high degree of agreement between modeled and metered loads

One degree of freedom minimization is useful as a quick check of model integrity, but more rigorous tests were performed. Electrical use, minimum air flow, and infiltration were set to unknown to determine model parameter convergence. The above parameters are often unknown when calibrating a building and provide an ample test for quick model

sensitivity which will be further tested with multiple degree of freedom fits and fault pattern analysis.

For three degrees of freedom analysis, infiltration, electrical use, and minimum air flow rate were fit and then a sensitivity analysis was performed. Due to influence of guess values, the calibrated parameter values for a non-malfunctioning building were entered as a starting point. As with the 1DOF method, error was only recorded when wind speed was above a specified threshold and, therefore, would have noticeable impact on the load of the building. Estimation of all three parameters was successful with a highly-accurate model being adjusted and parameter values adjusted accordingly, as demonstrated in Figure 87, Figure 88, and Table 3.

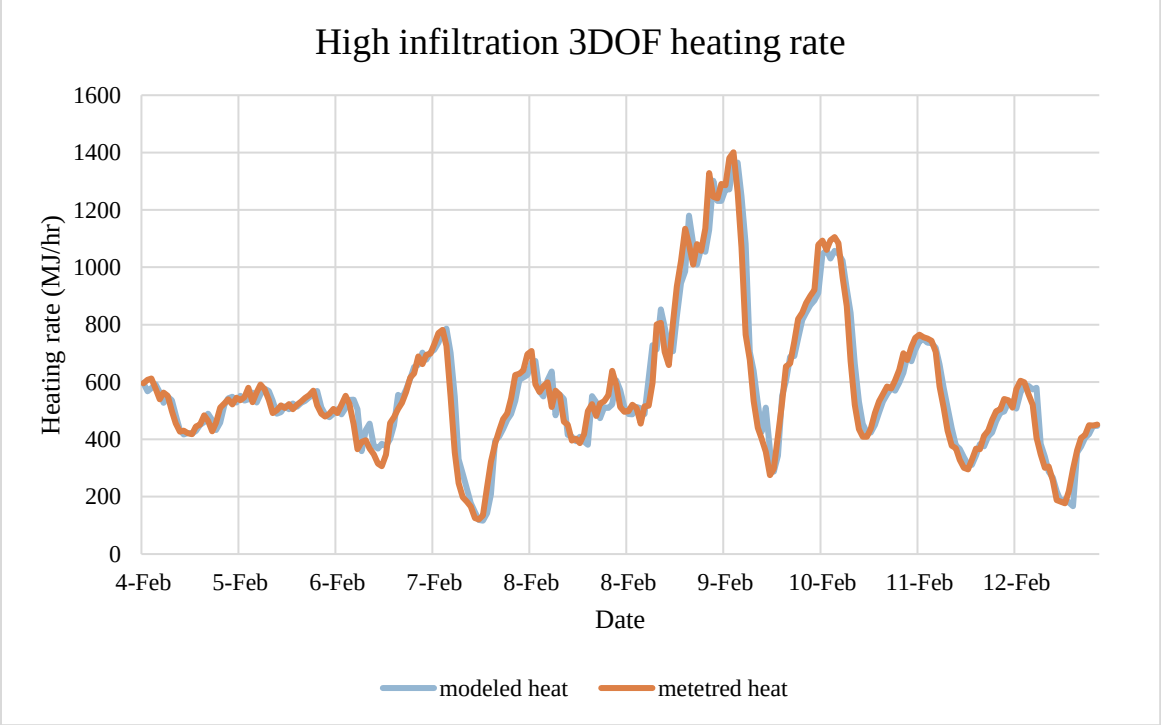

Figure 87: hourly heating rate of SPBM and metered data with high infiltration fault while also automatically calibrating minimum air flow rate and peak electrical fraction

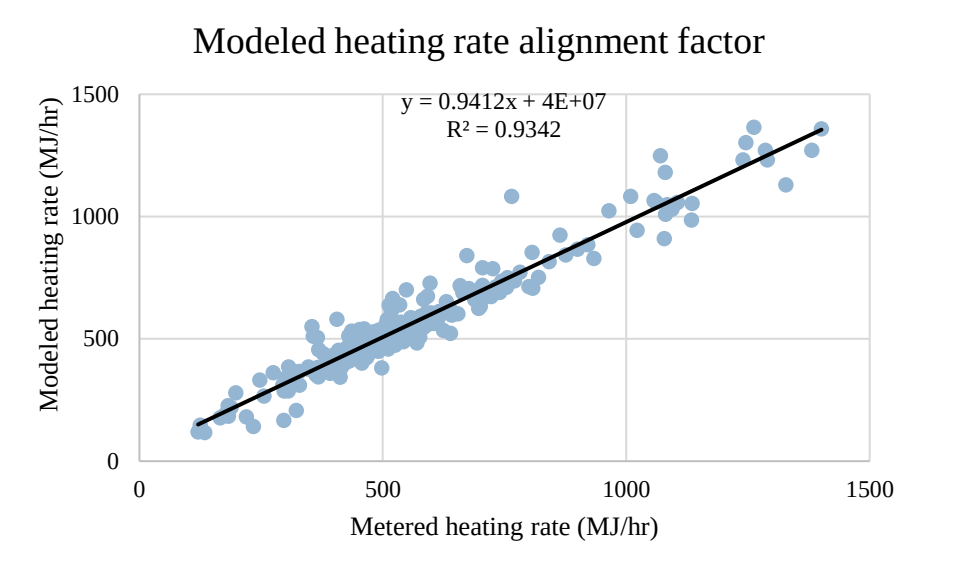

Figure 88: Alignment factor of SPBM and metered heating rate with high infiltration

Table 3 displays results for a sensitivity test in relation to both total load (δQ/δvar) and sum squared error (δSSE/δvar) with respect to each variable. Sensitivity analysis revealed that while infiltration has a relatively small impact on total building load, the SPBM is most sensitive to infiltration when compared to the other tested variables.

Table 3: Results of 3DOF infiltration fault automatic parameter estimation

	$\delta Q/\delta var$	$\delta SSE/\delta var$
INFILTRATION	1.59E+11	-4.31E+17
MINIMUM AIR FLOW RATE	4.98E+09	3.28E+16
PEAK ELECTRICAL FRACTION	-6.96E+09	-5.82E+16

Results from infiltration fault testing reveal both excellent model accuracy and high error sensitivity to infiltration. Confidence and accuracy displayed for infiltration

was expected from an understanding of how a physics-based model reacts to different parameters which was discussed in earlier sections.

7.1.2 Excessive Preheat

Excessive preheat is described in this paper as the use of an unnecessarily high preheat temperature setpoint as a quick and dirty solution to an underlying HVAC design problem. Namely, poorly designed mixed air inlet or cooling coil air inlet temperature sensor. Typically, a high preheat value is set by an operator so that air temperature sensors which are located before the cooling coil do not read a temperature below 7°C and have the AHU system trigger an emergency stop to prevent coil freeze. Therefore, a technician will manually override the preheat coil temperature from 13°C to 27°C; while this prevents false AHU shutdowns, it creates an immense amount of energy waste that is often forgotten once outside temperatures increase beyond the freeze warning threshold. Additionally, this sort of fault can also occur due to a leaking preheat valve.

A one degree of freedom minimization was tested first just to determine the accuracy of parameter estimation in relation to the overall change of the preheat temperature setpoint. The SPBM was able to get within half a degree of the setpoint which is more than adequate for fault detection. Results of the 1DOF fit are shown in Figure 89 through Figure 91 and display almost no error when compared to results for just five degrees divergence from actual settings. Additionally, the uncertainty of the result is well below a noticeable threshold of control (0.1°C).

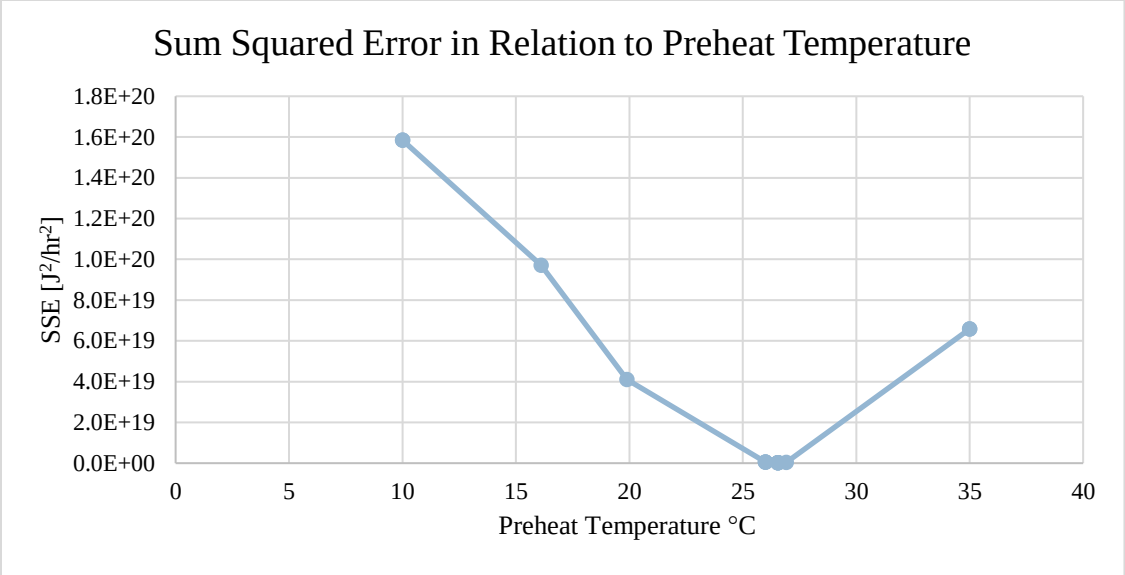

Figure 89: Error minimization results for 1DOF excessive preheat fit converges towards same value while demonstrating significant error reduction

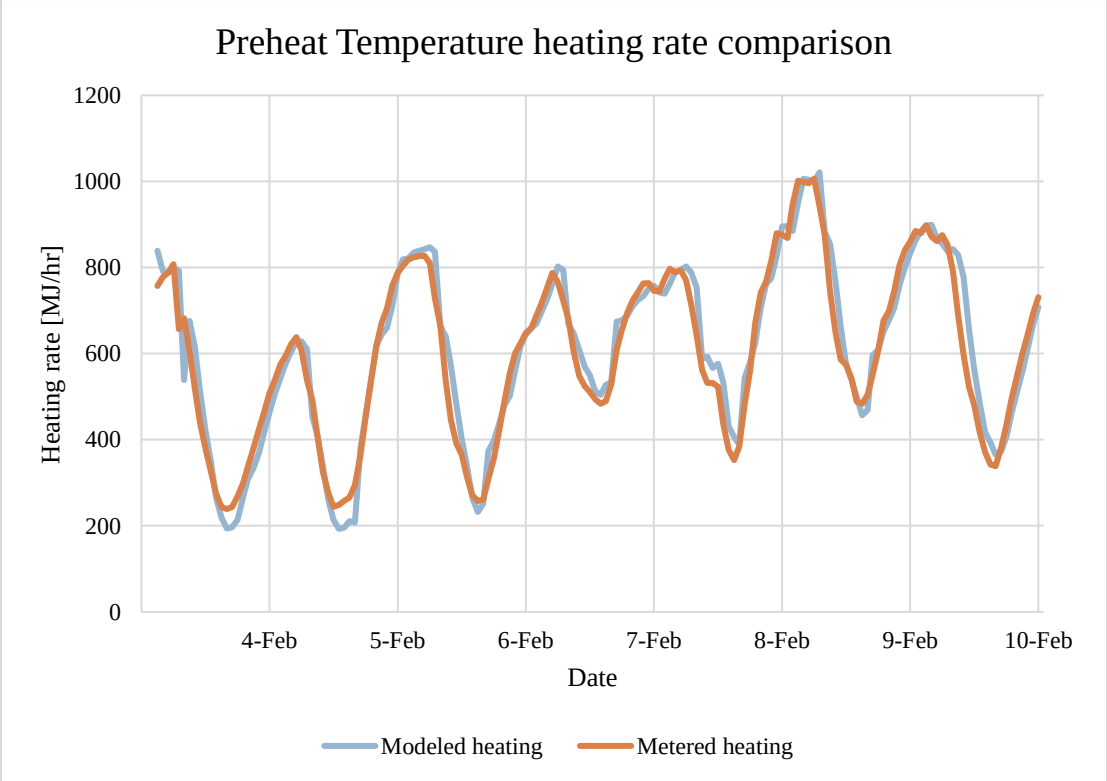

Figure 90: 1DOF excessive preheat hourly heating rate of SPBM and metered data with high infiltration fault

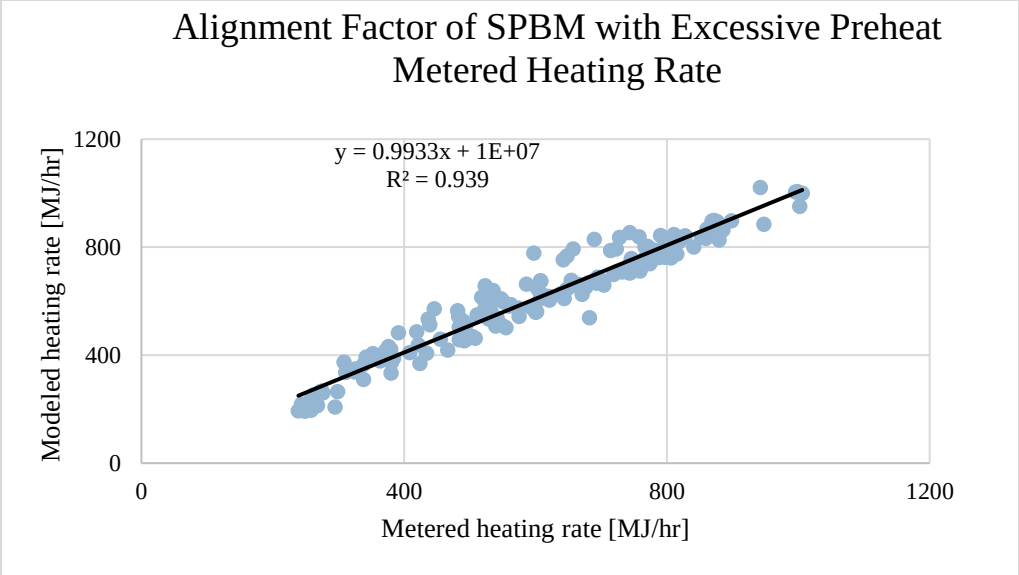

Figure 91:1DOF excessive preheat Alignment factor of SPBM and metered heating rate

As with the 1 and 3DOF model analysis of infiltration, excessive preheat had a similarly high level of convergence. As demonstrated in Figure 92, Figure 93, and Table 4, the SPBM was able to accurately replicate the fault state and associated parameter values.

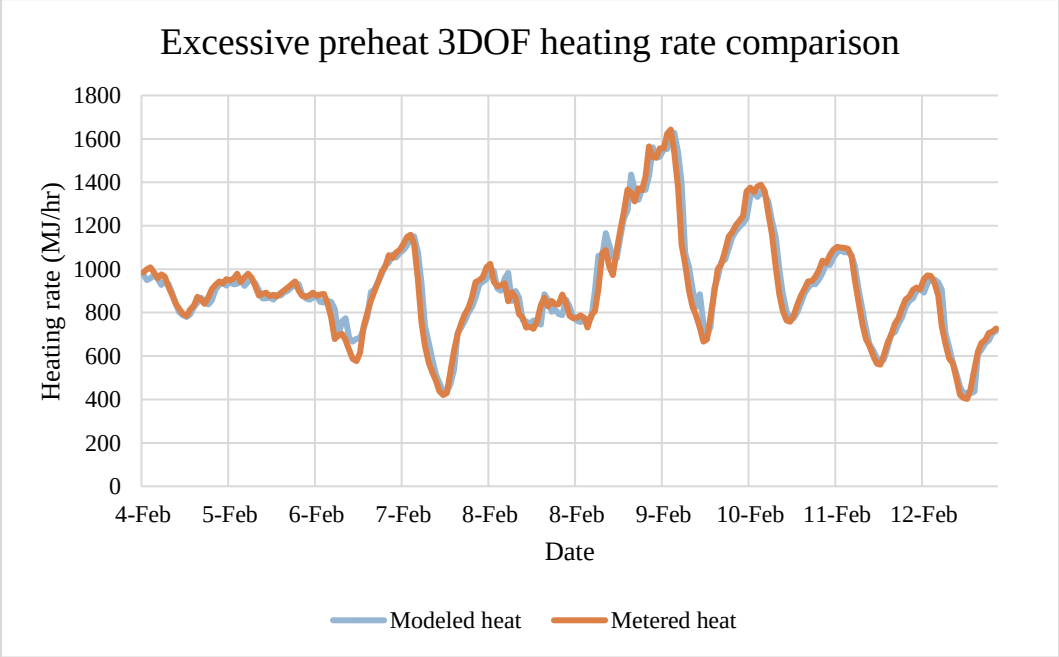

Figure 92: 3DOF analysis of excessive preheat fault detection while also automatically calibrating minimum air flow rate and peak electrical fraction

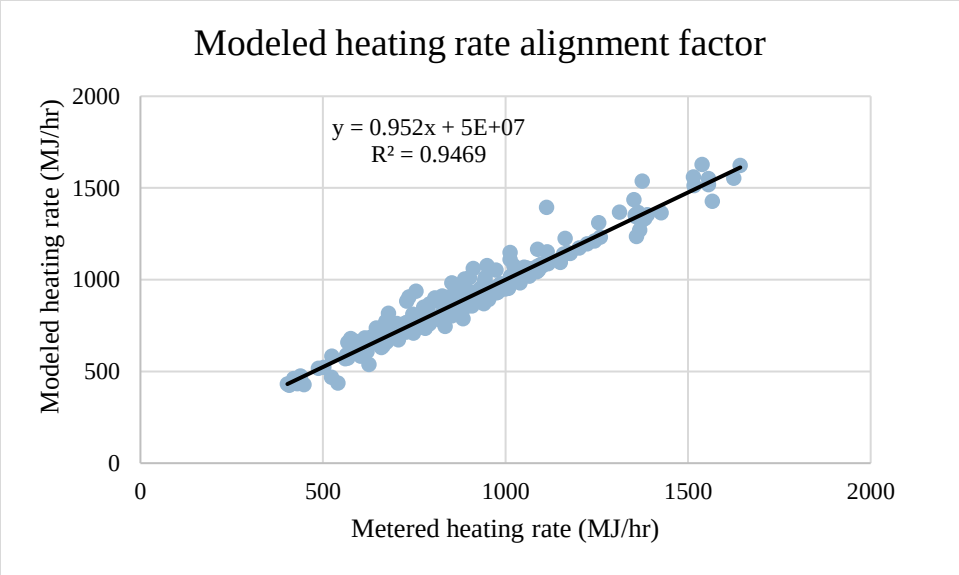

Figure 93: 3DOF alignment factor of hourly heating rate when testing excessive preheat fault detection displays high degree of SPBM accuracy despite no model calibration aside from preheat temperature being performed at such an extreme deviation from nominal operation

Table 4: Results of various variables tested for excessive preheat fault detection

	$\delta Q/\delta var$	UA	Uvar	$\delta SSE/\delta var$
Preheat temperature	1.16E+10	1.70E+17	6.22E-04	1.09E+17
Minimum air flow rate	1.72E+10	1.70E+17	4.19E-04	1.78E+17
Peak electrical fraction	-1.37E+10	1.70E+17	-5.27E-04	-1.21E+17

So far, the SPBM has been able to replicate the level of parameter estimation demonstrated in earlier calibration tests. The level of alignment is also noteworthy as a high alignment factor as well as visual trend inspection demonstrates the capabilities of a simplified physics-based model for fault detection.

7.1.3 Malfunctioning Occupancy Sensors

Unlike previous tests, calibration of Whitehead revealed that the building does not

enter temperature setback. Therefore, the baseline high-fidelity model needs to be adjusted away from the real building fit in order to establish a working version of the fault to compare against. Therefore, instead of using the high-fidelity model to generate faulty data, it was used to generate heating and cooling demands that are representative of how Whitehead should operate.

From analyzing multiple building performance characteristics, it was discovered that temperature setback is often noticeable with high heating demand spikes when the temperature setpoint changes early in the morning and the AHU needs to warm zones. A heating demand spike occurs because setback temperature and occupied temperature differ by typically 4 or 5 °C. Additionally, failure to enter unoccupied setback would cause both heating and cooling demand to elevate during unoccupied periods when compared to a functioning system.

While results for the 1DOF fit are similar to other fits with regards to uniqueness with error minimization, there was a slight decrease in model alignment when compared to other fault results. However, this difference in performance is more than likely due to the lower air flow rate brought about by the auto sizing in EnergyPlus requiring less heating energy at night which can be seen in the lower heating rates in Figure 95 and Figure 96 (minimum air flow was made constant for all faults when evaluating 4DOF and NN FD). Regardless, minimum finding was still successful as the error behaved predictably, as shown in Figure 94. Given the additional complexity and more aggressive changes in heating demand fault detection and identification was successful.

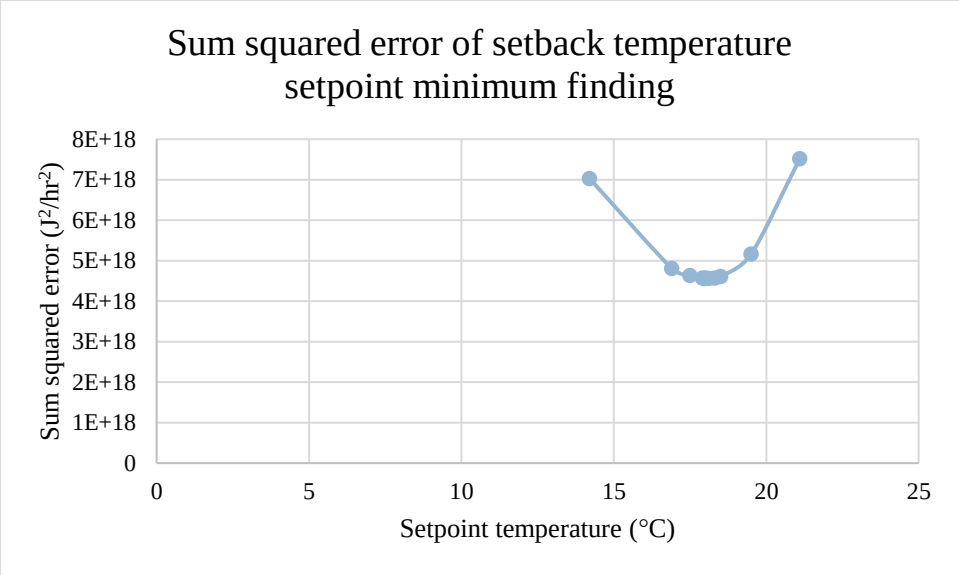

Figure 94: Error minimization results for 1DOF malfunctioning occupancy sensor fit

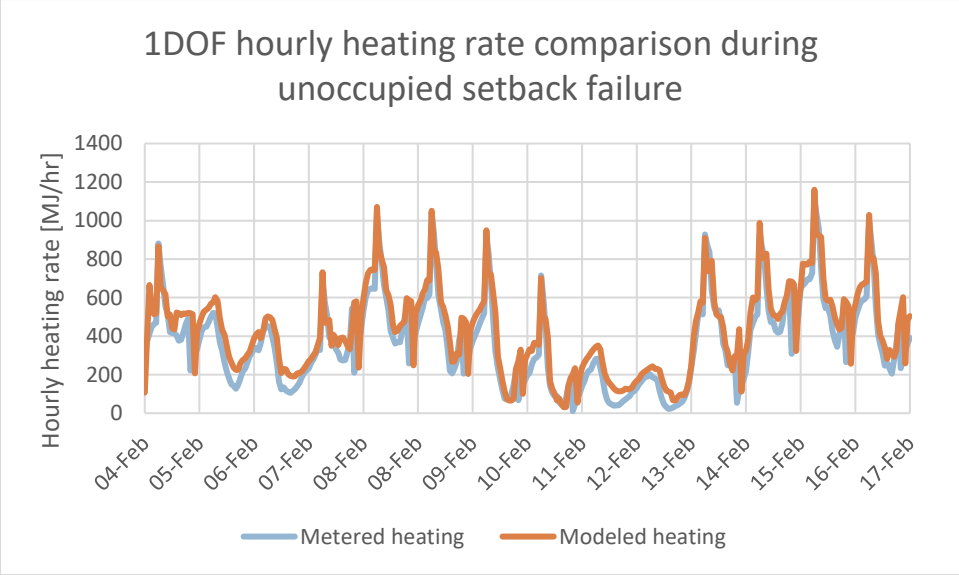

Figure 95: 1DOF excessive preheat hourly heating rate of SPBM and metered data with malfunctioning occupancy fault, although SPBM does demonstrate some overprediction

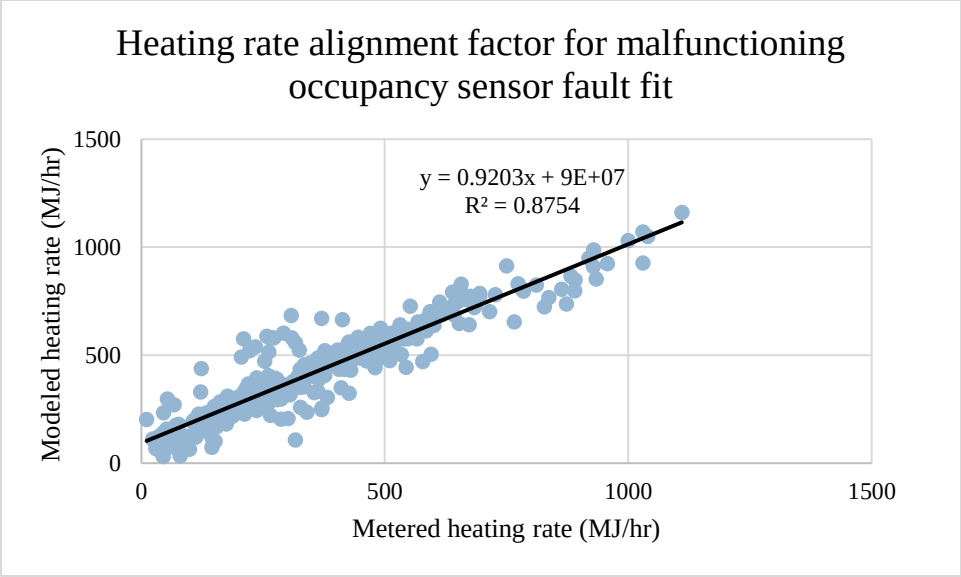

Figure 96:1DOF malfunctioning occupancy sensor fault fit alignment factor of SPBM and metered heating rate

While the results of determining the evening temperature setpoint were successful, a more realistic test would simply be between if unoccupied value ever switched from off '0' to on '1'. As such, this will be the base of future 4DOF tests between all the faults being examined. Additionally, to keep the tests consistent, all four faults were run with the same 3DOF additional parameters: peak electrical load fraction and minimum air flow. However, unoccupied temperature setback occurs in between peak loading. As such, this particular test was still able to achieve high alignment and minimal parameter error of 5% for the temperature setback (17.1°C instead of 18°C) as demonstrated in Table 5.

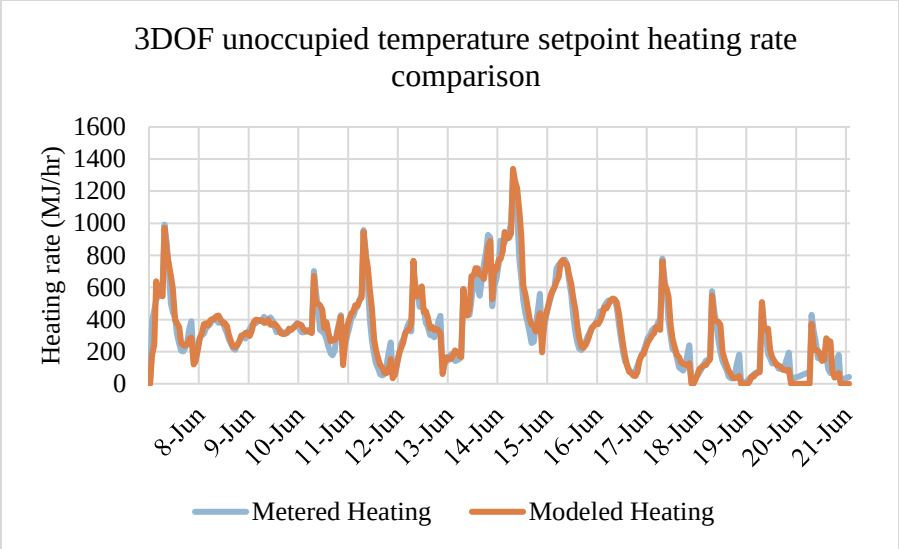

Figure 97: 3DOF excessive preheat hourly heating rate of SPBM and metered data with malfunctioning occupancy fault

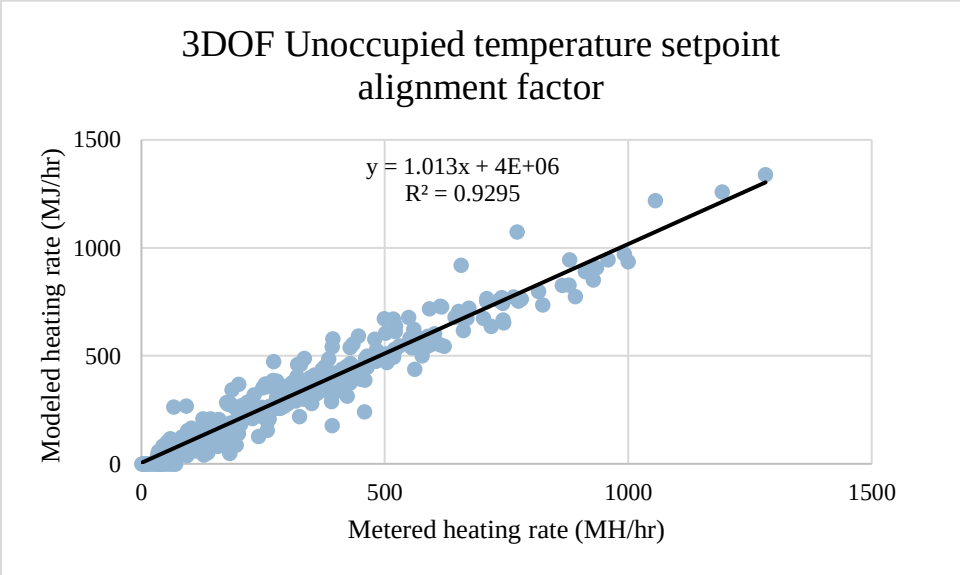

Figure 98:3DOF malfunctioning occupancy sensor fault fit alignment factor of SPBM and metered heating rate

Table 5: Results of various variables tested for not entering temperature setback fault detection

	$\delta Q/\delta var$	Uvar	$\delta SSE/\delta var$
Outdoor air flow rate	5.47E+09	0.000608	1.79E+17
Minimum air flow rate	-1.4E+10	0.000243	1.87E+16
Peak electrical fraction	3.97E+09	0.000837	6.81E+16

For actual fault detection between the proposed faults, a more rigorous set of parameters can be used to determine if evening temperature setback is occurring as well as adding evening lighting load to simulate the problems that arise from malfunctioning occupancy sensors resulting in a false positive occupancy.

7.1.4 Malfunctioning Outdoor Air Damper

Lastly, outdoor air flow rate control can either fault high or low. Too much outdoor air is delivered, which while improving occupant comfort, would increase energy consumption. Likewise, too little outdoor air can lead to poor indoor air quality either through excessive CO2 or other contaminants that can negatively affect occupant comfort and performance .

As a malfunctioning outdoor air damper has two fault states, a test for excess outdoor air was conducted first with a follow-up of too little outdoor air. Outdoor air has an immediate alteration on the AHU load as well as altering CO2 and humidity levels. Unlike infiltration, which is linked closely with air speed, outdoor air dampers have a constant change on mixed air properties arriving at heating and cooling coils in the AHU. If CO2 metering is added to heating and cooling load metering, the ability to detect outdoor air dampers increases in reliability.

Initial 1DOF fault testing revealed a strong relation between outdoor air flow rate and severity of fault. Figure 99 shows nearly an order of magnitude increase in SSE when compared to the true air flow rate.

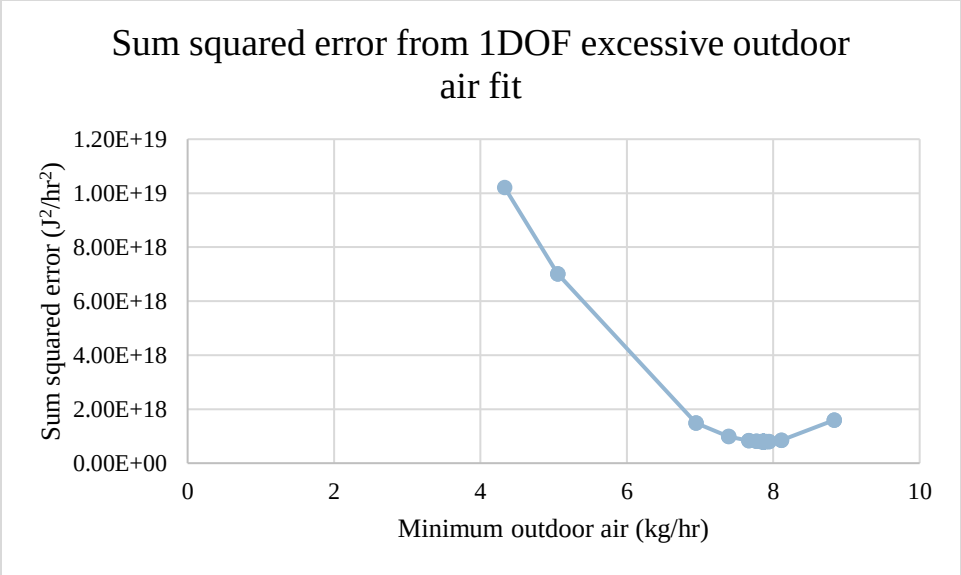

Figure 99: Error minimization results for 1DOF excessive outdoor air fit. While not as extended on the upper bound as other fault detection tests, the maximum air flow value evaluated represents the physical limitation of the Whitehead AHU.

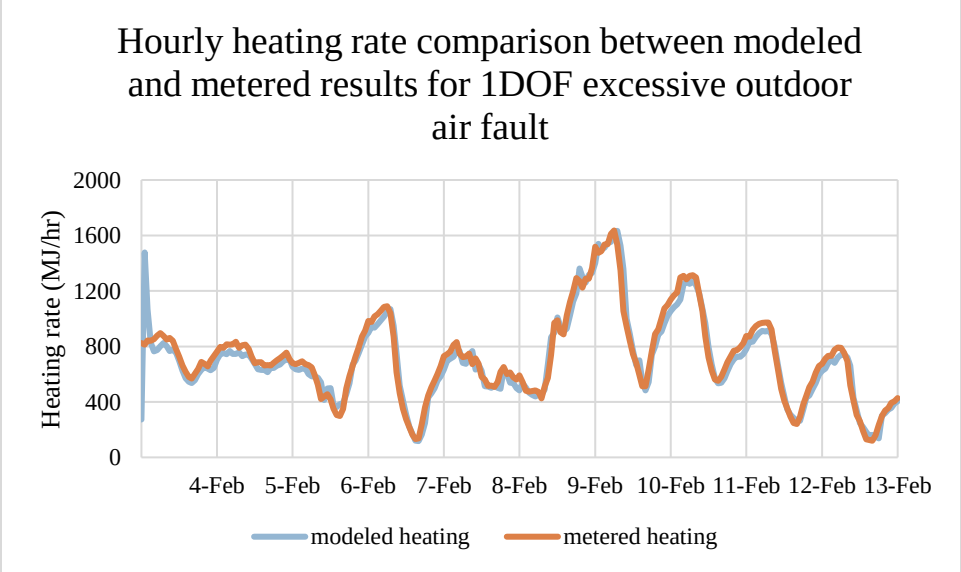

Figure 100: 1DOF excessive preheat hourly heating rate of SPBM and metered data with excessive outdoor air fault

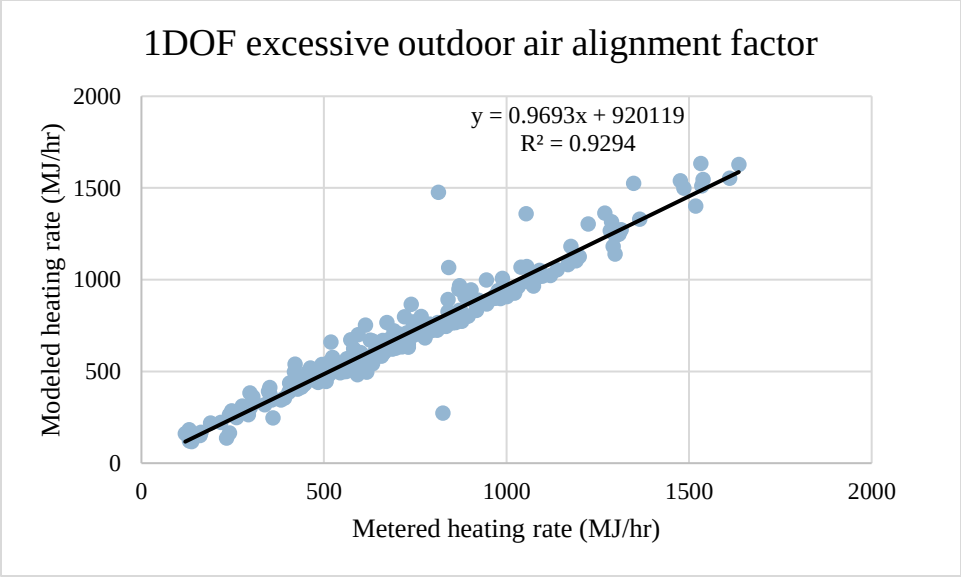

Figure 101:1DOF excessive outdoor air fault fit alignment factor of SPBM and metered heating rate

As with 1DOF fits, the accompanying 3DOF results in an adequate fit with reliable variable parameters.

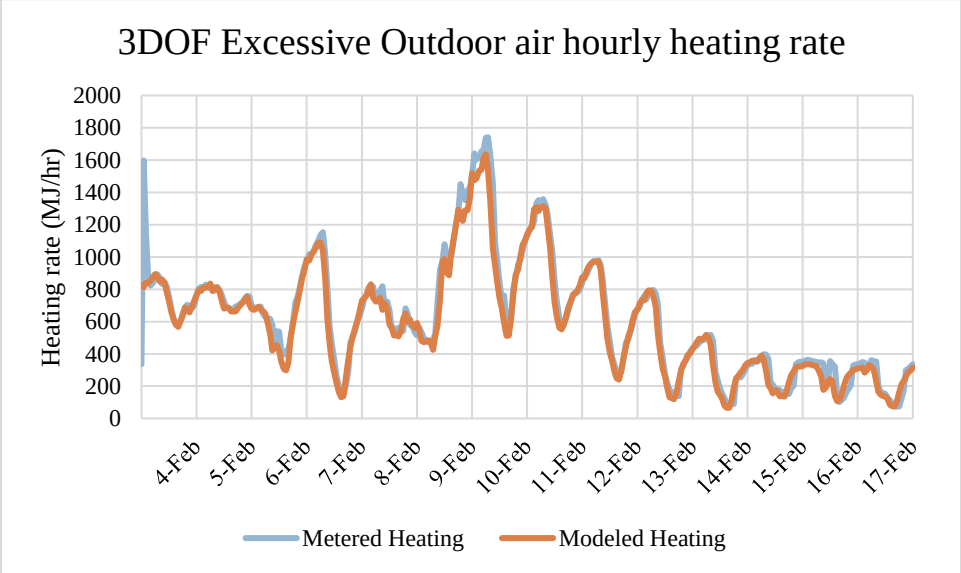

Figure 102: 3DOF excessive preheat hourly heating rate of SPBM and metered data with excessive outdoor air fault.

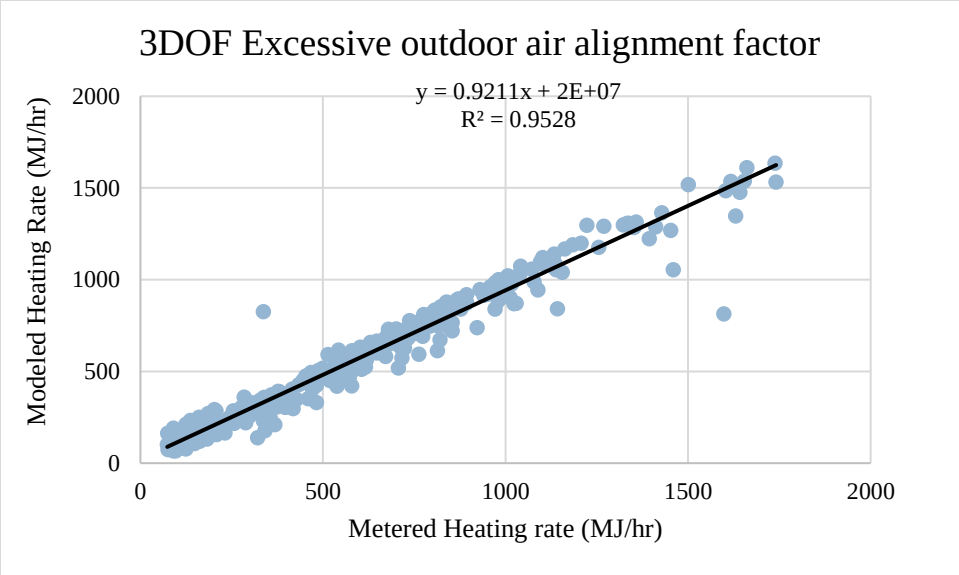

Figure 103: 3DOF excessive outdoor air fault fit alignment factor of SPBM and metered heating rate

Table 6: Results of various variables tested with excessive outdoor air fault detection

	$\delta Q/\delta var$	Uvar	$\delta SSE/\delta var$
Outdoor air flow rate	-1.4E+10	0.001118	2.82E+17
Minimum air flow rate	1.46E+10	0.001048	-1.5E+18
Peak electrical fraction	5.24E+09	0.002919	3.82E+16

These initial tests demonstrate that individual fault detection and identification with a SPBM is achievable and reliable. The following sections will test both Whitehead and Old CE during summer and winter conditions on their ability to distinguish which of four potential faults are occurring and even if multiple simultaneous faults can be identified.

7.2 Distinguishing Individual Faults from All Tested Faults

Having demonstrated that specific faults can be identified among other commonly

unknown values, it was time to test the faults against themselves. For this series of tests, there are six possible answers for each test: 1) Excessive infiltration, 2) Malfunctioning occupancy sensors 3) Unnecessary/excessive preheat and, 4) Malfunctioning outdoor air control system such as a faulty outdoor air damper. Unlike the previous tests, parameters for error and time of year for fault testing will be adjusted to suit each fault and minimize false reports.

7.2.1 Whitehead Four Degree of Freedom Fault Identification and Detection

Identifying faults within Whitehead was met with the same level of success that has been shown throughout this paper. Faults were found using sum squared error minimization and by adjusting fault parameters between correct operation and 100% failure. By utilizing both an error minimization search as well as predetermined values for the four different faults, true absolute minimum and uniqueness of model error can be tested.

No-fault performance was analyzed first to give baseline performance of the SPBM. Due to the complex nature of building energy modeling, and the established practice of using prediction intervals for model uncertainty for time series data, 95% prediction interval was used to evaluate how well faulty SPBM energy prediction compares to calibrated baseline performance. Ideally, a linear regression of metered and predicted energy use would result in a perfect 1:1 slope and no divergence; meaning that the model can perfectly replicate metered data for a given input. By comparing how well predicted loads fall within no-fault prediction intervals, this method allows for comparisons between different results by analyzing how many points fall within uncertainty bounds while 4DOF relative error changes can be used to approximate fault

identification confidence. Additionally, analysis of the number of points outside of 95% prediction interval was used to determine if a time series NN identified a fault. Results of SPBM calibration and prediction interval analysis of heating and cooling demand for Whitehead during winter and summer conditions are depicted below in Figure104 and Figure 105.

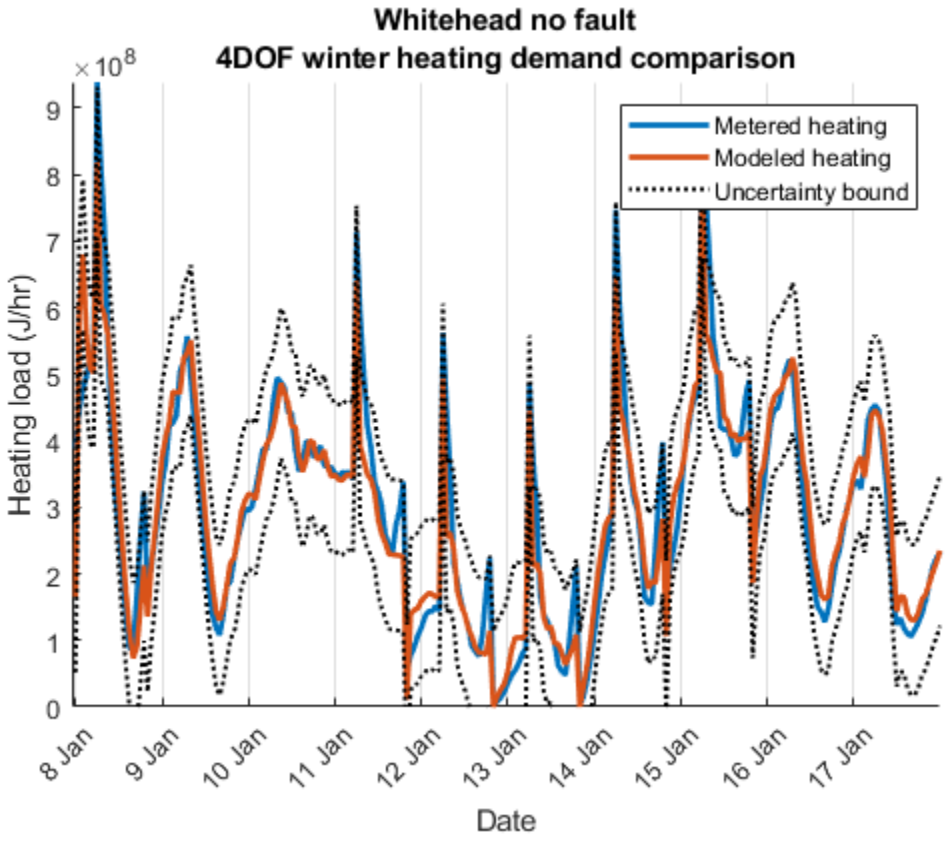

Figure 104A: Hourly heating demand represented as transient plot and alignment factor which demonstrates the high degree of accuracy of predicted load by the SPBM

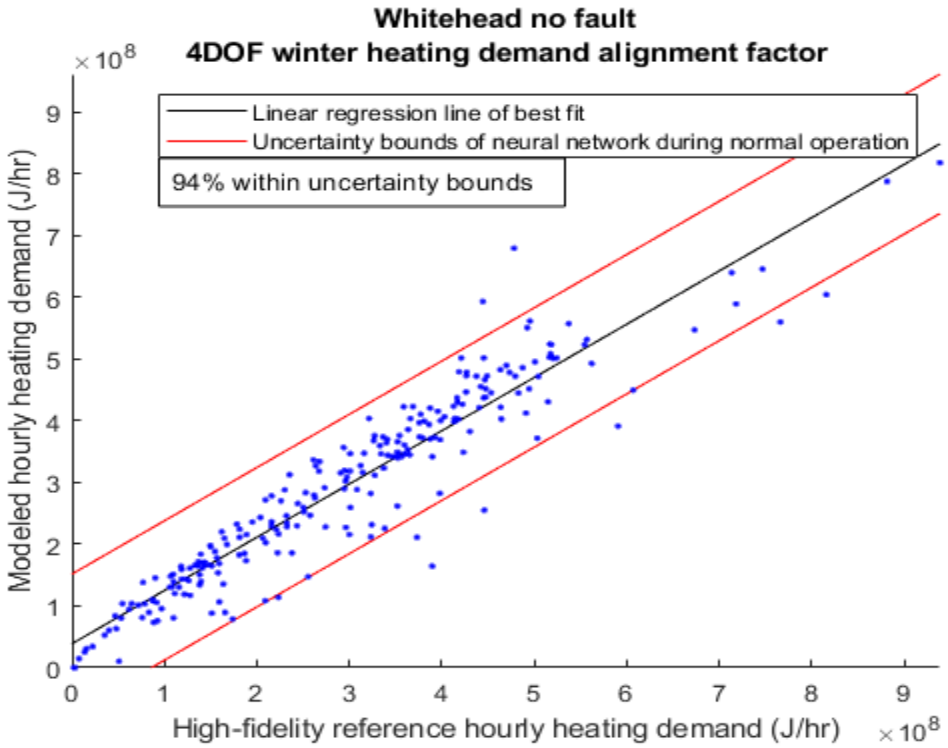

Figure 104B: Alignment factor of hourly heating demand represented as transient plot and alignment factor which demonstrates the high degree of accuracy of predicted load by the SPBM

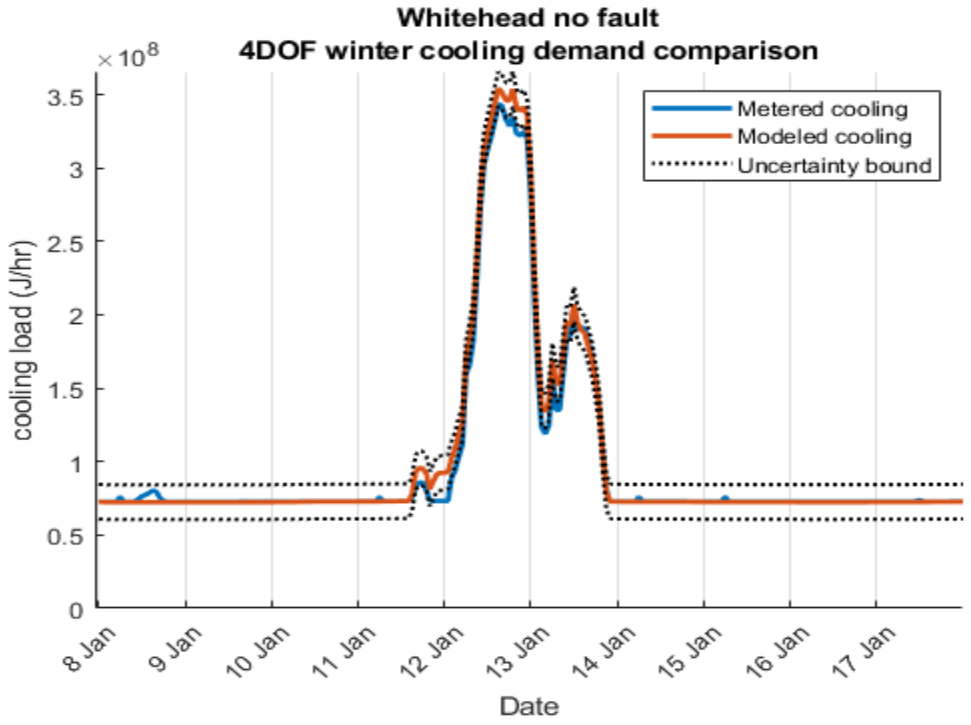

Figure 104C: Hourly cooling demand represented as transient plot and alignment factor which demonstrates the high degree of accuracy of predicted load by the SPBM

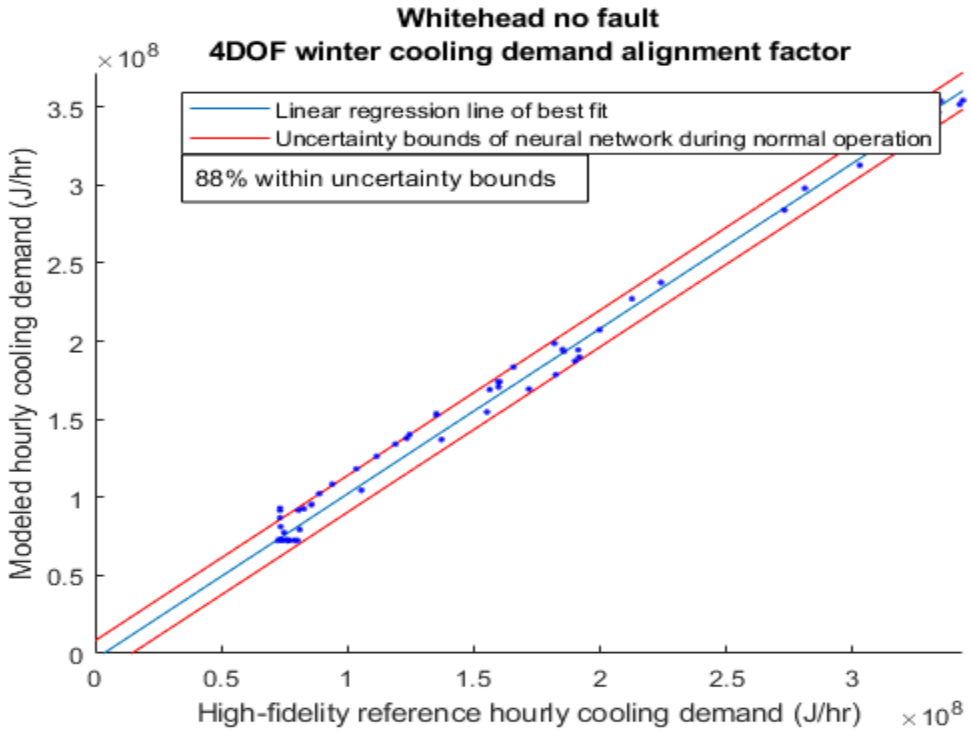

Figure 104D: Alignment factor of hourly cooling demand represented as transient plot and alignment factor which demonstrates the high degree of accuracy of predicted load by the SPBM

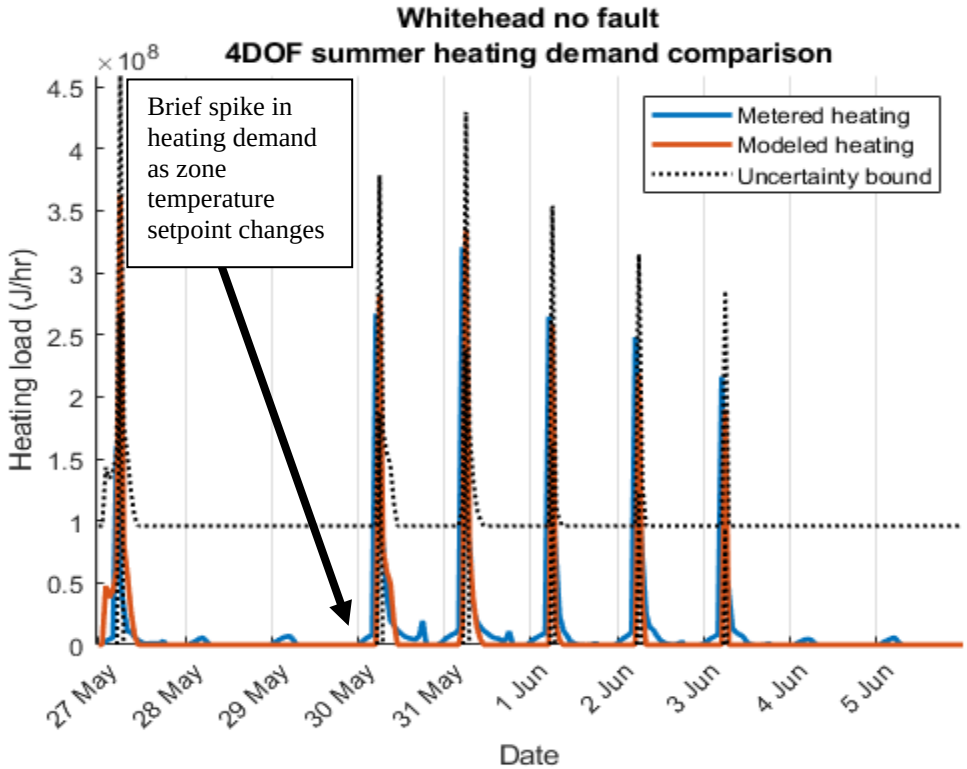

Figure 105A: No-fault heating demand for Whitehead for summer loading conditions

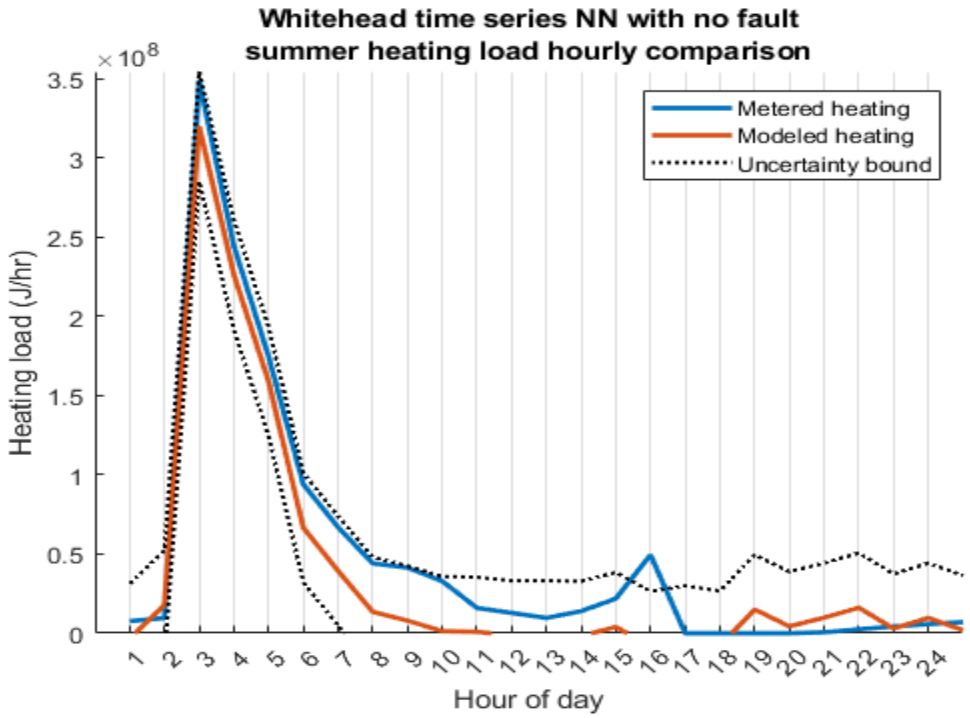

Figure 105B: No-fault heating demand for one day to more easily see how heating demand occurs during a brief spike for Whitehead during summer loading conditions

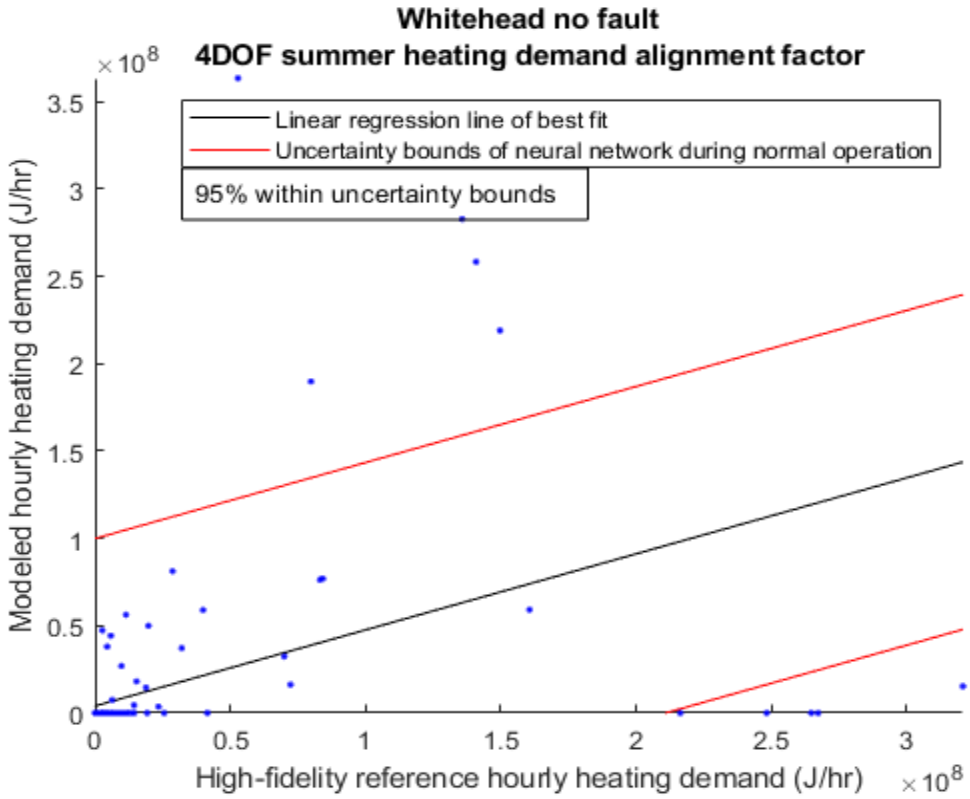

Figure 105C: Alignment factor of no-fault heating demand for Whitehead for summer loading conditions

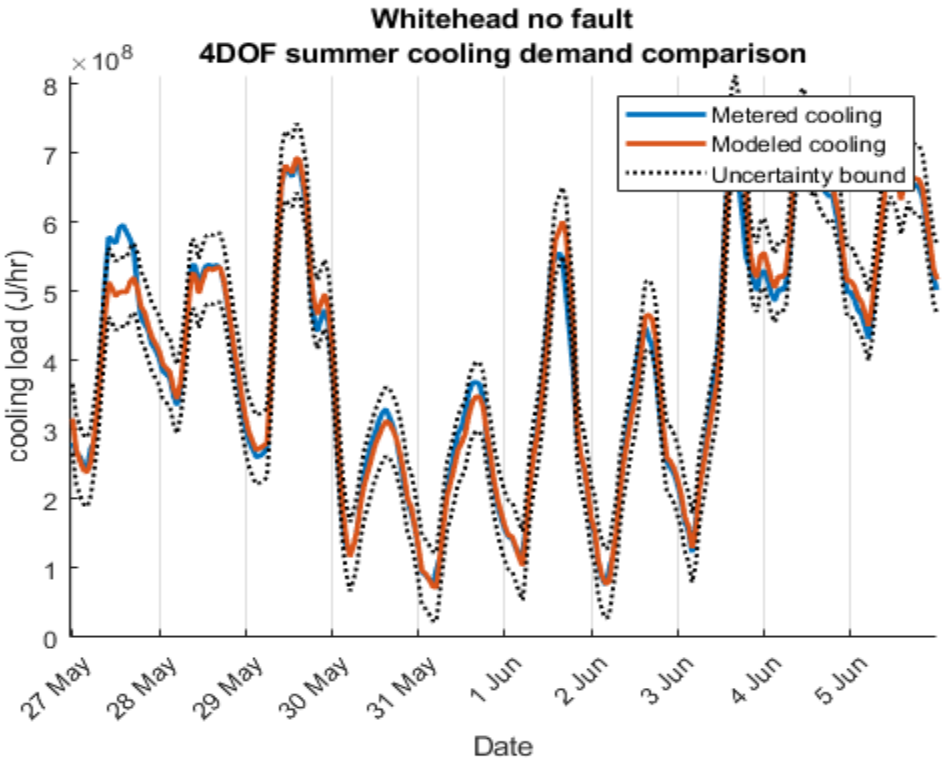

Figure 105D: No-fault cooling demand for Whitehead for summer loading conditions

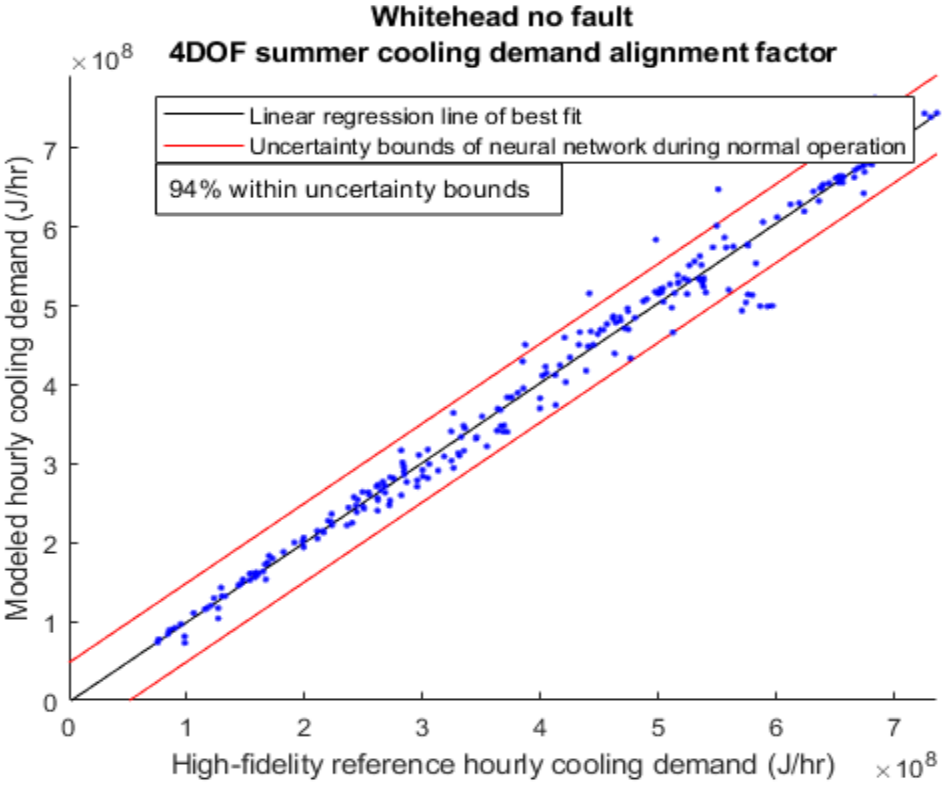

Figure 105E: Alignment factor of no-fault cooling demand for Whitehead for summer loading conditions

To better visualize changes in error in relation to changes in parameter values, Figure 106 demonstrates how altering values of the four potential fault parameters affects the sum squared error. All parameters are normalized to themselves, meaning a value of 1 corresponds to the value when no fault is occurring. For example, the infiltration coefficient under normal operation is 0.2 and would be represented as a relative value of 1 on the figure. If infiltration were to double (infiltration coefficient of 0.4), that would correspond with a relative value of 2. Notice on Figure 106 that when the relative parameter value of infiltration is 2, the relative error value is approximately 8. This means that doubling infiltration results in nearly eight times increase in sum squared error. While the below figure may be slightly enigmatic at first, it becomes extremely useful when discussing results of parameter identification.

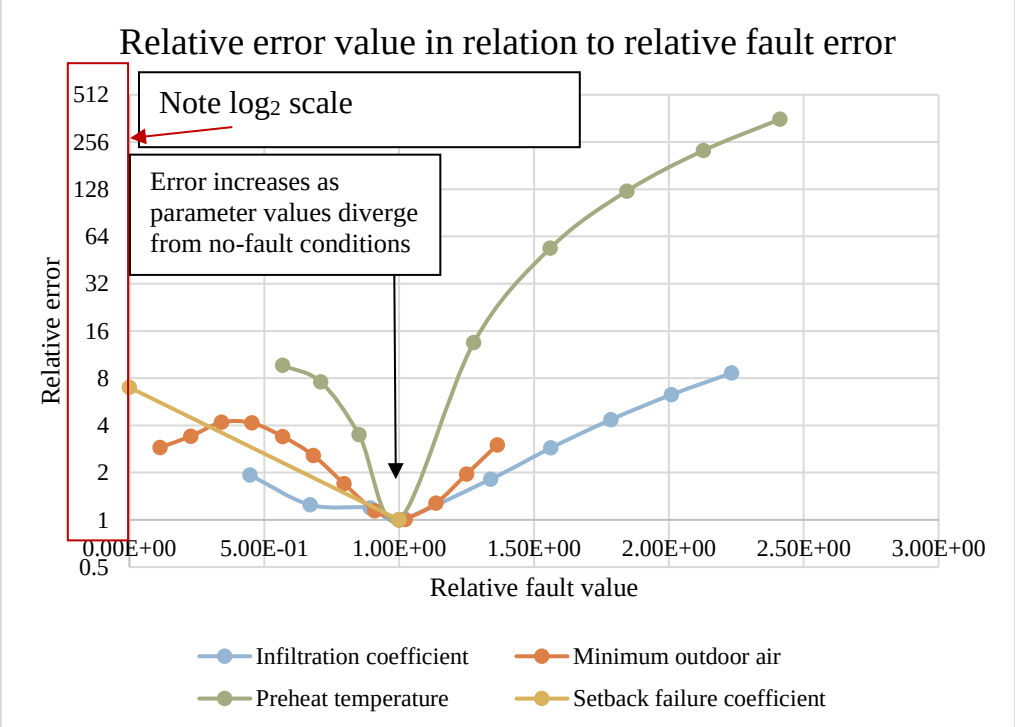

Figure 106: Visual representation of how relative changes in parameter values change error when no fault is occurring. Values represent multiples of no-fault parameter values and error; meaning changes along the vertical axis represents the multiple of error while changes along the horizontal axis represent multiples of parameter values

By comparing relative change in error to relative change in parameter also allows for visualization of model sensitivity to changes in different parameters. Increasing preheat temperature has the greatest change in error for a given change in parameter value while infiltration has the least sensitivity.

7.2.2 Excessive Infiltration

Infiltration is often a subtle source of error within the SPBM model. As discussed earlier in section 1.6 Infiltration, limiting error accumulation to periods of substantial wind speed allows for a more noticeable global minimum due to an increase in parameter sensitivity. Figure 107 through Figure 110 demonstrate the high degree of alignment that the SPBM is able to replicate after undergoing error minimization. Table 19 provides numerical values for errors associated with each of the possible causes of failure. The table lists a range of values for each fault to see how the error changes for each value while Figure 111 is a visual representation of how the error changes in relation to different failure values; here the error and potential failure values are represented fractionally, meaning an error of 1 is the error associated when the model is using parameter values that are associated with no-fault (as designed) operation. Additionally, a parameter value of 1 means the value is that of no-fault (as designed) operation. Likewise, an error value of ½ indicates that error has halved while an infiltration coefficient of 1.5 means that 50% more infiltration is occurring. For high infiltration, the high-fidelity model used a 1.4x increase in infiltration. By observing Figure 111 and Table 19, it is possible to see that the only parameter change that resulted in a lower error was infiltration. While the infiltration coefficient value was not the same as the high-fidelity model, finding the “true” value is not the objective of the SPBM, but rather

determining which of four possible faults may have caused the error. Therefore, in regard to model sensitivity, solution uniqueness, and fault detection, the SPBM demonstrates its aptitude for fault detection.

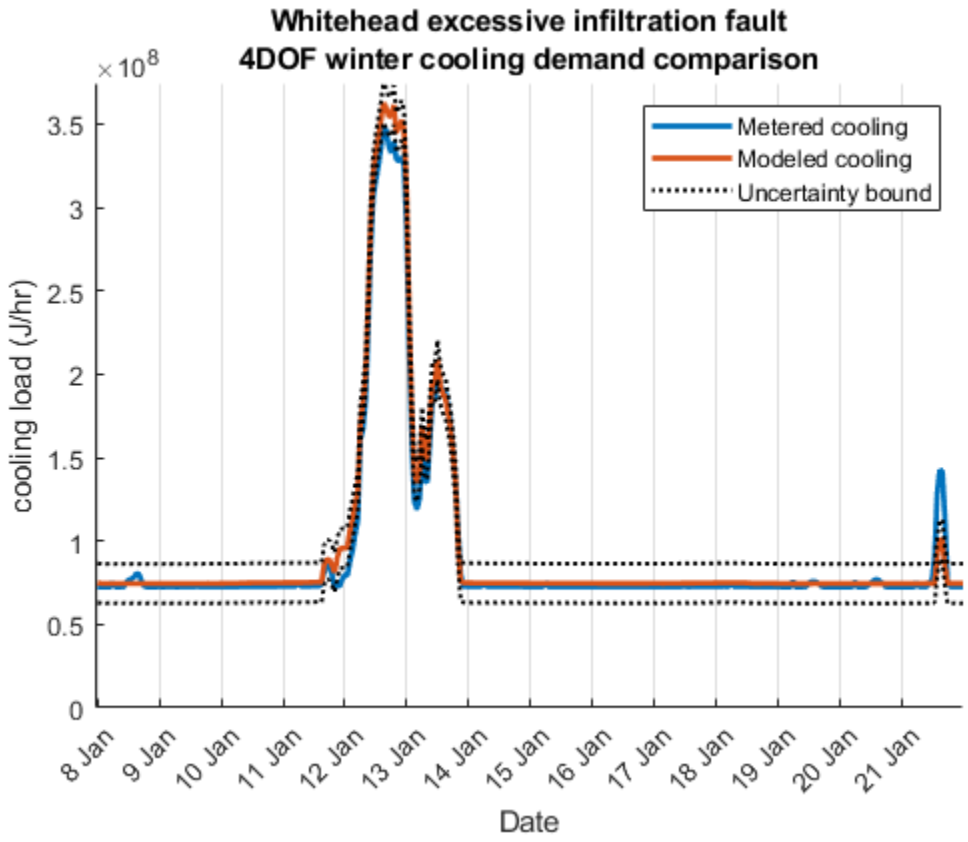

Figure 107: Hourly cooling rate for winter weather comparing SPBM and reference data when the building is experiencing a fault of excessive infiltration

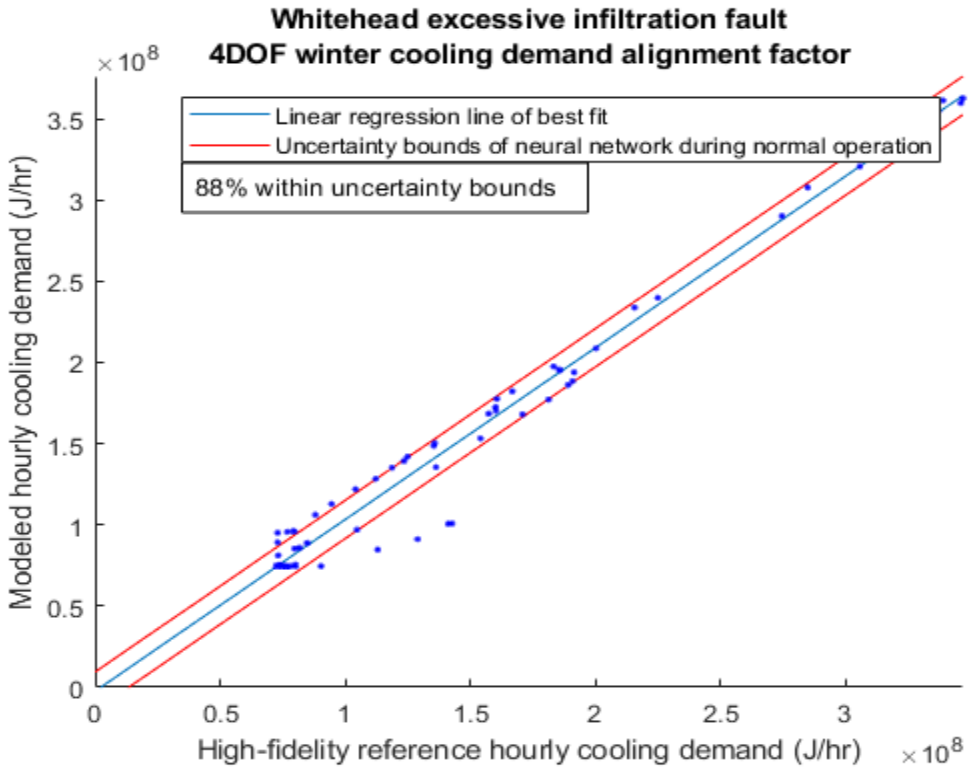

Figure 108: Hourly cooling rate alignment factor for Whitehead model experiencing excessive infiltration during winter weather

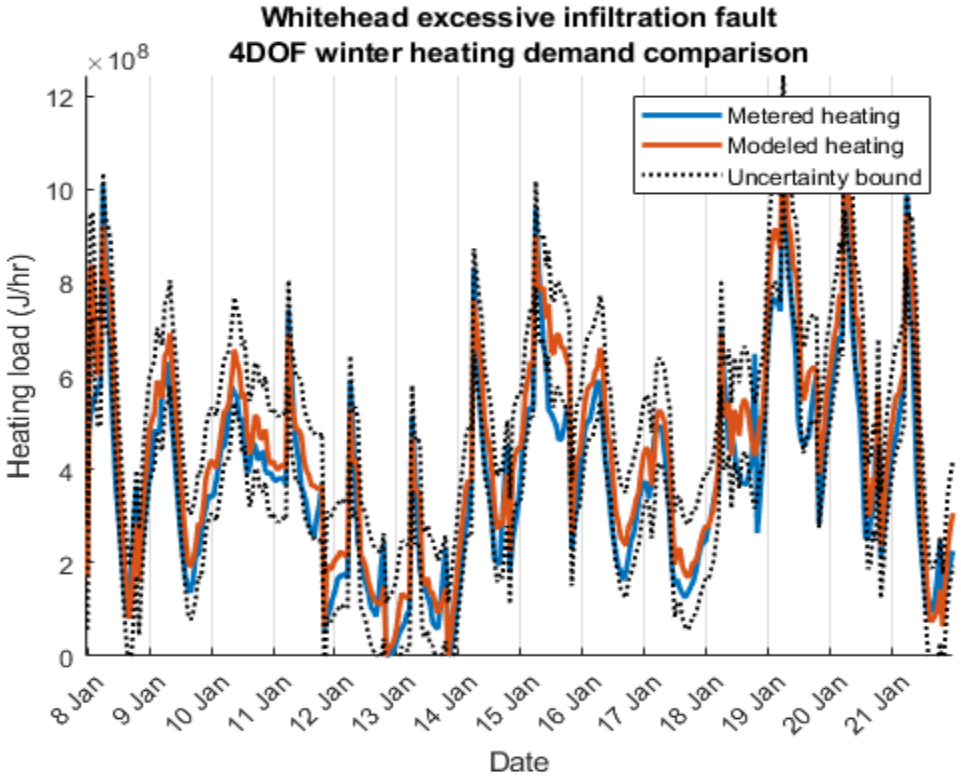

Figure 109: Hourly heating rate for winter weather comparing SPBM and reference data when the building is experiencing a fault of excessive infiltration

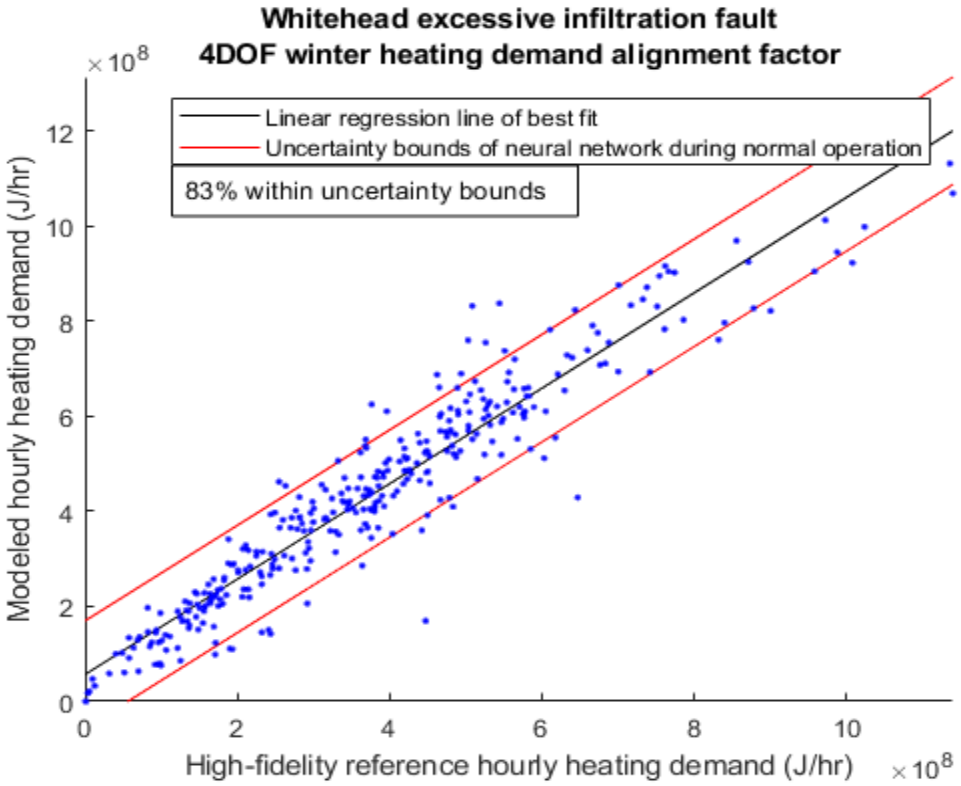

Figure 110: Hourly heating rate alignment factor for Whitehead model experiencing excessive infiltration during winter weather

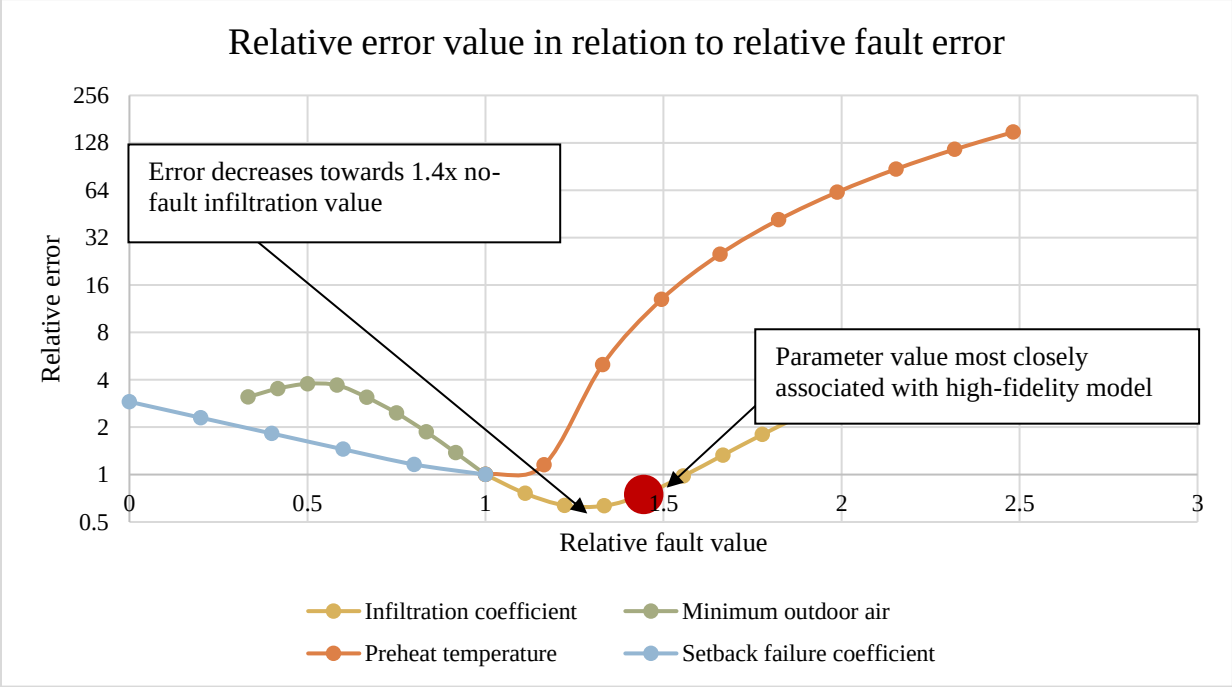

Figure 111: Visual representation of how magnitude of error changes across different magnitudes of the four possible faults. Excessive infiltration fault is being tested for automatic detection for Whitehead building during winter

Figure 111 shows how increasing infiltration from the nominal value (X value of 1 on the figure) decreases error to a point but then error increases. This is demonstrating that by increasing the SPBM infiltration parameter to that of the high-fidelity model value decreases error, but also that error begins to increase once modeled infiltration exceeds that of the reference data.

Continuing the investigation of excessive infiltration to the summer weather further demonstrates the versatility of the SPBM. While Figure 107 through Figure 111 demonstrate the heating-load driven fault detection abilities, Figure 112 through Figure 116 reveal that the SPBM is still achieving a more than acceptable level of model accuracy despite being subjected to completely different external load factors and primary energy demand. Unlike for winter weather, Figure 116 and Table 20 displays that insufficient outdoor air was not the only fault that caused a reduction in model error. However, the error reduction by the infiltration coefficient is over three times more significant than that of unoccupied setback fault. Additionally, error is only accounted for by monitoring the relative difference in heating and cooling load demand and not entering setback would increase the heating and cooling demand in a similar way to summer infiltration that occurs in the evening and weekends. Considering the objective of using the SPBM for automatic fault detection is not to determine the exact real-world value of the fault, but rather evaluate a spectrum of potential faults and use the results from these evaluation methods to suggest a possible cause of the fault.

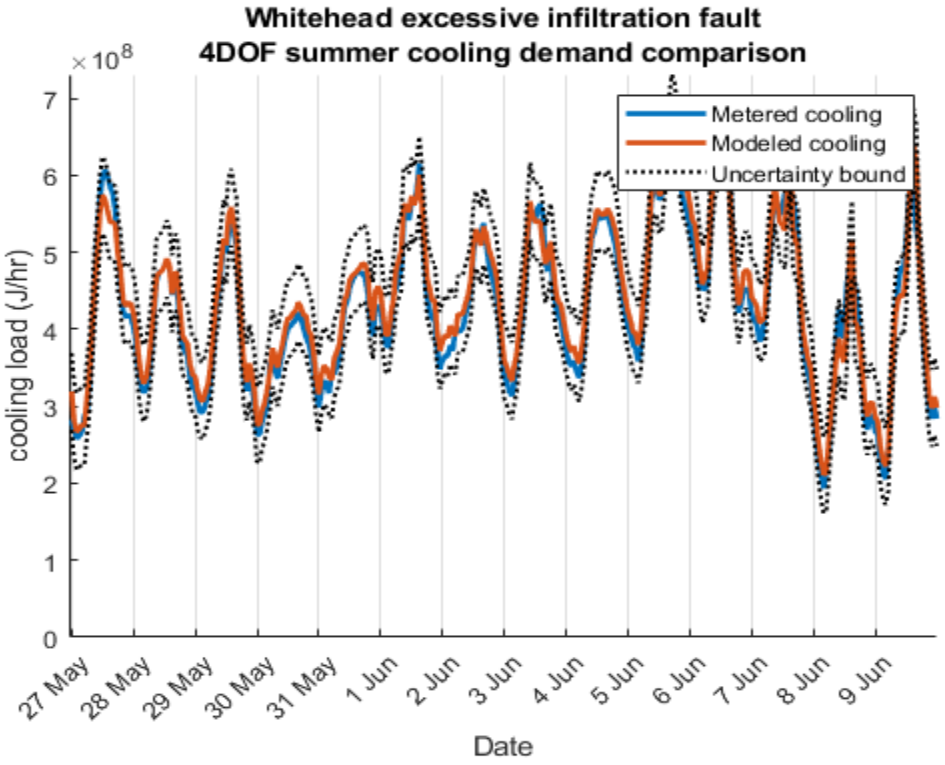

Figure 112: Hourly cooling rate for summer weather comparing SPBM and reference data when the building is experiencing a fault of excessive infiltration

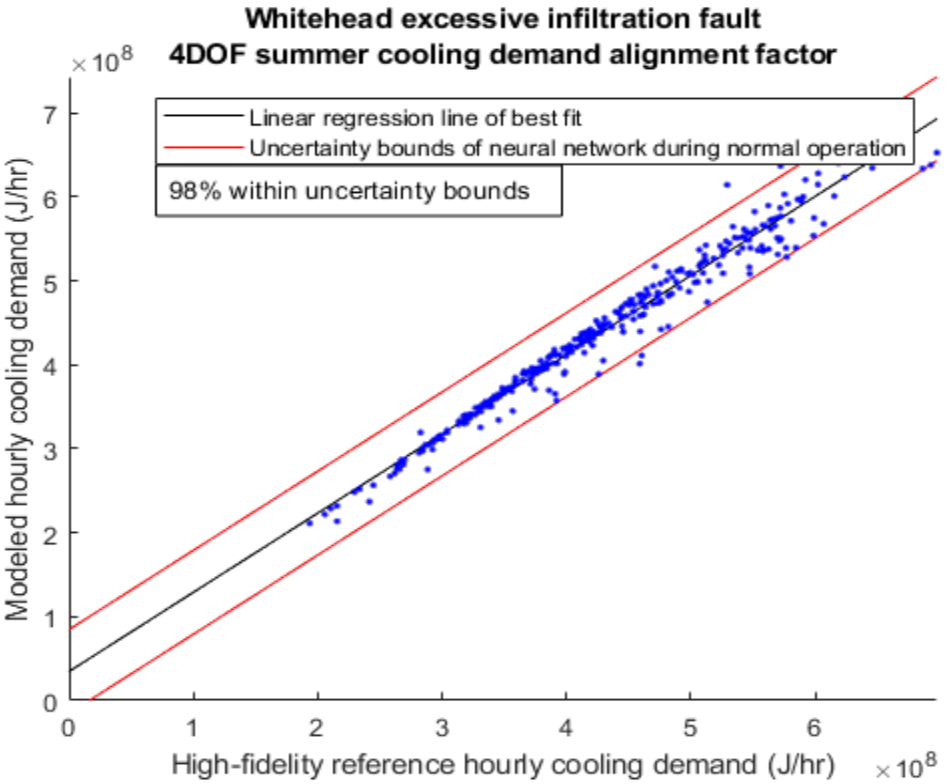

Figure 113: Hourly cooling rate alignment factor for Whitehead model experiencing excessive infiltration during summer weather

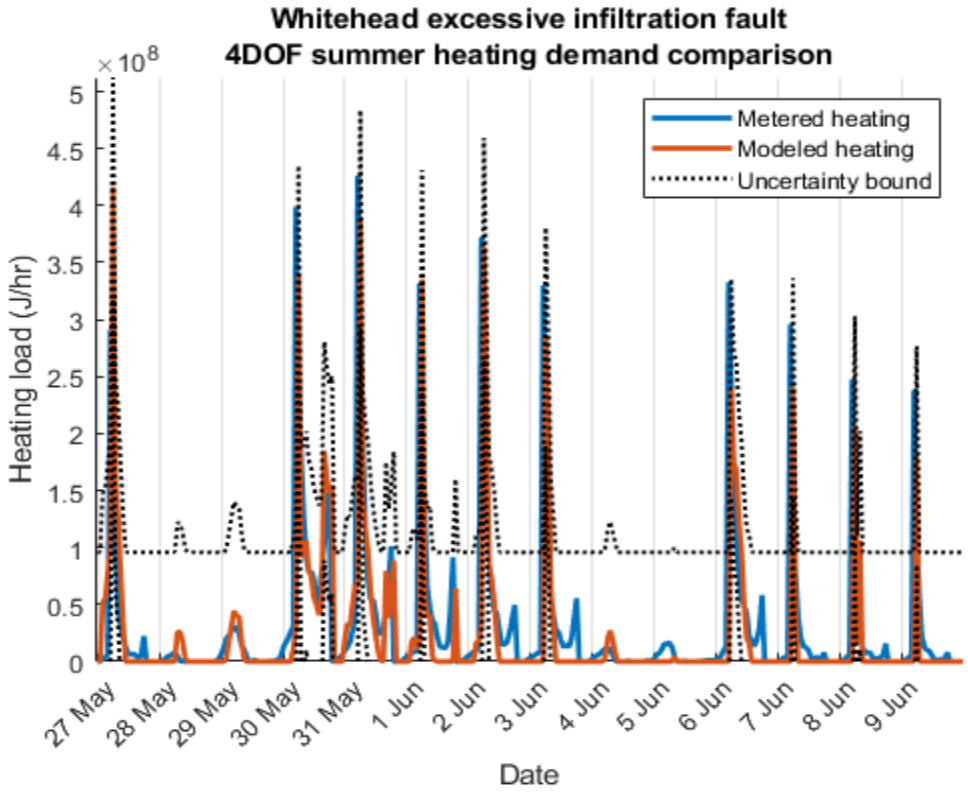

Figure 114: Hourly heating rate for summer weather comparing SPBM and reference data when the building is experiencing a fault of excessive infiltration

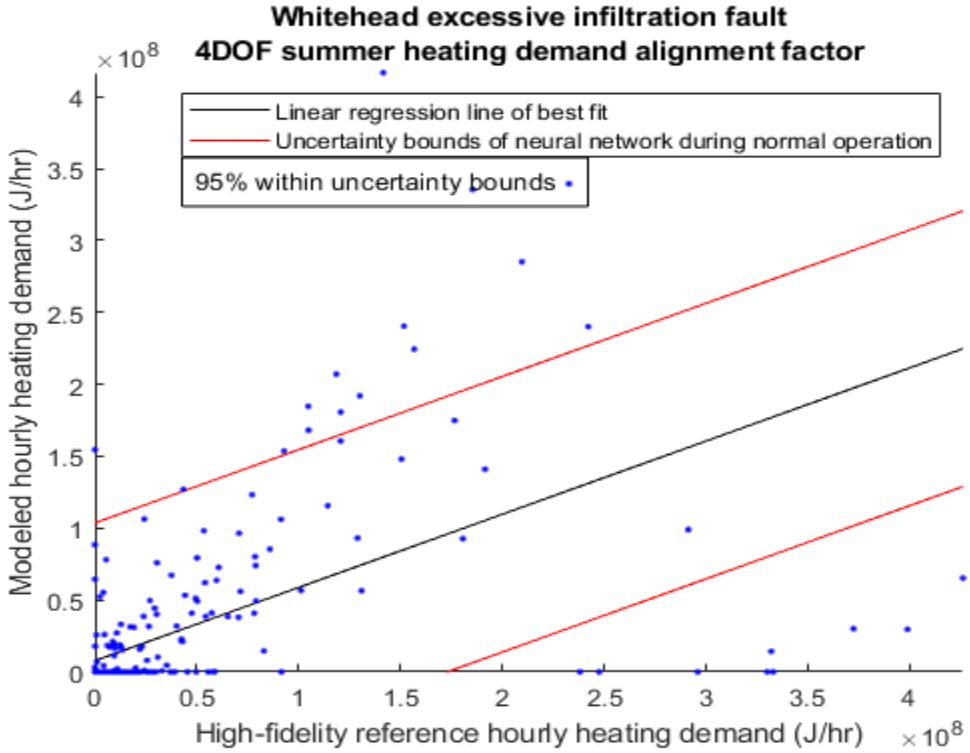

Figure 115: Hourly heating rate alignment factor for Whitehead model experiencing excessive infiltration during summer weather

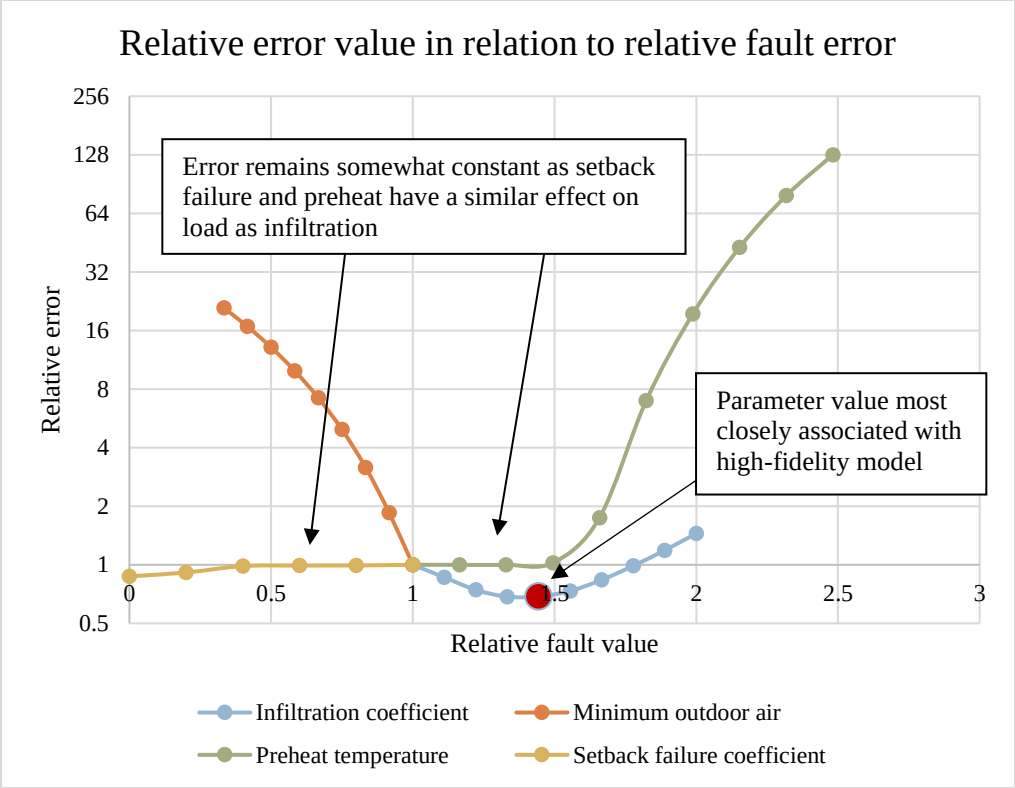

Figure 116: Visual representation of how magnitude of error changes across different magnitudes of the four possible faults. Excessive infiltration fault is being tested for automatic detection for Whitehead building during summer

Like with winter data, summer infiltration testing shows that error decreases as infiltration increases, but only to a point. Setback failure fault does show a slight reduction in error due to the low impact of infiltration in summer and because setback failure will increase energy demand, therefore lowering error.

Excessive infiltration presents the least impact on heating and cooling demand among the four faults that are being analyzed while also being the most difficult to detect in a real building. Old CE was discovered to have less significant infiltration load than Whitehead in addition to having a more complex AHU design. Therefore, analyzing how the SPBM and NN detects infiltration in a less sensitive building and with the presence of

other faults furthers the understanding of how simplified building fault detection programs behave.

7.2.3 No Setback

As explained earlier, setback is the action of widening the temperature setpoint during periods of building vacancy. While this fault can stem from numerous causes, the most likely cause experienced was from malfunctioning occupancy sensors. Malfunctioning occupancy sensors also keep lights on in zones where sensors detect (or believe to detect) occupants. Therefore, occupancy sensor fault adjusts both the temperature setpoint and internal load amount.

Figure 117 through Figure 121 again demonstrates how well the SPBM is able to align with a high-fidelity model. Figure 121 and displays the visual relative error associated with each of the four faults that are being evaluated while Table 21 lists numerical results from the tests. Just as with infiltration, only one parameter shows a decrease in error. However, the reduction in error here is over 85% between no-fault parameter values and full failure of temperature setback. Such a decisive reduction in error from only one parameter along with high modeled load alignment demonstrates both unique solutions and adaptability of the SPBM.

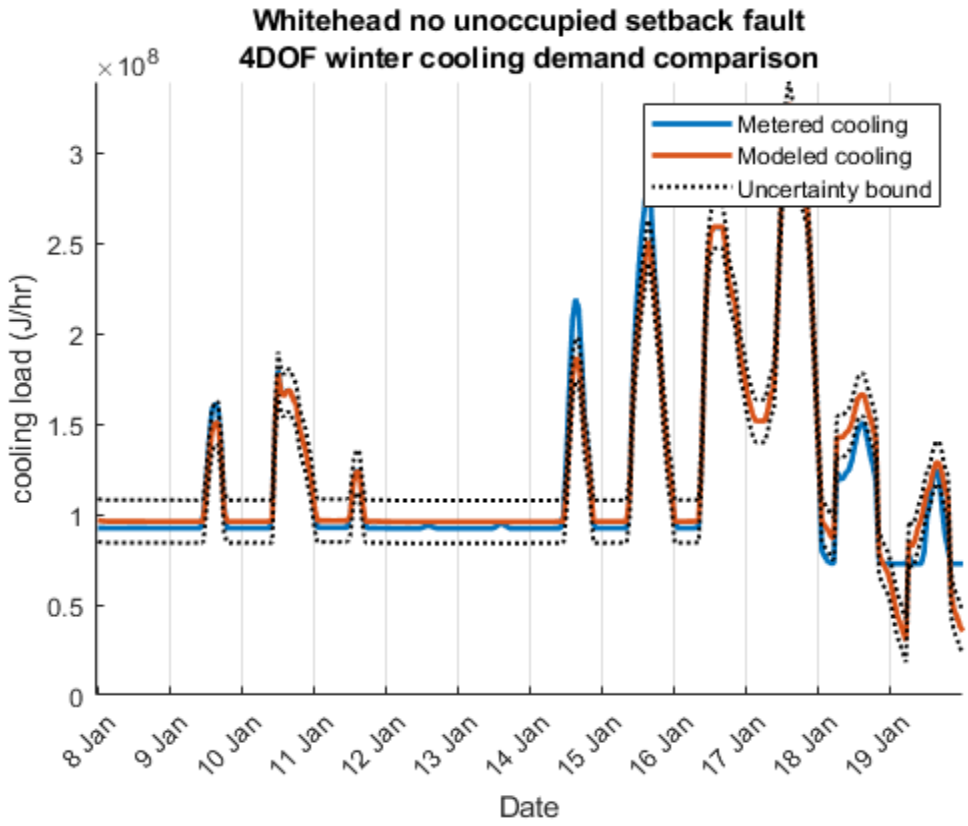

Figure 117: Hourly cooling rate for winter weather comparing SPBM and reference data when the building is experiencing a fault of not entering unoccupied setback

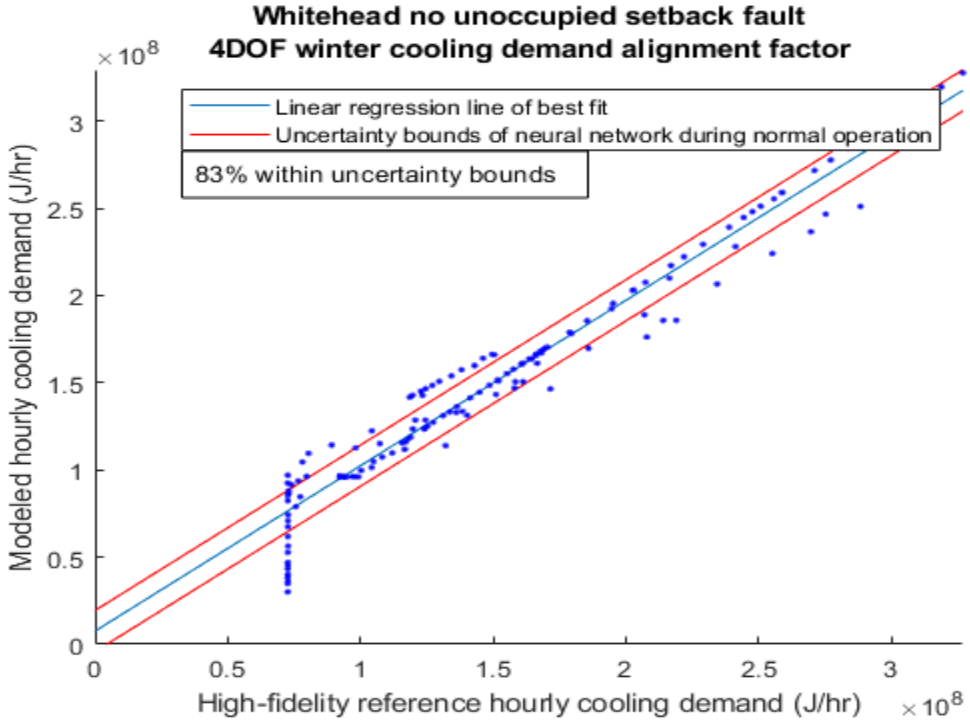

Figure 118: Hourly cooling rate alignment factor for Whitehead model experiencing no unoccupied setback fault during winter weather

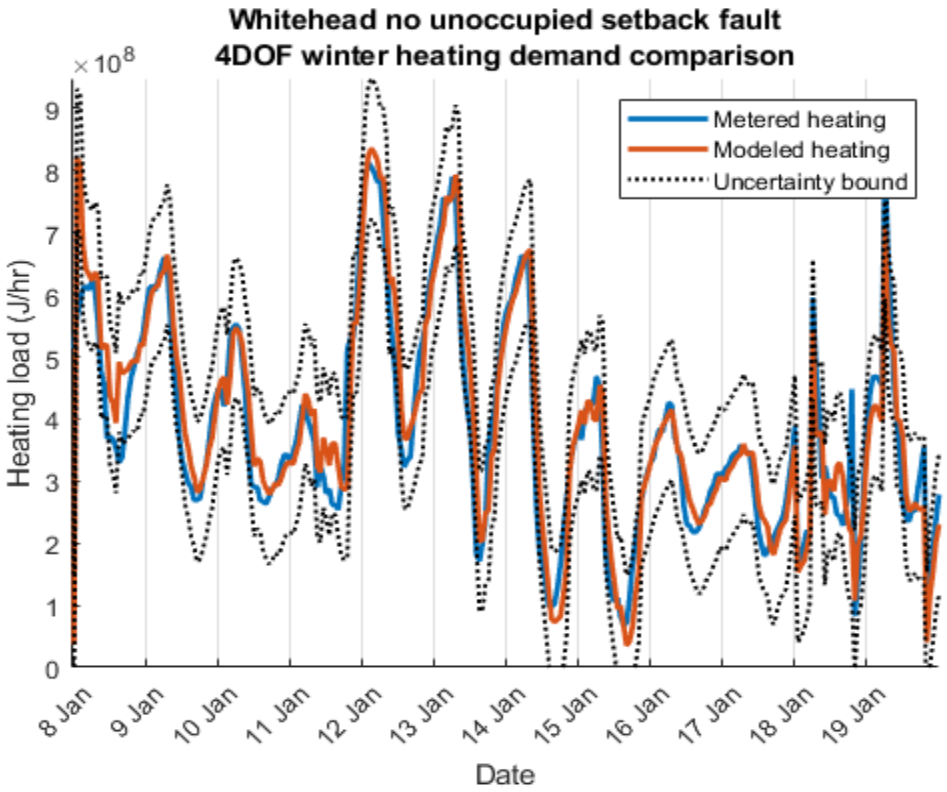

Figure 119: Hourly heating rate for winter weather comparing SPBM and reference data when the building is experiencing a fault of not entering unoccupied setback

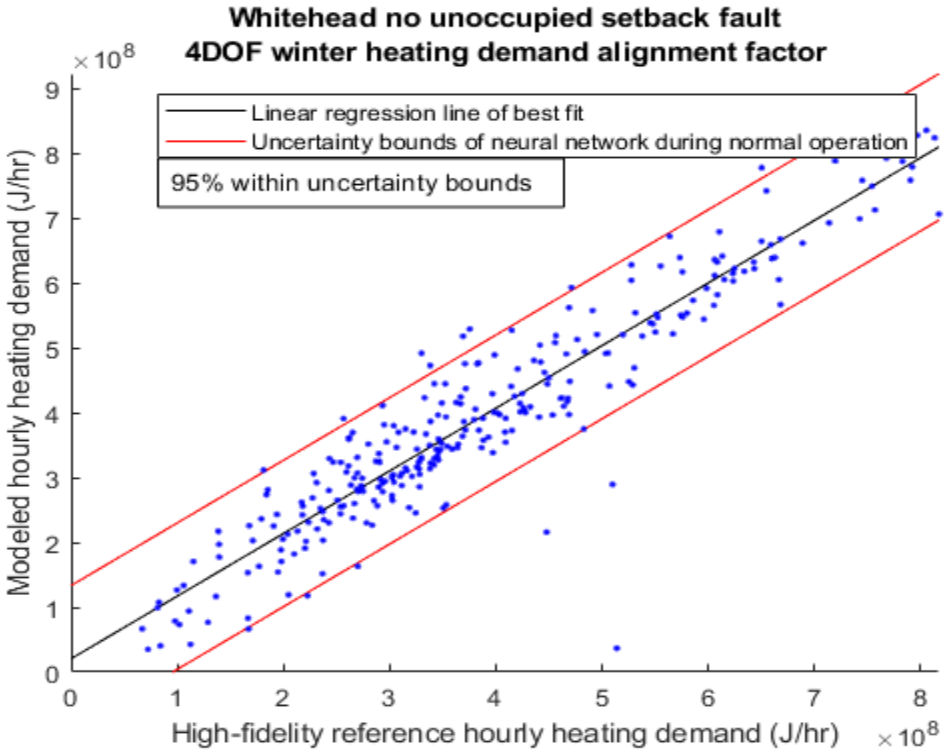

Figure 120: Hourly heating rate alignment factor for Whitehead model experiencing no unoccupied setback fault during winter weather

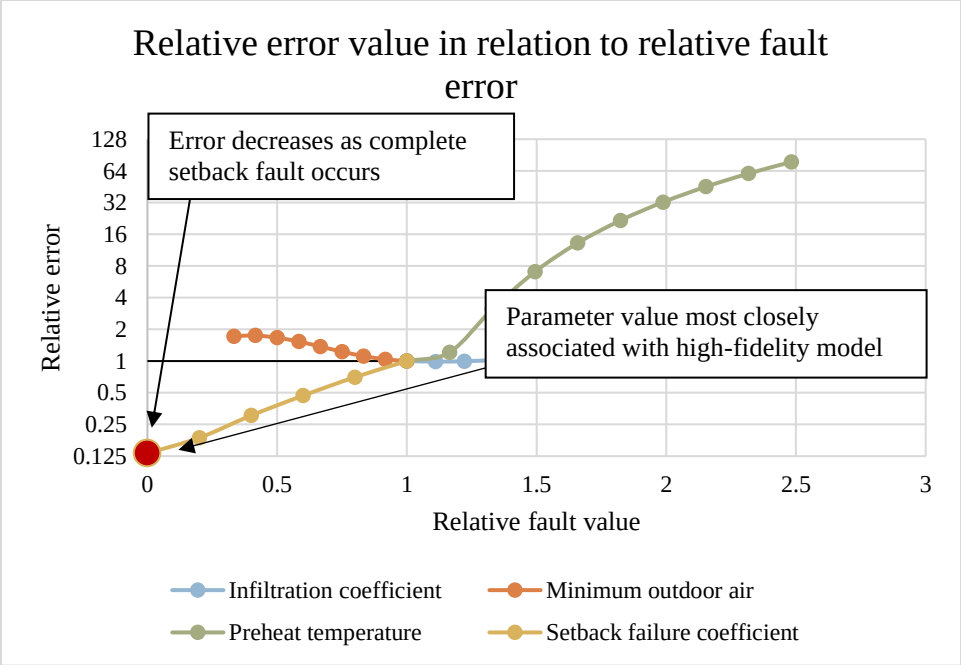

Figure 121: Visual representation of how magnitude of error changes across different magnitudes of the four possible faults. The fault of not entering unoccupied setback being tested for automatic detection for Whitehead building during winter

Unoccupied setback failure shows a clear decrease in error as the SPBM approaches a complete failure to enter setback. Error increase from other faults is decreased due to faults that increase load during unoccupied periods reducing error during that time.

Failure to enter setback during summer weather would increase cooling and heating demand during unoccupied times. The increase of cooling demand, as shown in Figure 122 and Figure 123, stems from having to cool return air that is at minimum occupied zone temperature setpoint, which is 4.5°C higher than an unoccupied zone temperature setpoint. Figure 124 and Figure 125 display heating demand increases during unoccupied periods due to having to maintain a higher minimum zone temperature despite having minimal zone loading. Together, the increase in both heating and cooling demand during summer weather would show a decrease in error for any fault that

accommodated these conditions, shown in Figure 126 and Table 22. However, reduction in error from not entering setback had the most noticeable and dramatic reduction in error of the tested faults. Given that not entering setback was the only fault that showed a reduction in error for both winter and summer loading conditions, it would be a safe assumption that automatic fault detection was successful for this fault test.

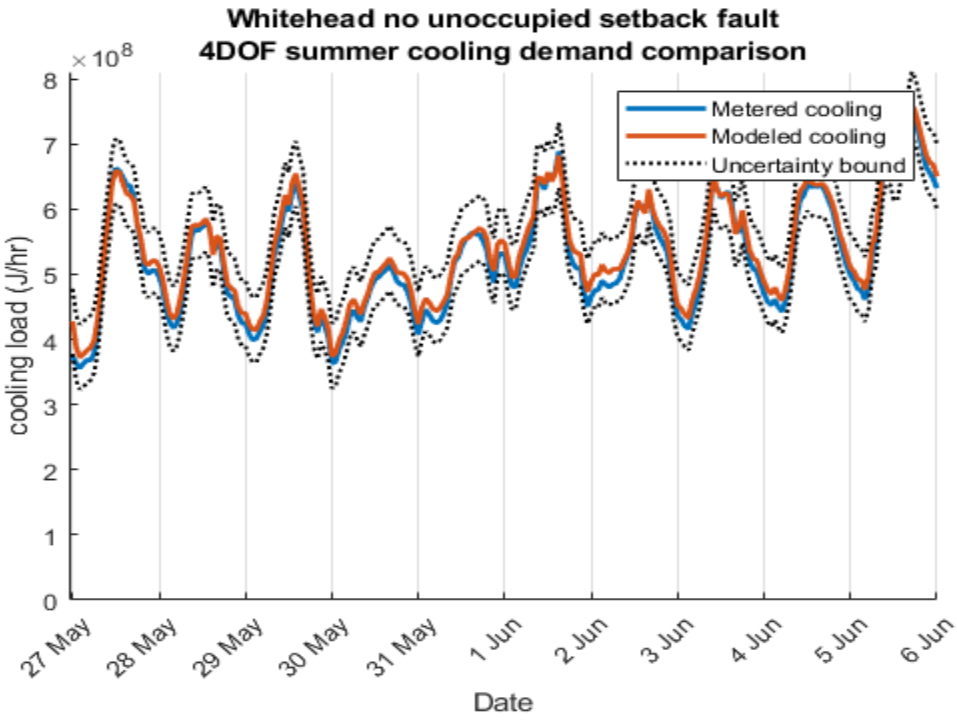

Figure 122: Hourly cooling rate for summer weather comparing SPBM and reference data when the building is experiencing a fault of not entering unoccupied setback

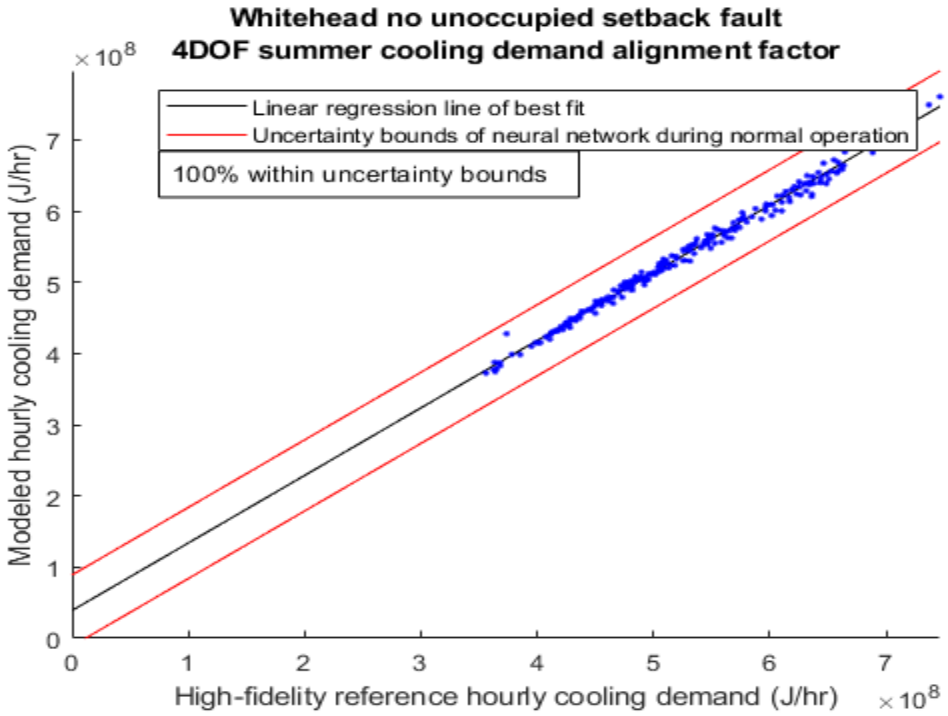

Figure 123: Hourly cooling rate alignment factor for Whitehead model experiencing no unoccupied setback fault during summer weather

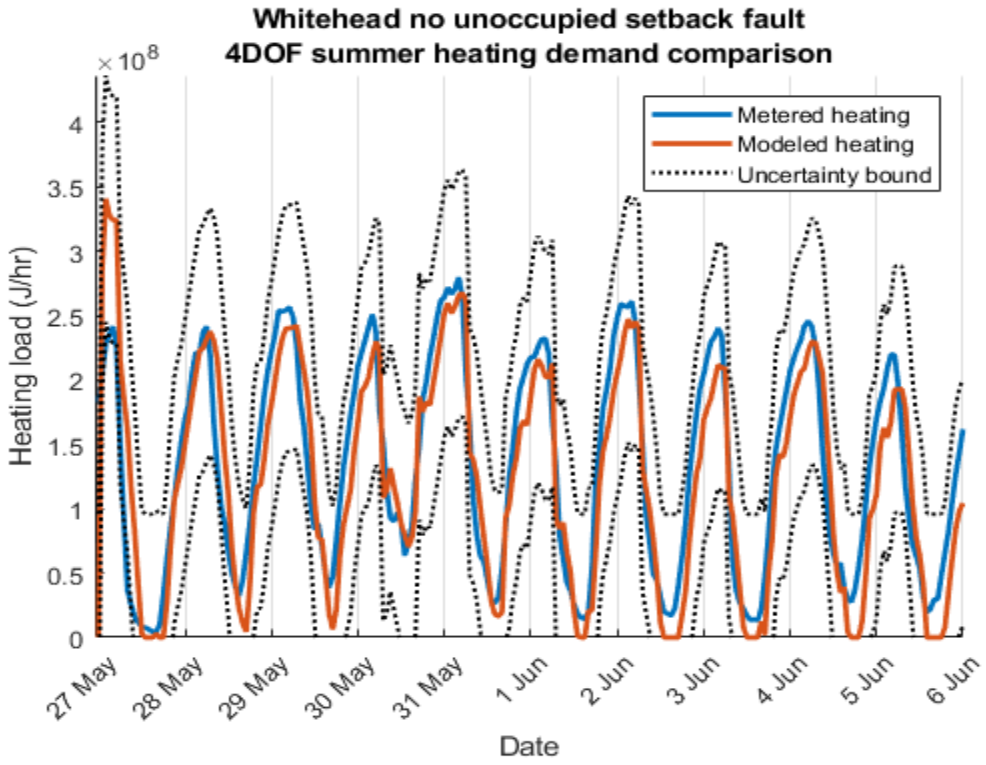

Figure 124: Hourly heating rate for summer weather comparing SPBM and reference data when the building is experiencing a fault of not entering unoccupied setback

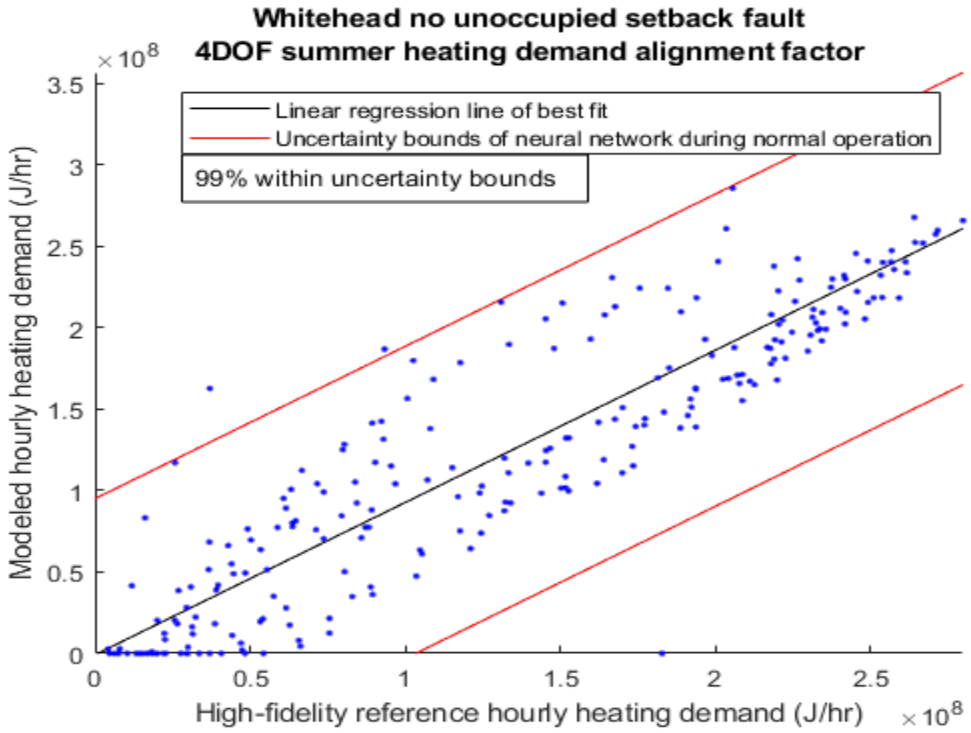

Figure 125: Hourly heating rate alignment factor for Whitehead model experiencing no unoccupied setback fault during summer weather

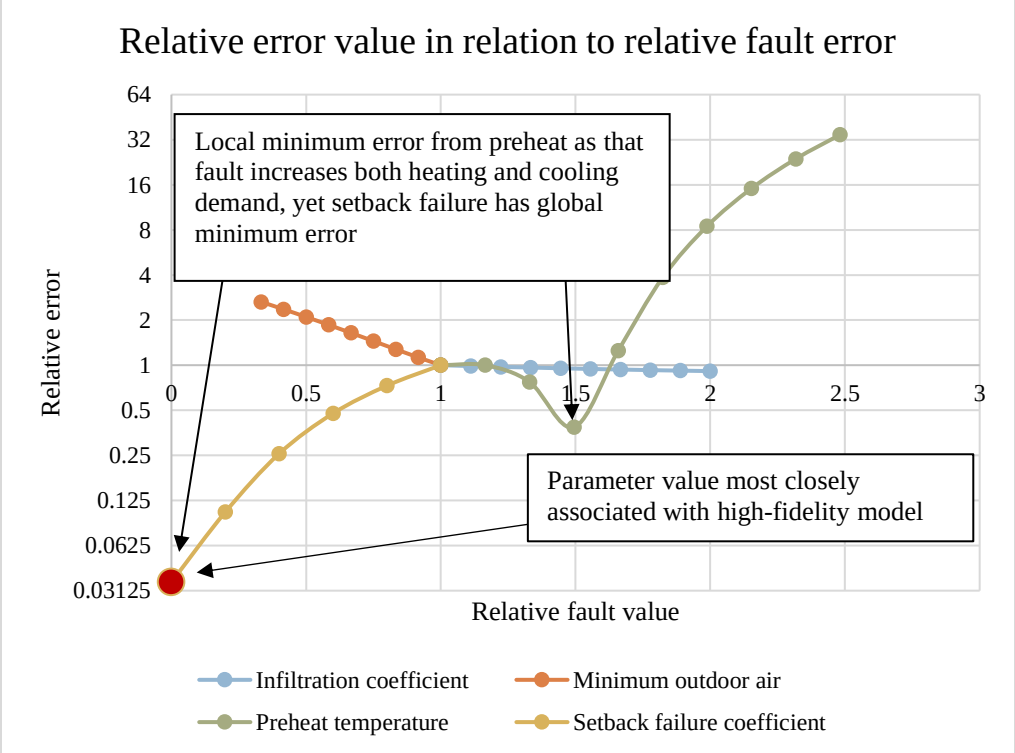

Figure 126: Visual representation of how magnitude of error changes across different magnitudes of the four possible faults. The fault of not entering unoccupied setback being tested for automatic detection for Whitehead building during summer

Unoccupied setback failure shows a greater reduction in error due to the increase in cooling demand required during summer. Infiltration and preheat faults also increase heating and cooling demand, so those faults also show a slight decrease in error, although a global minimum error still occurs for setback fault.

Failure to enter unoccupied setback and excessive infiltration both occur during different periods of the day. Likewise, fault detection can be limited to times in which faults are expected to occur in order to increase identification sensitivity. However, both excessive preheat and insufficient outdoor air faults occur at all times of operation, and therefore require different methods of ensuring confidence of fault identification.

7.2.4 Excessive Preheat

Excessive preheat is by far the most energy intensive fault being tested. To briefly review what excessive preheat entails, it means that the preheat temperature, which is usually set to the same desired supply temperature as the cooling coils, is set far above that specified supply temperature in an effort to prevent AHU cooling coils from freezing. While appropriate in extreme cases, high preheat setpoints are sometimes used as a solution to prevent overly sensitive or poorly designed AHUs from entering a false shutdown or from a leaking valve .

Examining the cooling and heating rates for winter weather that are displayed in Figure 127 through Figure 131 and Table 23 reveal overall less agreeable results from the SPBM when comparing to the high-fidelity reference model. However, considering the magnitude of both heating and cooling demand increase, the SPBM was still able to find an optimal solution and identify excessive preheat as a possible cause of building fault. Again, while other evaluated potential faults did demonstrate a reduction in error, any

fault that caused an increase in both heating and cooling load demand would lower the error. Due to this fault typically only existing during winter weather, it would be easy to confirm by looking at historical building energy consumption and looking for a sharp spike in heating and cooling demand sometime around winter. Additionally, excessive preheat has the highest increase in error when it is not the fault being evaluated, so comparing model results to a different period in time while keeping model parameters static would help rule out any potential false fault recommendations.

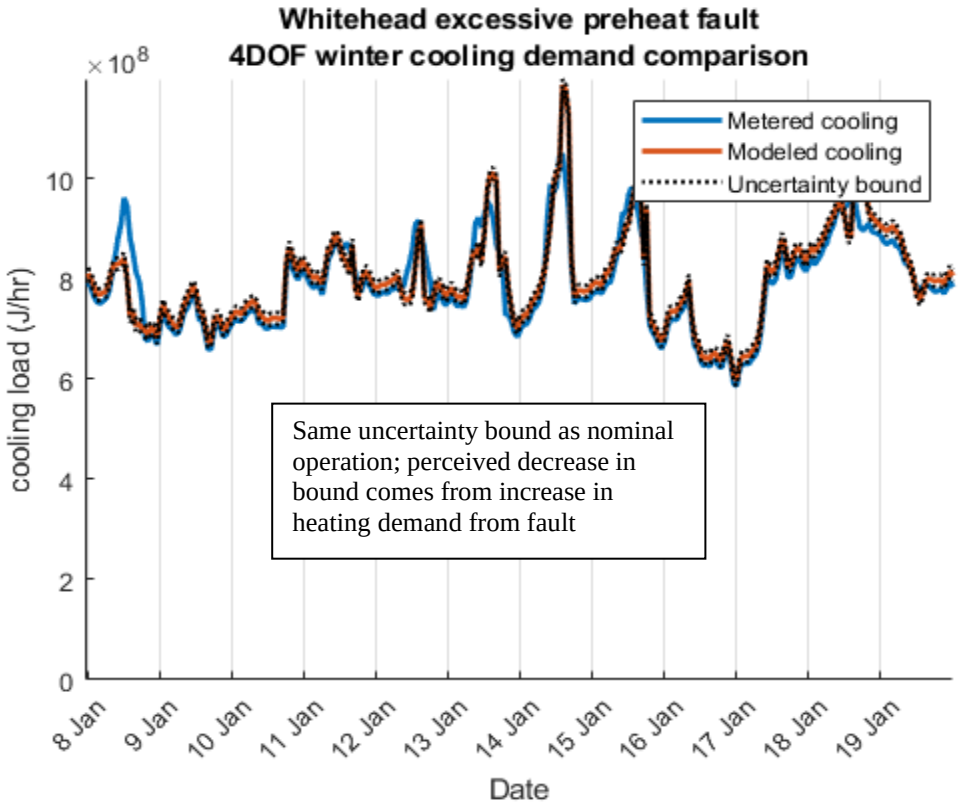

Figure 127: Hourly cooling rate for winter weather comparing SPBM and reference data when the building is experiencing a fault of excessive preheat

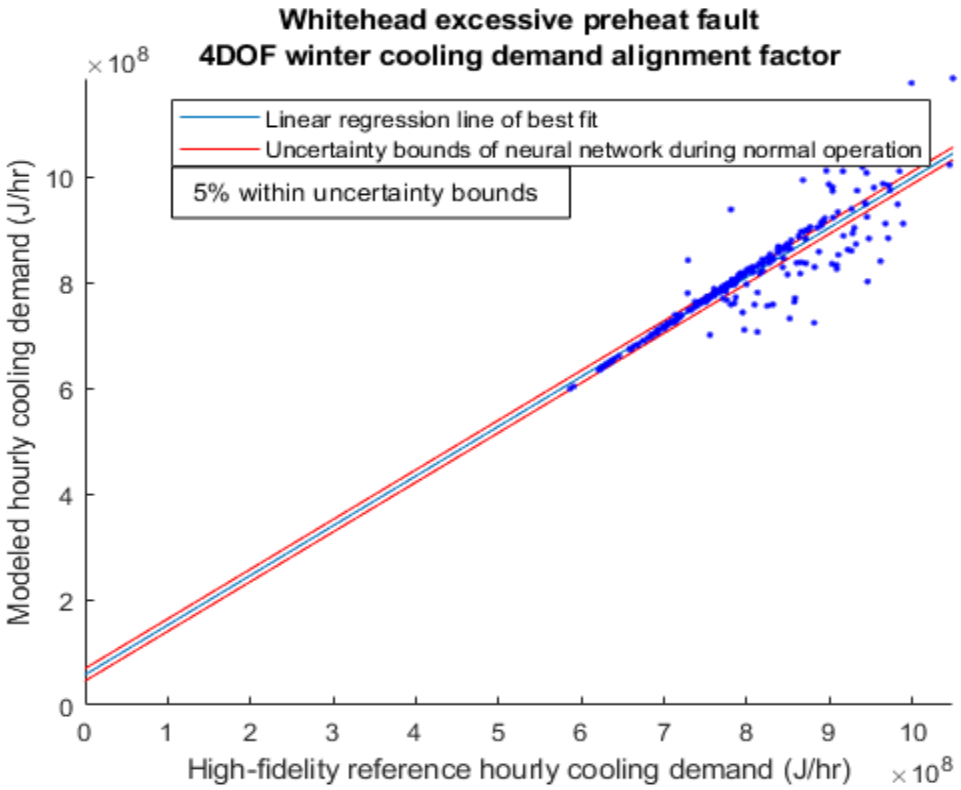

Figure 128: Hourly cooling rate alignment factor for Whitehead model experiencing excessive preheat fault during winter weather

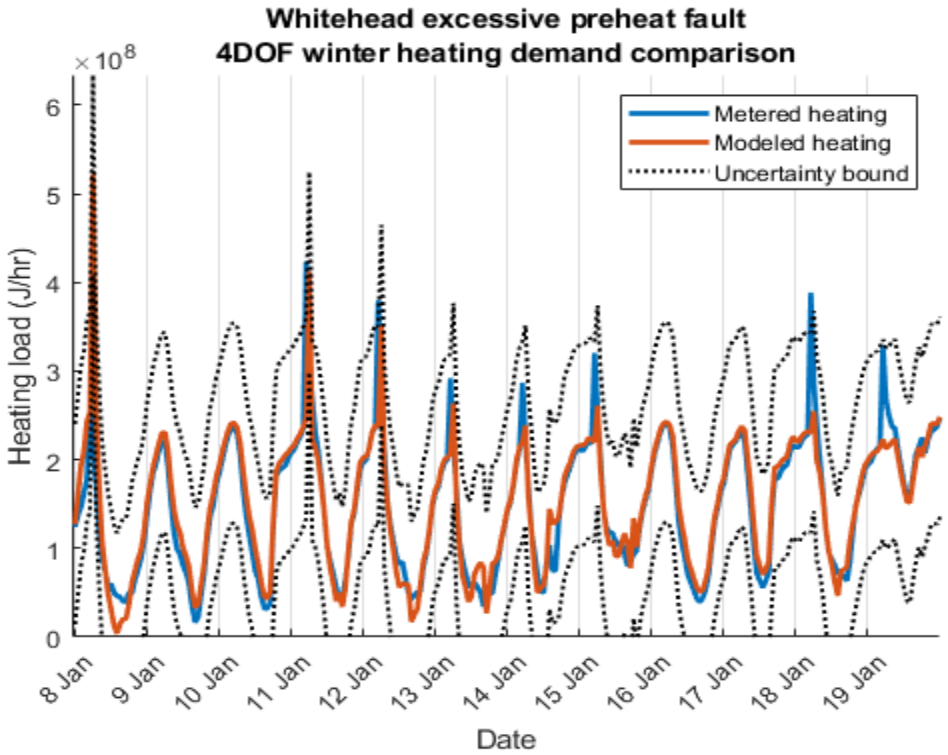

Figure 129: Hourly heating rate for winter weather comparing SPBM and reference data when the building is experiencing a fault of excessive preheat

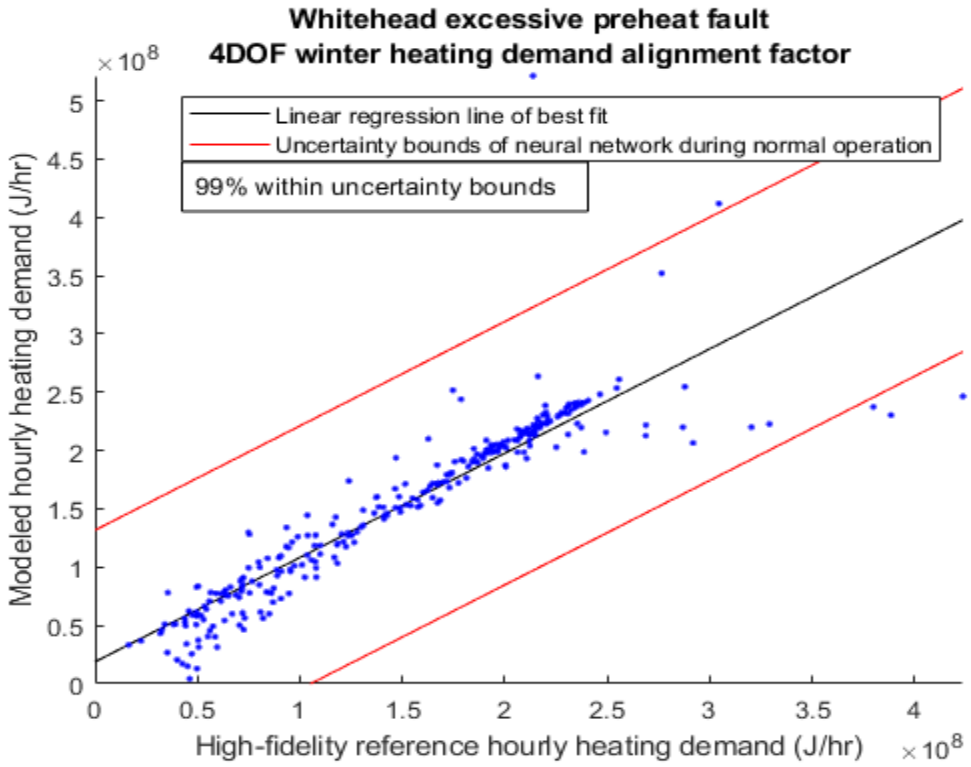

Figure 130: Hourly heating rate alignment factor for Whitehead model experiencing excessive preheat fault during winter weather

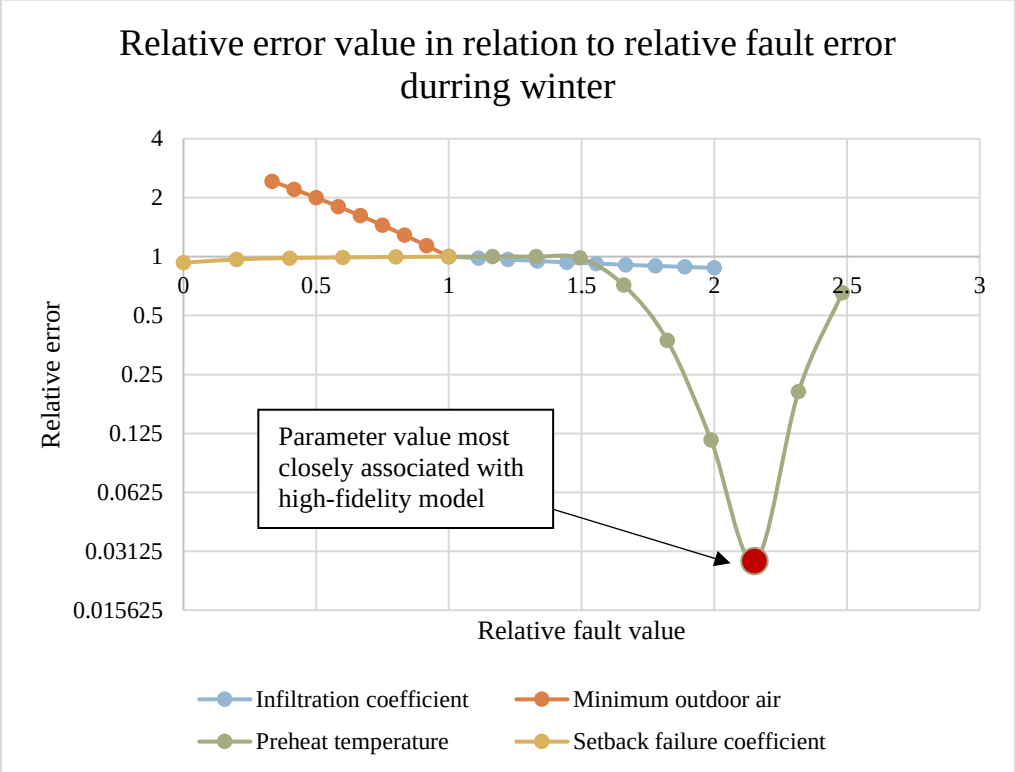

Figure 131: Visual representation of how magnitude of error changes across different magnitudes of the four possible faults. The fault of excessive preheat is being tested for automatic detection for Whitehead building during summer

Preheat fault has a dramatic impact on building load and an equally significant error. Due to the constant increase in both heating and cooling load, any fault that results in additional demand will lower error.

While excessive preheat fault should not be initiated in summer weather, it is possible that excessive preheat could occur from a leaking hot water valve. This scenario could result in a number of different preheat temperatures, but the test was conducted using the same parameters as the winter test for the sake of consistency between runs. Results for summer loading reveal similar results to that for winter. Figure 132 through Figure 135 visually show how the SPBM does have periods of over and under prediction, but the fault test results displayed in Figure 136 and Table 24 confirm the ability to estimate which of the potential faults may be causing the increase in energy consumption in the high-fidelity reference model.

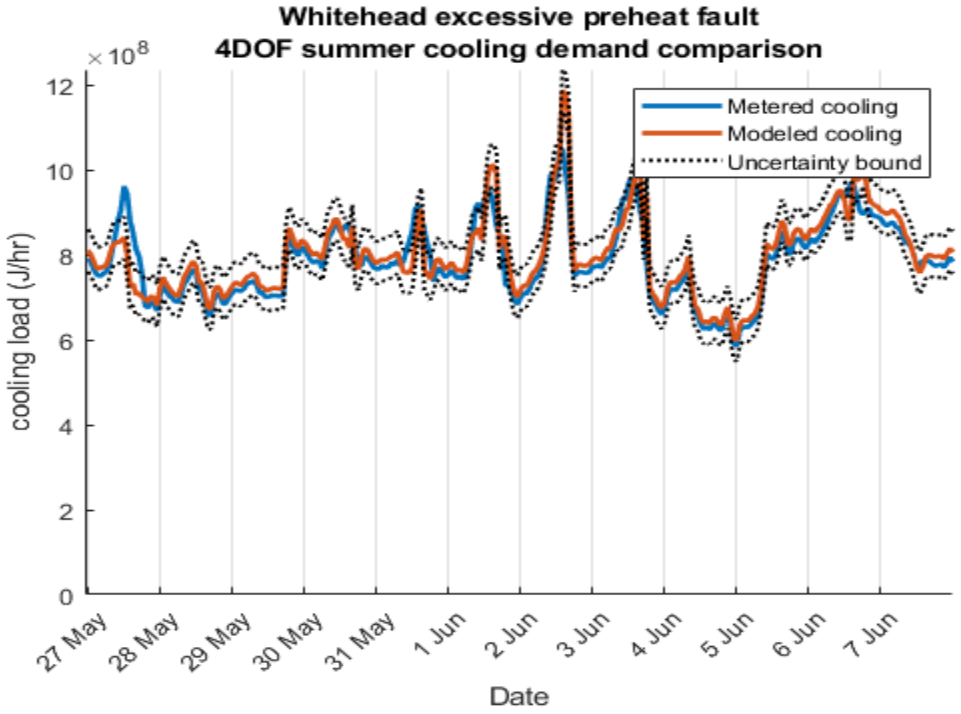

Figure 132: Hourly cooling rate for summer weather comparing SPBM and reference data when the building is experiencing a fault of excessive preheat

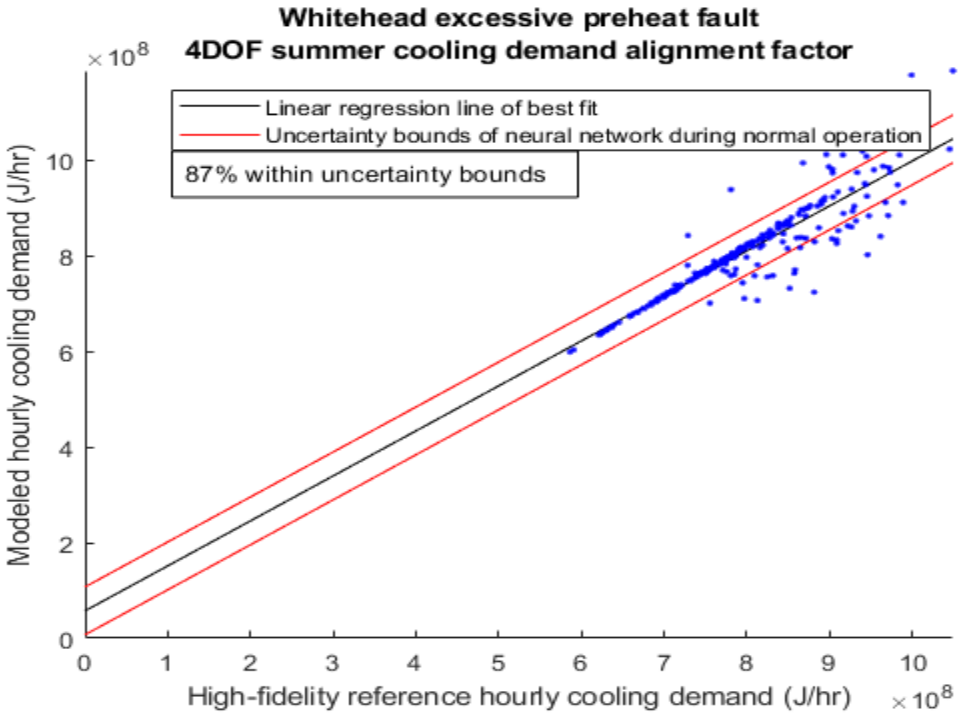

Figure 133: Hourly cooling rate alignment factor for Whitehead model experiencing excessive preheat fault during summer weather

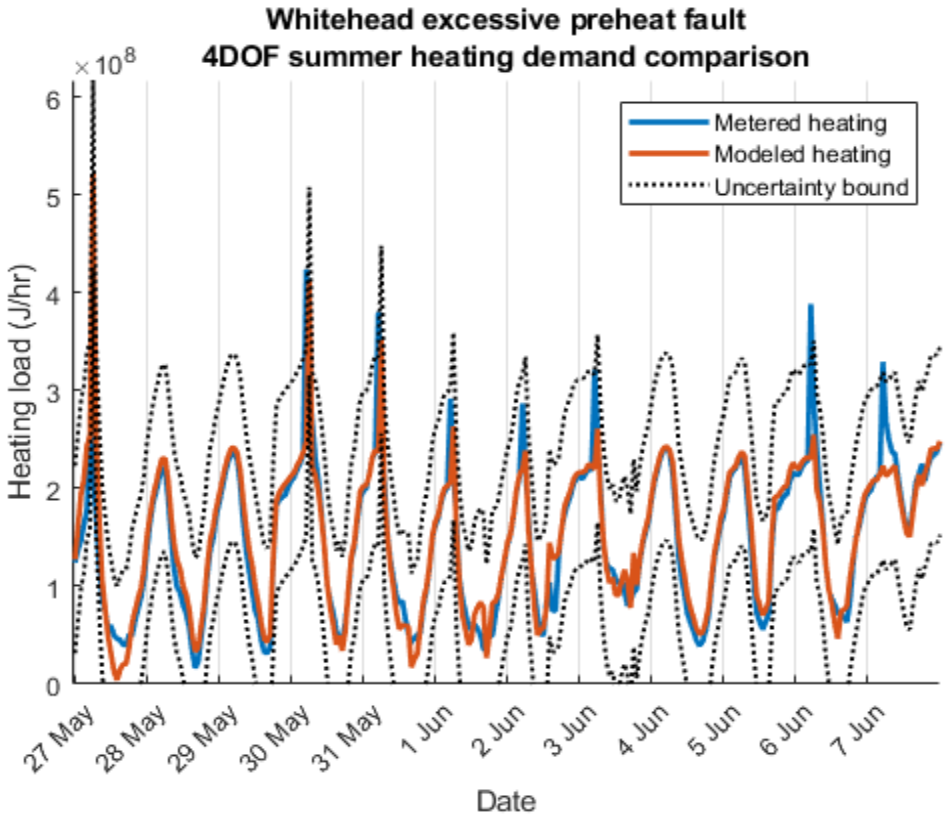

Figure 134: Hourly heating rate for summer weather comparing SPBM and reference data when the building is experiencing a fault of excessive preheat

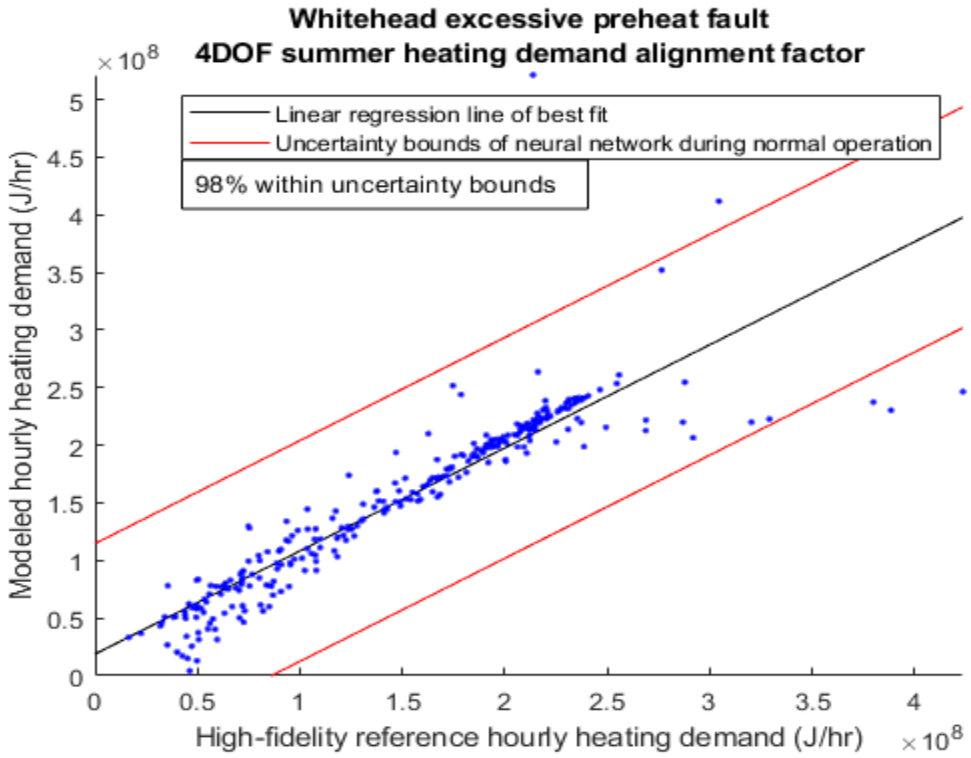

Figure 135: Hourly heating rate alignment factor for Whitehead model experiencing excessive preheat fault during summer weather

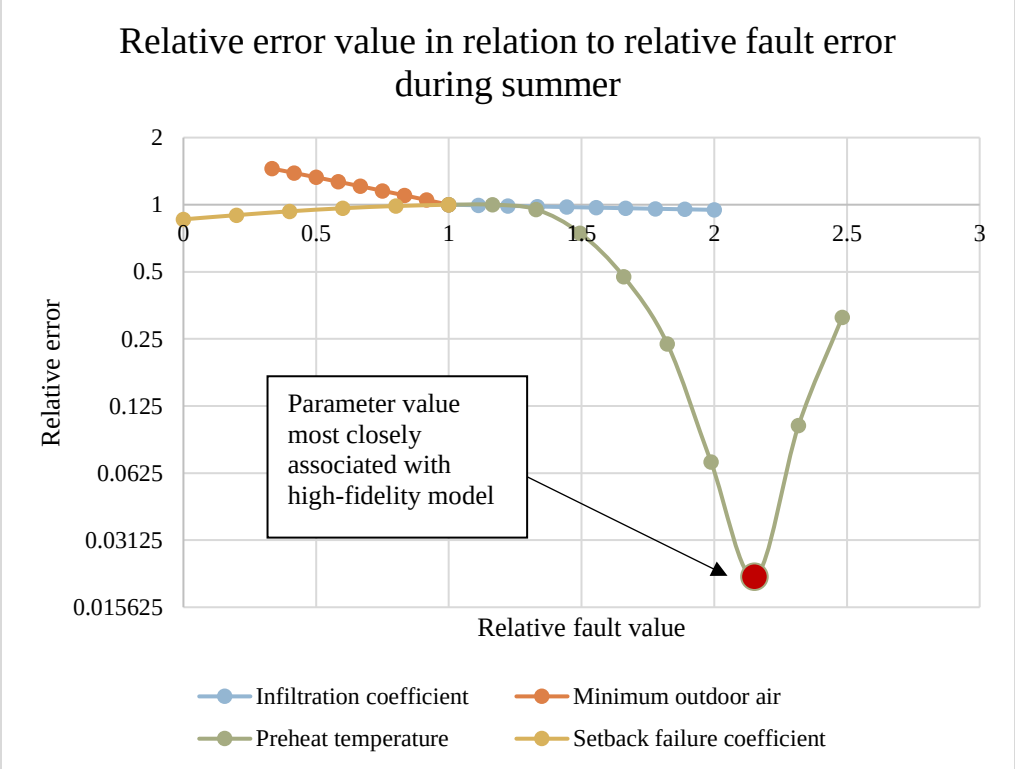

Figure 136: Visual representation of how magnitude of error changes across different magnitudes of the four possible faults. The fault of excessive preheating is being tested for automatic detection for Whitehead building during summer

Similar to winter conditions, excessive preheat in summer still has a large error from increased load yet a clear global minimum is still found.

Excessive preheat is by far the most energy intensive fault being analyzed for automatic fault detection and identification. While some of the results from automatic calibration had a significant number of data points fall outside the prediction interval established by the no-fault calibration, this was due to the no-fault data being nearly constant and the SPBM being in close alignment. However, the alignment factor between the SPBM and metered data remained excellent. While prediction interval data may raise suspicion, analysis of relative fault changes with respect to all the faults being analyzed revealed that excessive preheat had the most significant and consistent reduction in error.

7.2.5 Insufficient Outdoor Air

Insufficient outdoor air presents a unique challenge as testing has revealed that lowering outdoor air flow rates often appear as a reduction in cooling and heating load demand. However, low outdoor air flow rates may have negative health results on occupants . Given the global impact of COVID-19, it is not unreasonable to assume that prioritizing occupant health and disease prevention will become a higher priority for building managers and designers.

Evaluation of automatic fault detection results reveal an overall good performance of cooling load alignment, as demonstrated in Figure 137 and Figure 138. Even though less than 80% of data was within uncertainty bounds, the relatively low alignment was a result of a tight uncertainty under nominal conditions due to there being a near constant cooling demand while insufficient outdoor air resulted in increases in cooling load during

occupied periods. However, Figure 139 and Figure 140 demonstrate accuracy similar to nominal performance. Error reduction results presented in Figure 141 and Table 25 reveal a high degree of model sensitivity to lower outdoor air fault results. Evaluation of winter model results is perhaps the most representative result for SPBM automatic fault detection; the "true" value of outdoor air flow rate is not important, but rather the growth of error for every tested parameter aside from outdoor air flow rate for both winter and summer loading conditions.

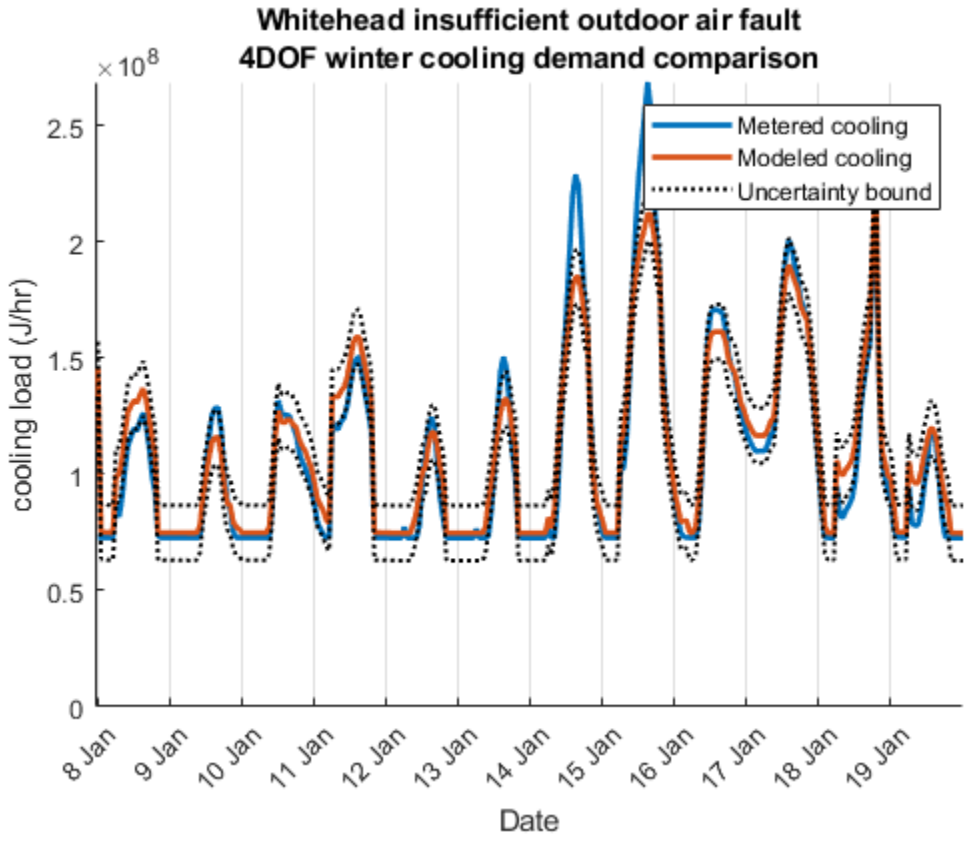

Figure 137: Hourly cooling rate for winter weather comparing SPBM and reference data when the building is experiencing a fault of insufficient outdoor air

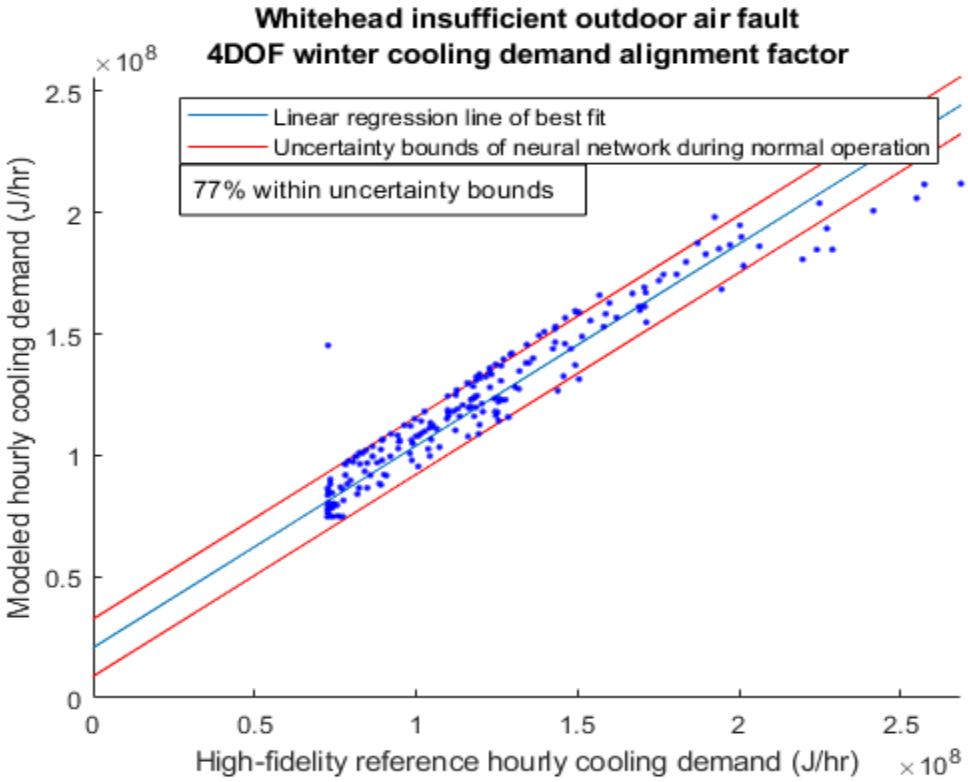

Figure 138: Hourly cooling rate alignment factor for Whitehead model experiencing insufficient outdoor air fault during winter weather

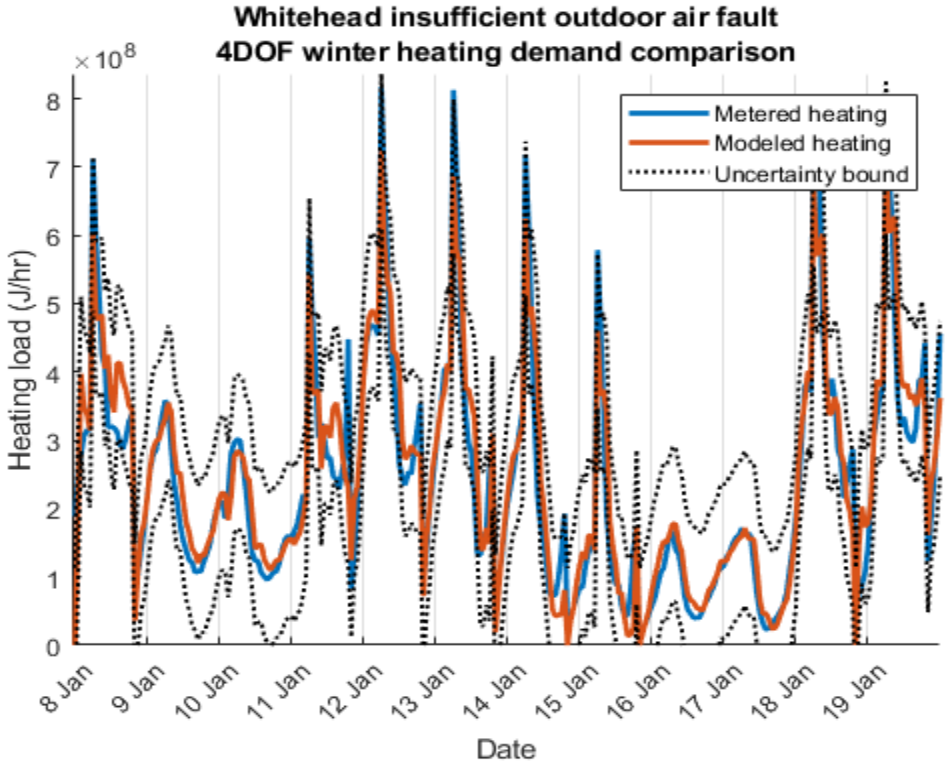

Figure 139: Hourly heating rate for winter weather comparing SPBM and reference data when the building is experiencing a fault of insufficient outdoor air

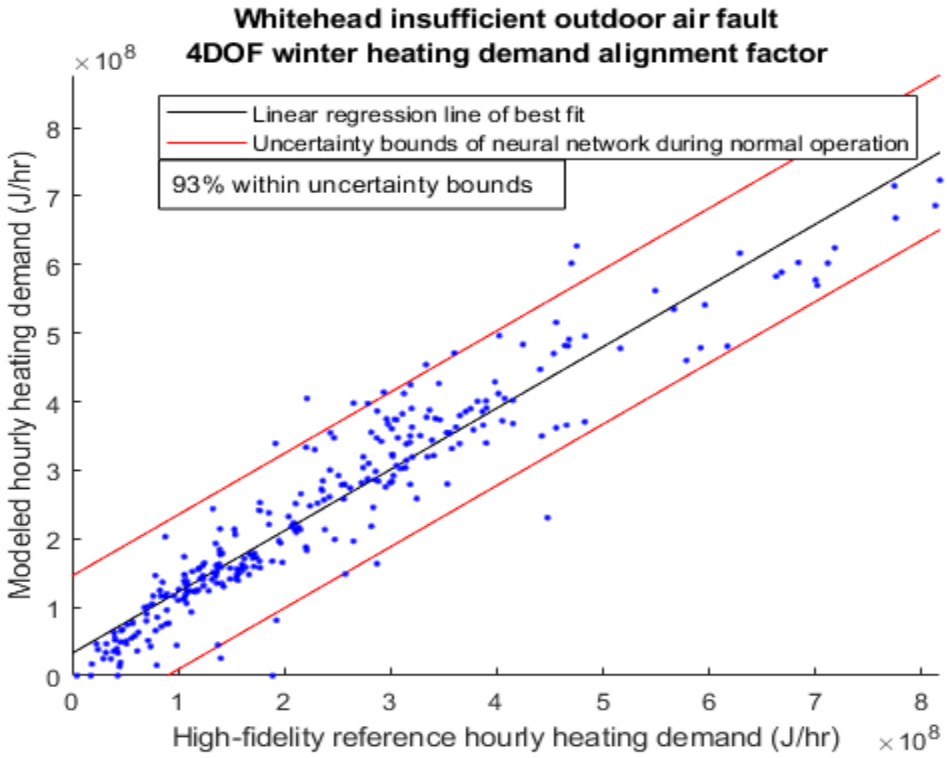

Figure 140: Hourly heating rate alignment factor for Whitehead model experiencing insufficient outdoor air fault during winter weather

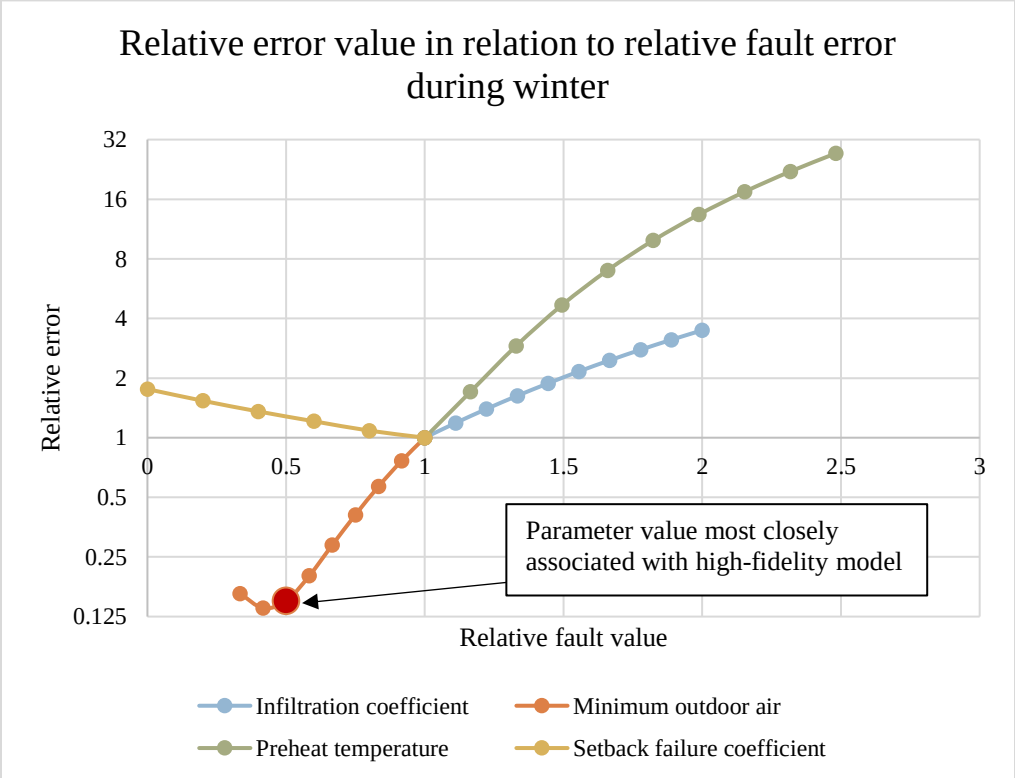

Figure 141: Visual representation of how magnitude of error changes across different magnitudes of the four possible faults. The fault of insufficient outdoor air is being tested for automatic detection for Whitehead building during winter

Insufficient outdoor air is unique among the four tested faults as it is the only fault that reduces load; therefore, other faults will show an increase in error as demand rises.

As stated for winter loading conditions, the SPBM displays adequate modeling ability when comparing to a high-fidelity reference model. Figure 142 through Figure 145 reflect previous summer loading results as well as the high level of agreement displayed for winter loading. Additionally, Figure 146 and Table 26 show the best summer loading results for automatic fault detection with only one of the four tested faults resulting in a reduction of error. These results are attributed to the reduction in heating and cooling demand that insufficient outdoor air provides while the other faults tend to display an increase in load demand when present.

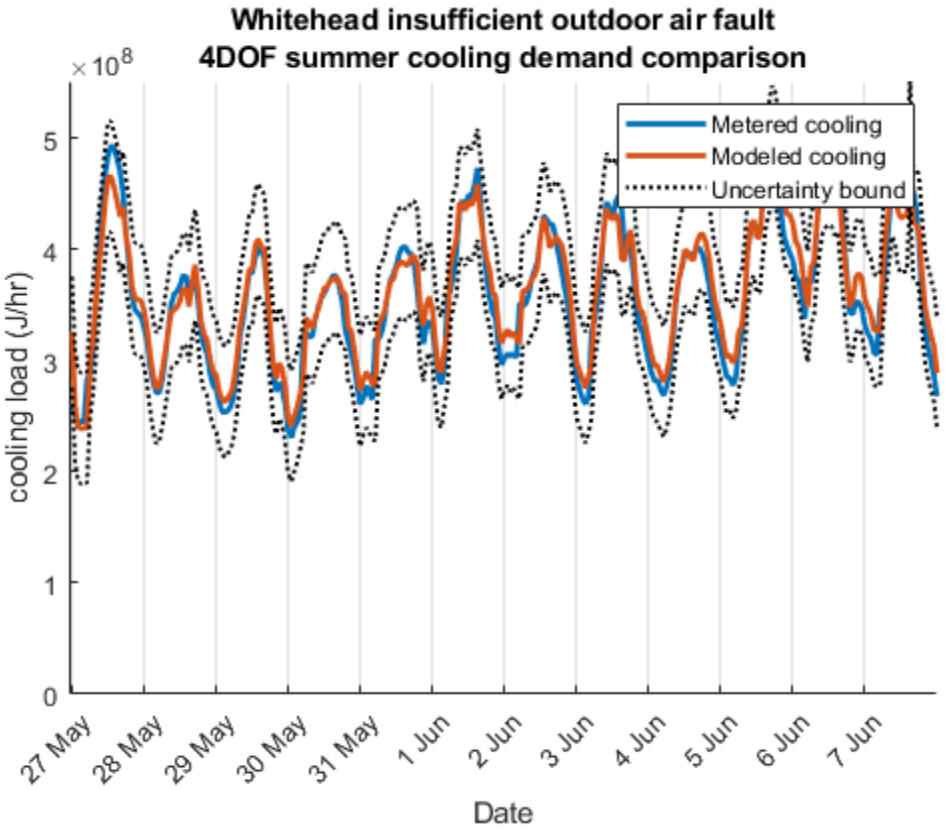

Figure 142: Hourly cooling rate for summer weather comparing SPBM and reference data when the building is experiencing a fault of insufficient outdoor air

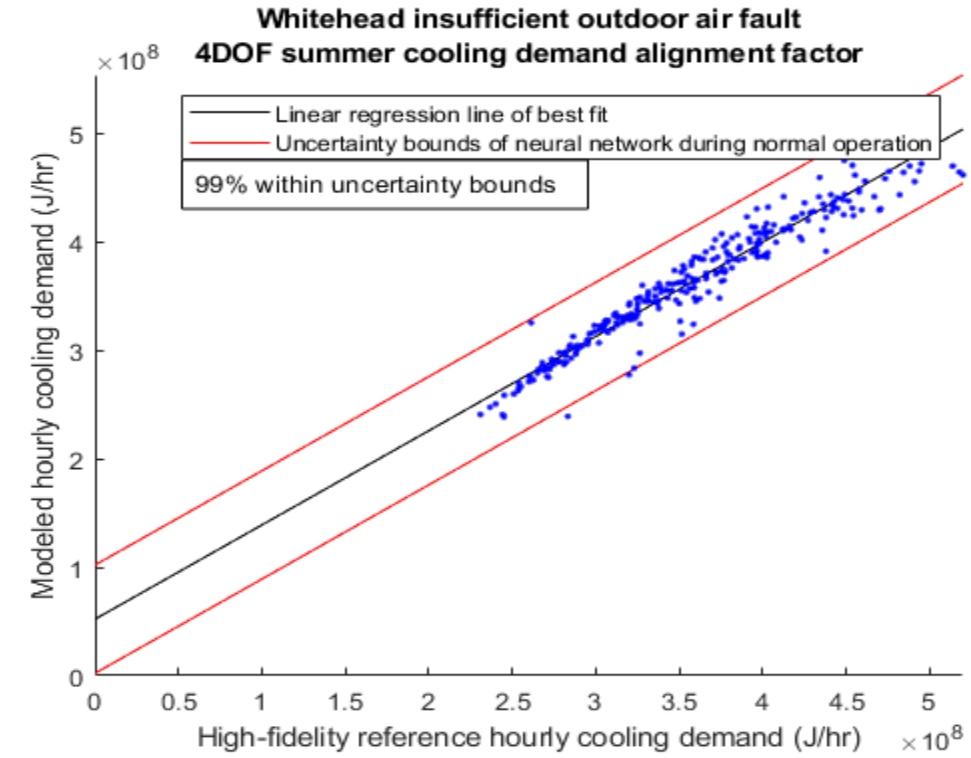

Figure 143: Hourly cooling rate alignment factor for Whitehead model experiencing insufficient outdoor air fault during summer weather

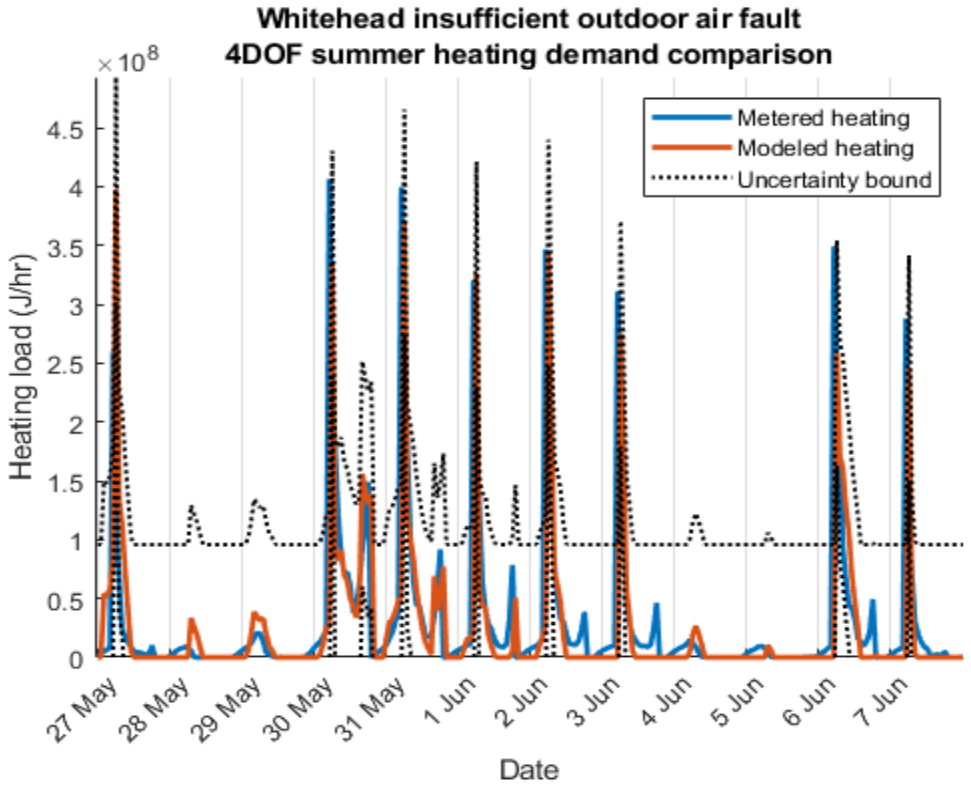

Figure 144: Hourly heating rate for summer weather comparing SPBM and reference data when the building is experiencing a fault of insufficient outdoor air

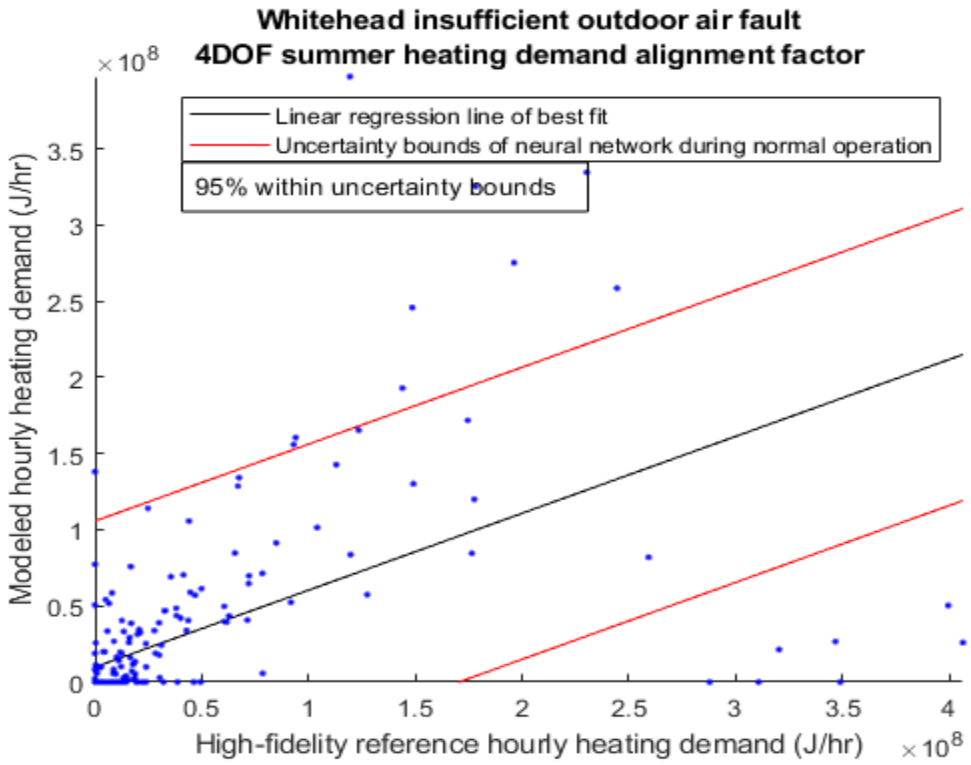

Figure 145: Hourly heating rate alignment factor for Whitehead model experiencing insufficient outdoor air fault during summer weather

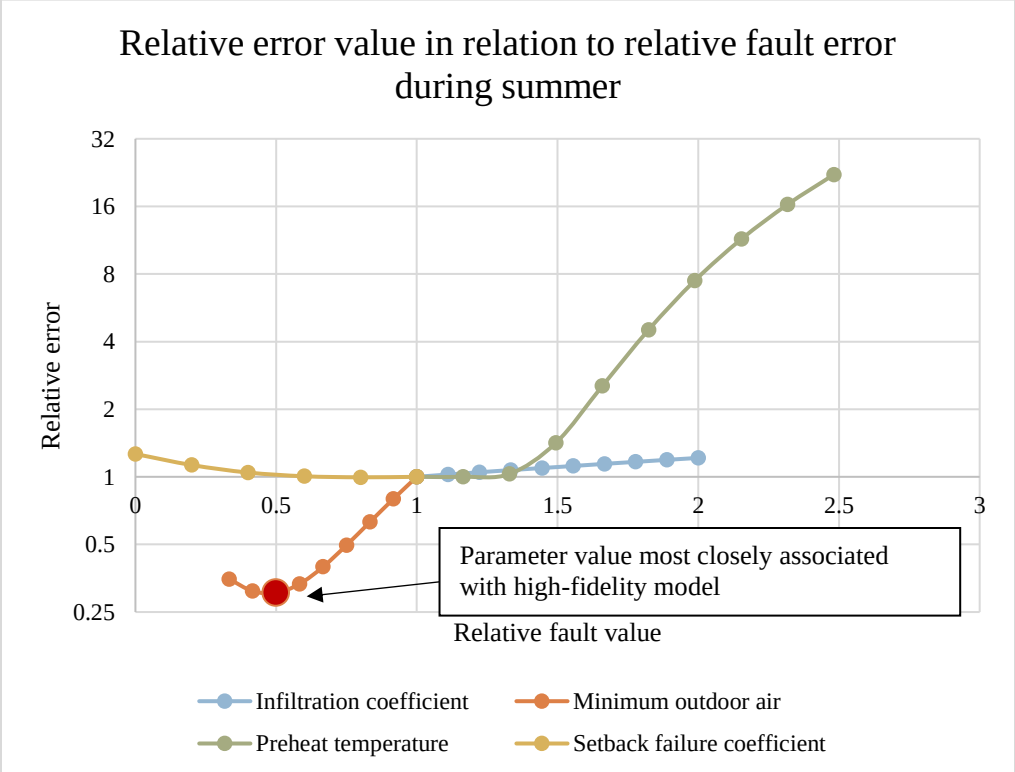

Figure 146: Visual representation of how magnitude of error changes across different magnitudes of the four possible faults. The fault of insufficient outdoor air is being tested for automatic detection for Whitehead building during summer

The increase in error from setback failure and infiltration is minimal as nominal parameter values already results in overprediction of loading. Nevertheless, minimum outdoor air fault was still successfully identified and classified.

As demonstrated above, the SPBM was able to replicate loading results of a high-fidelity reference model for all of the tested faults. Additionally, results demonstrated the uniqueness of how faults alter heating and cooling demands in a unique manner. As stated previously, Whitehead Building is being treated as a representation of a typical office building that experiences a similar internal load all year. However, Old CE is representative of a typical university classroom and office building with varying loads depending on the year. The following section will evaluate Old CE and see if the SPBM is capable of producing similar results for automatic fault detection that Whitehead Building demonstrated.

7.3 Old CE Automatic Fault Detection

To quickly review, Old CE is a legacy building that houses academic offices, classrooms that vary in use depending on the time of year, and a small library. Additionally, the HVAC configuration of Old CE is more complex than that of Whitehead's in that the building uses three separate air handling units, two total energy wheels, scheduled air flow rates, and outdoor air economizers. Despite an increase in complexity, the following analysis reveals that the SPBM more than capable of modeling this building. Nominal operation of Old CE for winter and summer is depicted in Figure 147; note how demand changes abruptly when the building switches between occupied and unoccupied states.

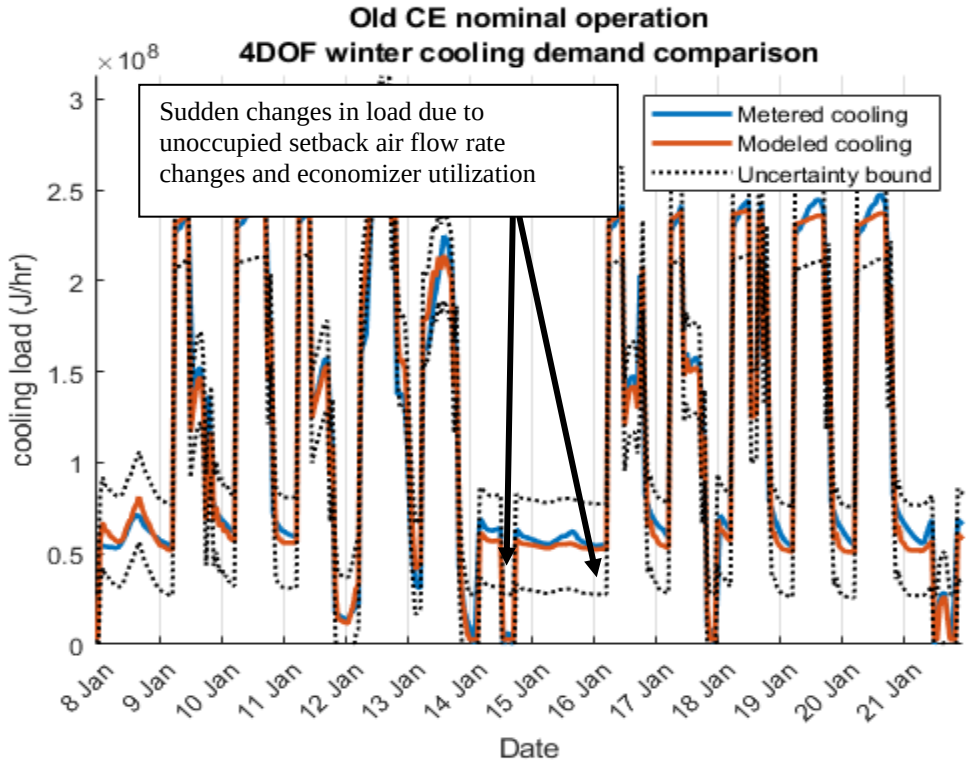

Figure 147A: SPBM cooling load accuracy during nominal operation of Old CE for winter weather

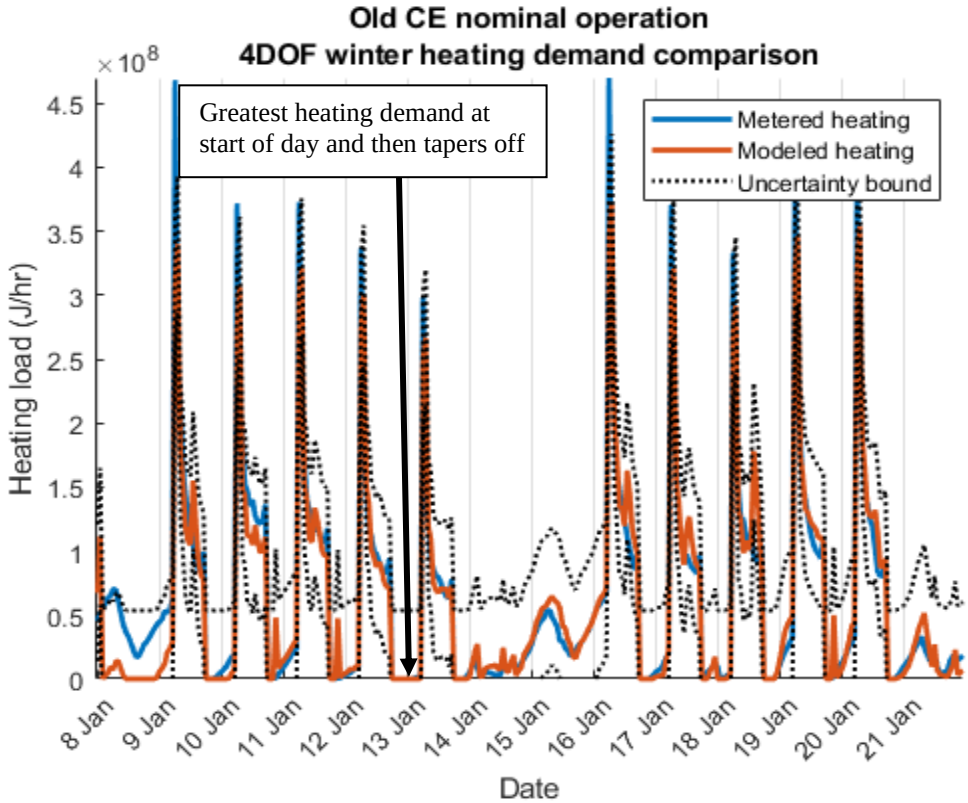

Figure 147B: SPBM heating load accuracy during nominal operation of Old CE for winter weather

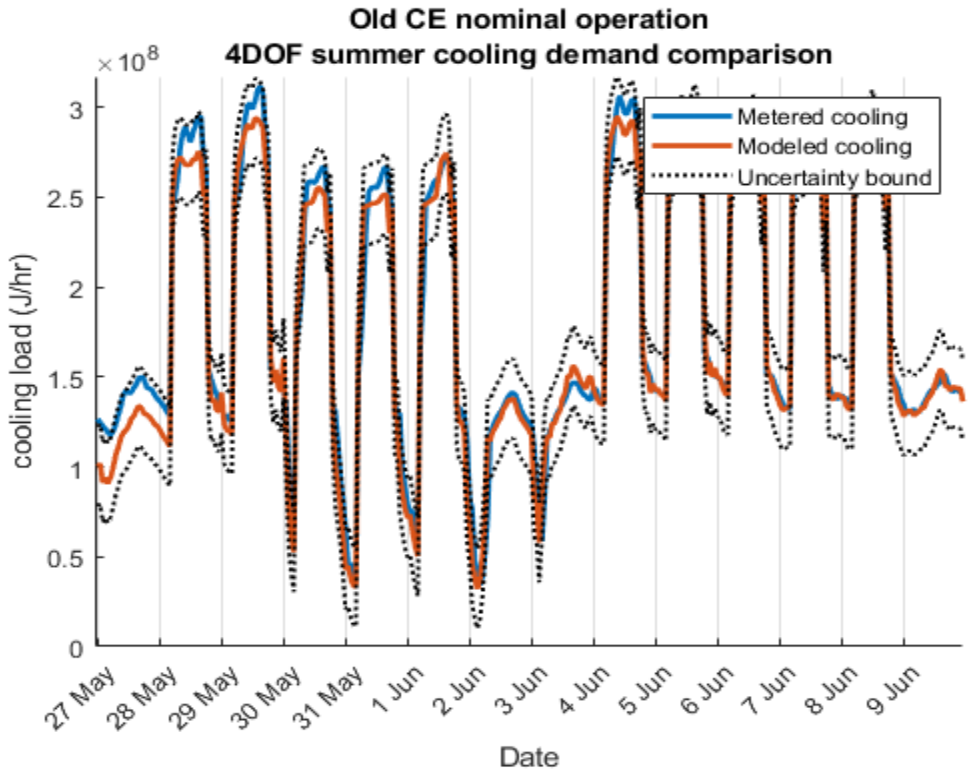

Figure 147C: SPBM cooling load accuracy during nominal operation of Old CE for summer weather

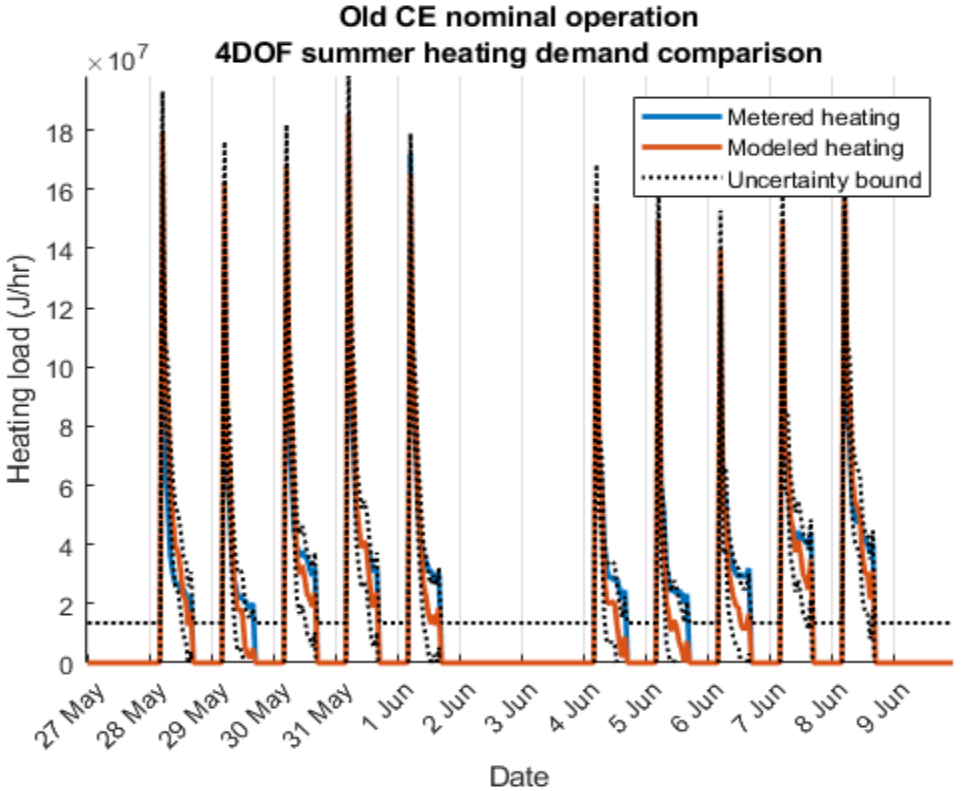

Figure 147D: SPBM heating load accuracy during nominal operation of Old CE for summer weather

It is theorized that the building, and therefore metered loads, experience a greater change in heating and cooling demand percent change per unit variance in HVAC system. The greater building sensitivity also makes automatic calibration easier and on average required fewer iterations to converge on a solution when compared to Whitehead automatic calibration. Old CE will be experiencing the same fault tests as Whitehead: excessive infiltration, not entering unoccupied setback, excessive preheat, and insufficient outdoor air.

7.3.1 Old CE Infiltration

Infiltration, as stated before, is when outdoor air enters through the building envelope. For purposes of model evaluation, and based on experience with building energy consumption analysis and the US Department of Energy, it is assumed that infiltration correlates with wind speed. It should be noted that determining the actual infiltration of a building is difficult without conducting field measurements.

Old CE demonstrated in the figures below and Table 27 that the building HVAC system is not as sensitive to infiltration as Whitehead while showing greater increase in error when testing the other faults. The reduction in sensitivity to infiltration is attributed to there being a basement level and much of the perimeter zones on higher levels being unoccupied providing less access for outdoor air to enter the building.

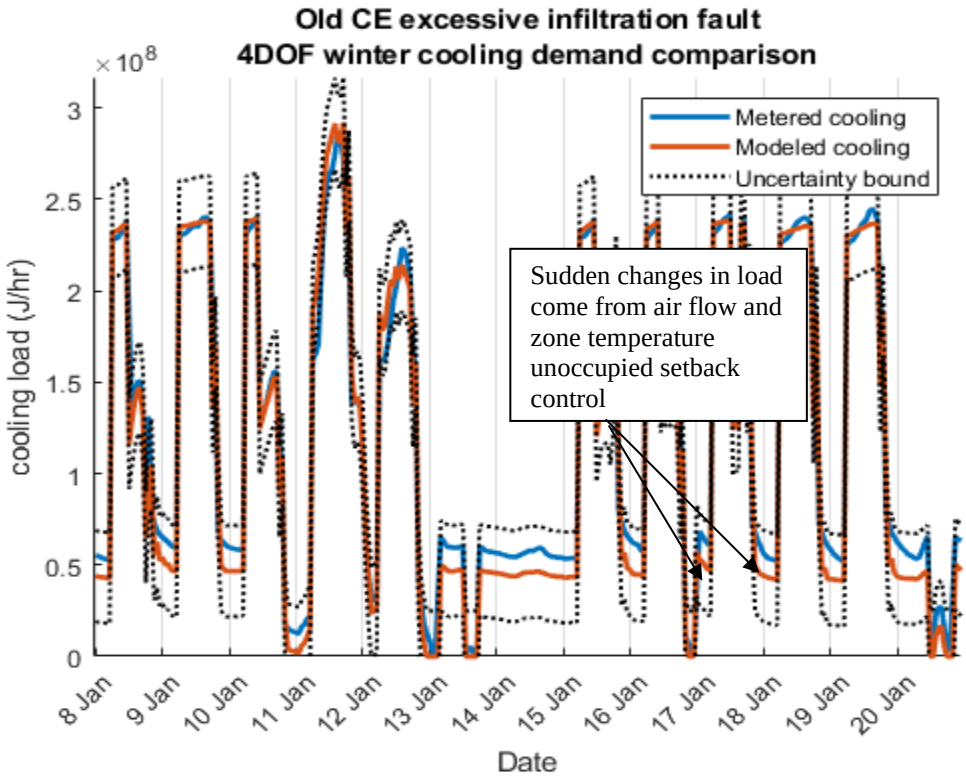

Figure 148: Hourly cooling rate for winter weather comparing SPBM and reference data when the building is experiencing a fault of excessive infiltration

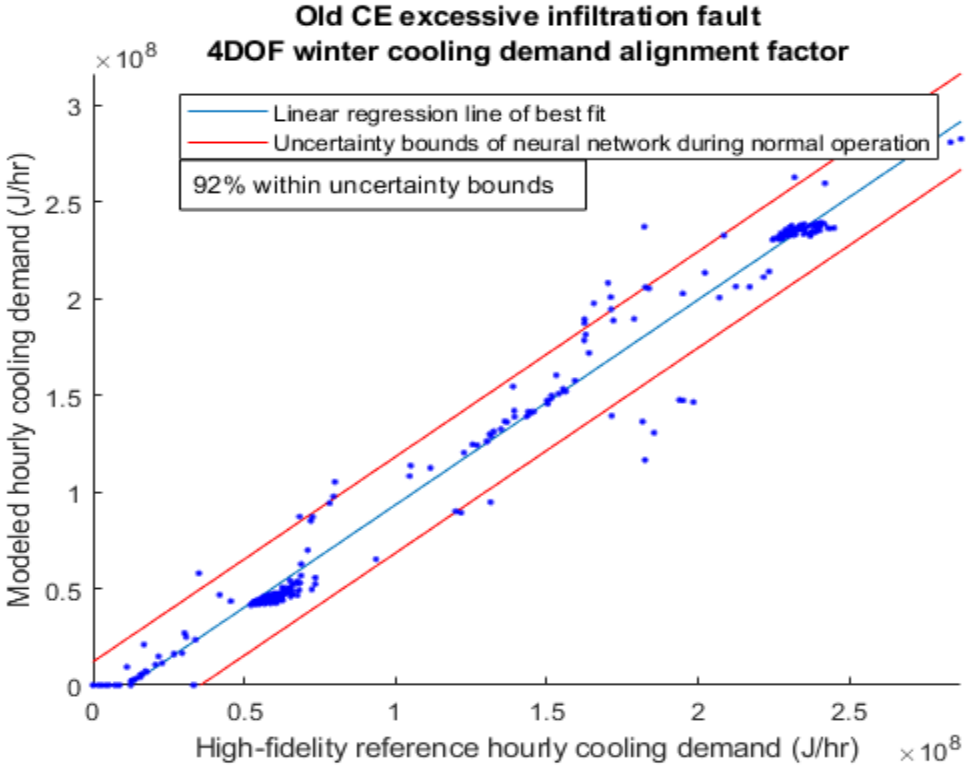

Figure 149: Hourly cooling rate alignment factor for Whitehead model experiencing excessive infiltration fault during winter weather

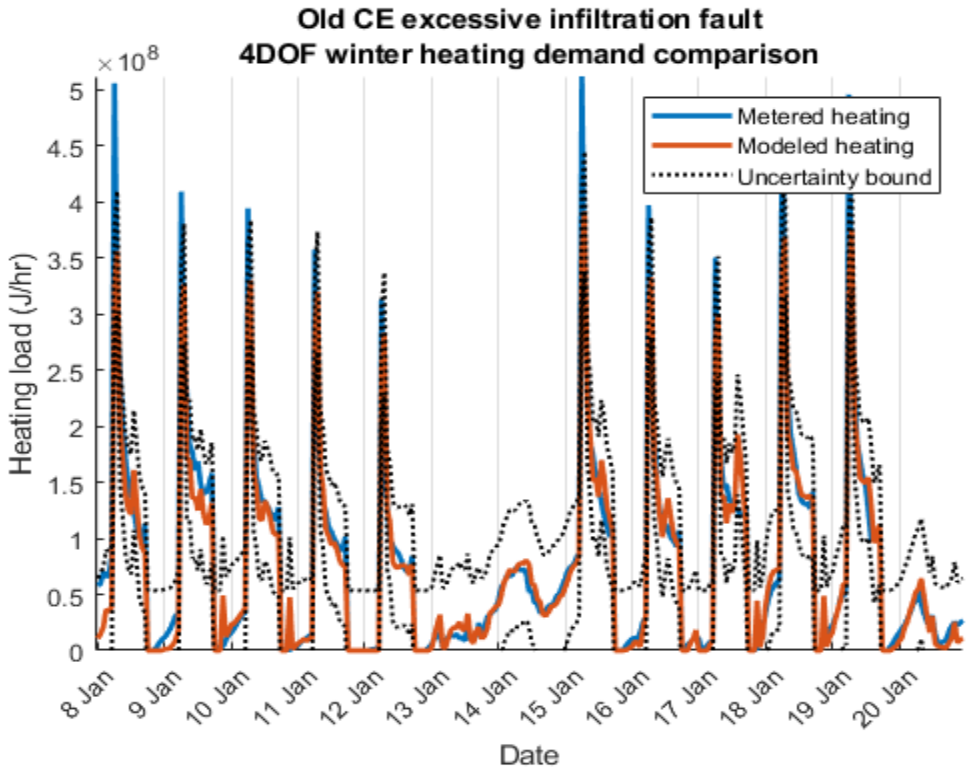

Figure 150: Hourly heating rate for winter weather comparing SPBM and reference data when the building is experiencing a fault of excessive infiltration

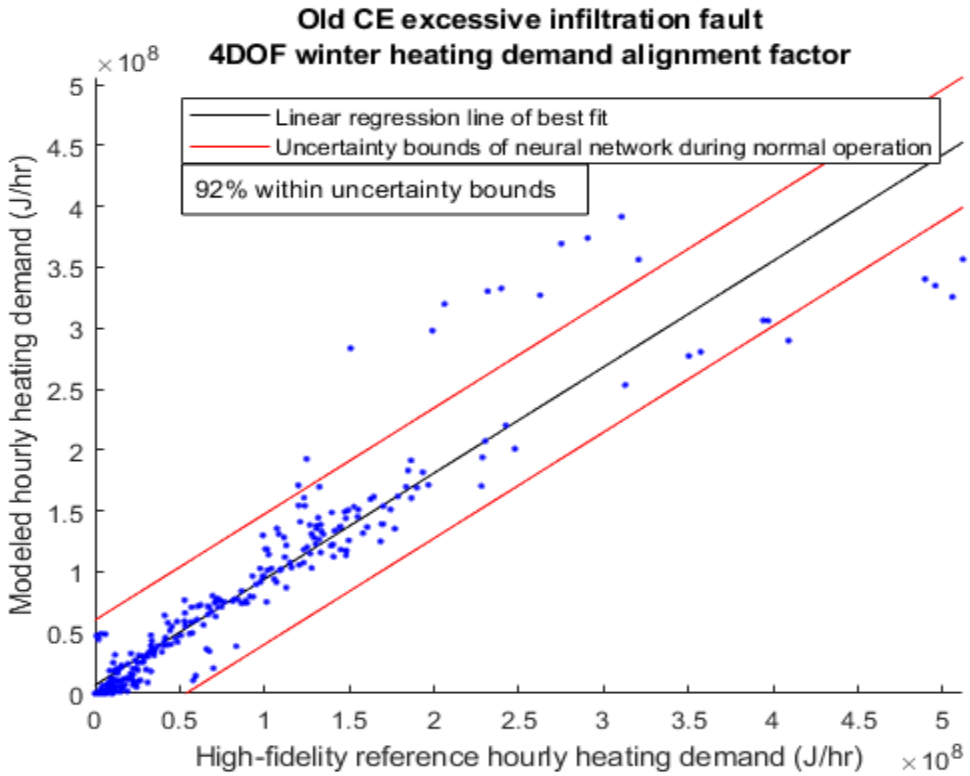

Figure 151: Hourly heating rate alignment factor for Whitehead model experiencing excessive infiltration fault during winter weather

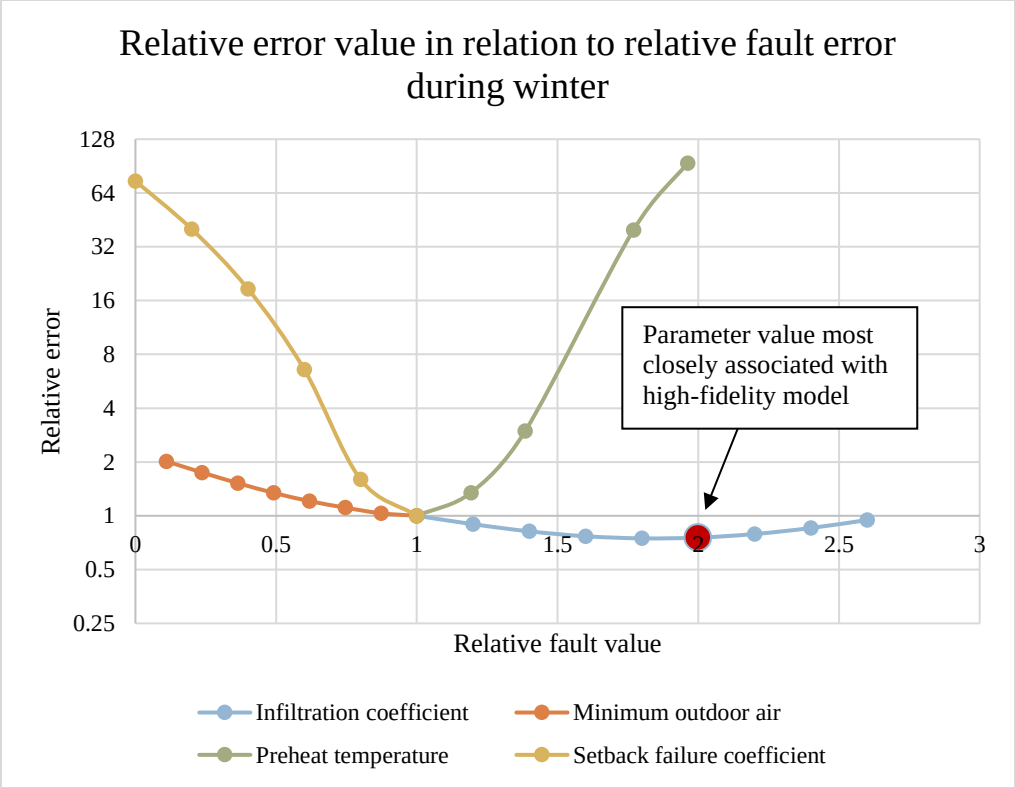

Figure 152: Visual representation of how magnitude of error changes across different magnitudes of the four possible faults. The fault of excessive infiltration is being tested for automatic detection for Old CE during winter

The error reduction for infiltration during winter weather is wider and shallower when compared to Whitehead. The broader error profile is due to there being less overall infiltration and the faulty infiltration high-fidelity parameter being twice that of nominal conditions (0.1 instead of 0.05 for nominal condition).

Modeled performance, as shown in Figure 153 through Figure 157, for excessive infiltration during summer weather for Old CE produced acceptable model accuracy. However, Figure 157 and Table 28 reveal that parameter estimation was less definitive than during winter weather, a trend mirrored during Whitehead testing. This reduced difference in error was due to Old CE not having a substantial amount of infiltration based on calibration efforts (a velocity wind speed coefficient for Old CE was less than

half the DOE2 recommended coefficient of 0.224). Additionally, wind speeds in summer were lower than in winter and often lower than the 5 m/s reference speed used by DOE2. However, given that CO2 monitoring in AHUs is not expensive and knowing the benefits of occupant health associated with outdoor air flow, infiltration error will be tested also using CO2 monitoring to see if any improvement can be made.

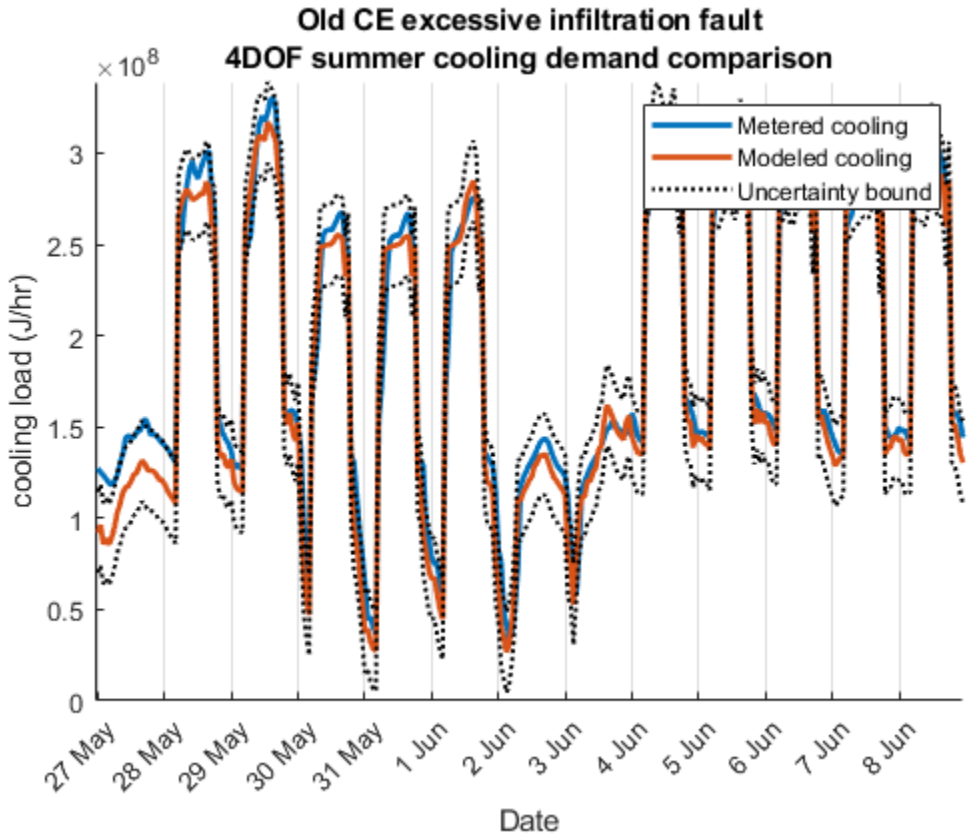

Figure 153: Hourly cooling rate for summer weather comparing SPBM and reference data when the building is experiencing a fault of excessive infiltration

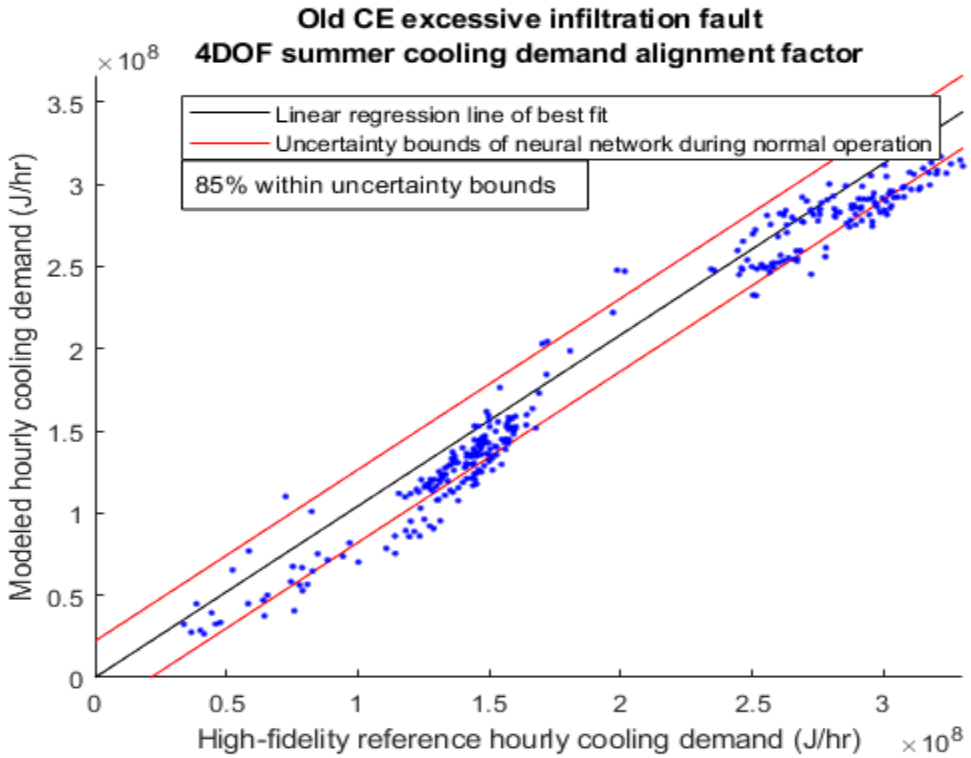

Figure 154: Hourly cooling rate alignment factor for Whitehead model experiencing excessive infiltration fault during summer weather

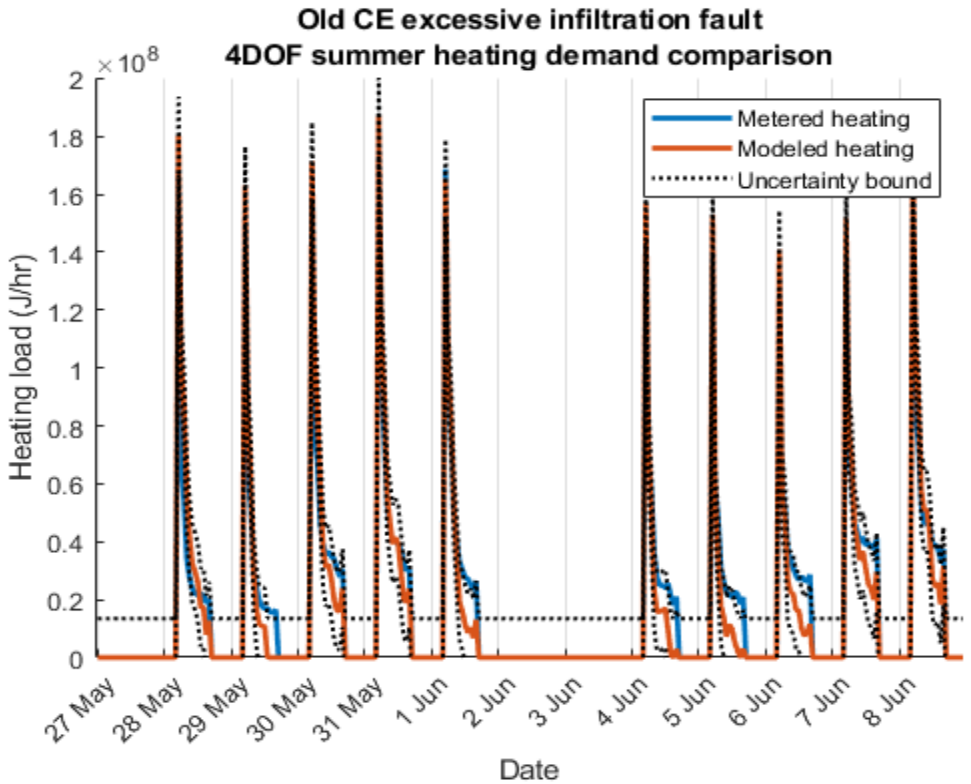

Figure 155: Hourly heating rate for summer weather comparing SPBM and reference data when the building is experiencing a fault of excessive infiltration

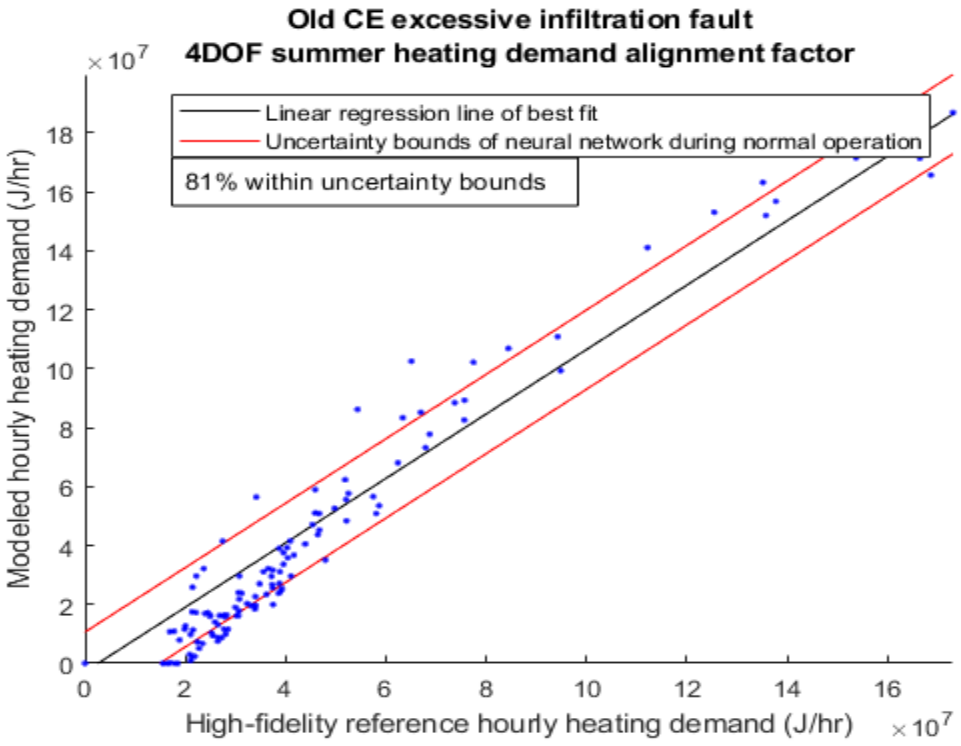

Figure 156: Hourly heating rate alignment factor for Whitehead model experiencing excessive infiltration fault during summer weather

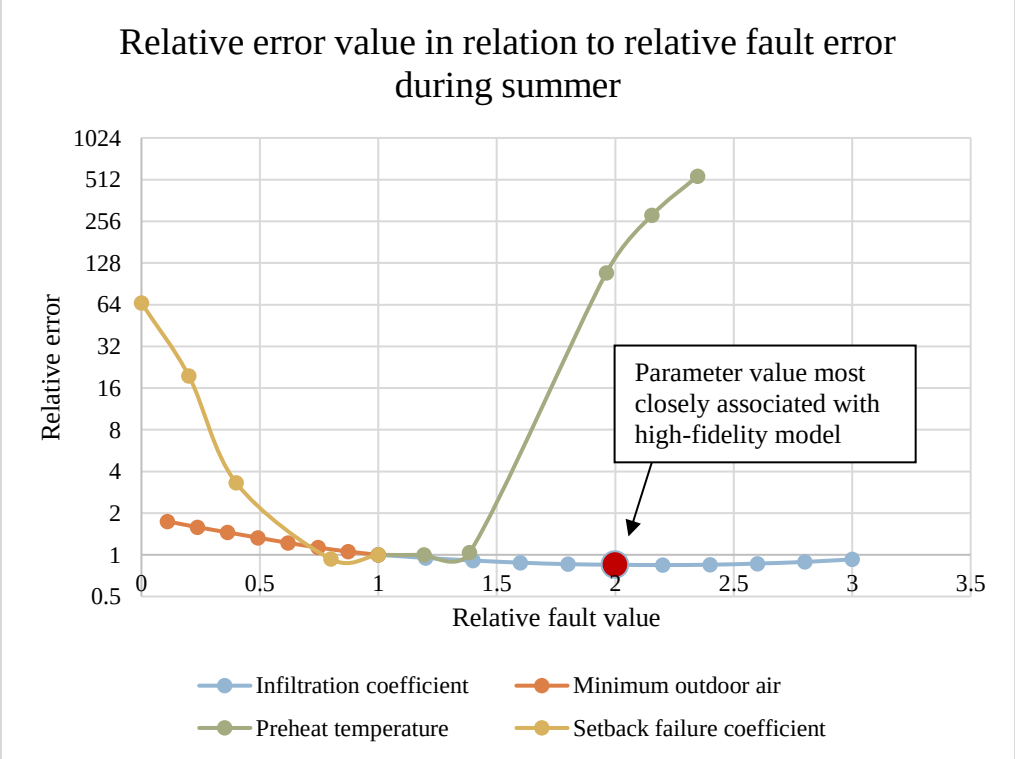

Figure 157: Visual representation of how magnitude of error changes across different magnitudes of the four possible faults. The fault associated with cooling load when testing excessive infiltration is being tested for automatic detection for Old CE during summer

Evaluation of Old CE with excessive infiltration using CO2 analysis resulted in a clear and unique result. Unoccupied setback and preheat failure do not affect air flow or zone CO2 contamination rates and therefore error remains unchanged for all parameter values, as shown in Figure 160 and Table 29. Reducing outdoor air flow rate increases CO2 concentration while infiltration lowers zone contaminate levels through increased outdoor air.

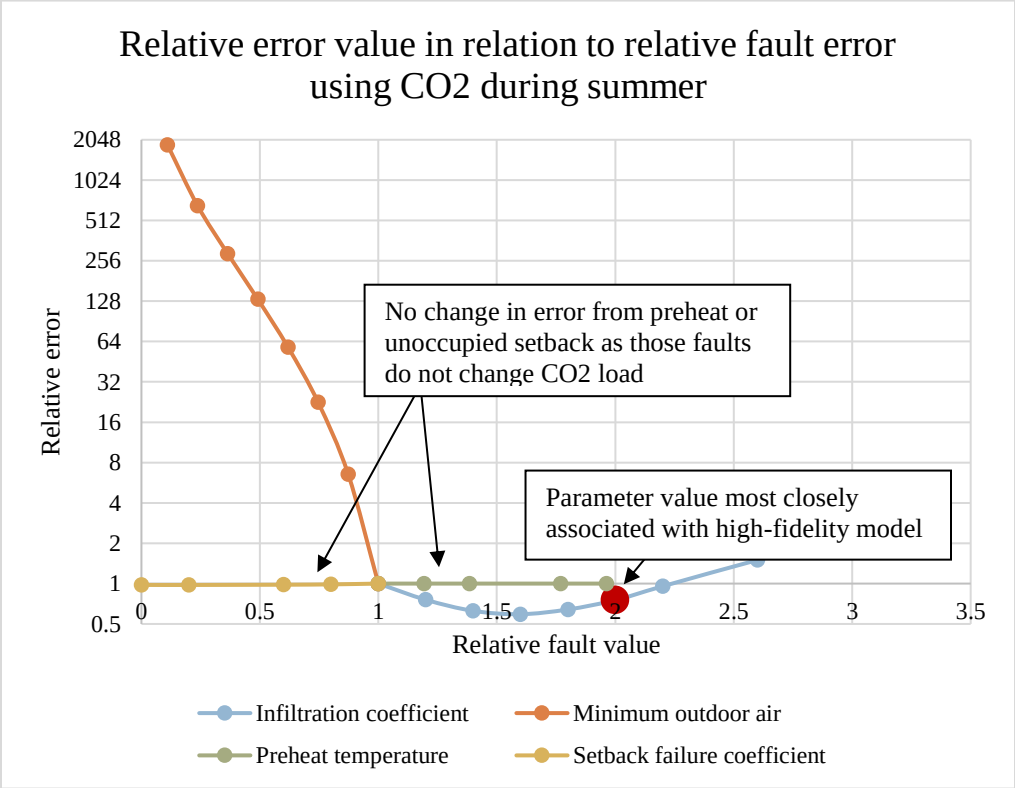

Figure 158: Visual representation of how magnitude of error changes across different magnitudes of the four possible faults. The fault associated with CO2 when testing excessive infiltration is being tested for automatic detection for Old CE during summer

SPBM results can be self-checking by keeping model parameters constant but evaluating error of multiple data points. Different error parameters can also be used with neural networks, but as stated before, a neural network has one output and would require a different NN for each parameter being tested.

7.3.2 Old CE no Unoccupied Setback

Failure to enter unoccupied setback has a more severe impact on energy use when compared to Whitehead. While Whitehead only altered zone temperature setpoints with unoccupied periods, Old CE implements a reduction in air flow rate in addition to widening zone temperature setpoints. On average, minimum air flow to zones is halved for unoccupied periods. Failure to reduce air flow not only increases both heating and cooling demand, but also produces a noticeable increase in heating load while simultaneously maintaining a constant cooling demand, as demonstrated in Figure 161 and Figure 159 respectively.

Increase in heating demand during unoccupied periods is caused from supply air at 13°C maintaining the same flow rate as during occupied periods without environmental or internal heating loads. Additionally, zone temperature setpoints during occupied periods are wider than during occupied periods, with the minimum air temperature being maintained at 21°C for occupied periods and 16.5°C for unoccupied periods.

Conversely, cooling demand remains nearly constant during winter weather when there is a failure to enter unoccupied setback. While one may expect a change in cooling demand during evenings, it is important to remember that zone temperatures often remain at their minimum setpoint during winter weather. Therefore, temperature of the retuning air does not fluctuate substantially throughout the day. Energy recovery wheels also dampen fluctuations of outdoor air temperatures which further reduces variations in cooling demand. Regardless of the challenges associated with modeling an energy

conscious building, there can sometimes be a benefit when it comes to automatic calibration and fault detection. As shown from Figure 159 through Figure 163, the SPBM demonstrated excellent cooling demand modeling performance and acceptable heating demand results. These results lead to a clear solution when evaluating fault identification in Figure 163 and Table 30.

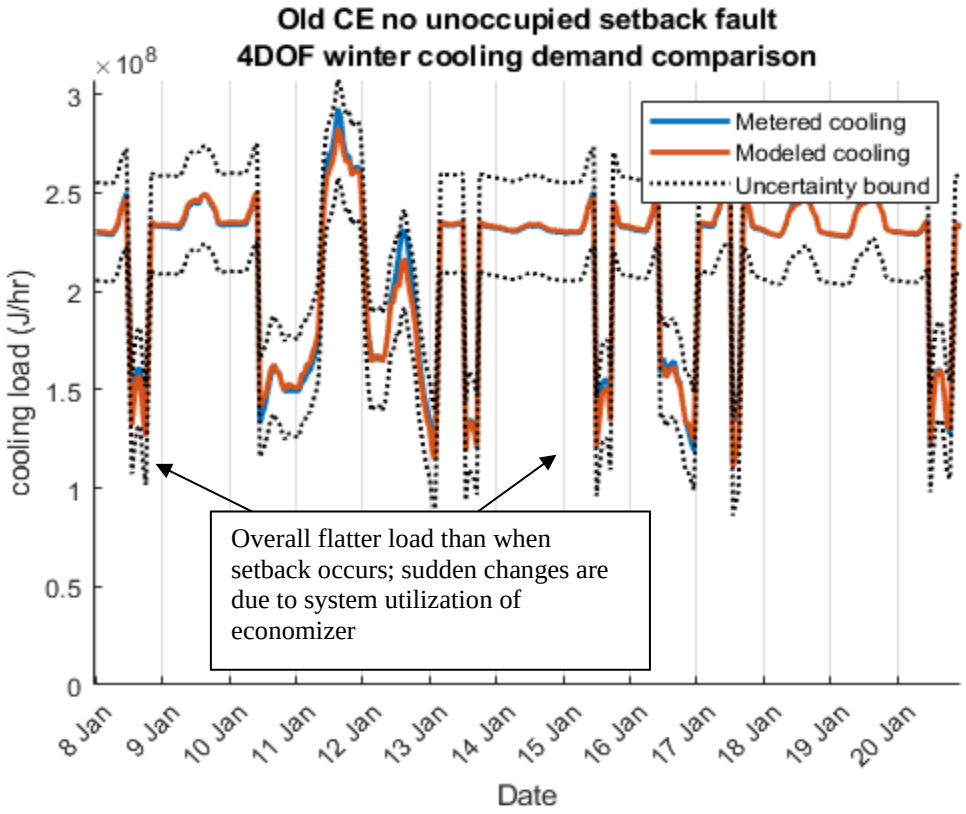

Figure 159: Hourly cooling rate for winter weather comparing SPBM and reference data when the building is experiencing a fault of not entering unoccupied setback

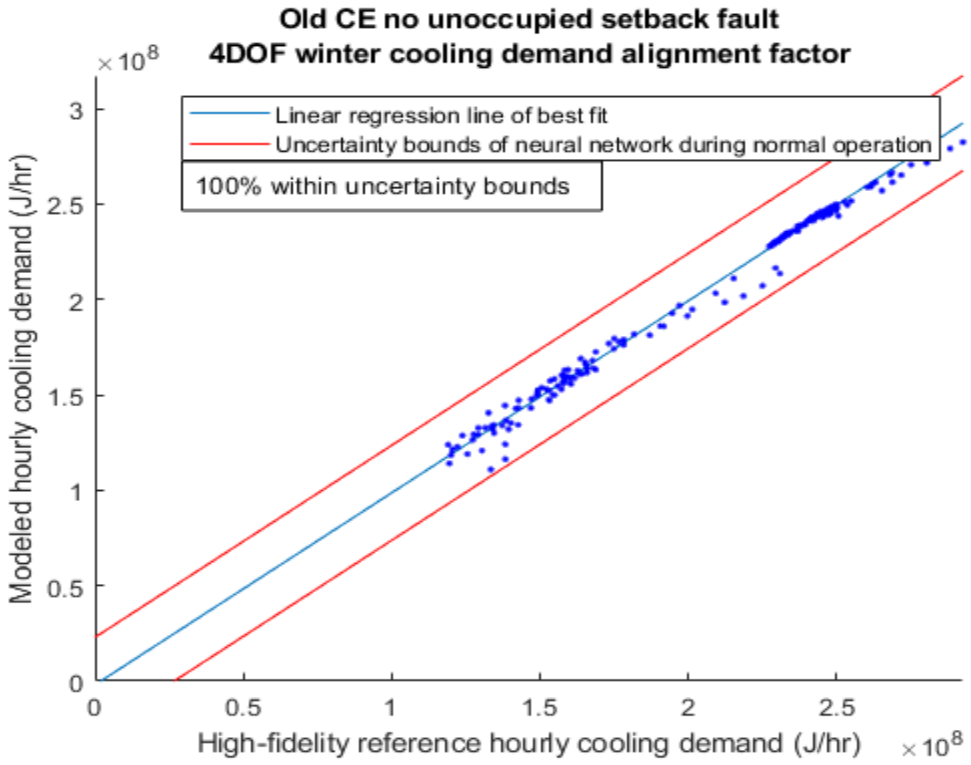

Figure 160: Hourly cooling rate alignment factor for Whitehead model not entering unoccupied setback fault during winter weather

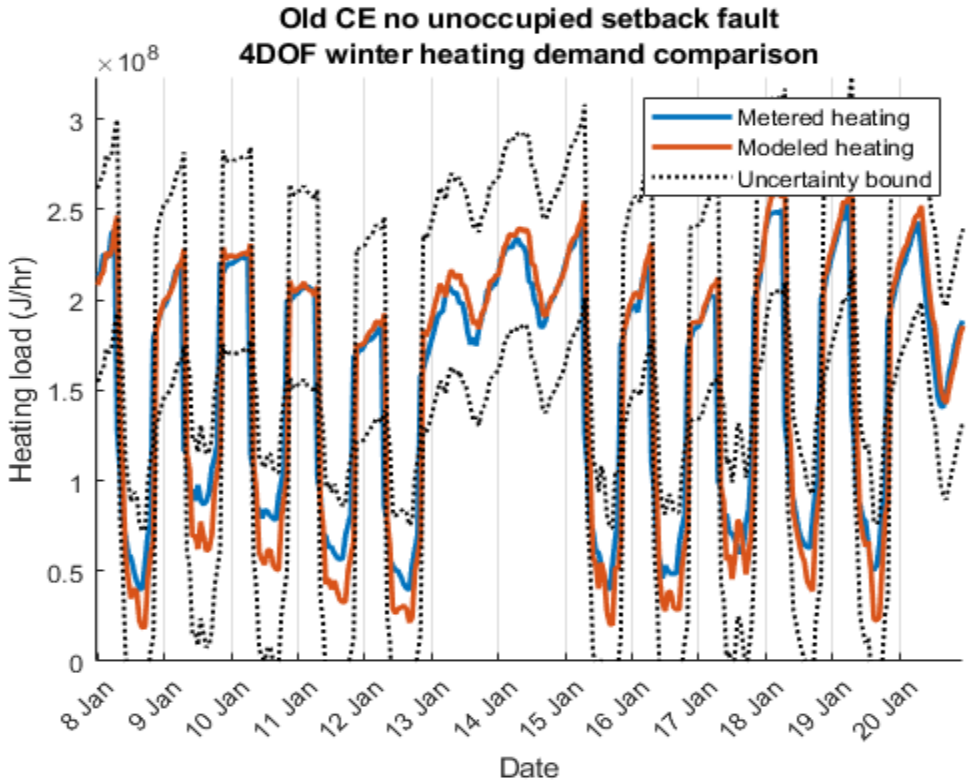

Figure 161: Hourly heating rate for winter weather comparing SPBM and reference data when the building is experiencing a fault of not entering unoccupied setback

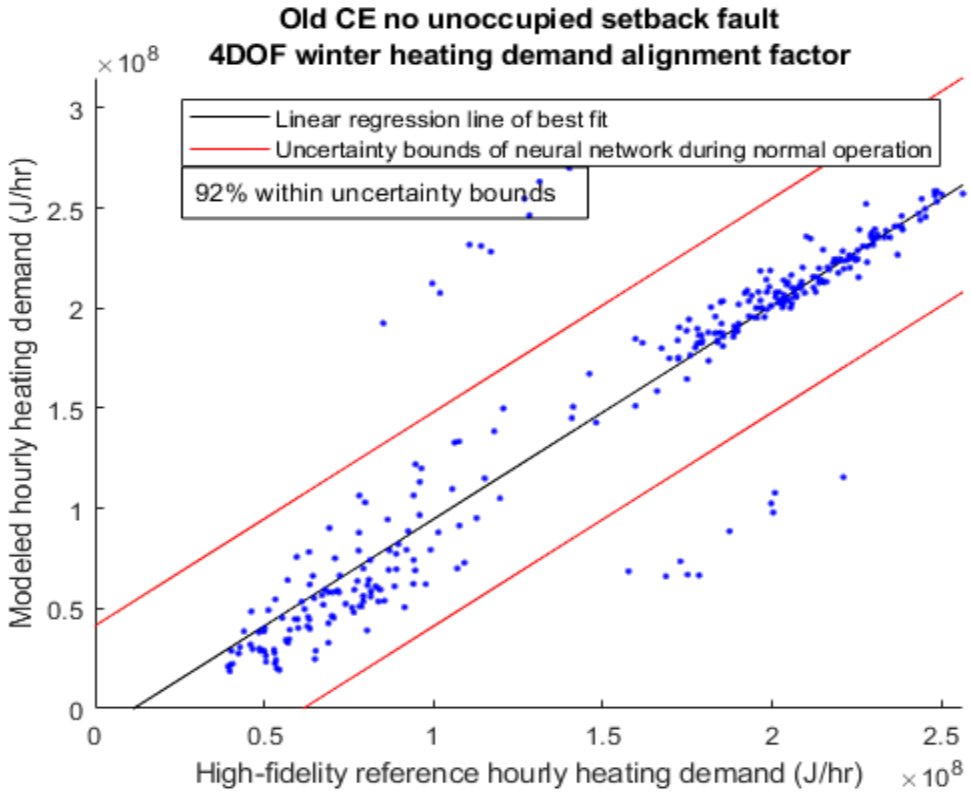

Figure 162: Hourly heating rate alignment factor for Whitehead model not entering unoccupied setback fault during winter weather

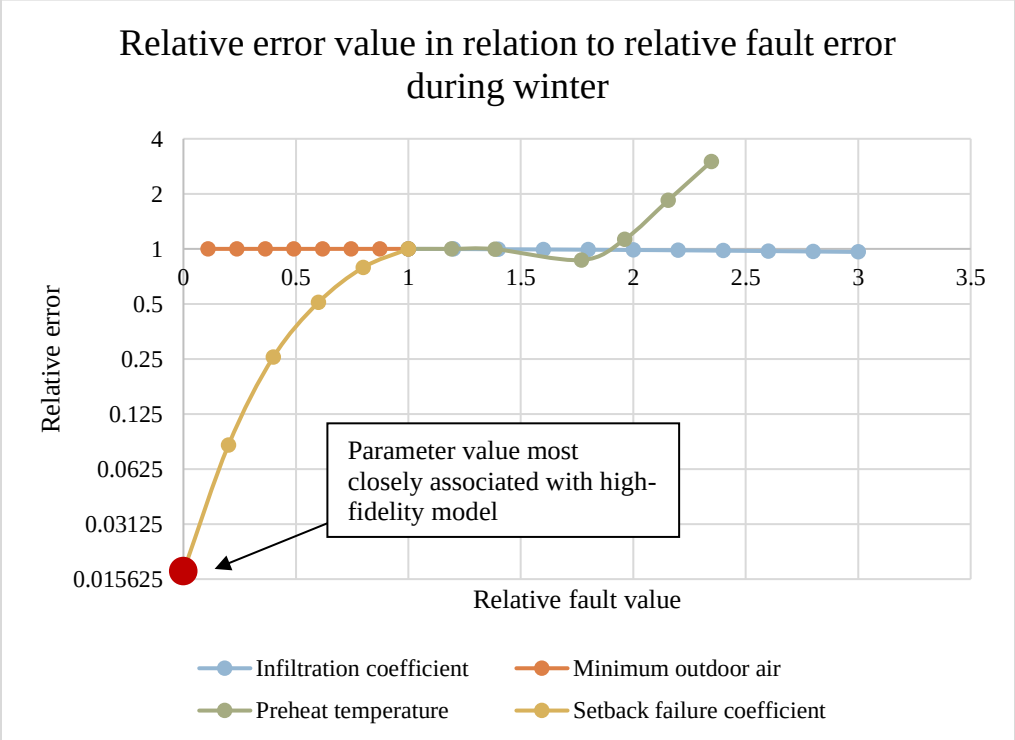

Figure 163: Visual representation of how magnitude of error changes across different magnitudes of the four possible faults. The fault of not entering unoccupied setback is being tested for automatic detection for Old CE during winter

Unlike infiltration, setback failure has a more significant impact on total building loading because both air flow rate and zone temperature changes during unoccupied periods.

Failure to enter unoccupied setback during summer weather displays similar performance to winter loading conditions. Cooling load is nearly constant as there is a diminished internal load due to fewer students and professors being on campus during summer semester. Heating demand during unoccupied periods still rises as occupants leave and internal equipment load is reduced; however, there is a more noticeable slope up in demand throughout unoccupied periods than was displayed during winter weather. It is theorized that the legacy construction of Old CE, with heavy brick, concrete, and relatively few windows made envelope thermal capacity have a greater impact on evening heating demand than the modern construction of Whitehead. Evaluating fault detection results in Figure 168 and in Table 31 reveal the largest reduction in error with a reduction of over 99%. Cooling load rate, as shown in Figure 164 and Figure 165, repeat the excellent agreement displayed earlier for Old CE when undergoing a failure to enter unoccupied setback for winter weather. Heating load rate shows acceptable agreement with a bias towards over prediction of demand, as demonstrated in Figure 166 and Figure 167.

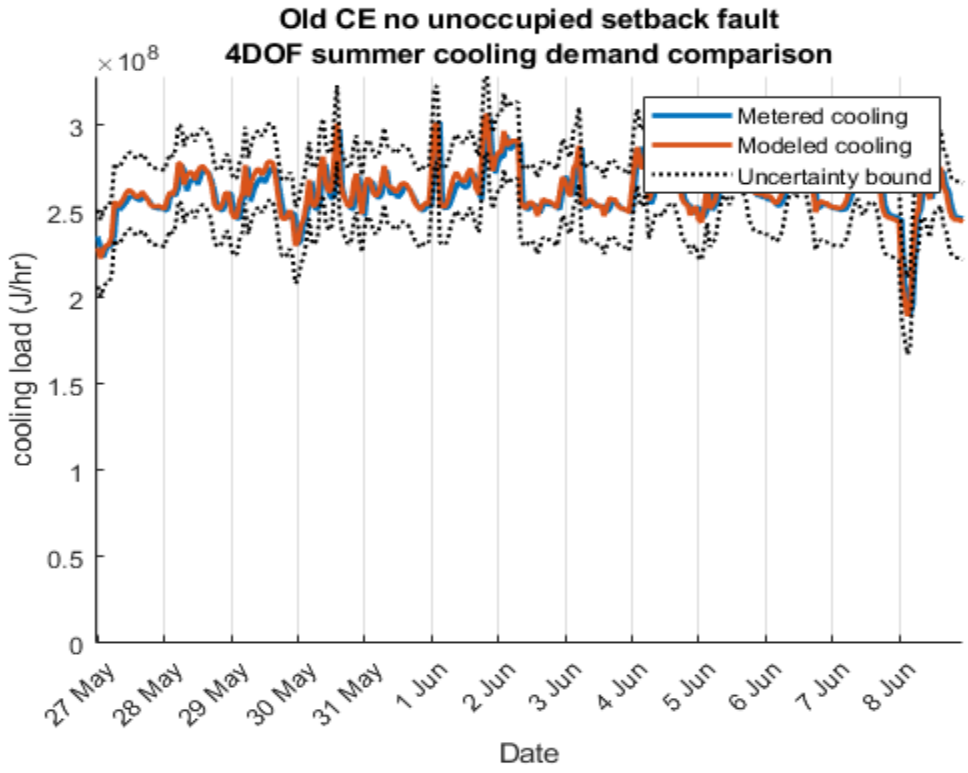

Figure 164: Hourly cooling rate for summer weather comparing SPBM and reference data when the building is experiencing a fault of not entering unoccupied setback

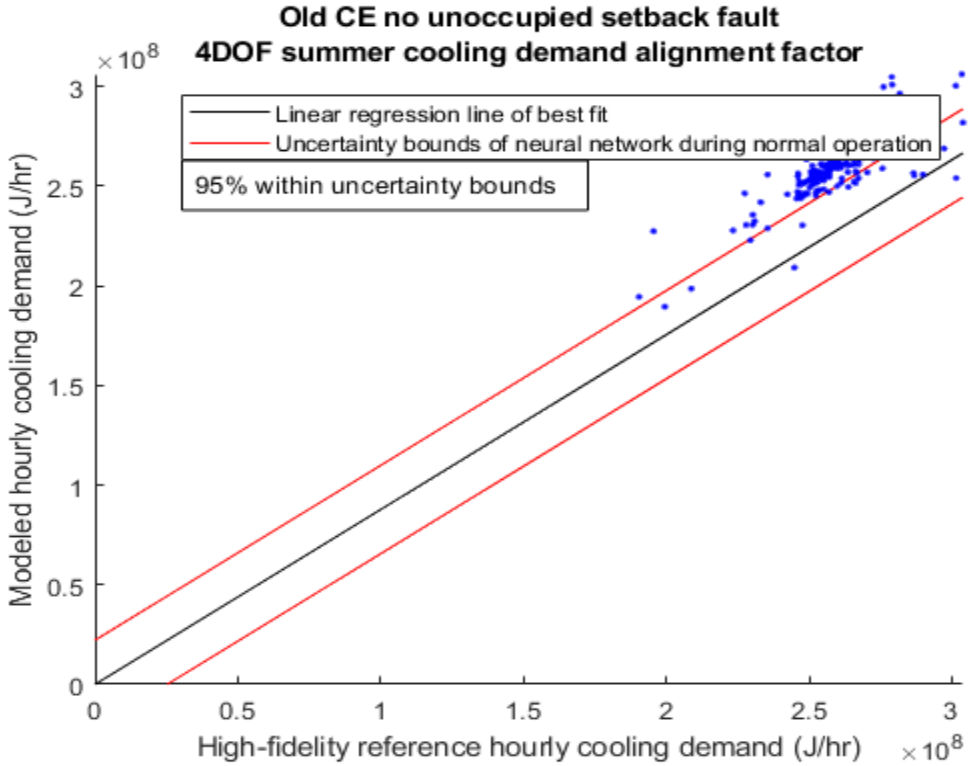

Figure 165: Hourly cooling rate alignment factor for Whitehead model not entering unoccupied setback fault during summer weather

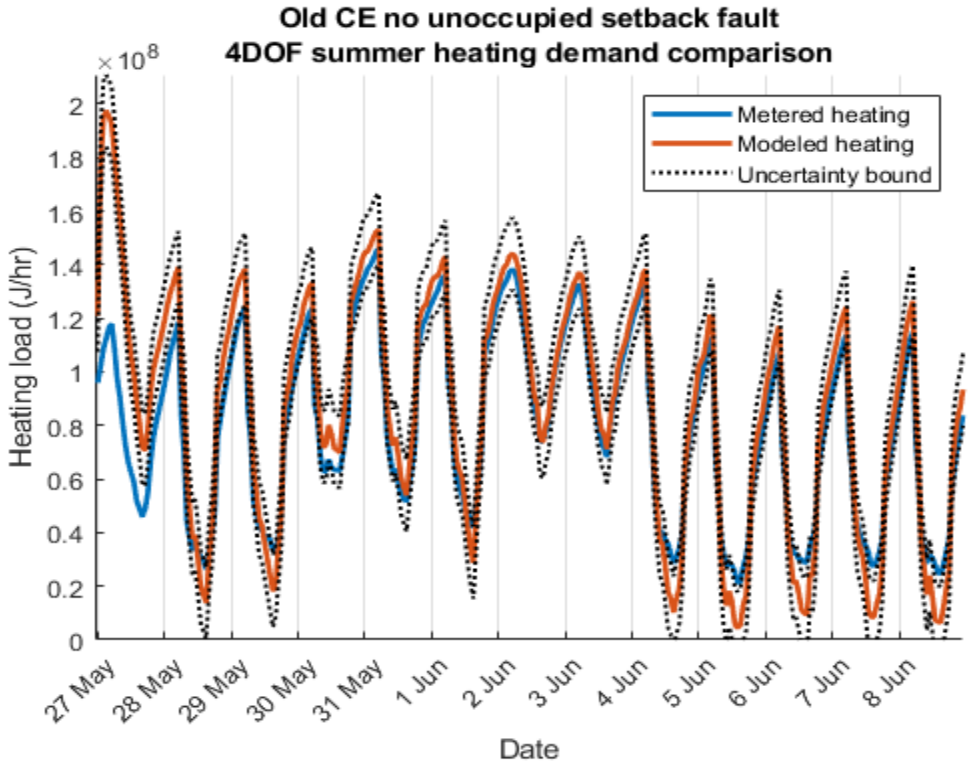

Figure 166: Hourly heating rate for summer weather comparing SPBM and reference data when the building is experiencing a fault of not entering unoccupied setback

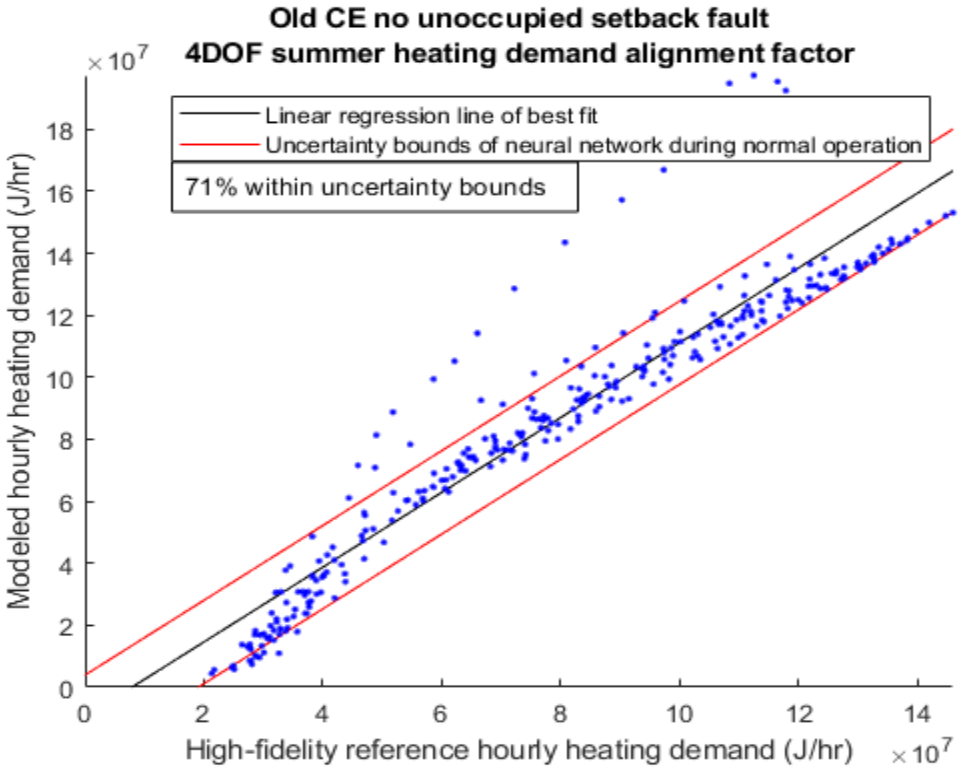

Figure 167: Hourly heating rate alignment factor for Whitehead model not entering unoccupied setback fault during summer weather

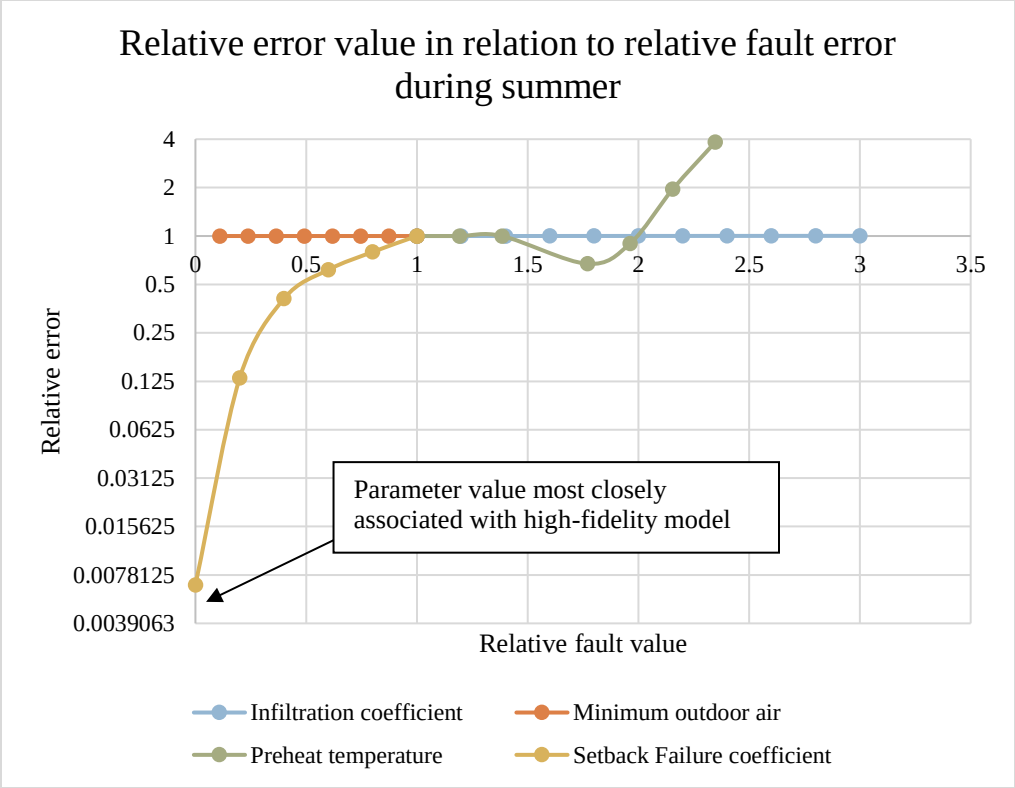

Figure 168: Visual representation of how magnitude of error changes across different magnitudes of the four possible faults. The fault of not entering unoccupied setback is being tested for automatic detection for Old CE during summer

Failure to enter unoccupied setback increases both heating and cooling demand, therefore faults such as excessive preheat which also increase heating and cooling demand will show a slight reduction in error too. Infiltration and outdoor air flow rate appear to not have a significant impact on error as the change in loading from unoccupied setback is so great.

As with all loads that depend on independent interior zones, a simplified building energy model can miss the minutia involved with small zones that experience either high or minimal amounts of environmental loading. Regardless, the SPBM has again demonstrated a reliable method for arriving at a unique solution for a potential fault.

7.3.3 Old CE Excessive Preheat

Excessive preheat, as discussed earlier, is most common during winter weather. An equal increase in heating and cooling demand is expected at all times when excessive preheat fault is occurring. Testing for excessive preheat fault employed the same tactic of comparing total heating and cooling demand and determining which fault reduced error the most. Figure 169 demonstrates that cooling rate increases during occupied times as air flow rate increases while Figure 170 highlights the overprediction in cooling rate for occupied periods and the excellent agreement for unoccupied periods. Again, Figure 171 and Figure 172 show heating rate spikes as occupied periods and internal loads rapidly shift. Even a broad fault search resulted in a clear and unique solution for minimum error, shown in Figure 173 and Table 32 , for a building with legacy construction and HVAC setup.

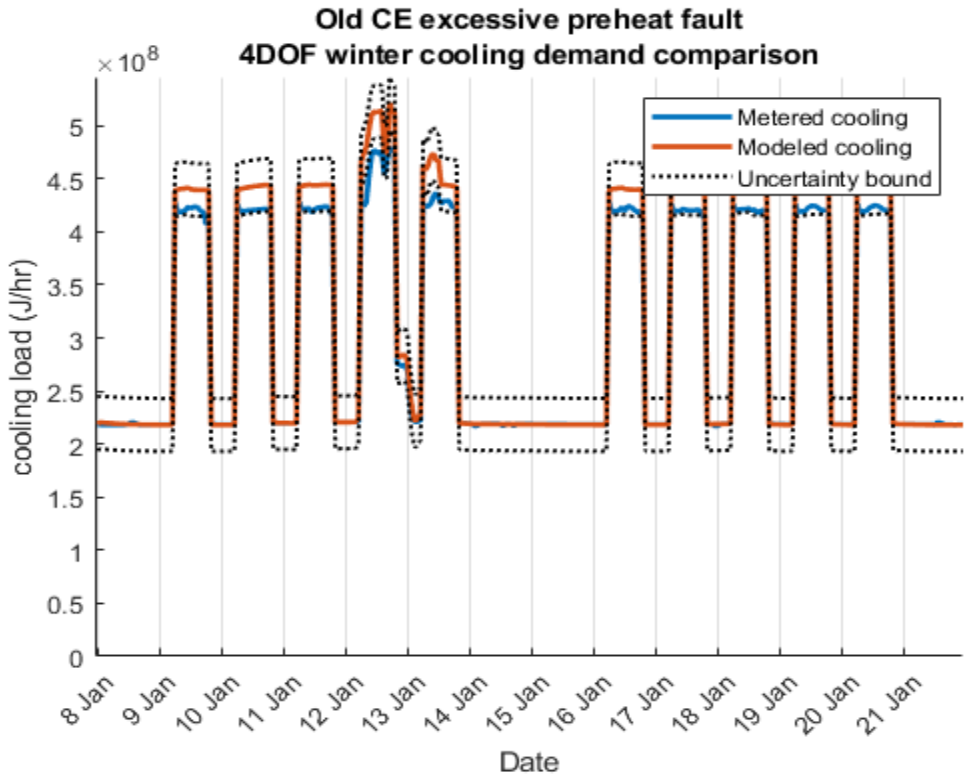

Figure 169: Hourly cooling rate for winter weather comparing SPBM and reference data when the building is experiencing a fault of excessive preheat

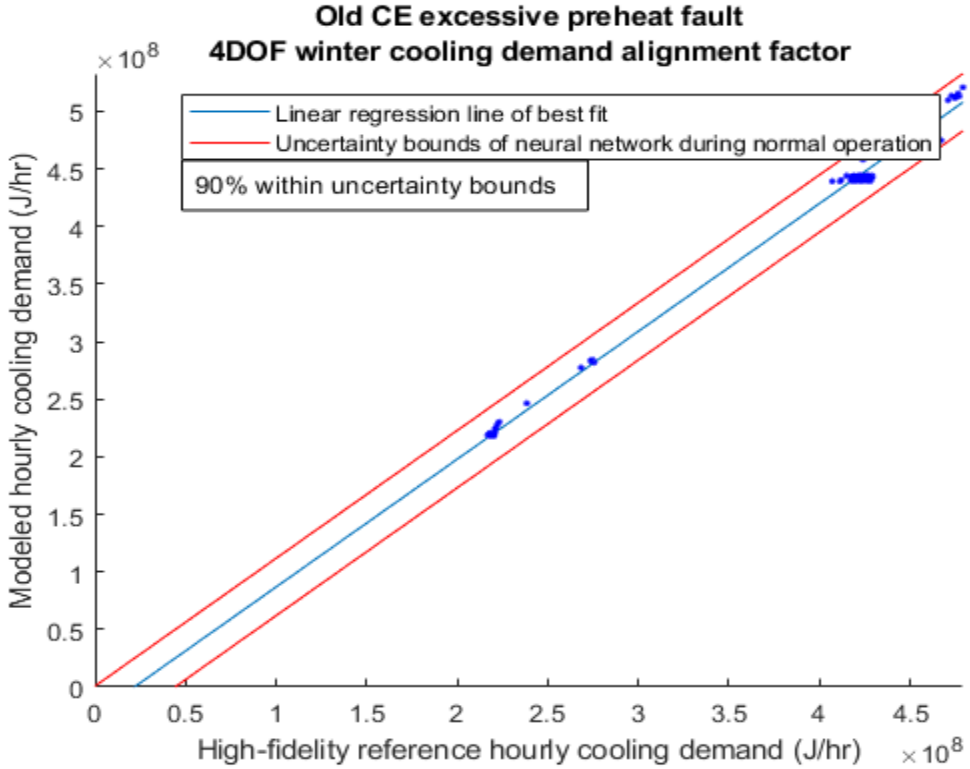

Figure 170: Hourly cooling rate alignment factor for Whitehead model experiencing excessive preheat fault during winter weather

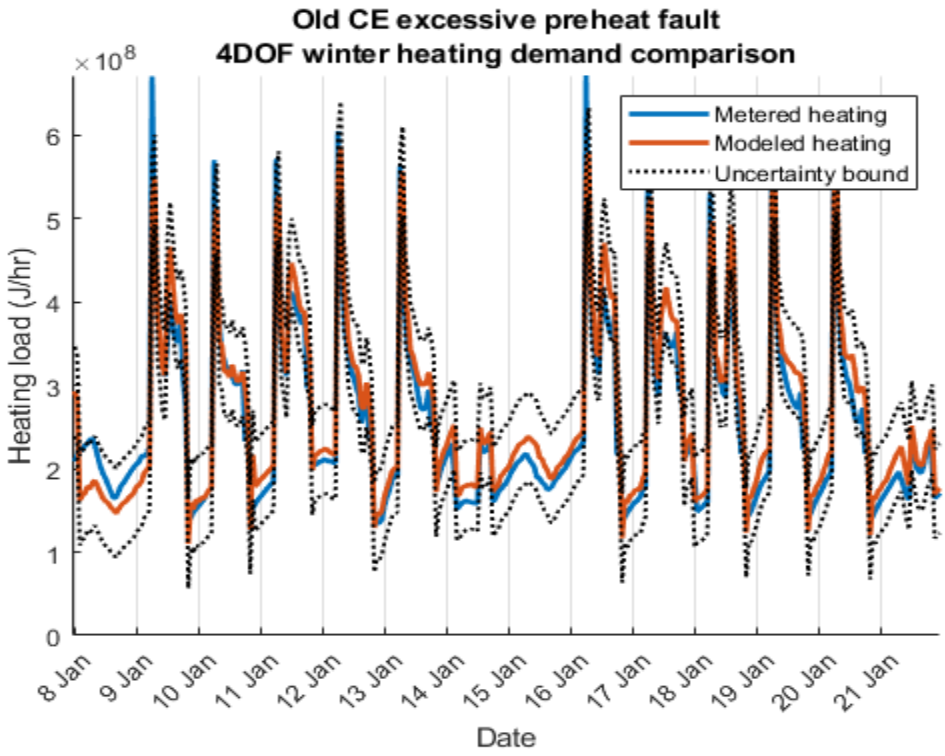

Figure 171: Hourly heating rate for winter weather comparing SPBM and reference data when the building is experiencing a fault of excessive preheat

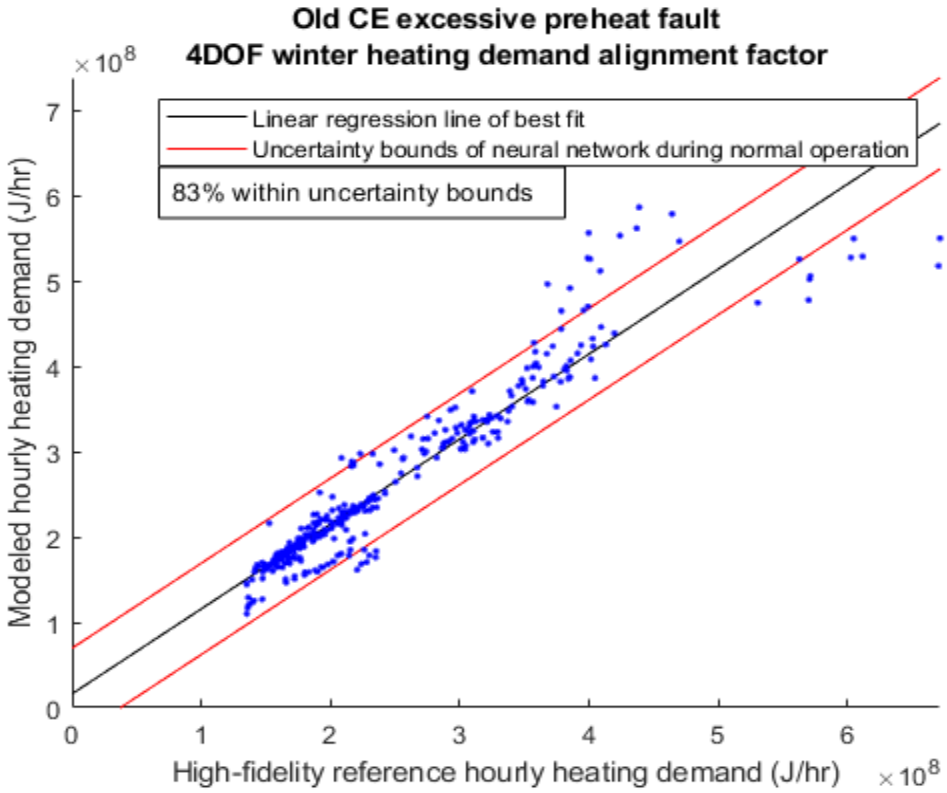

Figure 172: Hourly heating rate alignment factor for Whitehead model experiencing excessive preheat fault during winter weather

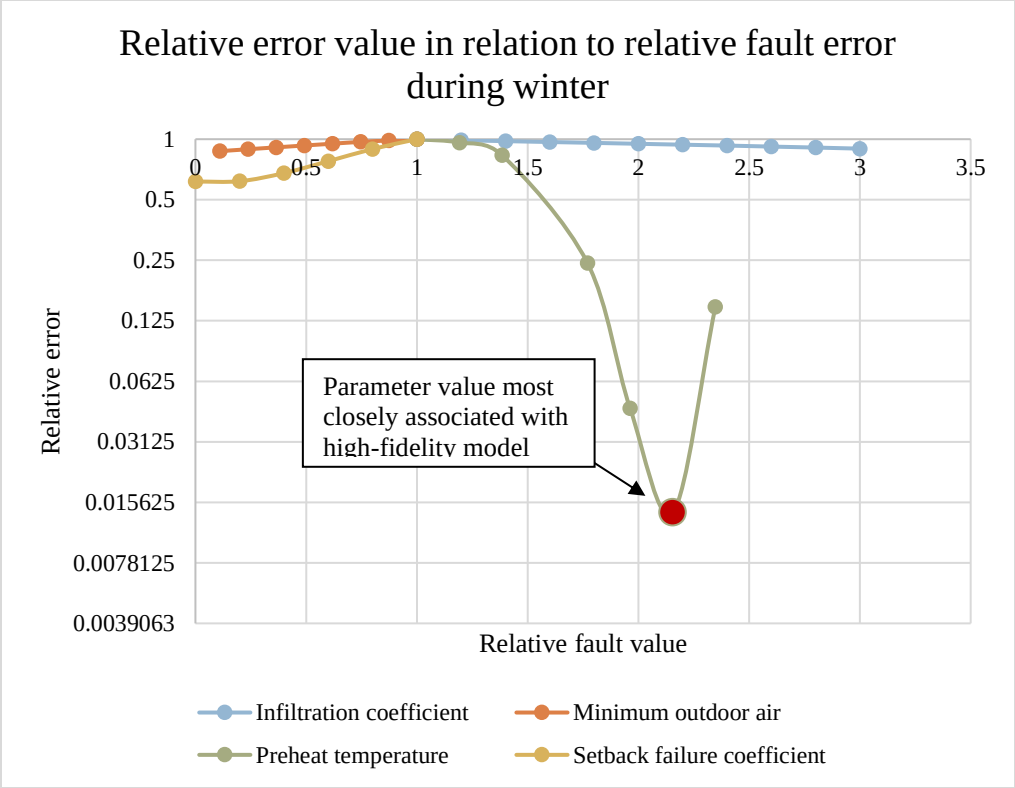

Figure 173: Visual representation of how magnitude of error changes across different magnitudes of the four possible faults. The fault of excessive preheat is being tested for automatic detection for Old CE during winter

Excessive preheat fault also has a dramatic impact on total building heating and cooling demand. Due to the loading characteristics of both excessive preheating and unoccupied setback failure, these two faults both show a reduction in error in each other's relative error analysis, though not nearly as great as the fault being tested.

Continuing off the success of excessive preheat of Old CE for winter weather, summer excessive preheating demonstrates a similar level of agreement. Overprediction in cooling demand, as represented by Figure 174 and Figure 175, are due to the preheat temperature with minimum error being slightly greater than the value used within the high-fidelity reference model. Similarly, Figure 176 and Figure 177 reveal a bias of higher heating demand from the SPBM. These biases towards overcooling and

overheating when compared to reference data is simply the product of not having the exact same preheat setpoint temperature. Analysis was done by using ‘as designed’ setpoints and using evenly spaced steps along a range of possible values. Figure 178 and Table 33 shows that the minimum error occurred on run 30 with a preheat temperature of 27.5°C, which is 0.5°C above the value used by the high-fidelity reference model. However, a clear minimum error is associated with excessive preheating is obtained, meaning that the intended purpose of fault detection and identification is successful even without a perfect load prediction.

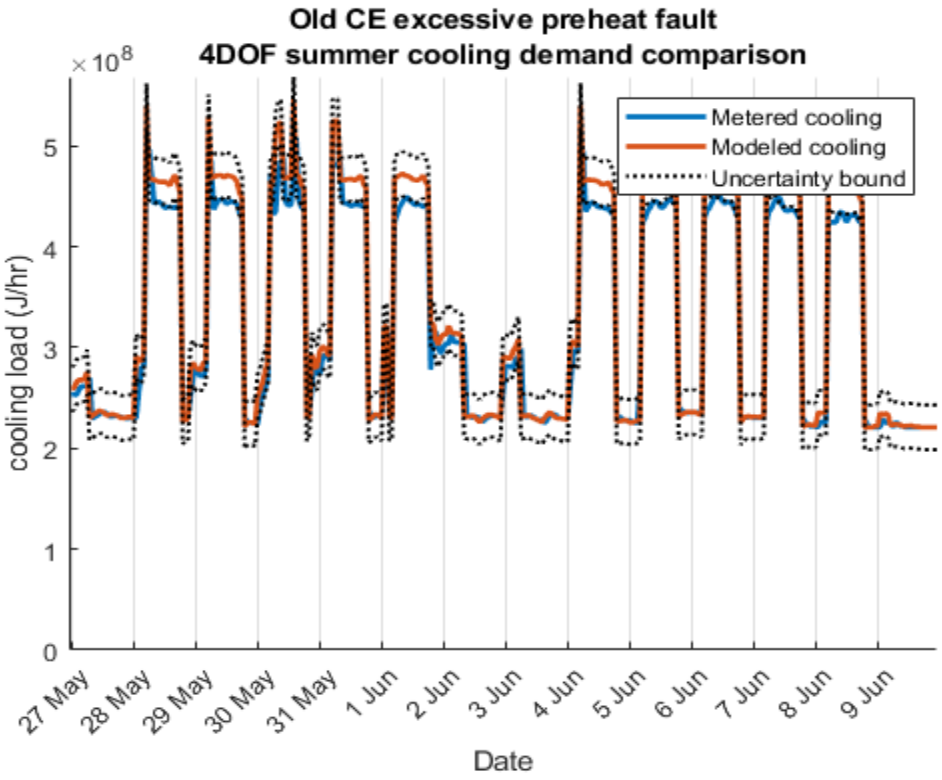

Figure 174: Hourly cooling rate for summer weather comparing SPBM and reference data when the building is experiencing a fault of excessive preheat

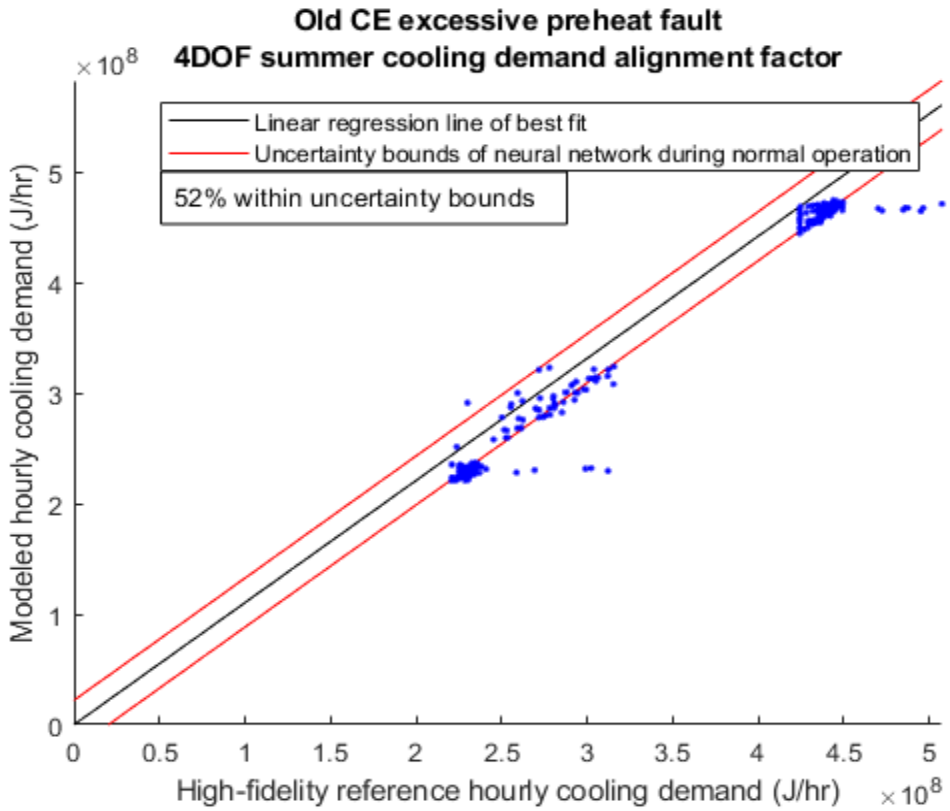

Figure 175: Hourly cooling rate alignment factor for Whitehead model experiencing excessive preheat fault during summer weather

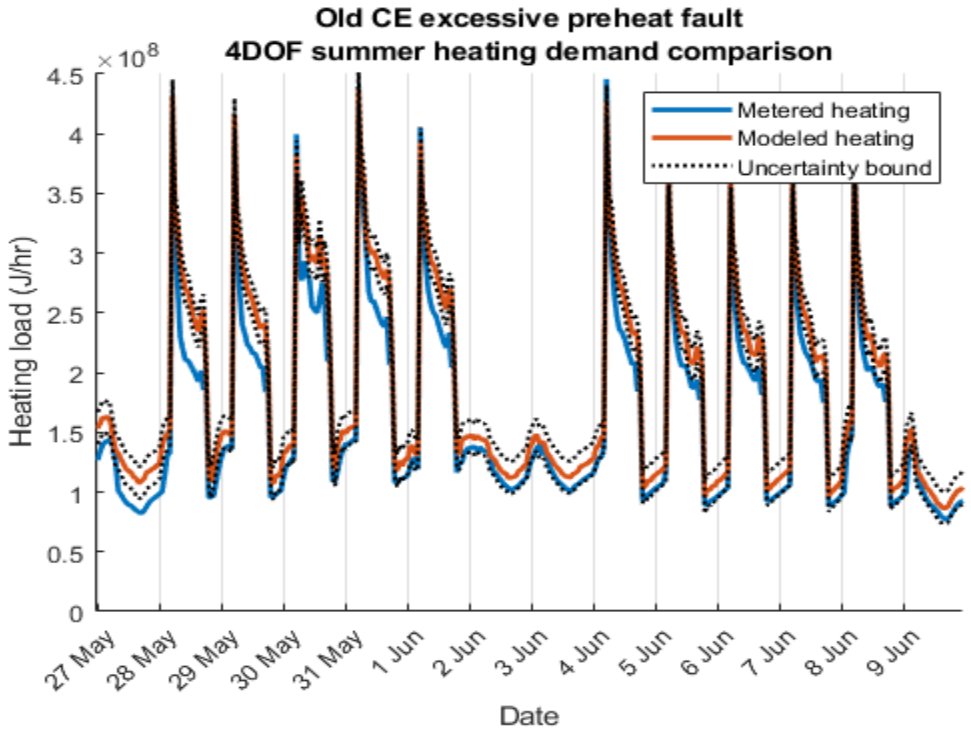

Figure 176: Hourly heating rate for summer weather comparing SPBM and reference data when the building is experiencing a fault of excessive preheat

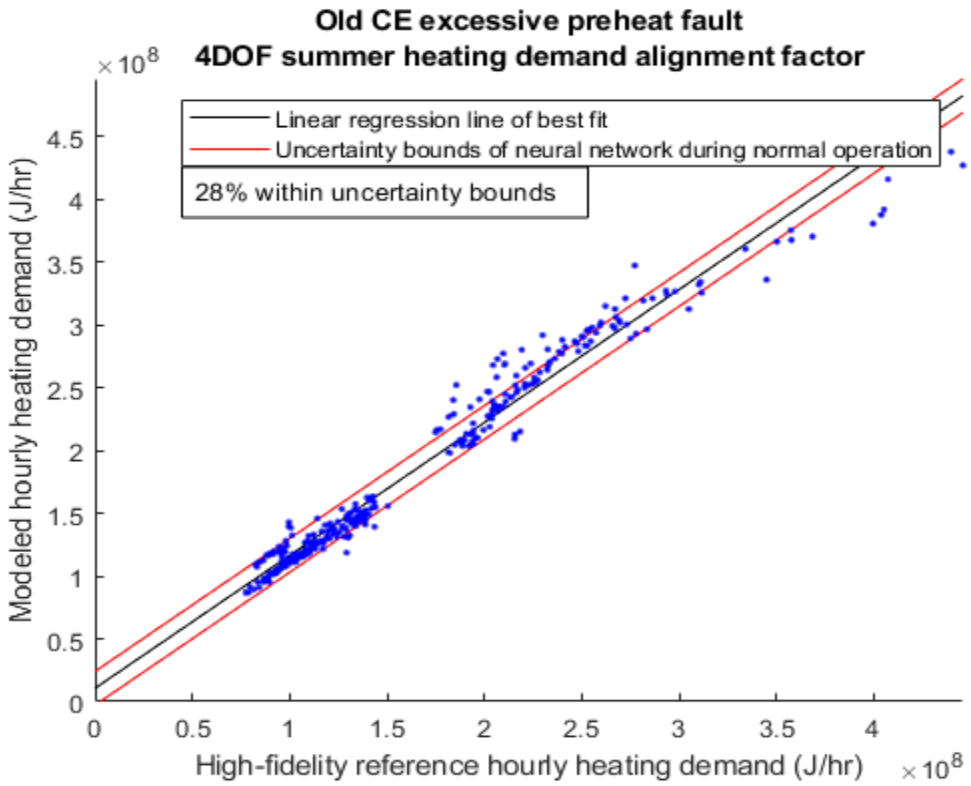

Figure 177: Hourly heating rate alignment factor for Whitehead model experiencing excessive preheat fault during summer weather

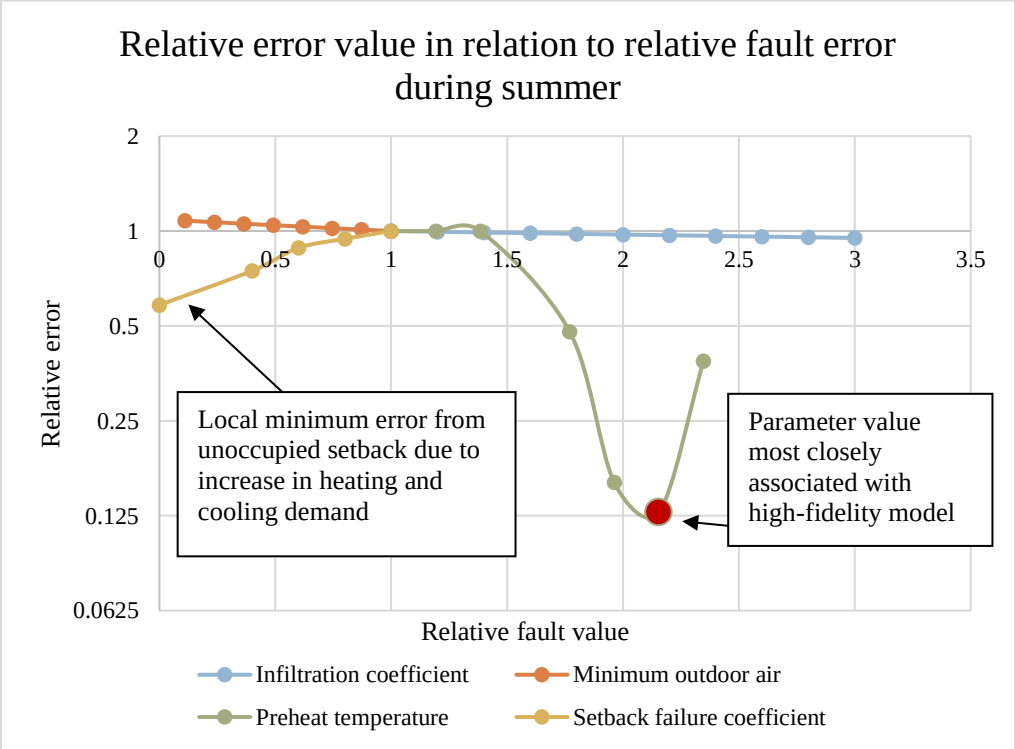

Figure 178: Visual representation of how magnitude of error changes across different magnitudes of the four possible faults. The fault of excessive preheat is being tested for automatic detection for Old CE during summer

Load impact from excessive preheating is less severe in summer as the air temperature entering the heating coils is of a higher temperature in summer than in winter, and therefore requires less preheating to match the same temperature setpoint.

As with Whitehead, relative error analysis revealed a clear and unique solution for minimum error and fault identification. Additionally, SPBM energy demand prediction alignment factors for all loading conditions were in strong agreement, further demonstrating simplified physics-based energy modeling as a reliable and predictable method of demand prediction.

7.3.4 Old CE Insufficient Outdoor Air

Insufficient outdoor air presents a unique kind of fault for building modeling. Due to outdoor air often being hotter than return air during the summer, and colder than return air for winter, supplying excessive amounts of outdoor air can sometimes come at a cost of increased cooling or heating load. Therefore, it has been advisable to supply the minimum amount of outdoor air required depending on the needs of a zone or building . However, elevated CO2 levels from insufficient outdoor air can be significant enough to impact occupant concentration. Additionally, insufficient outdoor air can potentially lead to viral infections. Therefore, insufficient outdoor air would have the potential to reduce energy consumption at the expense of occupant health. It is for the safety of the occupants that insufficient outdoor air fault is monitored.

Cooling performance is as to be expected with increases in demand during occupied periods and lowered demand during periods in which outdoor air economizer can operate (seen as sudden drops in demand in Figure 179). Figure 180 demonstrates a strong alignment factor over a wide range of operating conditions. Likewise, Figure 181

and Figure 182 continue the pattern of agreement with the high-fidelity reference model. Additionally, Figure 183 and Table 34 continue the other pattern of strong bias towards a unique solution for fault detection.

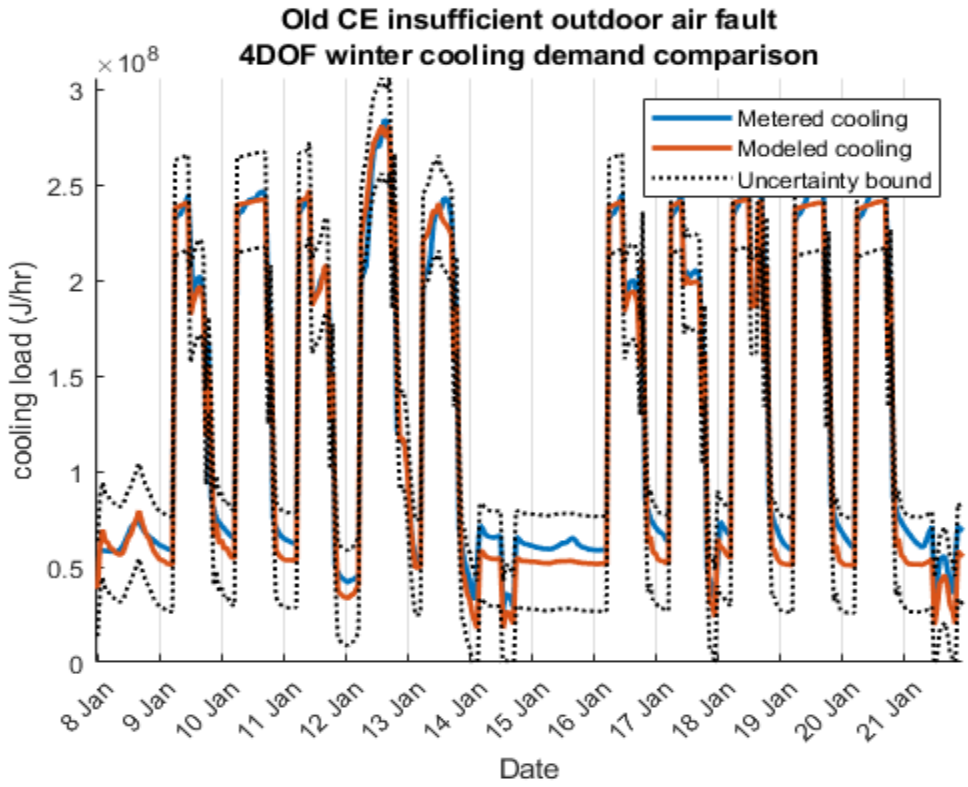

Figure 179: Hourly cooling rate for winter weather comparing SPBM and reference data when the building is experiencing a fault of insufficient outdoor air

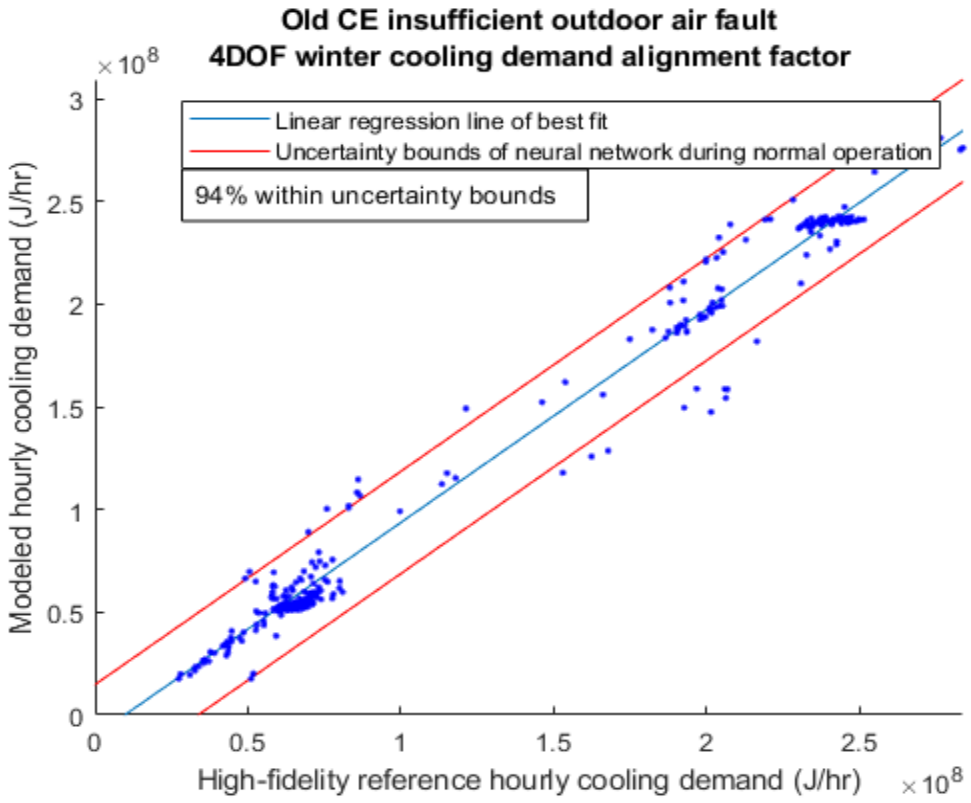

Figure 180: Hourly cooling rate alignment factor for Whitehead model experiencing insufficient outdoor air fault during winter weather

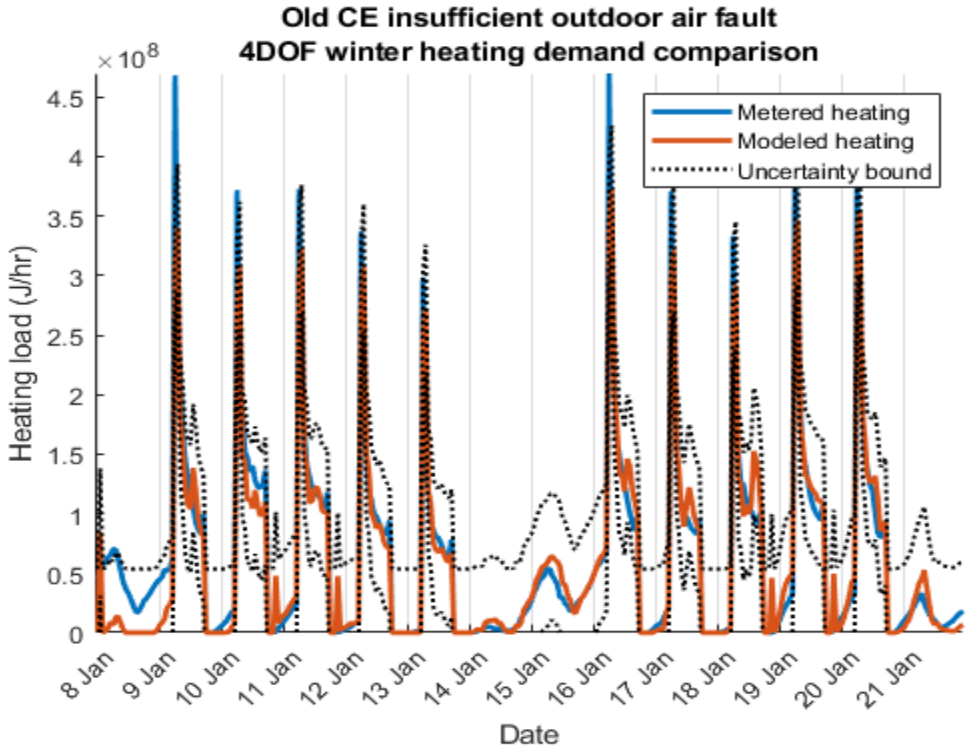

Figure 181: Hourly heating rate for winter weather comparing SPBM and reference data when the building is experiencing a fault of insufficient outdoor air

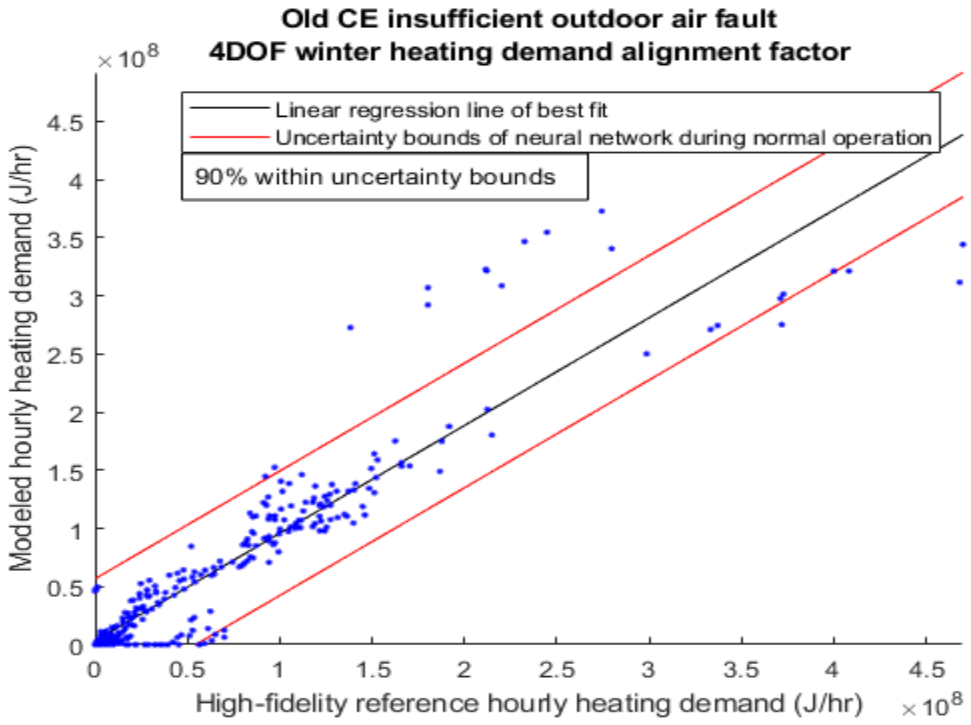

Figure 182: Hourly heating rate alignment factor for Whitehead model experiencing insufficient outdoor air fault during winter weather

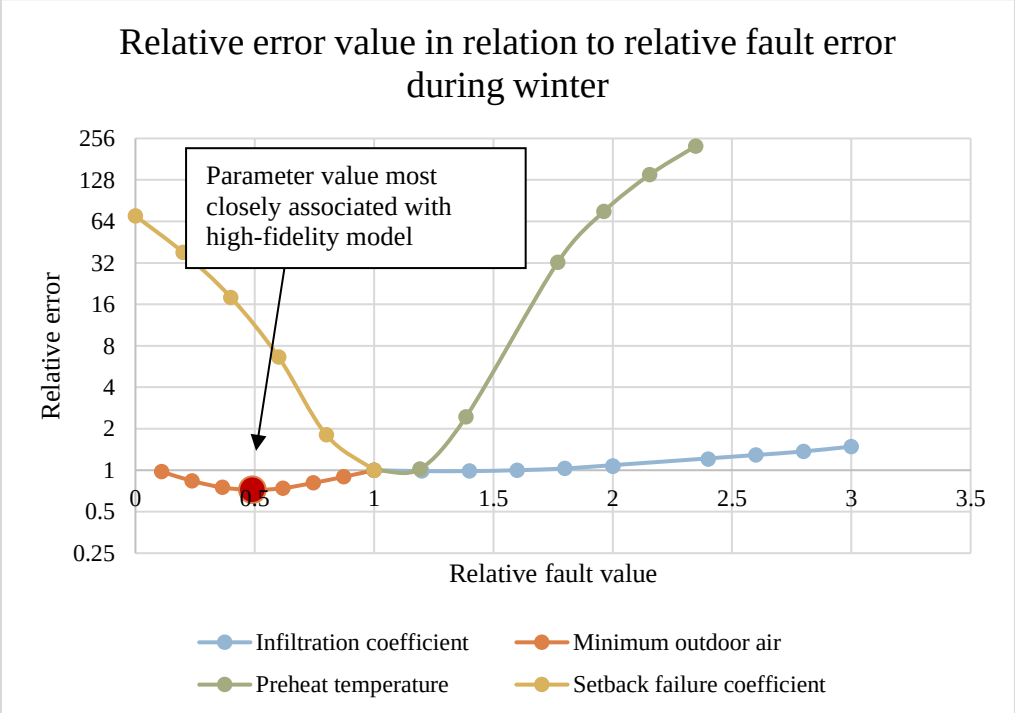

Figure 183: Visual representation of how magnitude of error changes across different magnitudes of the four possible faults. The fault of insufficient outdoor air is being tested for automatic detection for Old CE during winter and reveals a global minimum error associated when half the nominal outdoor air is testes, the same value as the high-fidelity model

Minimum outdoor air fault is similar to Whitehead as reducing outdoor air lowered energy demand. Therefore, any fault that increases loading would increase error.

Insufficient outdoor fault for summer weather for Old CE presents a unique series of results. However, load response, as featured in Figure 184 through Figure 187, again demonstrates the SPBM's energy modeling prowess. Figure 188 and Table 35 exposes that there was little to no reduction in error from any adjustments to fault parameters. A high degree of model accuracy while maintaining a near-constant error means that the SPBM is not sensitive enough to detect minute changes in load from different outdoor air flow rates. Initial tests used an extremely efficient (95%) total enthalpy wheel, but when evaluating a more realistic (70% efficiency) fault detection again provided conclusive and unique minimum error values. Additionally, testing the 95% efficient energy recovery while also monitoring CO2 provided an unambiguous result as to which potential fault was occurring.

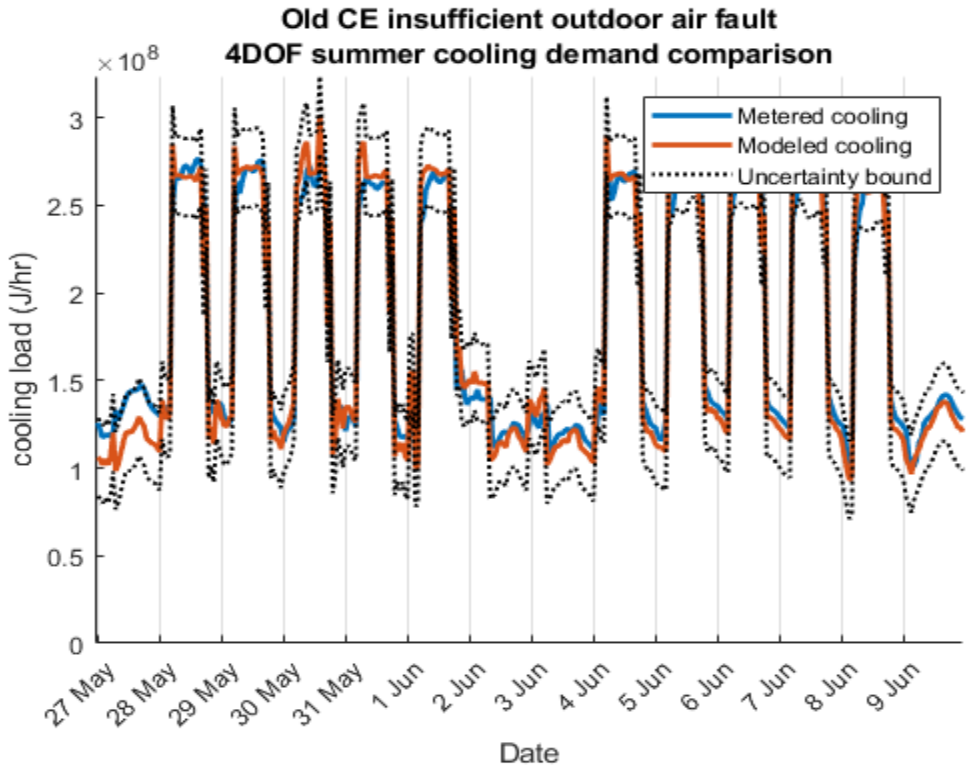

Figure 184: Hourly cooling rate for summer weather comparing SPBM and reference data when the building is experiencing a fault of insufficient outdoor air

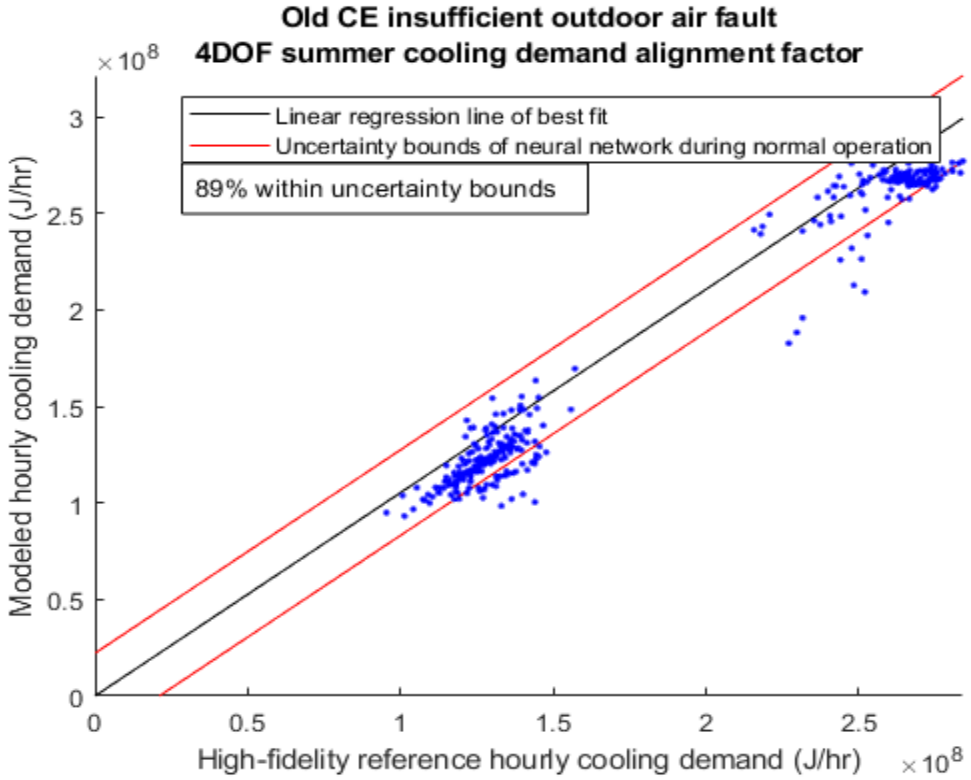

Figure 185: Hourly cooling rate alignment factor for Whitehead model experiencing insufficient outdoor air fault during summer weather

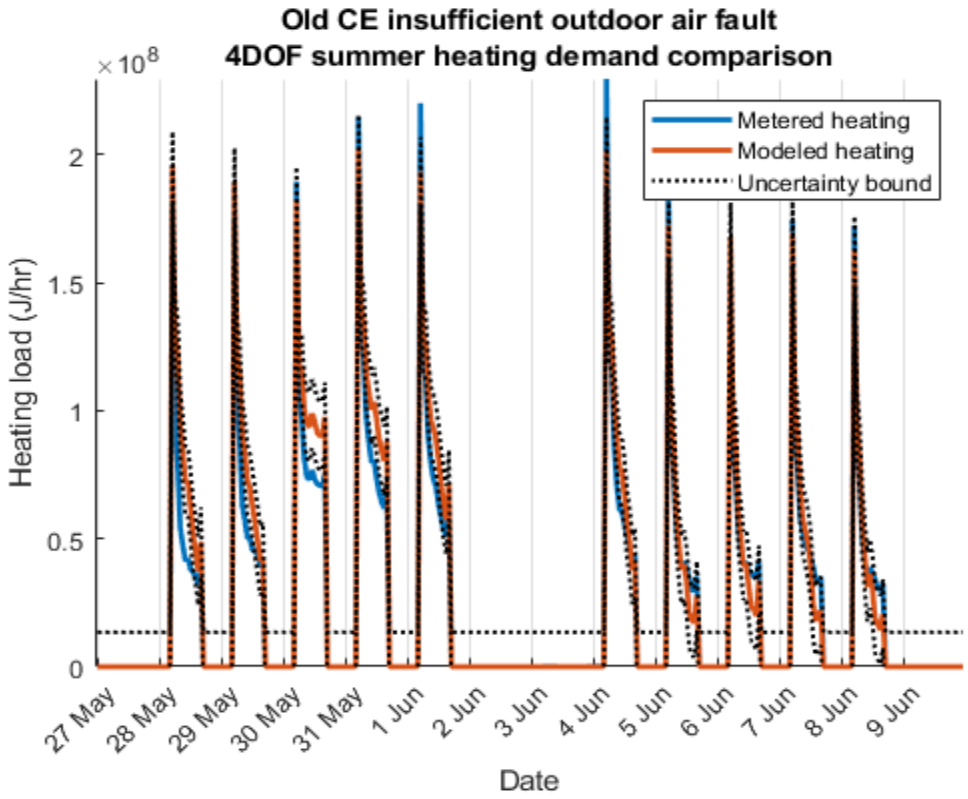

Figure 186: Hourly heating rate for summer weather comparing SPBM and reference data when the building is experiencing a fault of insufficient outdoor air

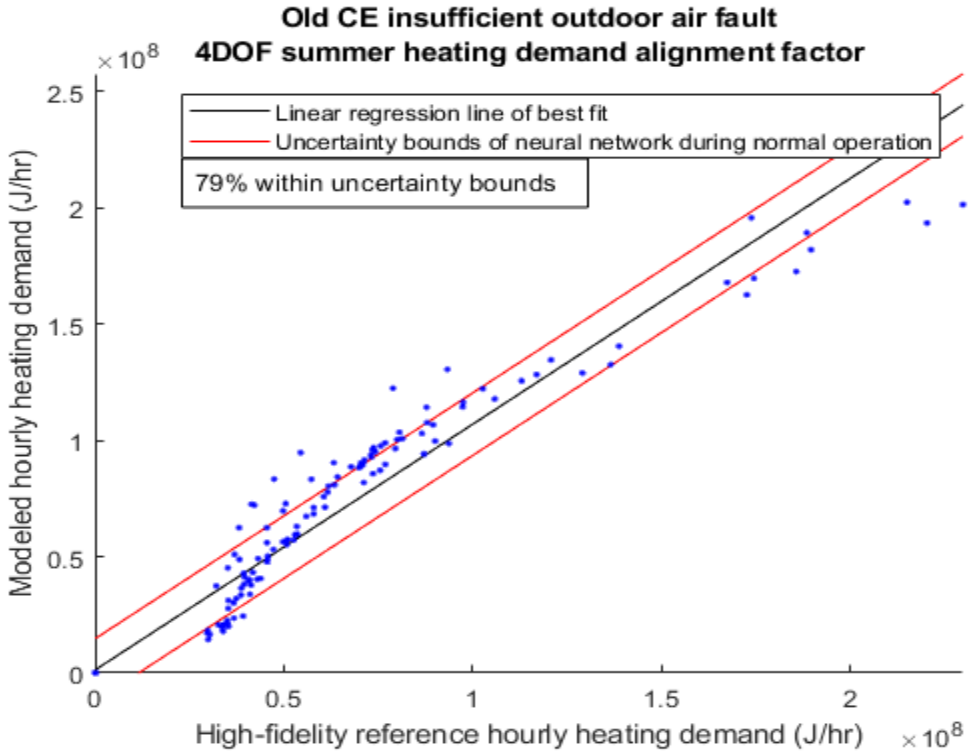

Figure 187: Hourly cooling rate alignment factor for Whitehead model experiencing insufficient outdoor air fault during summer weather

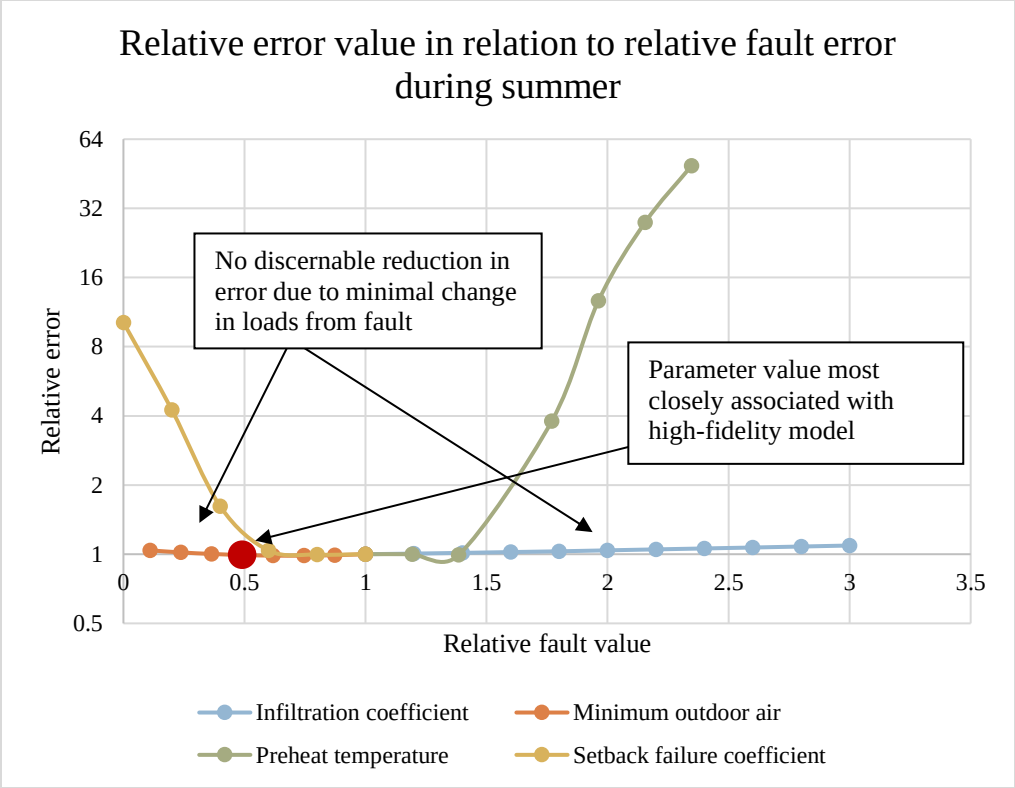

Figure 188: Visual representation of how magnitude of error changes across different magnitudes of the four possible faults. The fault of insufficient outdoor air is being tested for automatic detection for Old CE during summer

Changing outdoor air had little effect on error rates because heat recovery transferred nearly all of the thermal and latent energy from entering outdoor air to exhausting return air. Therefore, there was little change in building load between any outdoor air flow rate. This pattern was not seen in winter as Old CE utilizes an economizer that can bypass heat recovery when outdoor air has less enthalpy than return air.

Due to unrealistically high efficiency energy recovery in previous tests, there was no significant change in heating or cooling demand from changing outdoor air flow. However, a small decrease in total energy recovery efficiency to more realistic values

resulted in a clear and unique solution to error minimization as depicted in Figure 190 and Table 36.

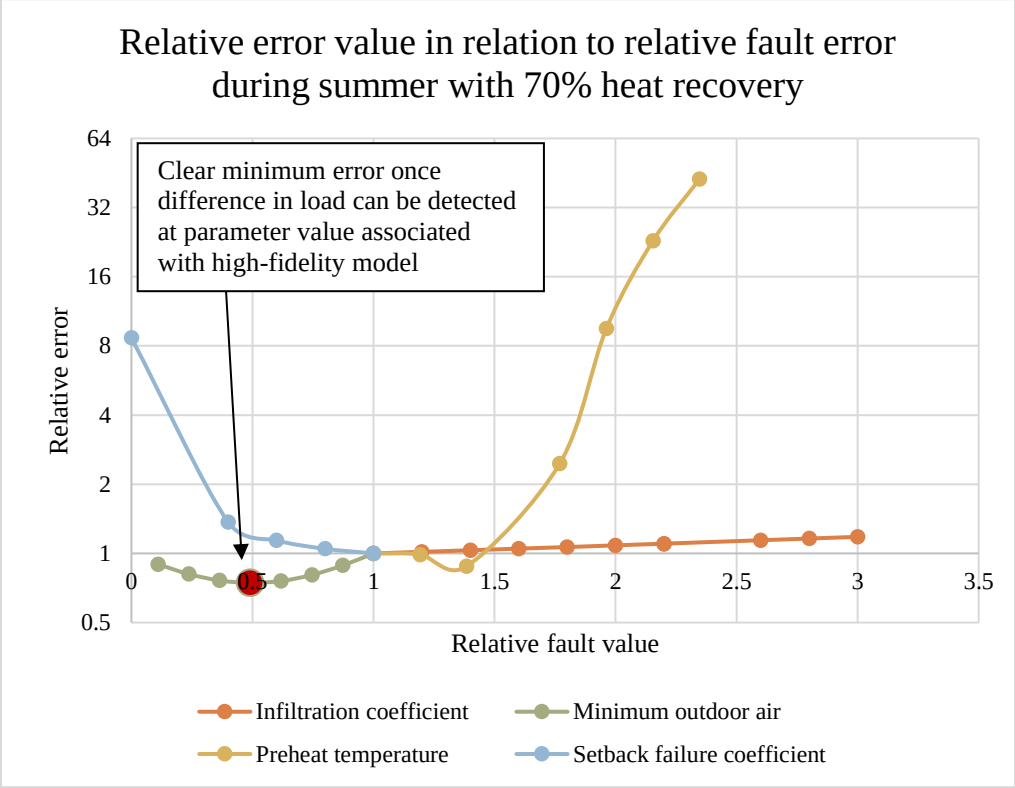

Figure 189: Visual representation of how magnitude of error changes across different magnitudes of the four possible faults. The fault of insufficient outdoor air is being tested for automatic detection for Old CE during summer

Being a physics-based model, more than one method of error minimization can be used to cross-check results. Figure 190 and Table 37 confirms error minimization results from previous tests by having the same parameter value produce the minimum value when using CO2 error minimization, an independent value from heating or cooling demand.

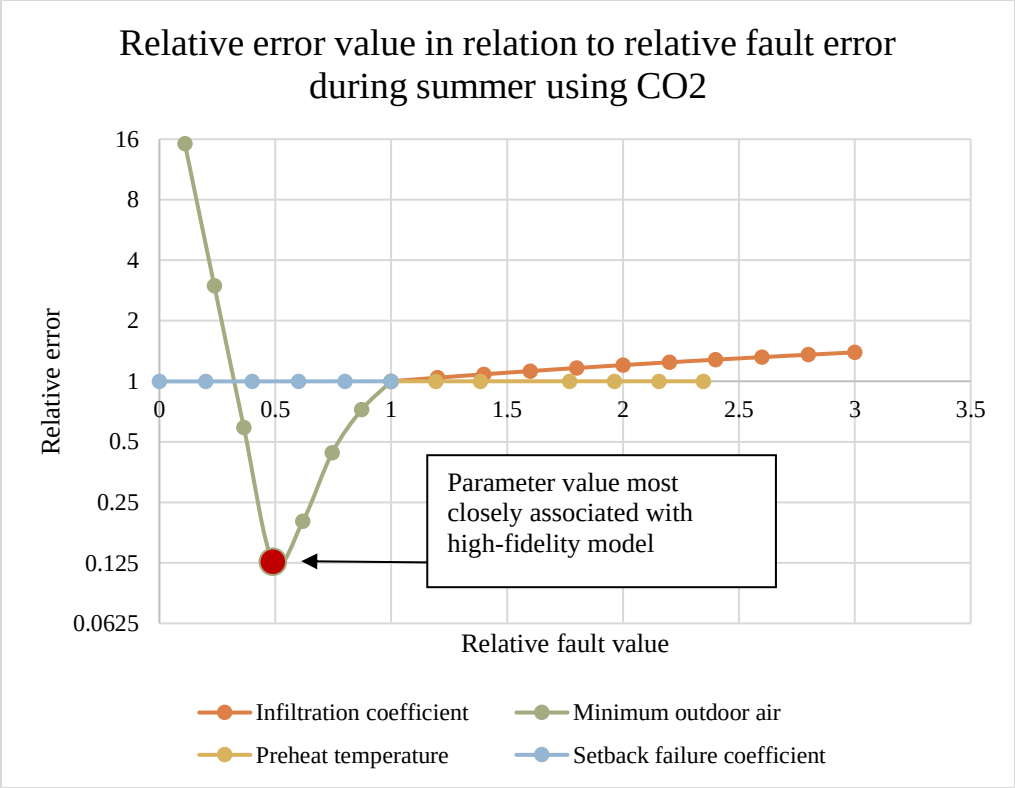

Figure 190: Visual representation of how magnitude of error changes when monitoring CO2 levels from return and supply air across different magnitudes of the four possible faults. The fault of insufficient outdoor air is being tested for automatic detection for Old CE during summer

Old CE proved to be a more challenging building to represent with a simplified physics-based model, but both energy demand prediction, fault detection, and fault identification tests were successful. Given the level of accuracy that parameter estimation has shown thus far, multiple simultaneous faults will be examined to determine how energy demand prediction and fault identification error minimization techniques compare to neural network-based fault detection and identification.

7.4 Multiple Simultaneous Faults

While individual faults occurring within a building has been shown to be well within the realm of ability of the SPBM, there is a possibility that multiple faults could simultaneously occur. Multiple fault analysis will focus on combining faults that both produced a reduction in error, such as excessive preheat combined with not entering unoccupied setback. By combining faults that both produced a reduction in error when individually analyzed, it will be possible to further explore uniqueness of detection and diagnosis of the SPBM.

Due to limitations in displaying higher-dimensional objects, a 4D plot was used where three parameter values (infiltration coefficient, preheat temperature setpoint, and minimum outdoor air) are along the axis while the size and color of the sphere at the corresponding XYZ location represents the error (larger meaning more error). The square root of error is plotted because the wide range of error values would make it difficult to discern the differences between similar parameter values. Old CE multi-fault analysis altered all four potential fault parameters so there will be three plots for each of the setback values (full setback, partial setback, and no setback.

7.4.1 Whitehead Excessive Preheat and Not Entering Setback

When either excessive preheating or a failure to enter unoccupied setback occurred, Whitehead experienced a dramatic increase in both heating and cooling load when compared to baseline operation. Therefore, it was theorized that both faults simultaneously occurring may lead to inconclusive results in terms of correct fault identification. However, evaluation of this set of combined faults resulted in a smooth

reduction in error towards a global minimum. For displaying error associated with multiple simultaneous faults, each of the three axes represent one of three potential faults (failure to enter unoccupied setback, excessive preheat, and excessive infiltration) while the size and color of the sphere at the vertex of the parameter values denotes error. Meaning that the direction of reduced error is the vector that points towards the smallest sphere, as seen in Figure 191. Analysis of these three faults revealed full unoccupied setback failure and excessive preheat of 30C° (same as the fault level in the high-fidelity model) resulted in the lowest error by two orders of magnitude compared to adjusting faults outside the two suspected faults.

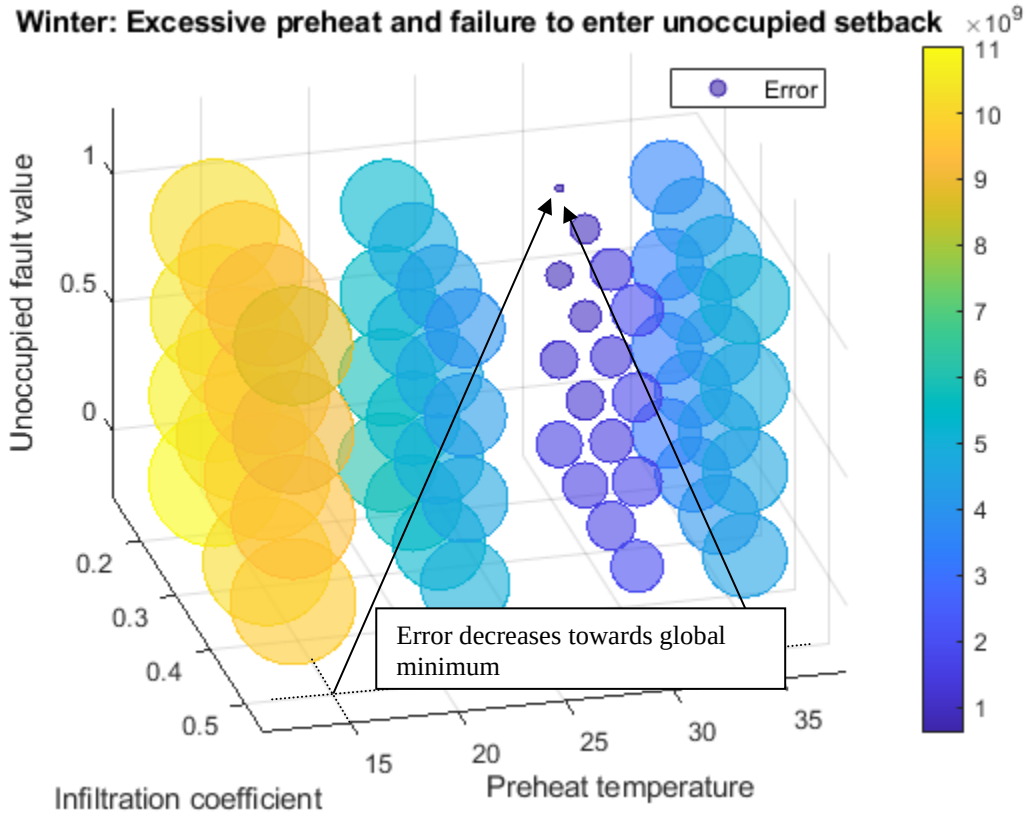

Figure 191A: Whitehead error plot during winter while experiencing two faults; excessive preheat and not entering setback. X, Y, and Z axis represent parameter values while size and color of spheres represent error associated with parameter values at the vertex of (X, Y, Z) parameter values

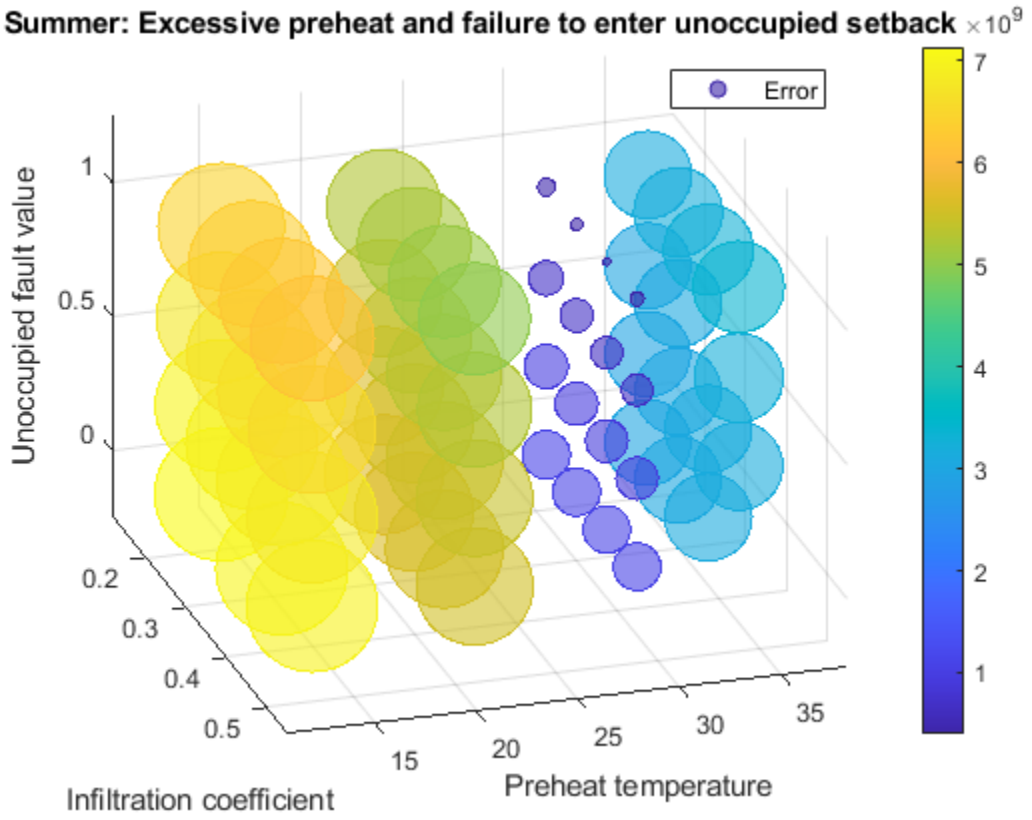

Figure 191B: Whitehead error plot during summer while experiencing two faults; excessive preheat and not entering setback. X, Y, and Z axis represent parameter values while size and color of spheres represent error associated with parameter values at the vertex of (X, Y, Z) parameter values

While winter and summer had differing values for infiltration associated with minimum error, excessive preheat and unoccupied setback fault parameter values associated with minimum error remained the same across both weather conditions. Additionally, infiltration has the least impact on energy demand while excessive preheat and unoccupied setback failure are the most energy intensive. Following tests will examine error minimization and fault identification with a high-intensity fault occurring along with infiltration.

7.4.2 Whitehead Excessive Preheat and Excessive Infiltration

As with not entering setback, excessive infiltration also produced a reduction in error when Whitehead was only experiencing excessive preheat. Due to the high energy demand of excessive preheat, error minimization is dominated by the temperature of the AHU heating coils. Figure 192 does demonstrate that increasing filtration while maintaining a normal preheat setpoint of 12°C lowers the error. However, when the preheat setpoint temperature matches that of the fault value, increasing infiltration beyond 0.32 (value used in high-fidelity model) significantly increases error. The discussed error result behavior reflects what is to be expected from multiple fault behavior and further enforces SPBM's ability to model realistic physical behavior.

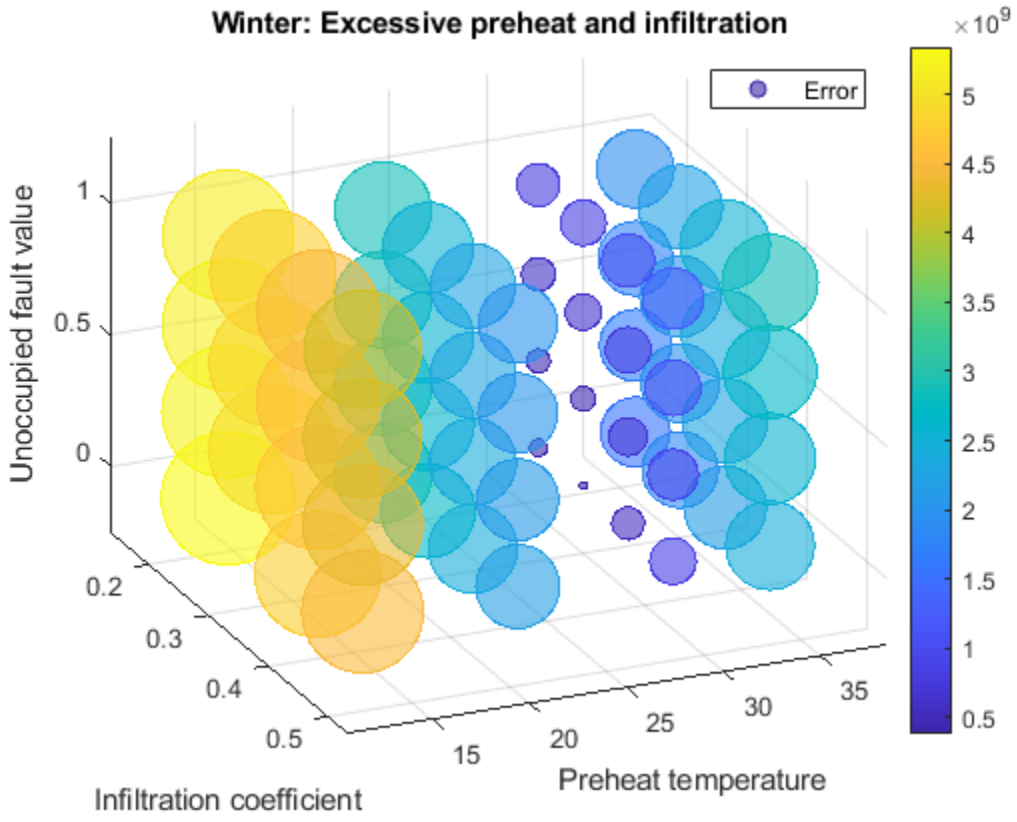

Figure 192A: Whitehead error plot while experiencing two faults; excessive preheat and not entering setback during winter

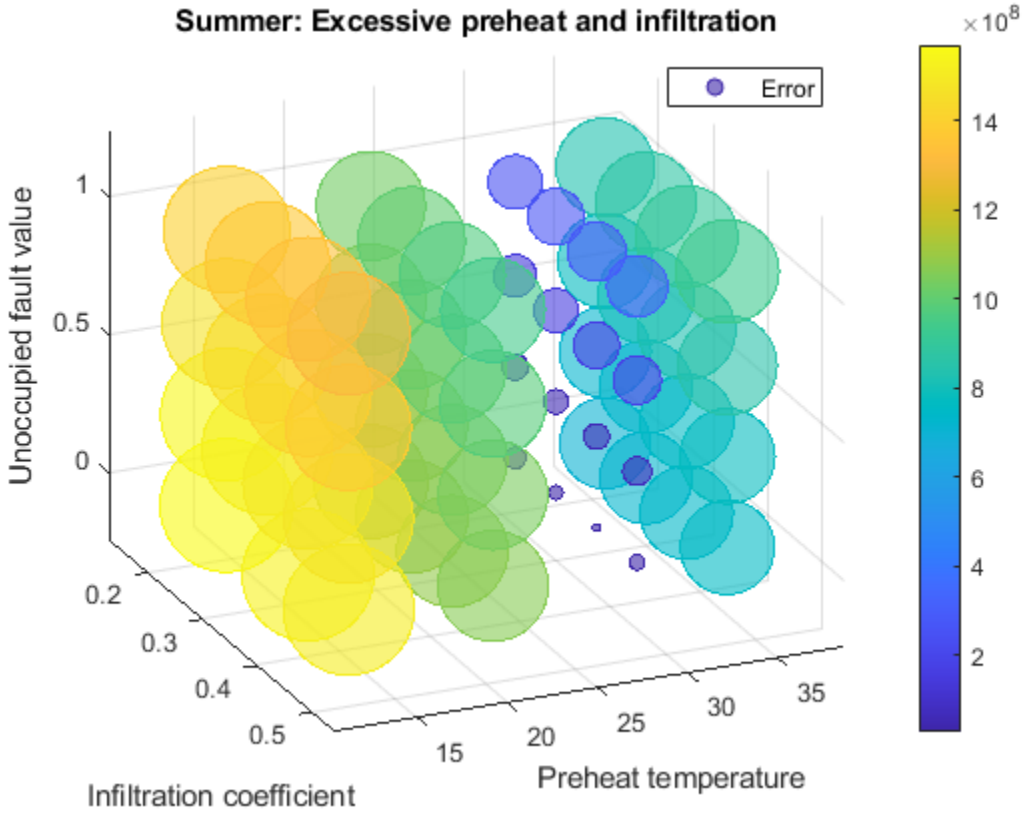

Figure 192B: Whitehead error plot while experiencing two faults; excessive preheat and not entering setback during summer

As with excessive preheat and failure to enter unoccupied setback, minimum error for winter and summer had slightly different infiltration coefficient values. As a reminder, the SPBM is not attempting to exactly match real-world parameter values but rather evaluate how altering parameter values changes relative error.

7.4.3 Whitehead Excessive Infiltration and Failure to Enter Unoccupied Setback

Excessive infiltration and a failure to enter unoccupied setback has demonstrated a convergence towards no setback and higher infiltration values. While Figure 193 shows different infiltration coefficient values for minimum error, the gradient of the error

converges towards excessive infiltration and setback failure. As such, results from error minimization still show a convergence towards increased infiltration and a failure to enter unoccupied setback.

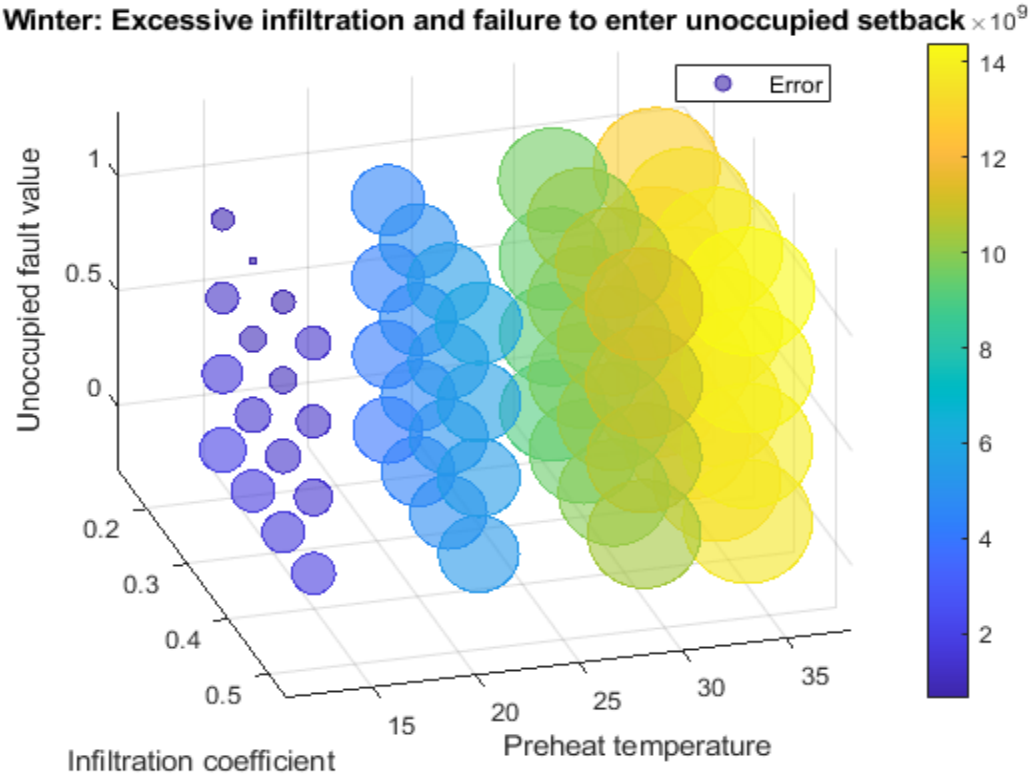

Figure 193A: Whitehead error plot while experiencing two faults; excessive infiltration and not entering setback during winter

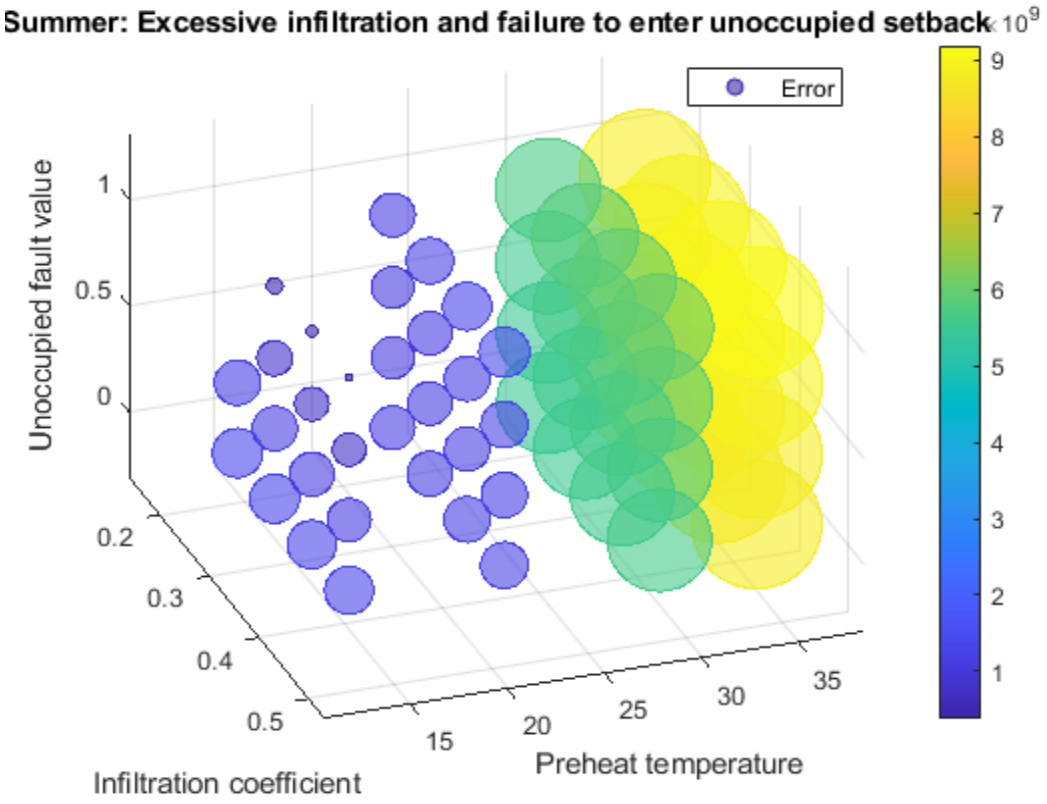

Figure 193B: Whitehead error plot while experiencing two faults; excessive infiltration and not entering setback during summer

Overall, a convergence towards a unique minimum error is attained by adjusting parameter values towards those of the high-fidelity model. In all cases, "as calibrated" parameter values produced significant error and would be representative of fault detection while error convergence is validation of fault identification.

7.4.4 Old CE Excessive Preheating and Failure to Enter Unoccupied Setback

Two different sets of multi-fault combinations were used when evaluating Old CE: excessive preheating with a failure to enter unoccupied setback, and excessive infiltration with insufficient outdoor air flow. All four fault parameters were adjusted for both of the two-fault conditions. By analyzing all four parameter values, it will be possible to determine if a global minimum error exists and if the SPBM converges

towards that minimum error.

Excessive preheat and unoccupied setback failure both produced sizable errors when evaluated separately and continue to have significant error variation when combined. Due to the four-parameter variations, different stages of occupied setback failure (full setback in Figure 194, partial setback in Figure 195, and setback failure in Figure 196) were plotted separately. As such, the minimum value on the error bar represents the minimum error for each plot and is important to note when comparing different stages of setback failure. For instance, minimum plotted error value (square root of true error) for full setback during winter is approximately 4.5E9[J/hr] in Figure 194 while full setback failure is less than 1E9[J/hr] in Figure 196. As such, the error scale represents minimum error for each plot and the lowest error scale represents the lowest overall error for each multi-fault test.

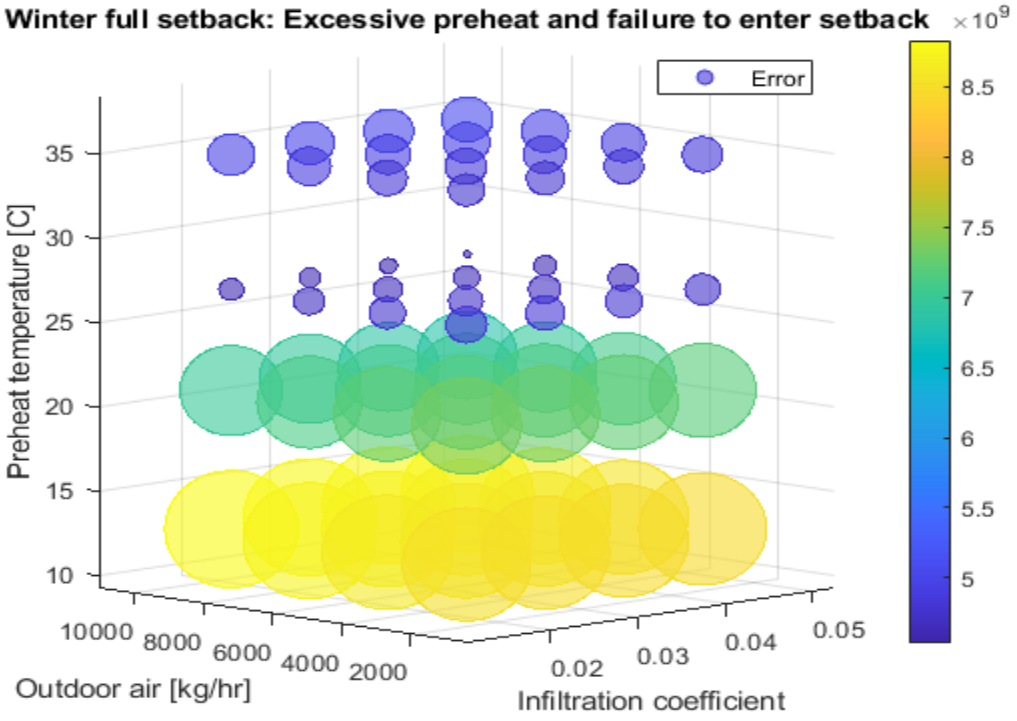

Figure 194A: Error associated with full setback when both excessive preheating and a failure to enter setback is occurring under winter environmental conditions

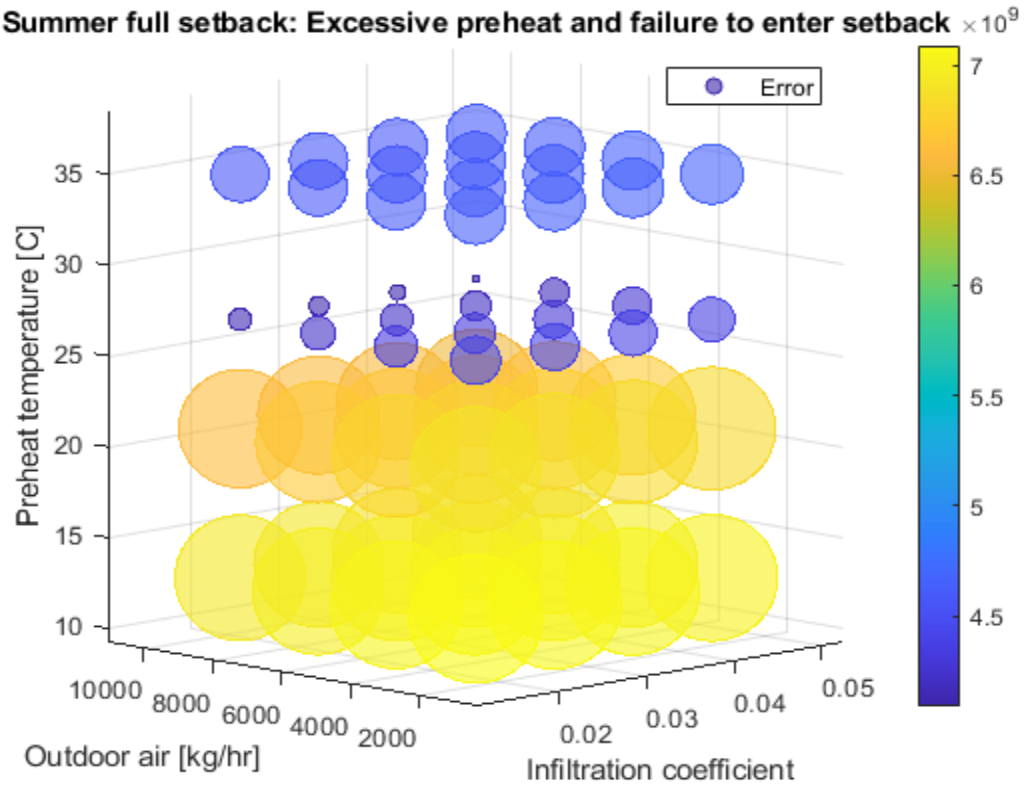

Figure 194B: Error associated with full setback when both excessive preheating and a failure to enter setback is occurring under summer environmental conditions

Partial setback refers to unoccupied temperature setpoint and air flow rates being halfway between occupied and full setback values. Both partial setback failure and complete setback failure have a minimum error associated with the maximum infiltration coefficient due to infiltration increasing load during unoccupied periods in addition to occupied periods.

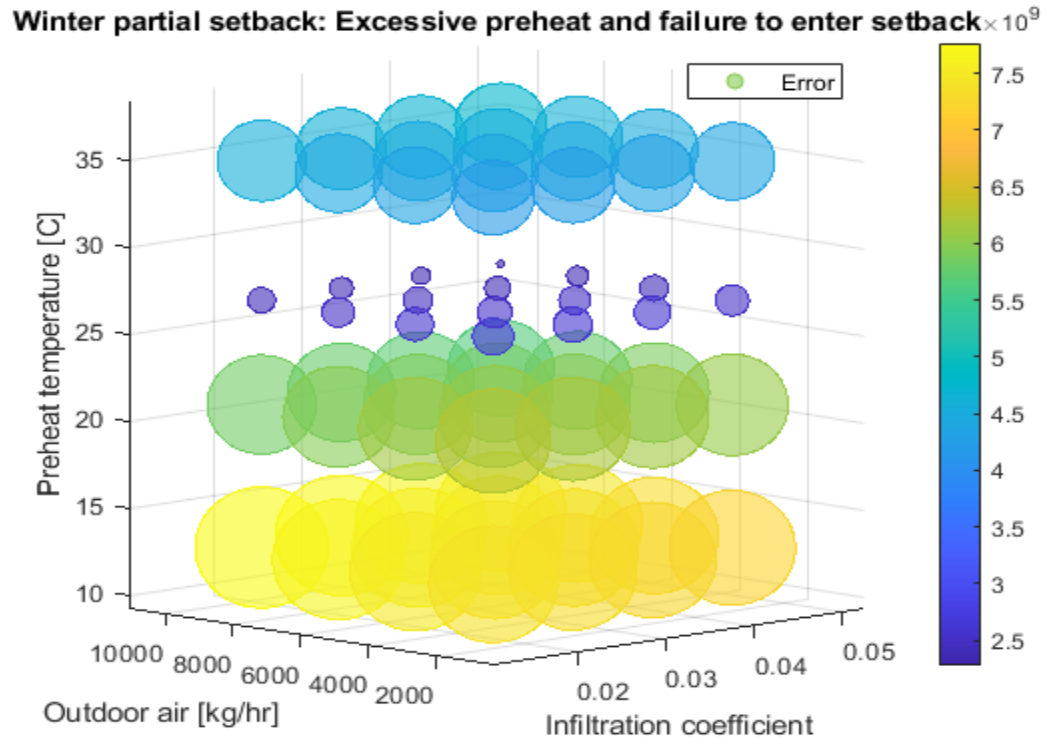

Figure 195A: Error associated with partial setback failure when both excessive preheating and a failure to enter setback is occurring under winter environmental conditions

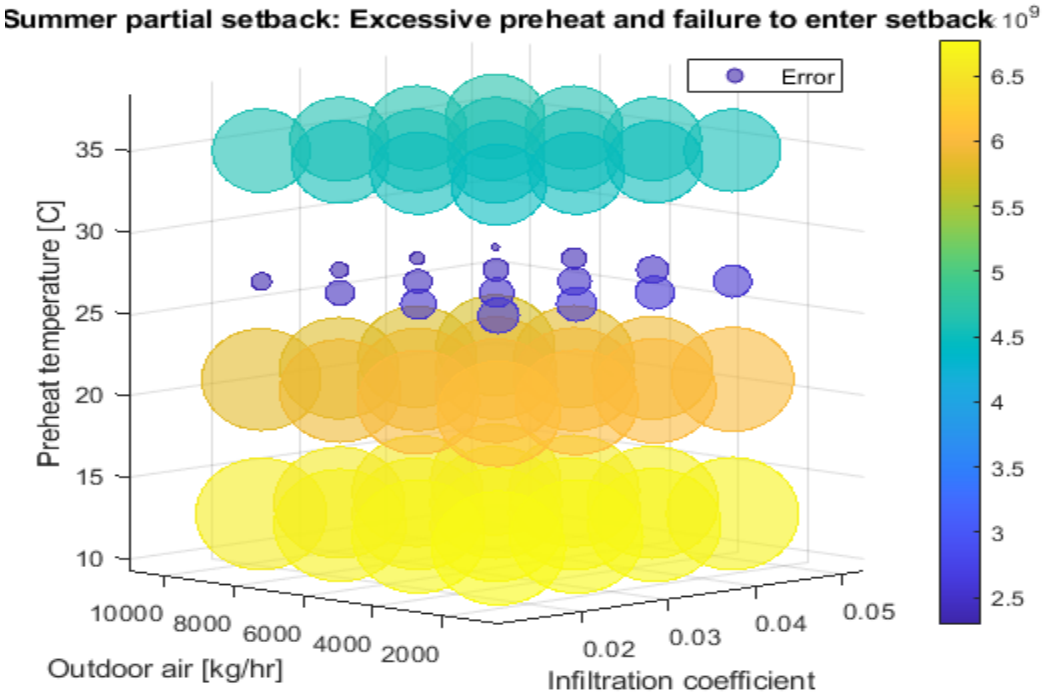

Figure 195B: Error associated with partial setback failure when both excessive preheating and a failure to enter setback is occurring under summer environmental conditions

Both winter and summer converge towards the same minimum error with associated parameters lining up with that of the high-fidelity test model.

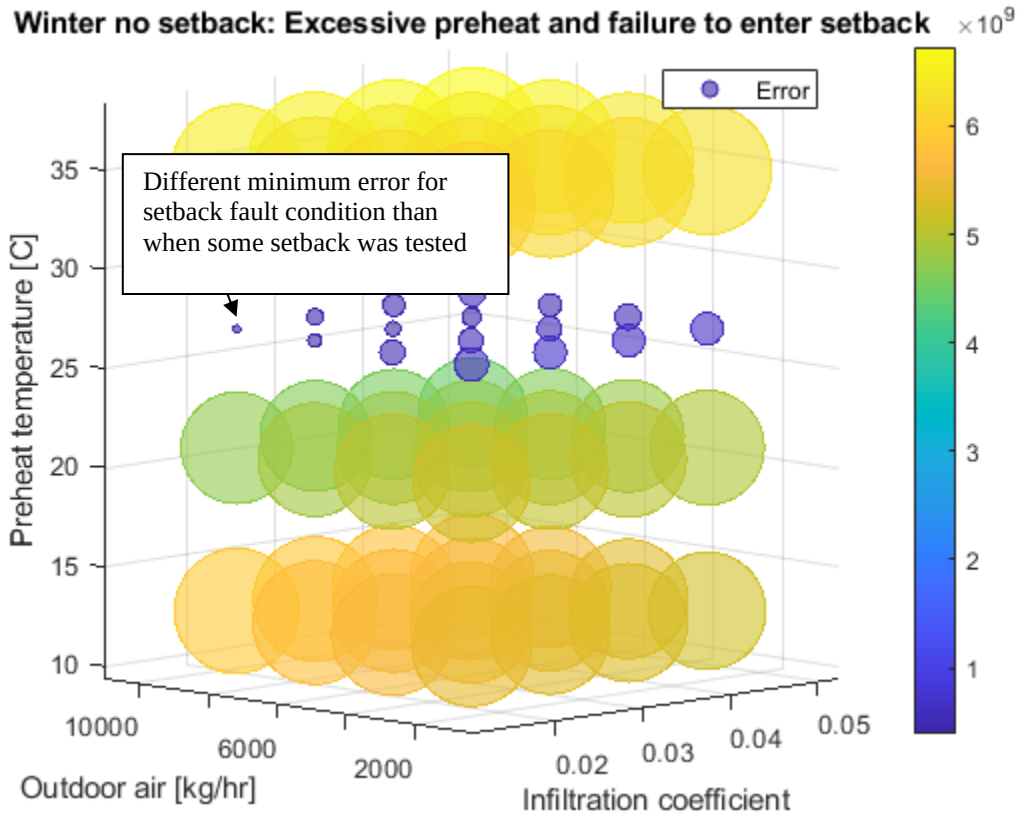

Figure 196A: Error associated with full setback failure when both excessive preheating and a failure to enter setback is occurring under winter environmental conditions

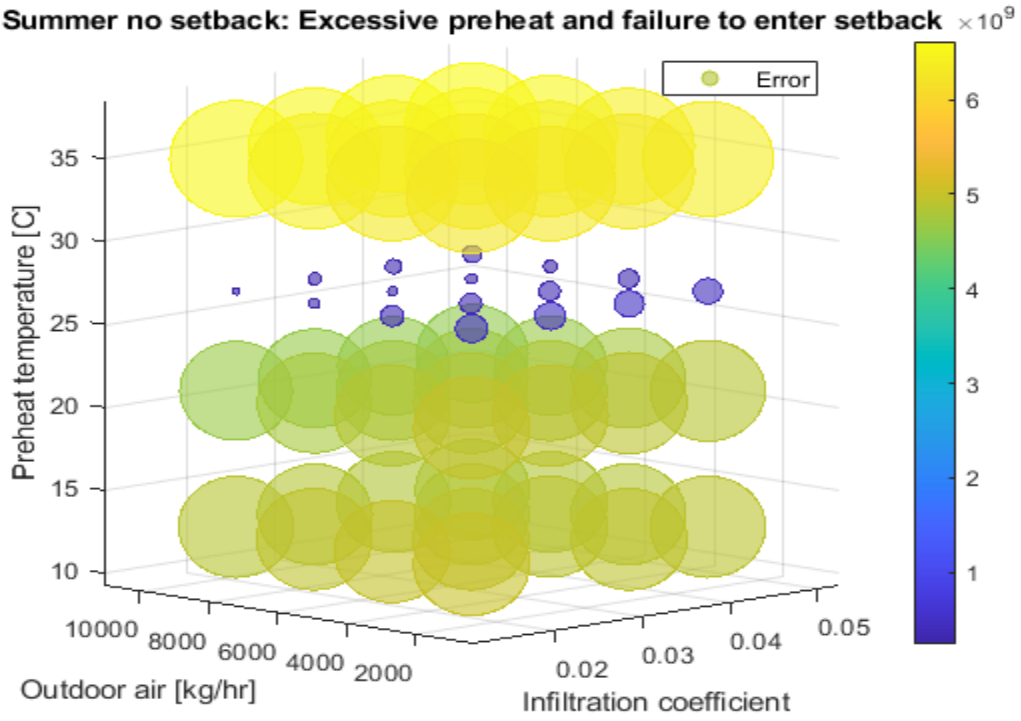

Figure 196B: Error associated with full setback failure when both excessive preheating and a failure to enter setback is occurring under summer environmental conditions

Both winter and summer tests of excessive preheating with failure to enter unoccupied setback converged towards the same parameter value as the high-fidelity reference model, which shows a clear and unique solution to this multi-fault identification test. Infiltration coefficient values for partial and full setback are the maximum value evaluated due to infiltration increasing heating and cooling demand.

7.4.5 Old CE Excessive Infiltration and Insufficient Outdoor Air

Excessive infiltration causes an increase in outdoor air entering building zones while insufficient outdoor air reduces fresh air to the AHUs. Additionally, both of these faults were subtle in their change to energy load error-based fault identification. Regardless of the expected difficulties, both winter and summer fault identification converged towards parameter values that are closest to those in the high-fidelity model;

as shown in Figure 197.

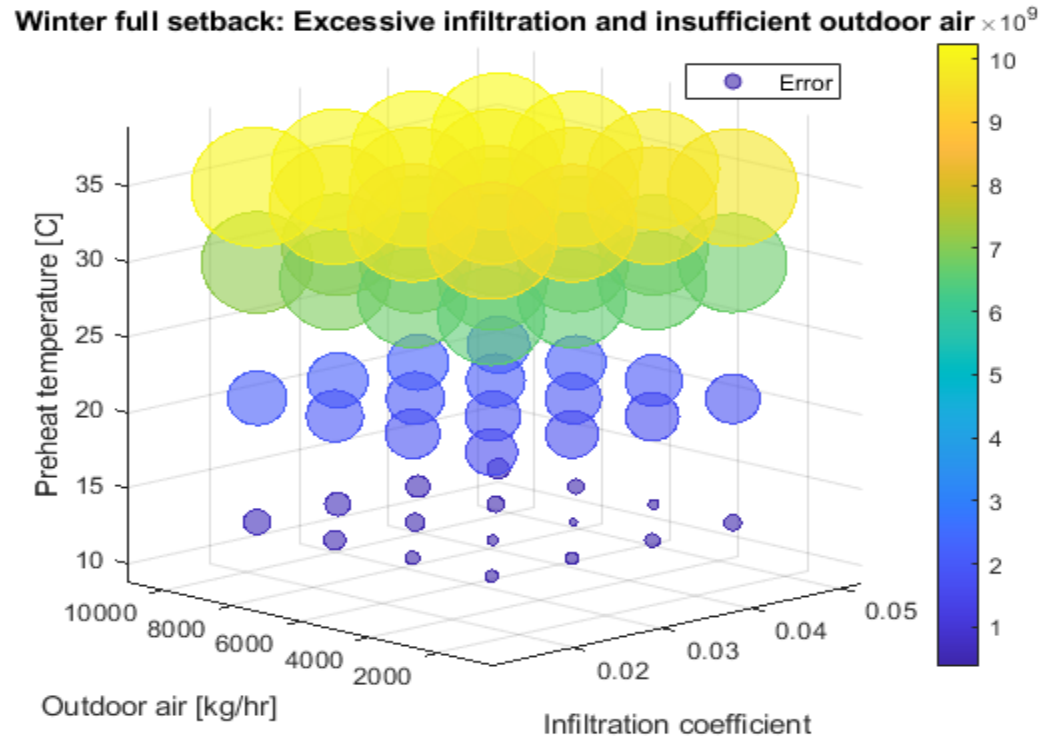

Figure 197A: Error associated with no setback failure when both excessive infiltration and insufficient outdoor air is occurring during winter

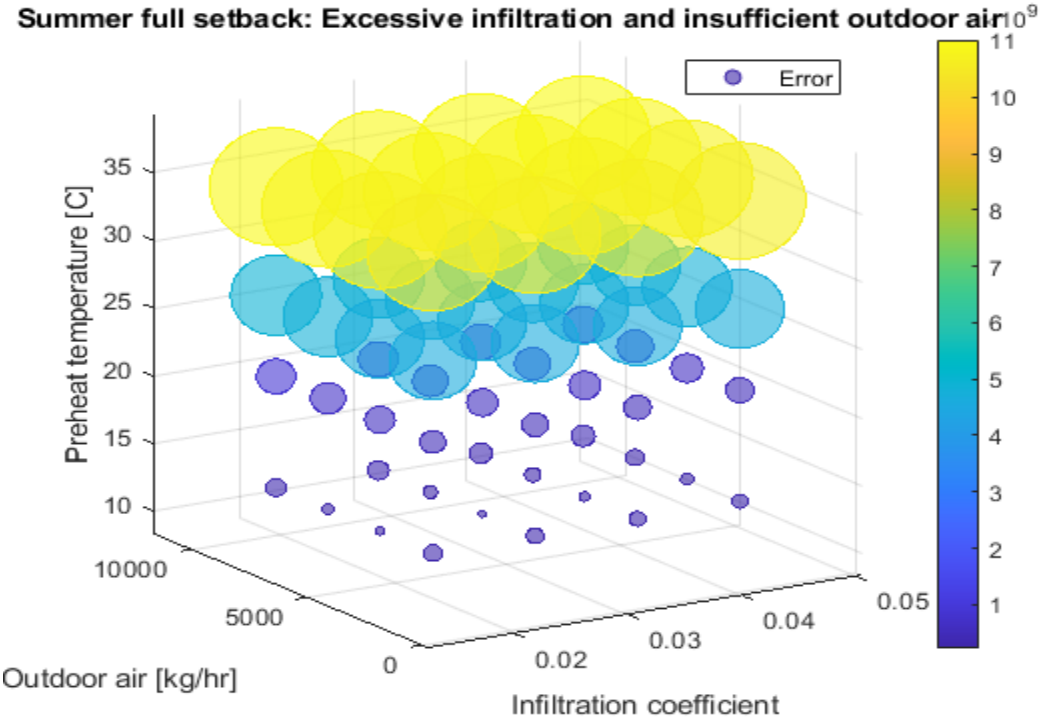

Figure 197B: Error associated with no setback failure when both excessive infiltration and insufficient outdoor air is occurring during winter

Partial setback results in Figure 198 no longer converge towards the same minimum outdoor air flow or infiltration coefficient due to the intensity of error associated with partial setback. For example, the minimum error when partial setback failure is occurring is more than double that of no setback failure.

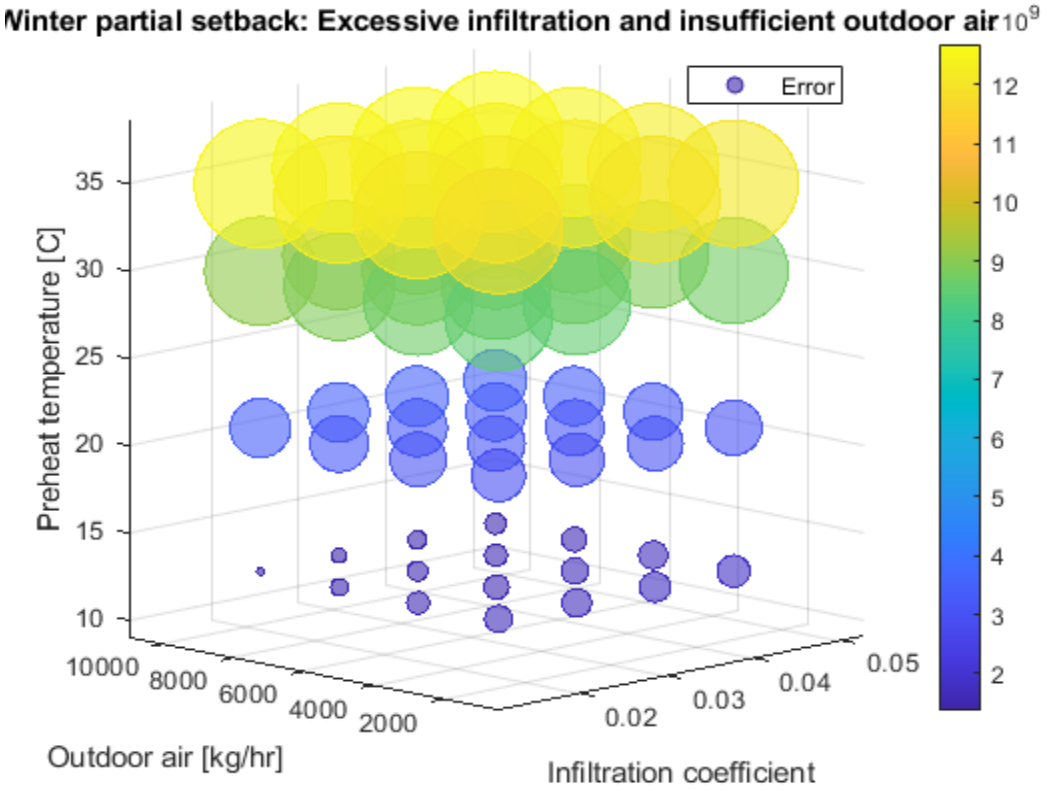

Figure 198A: Error associated with partial setback failure when both excessive infiltration and insufficient outdoor air is occurring under winter environmental conditions

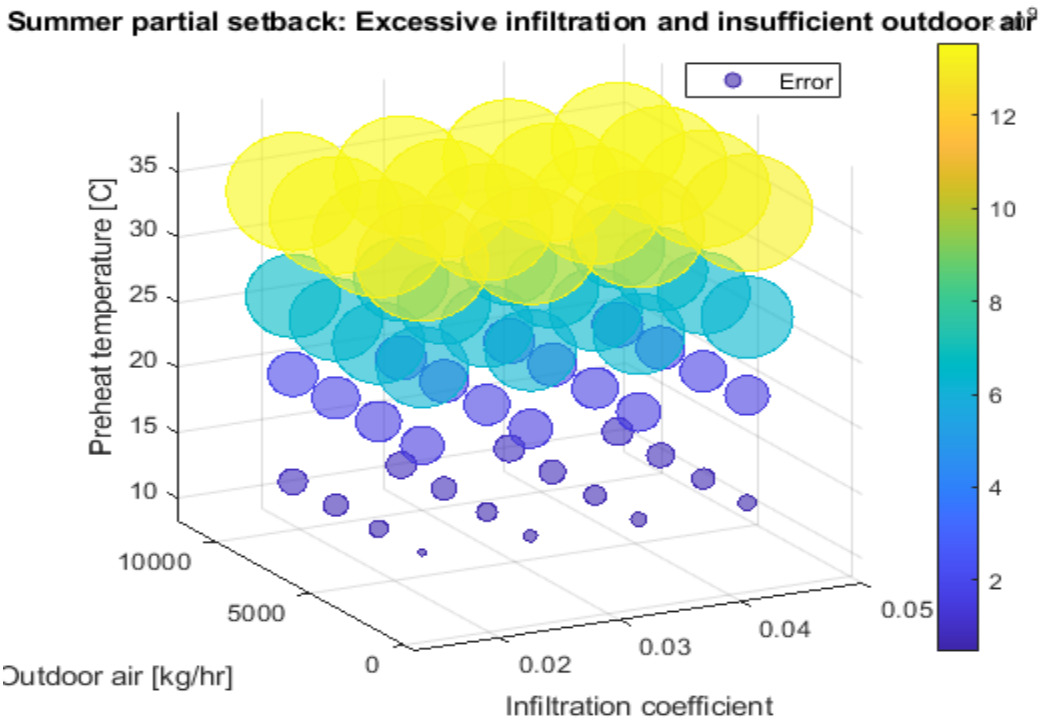

Figure 198B: Error associated with partial setback failure when both excessive infiltration and insufficient outdoor air is occurring under summer environmental conditions

A similar non-convergence of parameter values is observed when no setback occurs due to having such a severe error that it exceeds that from infiltration and insufficient outdoor air. However, Figure 199 has the same minimum occurring at the same outdoor air and infiltration parameter values as partial setback for both winter and summer. Different minimum error values when partial and no setback conditions were evaluated stems from the severity of failing to enter setback is greater than infiltration or insufficient outdoor air. While a local minimum for each setback condition exists, a clear global minimum lies at the expected parameter values. Also of note is that minimum error when entering setback does not occur (Figure 199) is double that of partial setback (Figure 198) and four times that of full setback (Figure 197). The plotted error is the square root of the total sum squared error, so the minimum error of full setback failure is 16 times that of no setback fault.

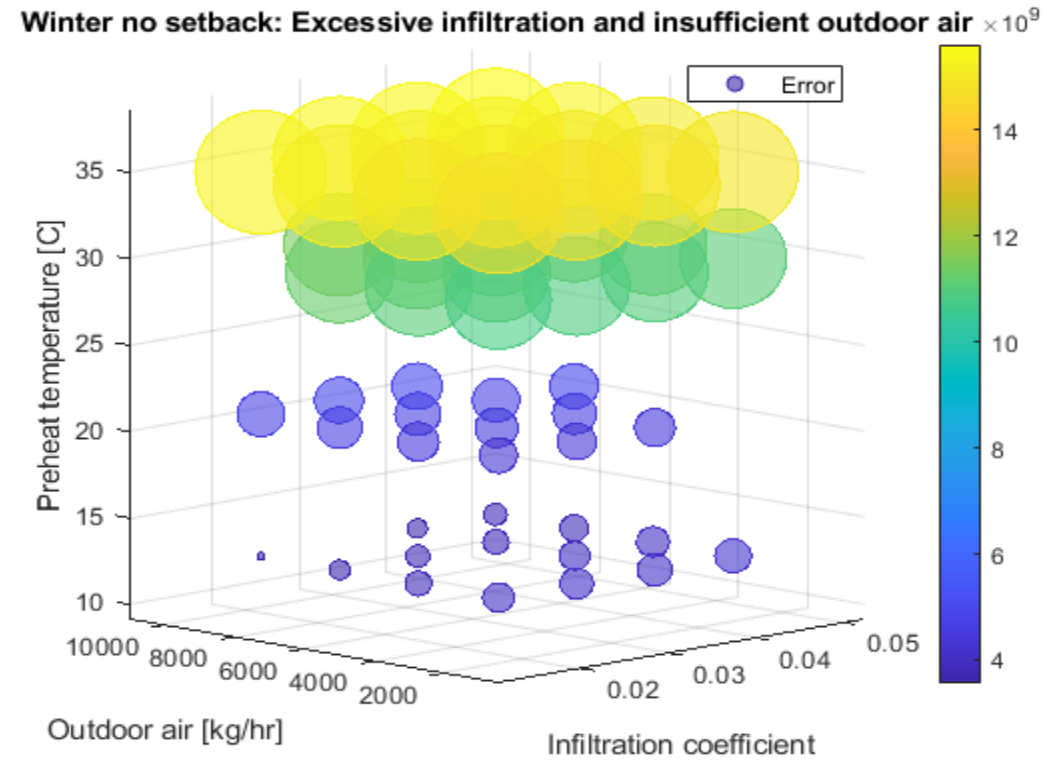

Figure 199A: Error associated with full setback failure when both excessive infiltration and insufficient outdoor air is occurring under winter environmental conditions

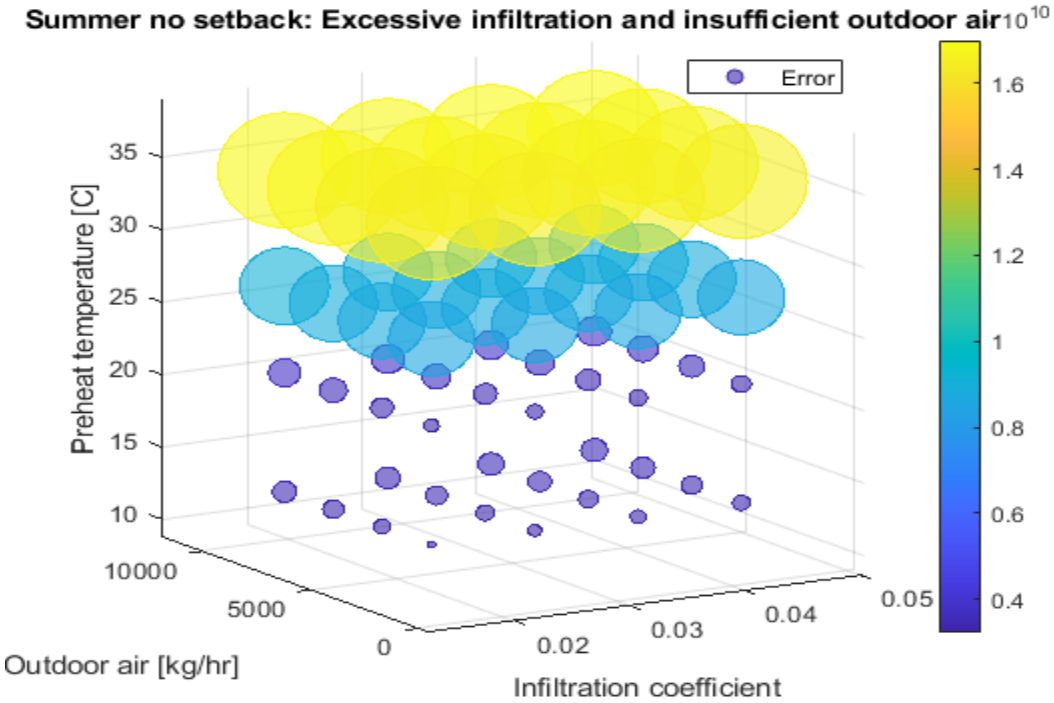

Figure 199B: Error associated with full setback failure when both excessive infiltration and insufficient outdoor air is occurring under summer environmental conditions

Both Whitehead and Old CE displayed convergence towards parameter values associated with the values of the high-fidelity reference model. Additionally, all single and multi-fault tests have shown a clear optimal value and predictable error. As such, it can be said that the SPBM is capable of detecting and identifying unique parameter values associated with different kinds of faults.

CHAPTER 8. NEURAL NETWORK FAULT DETECTION

Much of this paper has focused on a physics-based simulation approach to fault detection and building modeling due to flexibility, ease of calibration, and that the SPBM model required unique development. However, another simplified technique for modeling buildings comes from neural networks. Some research has shown that it is possible to achieve a higher accuracy with energy consumption prediction with a neural network than a high-fidelity model in some instances. Additionally, neural networks can be successfully used for automatic fault detection . However, neural networks require data to train and learn the input/output relations. Requiring training data for faults is problematic because it requires either artificial fault data gathered from a detailed model or operating a building under fault conditions.

Fault detection by neural networks will employ two different techniques: 1) train a neural network to predict heating and cooling loads and determine when and how a divergence occurs when under a fault condition 2) train a neural network under normal and fault conditions in order for it to classify input data as either no fault or one of four faults. These two methods of evaluation will allow for analysis of neural networks as a standalone building fault detection solution and as a supplement to already existing high-fidelity models.

Before continuing, it is important to remember that there is a difference between fault detection and fault identification. Fault detection can be achieved by noting significant and sustained deviations from expected energy consumption levels while fault identification attempts to categorize deviations into potential causes. Both methods will

be explored in this section, beginning with establishing to what degree faults cause deviations in results and then using networks to diagnose building behavior. Comparing these two states of the art fault detection and diagnosis methods with results from the SPBM will provide a practical baseline for result evaluation.

8.1 Time Series Neural Network Fault Detection

Time series neural network fault detection is based on deviation from expected input and output pattern relations . Inputs for time series networks include time, outdoor air temperature, outdoor air humidity, direct solar radiation, diffuse solar radiation, wind speed, wind direction, and building electrical load. Using the above inputs, a network is trained using Bayesian Regularization with either heating or cooling load data as the output. Bayesian Regularization was chosen for being robust, less susceptible to overfitting, and better suited to noisy or difficult data sets when compared to the other available options of Levenberg-Marquardt or Scaled Conjugate Gradient. For this paper, a fault is considered detected when heating or cooling load significantly deviate from expected input/output relations that are generated by the time series NN linear regression line and uncertainty bounds that were calculated under nominal conditions.

Two different input/ouput relations were tested for time series neural networks. NARX (Nonlinear Autoregressive with External (Exogenous) Input), where the predicted value relies on weather, metered electrical data, as well as metered heating and cooling loads. While the other method, NIO (Nonlinear Input-Output), only relies on weather and metered electrical data for predicting loads. Testing showed that NARX had better accuracy while NIO has better divergence when faulty data is used for load prediction.

Initial results using NARX resulted in excellent fit with an R^2 value of approximately 0.99. Heating and cooling model results for both winter and summer conditions in Figure 200 helps visualize the high level of accuracy. However, this network type did not significantly deviate from expected outputs for insufficient outdoor air, excessive infiltration, and not entering setback for winter weather. Excessive preheat fault and not entering setback during summer weather did produce some deviance. While not deviating from metered loads may appear to be a sign of good modeling, further testing resulted in no fault being detected aside from excessive preheat or not entering setback during summer weather.

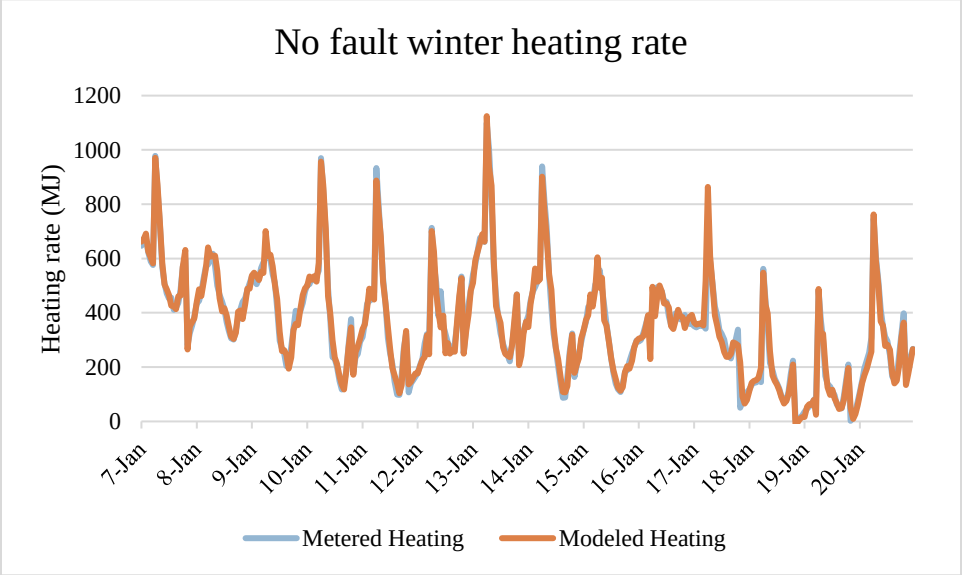

Figure 200A: NARX 10 neurons and 12 delay neural network heating load prediction for Whitehead during winter. While model accuracy is exceptional, the NN is incapable of divergence for tested faults

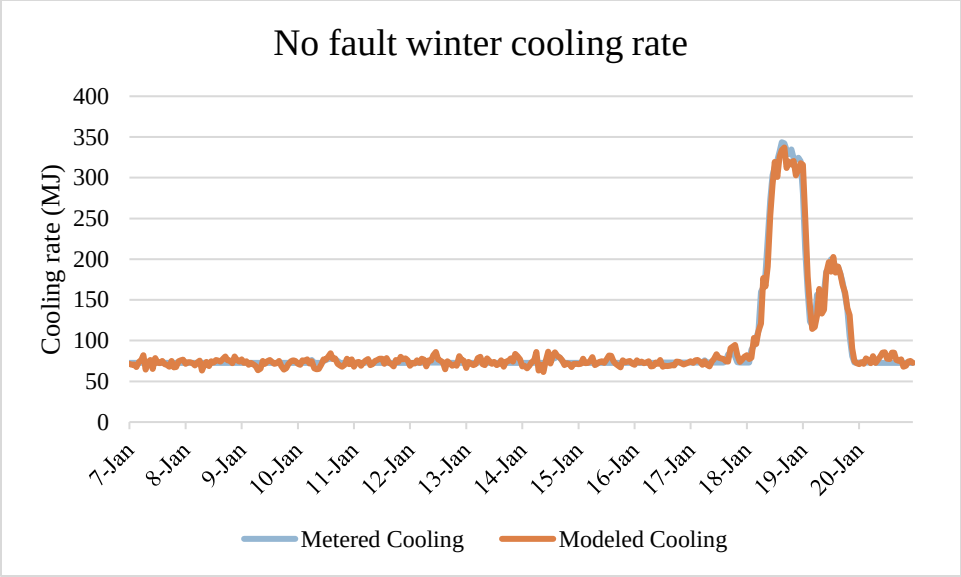

Figure 200B: NARX 10 neurons and 12 delay neural network cooling load prediction for Whitehead during winter. While model accuracy is exceptional, the NN is incapable of divergence for tested faults

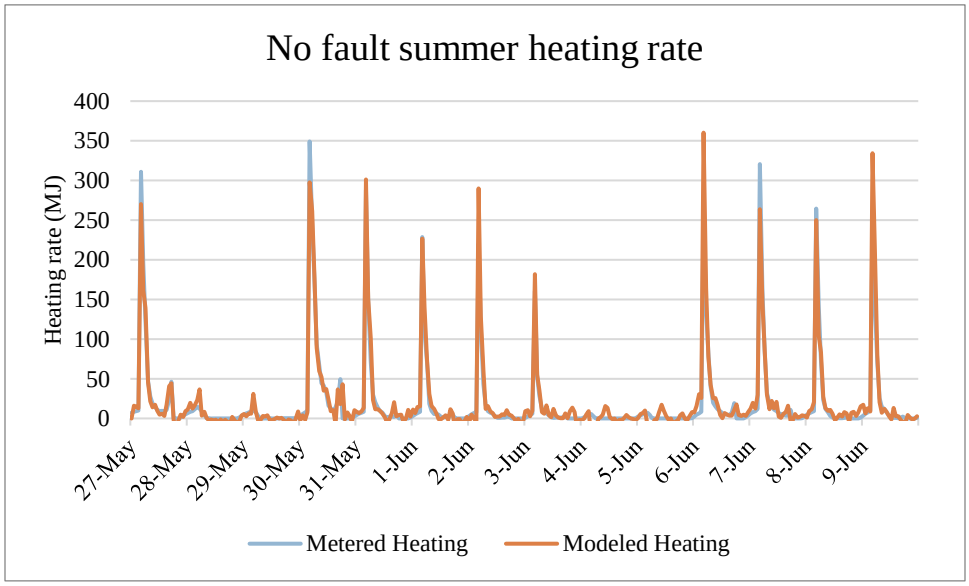

Figure 200C: NARX 10 neurons and 12 delay neural network heating load prediction for Whitehead during summer. While model accuracy is exceptional, the NN is incapable of divergence for tested faults

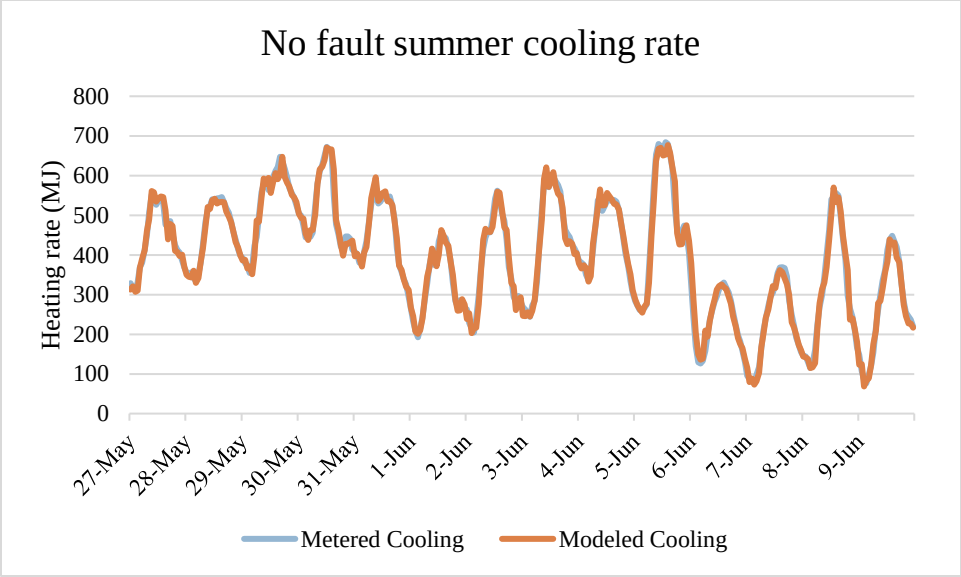

Figure 200D: NARX 10 neurons and 12 delay neural network cooling load prediction for Whitehead. While model accuracy is exceptional, the NN is incapable of divergence for tested faults

Moving away from NARX time series energy modeling did maintain excellent energy prediction (R^2 greater than 0.98) and resulted in some deviation for fault parameters. The excellent fitting of NARX neural networks for all faults might explain why energy prediction research is so popular while neural network fault detection is least popular as neural networks are adept at pattern recognition but poor at extrapolation . However, deviation displayed by nonlinear input/output raises the question if there is an ideal number of hidden neurons and delays that would produce a best-case network. While it is possible that optimum specifications exist, it is impossible to know what that case is unless tested .

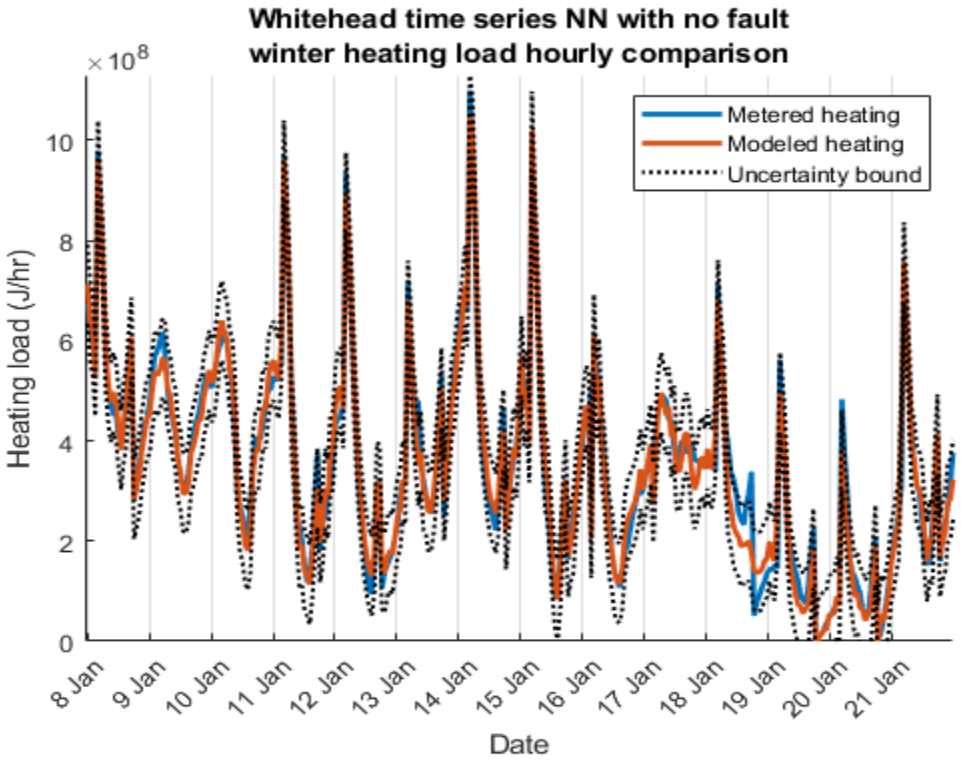

Figure 201A: Nonlinear 10 neurons and 12 delay neural network heating load prediction for Whitehead during winter. Time series NN displays excellent agreement with metered load, though not to the same degree as NARX.

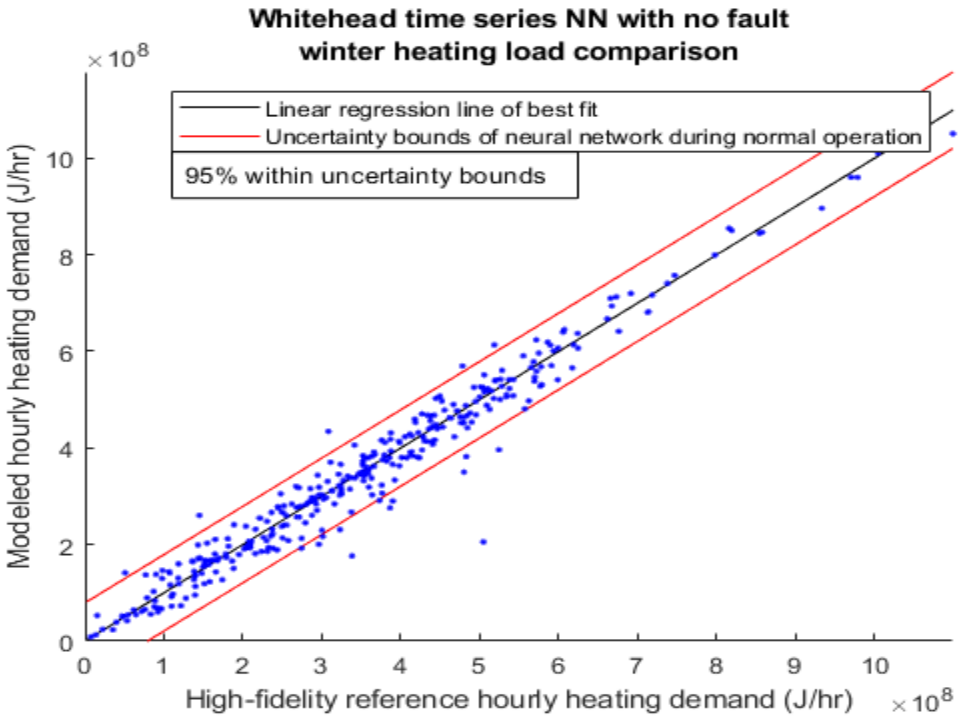

Figure 201B: Nonlinear 10 neurons and 12 delay neural network heating load alignment factor for Whitehead during winter. Time series NN displays excellent agreement with metered load, though not to the same degree as NARX.

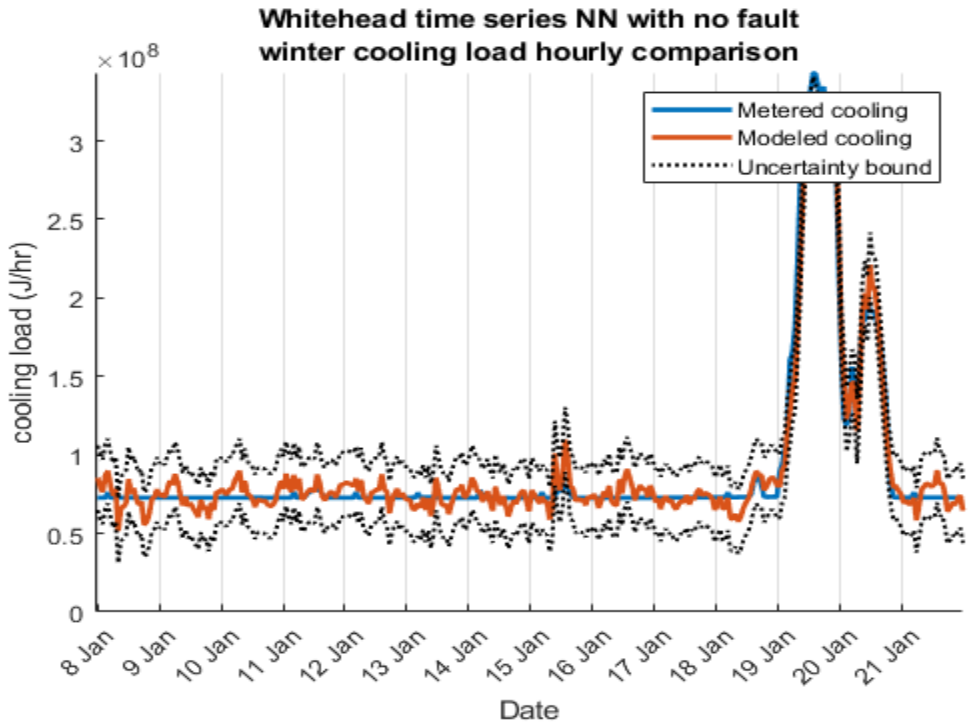

Figure 201C: Nonlinear 10 neurons and 12 delay neural network cooling load prediction for Whitehead during winter. Time series NN displays excellent agreement with metered load, though not to the same degree as NARX.

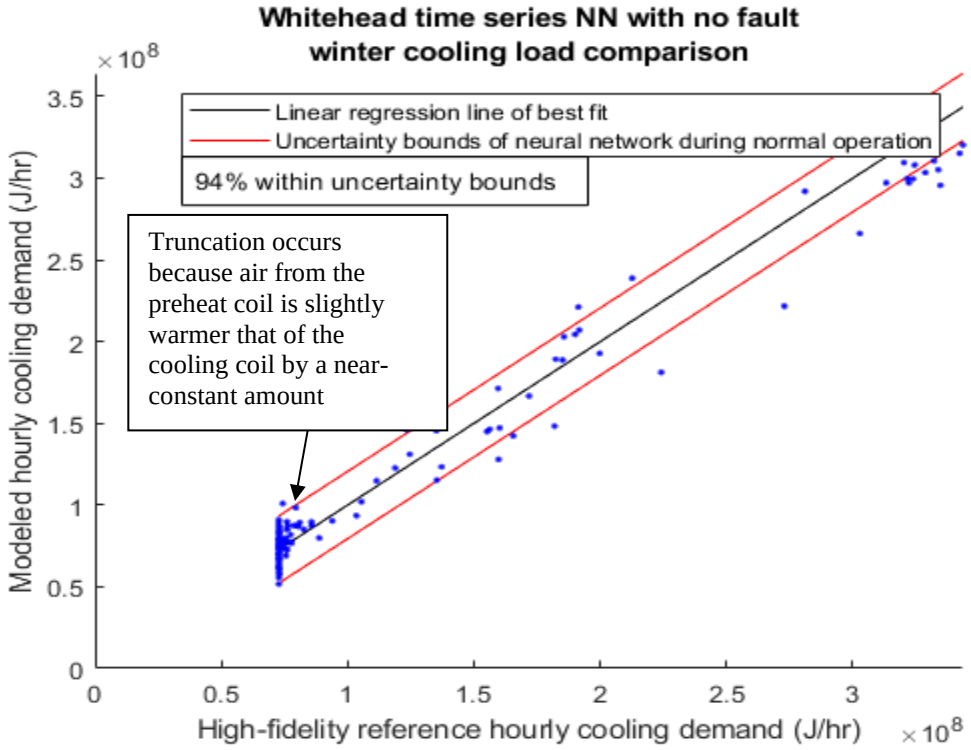

Figure 201D: Nonlinear 10 neurons and 12 delay neural network cooling load alignment factor for Whitehead during winter. Time series NN displays excellent agreement with metered load, though not to the same degree as NARX.

Winter time series NN displays the overall load matching expected of a well trained system for heating load but random noise for cooling load prediction in Figure 201. The noise comes from random variations that the network learned during training that allows it to respond to increases in load and deviations under fault conditions.

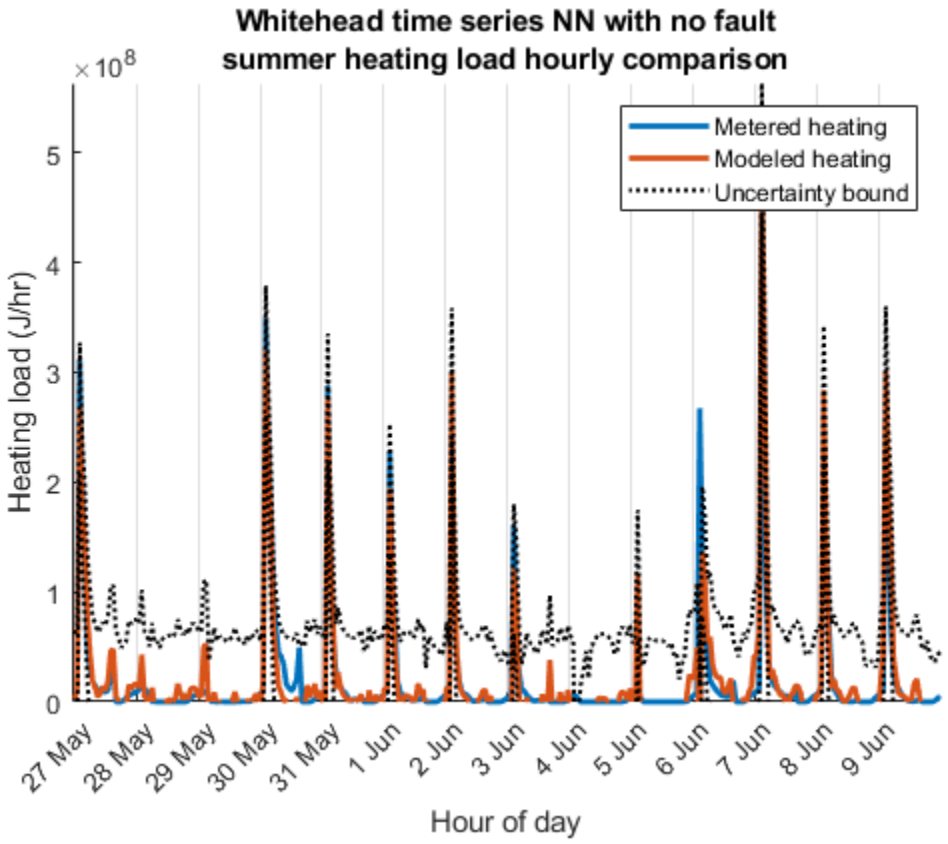

Figure 202A: Nonlinear 10 neurons and 12 delay neural network heating load prediction for Whitehead during summer. Time series NN displays excellent agreement with metered load, though not to the same degree as NARX.

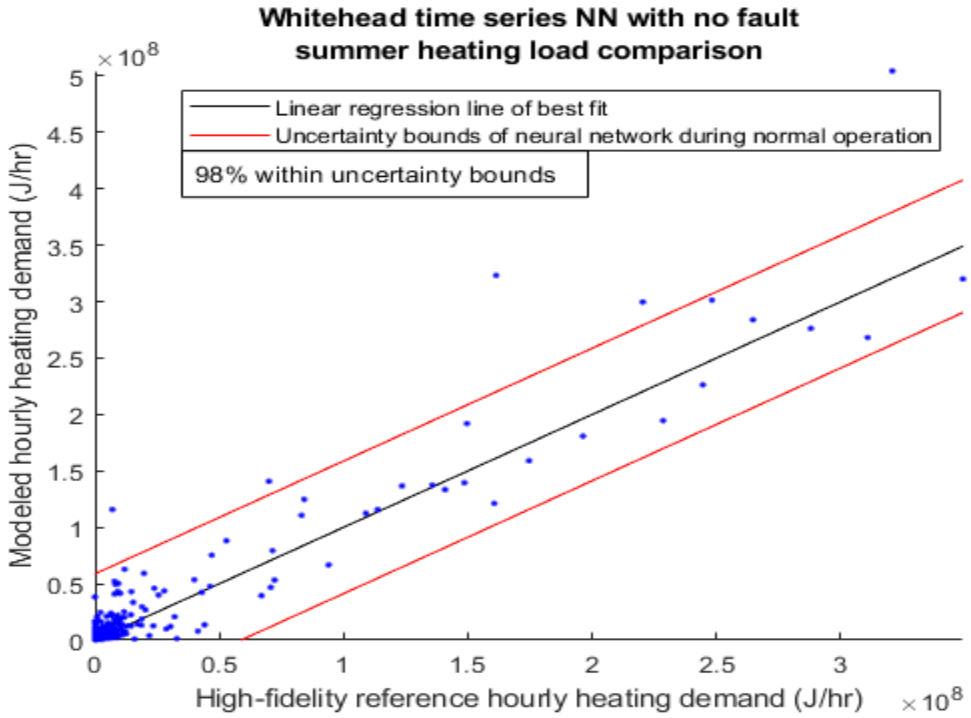

Figure 202B: Nonlinear 10 neurons and 12 delay neural network heating load alignment factor for Whitehead during summer. Time series NN displays excellent agreement with metered load, though not to the same degree as NARX.

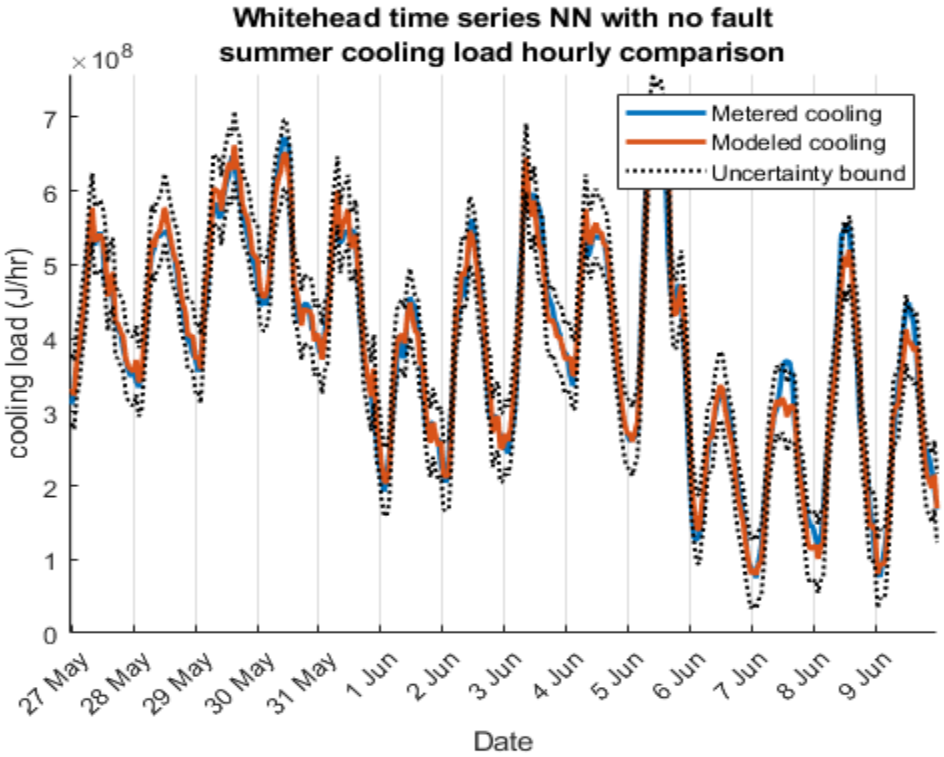

Figure 202C: Nonlinear 10 neurons and 12 delay neural network cooling load prediction for Whitehead during summer. Time series NN displays excellent agreement with metered load, though not to the same degree as NARX.

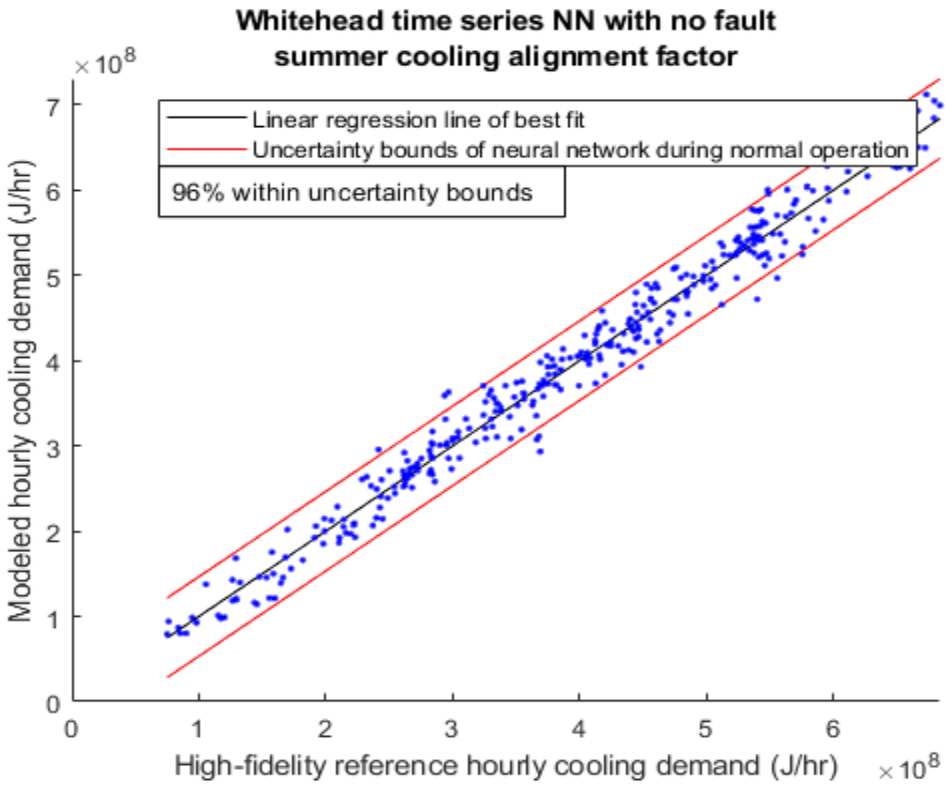

Figure 202D: Nonlinear 10 neurons and 12 delay neural network cooling load alignment factor for Whitehead during summer. Time series NN displays excellent agreement with metered load, though not to the same degree as NARX.

Neural network time series have been used for fault detection by observing deviations away from expected outputs for given inputs. Therefore, using time series will not necessarily identify which fault is occurring. However, given that building loads are physical, it may be possible to see how and where deviations from expected results occur and use that information to piece together a plausible fault.

8.1.1 Whitehead Excessive Infiltration

Excessive infiltration is a fault that one would expect to align strongly with outdoor air wind speed and outdoor air temperature. However, no strong correlation between excessive deviation of predicted load and wind speed were observed for time series neural network testing. It is possible that an increase in electrical use due to an

increase in HVAC demand is what caused the deviation from metered data. As mentioned before, analyzing the structure of a neural network does not bring insightful information on how the network changes for particular inputs. Regardless, Figure 203 and Figure 204 displays the deviation from predicted load that would be expected during occurrence of a fault in the form of increased demand from the dominate loads for each season.

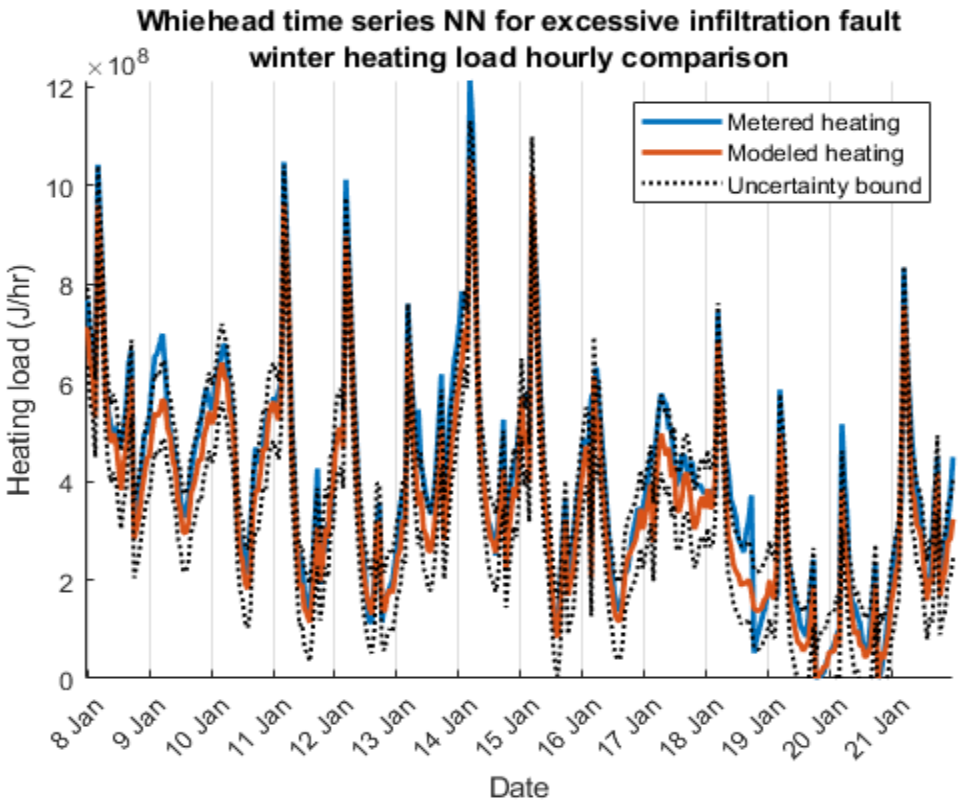

Figure 203A: Predicted heating load for Whitehead while experiencing excessive infiltration fault condition during winter

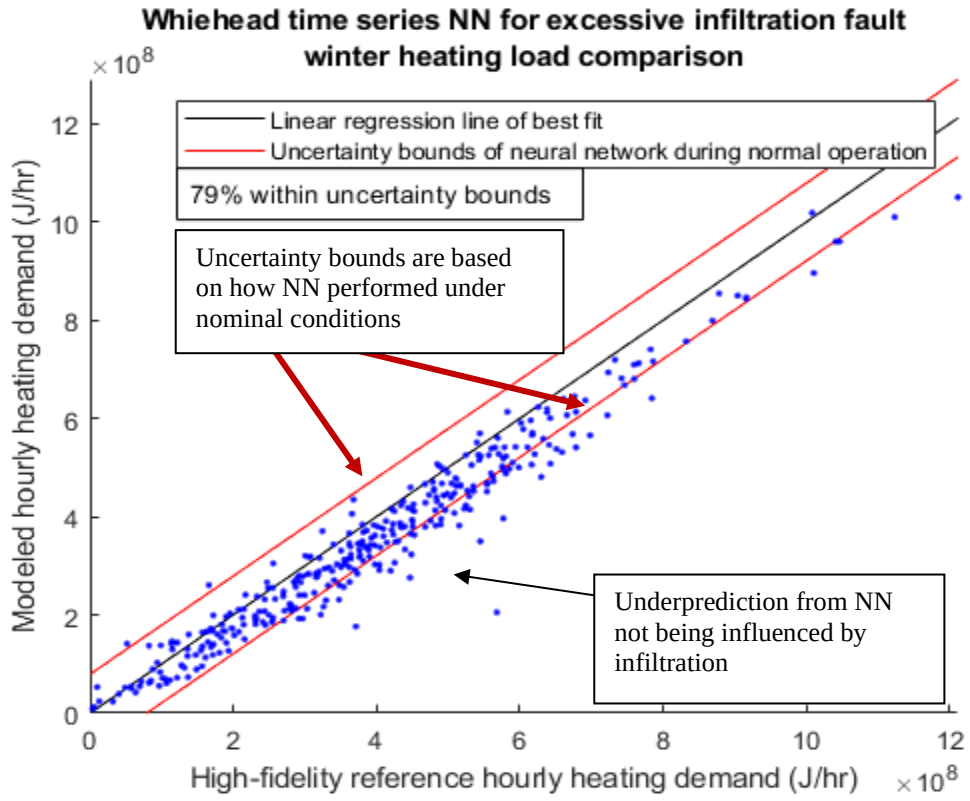

Figure 203B: Alignment factor for heating load for Whitehead while experiencing excessive infiltration fault condition during winter

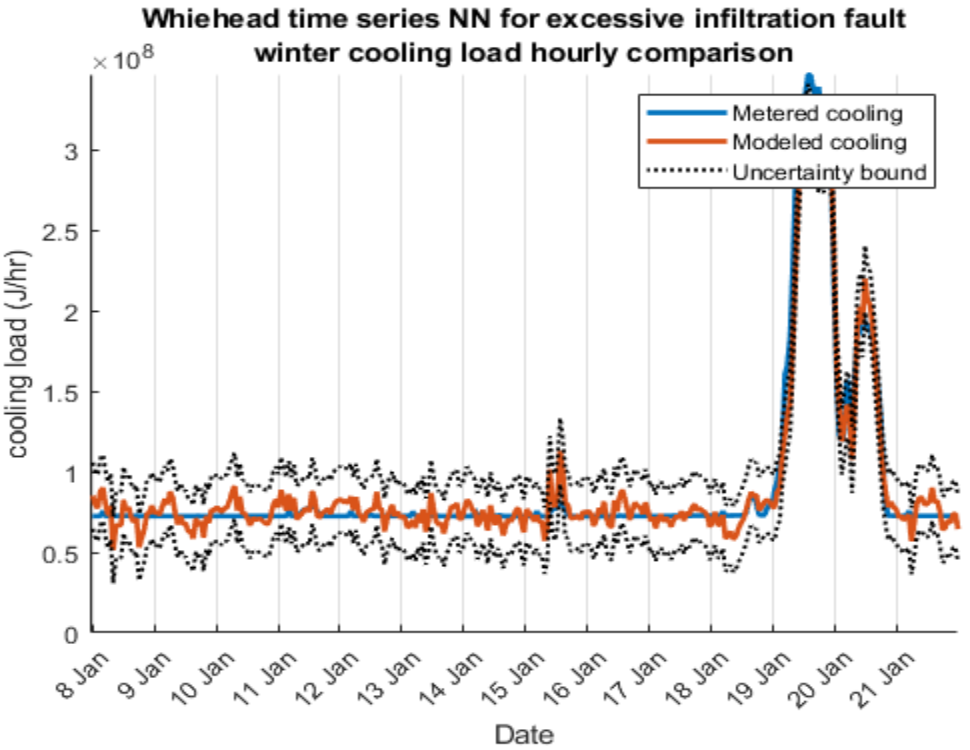

Figure 203C: Predicted cooling load for Whitehead while experiencing excessive infiltration fault condition during winter

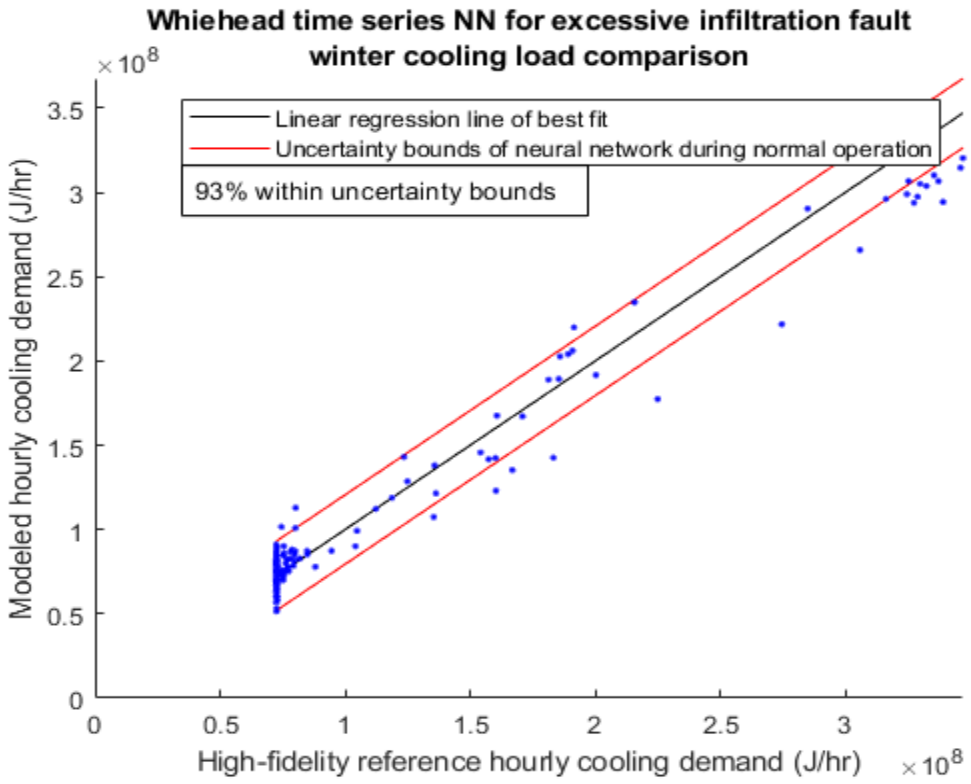

Figure 203D: Cooling load alignment factor for Whitehead while experiencing excessive infiltration fault condition during winter

Figure 203 shows nearly the same cooling load prediction as nominal conditions because winter weather infiltration would not increase cooling demand within zones. However, heating load is underpredicted as the trained network is not anticipating an elevated level of outdoor air entering zones. Figure 204 reveals that infiltration tends to alter the primary load as heating demand in summer is relatively unchanged while cooling demand increased in metered data.

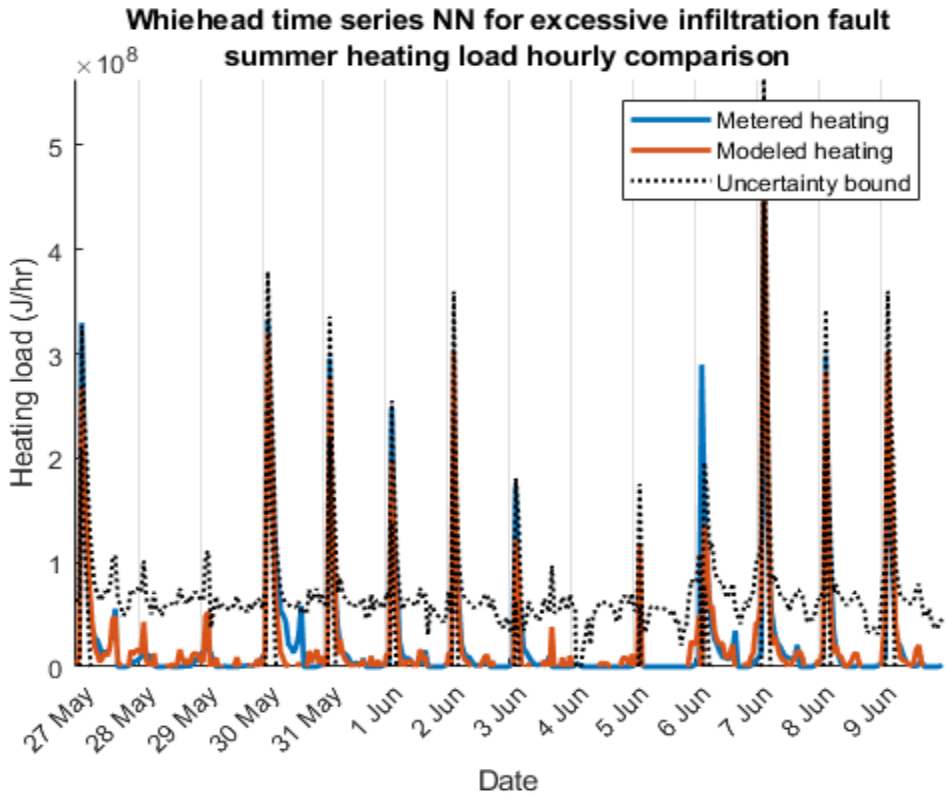

Figure 204A: Predicted heating load for Whitehead while experiencing excessive infiltration fault condition during summer

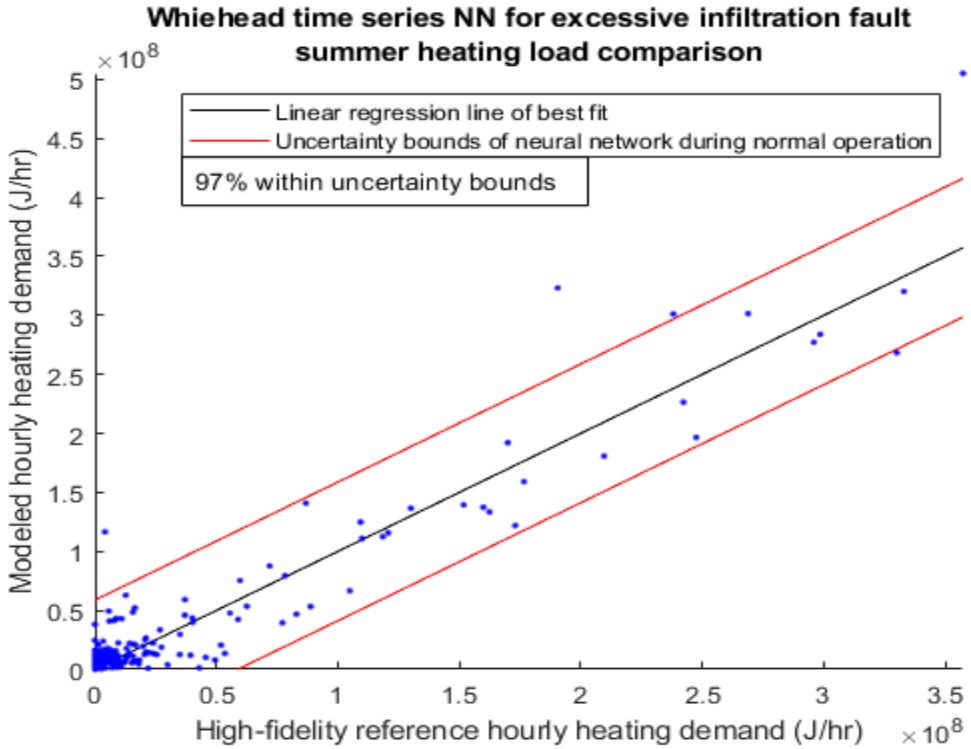

Figure 204B: Alignment factor of heating load for Whitehead while experiencing excessive infiltration fault condition during summer

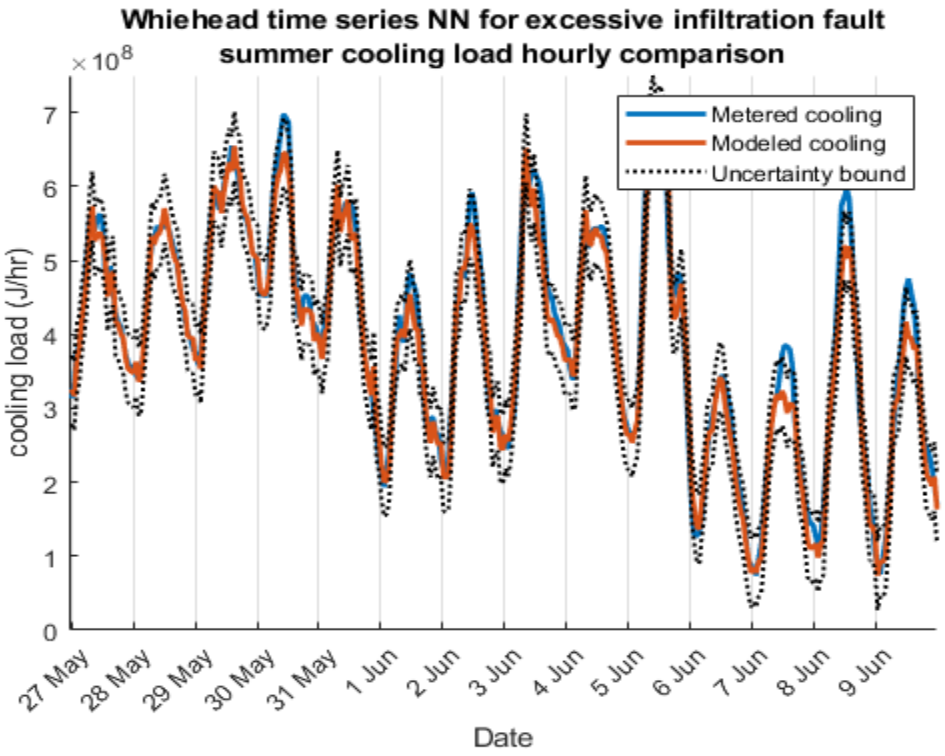

Figure 204C: Predicted cooling load for Whitehead while experiencing excessive infiltration fault condition during summer

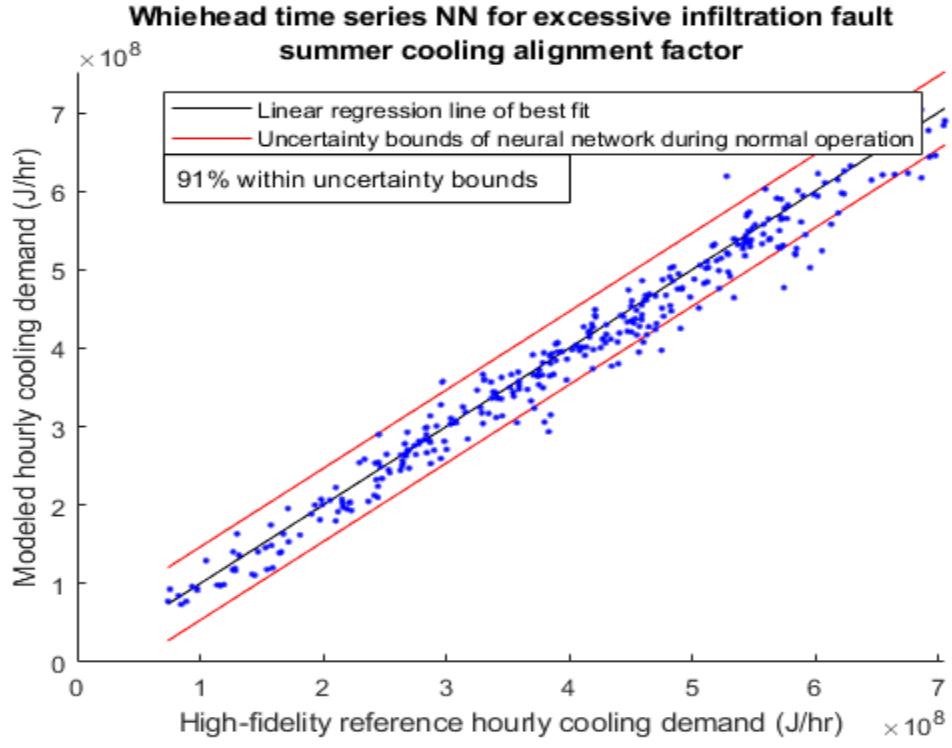

Figure 204D: Alignment factor of heating load for Whitehead while experiencing excessive infiltration fault condition during summer

Winter heating demand displayed a characteristic divergence from 1:1 alignment and a significant number of points outside the prediction interval. However, no divergence was observed from cooling demand prediction due to infiltration not having a significant impact on cooling performance. Summer demand for winter and summer conditions shows no statistically significant change from metered data. While NNs are faster and less complicated to calibrate than a SPBM, there is a downside in that parameters cannot be adjusted once the model is trained to check for how different faults alter error values like the SPBM did for relative error analysis. This drawback becomes more apparent for low sensitivity faults such as infiltration where fault identification finds a minimum error value by adjusting parameter values and where there is a small change in energy demand between no-fault and faulty metered data.

8.1.2 Whitehead Not Entering Unoccupied Setback

Not entering setback is a fault that should only present itself during unoccupied hours, a perfect example of how automated fault detection could be utilized. Figure 205 reveals some periods of agreement during occupied hours with the heating load during winter. However, cooling load prediction deviation occurs for multiple days during a period of time in which the building was in occupied mode. Summer demand prediction was less definitive than winter loading but still within detection range. Heating demand during summer loading showed significant deviation when non-zero demand occurred while cooling demand displayed a clear bias towards overprediction. Overall, analysis of setback fault results in clear identification of a system error regardless of season.

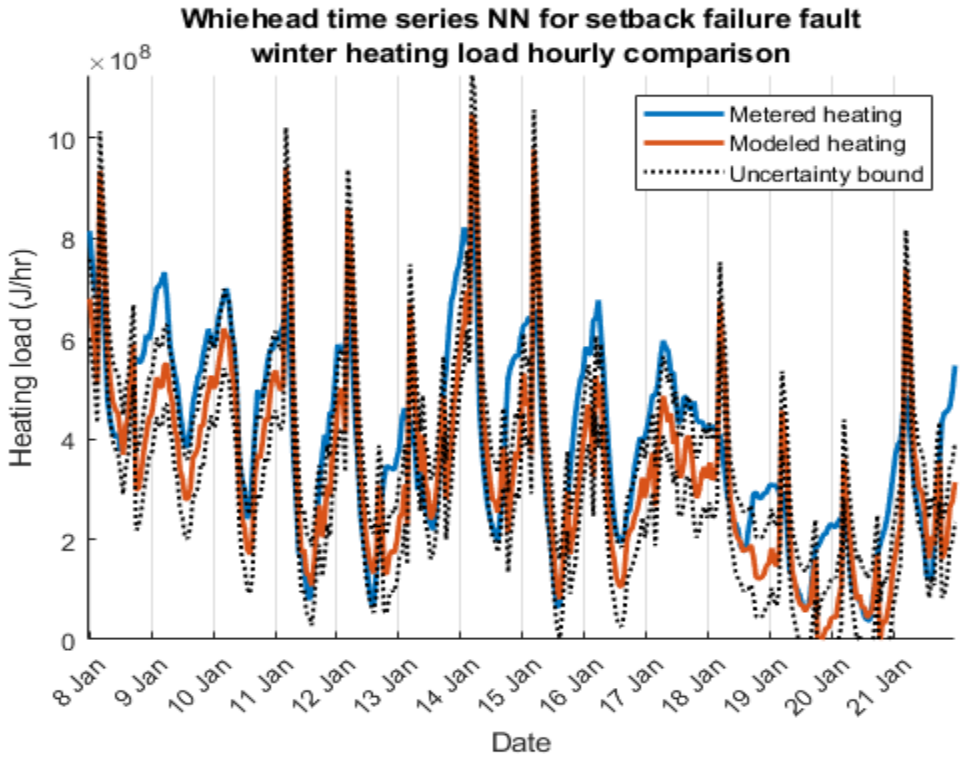

Figure 205A: Predicted heating load for Whitehead while not entering unoccupied setback during winter

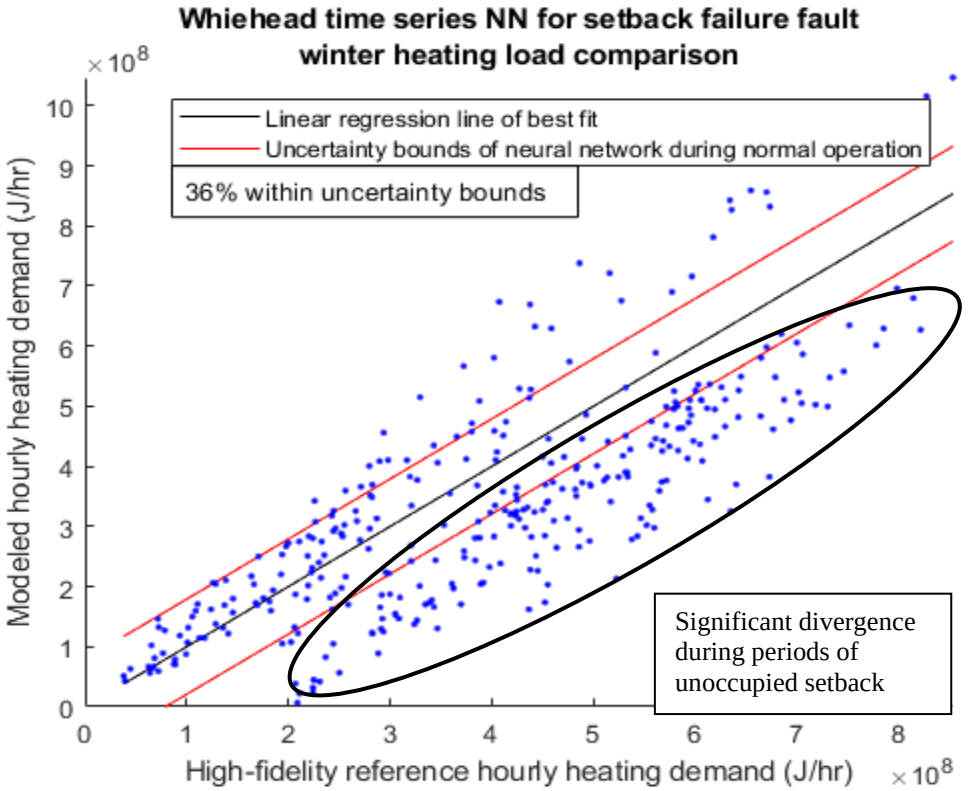

Figure 205B: Alignment factor of heating load for Whitehead while not entering unoccupied setback during winter

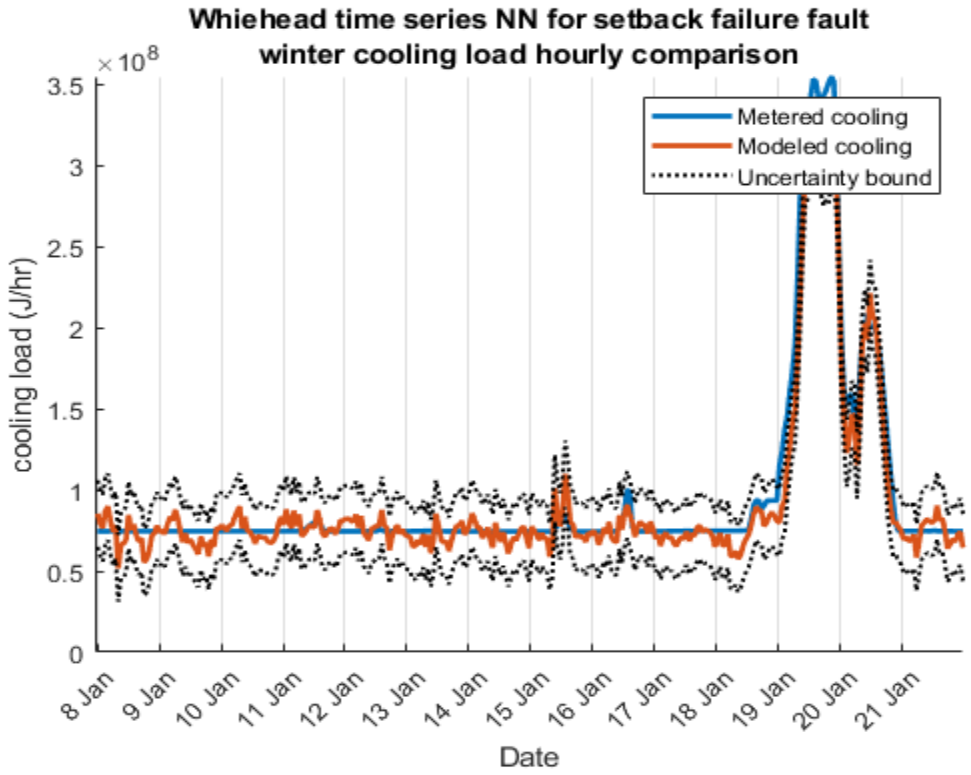

Figure 205C: Predicted cooling load for Whitehead while not entering unoccupied setback during winter

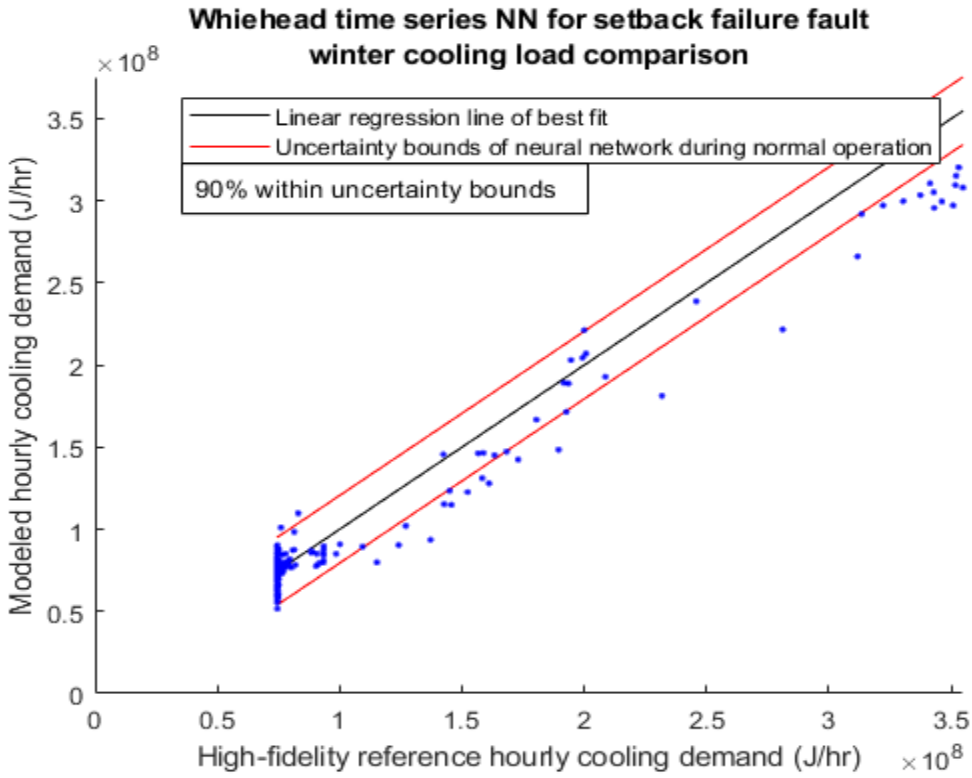

Figure 205D: Alignment factor of cooling load for Whitehead while not entering unoccupied setback during winter

Both Figure 205 for winter and Figure 206 for summer have divergence for heating load prediction. The difference between predicted and metered loads comes from the increase in heating demand that unoccupied setback failure causes by requiring zones to essentially warm the 14C° supply air to the minimum zone temperature of 21C°.

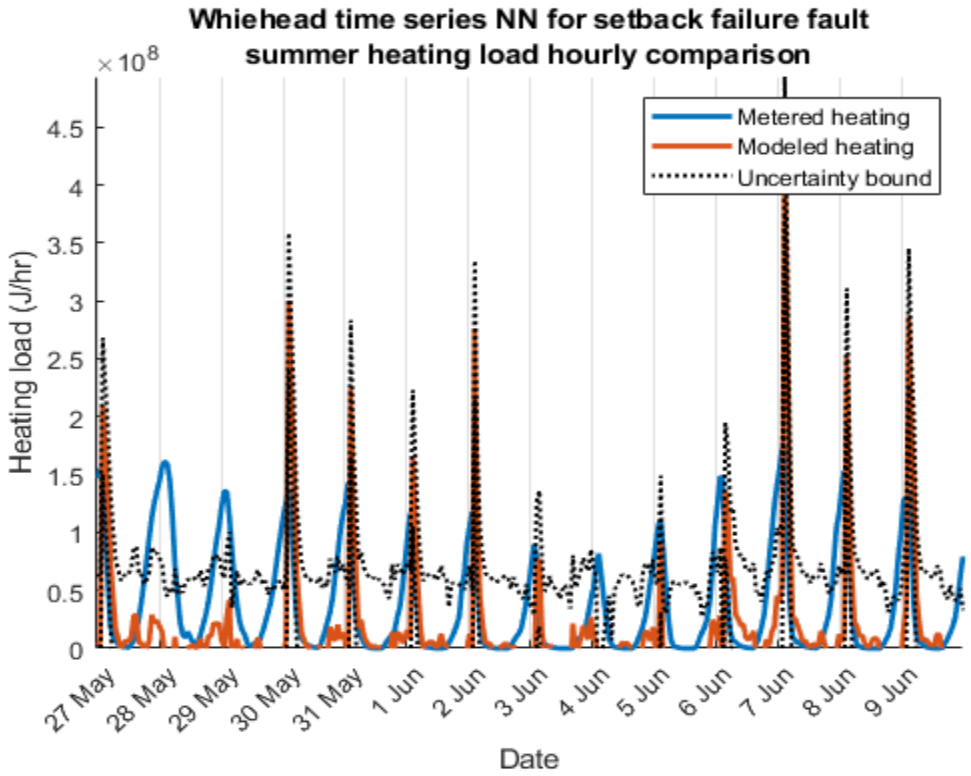

Figure 206A: Predicted heating load for Whitehead while not entering unoccupied setback during summer

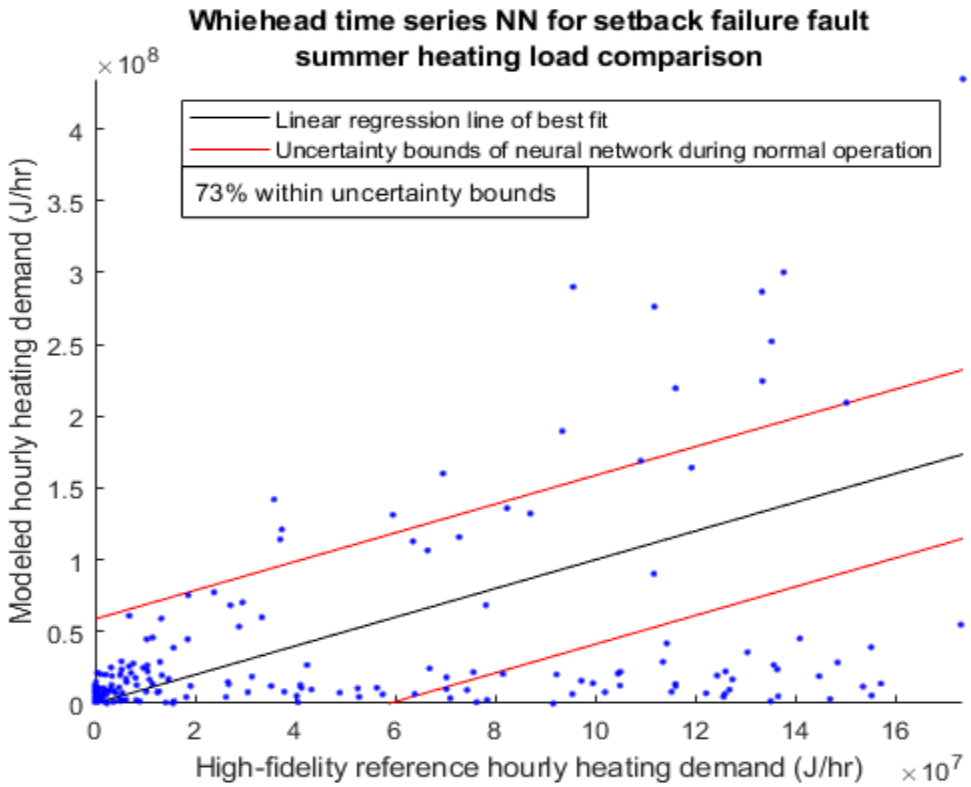

Figure 206B: Alignment factor of cooling load for Whitehead while not entering unoccupied setback during summer

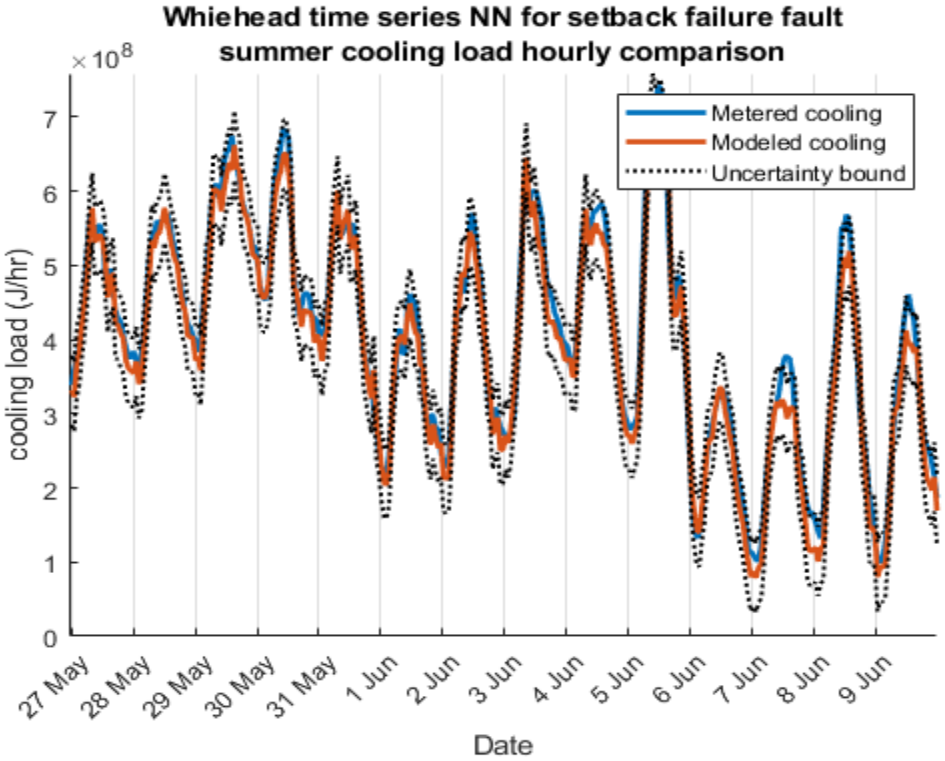

Figure 206C: Predicted cooling load for Whitehead while not entering unoccupied setback during summer

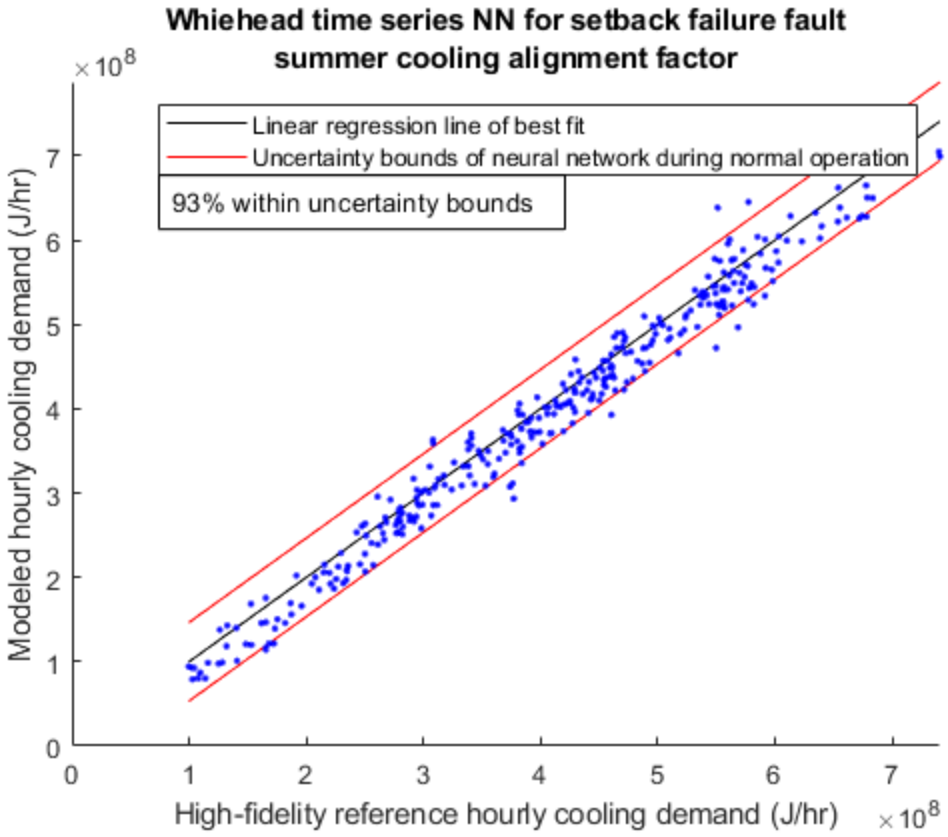

Figure 206D: Alignment factor of cooling load for Whitehead while not entering unoccupied setback during summer

Failure to enter unoccupied setback is a fault that can be difficult to detect due to the fault occurring when the building is vacant. However, model-based fault detection and identification methods tested have all proven to be able to correctly identify this fault. Further research could include determining minimum training periods required for NNs to detect faults. Due to the simplistic and low energy demand associated with failure to enter unoccupied setback, it may be possible for a building operator to purposefully induce this fault so that a NN can be trained with metered data.

8.1.3 Whitehead Excessive Preheat

Excessive preheat is the most extreme load fault being investigated, and Figure 208 displays the vast energy waste associated with this fault. Severity of the lost energy is

reflected in the magnitude of the deviation from metered data that was estimated by the neural network time series. For winter, a near constant increase in heating and cooling load was observed due to cooling coils needing to continuously lower supply air by 15°C from the preheat coils as shown in Figure 207. For this fault, it appears that both the SPBM and a time series neural network are equally adept at detecting changes in load demand.

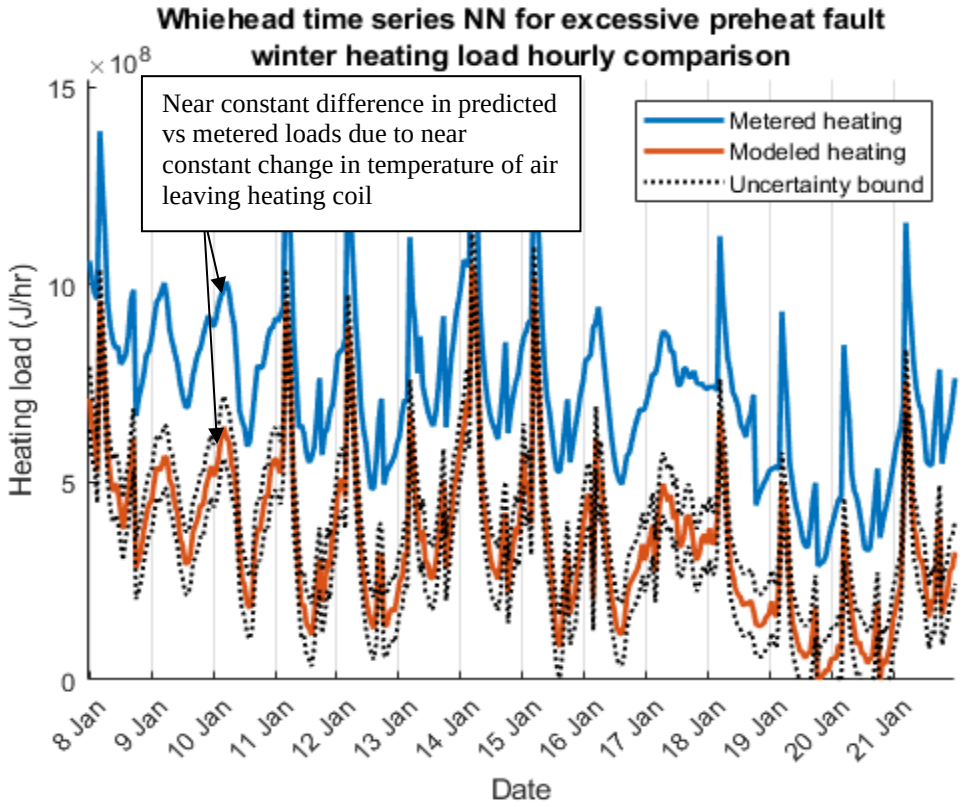

Figure 207A: Predicted heating load for Whitehead while experiencing excessive preheat fault condition during winter

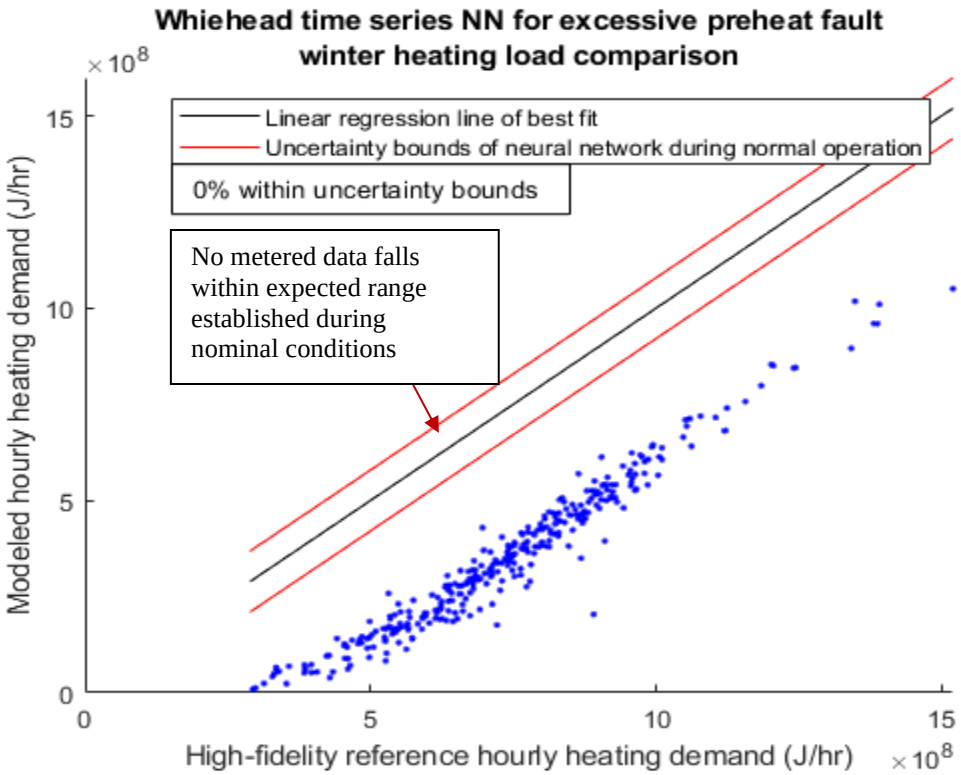

Figure 207B: Alignment factor of heating load for Whitehead while experiencing excessive preheat fault condition during winter

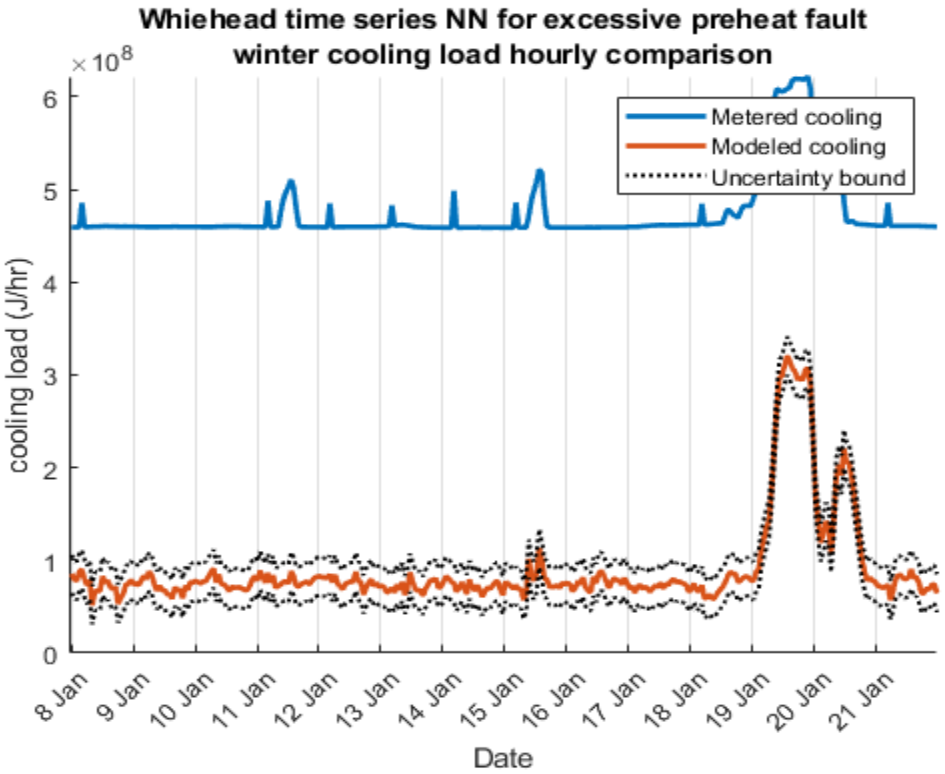

Figure 207C: Predicted cooling load for Whitehead while experiencing excessive preheat fault condition during winter

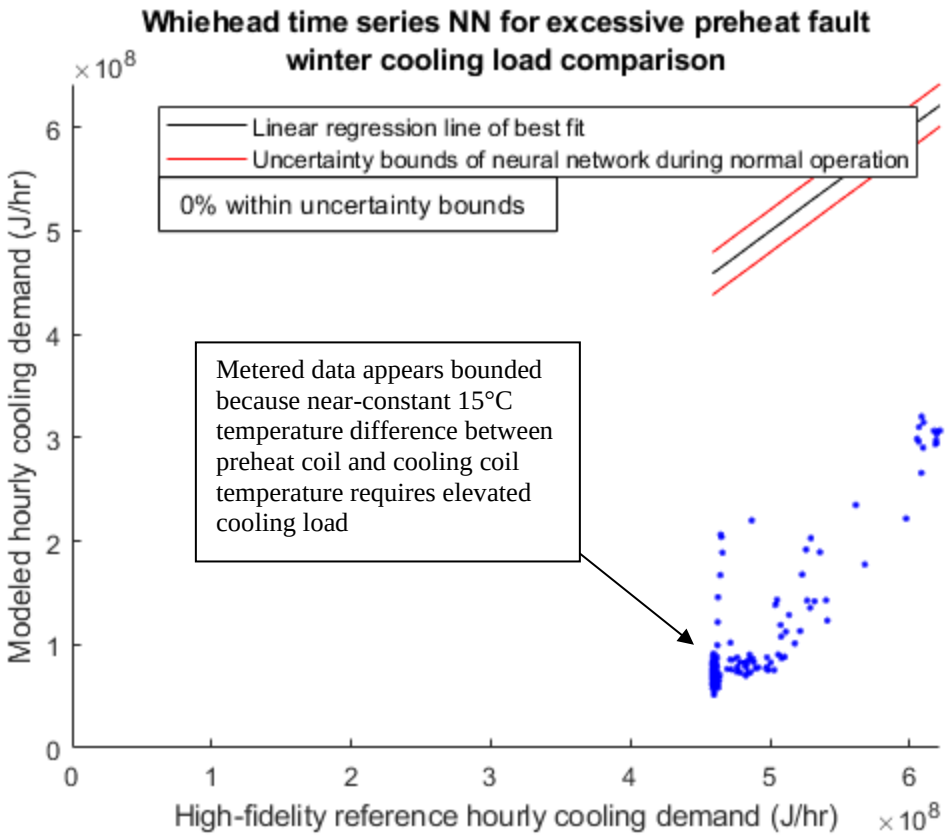

Figure 207D: Alignment factor of cooling load for Whitehead while experiencing excessive preheat fault condition during winter

During winter, excessive preheating causes a near-constant increase in both heating and cooling demand. Summer loading is not as constant due to mixed air temperature being hotter and more humid than during winter and the excessive preheat temperature setpoint of 28°C sometimes being matched by the temperature of air supplied to the AHU as depicted in Figure 208.

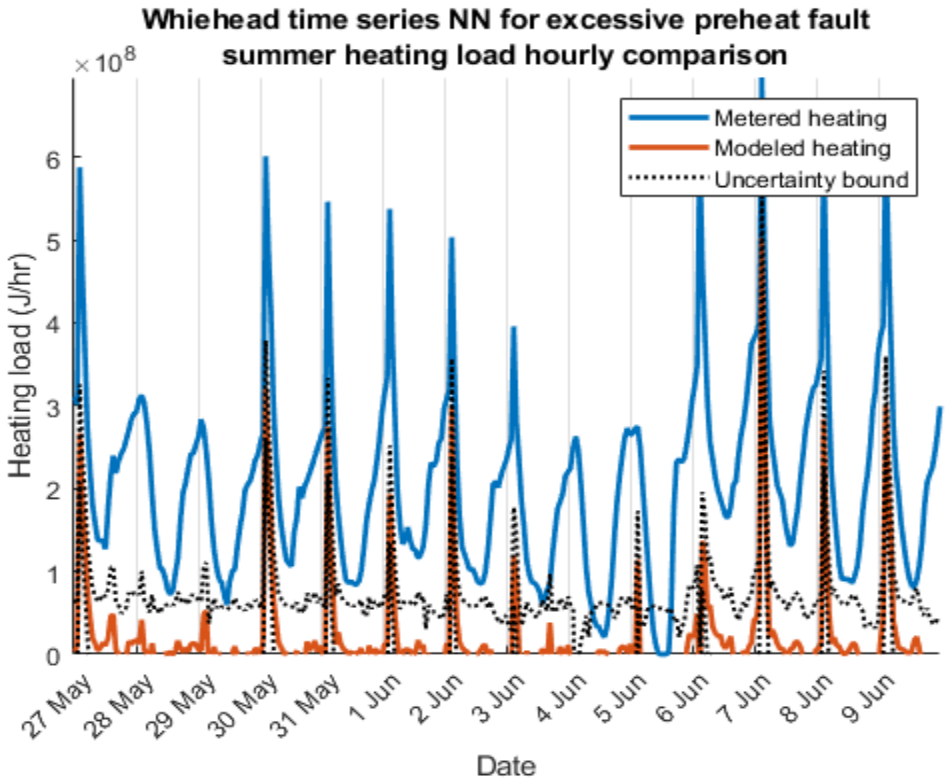

Figure 208A: Predicted heating load for Whitehead while experiencing excessive preheat fault condition during summer

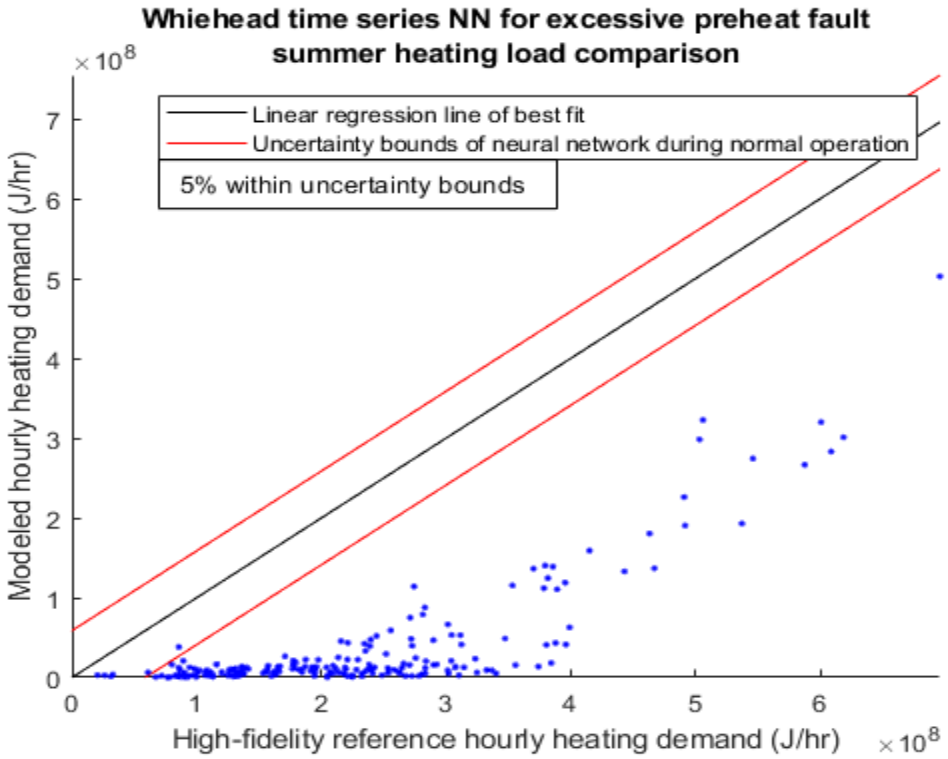

Figure 208B: Alignment factor of heating load for Whitehead while experiencing excessive preheat fault condition during summer

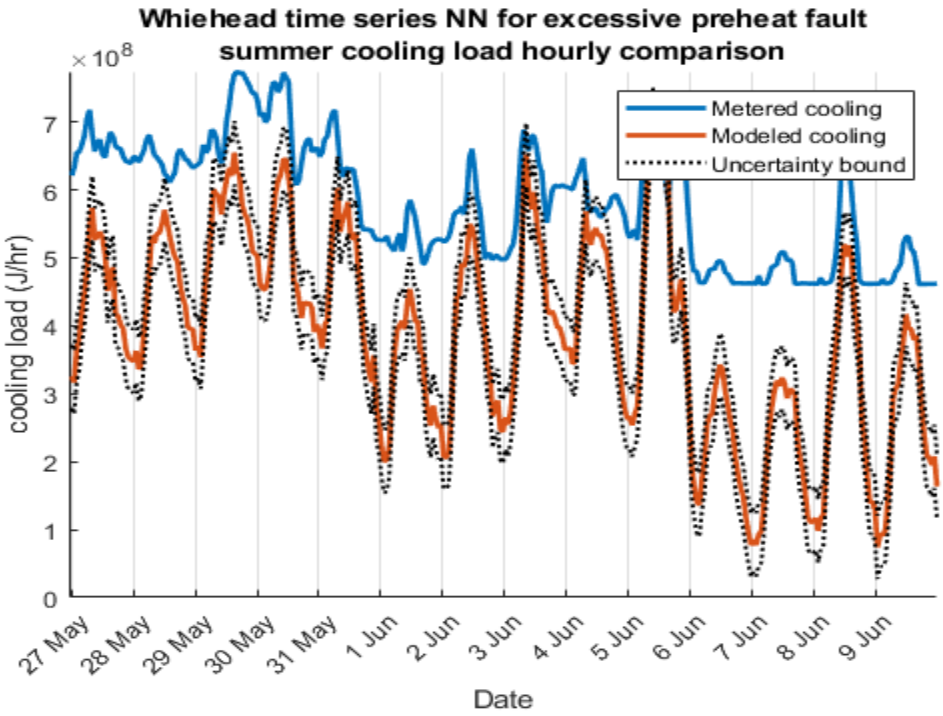

Figure 208C: Predicted cooling load for Whitehead while experiencing excessive preheat fault condition during summer

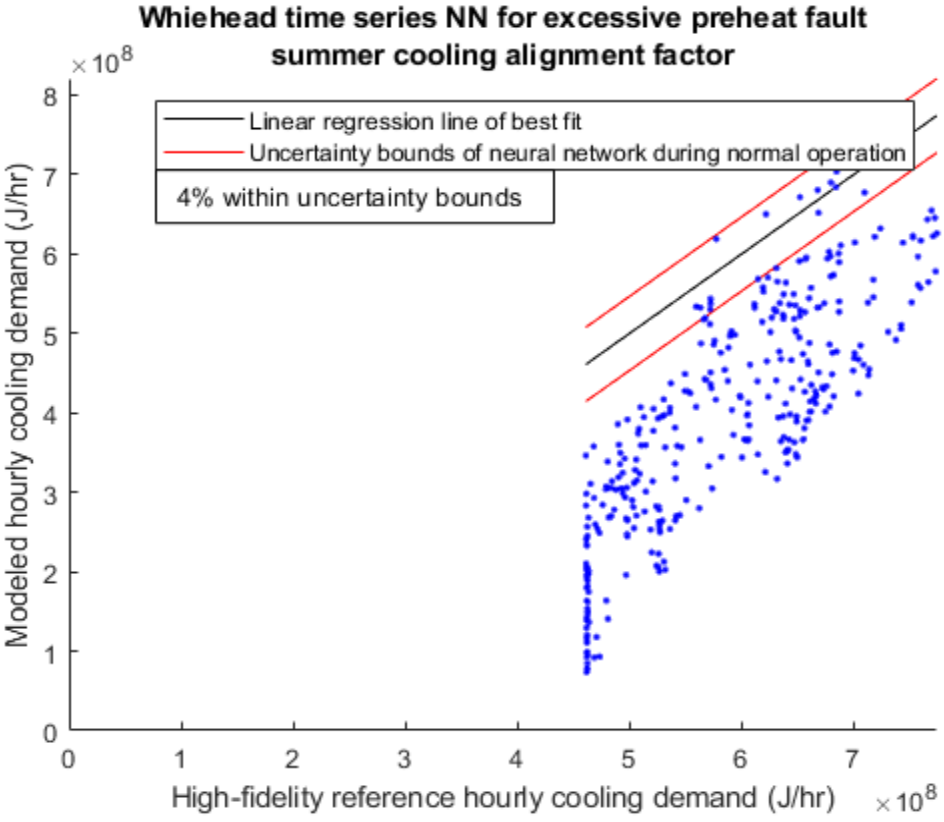

Figure 208D: Alignment factor of cooling load for Whitehead while experiencing excessive preheat fault condition during summer

Using the prediction interval from no-fault data resulted in no points falling within range of metered data during winter and a statistically insignificant portion of data during summer. Given that excessive preheating causes such a significant alteration of both heating and cooling demand, and therefore conditions well outside the trained data set, it is expected that a time series NN would not extrapolate well.

8.1.4 Whitehead Insufficient Outdoor Air

Insufficient outdoor air fault presents a unique deviation from the other faults as, typically, reducing outdoor air lowers load demand. As shown in Figure 209 and Figure 210, metered loads are consistently lower than those predicted by the time series neural network. Lower energy consumption than expected due to insufficient outdoor air may result in lower energy costs but at potential harm to building occupants. Given that this fault is the only one that has a direct impact on the health of building occupants, reduced building heating and cooling demand should be a red flag for building operators.

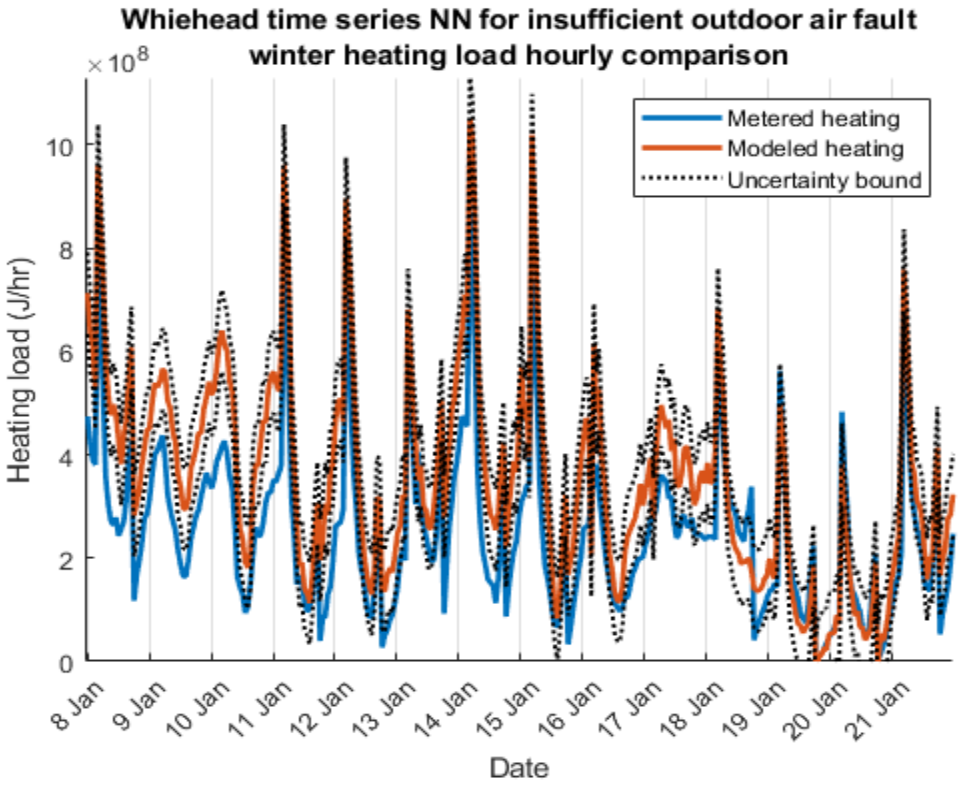

Figure 209A: Predicted heating load for Whitehead experiencing insufficient outdoor air flow fault during winter

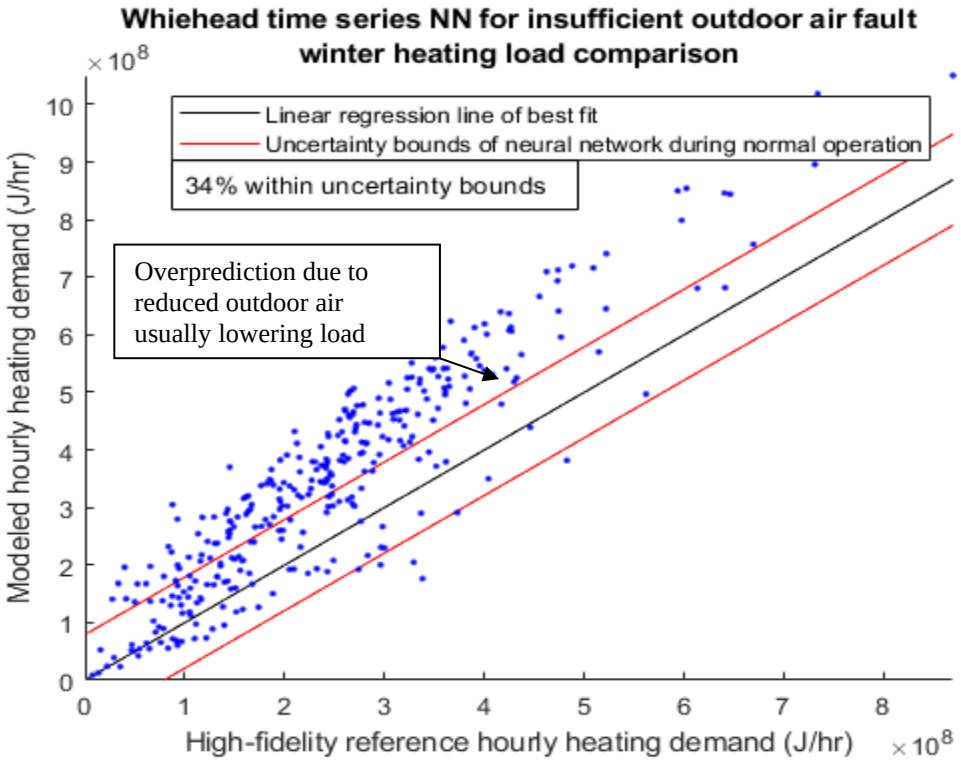

Figure 209B: Alignment factor of heating load for Whitehead experiencing insufficient outdoor air flow fault during winter

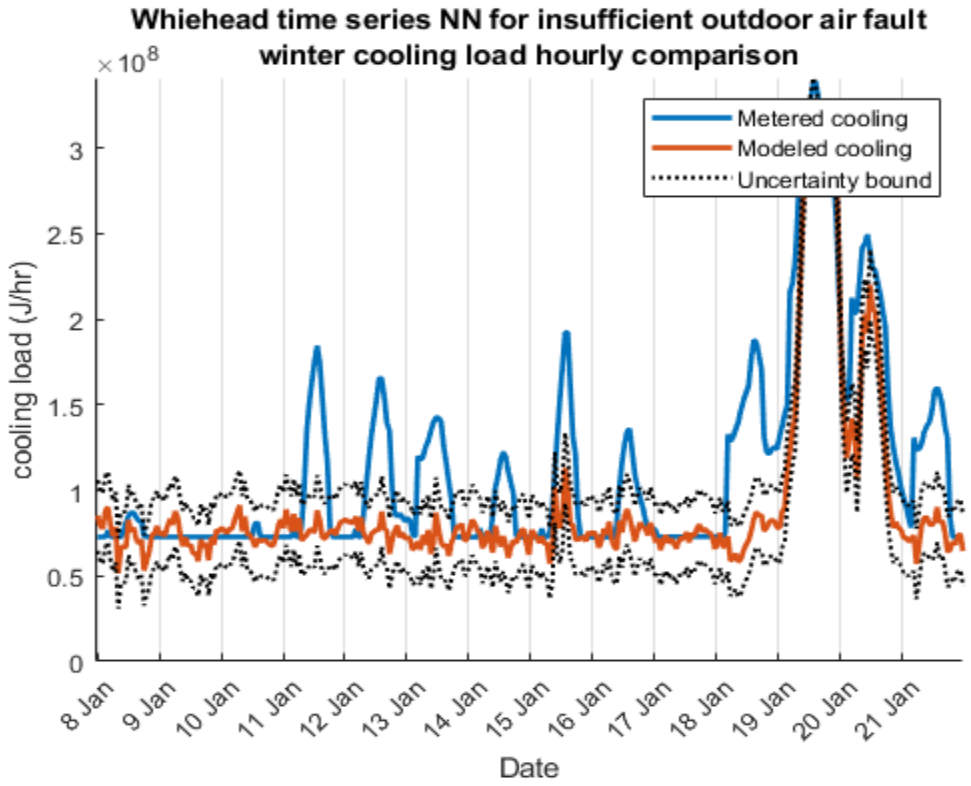

Figure 209C: Predicted cooling load for Whitehead experiencing insufficient outdoor air flow fault during winter

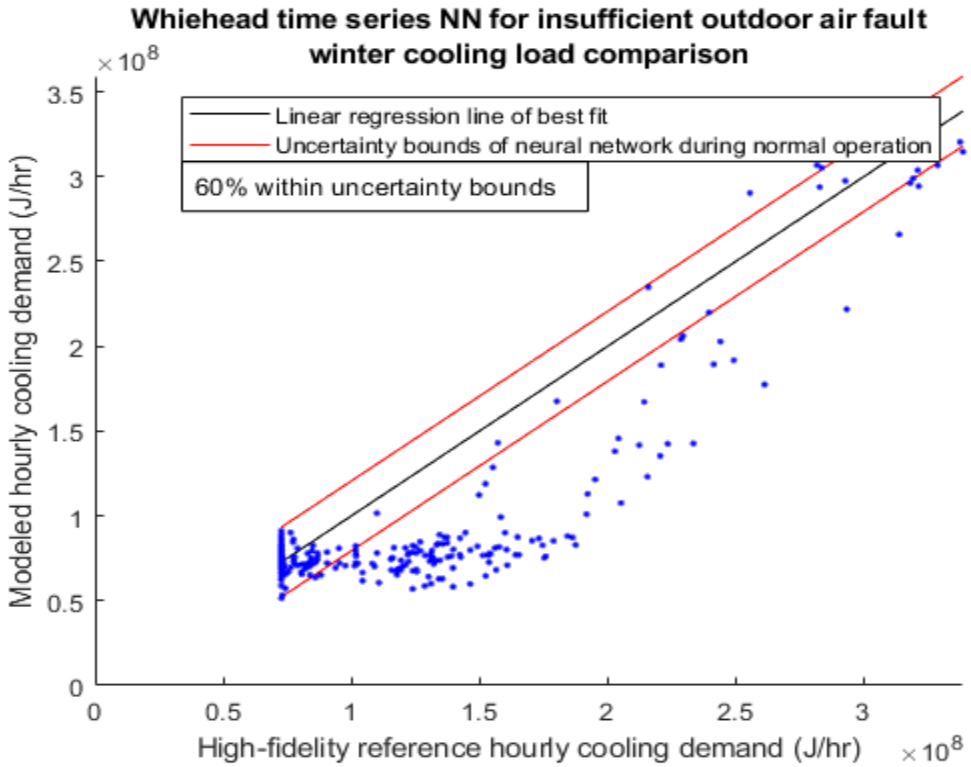

Figure 209D: Alignment factor of cooling load for Whitehead experiencing insufficient outdoor air flow fault during winter

Summer load analysis reveals that metered data is significantly lower than that from predicted loads. As with winter, reducing outdoor air decreases energy use but can potentially impact occupant health.

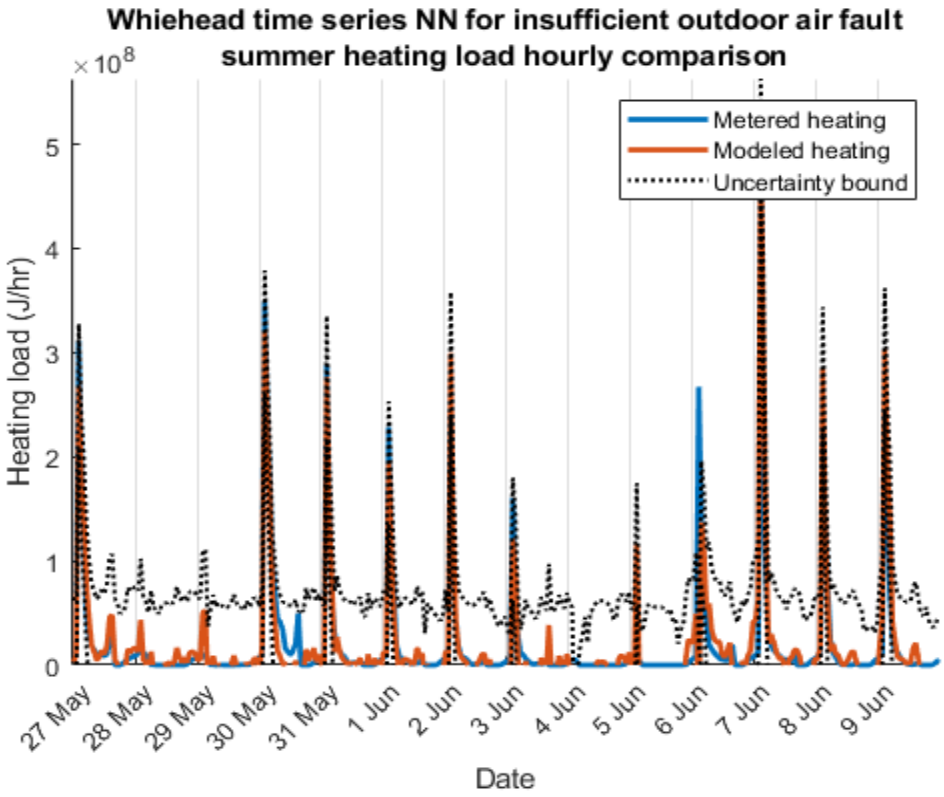

Figure 210A: Predicted heating load for Whitehead experiencing insufficient outdoor air flow fault during summer

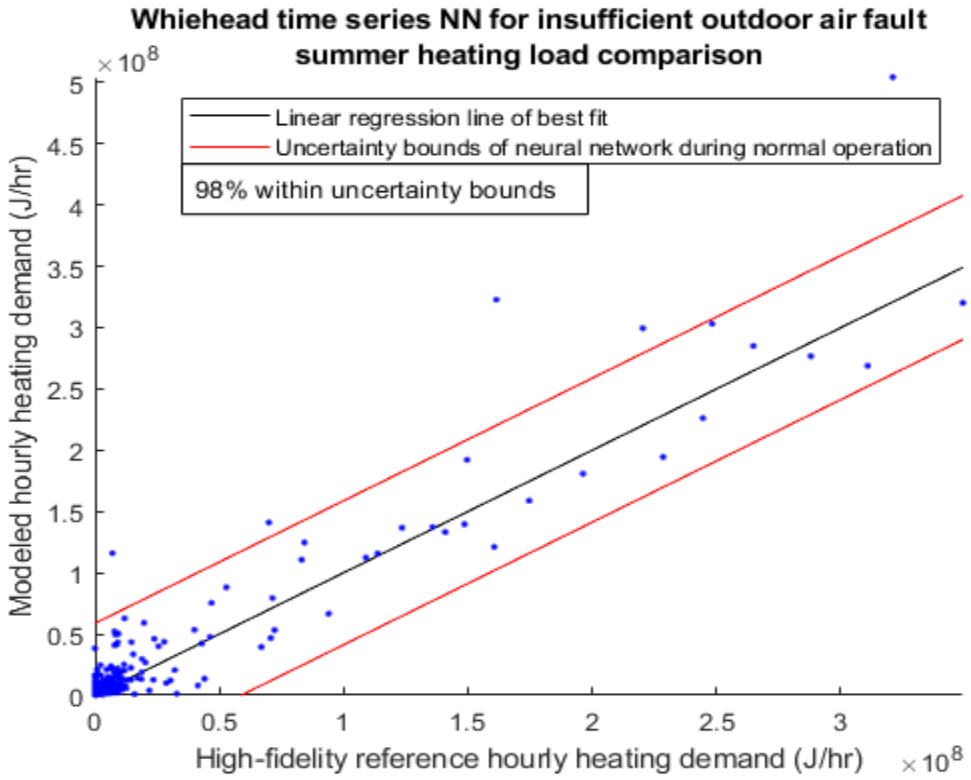

Figure 210B: Alignment factor of heating load for Whitehead experiencing insufficient outdoor air flow fault during summer

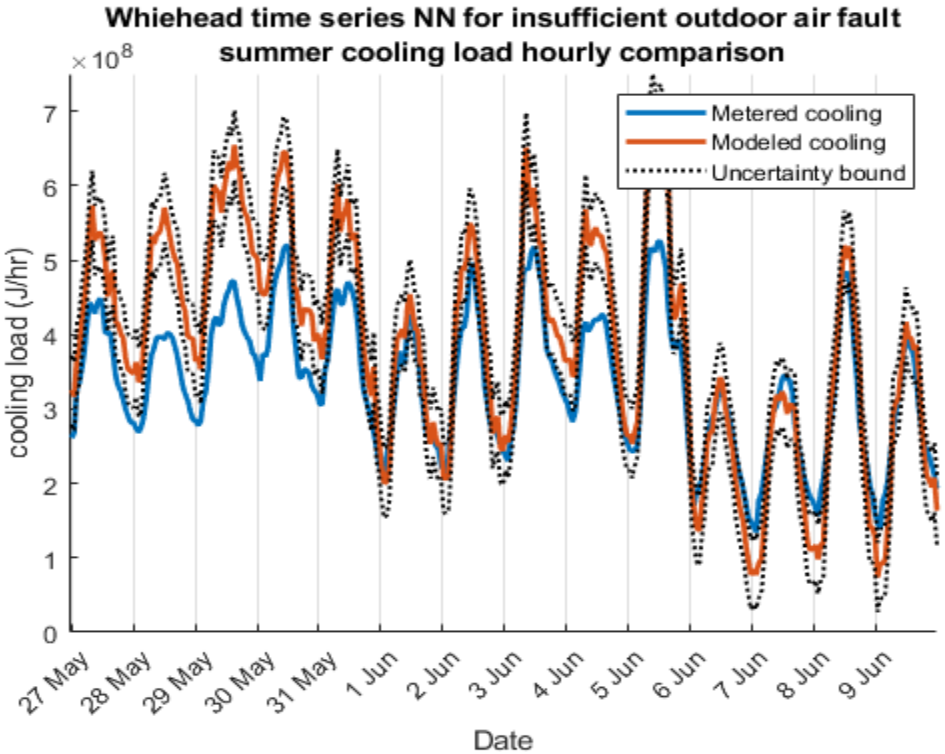

Figure 210C: Predicted cooling load for Whitehead experiencing insufficient outdoor air flow fault during summer

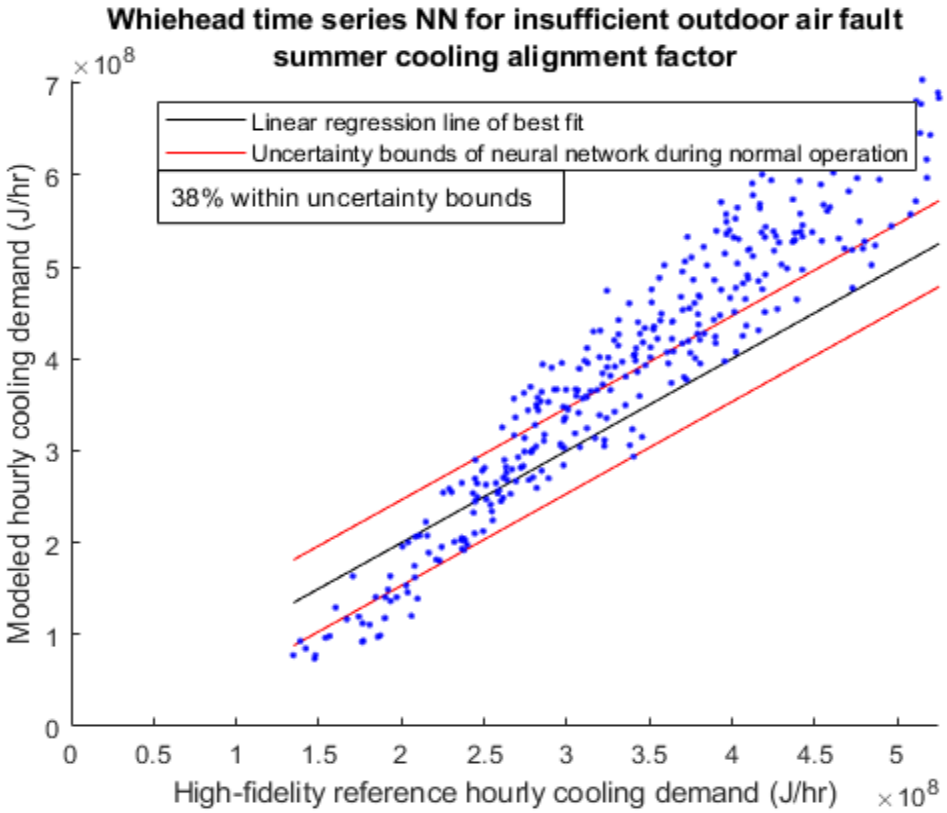

Figure 210D: Alignment factor of cooling load for Whitehead experiencing insufficient outdoor air flow fault during summer

Insufficient outdoor air fault test reveals a benefit to model-based fault detection and identification. Energy demand is lower for fault conditions, and one may assume this building experienced lower load demand rather than from a fault occurring. This test highlights the importance of automatic fault detection as some faults such as insufficient outdoor air may not result in complaints from occupants or may be missed by energy use assessment.

8.1.5 Whitehead Multiple Faults: Excessive Preheat and Not Entering Unoccupied Setback

Multiple simultaneous faults are evaluated to determine how compounding alterations in load affect predicted load deviations. Given that a time series neural

network is bound by the inputs and outputs used while training, it is not possible for the neural network to produce a definitive answer for what fault is occurring. Despite this limitation, it is still possible to detect a fault due to divergence from metered data. While one might expect an enhanced deviation from multiple simultaneous faults, Figure 211 reveals that concurrent faults produce an additive deviation. On their own, excessive preheat and a failure to enter unoccupied setback both produced dramatic deviations from predicted load levels; therefore, it comes as no surprise that combining two high-impact faults would produce an even greater deviation from metered values.

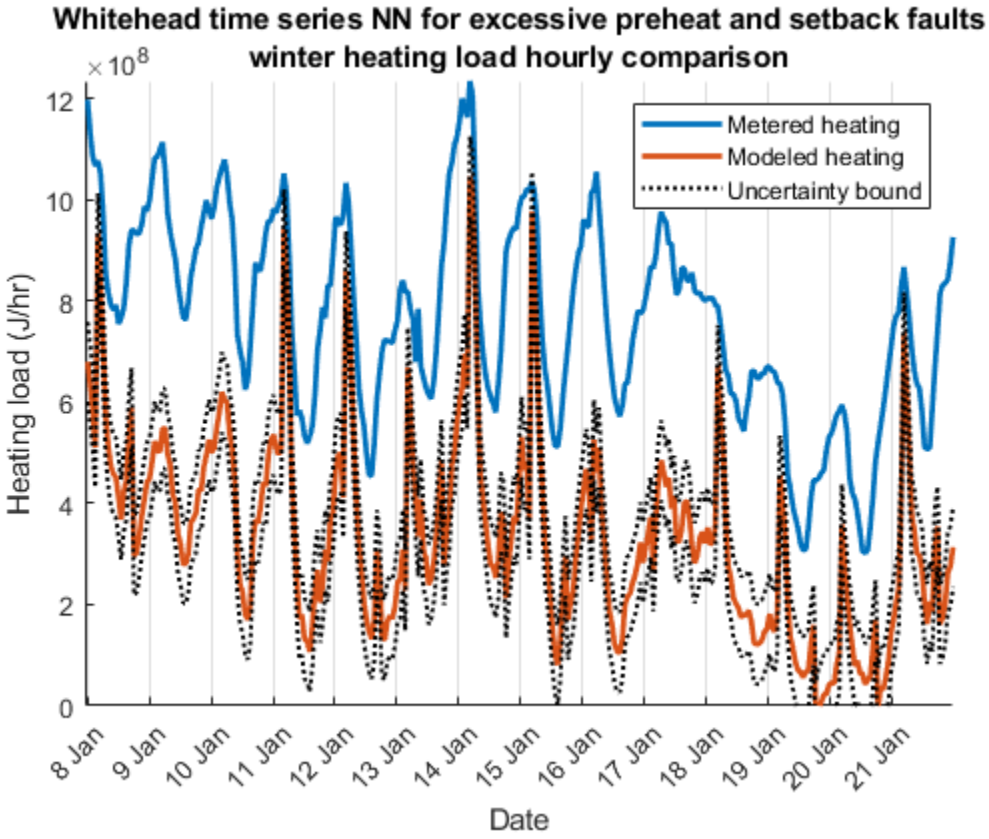

Figure 211A: Predicted heating load for Whitehead experiencing both excessive preheat and a failure to enter unoccupied setback during winter

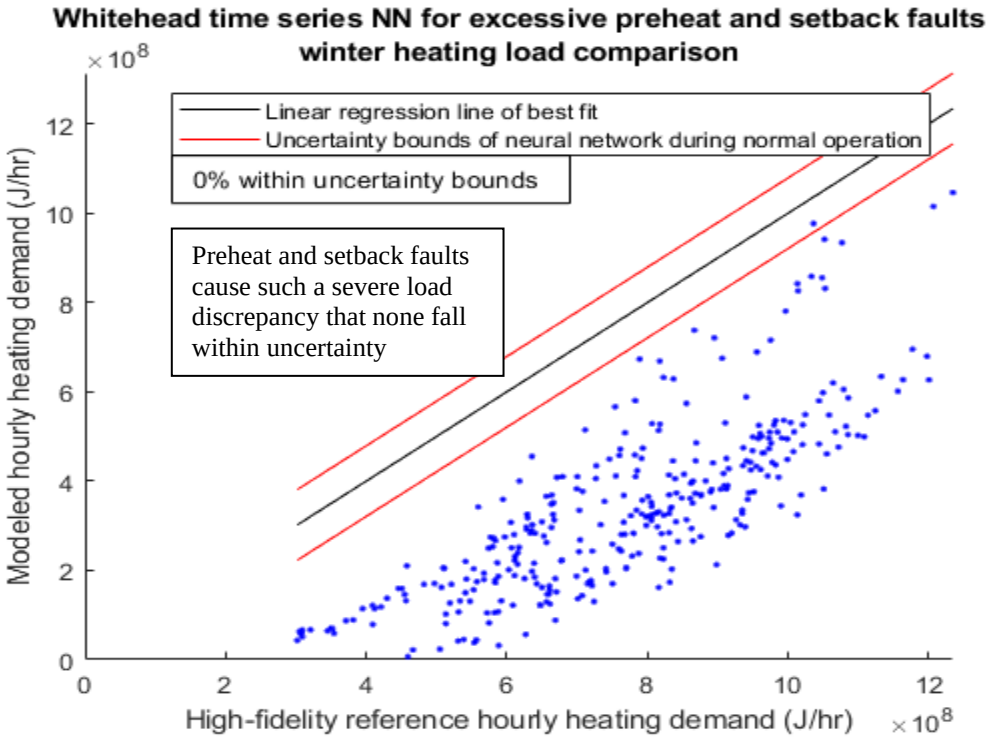

Figure 211B: Alignment factor of heating load for Whitehead experiencing both excessive preheat and a failure to enter unoccupied setback during winter

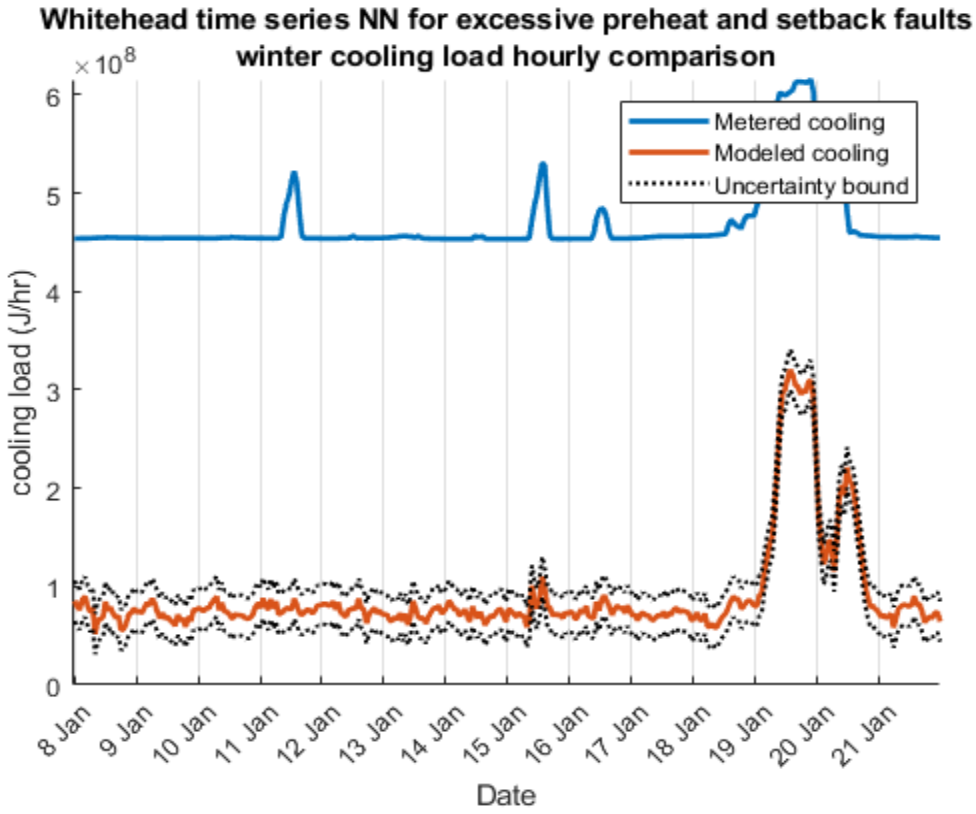

Figure 211C: Predicted cooling load for Whitehead experiencing both excessive preheat and a failure to enter unoccupied setback during winter

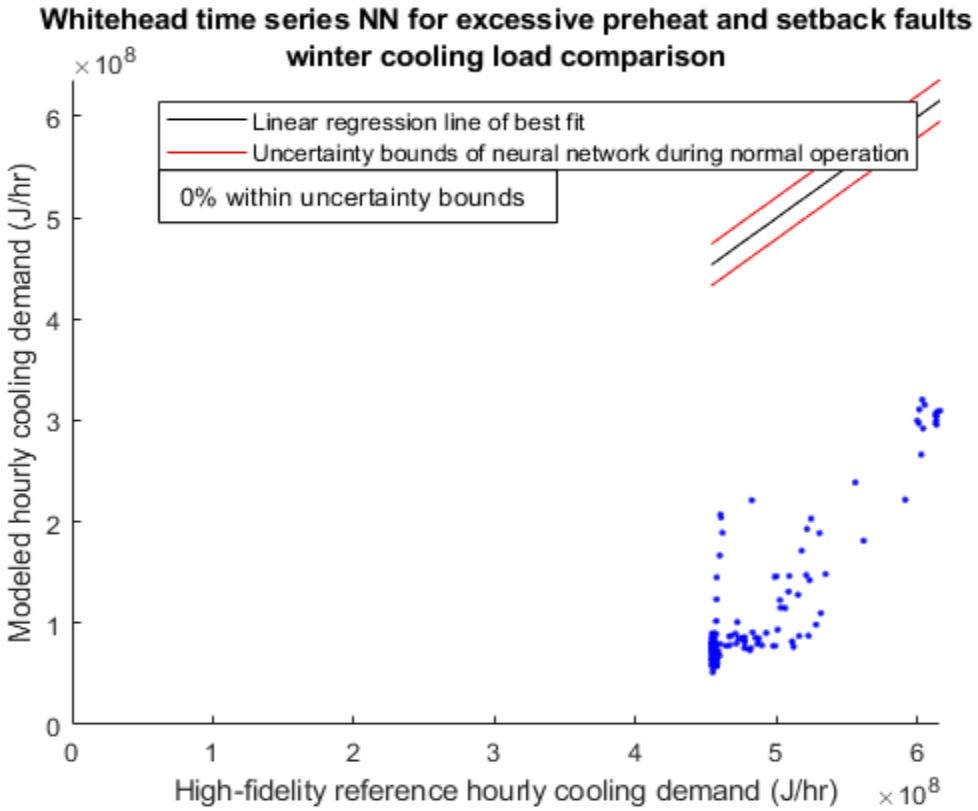

Figure 211D: Alignment factor of cooling load for Whitehead experiencing both excessive preheat and a failure to enter unoccupied setback during winter

Summer fault detection testing also has a definitive result when both preheat and unoccupied setback faults are present. Both of these faults increase heating and cooling demand, therefore it is expected that the trained NN would underpredict loading.

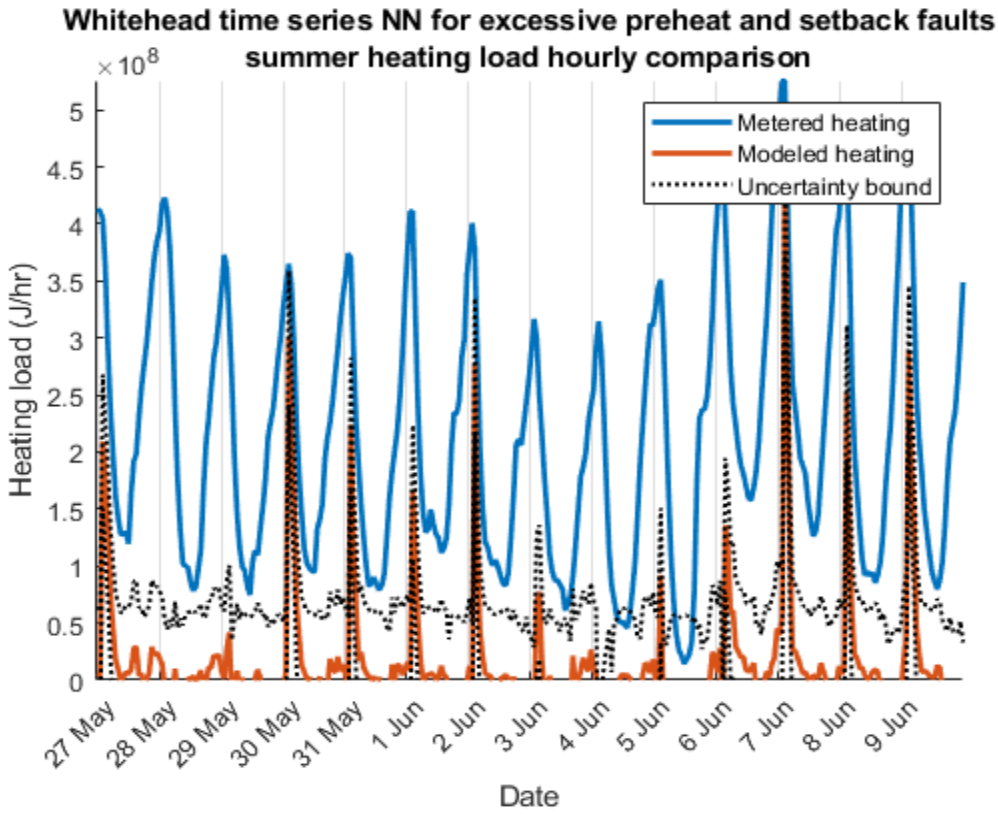

Figure 212A: Predicted heating load for Whitehead experiencing both excessive preheat and a failure to enter unoccupied setback during summer

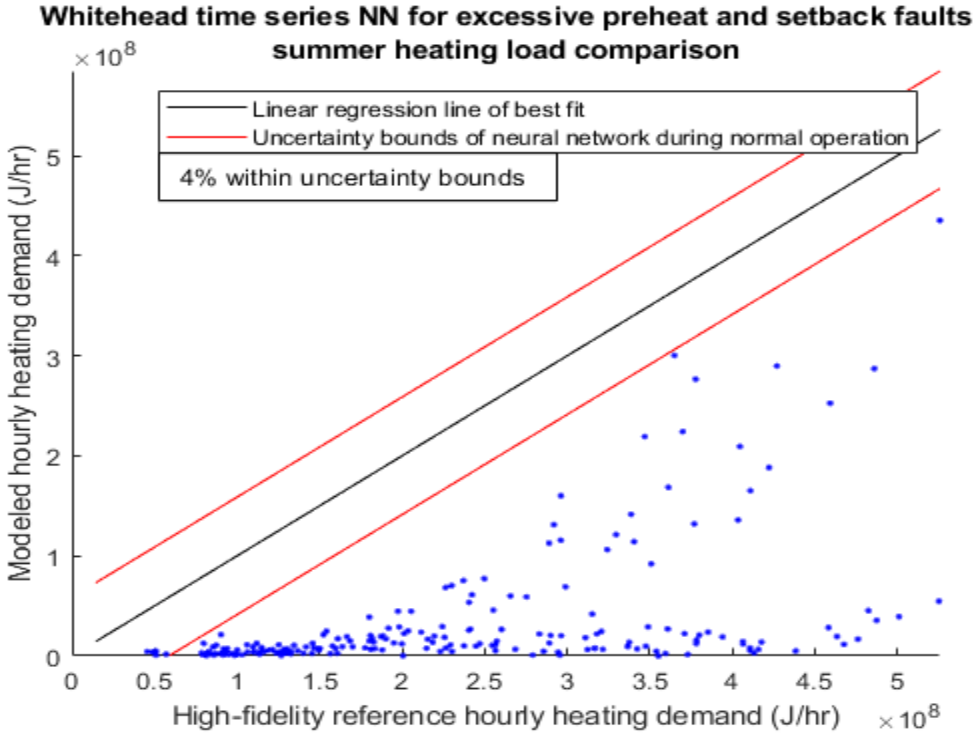

Figure 212B: Alignment factor of heating load for Whitehead experiencing both excessive preheat and a failure to enter unoccupied setback during summer

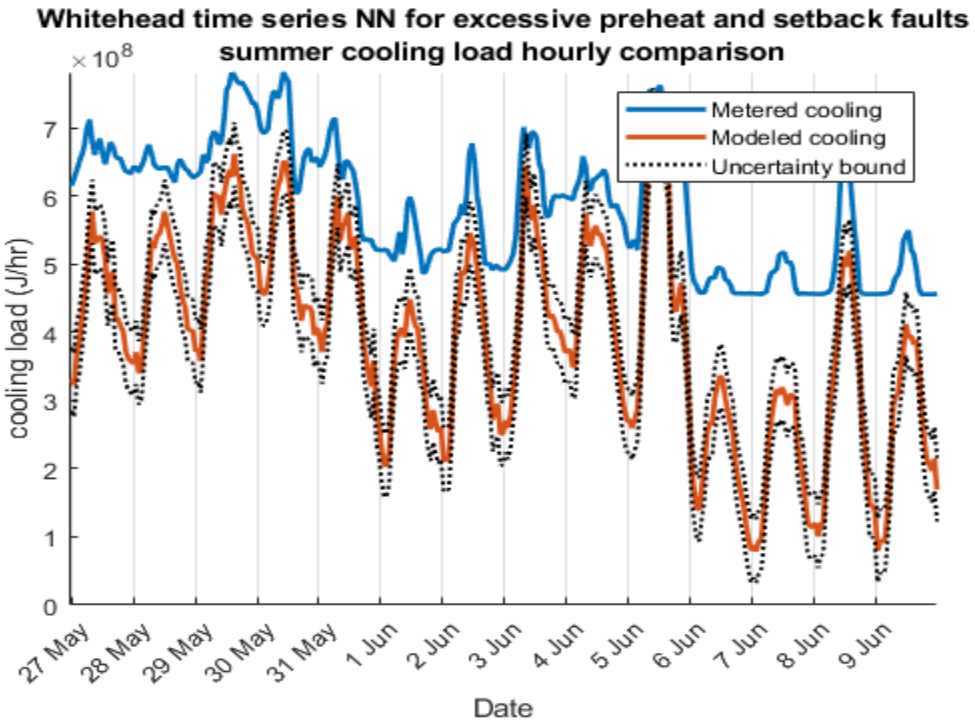

Figure 212C: Predicted cooling load for Whitehead experiencing both excessive preheat and a failure to enter unoccupied setback during summer

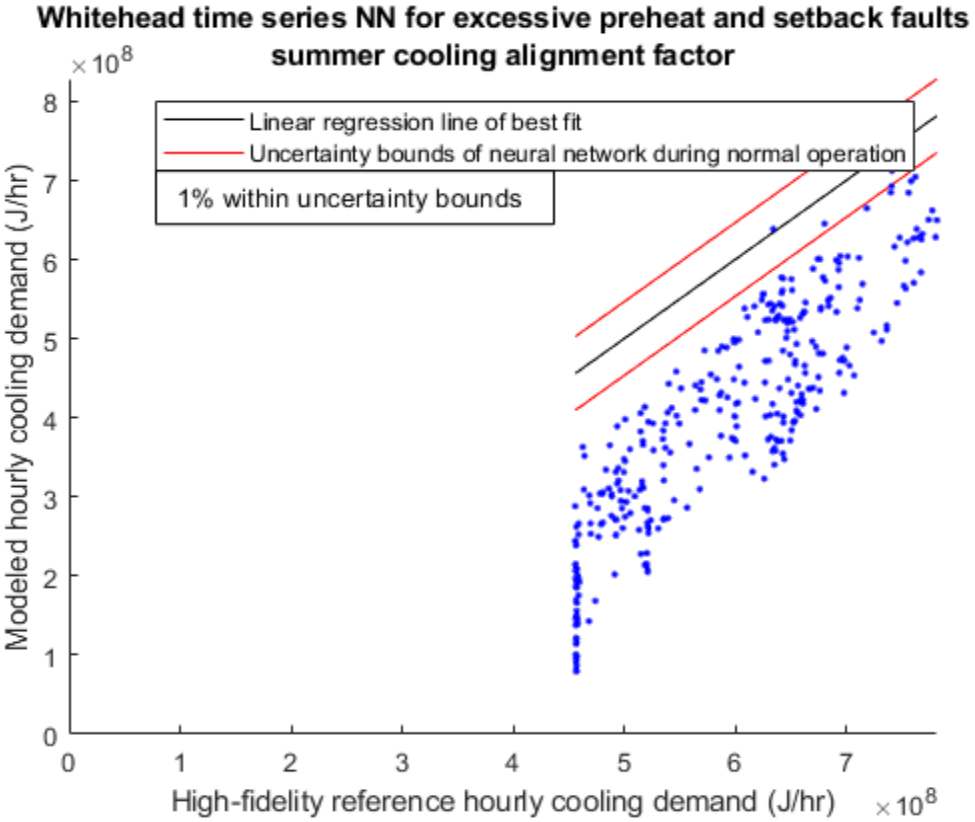

Figure 212D: Alignment factor of cooling load for Whitehead experiencing both excessive preheat and a failure to enter unoccupied setback during summer

Combining multiple high-energy deviation faults reveals how time series NNs are only capable of detecting faults, not classification. Figure 211 and Figure 212 may appear similar to Figure 207 and Figure 208, but there are two severe faults occurring in this most recent test.

8.1.6 Whitehead Multiple Faults: Excessive Preheat and Excessive Infiltration

Excessive preheating and infiltration show additive deviation in Figure 213 similar to when excessive preheating was coupled with a failure to enter unoccupied setback as shown in Figure 211. Additionally, predicted loads were substantially different from metered loads, as was the case in the previous section. The final test for Whitehead involves two subtle faults, a failure to enter unoccupied setback concurrent with excessive infiltration fault. Section 8.1.7 Whitehead multiple faults: excessive infiltration and failure to enter unoccupied setback explores how the apparent additive divergence can aid in finding multiple points of failure when faults are potentially too subtle to individually notice.

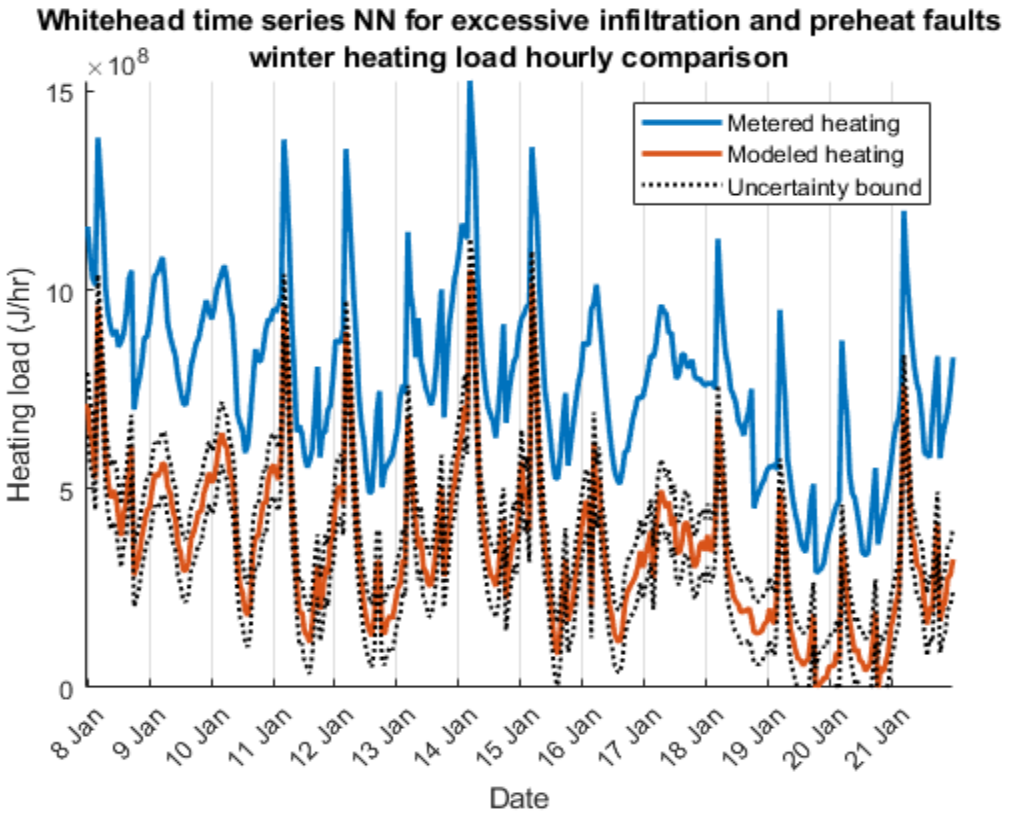

Figure 213A: Predicted heating load for Whitehead experiencing both excessive preheat and excessive infiltration during winter

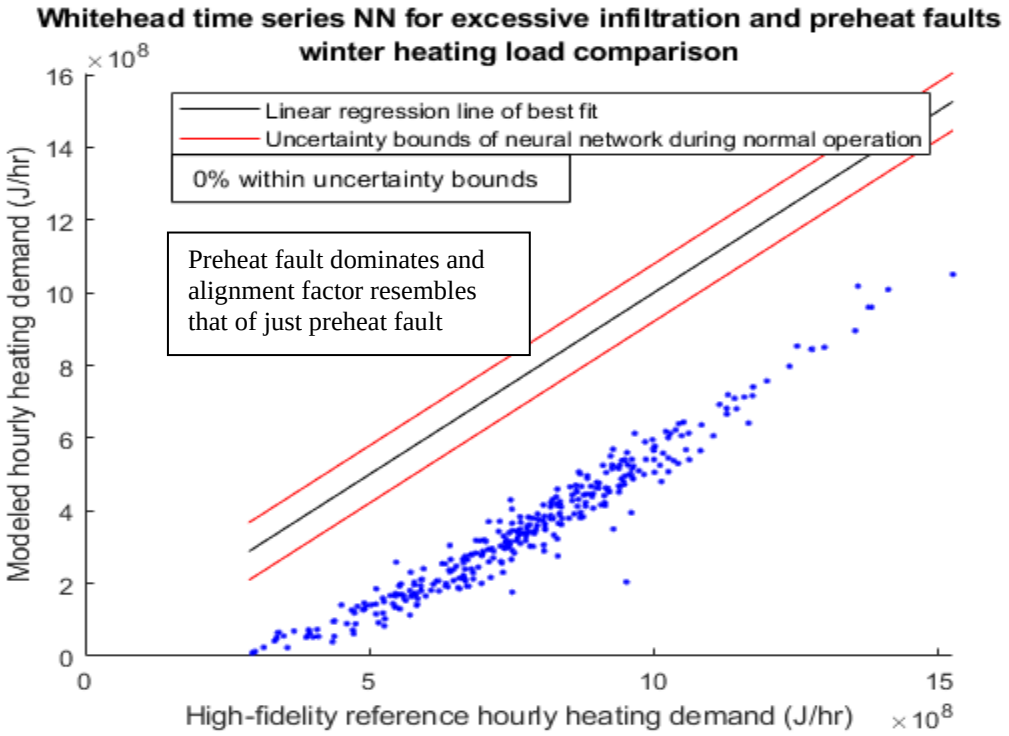

Figure 213B: Alignment factor of heating load for Whitehead experiencing both excessive preheat and excessive infiltration during winter

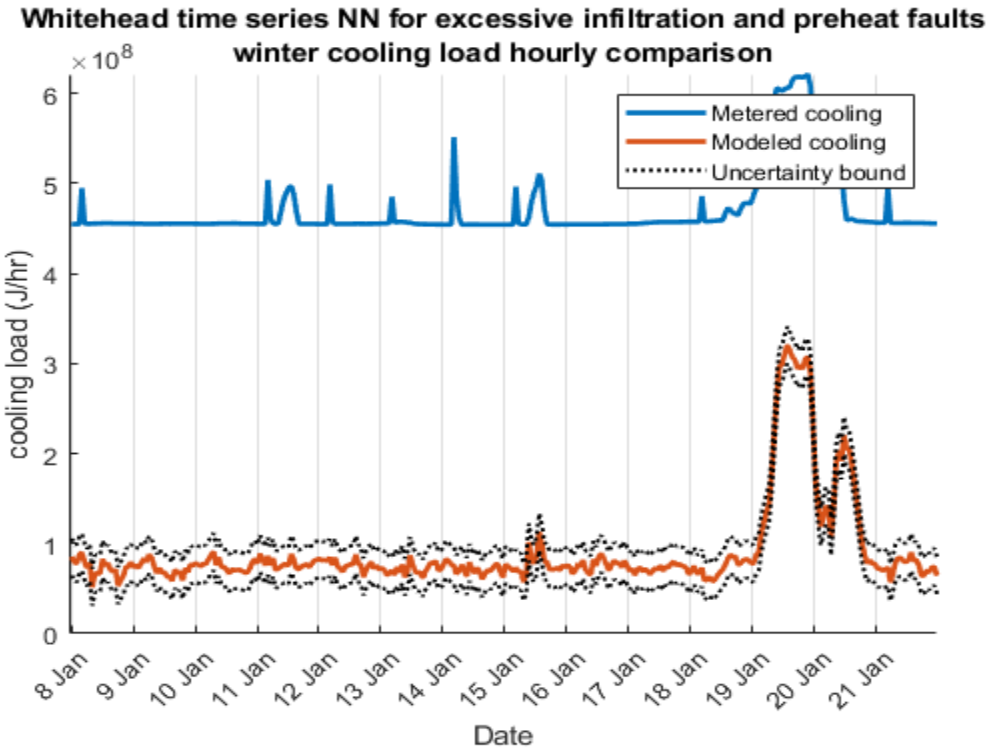

Figure 213C: Predicted cooling load for Whitehead experiencing both excessive preheat and excessive infiltration during winter

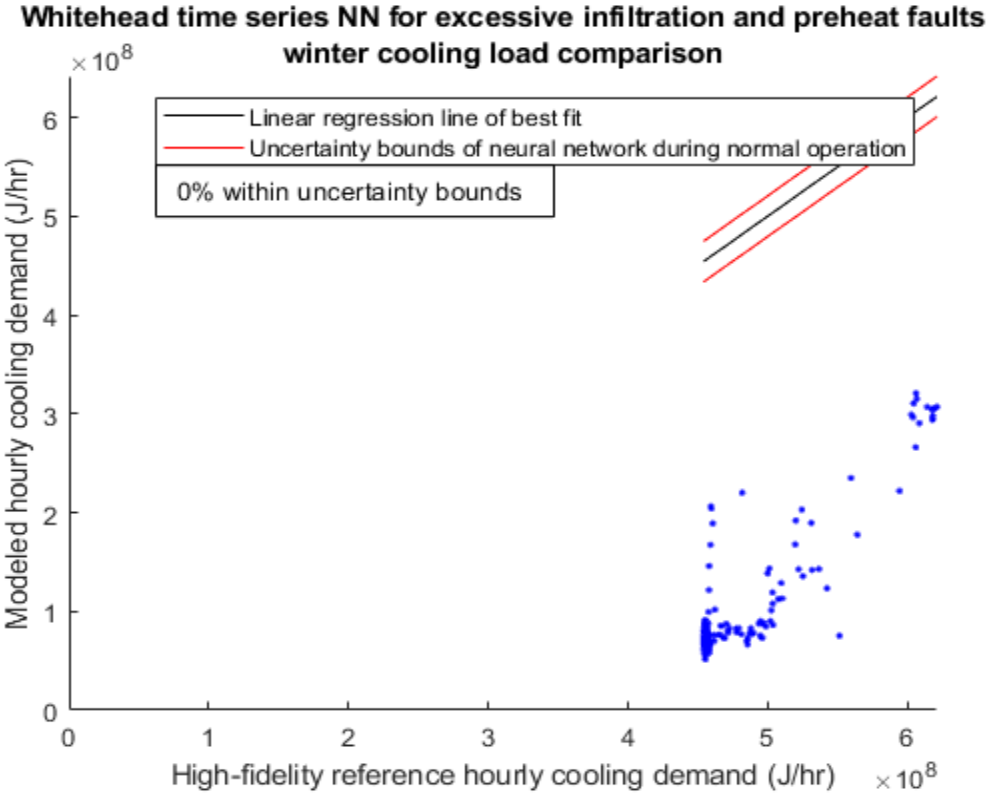

Figure 213D: Alignment factor of cooling load for Whitehead experiencing both excessive preheat and excessive infiltration during winter

Both winter and summer analysis reveal how time series NNs tend to “add together” the faults that are occurring.

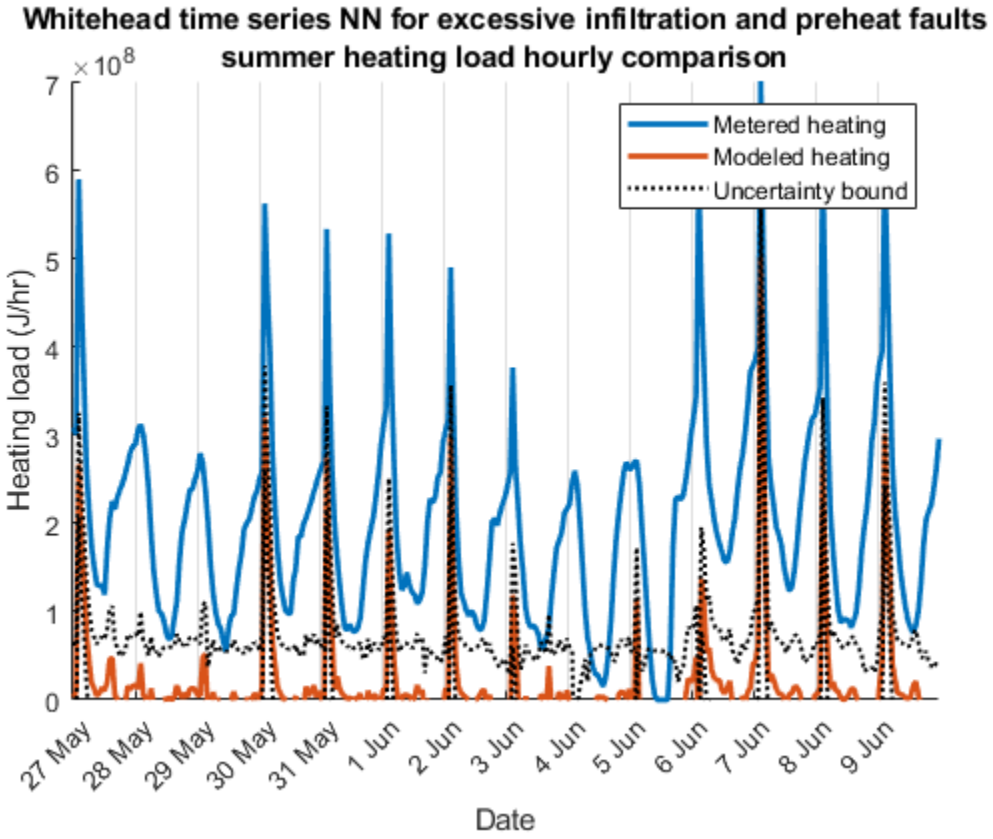

Figure 214A: Predicted heating load for Whitehead experiencing both excessive preheat and excessive infiltration during summer

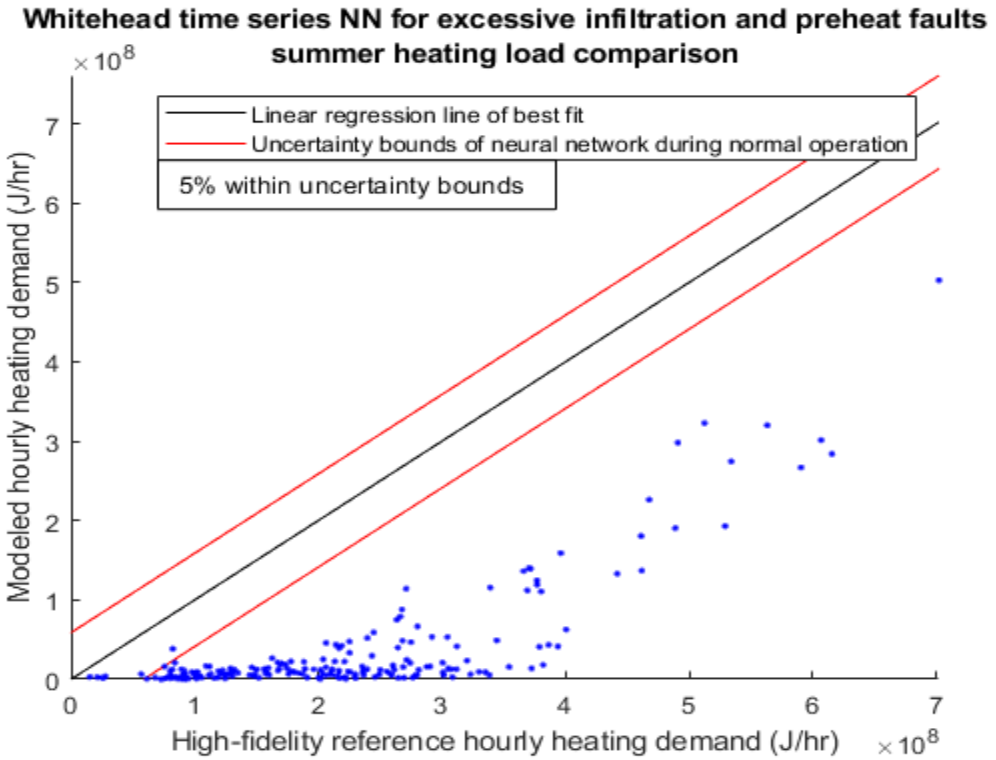

Figure 214B: Alignment factor of heating load for Whitehead experiencing both excessive preheat and excessive infiltration during summer

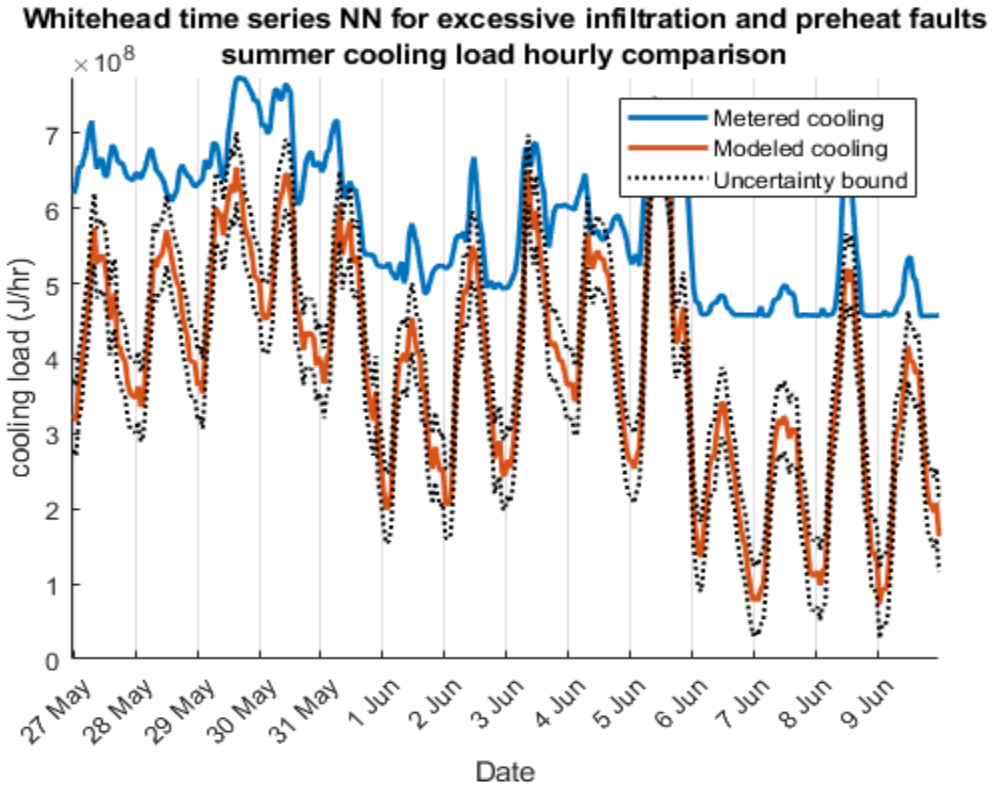

Figure 214C: Predicted cooling load for Whitehead experiencing both excessive preheat and excessive infiltration during summer

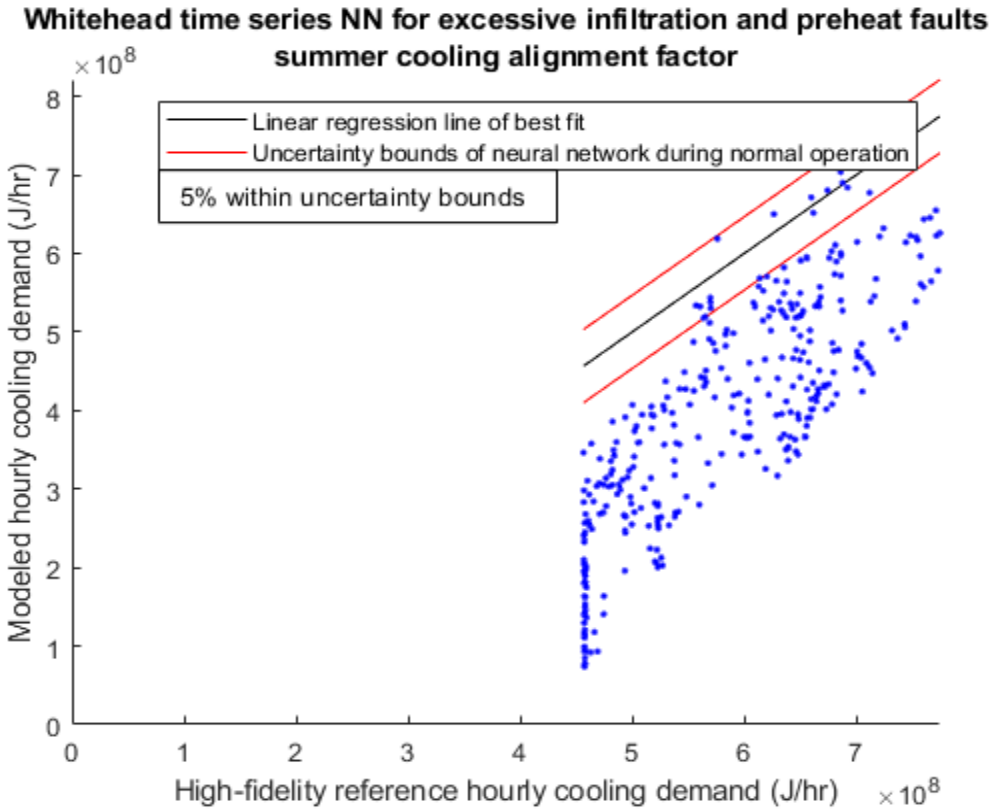

Figure 214D: Alignment factor of cooling load for Whitehead experiencing both excessive preheat and excessive infiltration during summer

Combining excessive preheat with infiltration again produced results similar to Figure 208, which only identifies that a fault is occurring. The next section will examine how combining two subtle faults may alter time series NN energy prediction. Additionally, multiple fault analysis will be conducted by decision tree NN as a method of using machine learning to classify and identify faults.

8.1.7 Whitehead Multiple Faults: Excessive Infiltration and Failure to Enter Unoccupied Setback

While the previous compound faults have involved excessive preheat, a fault with a pronounced increase in load demand, the last combination will involve excessive infiltration and a failure to enter unoccupied setback which both produced subtle

alterations to loading. When comparing the predicted and metered loads, winter demand appears dominated by a failure to enter unoccupied setback, which is evident by the sustained underestimation of heating loads during evening and weekend periods as seen in Figure 215.

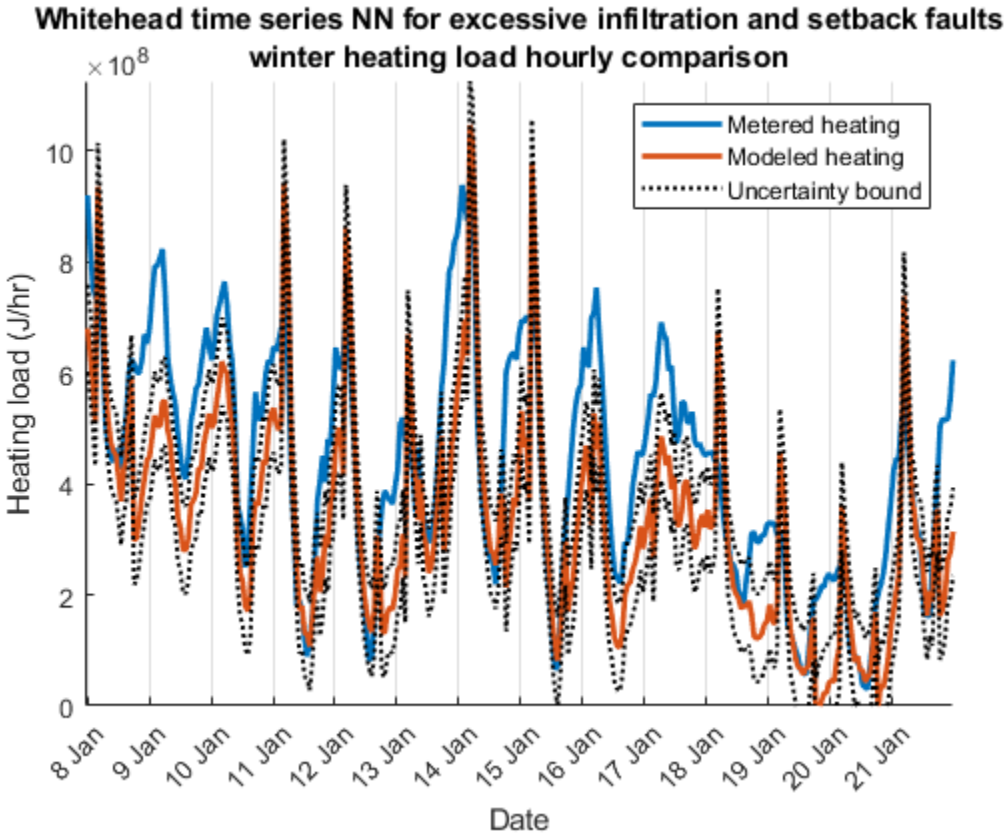

Figure 215A: Predicted heating load for Whitehead experiencing both excessive infiltration and a failure to enter unoccupied setback during winter

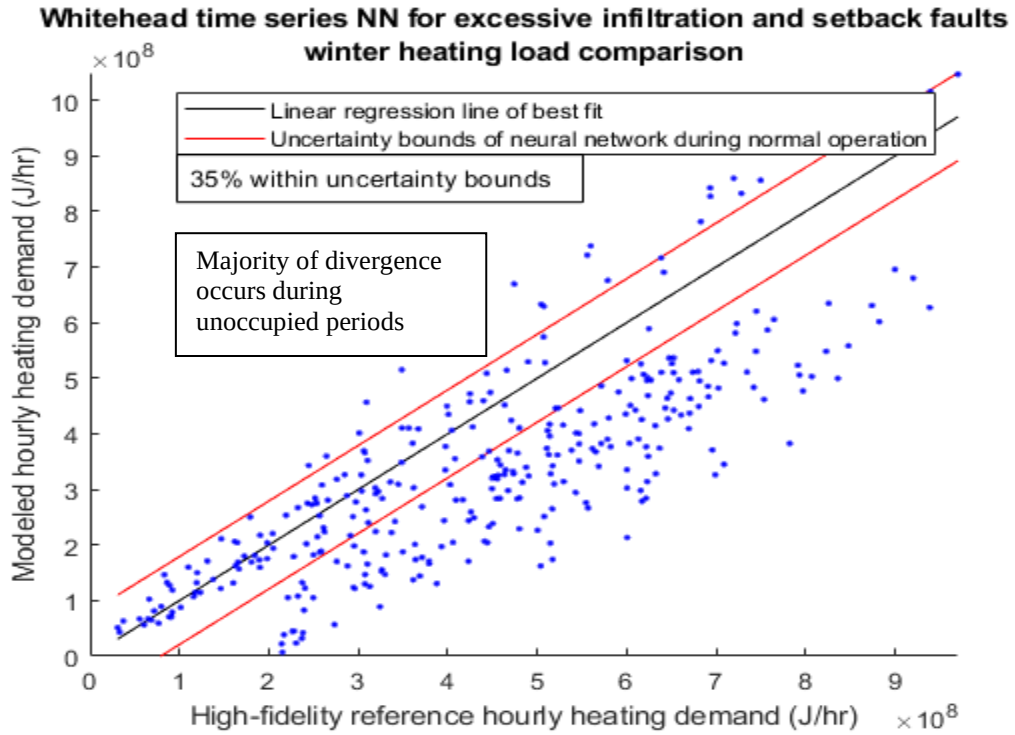

Figure 215B: Alignment factor of heating load for Whitehead experiencing both excessive infiltration and a failure to enter unoccupied setback during winter

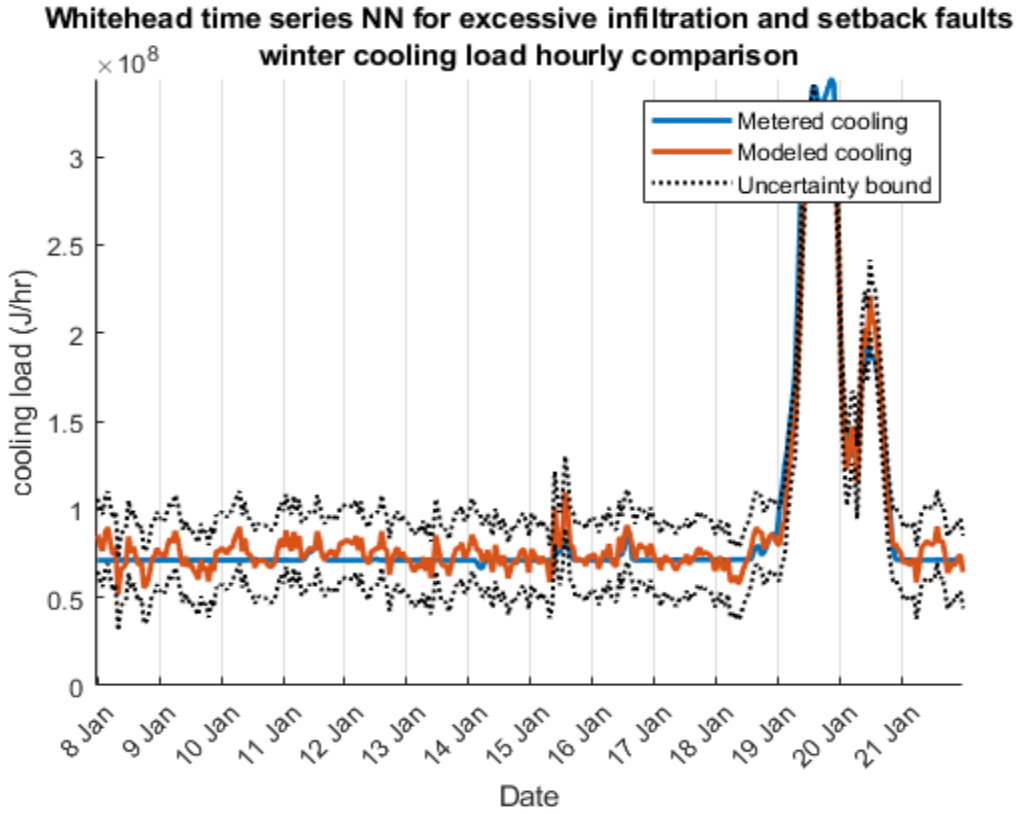

Figure 215C: Predicted cooling load for Whitehead experiencing both excessive infiltration and a failure to enter unoccupied setback during winter

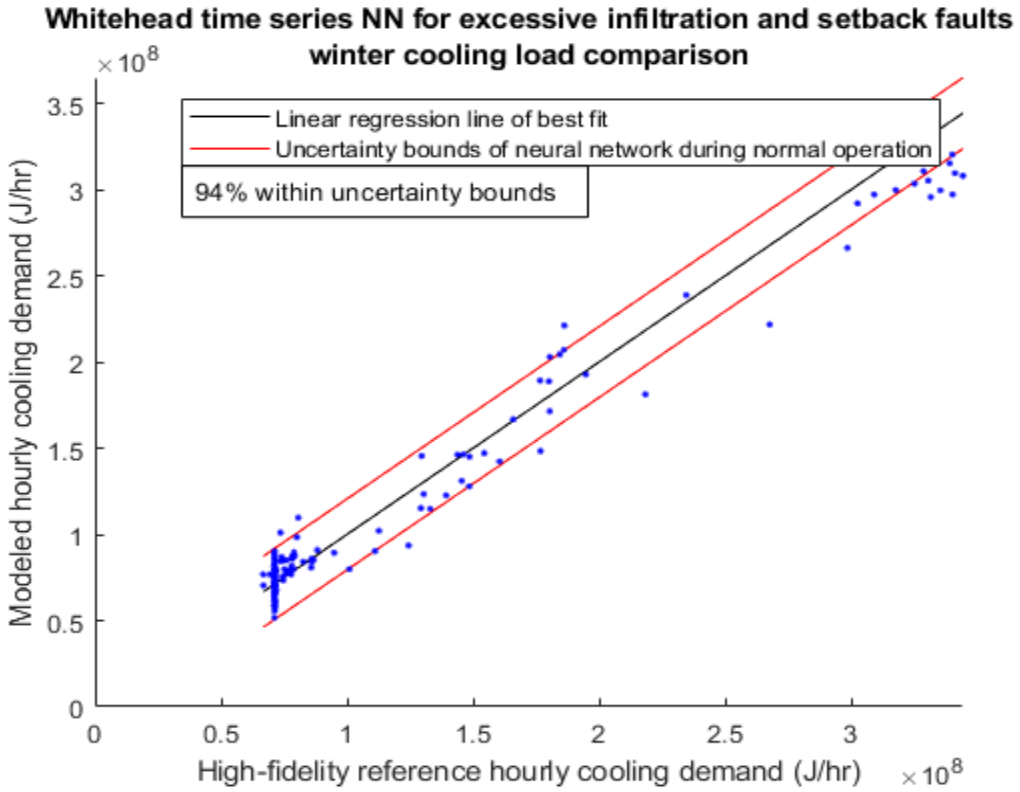

Figure 215D: Alignment factor of cooling load for Whitehead experiencing both excessive infiltration and a failure to enter unoccupied setback during winter

Loads deviation during summer in Figure 216 have both excessive heating, which is similar to Figure 206, and elevated cooling as depicted in Figure 204 meaning that multiple faults tend to act in an additive manner.

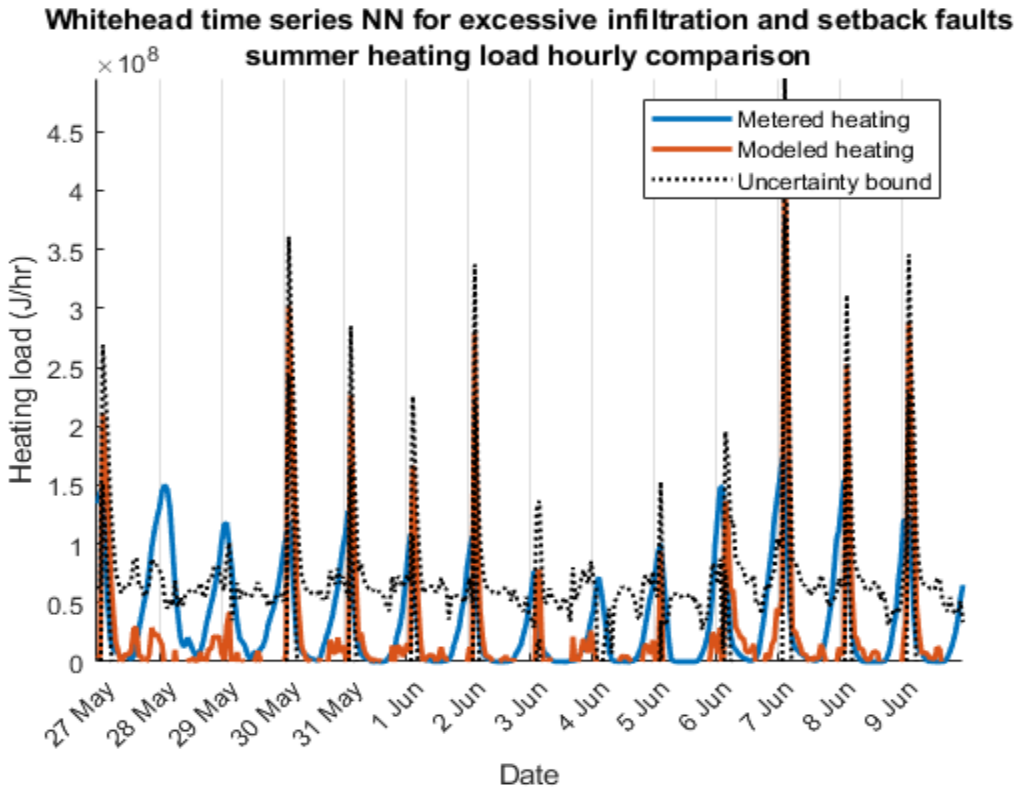

Figure 216A: Predicted heating load for Whitehead experiencing both excessive infiltration and a failure to enter unoccupied setback during summer

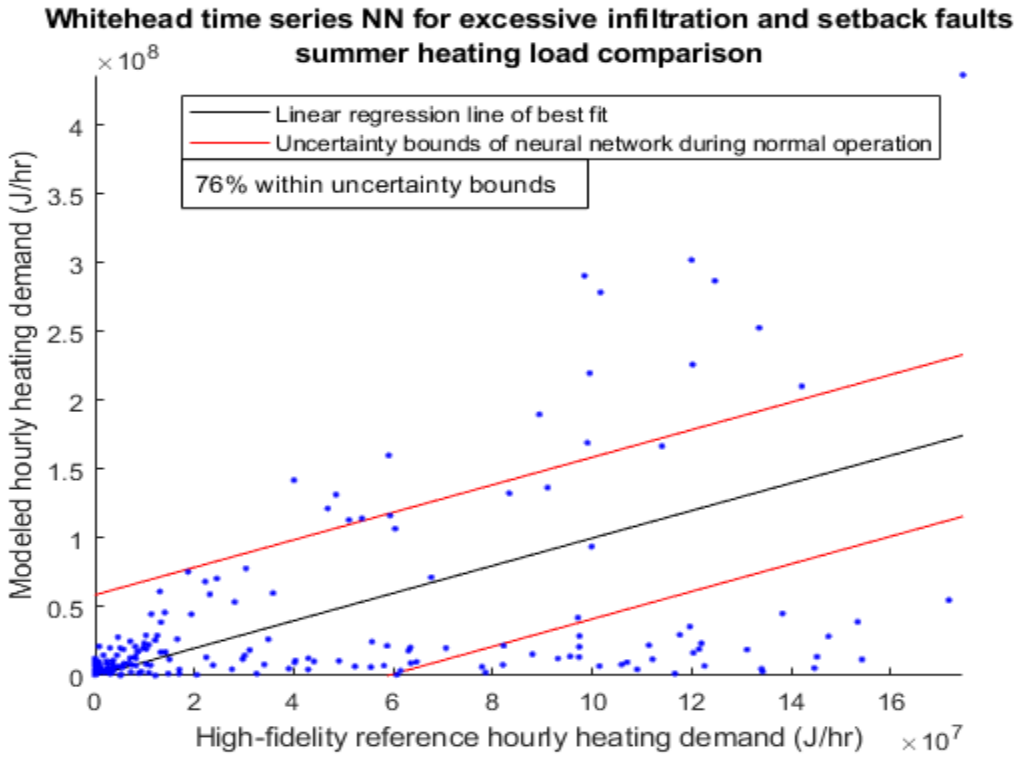

Figure 216B: Alignment factor of heating load for Whitehead experiencing both excessive infiltration and a failure to enter unoccupied setback during summer

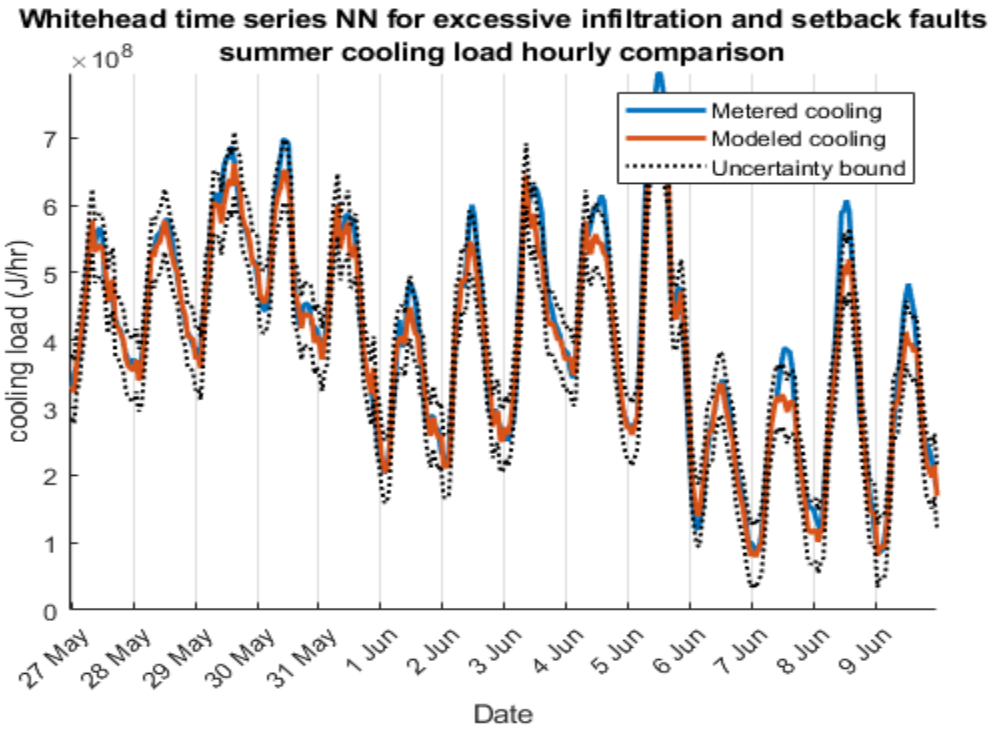

Figure 216C: Predicted cooling load for Whitehead experiencing both excessive infiltration and a failure to enter unoccupied setback during summer

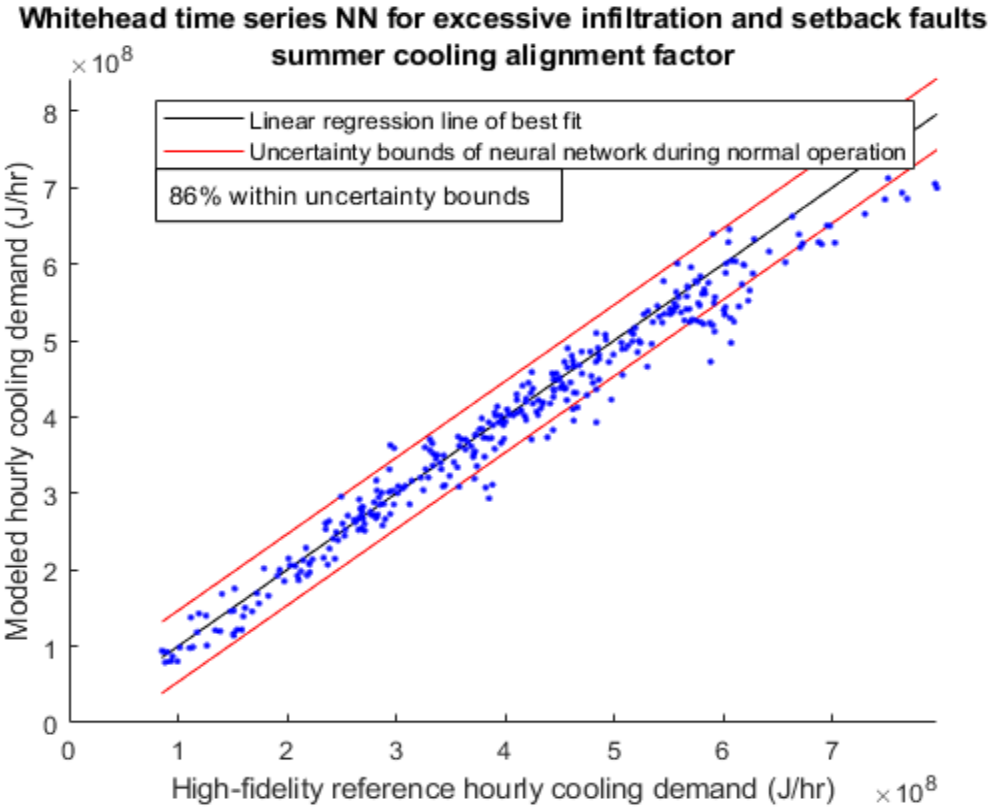

Figure 216D: Alignment factor of cooling load for Whitehead experiencing both excessive infiltration and a failure to enter unoccupied setback during summer

Again, it is not possible for a time series neural network to extrapolate the cause of a fault without given information about component status and being trained on that data. However, fault identification with neural networks will be explored in section 8.3 Deep learning data classification.

8.2 Old CE Times Series Fault Detection

Old CE presents a more complicated pattern and therefore less accurate neural network energy prediction. While NARX neural networks was able to produce excellent accuracy on trained data (R^2 over 0.98 for heating and cooling load) results for untrained weather was less than ideal. Despite a less than desirable result for no-fault data, NARX neural network deviation was so small as to be almost imperceivable for all faults aside from not entering setback during winter weather. Comparing R^2 between faults revealed that all but insufficient outdoor air had a higher R^2 value for heating load comparison than the training data. Cooling meter data was better with only excessive infiltration being marginally better fit (0.83 as opposed to 0.81 for no-fault data). These results were not satisfactory and therefore more iterations of neural networks for Old CE were evaluated.

A lack of satisfactory results is a common problem with neural networks; they require analysis to determine if a model is adequate. As stated earlier, it is impossible to know what the optimal configuration of a network is before comparing the outcomes of different models. Numerous different configurations of neurons and delays were tested until a configuration was found that had acceptable load prediction when no fault was occurring while also displaying significant deviation during faulty operation.

Reducing the number of neurons and delays for nonlinear neural networks did slightly increase deviation for the fault of not entering setback and excessive preheat but did not substantially increase deviation for infiltration or insufficient outdoor air. Further reducing neurons and delays did exacerbate deviation for fault conditions but also reduced energy prediction accuracy when no fault was occurring, which left the results indistinguishable between no fault and a fault of insufficient outdoor air or excessive infiltration occurring. Dramatically increasing node and delay count resulted in no statistically significant change in no-fault energy prediction while also not demonstrating an increase in deviation when excessive infiltration or insufficient outdoor faults were present. While it is possible that an extreme number of nodes and lookback samples may have the desired results, 40 nodes with 20 lookback points already took over 8 hours to train using parallel computing on over 4000 cores.

To simplify comparisons, a 10 neuron and 12 lookback nonlinear input-output neural network was used for analysis to more easily compare neural network results to those of Whitehead. Results were acceptable but with more deviation than occurred when calibrating to Whitehead metered data. Additionally, fault detection tests for all faults but insufficient outdoor air were successful.

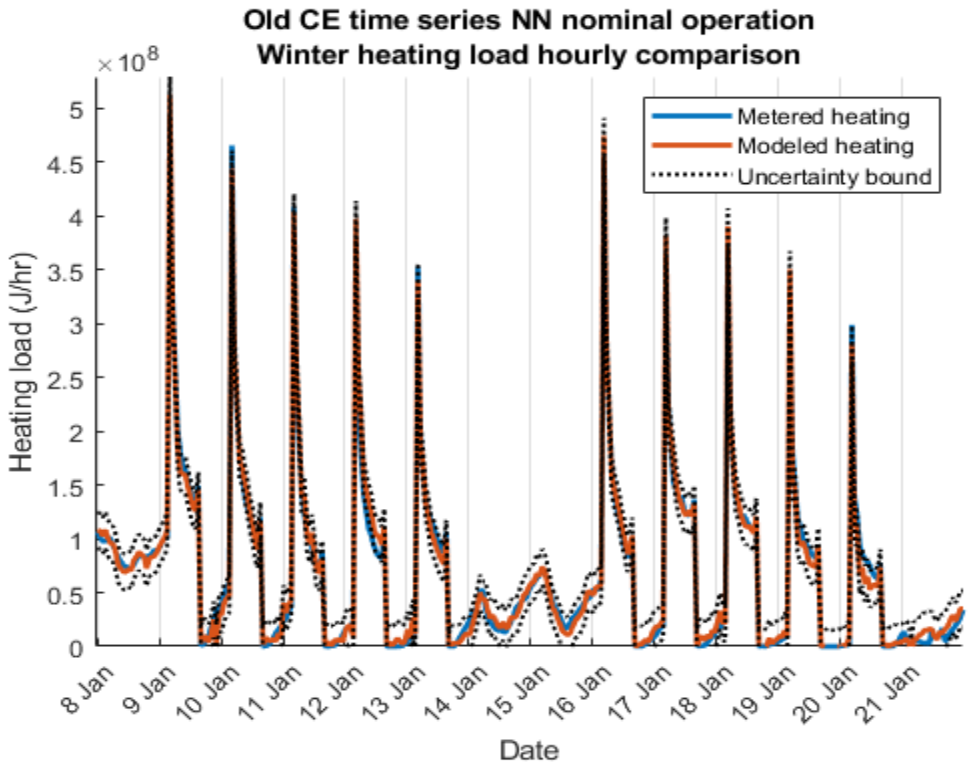

Figure 217A: Hourly heating load comparison of 10 neuron and 12 delay time series neural network for Old CE during winter

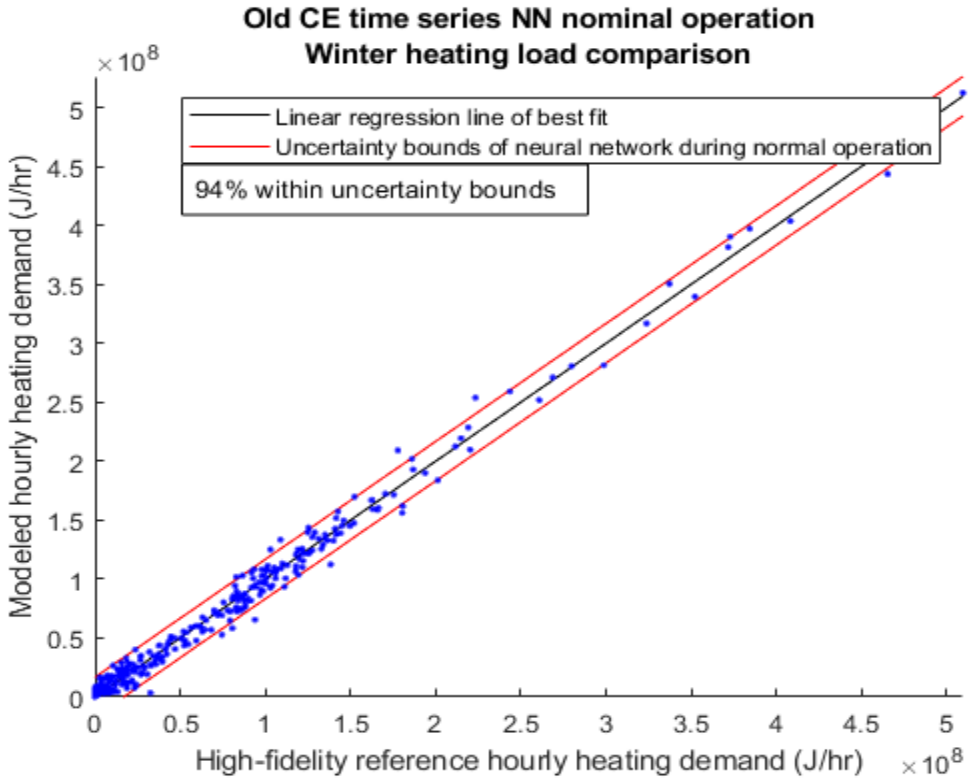

Figure 217B: Alignment factor of heating load comparison of 10 neuron and 12 delay time series neural network for Old CE during winter

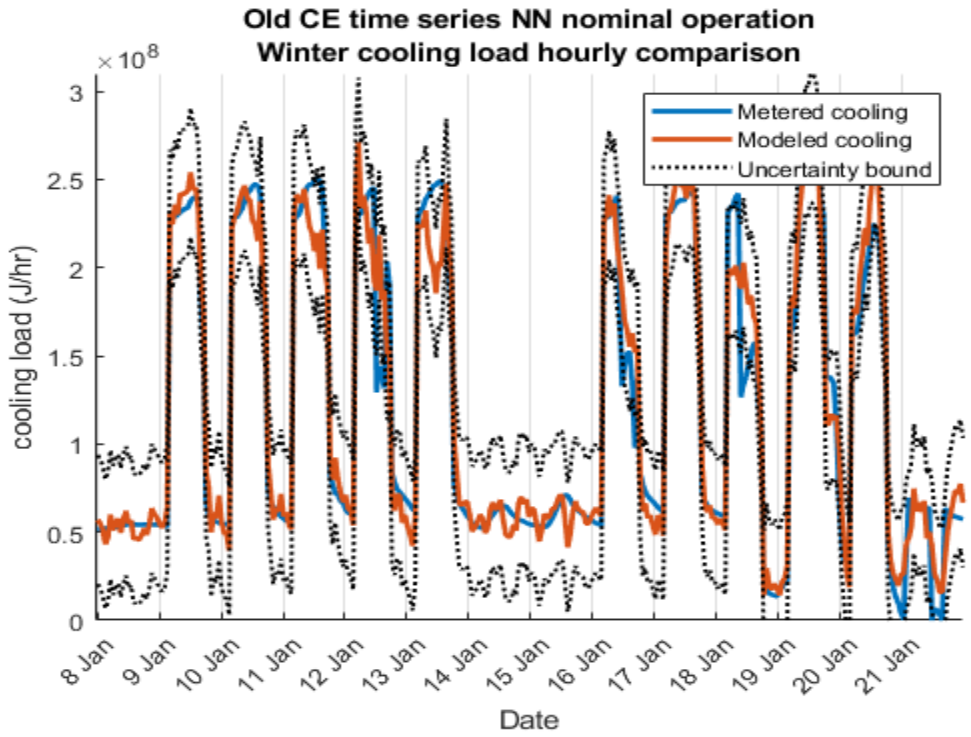

Figure 217C: Hourly cooling load comparison of 10 neuron and 12 delay time series neural network for Old CE during winter

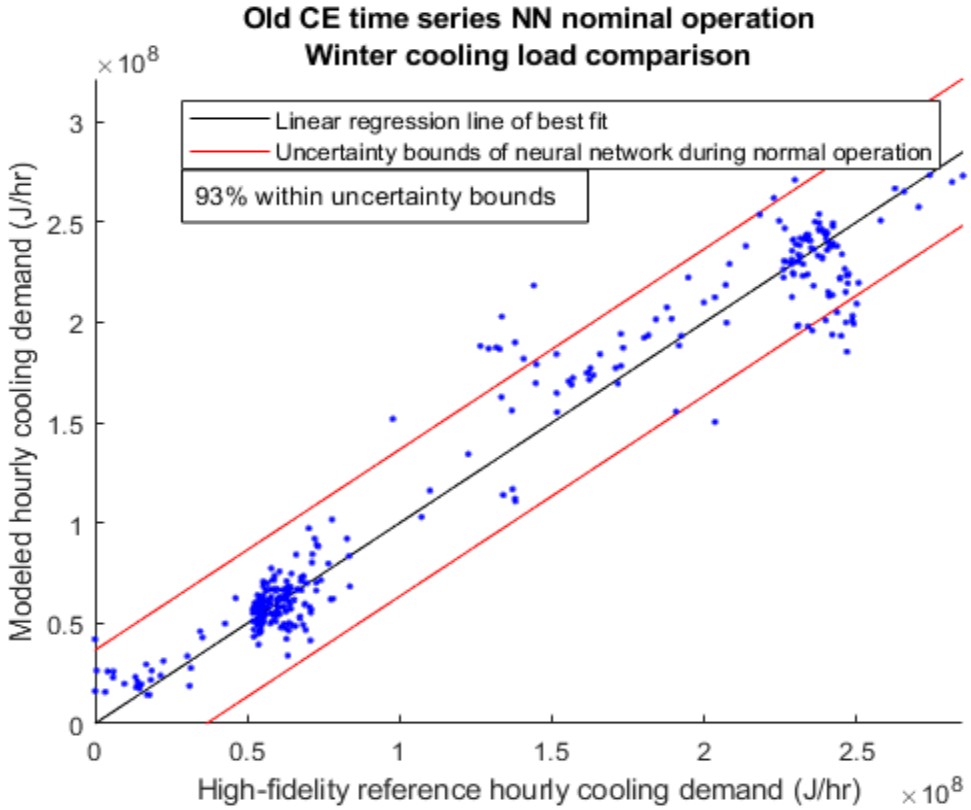

Figure 217D: Alignment factor of hourly cooling load comparison of 10 neuron and 12 delay time series neural network for Old CE during winter

Winter and summer analysis, in Figure 217 and Figure 218 respectively, reveals time series NN load prediction demonstrates a broad level agreement with metered data while missing on some seemingly random spikes in load. As with Whitehead time series NN testing, a balance needed to be found between nominal load accuracy and faulty operation deviation.

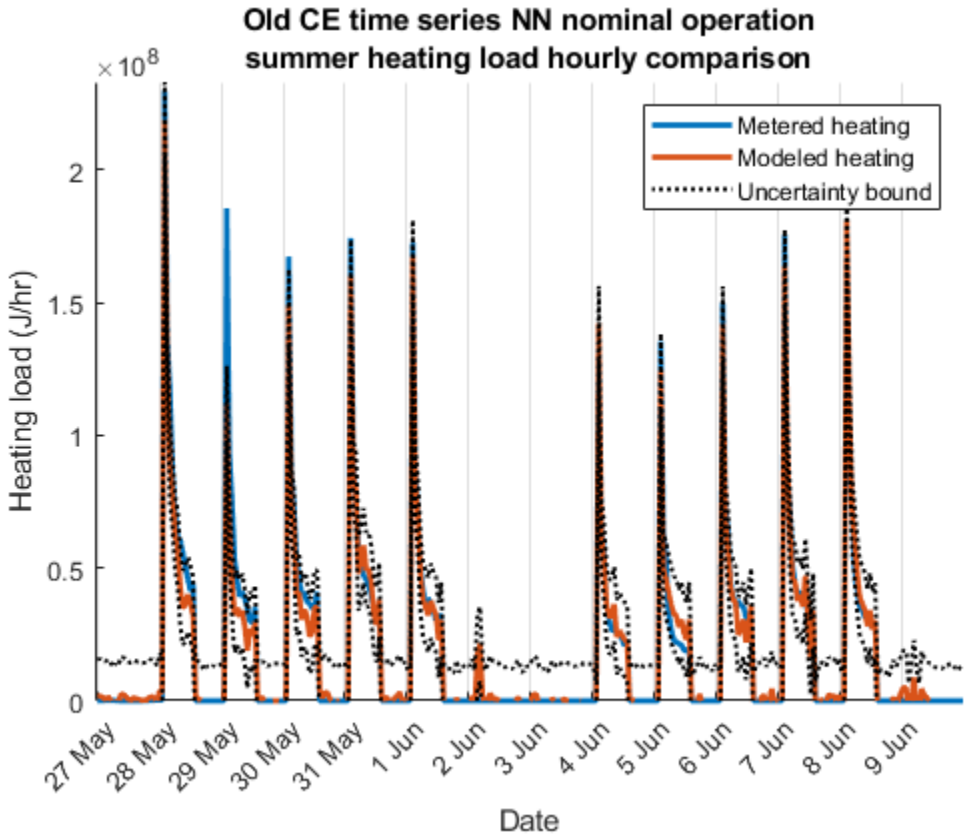

Figure 218A: Hourly heating load comparison of 10 neuron and 12 delay time series neural network for Old CE

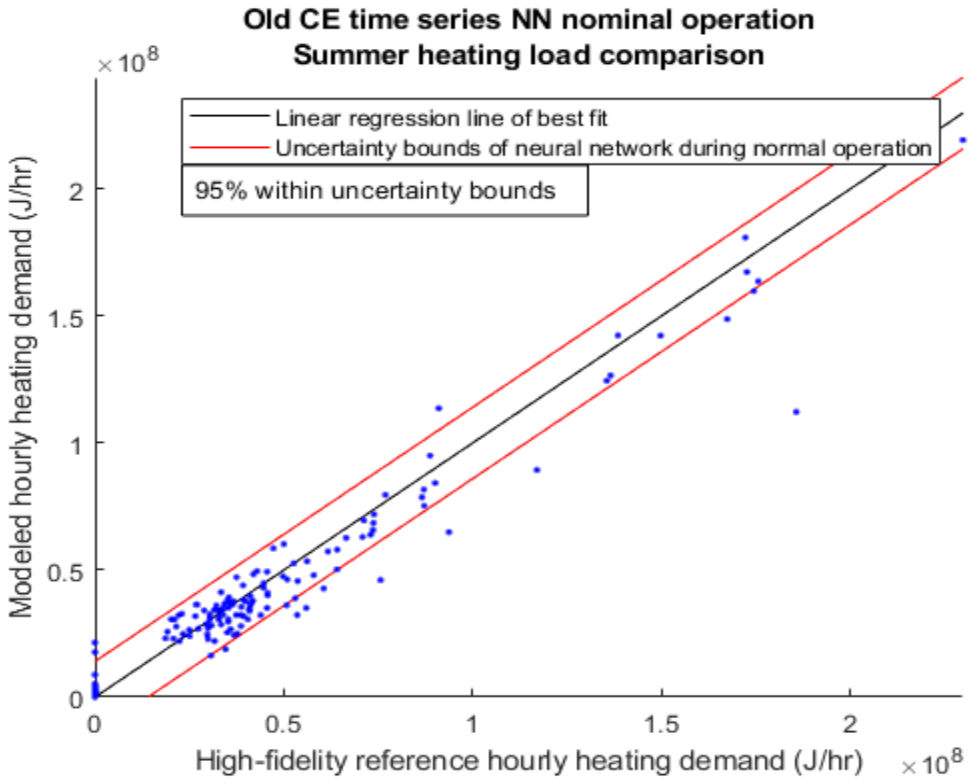

Figure 218B: Alignment factor of hourly heating load comparison of 10 neuron and 12 delay time series neural network for Old CE

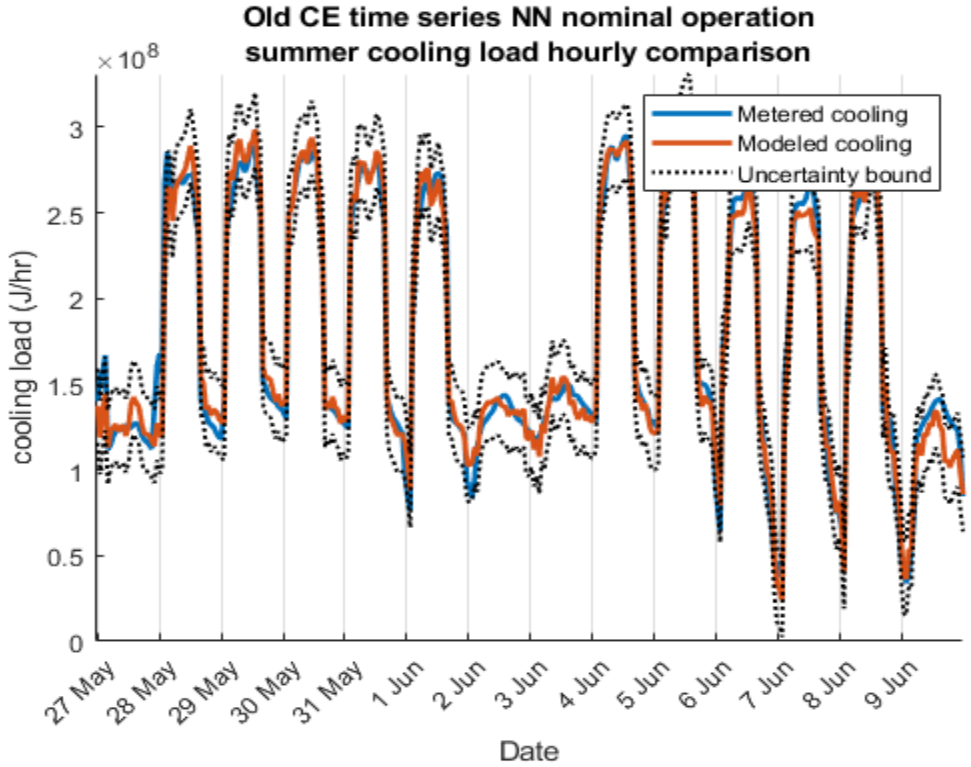

Figure 218C: Hourly cooling load comparison of 10 neuron and 12 delay time series neural network for Old CE

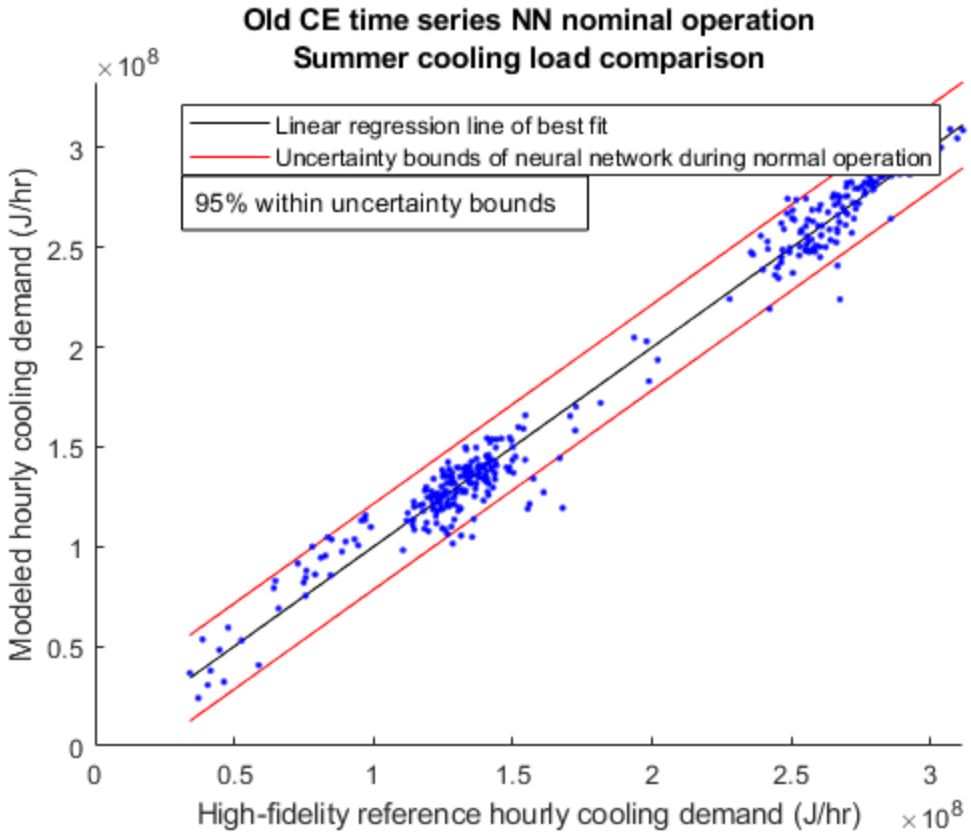

Figure 218D: Alignment factor of hourly cooling load comparison of 10 neuron and 12 delay time series neural network for Old CE

Analysis of time series predicted load results depict heating and cooling demands that are largely representative of metered data but with some periods of significant deviation. NN calibration for fault detection requires a balance of no-fault accuracy and limited prediction interval while also not overfitting such that faults are not differentiable from no-fault performance.

8.2.1 Old CE Excessive Infiltration

Excessive infiltration was a subtle load to detect in Whitehead, a building without evening air flow setback and energy recovery systems. As such, a renovated, low load, and energy conscious building such as Old CE is primarily impacted by infiltration by altering zone load demand rather than through altering return air properties. Figure 219

reveals a decrease in predicted heating demand when compared to metered data for winter weather. In section 5.3.1. Old CE Infiltration, revealed that infiltration was a subtle but detectable fault when using physics-based simulation, but results are more difficult to find exclusively through time series deviation from metered data.

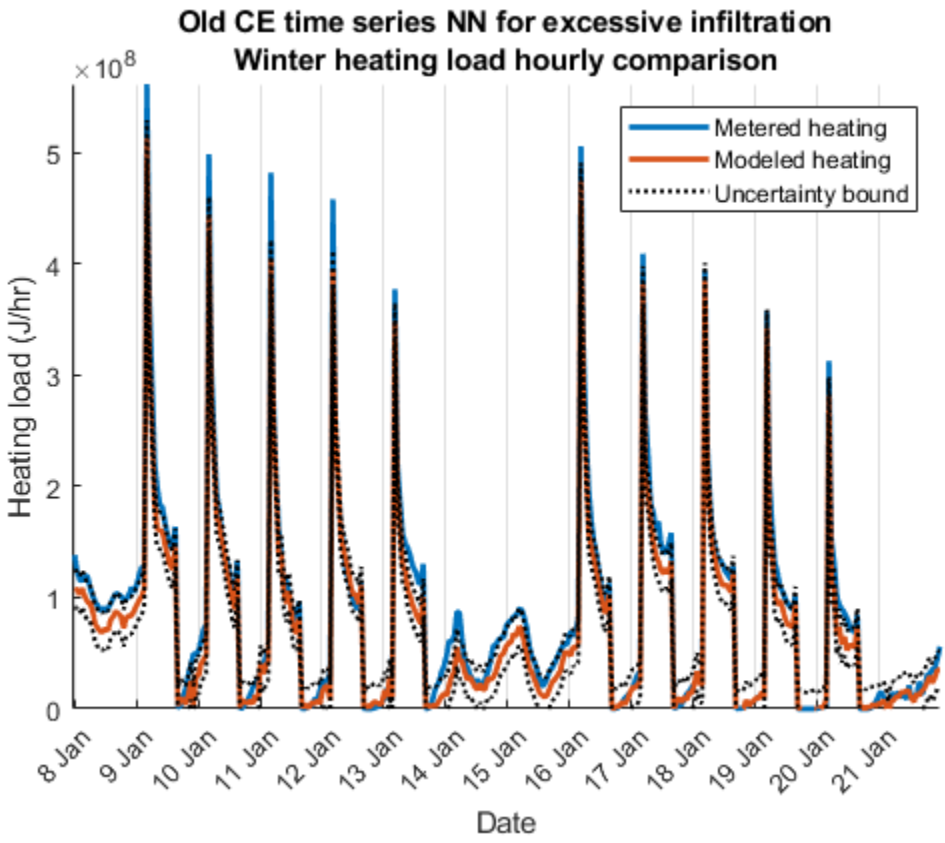

Figure 219A: Predicted heating loads for Old CE while experiencing excessive infiltration fault condition during winter

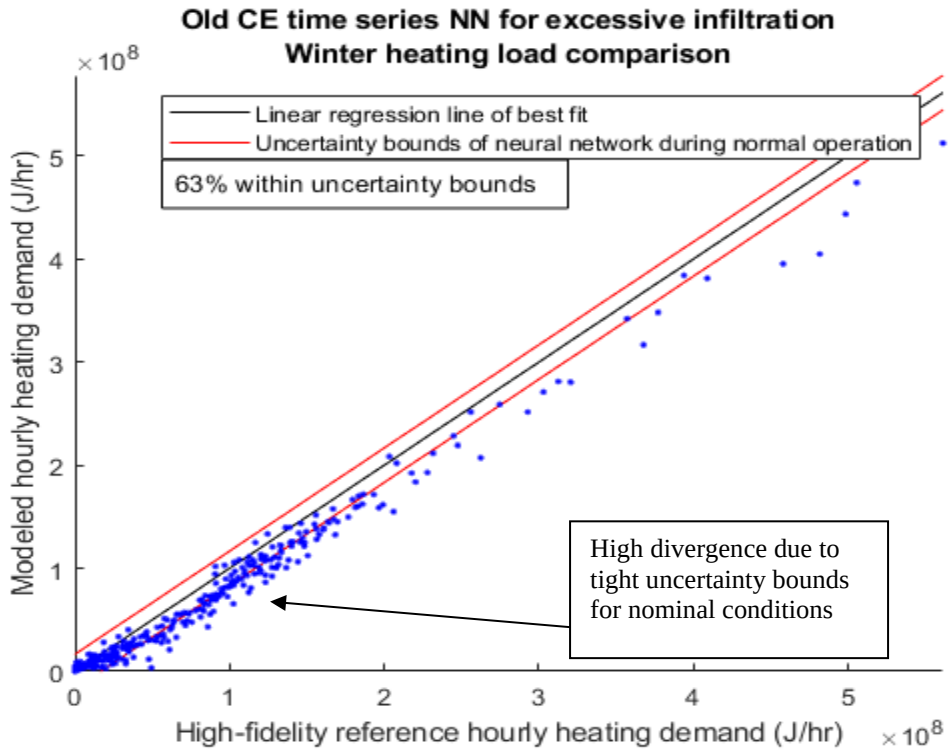

Figure 219B: Alignment factor of predicted heating load for Old CE while experiencing excessive infiltration fault condition during winter

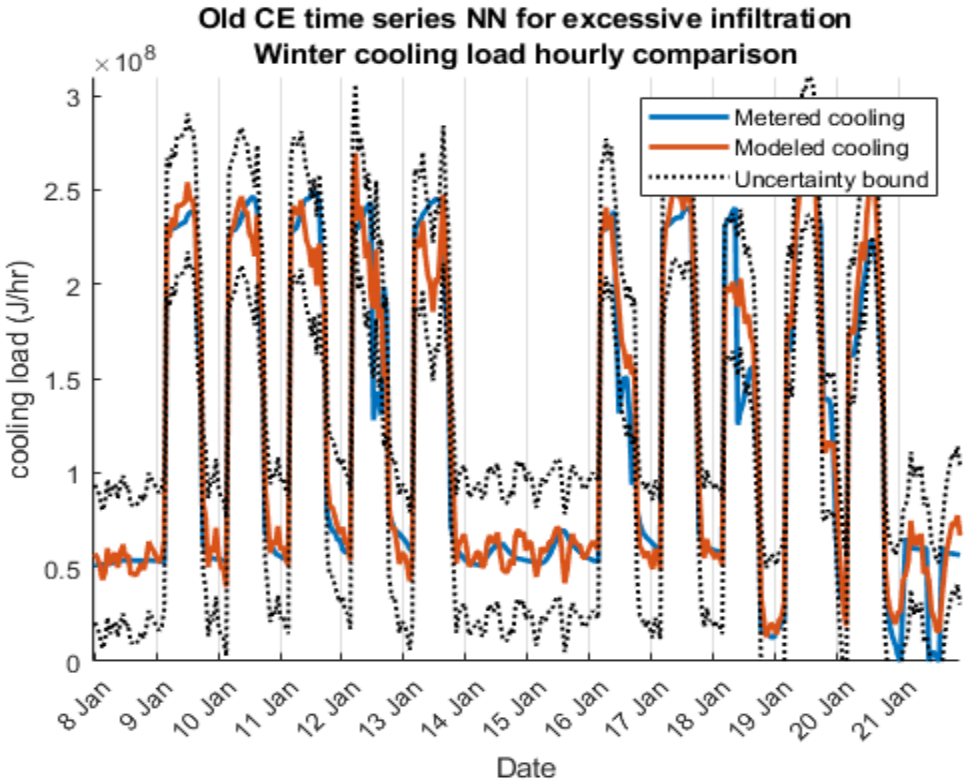

Figure 219C: Predicted cooling load for Old CE while experiencing excessive infiltration fault condition during winter

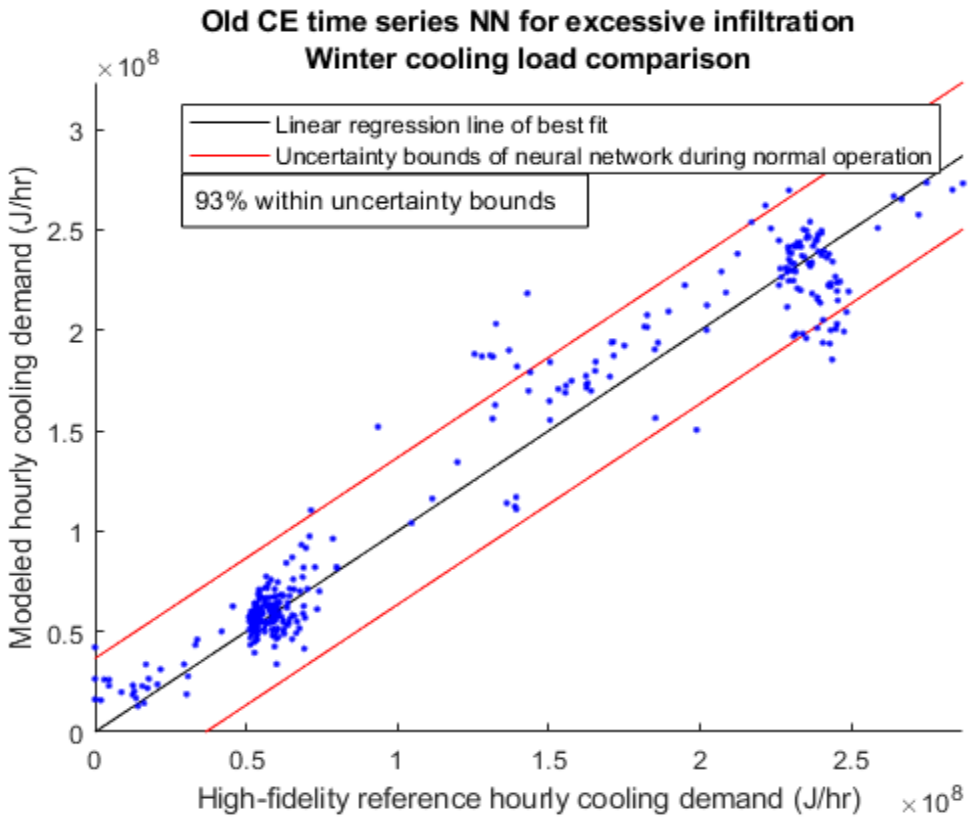

Figure 219D: Alignment factor of predicted cooling load for Old CE while experiencing excessive infiltration fault condition during winter

While winter testing has a noticeable deviation in heating load, no statistically significant change can be found for summer conditions in Figure 220. Infiltration has a relatively low impact on building loads during summer as wind speeds and temperature difference between indoor and outdoor air is reduced.

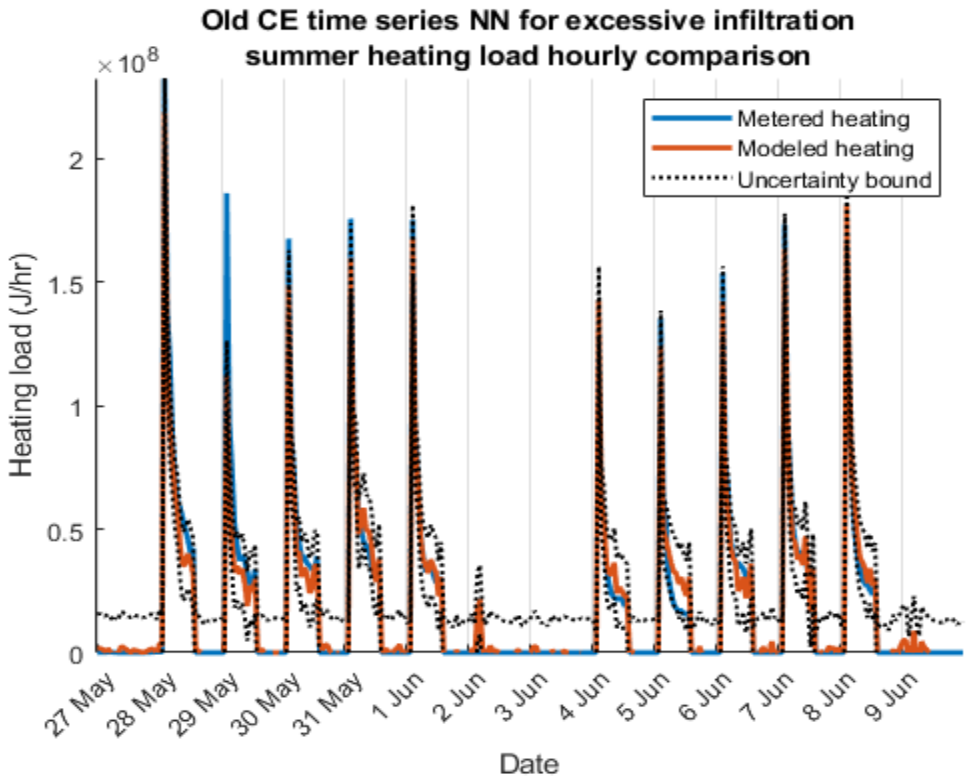

Figure 220A: Predicted heating load for Old CE while experiencing excessive infiltration fault condition during summer

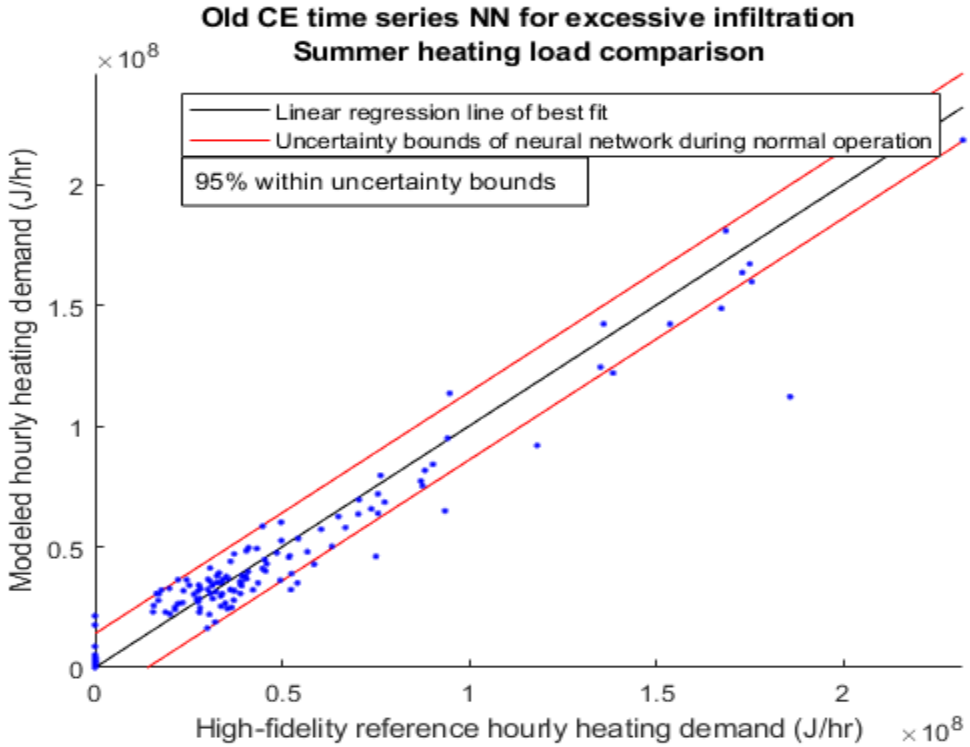

Figure 220B: Alignment factor of predicted heating load for Old CE while experiencing excessive infiltration fault condition during summer

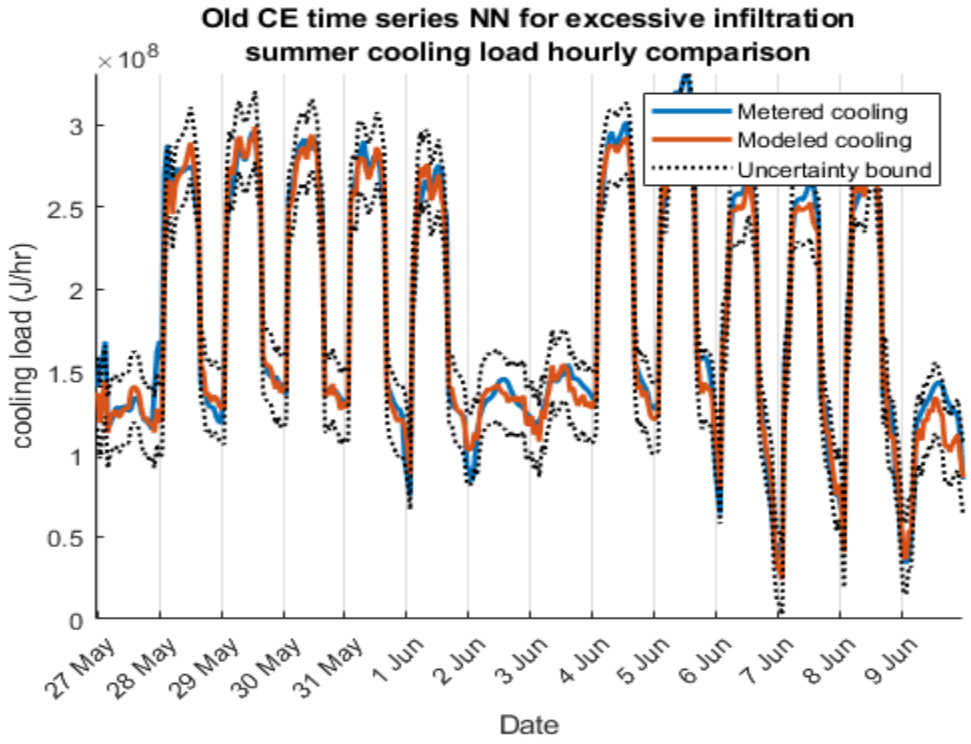

Figure 220C: Predicted cooling load for Old CE while experiencing excessive infiltration fault condition during summer

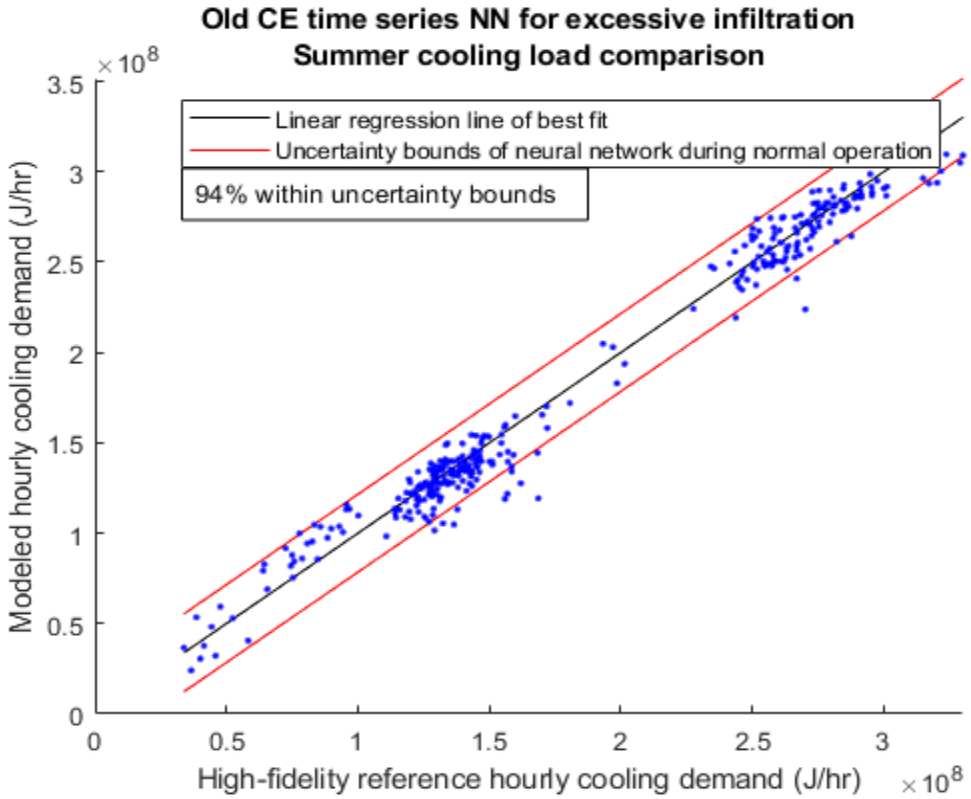

Figure 220D: Alignment factor of predicted cooling load for Old CE while experiencing excessive infiltration fault condition during summer

Predicted energy demand during an excessive infiltration fault reflected results from the SPBM test. Winter conditions produced noticeable deviation from metered data while summer results were statistically indistinguishable. It is theorized that winter conditions produce more significant demands on zone heating as zone temperature is often near the minimum setpoint and that outdoor air would be significantly cooler and less humid than interior conditions. Summer outdoor air can be hotter and more humid than interior zone temperatures but rarely was a zone at the maximum setpoint temperature, so increased infiltration did not produce additional zone cooling demand and infiltration therefore would only slightly increase demand at cooling coils.

8.2.2 Old CE Not Entering Unoccupied Setback

Failure to enter unoccupied setback displays significant deviation from metered load data. Heating load comparison for winter in Figure 221 revealed an alignment slope for linear regression far different from the ideal 1:1 relation.

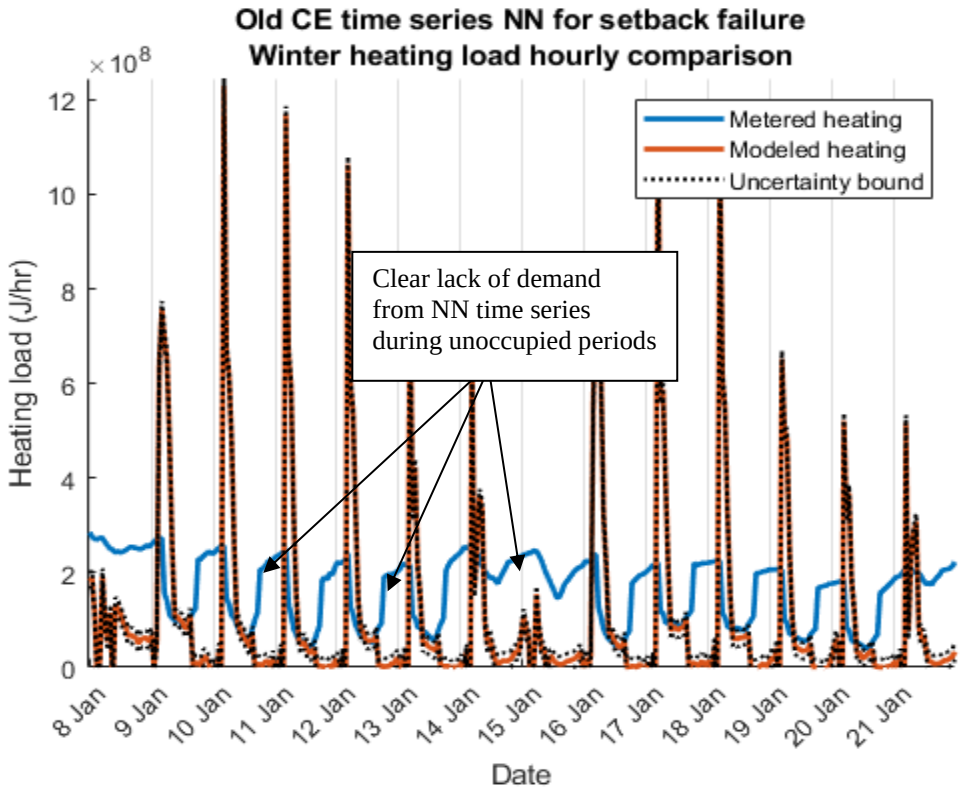

Figure 221A: Predicted heating load for Old CE while a failure to enter unoccupied setback fault is occurring during winter

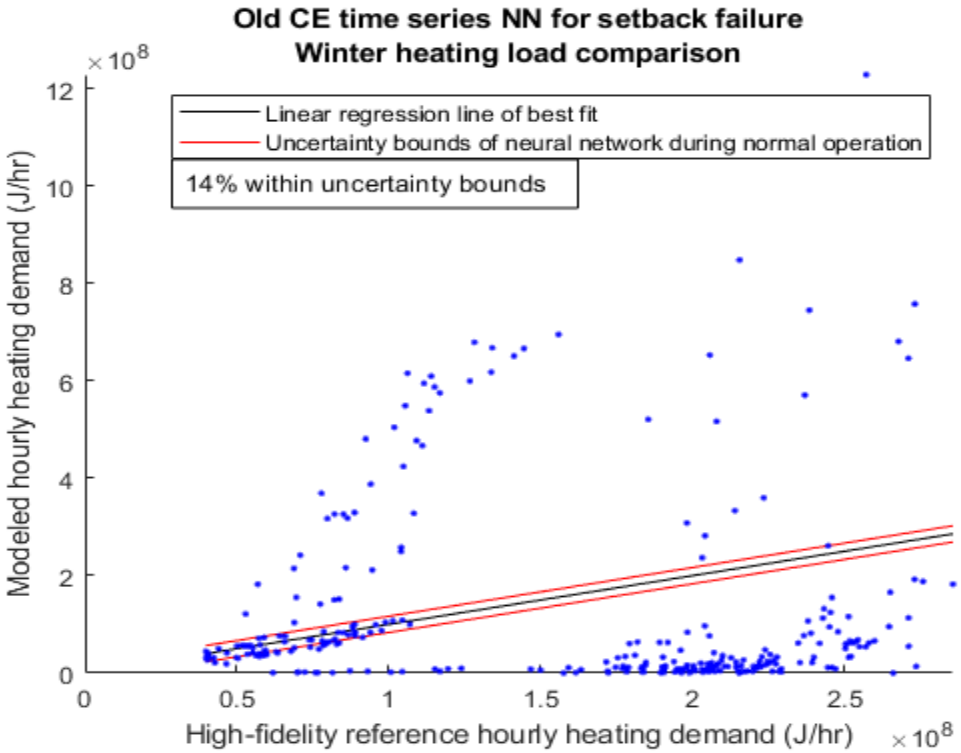

Figure 221B: Alignment factor of predicted heating load for Old CE while a failure to enter unoccupied setback fault is occurring during winter

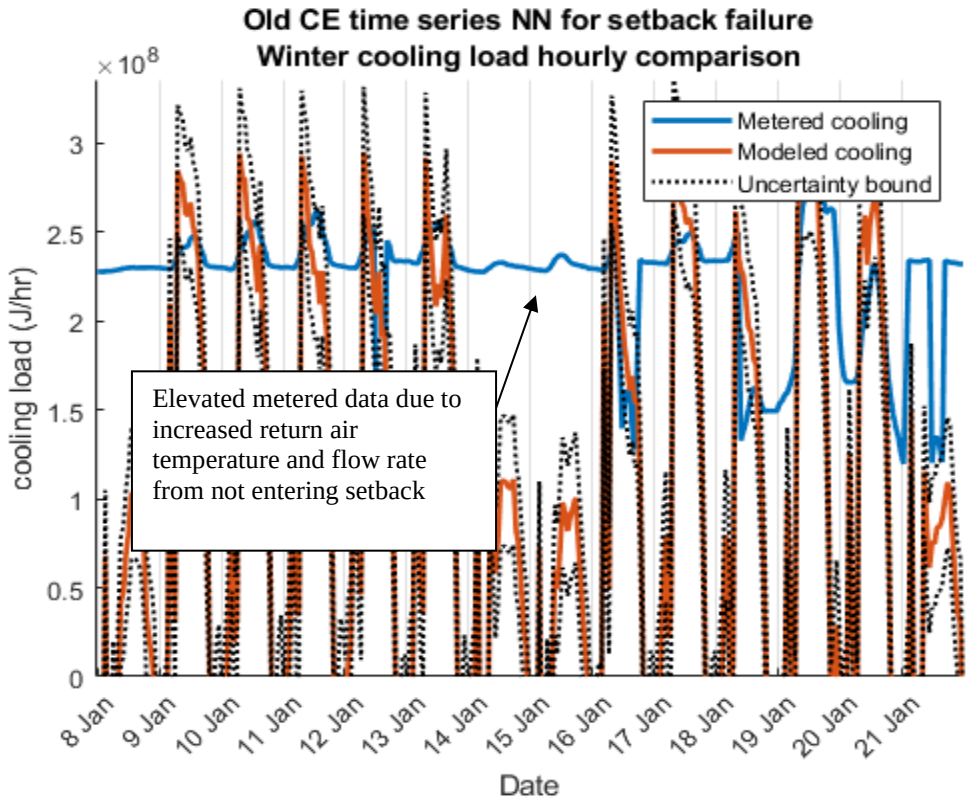

Figure 221C: Predicted cooling load for Old CE while a failure to enter unoccupied setback fault is occurring during winter

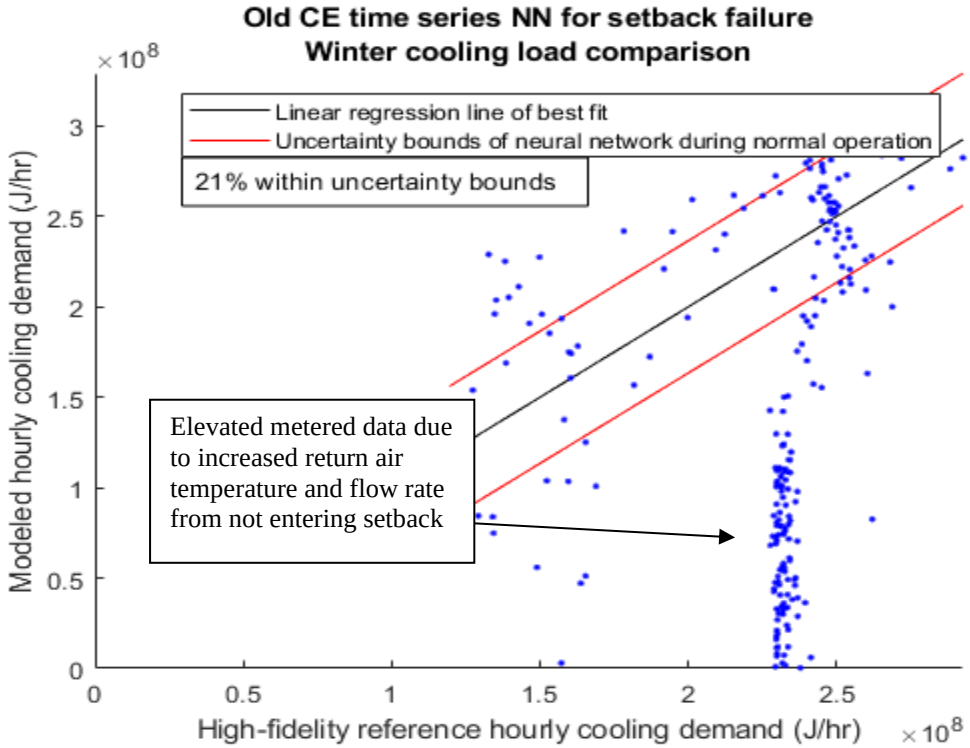

Figure 221D: Alignment factor of predicted cooling loads for Old CE while a failure to enter unoccupied setback fault is occurring during winter

Summer heating alignment factor in Figure 222 has nearly a 1:10 slope, which is indicative of modeled underprediction. Because the time series NN was trained under nominal conditions, there only difference between training data and unoccupied setback data would be changes in electrical use during nights and weekends. Therefore, the NN may interpret this change as an increase in cooling demand rather than a need for additional heating.

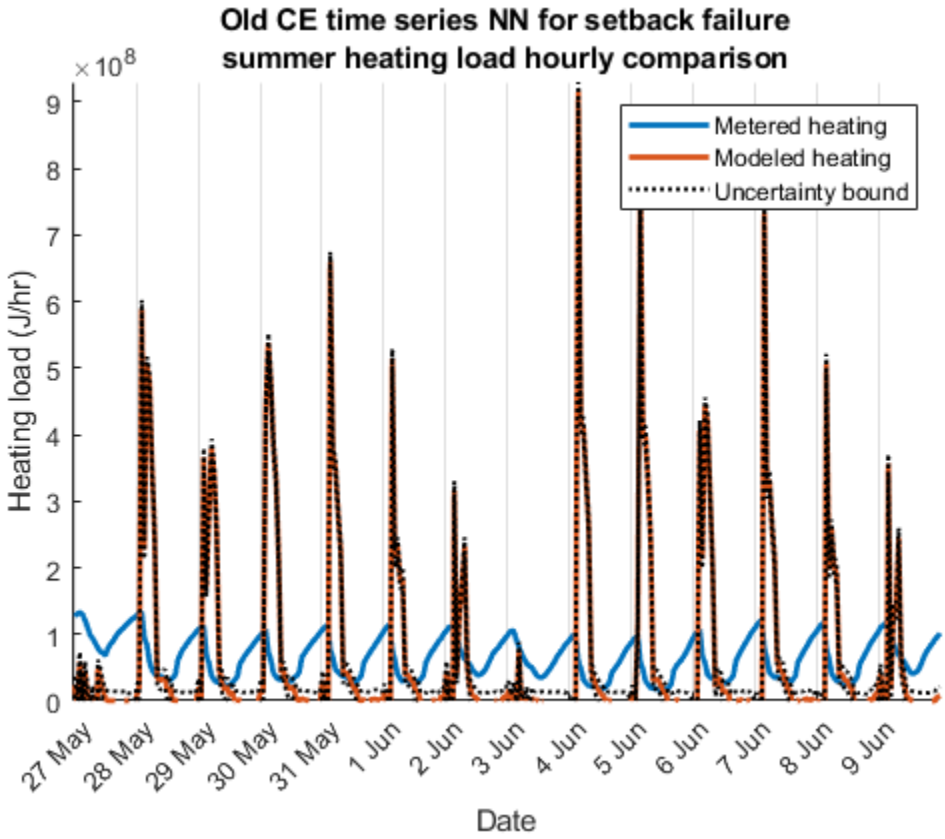

Figure 222A: Predicted heating load for Old CE while a failure to enter unoccupied setback fault is occurring during summer

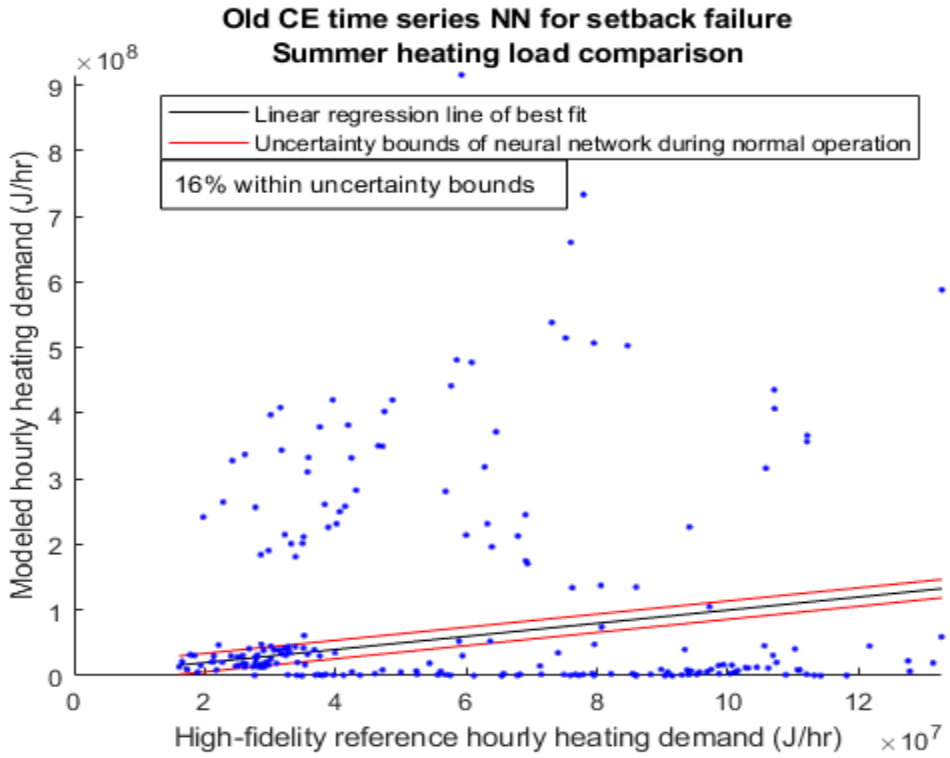

Figure 222B: Alignment factor of predicted heating load for Old CE while a failure to enter unoccupied setback fault is occurring during summer

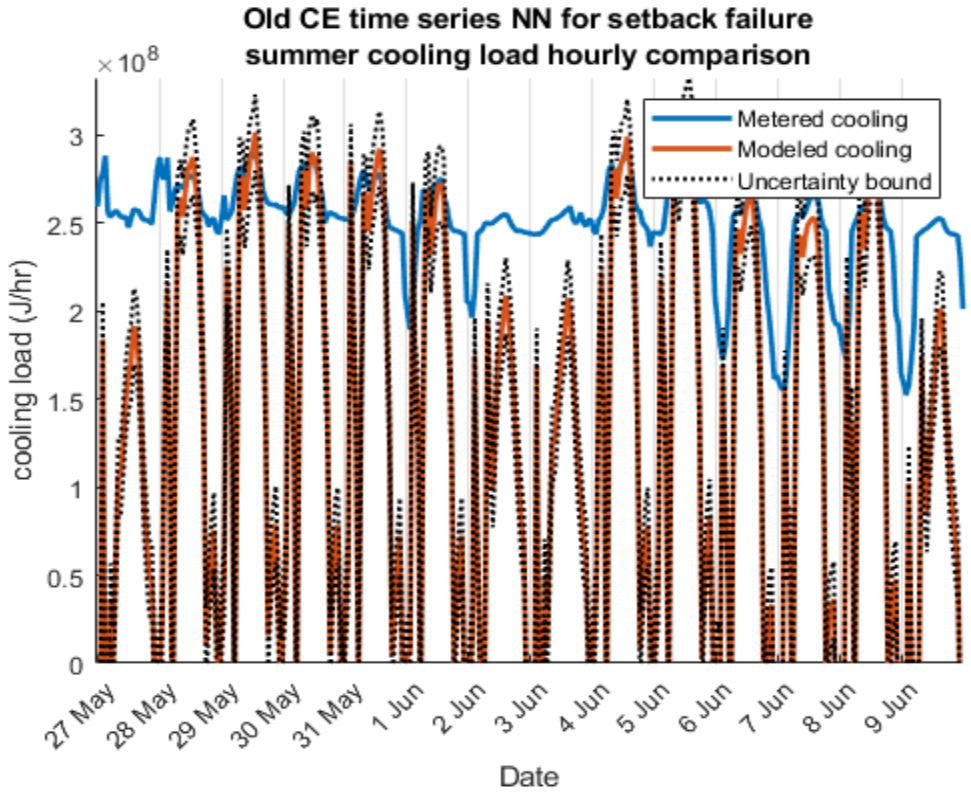

Figure 222C: Predicted cooling load for Old CE while a failure to enter unoccupied setback fault is occurring during summer

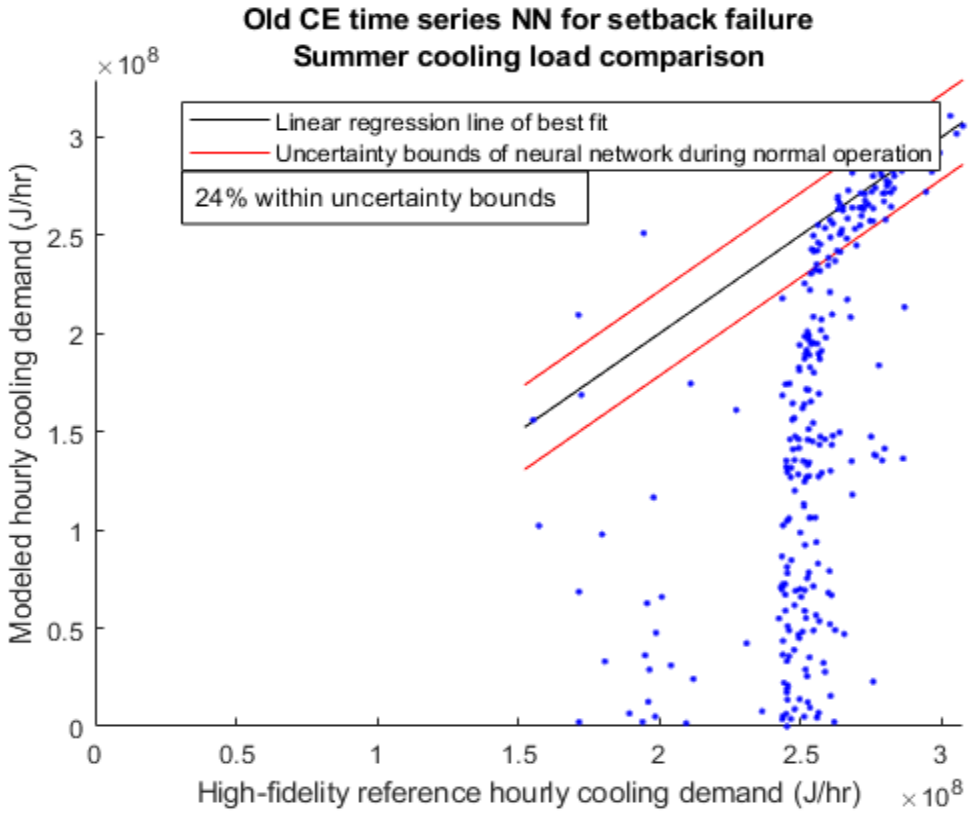

Figure 222D: Alignment factor of predicted cooling load for Old CE while a failure to enter unoccupied setback fault is occurring during summer

Such a significant change in predicted load is attributed to a lack of drop of both heating and cooling demand that is associated with unoccupied setback. The NN was trained with 'time of day' and 'day of week' information, so it is possible that the network reduced demand during those periods.

8.2.3 Old CE Excessive Preheat

Unsurprisingly, excessive preheating fault has the most significant deviation from predicted load demand. Due to the efficiency of Old CE and its HVAC system, both heating and cooling loads are noticeably altered from those predicted by the neural network for winter test periods in Figure 223. A noticeable shift in cooling and heating load occurs when air flow rates increase for occupied times; both heating and cooling

demand changes because the 16°C temperature change between preheated air and cooled air remains nearly constant while air flow rate substantially increases for occupied periods. Noticing differences in how predicted and metered energy behave in relation to each other is important when using these results to deduce a plausible fault that may be responsible for these changes.

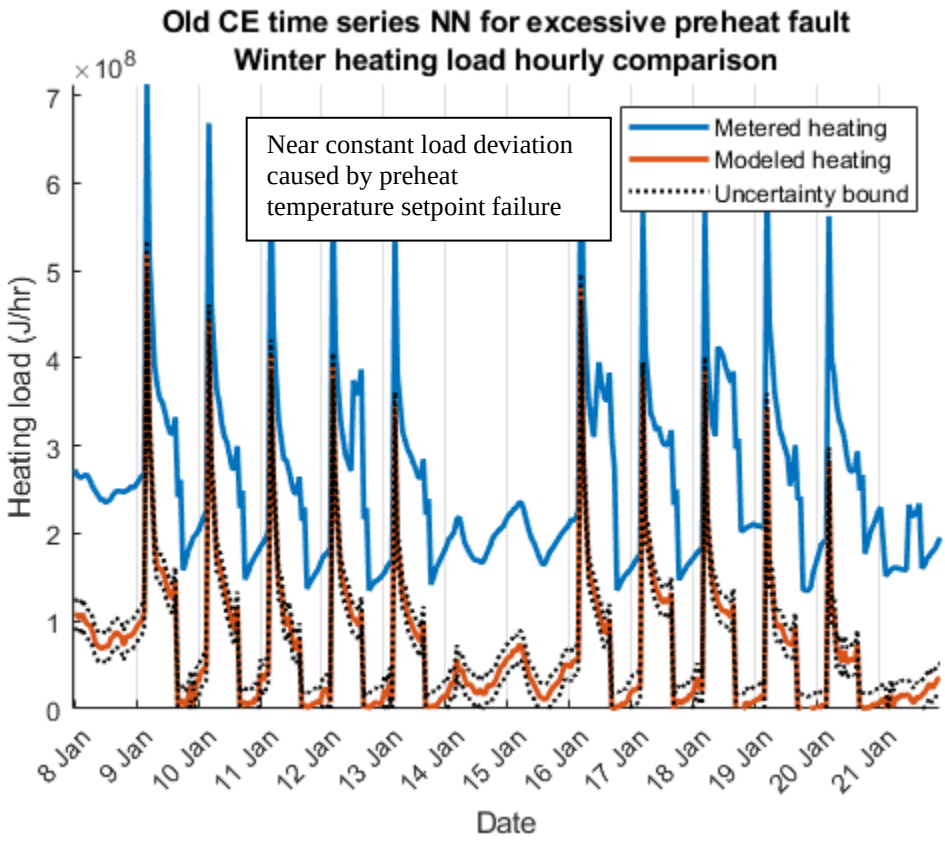

Figure 223A: Predicted heating load for Old CE while experiencing excessive preheat fault condition during winter

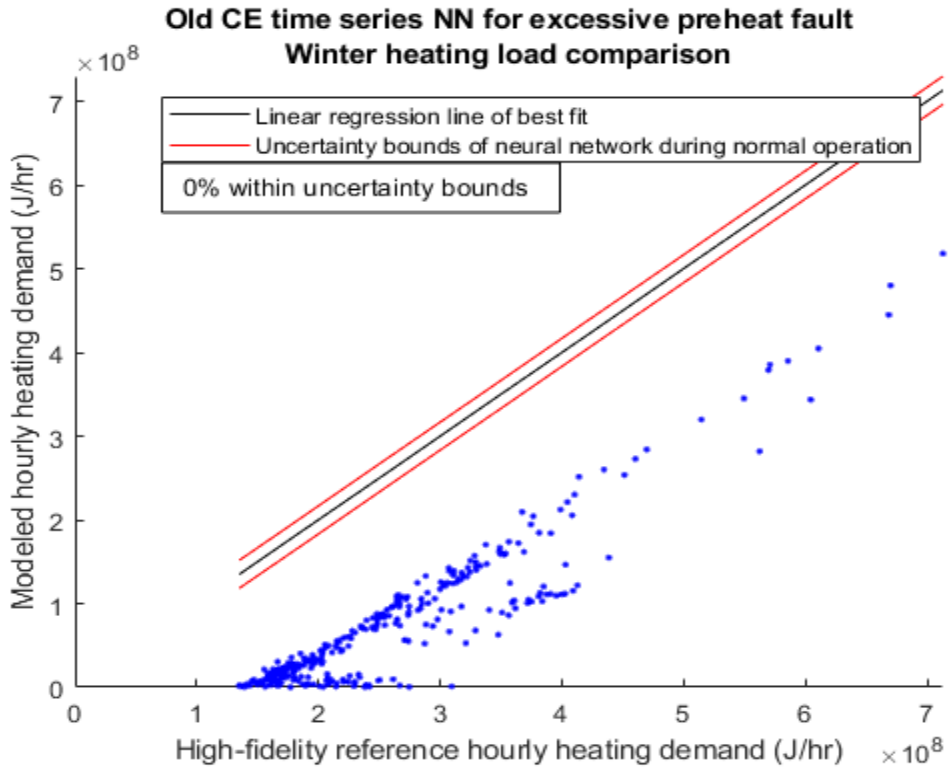

Figure 223B: Alignment factor of predicted heating load for Old CE while experiencing excessive preheat fault condition during winter

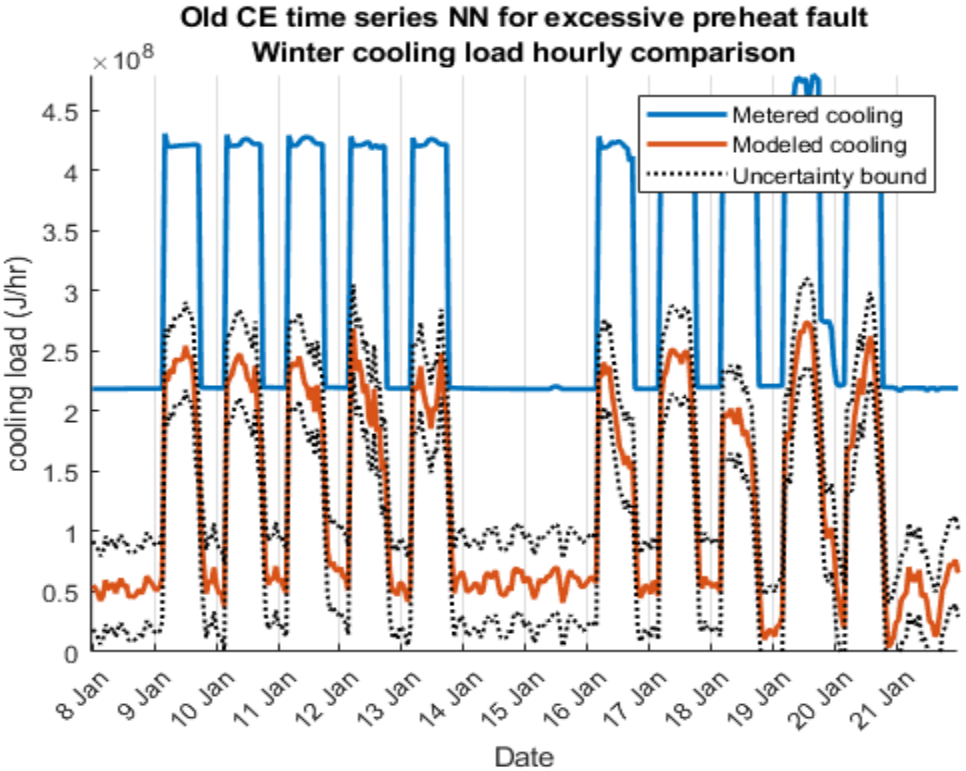

Figure 223C: Predicted cooling load for Old CE while experiencing excessive preheat fault condition during winter

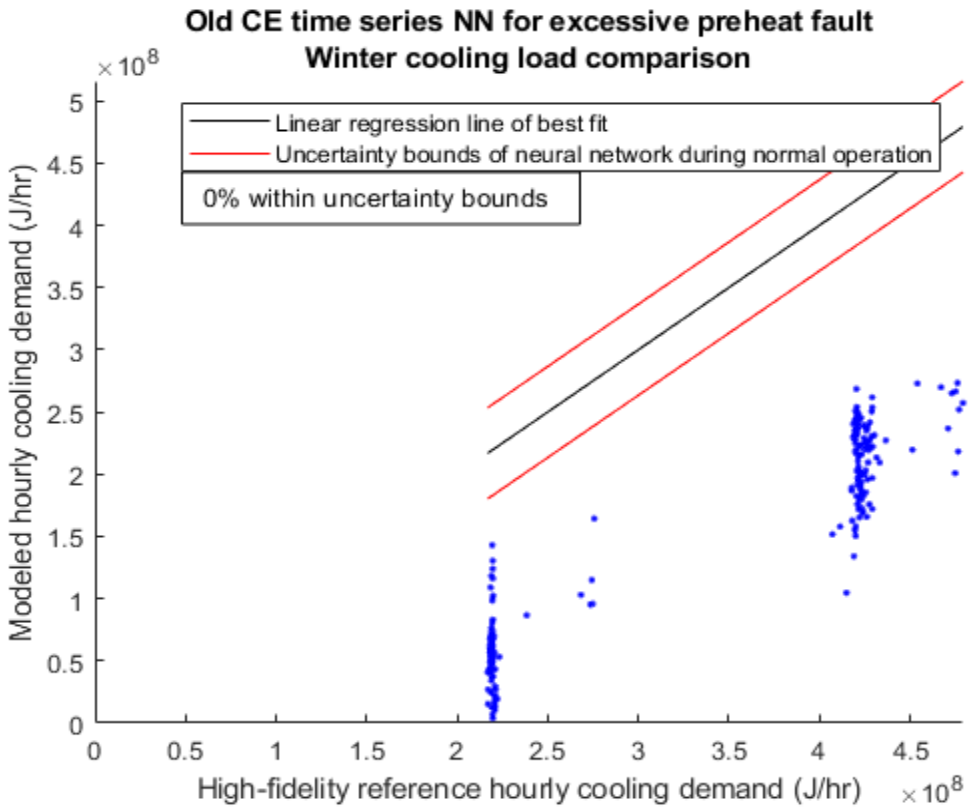

Figure 223D: Alignment factor of predicted cooling loads for Old CE while experiencing excessive preheat fault condition during winter

Figure 224 maintains the increase in demand from metered data that was evident during winter conditions. As with setback failure testing, the only change to input data for the NN would be whatever electrical increase occurs from higher hot and chilled water pumping; yet it is impossible to understand how this trained network may interpret this change in data due to the nature of neural network structures.

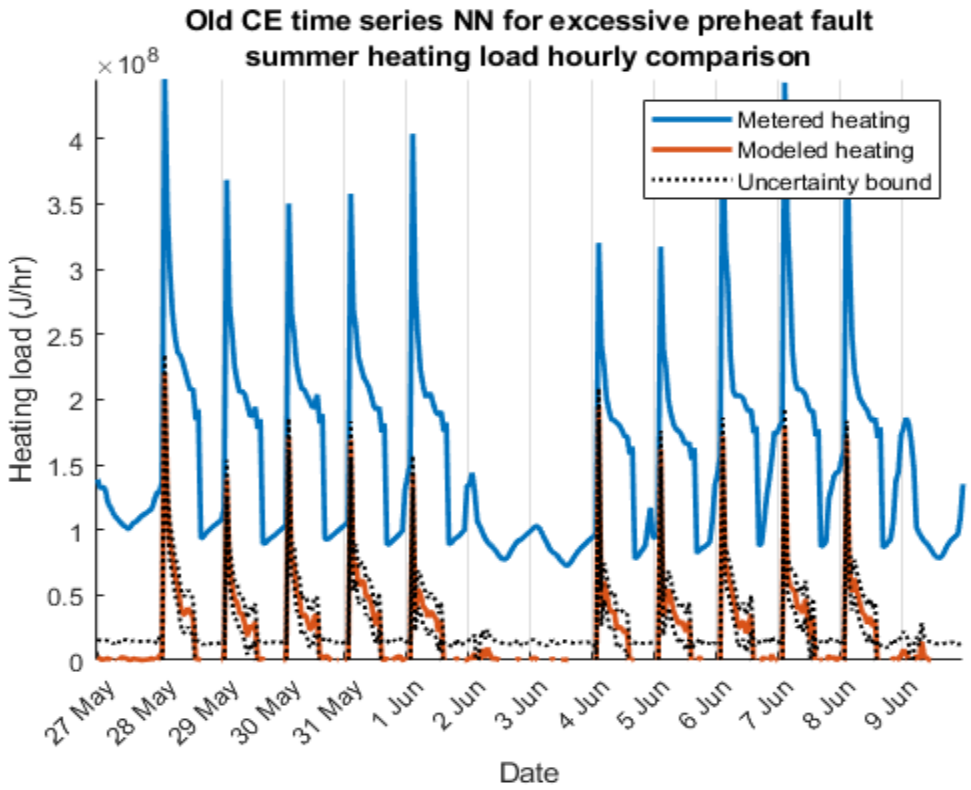

Figure 224A: Predicted heating load for Old CE while experiencing excessive preheat fault condition during summer

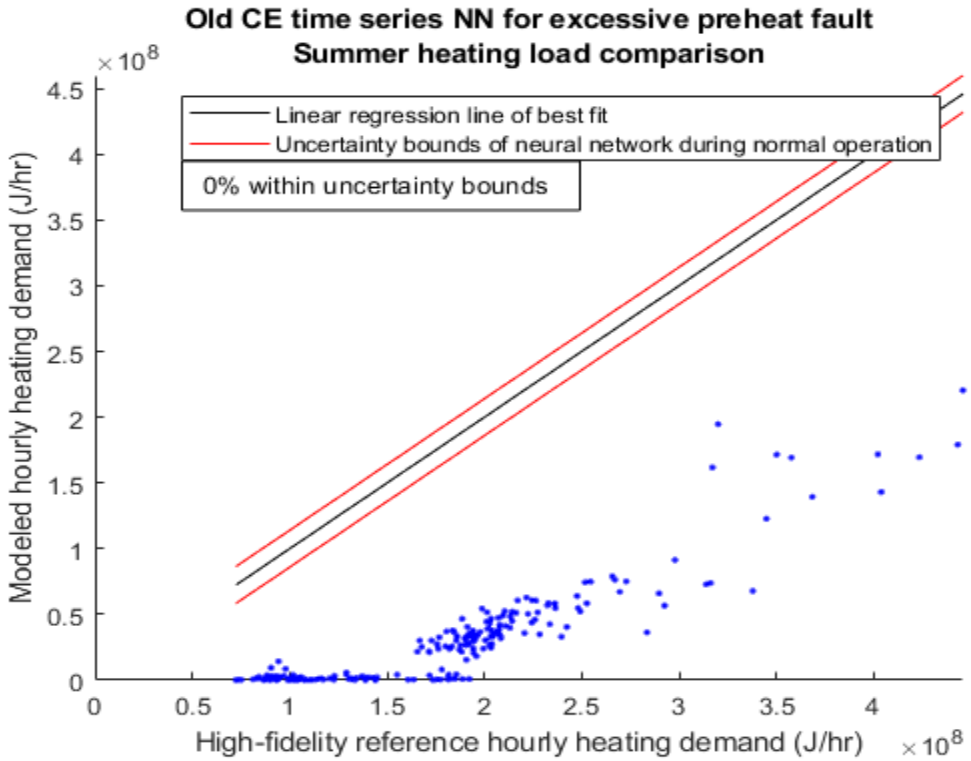

Figure 224B: Alignment factor of predicted heating load for Old CE while experiencing excessive preheat fault condition during summer

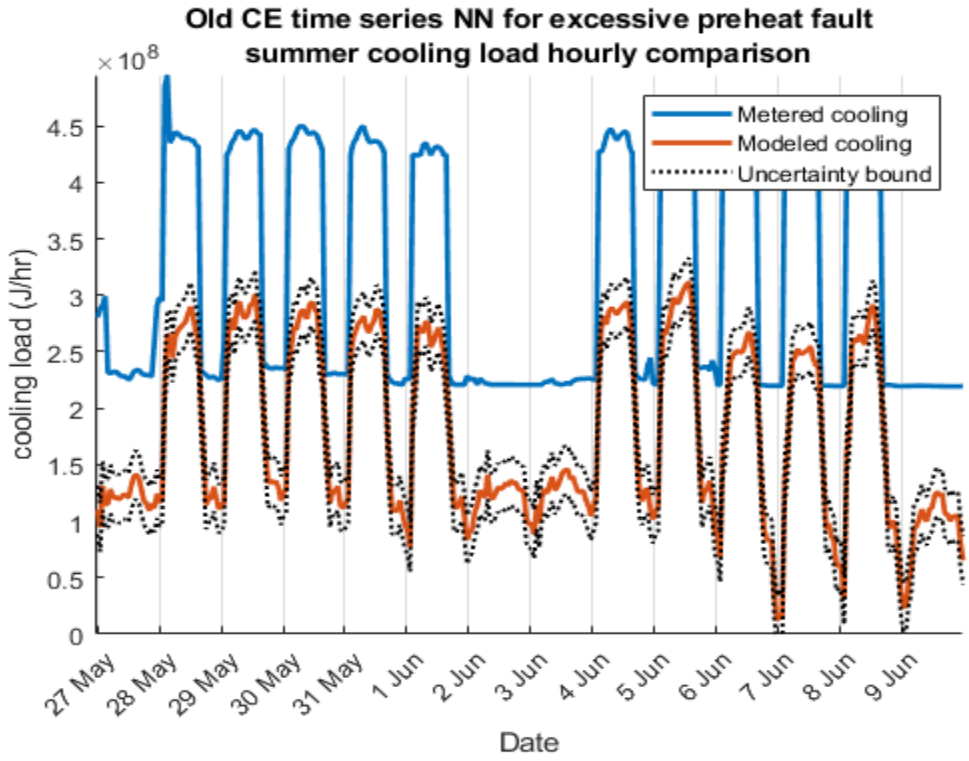

Figure 224C: Predicted cooling load for Old CE while experiencing excessive preheat fault condition during summer

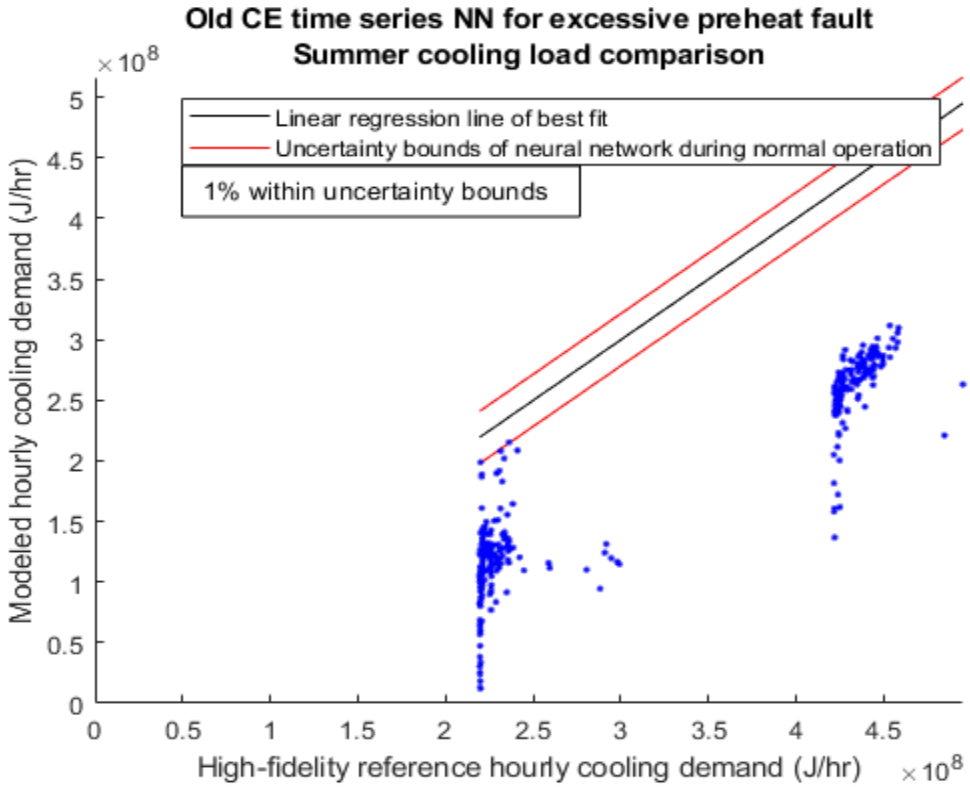

Figure 224D: Alignment factor of predicted cooling loads for Old CE while experiencing excessive preheat fault condition during summer

The above figures demonstrate how excessive preheating only affects AHU heating and cooling demand. NN predicted loads appear to follow a similar transient profile as metered data but reduced by a constant value. This behavior is due to preheat coils within the AHU heating air well above supply temperature and then cooling coils needing to remove the thermal energy that was just added to the supply air. Excessive preheat only affecting AHU demand also means that occupants would not be uncomfortable and would not file maintenance requests as they might with other faults.

8.2.4 Old CE Insufficient Outdoor Air

Insufficient outdoor air presented a challenge for physics-based fault detection in section 5.3.4. Old CE Insufficient Outdoor Air during summer loading with no conclusive results being identified while high-efficiency heat recovery was occurring. Similar results were displayed in Figure 225 and Figure 226 by the time series neural network even though heat recover efficiency was reduced. There is a slight underprediction for cooling load, but no confidence of a fault can exist when 92% of data points fall within uncertainty bands. While time series neural networks may be unable to statistically determine when some faults are occurring, decision trees have been shown to be suitable for fault identification and are explored in section 8.3 Deep learning data classification.

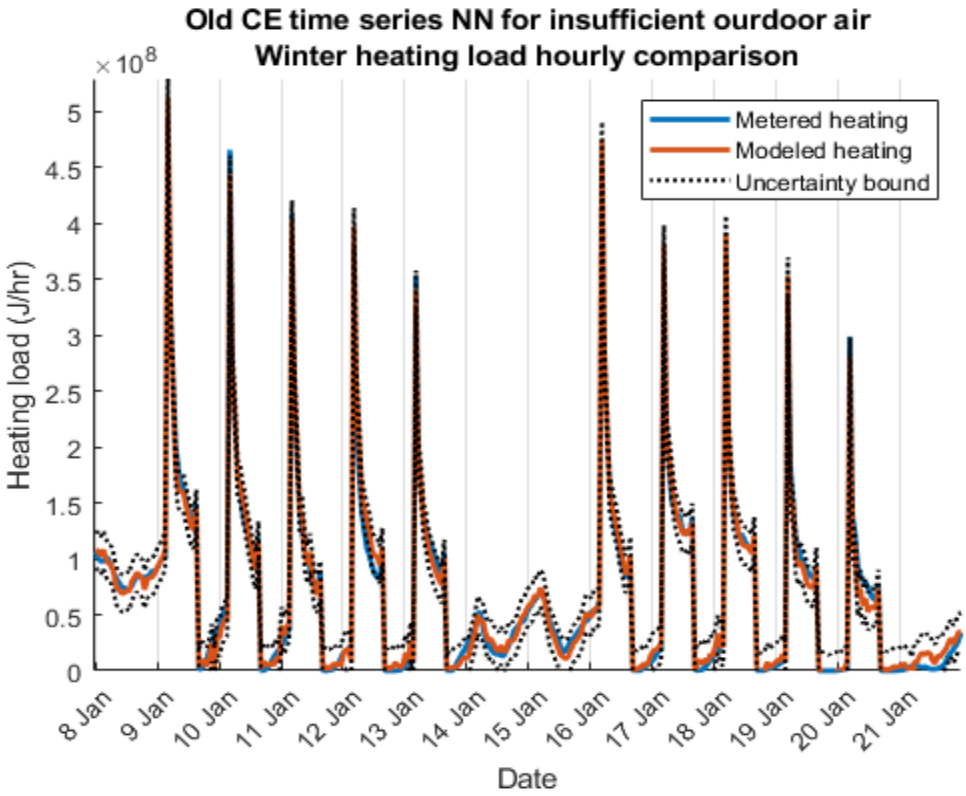

Figure 225A: Predicted heating load for Old CE while experiencing insufficient outdoor air fault condition during winter

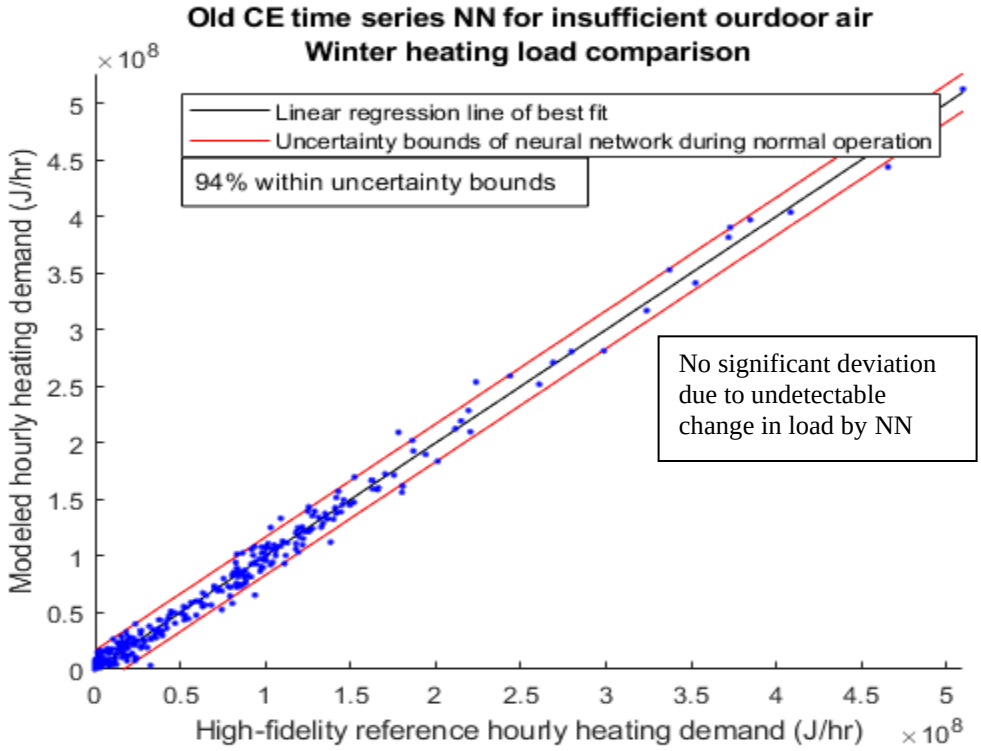

Figure 225B: Alignment factor of predicted heating load for Old CE while experiencing insufficient outdoor air fault condition during winter

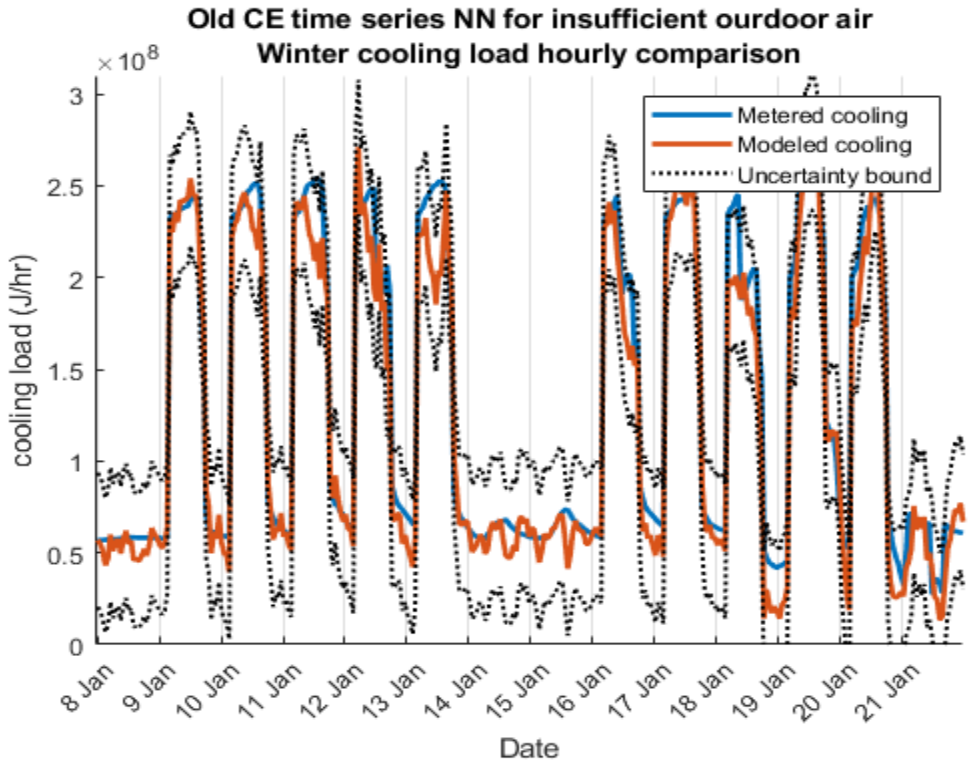

Figure 225C: Predicted cooling load for Old CE while experiencing insufficient outdoor air fault condition during winter

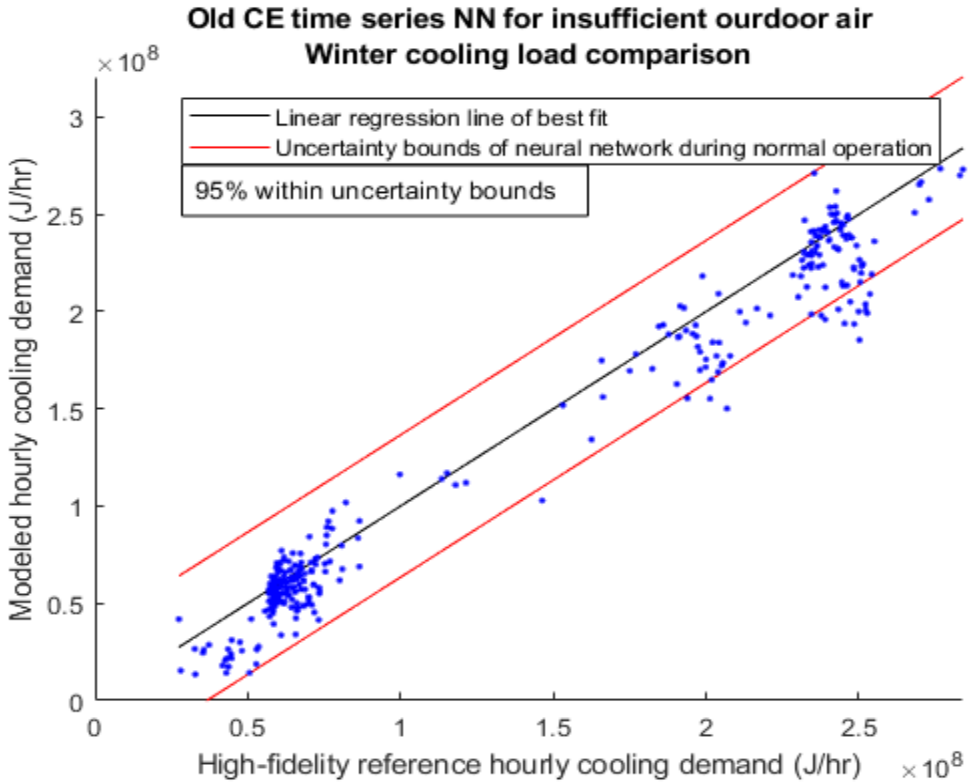

Figure 225D: Alignment factor of predicted cooling load for Old CE while experiencing insufficient outdoor air fault condition during winter

As stated above, there is almost no change in metered or predicted loads when there is insufficient outdoor air simply due to the high efficiency of the heat recovery system that was utilized in the high-fidelity model.

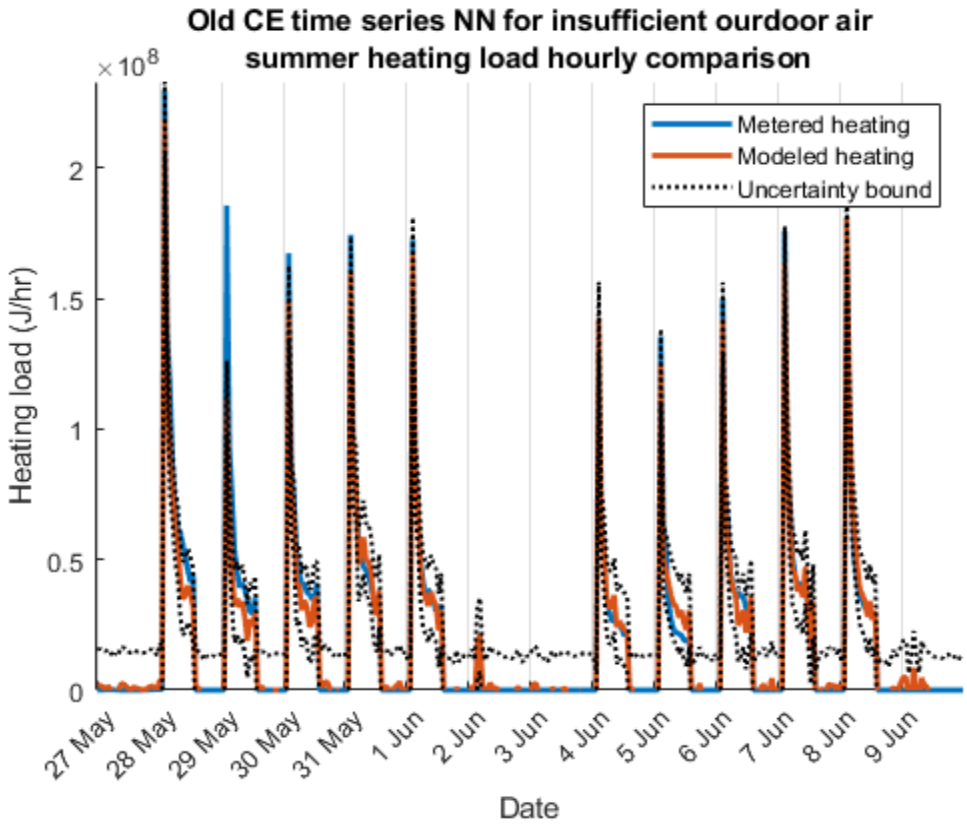

Figure 226A: Predicted heating load for Old CE while experiencing insufficient outdoor air fault condition during summer

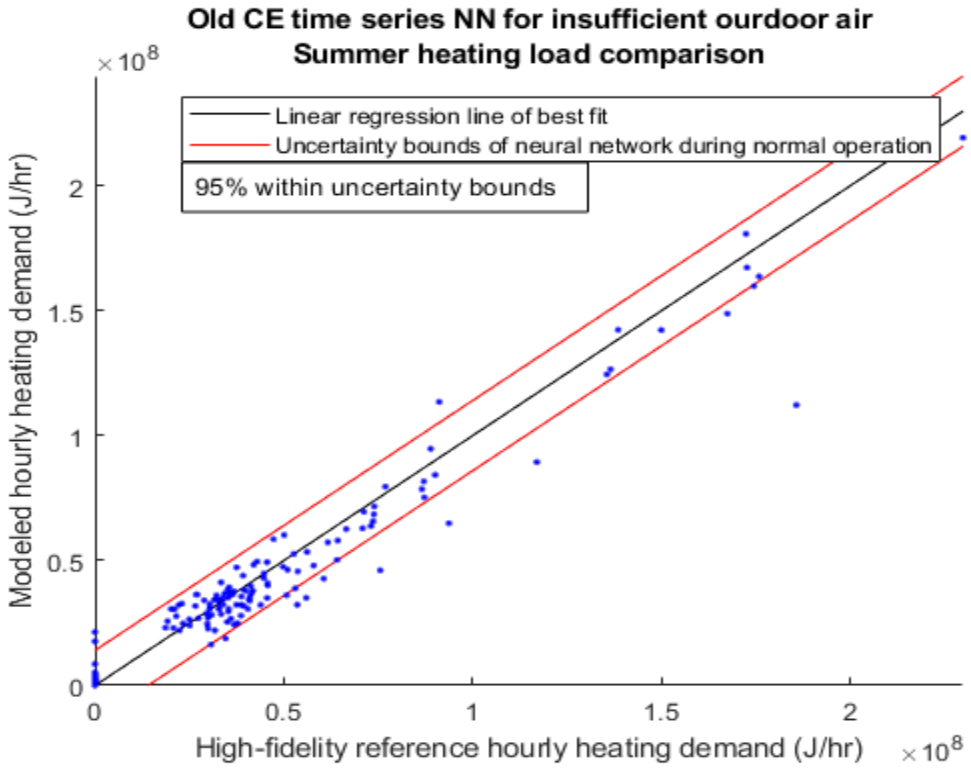

Figure 226B: Alignment factor of predicted heating load for Old CE while experiencing insufficient outdoor air fault condition during summer

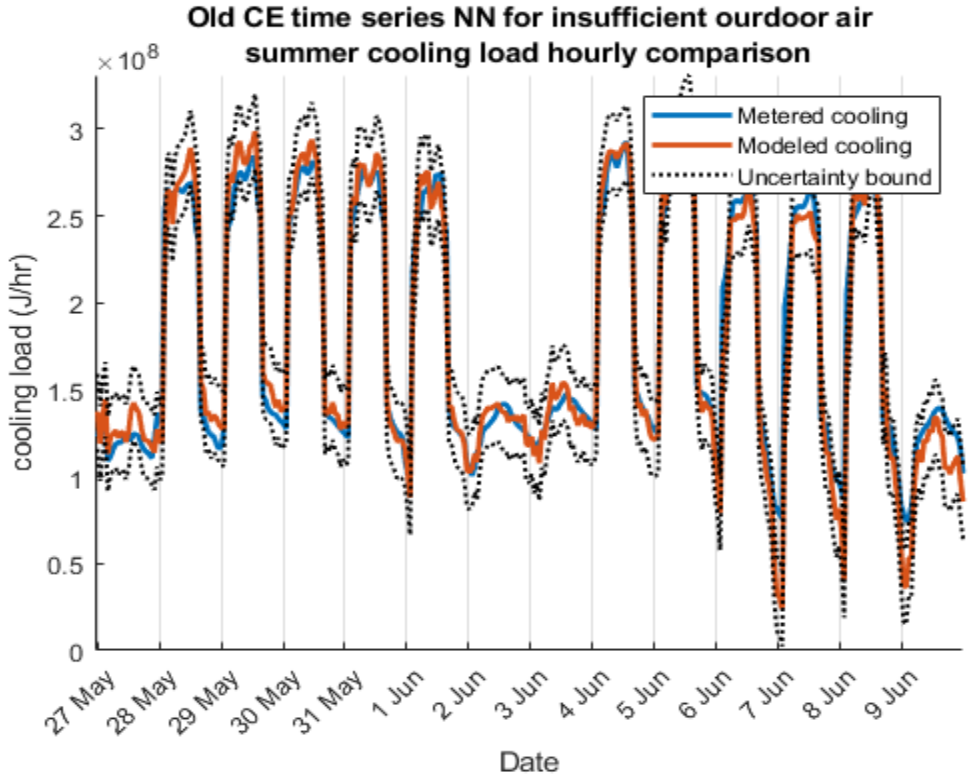

Figure 226C: Predicted cooling load for Old CE while experiencing insufficient outdoor air fault condition during summer

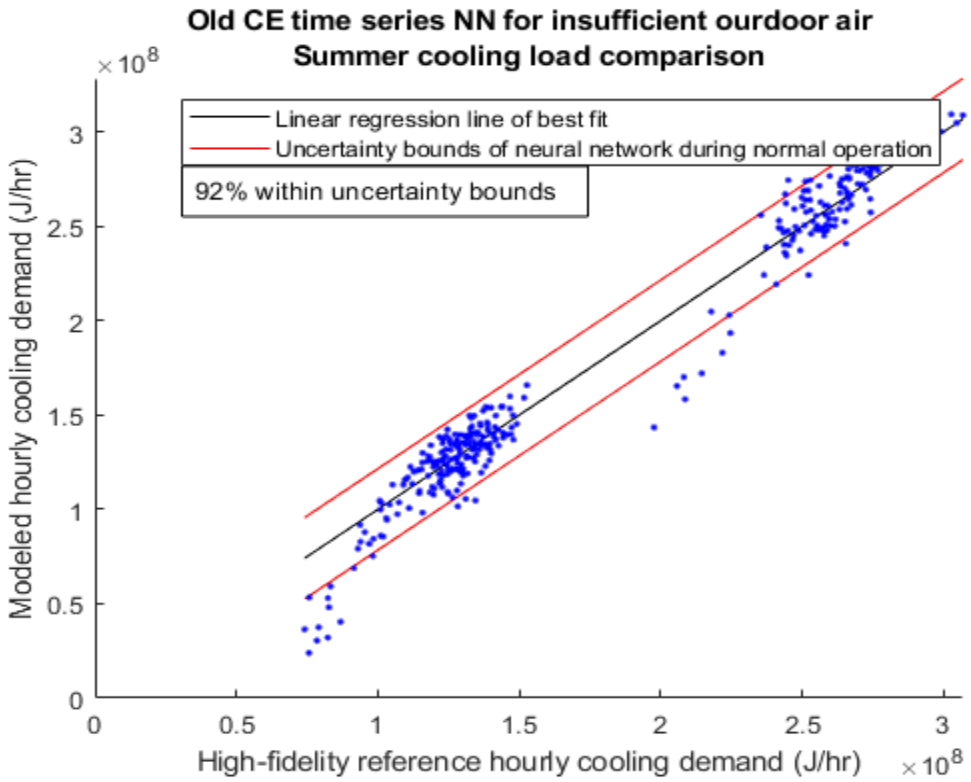

Figure 226D: Alignment factor of predicted cooling load for Old CE while experiencing insufficient outdoor air fault condition during summer

Old CE demonstrated how reliance on deviation from predicted energy demand may not always be successful. Additionally, if faulty data is not available in which to test a time series neural network, it may be difficult to know if and when a trained NN has been overfitted and not deviating when faults are occurring. Future research on time series neural networks for building fault detection could include analysis of parameter sensitivity manipulation to increase the possibility of divergence for specific faults.

8.2.5 Old CE Multiple Faults: Excessive Preheating and Failure to Enter Unoccupied Setback

Combining a failure to enter unoccupied setback with excessive preheat depicts the additive property of fault deviation. Continuously elevated loading stems from excessive preheat fault while significant changes in load come from the fault of failing to

enter unoccupied setback. Figure 223 and Figure 224 displays a near-uniform increase in heating demand over predicted load values, which is expected from an excessive preheat fault failure. Failure to enter evening setback produces significant deviation from metered values only during unoccupied periods, as demonstrated in Figure 221 and Figure 222. As expected, both excessive preheating while also not entering unoccupied setback produces results that encapsulates the near-constant deviation produced by excessive preheating while also demonstrating a more pronounced deviation during unoccupied hours, as seen in Figure 227 and Figure 228.

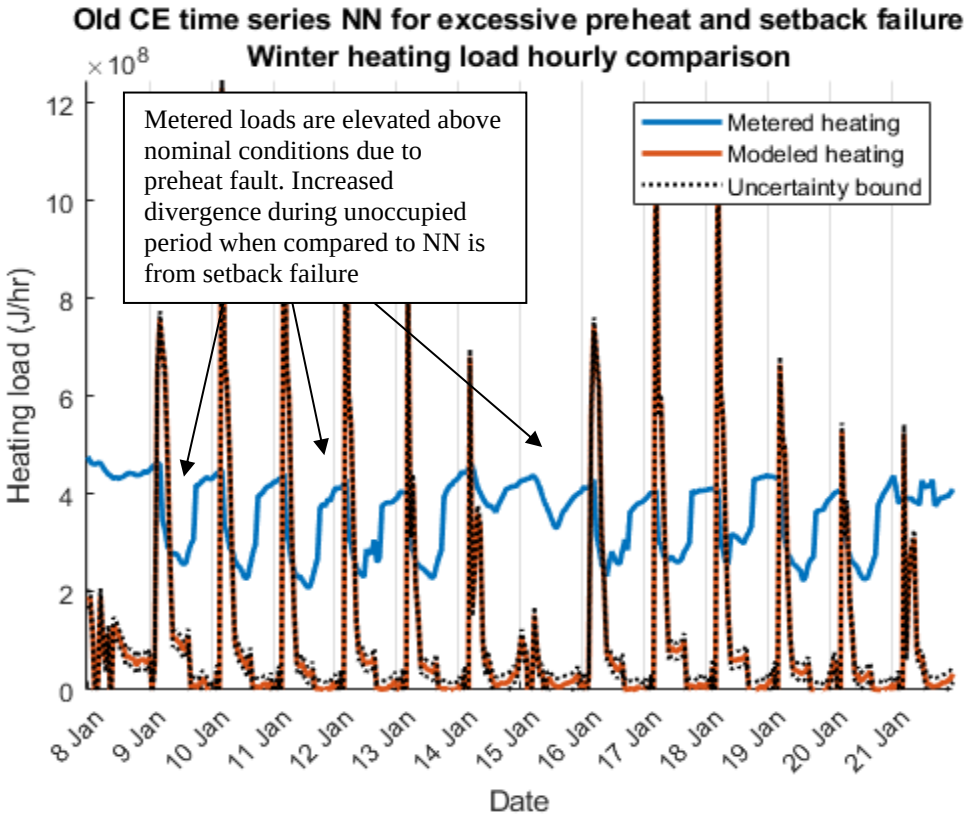

Figure 227A: Predicted heating load for Old CE while a failure to enter unoccupied setback in addition to excessive preheat faults are occurring during winter

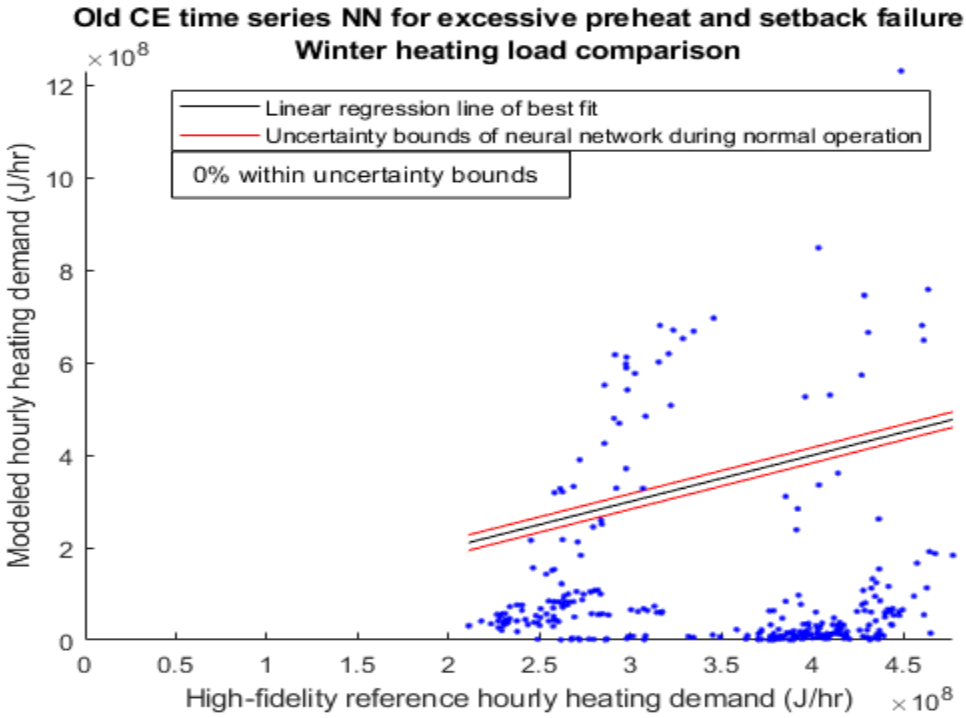

Figure 227B: Alignment factor of predicted heating load for Old CE while a failure to enter unoccupied setback in addition to excessive preheat faults are occurring during winter

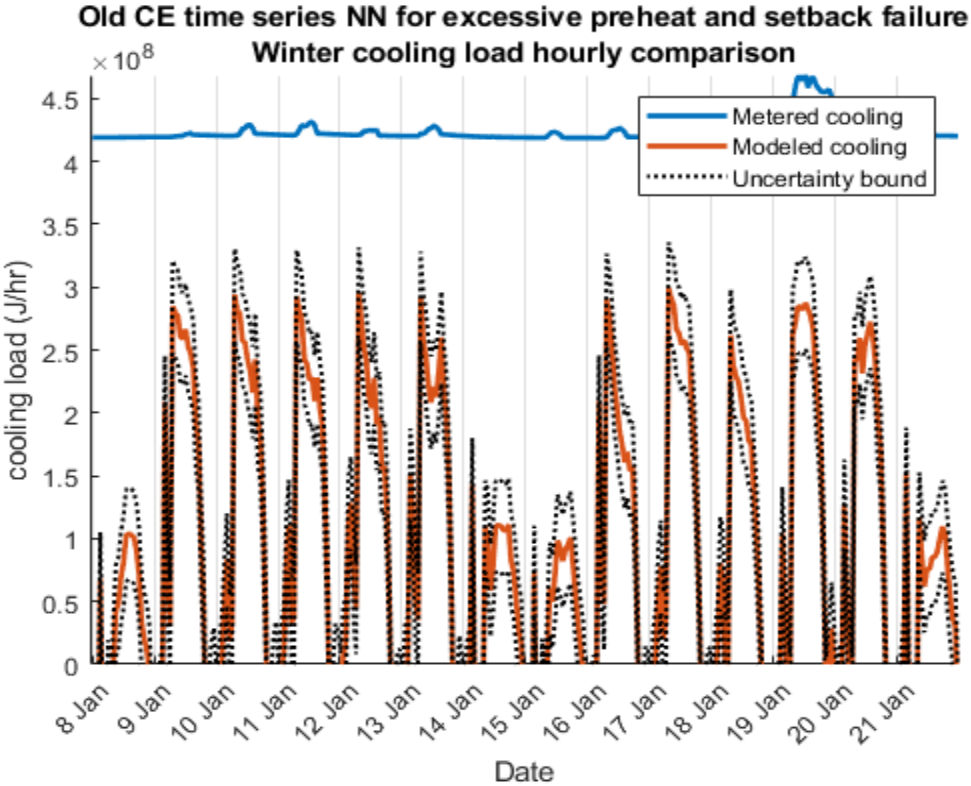

Figure 227C: Predicted cooling load for Old CE while a failure to enter unoccupied setback in addition to excessive preheat faults are occurring during winter

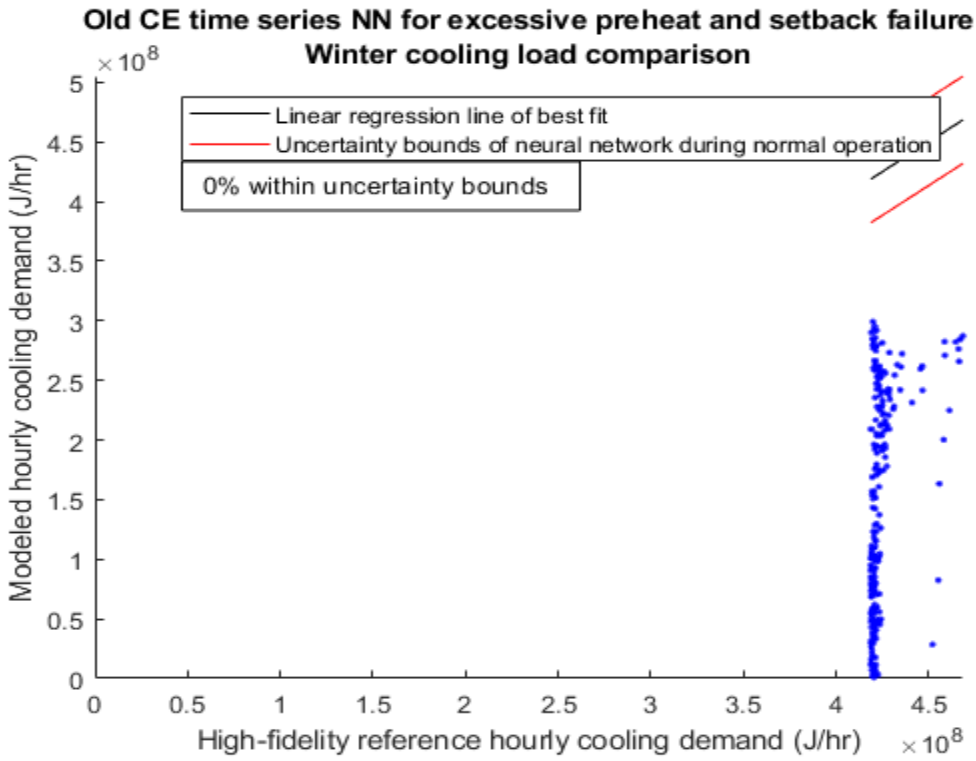

Figure 227D: Alignment factor of predicted cooling load for Old CE while a failure to enter unoccupied setback in addition to excessive preheat faults are occurring during winter

Similar to Whitehead time series NN multi-fault analysis, Old CE time series NNs behave in an additive manner when dealing with multiple faults. Meaning that deviation magnitude from each fault combine when multiple faults are present.

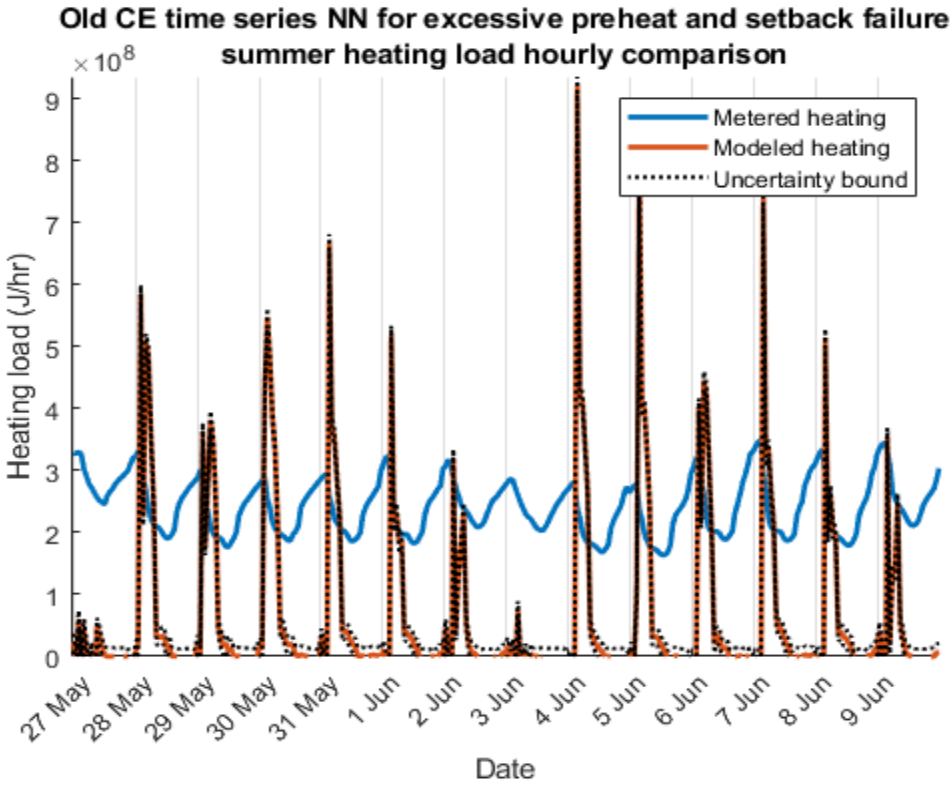

Figure 228A: Predicted heating load for Old CE while a failure to enter unoccupied setback in addition to excessive preheat faults are occurring during summer

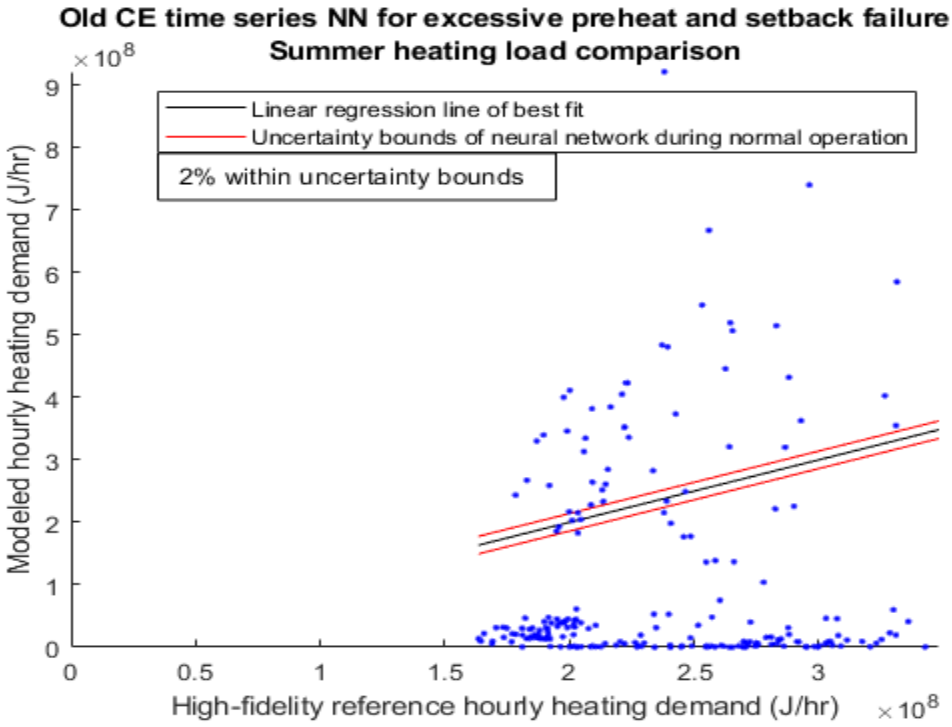

Figure 228B: Alignment factor of predicted heating load for Old CE while a failure to enter unoccupied setback in addition to excessive preheat faults are occurring during summer

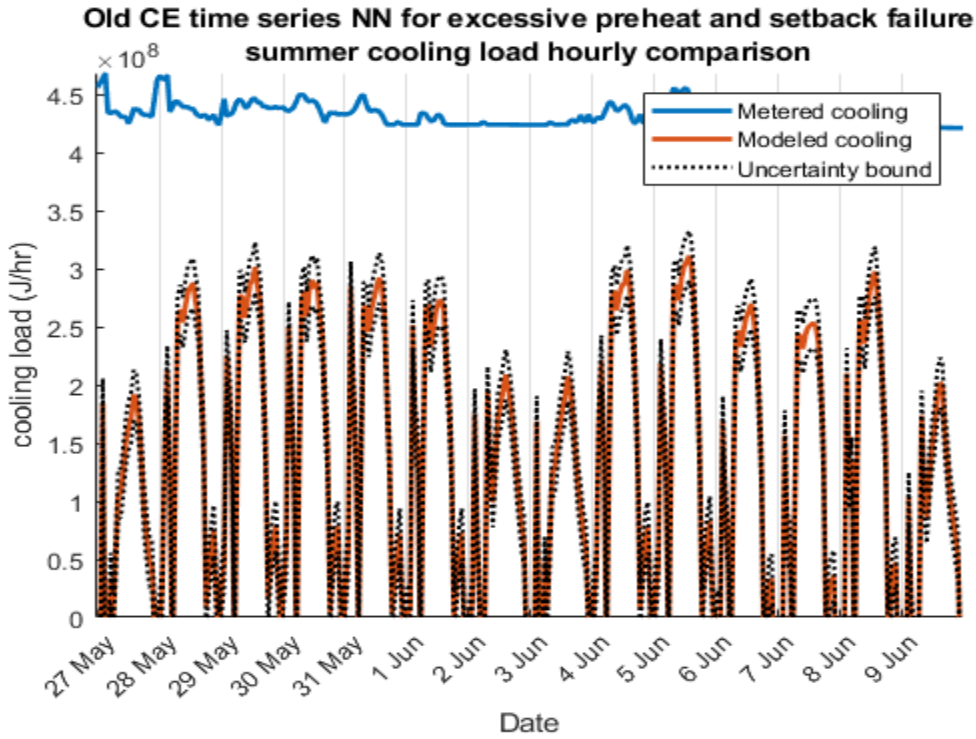

Figure 228C: Predicted cooling load for Old CE while a failure to enter unoccupied setback in addition to excessive preheat faults are occurring during summer

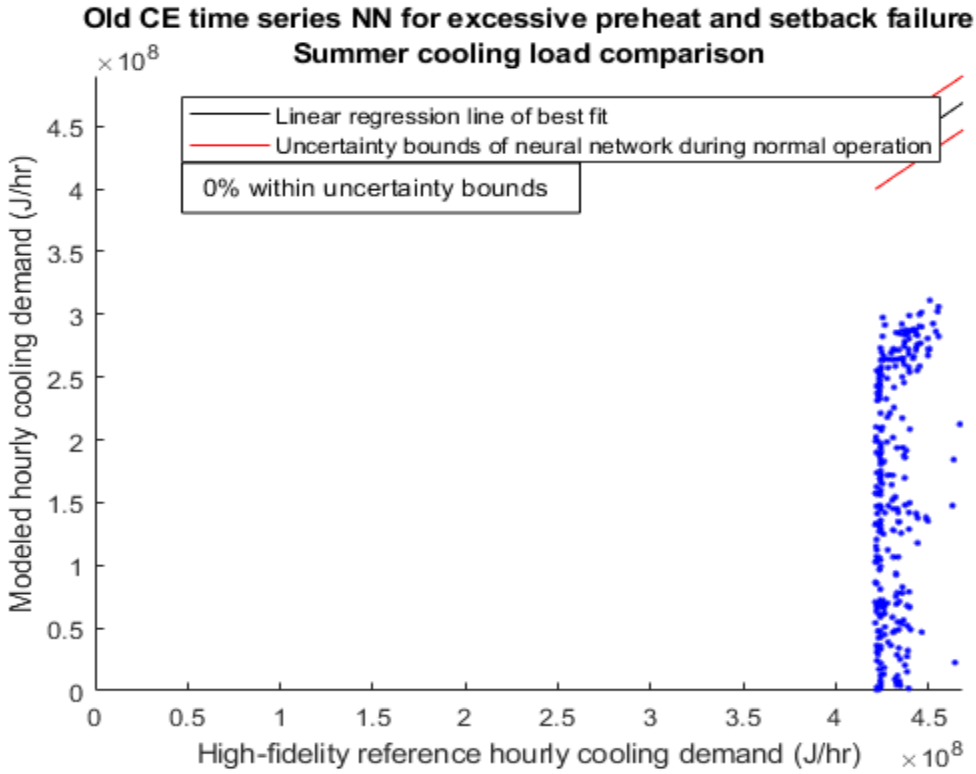

Figure 228D: Alignment factor of predicted cooling load for Old CE while a failure to enter unoccupied setback in addition to excessive preheat faults are occurring during summer

Combining two faults that each produce significant deviation of predicted demand from metered energy, unsurprisingly, resulted in significant portions of predicted demand to fall outside metered prediction windows. Therefore, it is evident that more significant changes in metered demand from no-fault training data causes the most severe deviation of NN predicted loads.

8.2.5 Old CE Multiple Faults: Insufficient Outdoor Air and Excessive Infiltration

Insufficient outdoor air and excessive infiltration both induced subtle alterations in differences between predicted and metered loads. Figure 229 displays a similar heating rate prediction deviation as Figure 219 displays for excessive infiltration. Likewise, winter cooling prediction deviation in Figure 229 matches that of insufficient outdoor air, as depicted in Figure 225.

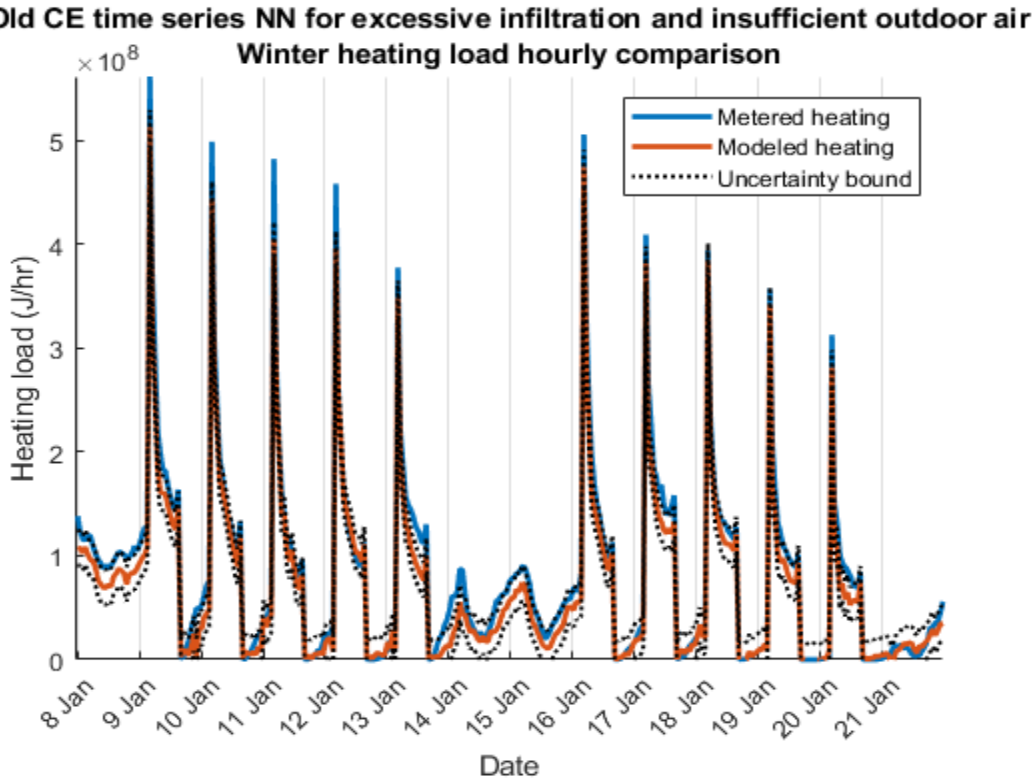

Figure 229A: Predicted heating load for Old CE while experiencing insufficient outdoor air in addition to excessive infiltration during winter

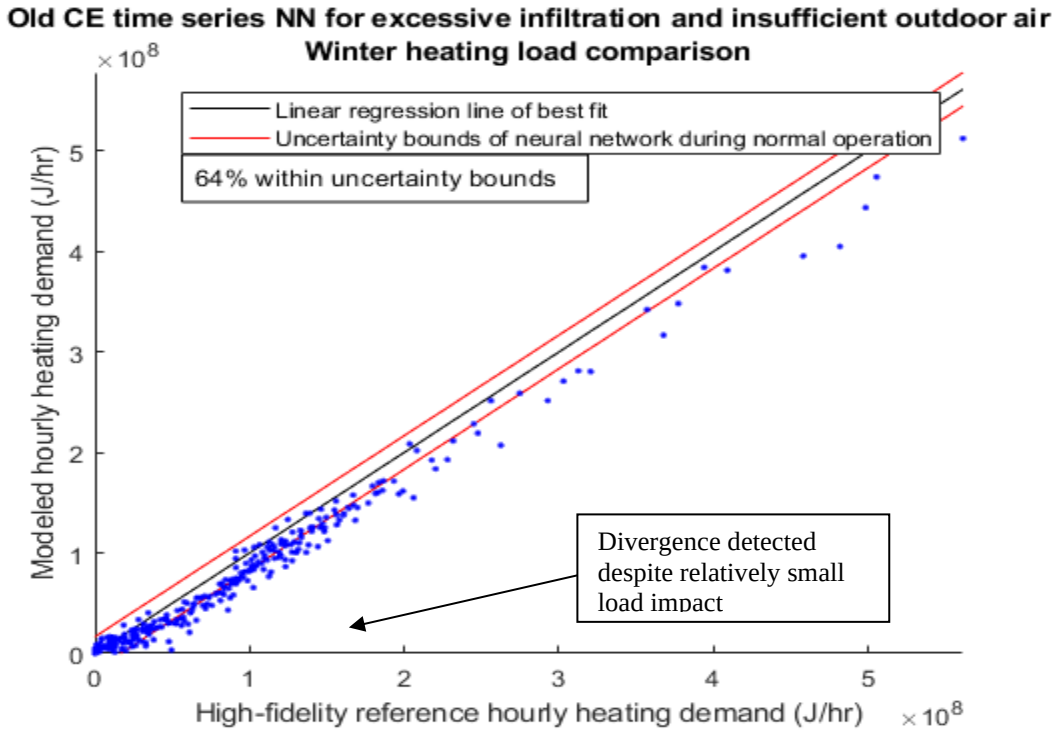

Figure 229B: Alignment factor of predicted heating load for Old CE while experiencing insufficient outdoor air in addition to excessive infiltration during winter

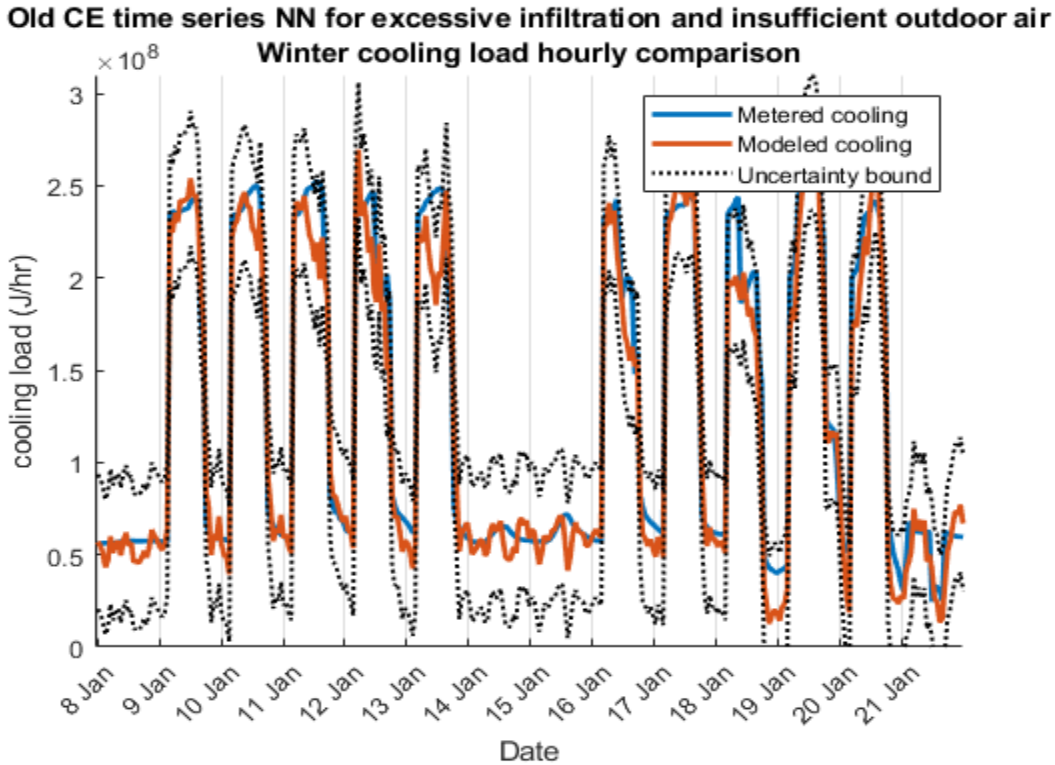

Figure 229C: Predicted cooling load for Old CE while experiencing insufficient outdoor air in addition to excessive infiltration during winter

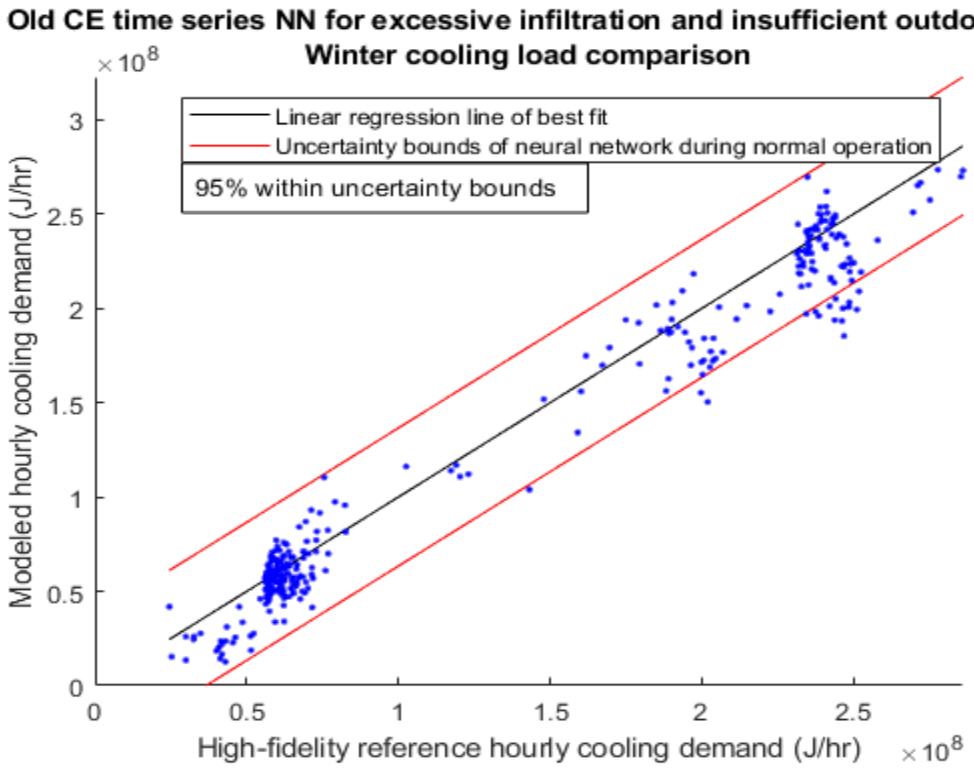

Figure 229D: Alignment factor of predicted cooling load for Old CE while experiencing insufficient outdoor air in addition to excessive infiltration during winter

Summer load prediction deviation in Figure 230 remains statistically insignificant despite two faults simultaneously occurring which suggests that load deviation from nominal performance needs to be of sufficient magnitude to be detected.

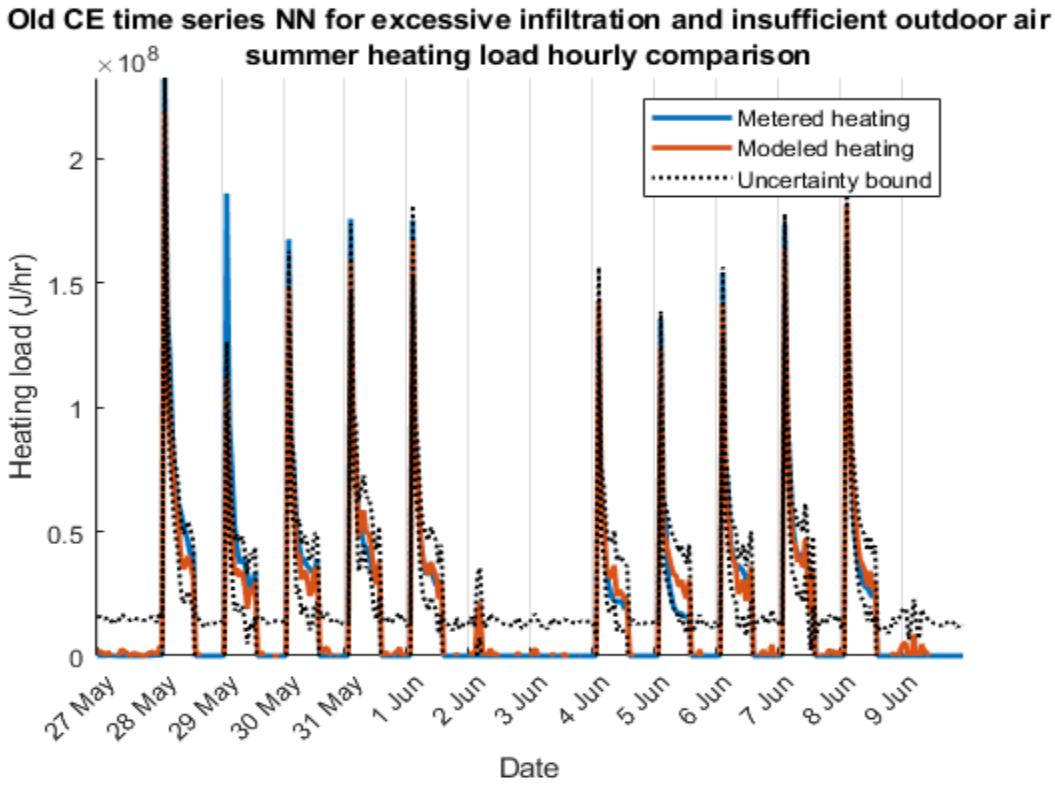

Figure 230A: Predicted heating load for Old CE while experiencing insufficient outdoor air in addition to excessive infiltration during summer

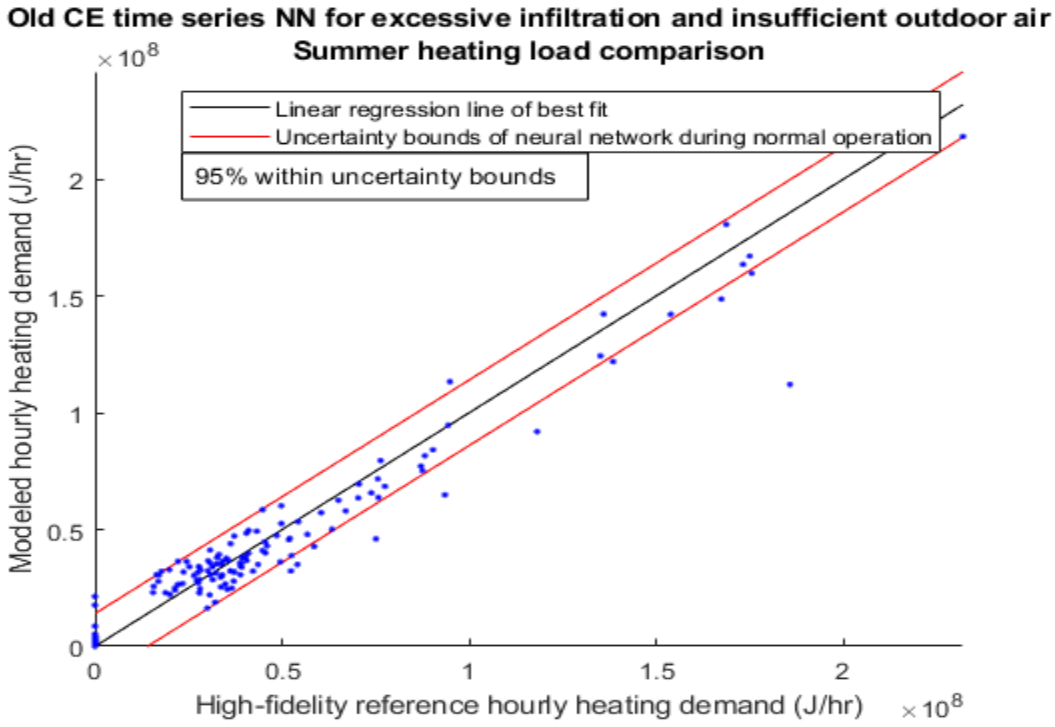

Figure 230B: Alignment factor of predicted heating load for Old CE while experiencing insufficient outdoor air in addition to excessive infiltration during summer

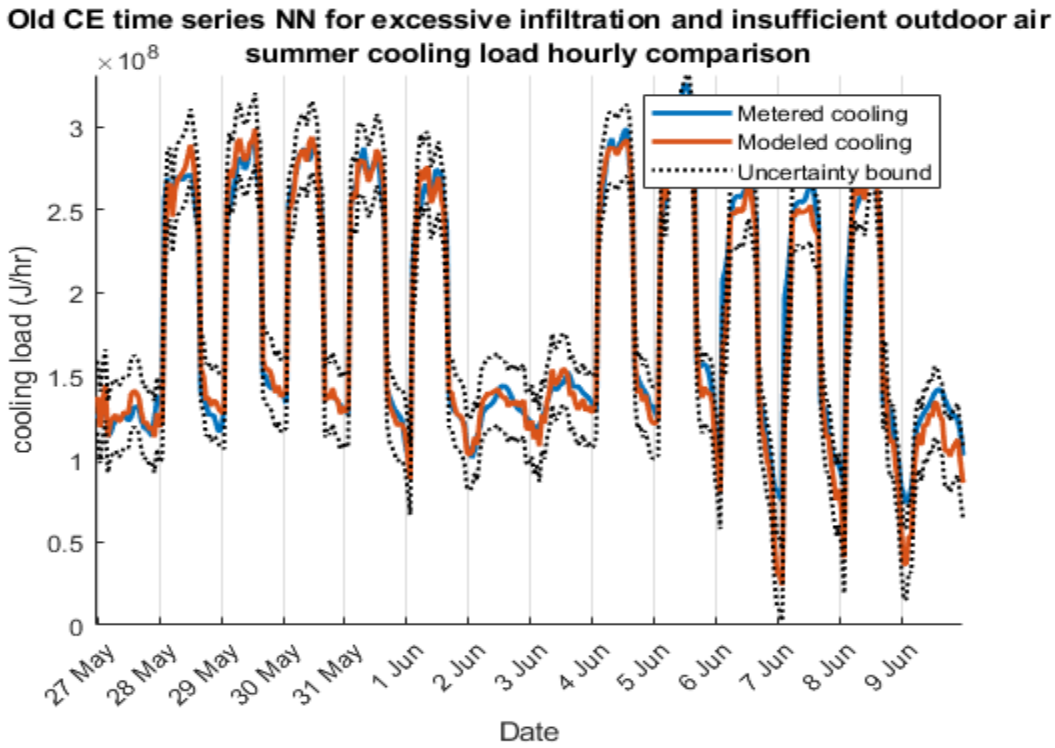

Figure 230C: Predicted cooling load for Old CE while experiencing insufficient outdoor air in addition to excessive infiltration during summer

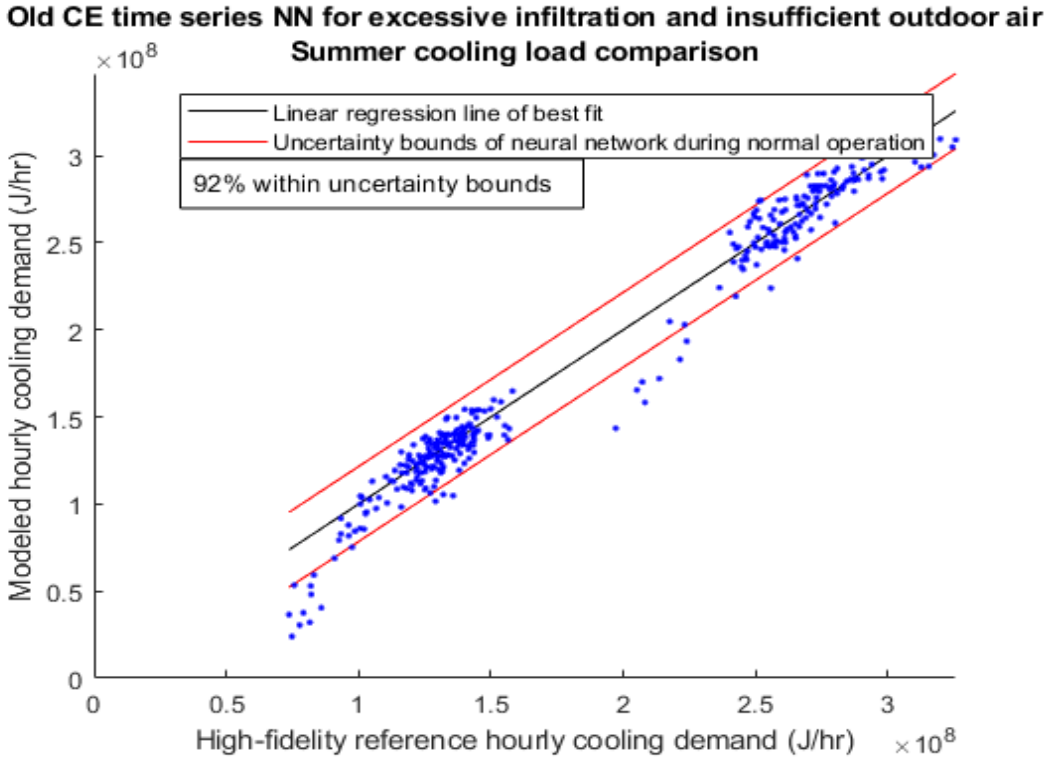

Figure 230D: Alignment factor of predicted cooling load for Old CE while experiencing insufficient outdoor air in addition to excessive infiltration during summer

Time series neural networks have demonstrated that they are capable of excellent energy use prediction, even during periods and conditions where the network was not trained. However, adaptability to suit different occasions is a detriment when fault detection is desired; because it is difficult to detect a fault given the limited amount of input/output data if modeled loading always closely matches metered results. However, time series are not the only use for neural networks; deep learning decision trees have been implemented for fault identification in some circumstances. Therefore, trees will be investigated to see if they offer an acceptable source of fault detection using neural networks.

8.3 Deep Learning Data Classification

While time series NIO neural networks thus far have been shown to be adept at energy use modeling, they have struggled with fault detection in some situations. However, deep learning decision trees have been shown to be a promising method of implementing fault identification through simplified modeling . While time series NNs can be used to compare metered and predicted loading to detect faults, decision trees sort data to identify faults. The objective of this section is to explore how well decision trees worked in comparison to time series neural networks and to SPBM fault identification and classification.

As stated in the literature review, decision trees can be used to discover patterns in data as well as data classification. Time series neural networks and deep learning decision trees were trained on a year of data that omitted two weeks from winter and summer that are used for testing. Omitting testing periods from training data was done to not give an advantage to decision trees by testing faults with the same data that the tree

was trained with and was the same time period used for fault detection and identification by the SPBM. However, the decision trees were trained with all four potential faults in addition to data gathered while no faults were occurring.

To understand the process of decision trees, first they are trained on data for all operating modes (all four faults as well as non-faulty operation). After training, the NNs are fed data for two weeks in winter and two weeks in summer where either one of four faults is occurring, or the building is operating as intended. The NN then sorts each hour of data into the five potential outcomes and the result with the highest number is considered to be the state in which the building is operating. Because two weeks of hourly data is being used, a perfect score is 337 (where all 337 discrete hours of operation land in the same sorted bin).

Whitehead performed rather well in decision tree fault classification test. Winter months displayed slightly more convergence towards being identified as the state of the building being tested. When comparing the results of summer testing from Table 8 to winter testing in Table 7, it is apparent that decision tree fault identification is well suited to this level of building complexity. Unfortunately, results from classifying faults from Old CE were not as definitive. As a note, it is often desirable to compare results of this nature with a confusion matrix which displays classification tests as columns and test results in rows; meaning correct classifications fall along the main diagonal of the matrix while incorrect classifications fall outside the main diagonal.

Table 7: Whitehead winter test fault identification neural network decision tree confusion matrix classification. Columns represent different fault identification tests while rows show results from tests. The main diagonal of the matrix is where the tested fault and predicted fault match (correct data sort)

	Test: no fault	Test: excessive infiltration	Test: failure to enter unoccupied setback	Test: excessive preheat	Test: insufficient outdoor air
Prediction: no fault	263	33	10	0	31
Prediction: excessive infiltration	21	275	7	0	6
Prediction: failure to enter setback	20	13	310	0	3
Prediction: excessive preheat	0	0	0	337	0
Prediction: insufficient outdoor air	33	16	10	0	297

Table 8: Whitehead summer test fault identification neural network decision tree confusion matrix classification

	Test: no fault	Test: excessive infiltration	Test: failure to enter unoccupied setback	Test: excessive preheat	Test: insufficient outdoor air
Prediction: no fault	188	88	10	0	29
Prediction: excessive infiltration	89	201	3	0	9
Prediction: failure to enter setback	25	17	310	0	12
Prediction: excessive preheat	0	0	0	337	0
Prediction: insufficient outdoor air	35	31	14	0	287

Multiple simultaneous faults were also analyzed to see how a fault classification neural network would handle data outside of its training set. While the fault classification tree was trained with all faults individually occurring, multiple simultaneous faults were

not part of training. Ideally, either both faults or the most energy-intensive fault would be selected. Winter testing resulted in one successful identification when excessive infiltration and a failure to enter unoccupied setback occurred, as recorded in Table 9. Summer testing in Table 10 was partially successful with at least one of the occurring faults being identified for all tests. Additionally, multi-fault testing results suggests that whatever fault produces a more significant deviation from nominal load will be given classification priority.

Table 9: Whitehead winter test fault identification neural network decision tree confusion matrix classification for multiple simultaneous faults

	Test: Excessive preheat and not entering setback	Test: Excessive preheat and infiltration	Test: Excessive infiltration and failure to enter setback
Prediction: no fault	0	40	23
Prediction: excessive infiltration	0	9	124
Prediction: failure to enter setback	6	3	179
Prediction: excessive preheat	95	92	0
Prediction: insufficient outdoor air	236	194	11

Table 10: Whitehead winter test fault identification neural network decision tree confusion matrix classification for multiple simultaneous faults

	Test: Excessive preheat and not entering setback	Test: Excessive preheat and infiltration	Test: Excessive infiltration and failure to enter setback
Prediction: no fault	0	0	17
Prediction: excessive infiltration	0	0	6
Prediction: failure to enter setback	0	0	290
Prediction: excessive preheat	337	337	0
Prediction: insufficient outdoor air	0	0	24

While Whitehead was able to identify individual faults and some simultaneous faults with high accuracy, classification of faults for Old CE resulted in misclassifications to exceed correct identifications. Multiple techniques were used to attempt to find an optimal solution including principal command analysis, using different data inputs, multiple optimization criteria, various misclassification indices, and optimizing past 1000 iterations. As with SPBM and time series testing, winter data did produce four out of five correct results while summer correctly classified three out of five faults: shown in Table 11 and Table 12 respectively.

Table 11: Old CE winter test fault identification neural network decision tree confusion matrix classification

	Test: no fault	Test: excessive infiltration	Test: failure to enter unoccupied setback	Test: excessive preheat	Test: insufficient outdoor air
Prediction: no fault	248	175	25	0	100
Prediction: excessive infiltration	55	136	1	0	19
Prediction: failure to enter setback	9	0	310	0	4
Prediction: excessive preheat	0	0	0	337	0
Prediction: insufficient outdoor air	25	26	1	0	214

Table 12: Old CE winter test fault identification neural network decision tree confusion matrix classification

	Test: no fault	Test: excessive infiltration	Test: failure to enter unoccupied setback	Test: excessive preheat	Test: insufficient outdoor air
Prediction: no fault	296	284	1	0	273
Prediction: excessive infiltration	9	42	0	0	1
Prediction: failure to enter setback	0	1	336	0	1
Prediction: excessive preheat	0	0	0	337	0
Prediction: insufficient outdoor air	32	10	0	0	62

Less efficient heat recovery was tested to see if results were improved similar to SPBM fault identification. Overall, results were improved, especially for summer

conditions. Table 13 does display a slight decrease in accuracy when no fault is occurring, which is accompanied by an increase in false classifications as an excessive infiltration fault. However, correct classification when excessive infiltration is occurring went up considerably. Table 14 shows 173 of 337 (51%) correct classifications for excessive infiltration during summer conditions, a substantial increase of 12% correct classifications in Table 12 before heat recovery was adjusted. Similar to the increase in accuracy from excessive infiltration, insufficient outdoor air was correctly classified at an almost perfect rate of 94%. Both insufficient outdoor air and excessive infiltration are primarily low-impact faults that are seen through subtle changes in AHU heating and cooling loads.

Infiltration is a subtle fault to detect as changes to zone demand and return air conditions noticeably occur when exterior air conditions are substantially different from indoor air conditions and can often be misidentified as an increase in building usage. During high-fidelity model calibration, it was identified that Old CE has a relatively low level of infiltration; combine an efficient AHU system and detecting a subtle fault becomes even more difficult. Although parameter-specific adjustments are not possible with a neural network, this demonstrates that a decision tree is capable of being correct in a majority of situations when enough training data is available.

Insufficient outdoor air is an energy load that exclusively affects AHU energy demand and has no impact on zone loads for the AHU systems being explored in this paper. Whitehead and Old CE do not have CO2 demand control ventilation or dedicated outdoor air units; so, the only influence outdoor air flow rate has on energy consumption is by altering the mixed air temperature and humidity. Obviously, incoming outdoor air

enthalpy approaches that of return air as energy recovery system approaches perfect efficiency. At 95% efficiency, there is almost no difference between air leaving energy recovery and return air. SPBM fault identification faced similar difficulty during summer insufficient outdoor air conditions. Regardless, decision tree neural network was able to correctly identify low outdoor air for both winter and summer loading when heat recovery was lowered to a more realistic 70%.

Table 13: Old CE with less efficient heat recovery winter test fault identification neural network decision tree confusion matrix classification

	Test: no fault	Test: excessive infiltration	Test: failure to enter unoccupied setback	Test: excessive preheat	Test: insufficient outdoor air
Prediction: no fault	190	104	3	0	11
Prediction: excessive infiltration	129	221	8	0	9
Prediction: failure to enter setback	7	0	324	0	0
Prediction: excessive preheat	0	0	0	337	0
Prediction: insufficient outdoor air	11	12	2	0	317

Table 14: Old CE with less efficient heat recovery summer test fault identification neural network decision tree confusion matrix classification

	Test: no fault	Test: excessive infiltration	Test: failure to enter unoccupied setback	Test: excessive preheat	Test: insufficient outdoor air
Prediction: no fault	123	60	1	0	12
Prediction: excessive infiltration	85	173	0	0	7
Prediction: failure to enter setback	4	2	336	0	4
Prediction: excessive preheat	0	0	0	337	0
Prediction: insufficient outdoor air	125	102	0	0	314

Multiple simultaneous faults for Old CE resulted in classification of whichever fault has a higher energy impact. Winter tests resulted in a minimum correct classification

percentage of 98.5% while summer was correct at least 87%. When comparing results from Table 15 and Table 16 to those of single-fault classifications, it appears that the neural network struggles with identifying excessive infiltration but excels at the other three faults and will default to whichever of those three faults have the greatest change from normal operation.

Table 15: Old CE with less efficient heat recovery with multiple simultaneous fault winter identification neural network decision tree confusion matrix classification

	Excessive infiltration and insufficient outdoor air	Test: Excessive preheat and failure to enter unoccupied setback
Prediction: no fault	5	0
Prediction: excessive infiltration	21	0
Prediction: failure to enter setback	0	0
Prediction: excessive preheat	0	337
Prediction: insufficient outdoor air	311	0

Table 16: Old CE with less efficient heat recovery with multiple simultaneous fault summer identification neural network decision tree confusion matrix classification

	Excessive infiltration and insufficient outdoor air	Test: Excessive preheat and failure to enter unoccupied setback
Prediction: no fault	42	0
Prediction: excessive infiltration	39	0
Prediction: failure to enter setback	3	0
Prediction: excessive preheat	0	337
Prediction: insufficient outdoor air	253	0

To conclude the classification tree section, neural network-based fault classification is an effective and efficient method of classifying faults for buildings that are able to record data under faulty operation. As mentioned before, neural networks are poor at extrapolation and because decision trees classify data into bins, classification trees require training data for faults that wish to be identified. However, if reliable data for faulty operations are available, then decision tree neural networks are a reasonably accurate method of fault classification.

8.4 Conclusion

Analysis conducted in this chapter covered how two different time series neural networks and a decision tree can be used for automatic fault detection and identification. NARX time series demonstrated excellent load prediction but was unable to detect most tested faults. NIO time series had similar fault detection results to the SPBM but lacked an ability to classify data. Conversely, decision trees are capable of classifying data by faults in some situations but require data from faulty building operation in order to be properly trained. Therefore, it is recommended that future research investigate combining NIO, decision trees, and the SPBM for a potentially all-encompassing fault detection and identification package.

CHAPTER 9. NOISE AND IMPERFECT REFERENCE DATA IN FAULT DETECTION

Given the exact nature of high-fidelity models, a concern that would arise is how natural variation from using real-world meters would change comparisons between SPBM and reference data. To test variation in metered data, a random ±5% change was applied to each point of hourly heating and cooling reference data. Excessive infiltration fault identification was chosen for this test as it was the fault with the least amount of energy use deviation from normal operation, and therefore, the most difficult fault to identify. Figure 231 and Figure 232 reveals no change in parameter identification results. While error increased for all test values (which is to be expected), the overall heating and cooling reference data still followed an overall pattern of increased load associated with increased infiltration. While there may be a point in which sensor or meter miscalibration or noise may result in reference data that is no longer useful in fault identification, this test demonstrates that the SPBM does not require “prefect” reference data to correctly identify a building fault.

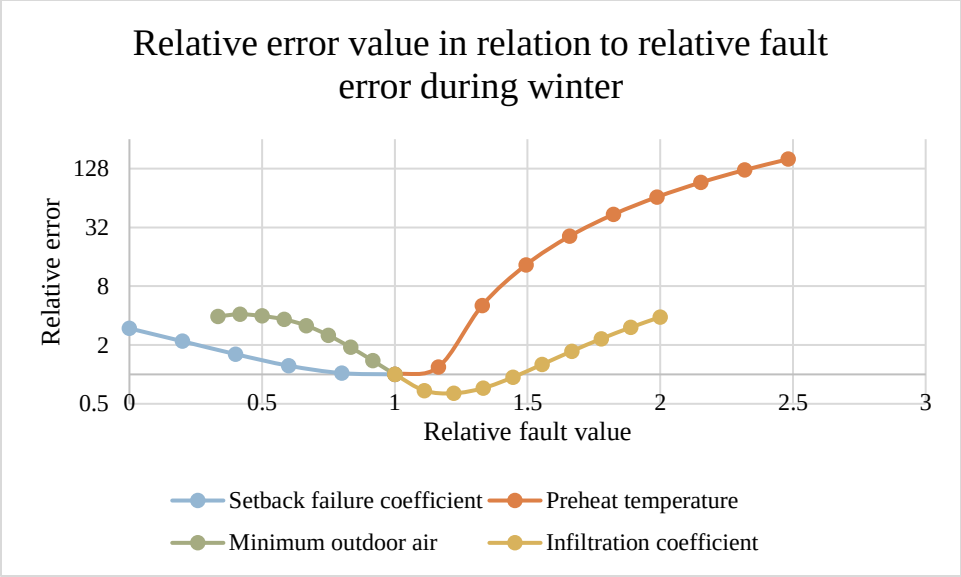

Figure 231: Visual representation of how magnitude of error changes across different magnitudes of the four possible faults when reference data is noisy. Excessive infiltration fault is being tested for automatic detection for Whitehead building during winter.

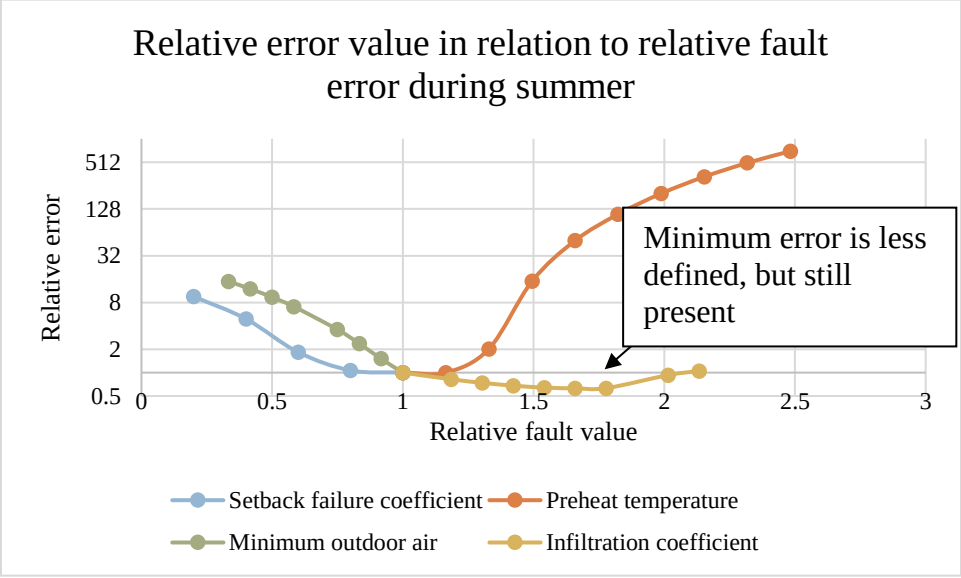

Figure 232: Visual representation of how magnitude of error changes across different magnitudes of the four possible faults when reference data is noisy. Excessive infiltration fault is being tested for automatic detection for Whitehead building during winter

Analysis of noisy infiltration data on time series neural network fault detection revealed that the primary demand load (heating during winter, cooling during summer)

experienced noticeable deviation away from 2σ bounds established for training data. Even so, summer deviation was minimal with more than 90% of data falling within uncertainty limits, as shown in Figure 233 to Figure 236. Winter deviation of heating load demand prediction was more conclusive with nearly 24% of data outside 2σ bands.

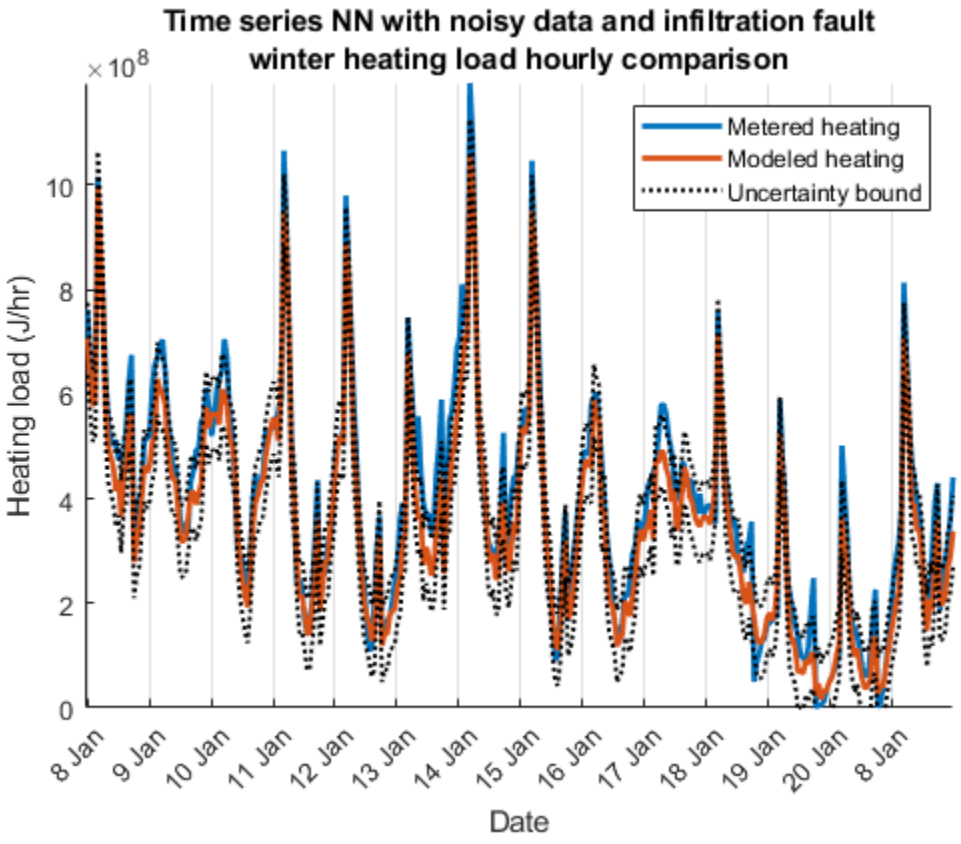

Figure 233: Hourly time series neural network predicted heating load and modeled heating load for winter while experiencing high infiltration fault and noisy data

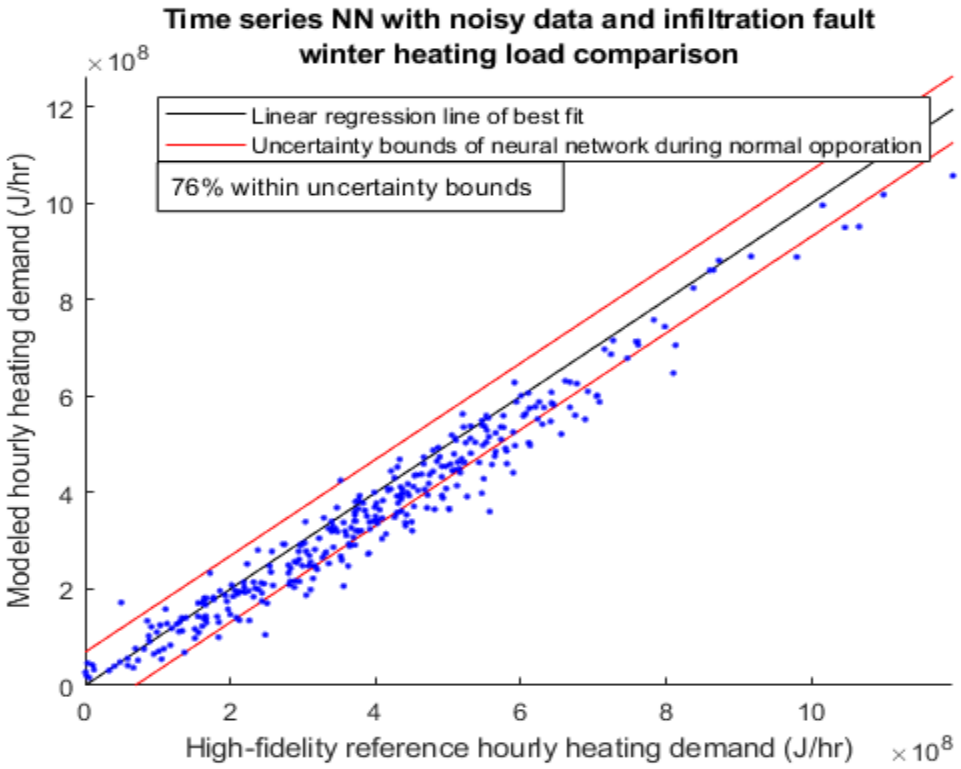

Figure 234: Scatter plot of time series neural network predicted heating demand compared against noisy metered infiltration fault data for winter

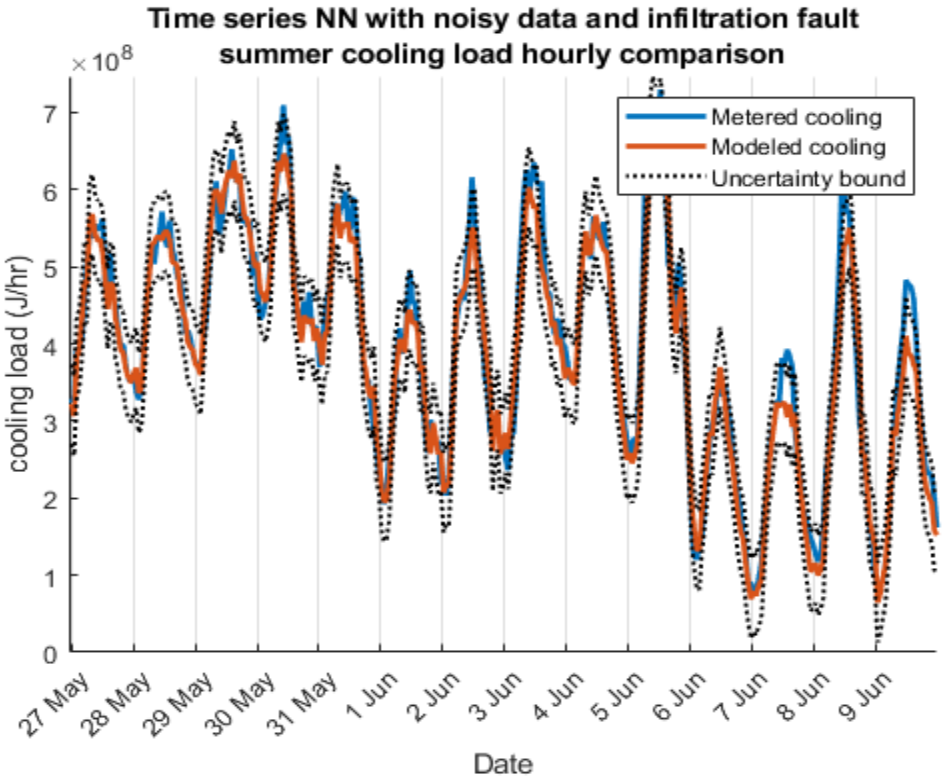

Figure 235: Hourly time series neural network predicted heating load and modeled cooling load for summer while experiencing high infiltration fault and noisy data

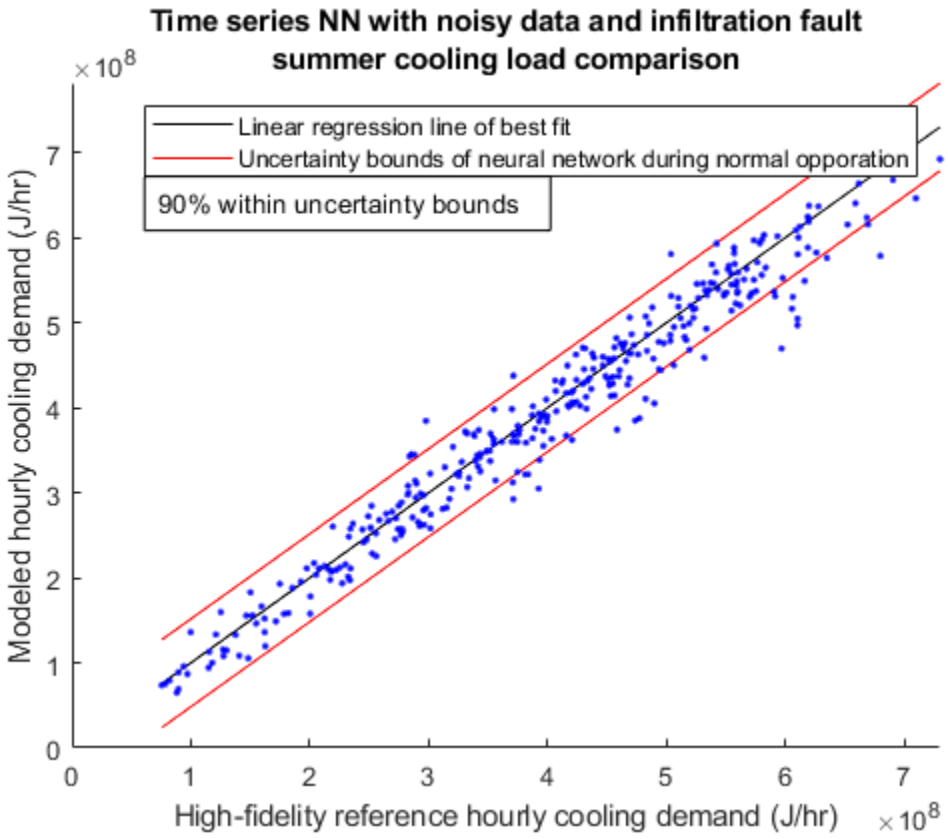

Figure 236: Scatter plot of time series neural network predicted cooling demand compared against noisy metered infiltration fault data for summer

Fault classification using a neural network with noisy data had significantly reduced accuracy when compared to non-noisy training. Winter fault identification failed to correctly distinguish between no fault and excessive infiltration fault even 50% of the time, results listed below in Table 17. Summer testing resulted in 53% correct prediction when infiltration was occurring, but 42% accuracy was achieved under no-fault conductions. By evaluating the SPBM fault identification results from Figure 232, neural network time series scatter plot from Figure 236, and neural network classification tree results in Table 18, it appears that random noise made the decision tree less sensitive to a specific infiltration parameter value. As such, a wider range of data can “fall in” to infiltration classification.

Table 17: Fault classification of noisy no-fault and excessive infiltration fault data for wintertime period

	Test: no fault	Test: excessive infiltration
Prediction: no fault	162	140
Prediction: excessive infiltration	86	135
Prediction: failure to enter setback	45	33
Prediction: excessive preheat	0	0
Prediction: insufficient outdoor air	44	29

Table 18: Fault classification of noisy no-fault and excessive infiltration fault data for wintertime period

	Test: no fault	Test: excessive infiltration
Prediction: no fault	140	96
Prediction: excessive infiltration	117	179
Prediction: failure to enter setback	22	14
Prediction: excessive preheat	0	0
Prediction: insufficient outdoor air	58	48

All the methods explored were able to either detect or classify a subtle fault using building energy data comparison and training. Sensors required to calculate liquid thermal energy transfer are easily available with less than 1% variance while air flow meters can have an accuracy variance of 3%. Given the above results for the most sensitive fault to detect and how fault classification and detection was possible, these tests provide reasonable confidence that all tested fault detection and identification methods in this paper will be sufficiently able to handle noise with more energy intensive faults.

CHAPTER 10. CONCLUSION AND FUTURE PLANS

This paper, as proposed, has set out to demonstrate the capabilities of a simplified physics-based building energy model in terms of its ability to accurately replicate heating and cooling load demand of more sophisticated high-fidelity models. As a similar all-encompassing simplified physics-based model developed for fault detection does not exist for comparison, it was also compared against neural networks, a popular tool for minimal parameter building energy prediction and fault detection. By comparing results from a high-fidelity model, neural networks, and the SPBM, it was possible to evaluate the strengths and weaknesses of the different modeling techniques.

This thesis set out to answer a number of questions:

1) Can a SPBM be calibrated to match building performance?

To briefly summarize, this paper demonstrated that the SPBM is capable of accurate building energy load modeling and can obtain similar performance to a high-fidelity model once fitted.

2) Can a neural network also be tuned to match building performance?

Neural networks are also capable of being trained such that predicted energy demand is similar to metered data.

3) Can either a SPBM or neural network identify building and system faults?

Fault detection and fault identification of one fault can be achieved by the SPBM and NNs as long as there is a sufficient change in metered data.

4) Can multiple faults be identified?

The SPBM and NNs are capable of detecting multiple simultaneous faults. However, only the SPBM was able to identify multiple simultaneous faults.

5) and in which situations are either a SPBM or neural network more suitable?

Fault detection with a neural network requires a noticeable deviation from nominal heating or cooling demand, while also maintaining acceptable accuracy when no fault is occurring. Therefore, a SPBM is more suited to general cases when a high-fidelity model or metered data under faulty conditions is not available because it is able to mimic thermodynamic responses of a building. However, a time series neural network can be effective if nominal performance data is available and only fault detection is desired.

Future works could explore a number of different topics for SPBM applications and improvements. Given the prowess for fault identification and transient response, it seems that demand control prediction would be a simple yet effective implementation. An improvement to the current SPBM could be a way to further increase computation speed. Some promising work was done to dramatically increase simulation speed, but the program used for coding (EES) is not suitable for product release. Improvements for neural networks could be use of more advanced or custom-made algorithms with different parameters or weightings. Research on combining the SPBM with NNs presented in this paper for use in increasing fault detection and identification accuracy and confidence will also be explored.

To summarize, a simplified physics-based building energy model is uniquely able to sufficiently represent building energy demands, detect faults, and identify which faults are occurring without needing data on how a building reacts when in a faulty situation.

While a neural network can accomplish some of the tasks of the SPBM, and at a fraction of the time, a reliance on an abundance of training data under different conditions makes machine learning an unsuitable replacement for physics-based modeling but rather a fantastic supplementation when the training data is available.

Overall, the proposed research was conducted with uniform success. The SPBM demonstrated an ability to match performance of both real buildings and high-fidelity models. Additionally, single faults and multiple simultaneous faults, were able to be detected and identified for cases in which a statistically significant change in load occured. Likewise, neural network time series and decision tree testing resulted in detection or identification of individual and simultaneous faults when sufficient alteration of metered load was present. Therefore, it can be said that the results presented in this paper achieved the stated goals with sufficient academic rigor.

APPENDIX

A.1 Completed Tasks

Task	Task title	Task description	Results and expectations
1	Investigate models for opaque walls and roofs	Compared simplified models with existing detailed models and identified component models that can adequately represent actual thermally capacitive walls and roofs.	Determined required inputs to achieve acceptable agreement with sophisticated models
2	Preliminary investigation of parameter estimation methods for conductive loads	Conducted parameter estimation exercise for each proposed wall or roof model. Found parameters giving least SSE for each simplified model when compared with detailed model for representative design cooling day.	Discovered that two node R-C system is sufficient and capacitance distribution is critical
3	Investigate models for fenestration	Compared simplified models with reflection and absorption with existing detailed models and identify an adequate fenestration model; all solar heat assumed to be absorbed in the floor.	Created acceptable radiation model
4	Develop simplified HVAC model	Incorporated ventilation load, VAV for capacity control; coolant modulation to maintain specific SA temperature, and specified supply air temperature and humidity to represent expected dehumidification performance for moist air.	Created baseline HVAC system with basic temperature and humidity control
5	Thermodynamic modeling	Developed rigorous thermodynamic model for building spaces and HVAC systems allowing consistent treatment of energy and mass conservation and transient effects.	Confirmed and agreement with modern models
6	Include internal equipment, lighting, and people loads	Internal load modeled based on fractional schedules.	Demonstrated adequate internal load simplification
7	Further investigation of parameter estimation methods	Automatically calibrated multiple parameter values simultaneously. Using only heating and cooling values, parameter value estimation was done on HVAC setpoints, envelope material properties, maximum internal load, and maximum occupancy.	Successful with available algorithm and software

8	Develop Neural Networks with real building data	Trained multiple neural networks with various conditions and input parameters to find a set of networks that respond well to training and output response	Created a set of networks for use in building modeling

A.2 Completed Tasks for Presented Thesis

Task	Title	Description	Results
1	Create detailed DesignBuilder model of two representative buildings	Apply knowledge of schedules and internal loads to DesignBuilder models. After calibrating the DesignBuilder models, outputs will be gathered so that the SPBM and NN can be trained on this data set.	Models were able to replicate heating and cooling metered data within 10% error
2	Simulate faults of two representative buildings with DesignBuilder models	Operate DesignBuilder model under numerous different faults and fault conditions.	Data was generated to mimic results expected when buildings operate under faulty conditions
3	Refine interior air and moisture model	Add adjustable internal air temperature setpoints to allow for internal air temperature changes. Explore internal sources of internal water vapor and contamination (CO_2) generation.	Realistic temperature deadband, CO2, and humidity modeling for all parts of AHU system
4	Test SPBM fault-modeling	Evaluate fault-modeling for fault detection effectiveness and impact. Develop specifications for optimal fault detection methods.	Methods for detecting and identifying faults was demonstrated such that a unique solution could be found
5	Identify effectiveness of NN fault detection	Creation and evaluation of multiple NN systems to determine how parameters change outputs when a building operates with a fault.	Both time series and decision tree neural networks were evaluated. Results showed that these methods are broadly able to detect or identify faults in conditions where sufficient change in loading occurs
6	Identify effectiveness of detecting multiple simultaneous faults	Create multiple faults, possibly starting at different times, to see which model is better suited for identifying multiple simultaneous faults.	All methods were able to detect that a fault was occurring when multiple simultaneous faults were evaluated. However, only the SPBM was capable of

			converging towards a solution that identified both faults

A.3 Tables

Table 19: Values for error associated with a corresponding potential fault values when running a high-infiltration test for winter weather for Whitehead

ERROR	INFILTRATION COEFFICIENT	MINIMUM OUTDOOR AIR [kg/s]	PREHEAT TEMPERATURE	SETBACK FAILURE COEFFICIENT
7.48E+17	0.224	4.4	14.1	0.001
5.68E+17	0.2489	4.4	14.1	0.001
4.77E+17	0.2738	4.4	14.1	0.001
4.73E+17	0.2987	4.4	14.1	0.001
5.59E+17	0.3236	4.4	14.1	0.001
7.31E+17	0.3484	4.4	14.1	0.001
9.93E+17	0.3733	4.4	14.1	0.001
1.34E+18	0.3982	4.4	14.1	0.001
1.78E+18	0.4231	4.4	14.1	0.001
2.31E+18	0.448	4.4	14.1	0.001
1.03E+18	0.224	4.033	14.1	0.001
1.40E+18	0.224	3.667	14.1	0.001
1.84E+18	0.224	3.3	14.1	0.001
2.31E+18	0.224	2.933	14.1	0.001
2.76E+18	0.224	2.567	14.1	0.001
2.82E+18	0.224	2.2	14.1	0.001
2.63E+18	0.224	1.833	14.1	0.001
2.33E+18	0.224	1.467	14.1	0.001
1.94E+18	0.224	1.1	14.1	0.001
8.61E+17	0.224	4.4	16.42	0.001
3.73E+18	0.224	4.4	18.74	0.001
9.68E+18	0.224	4.4	21.07	0.001
1.88E+19	0.224	4.4	23.39	0.001
3.10E+19	0.224	4.4	25.71	0.001
4.65E+19	0.224	4.4	28.03	0.001
6.51E+19	0.224	4.4	30.36	0.001
8.69E+19	0.224	4.4	32.68	0.001
1.12E+20	0.224	4.4	35	0.001
8.67E+17	0.224	4.4	14.1	0.2008
1.08E+18	0.224	4.4	14.1	0.4006
1.36E+18	0.224	4.4	14.1	0.6004
1.72E+18	0.224	4.4	14.1	0.8002
2.17E+18	0.224	4.4	14.1	1

Table 20: Values for error associated with a corresponding potential fault values when running a high-infiltration test for summer weather for Whitehead

SUM SQUARED ERROR	INFILTRATION COEFFICIENT	MINIMUM OUTDOOR AIR [kg/s]	PREHEAT TEMPERATURE	SETBACK FAILURE COEFFICIENT
1.09E+17	0.224	4.4	14.1	0.001
9.39E+16	0.2489	4.4	14.1	0.001
8.09E+16	0.2738	4.4	14.1	0.001
7.47E+16	0.2987	4.4	14.1	0.001
7.48E+16	0.3236	4.4	14.1	0.001
7.99E+16	0.3484	4.4	14.1	0.001
9.11E+16	0.3733	4.4	14.1	0.001
1.08E+17	0.3982	4.4	14.1	0.001
1.29E+17	0.4231	4.4	14.1	0.001
1.58E+17	0.448	4.4	14.1	0.001
2.02E+17	0.224	4.033	14.1	0.001
3.45E+17	0.224	3.667	14.1	0.001
5.40E+17	0.224	3.3	14.1	0.001
7.85E+17	0.224	2.933	14.1	0.001
1.08E+18	0.224	2.567	14.1	0.001
1.43E+18	0.224	2.2	14.1	0.001
1.83E+18	0.224	1.833	14.1	0.001
2.28E+18	0.224	1.467	14.1	0.001
2.78E+18	0.224	1.1	14.1	0.001
1.09E+17	0.224	4.4	16.42	0.001
1.09E+17	0.224	4.4	18.74	0.001
1.11E+17	0.224	4.4	21.07	0.001
1.90E+17	0.224	4.4	23.39	0.001
7.59E+17	0.224	4.4	25.71	0.001
2.12E+18	0.224	4.4	28.03	0.001
4.66E+18	0.224	4.4	30.36	0.001
8.60E+18	0.224	4.4	32.68	0.001
1.40E+19	0.224	4.4	35	0.001
1.08E+17	0.224	4.4	14.1	0.2008
1.08E+17	0.224	4.4	14.1	0.4006
1.07E+17	0.224	4.4	14.1	0.6004
9.94E+16	0.224	4.4	14.1	0.8002
9.50E+16	0.224	4.4	14.1	1

Table 21: Values for error associated with a corresponding potential fault values when running a failure to enter setback test for winter weather for Whitehead

SUM SQUARED ERROR	INFILTRATION COEFFICIENT	MINIMUM OUTDOOR AIR [kg/s]	PREHEAT TEMPERATURE	SETBACK FAILURE COEFFICIENT
4.12E+18	0.224	4.4	14.1	0.001
4.07E+18	0.2489	4.4	14.1	0.001
4.11E+18	0.2738	4.4	14.1	0.001
4.21E+18	0.2987	4.4	14.1	0.001
4.38E+18	0.3236	4.4	14.1	0.001
4.61E+18	0.3484	4.4	14.1	0.001
4.89E+18	0.3733	4.4	14.1	0.001
5.25E+18	0.3982	4.4	14.1	0.001
5.68E+18	0.4231	4.4	14.1	0.001
6.17E+18	0.448	4.4	14.1	0.001
4.29E+18	0.224	4.033	14.1	0.001
4.59E+18	0.224	3.667	14.1	0.001
5.06E+18	0.224	3.3	14.1	0.001
5.66E+18	0.224	2.933	14.1	0.001
6.32E+18	0.224	2.567	14.1	0.001
6.87E+18	0.224	2.2	14.1	0.001
7.22E+18	0.224	1.833	14.1	0.001
7.10E+18	0.224	1.467	14.1	0.001
6.76E+18	0.224	1.1	14.1	0.001
4.99E+18	0.224	4.4	16.42	0.001
1.28E+19	0.224	4.4	18.74	0.001
2.91E+19	0.224	4.4	21.07	0.001
5.46E+19	0.224	4.4	23.39	0.001
8.93E+19	0.224	4.4	25.71	0.001
1.33E+20	0.224	4.4	28.03	0.001
1.87E+20	0.224	4.4	30.36	0.001
2.49E+20	0.224	4.4	32.68	0.001
3.21E+20	0.224	4.4	35	0.001
2.90E+18	0.224	4.4	14.1	0.2008
1.94E+18	0.224	4.4	14.1	0.4006
1.25E+18	0.224	4.4	14.1	0.6004
7.70E+17	0.224	4.4	14.1	0.8002
5.49E+17	0.224	4.4	14.1	1

Table 22: Values for error associated with a corresponding potential fault values when running a failure to enter setback test for summer weather for Whitehead

SUM SQUARED ERROR	INFILTRATION COEFFICIENT	MINIMUM OUTDOOR AIR [kg/s]	PREHEAT TEMPERATURE	SETBACK FAILURE COEFFICIENT
4.66E+18	0.224	4.4	14.1	0.001
4.60E+18	0.2489	4.4	14.1	0.001
4.54E+18	0.2738	4.4	14.1	0.001
4.49E+18	0.2987	4.4	14.1	0.001
4.44E+18	0.3236	4.4	14.1	0.001
4.40E+18	0.3484	4.4	14.1	0.001
4.36E+18	0.3733	4.4	14.1	0.001
4.32E+18	0.3982	4.4	14.1	0.001
4.29E+18	0.4231	4.4	14.1	0.001
4.25E+18	0.448	4.4	14.1	0.001
5.25E+18	0.224	4.033	14.1	0.001
5.95E+18	0.224	3.667	14.1	0.001
6.75E+18	0.224	3.3	14.1	0.001
7.65E+18	0.224	2.933	14.1	0.001
8.66E+18	0.224	2.567	14.1	0.001
9.78E+18	0.224	2.2	14.1	0.001
1.10E+19	0.224	1.833	14.1	0.001
1.23E+19	0.224	1.467	14.1	0.001
1.38E+19	0.224	1.1	14.1	0.001
4.66E+18	0.224	4.4	16.42	0.001
3.60E+18	0.224	4.4	18.74	0.001
1.80E+18	0.224	4.4	21.07	0.001
5.84E+18	0.224	4.4	23.39	0.001
1.79E+19	0.224	4.4	25.71	0.001
3.94E+19	0.224	4.4	28.03	0.001
7.05E+19	0.224	4.4	30.36	0.001
1.11E+20	0.224	4.4	32.68	0.001
1.61E+20	0.224	4.4	35	0.001
3.40E+18	0.224	4.4	14.1	0.2008
2.22E+18	0.224	4.4	14.1	0.4006
1.20E+18	0.224	4.4	14.1	0.6004
4.87E+17	0.224	4.4	14.1	0.8002
1.66E+17	0.224	4.4	14.1	1

Table 23: Values for error associated with a corresponding potential fault values when an excessive preheat temperature failure test for winter weather for Whitehead

SUM SQUARED ERROR	INFILTRATION COEFFICIENT	MINIMUM OUTDOOR AIR [kg/s]	PREHEAT TEMPERATURE	SETBACK FAILURE COEFFICIENT
2.52E+19	0.224	4.4	14.1	0.001
2.47E+19	0.2489	4.4	14.1	0.001
2.43E+19	0.2738	4.4	14.1	0.001
2.39E+19	0.2987	4.4	14.1	0.001
2.35E+19	0.3236	4.4	14.1	0.001
2.32E+19	0.3484	4.4	14.1	0.001
2.29E+19	0.3733	4.4	14.1	0.001
2.26E+19	0.3982	4.4	14.1	0.001
2.23E+19	0.4231	4.4	14.1	0.001
2.20E+19	0.448	4.4	14.1	0.001
2.86E+19	0.224	4.033	14.1	0.001
3.24E+19	0.224	3.667	14.1	0.001
3.64E+19	0.224	3.3	14.1	0.001
4.07E+19	0.224	2.933	14.1	0.001
4.54E+19	0.224	2.567	14.1	0.001
5.03E+19	0.224	2.2	14.1	0.001
5.56E+19	0.224	1.833	14.1	0.001
6.11E+19	0.224	1.467	14.1	0.001
6.70E+19	0.224	1.1	14.1	0.001
2.52E+19	0.224	4.4	16.42	0.001
2.52E+19	0.224	4.4	18.74	0.001
2.48E+19	0.224	4.4	21.07	0.001
1.80E+19	0.224	4.4	23.39	0.001
9.39E+18	0.224	4.4	25.71	0.001
2.91E+18	0.224	4.4	28.03	0.001
6.99E+17	0.224	4.4	30.36	0.001
5.14E+18	0.224	4.4	32.68	0.001
1.65E+19	0.224	4.4	35	0.001
2.51E+19	0.224	4.4	14.1	0.2008
2.49E+19	0.224	4.4	14.1	0.4006
2.48E+19	0.224	4.4	14.1	0.6004
2.44E+19	0.224	4.4	14.1	0.8002
2.34E+19	0.224	4.4	14.1	1

Table 24: Values for error associated with a corresponding potential fault values when running an excessive preheat temperature fault test for summer weather for Whitehead

SUM SQUARED ERROR	INFILTRATION COEFFICIENT	MINIMUM OUTDOOR AIR [kg/s]	PREHEAT TEMPERATURE	SETBACK FAILURE COEFFICIENT
5.91E+19	0.224	4.4	14.1	0.001
5.87E+19	0.2489	4.4	14.1	0.001
5.83E+19	0.2738	4.4	14.1	0.001
5.80E+19	0.2987	4.4	14.1	0.001
5.76E+19	0.3236	4.4	14.1	0.001
5.73E+19	0.3484	4.4	14.1	0.001
5.70E+19	0.3733	4.4	14.1	0.001
5.66E+19	0.3982	4.4	14.1	0.001
5.63E+19	0.4231	4.4	14.1	0.001
5.60E+19	0.448	4.4	14.1	0.001
6.20E+19	0.224	4.033	14.1	0.001
6.50E+19	0.224	3.667	14.1	0.001
6.82E+19	0.224	3.3	14.1	0.001
7.15E+19	0.224	2.933	14.1	0.001
7.49E+19	0.224	2.567	14.1	0.001
7.84E+19	0.224	2.2	14.1	0.001
8.20E+19	0.224	1.833	14.1	0.001
8.58E+19	0.224	1.467	14.1	0.001
8.97E+19	0.224	1.1	14.1	0.001
5.91E+19	0.224	4.4	16.42	0.001
5.62E+19	0.224	4.4	18.74	0.001
4.40E+19	0.224	4.4	21.07	0.001
2.81E+19	0.224	4.4	23.39	0.001
1.40E+19	0.224	4.4	25.71	0.001
4.13E+18	0.224	4.4	28.03	0.001
1.26E+18	0.224	4.4	30.36	0.001
6.04E+18	0.224	4.4	32.68	0.001
1.85E+19	0.224	4.4	35	0.001
5.83E+19	0.224	4.4	14.1	0.2008
5.69E+19	0.224	4.4	14.1	0.4006
5.52E+19	0.224	4.4	14.1	0.6004
5.30E+19	0.224	4.4	14.1	0.8002
5.08E+19	0.224	4.4	14.1	1

Table 25: Values for error associated with a corresponding potential fault values when running an insufficient outdoor air fault test for winter weather for Whitehead

SUM SQUARED ERROR	INFILTRATION COEFFICIENT	MINIMUM OUTDOOR AIR [kg/s]	PREHEAT TEMPERATURE	SETBACK FAILURE COEFFICIENT
5.34E+18	0.224	4.4	14.1	0.001
6.34E+18	0.2489	4.4	14.1	0.001
7.46E+18	0.2738	4.4	14.1	0.001
8.70E+18	0.2987	4.4	14.1	0.001
1.01E+19	0.3236	4.4	14.1	0.001
1.15E+19	0.3484	4.4	14.1	0.001
1.31E+19	0.3733	4.4	14.1	0.001
1.49E+19	0.3982	4.4	14.1	0.001
1.67E+19	0.4231	4.4	14.1	0.001
1.86E+19	0.448	4.4	14.1	0.001
4.09E+18	0.224	4.033	14.1	0.001
3.03E+18	0.224	3.667	14.1	0.001
2.18E+18	0.224	3.3	14.1	0.001
1.54E+18	0.224	2.933	14.1	0.001
1.07E+18	0.224	2.567	14.1	0.001
7.99E+17	0.224	2.2	14.1	0.001
7.38E+17	0.224	1.833	14.1	0.001
8.74E+17	0.224	1.467	14.1	0.001
1.18E+18	0.224	1.1	14.1	0.001
9.12E+18	0.224	4.4	16.42	0.001
1.55E+19	0.224	4.4	18.74	0.001
2.50E+19	0.224	4.4	21.07	0.001
3.74E+19	0.224	4.4	23.39	0.001
5.29E+19	0.224	4.4	25.71	0.001
7.15E+19	0.224	4.4	28.03	0.001
9.33E+19	0.224	4.4	30.36	0.001
1.18E+20	0.224	4.4	32.68	0.001
1.46E+20	0.224	4.4	35	0.001
5.80E+18	0.224	4.4	14.1	0.2008
6.47E+18	0.224	4.4	14.1	0.4006
7.25E+18	0.224	4.4	14.1	0.6004
8.21E+18	0.224	4.4	14.1	0.8002
9.40E+18	0.224	4.4	14.1	1

Table 26: Values for error associated with a corresponding potential fault values when running an insufficient outdoor air fault test for summer weather for Whitehead

SUM SQUARED ERROR	INFILTRATION COEFFICIENT	MINIMUM OUTDOOR AIR [kg/s]	PREHEAT TEMPERATURE	SETBACK FAILURE COEFFICIENT
3.33E+18	0.224	4.4	14.1	0.001
3.41E+18	0.2489	4.4	14.1	0.001
3.49E+18	0.2738	4.4	14.1	0.001
3.57E+18	0.2987	4.4	14.1	0.001
3.65E+18	0.3236	4.4	14.1	0.001
3.72E+18	0.3484	4.4	14.1	0.001
3.81E+18	0.3733	4.4	14.1	0.001
3.89E+18	0.3982	4.4	14.1	0.001
3.97E+18	0.4231	4.4	14.1	0.001
4.05E+18	0.448	4.4	14.1	0.001
2.66E+18	0.224	4.033	14.1	0.001
2.10E+18	0.224	3.667	14.1	0.001
1.65E+18	0.224	3.3	14.1	0.001
1.32E+18	0.224	2.933	14.1	0.001
1.11E+18	0.224	2.567	14.1	0.001
1.01E+18	0.224	2.2	14.1	0.001
1.03E+18	0.224	1.833	14.1	0.001
1.17E+18	0.224	1.467	14.1	0.001
1.42E+18	0.224	1.1	14.1	0.001
3.33E+18	0.224	4.4	16.42	0.001
3.43E+18	0.224	4.4	18.74	0.001
4.72E+18	0.224	4.4	21.07	0.001
8.45E+18	0.224	4.4	23.39	0.001
1.50E+19	0.224	4.4	25.71	0.001
2.49E+19	0.224	4.4	28.03	0.001
3.81E+19	0.224	4.4	30.36	0.001
5.44E+19	0.224	4.4	32.68	0.001
7.39E+19	0.224	4.4	35	0.001
3.32E+18	0.224	4.4	14.1	0.2008
3.35E+18	0.224	4.4	14.1	0.4006
3.48E+18	0.224	4.4	14.1	0.6004
3.76E+18	0.224	4.4	14.1	0.8002
4.21E+18	0.224	4.4	14.1	1

Table 27: Values for error associated with a corresponding potential fault values when running an excessive infiltration fault test during winter weather for Old CE

SUM SQUARED ERROR	INFILTRATION	UNOCCUPIED SETBACK COEFFICIENT	PREHEAT TEMPERATURE	MINIMUM OUTDOOR AIR [kg/hr]
8.08E+16	0.018	1	12.78	9108
1.23E+17	0.018	0.8	12.78	9108
3.38E+17	0.018	0.6	12.78	9108
8.12E+17	0.018	0.4	12.78	9108
1.61E+18	0.018	0.2	12.78	9108
2.84E+18	0.018	0	12.78	9108
8.08E+16	0.018	1	12.78	9108
7.31E+16	0.0216	1	12.78	9108
6.66E+16	0.0252	1	12.78	9108
6.31E+16	0.0288	1	12.78	9108
6.29E+16	0.0324	1	12.78	9108
6.56E+16	0.036	1	12.78	9108
7.14E+16	0.0396	1	12.78	9108
8.03E+16	0.0432	1	12.78	9108
9.22E+16	0.0468	1	12.78	9108
1.07E+17	0.0504	1	12.78	9108
1.27E+17	0.054	1	12.78	9108
8.05E+16	0.018	1	12.78	7950
8.06E+16	0.018	1	12.78	6791
7.98E+16	0.018	1	12.78	5633
7.88E+16	0.018	1	12.78	4475
7.73E+16	0.018	1	12.78	3317
7.55E+16	0.018	1	12.78	2158
7.49E+16	0.018	1	12.78	1000
9.46E+16	0.018	1	15.24	9108
1.44E+17	0.018	1	17.7	9108
1.10E+18	0.018	1	20.16	9108
2.49E+18	0.018	1	22.62	9108
4.64E+18	0.018	1	25.08	9108
7.54E+18	0.018	1	27.54	9108

Table 28: Values for cooling demand error associated with a corresponding potential fault values when running an excessive infiltration fault test during summer weather for Old CE

SUM SQUARED ERROR	INFILTRATION	UNOCCUPIED SETBACK COEFFICIENT	PREHEAT TEMPERATURE	MINIMUM OUTDOOR AIR [kg/hr]
1.19E+17	0.018	1	12.78	9108
1.05E+17	0.018	0.8	12.78	9108
1.05E+17	0.018	0.6	12.78	9108
2.24E+17	0.018	0.4	12.78	9108
5.60E+17	0.018	0.2	12.78	9108
1.19E+17	0.018	0	12.78	9108
1.16E+17	0.018	1	12.78	9108
1.14E+17	0.0216	1	12.78	9108
1.11E+17	0.0252	1	12.78	9108
1.11E+17	0.0288	1	12.78	9108
1.11E+17	0.0324	1	12.78	9108
1.12E+17	0.036	1	12.78	9108
1.14E+17	0.0396	1	12.78	9108
1.15E+17	0.0432	1	12.78	9108
1.18E+17	0.0468	1	12.78	9108
1.19E+17	0.0504	1	12.78	9108
1.19E+17	0.054	1	12.78	9108
1.20E+17	0.018	1	12.78	7950
1.22E+17	0.018	1	12.78	6791
1.25E+17	0.018	1	12.78	5633
1.28E+17	0.018	1	12.78	4475
1.32E+17	0.018	1	12.78	3317
1.19E+17	0.018	1	12.78	2158
1.13E+17	0.018	1	12.78	1000
1.14E+17	0.018	1	15.24	9108
2.43E+17	0.018	1	17.7	9108
1.04E+18	0.018	1	20.16	9108
2.59E+18	0.018	1	22.62	9108
4.90E+18	0.018	1	25.08	9108

Table 29: Values associated CO2-based error minimization for Old CE experiencing excessive infiltration during summer weather

SUM SQUARED ERROR	INFILTRATION	UNOCCUPIED SETBACK COEFFICIENT	PREHEAT TEMPERATURE	MINIMUM OUTDOOR AIR [kg/hr]
1.56E+03	0.018	1	12.78	9108
1.54E+03	0.018	0.8	12.78	9108
1.53E+03	0.018	0.6	12.78	9108
1.52E+03	0.018	0.4	12.78	9108
1.52E+03	0.018	0.2	12.78	9108
1.52E+03	0.018	0	12.78	9108
1.56E+03	0.018	1	12.78	9108
1.18E+03	0.0216	1	12.78	9108
9.75E+02	0.0252	1	12.78	9108
9.20E+02	0.0288	1	12.78	9108
9.98E+02	0.0324	1	12.78	9108
1.17E+03	0.036	1	12.78	9108
1.49E+03	0.0396	1	12.78	9108
1.87E+03	0.0432	1	12.78	9108
2.33E+03	0.0468	1	12.78	9108
2.87E+03	0.0504	1	12.78	9108
3.46E+03	0.054	1	12.78	9108
1.02E+04	0.018	1	12.78	7950
3.51E+04	0.018	1	12.78	6791
9.06E+04	0.018	1	12.78	5633
2.06E+05	0.018	1	12.78	4475
4.51E+05	0.018	1	12.78	3317
1.03E+06	0.018	1	12.78	2158
2.92E+06	0.018	1	12.78	1000
1.56E+03	0.018	1	15.24	9108
1.56E+03	0.018	1	17.7	9108
1.56E+03	0.018	1	20.16	9108
1.56E+03	0.018	1	22.62	9108
1.56E+03	0.018	1	25.08	9108
1.56E+03	0.018	1	27.54	9108
1.56E+03	0.018	1	30	9108

Table 30: Values for error associated with a corresponding potential fault values when running a fault test for not entering unoccupied setback for winter for Old CE

SUM SQUARED ERROR	INFILTRATION	UNOCCUPIED SETBACK COEFFICIENT	PREHEAT TEMPERATURE	MINIMUM OUTDOOR AIR [kg/hr]
1.51E+19	0.018	1	12.78	9108
1.19E+19	0.018	0.8	12.78	9108
7.67E+18	0.018	0.6	12.78	9108
3.86E+18	0.018	0.4	12.78	9108
1.27E+18	0.018	0.2	12.78	9108
2.59E+17	0.018	0	12.78	9108
1.51E+19	0.018	1	12.78	9108
1.50E+19	0.0216	1	12.78	9108
1.50E+19	0.0252	1	12.78	9108
1.50E+19	0.0288	1	12.78	9108
1.49E+19	0.0324	1	12.78	9108
1.49E+19	0.036	1	12.78	9108
1.48E+19	0.0396	1	12.78	9108
1.47E+19	0.0432	1	12.78	9108
1.47E+19	0.0468	1	12.78	9108
1.46E+19	0.0504	1	12.78	9108
1.45E+19	0.054	1	12.78	9108
1.51E+19	0.018	1	12.78	7950
1.51E+19	0.018	1	12.78	6791
1.51E+19	0.018	1	12.78	5633
1.51E+19	0.018	1	12.78	4475
1.51E+19	0.018	1	12.78	3317
1.51E+19	0.018	1	12.78	2158
1.51E+19	0.018	1	12.78	1000
1.51E+19	0.018	1	15.24	9108
1.50E+19	0.018	1	17.7	9108
1.45E+19	0.018	1	20.16	9108
1.31E+19	0.018	1	22.62	9108
1.70E+19	0.018	1	25.08	9108
2.77E+19	0.018	1	27.54	9108
4.53E+19	0.018	1	30	9108

Table 31: Values for error associated with a corresponding potential fault values when running a fault test for not entering unoccupied setback for summer for Old CE

SUM SQUARED ERROR	INFILTRATION	UNOCCUPIED SETBACK COEFFICIENT	PREHEAT TEMPERATURE	MINIMUM OUTDOOR AIR [kg/hr]
8.37E+18	0.018	1	12.78	9108
6.66E+18	0.018	0.8	12.78	9108
5.16E+18	0.018	0.6	12.78	9108
3.41E+18	0.018	0.4	12.78	9108
1.10E+18	0.018	0.2	12.78	9108
5.67E+16	0.018	0	12.78	9108
8.37E+18	0.018	1	12.78	9108
8.37E+18	0.0216	1	12.78	9108
8.37E+18	0.0252	1	12.78	9108
8.38E+18	0.0288	1	12.78	9108
8.38E+18	0.0324	1	12.78	9108
8.38E+18	0.036	1	12.78	9108
8.38E+18	0.0396	1	12.78	9108
8.38E+18	0.0432	1	12.78	9108
8.39E+18	0.0468	1	12.78	9108
8.39E+18	0.0504	1	12.78	9108
8.39E+18	0.054	1	12.78	9108
8.37E+18	0.018	1	12.78	7950
8.37E+18	0.018	1	12.78	6791
8.37E+18	0.018	1	12.78	5633
8.37E+18	0.018	1	12.78	4475
8.37E+18	0.018	1	12.78	3317
8.37E+18	0.018	1	12.78	2158
8.37E+18	0.018	1	12.78	1000
8.37E+18	0.018	1	15.24	9108
8.37E+18	0.018	1	17.7	9108
8.27E+18	0.018	1	20.16	9108
5.62E+18	0.018	1	22.62	9108
7.52E+18	0.018	1	25.08	9108
1.64E+19	0.018	1	27.54	9108
3.21E+19	0.018	1	30	9108

Table 32: Values for error associated with a corresponding potential fault values when running a fault test for excessive preheat during winter weather for Old CE

SUM SQUARED ERROR	INFILTRATION	UNOCCUPIED SETBACK COEFFICIENT	PREHEAT TEMPERATURE	MINIMUM OUTDOOR AIR [kg/hr]
4.16E+19	0.018	1	12.78	9108
3.71E+19	0.018	0.8	12.78	9108
3.23E+19	0.018	0.6	12.78	9108
2.82E+19	0.018	0.4	12.78	9108
2.57E+19	0.018	0.2	12.78	9108
2.56E+19	0.018	0	12.78	9108
4.16E+19	0.018	1	12.78	9108
4.11E+19	0.0216	1	12.78	9108
4.06E+19	0.0252	1	12.78	9108
4.02E+19	0.0288	1	12.78	9108
3.98E+19	0.0324	1	12.78	9108
3.94E+19	0.036	1	12.78	9108
3.90E+19	0.0396	1	12.78	9108
3.86E+19	0.0432	1	12.78	9108
3.82E+19	0.0468	1	12.78	9108
3.78E+19	0.0504	1	12.78	9108
3.73E+19	0.054	1	12.78	9108
4.10E+19	0.018	1	12.78	7950
4.03E+19	0.018	1	12.78	6791
3.95E+19	0.018	1	12.78	5633
3.87E+19	0.018	1	12.78	4475
3.78E+19	0.018	1	12.78	3317
3.70E+19	0.018	1	12.78	2158
3.62E+19	0.018	1	12.78	1000
4.00E+19	0.018	1	15.24	9108
3.45E+19	0.018	1	17.7	9108
2.35E+19	0.018	1	20.16	9108
1.01E+19	0.018	1	22.62	9108
1.91E+18	0.018	1	25.08	9108
5.78E+17	0.018	1	27.54	9108
6.09E+18	0.018	1	30	9108

Table 33: Values for error associated with a corresponding potential fault values when running an excessive preheat temperature fault test during summer weather for Old CE

SUM SQUARED ERROR	INFILTRATION	UNOCCUPIED SETBACK COEFFICIENT	PREHEAT TEMPERATURE	MINIMUM OUTDOOR AIR [kg/hr]
2.40E+19	0.018	1	12.78	9108
2.26E+19	0.018	0.8	12.78	9108
2.12E+19	0.018	0.6	12.78	9108
1.79E+19	0.018	0.4	12.78	9108
1.40E+19	0.018	0.2	12.78	9108
2.40E+19	0.018	0	12.78	9108
2.38E+19	0.018	1	12.78	9108
2.37E+19	0.0216	1	12.78	9108
2.36E+19	0.0252	1	12.78	9108
2.35E+19	0.0288	1	12.78	9108
2.34E+19	0.0324	1	12.78	9108
2.32E+19	0.036	1	12.78	9108
2.31E+19	0.0396	1	12.78	9108
2.30E+19	0.0432	1	12.78	9108
2.29E+19	0.0468	1	12.78	9108
2.28E+19	0.0504	1	12.78	9108
2.42E+19	0.054	1	12.78	9108
2.45E+19	0.018	1	12.78	7950
2.47E+19	0.018	1	12.78	6791
2.50E+19	0.018	1	12.78	5633
2.53E+19	0.018	1	12.78	4475
2.56E+19	0.018	1	12.78	3317
2.59E+19	0.018	1	12.78	2158
2.40E+19	0.018	1	12.78	1000
2.39E+19	0.018	1	15.24	9108
2.17E+19	0.018	1	17.7	9108
1.15E+19	0.018	1	20.16	9108
3.82E+18	0.018	1	22.62	9108
3.07E+18	0.018	1	25.08	9108
9.26E+18	0.018	1	27.54	9108
2.40E+19	0.018	1	30	9108

Table 34: Values for error associated with a corresponding potential fault values when running an insufficient outdoor air fault test during winter weather for Old CE

SUM SQUARED ERROR	INFILTRATION	UNOCCUPIED SETBACK COEFFICIENT	PREHEAT TEMPERATURE	MINIMUM OUTDOOR AIR [kg/hr]
2.40E+19	0.018	1	12.78	9108
2.26E+19	0.018	0.8	12.78	9108
2.12E+19	0.018	0.6	12.78	9108
1.79E+19	0.018	0.4	12.78	9108
1.40E+19	0.018	0.2	12.78	9108
2.40E+19	0.018	0	12.78	9108
2.38E+19	0.018	1	12.78	9108
2.37E+19	0.0216	1	12.78	9108
2.36E+19	0.0252	1	12.78	9108
2.35E+19	0.0288	1	12.78	9108
2.34E+19	0.0324	1	12.78	9108
2.32E+19	0.036	1	12.78	9108
2.31E+19	0.0396	1	12.78	9108
2.30E+19	0.0432	1	12.78	9108
2.29E+19	0.0468	1	12.78	9108
2.28E+19	0.0504	1	12.78	9108
2.42E+19	0.054	1	12.78	9108
2.45E+19	0.018	1	12.78	7950
2.47E+19	0.018	1	12.78	6791
2.50E+19	0.018	1	12.78	5633
2.53E+19	0.018	1	12.78	4475
2.56E+19	0.018	1	12.78	3317
2.59E+19	0.018	1	12.78	2158
2.40E+19	0.018	1	12.78	1000
2.39E+19	0.018	1	15.24	9108
2.17E+19	0.018	1	17.7	9108
1.15E+19	0.018	1	20.16	9108
3.82E+18	0.018	1	22.62	9108
3.07E+18	0.018	1	25.08	9108
9.26E+18	0.018	1	27.54	9108
	0.018	1	30	9108

Table 35: Values for error associated with a corresponding potential fault values when running an insufficient outdoor air fault test during summer weather for Old CE

SUM SQUARED ERROR	INFILTRATION	UNOCCUPIED SETBACK COEFFICIENT	PREHEAT TEMPERATURE	MINIMUM OUTDOOR AIR [kg/hr]
3.23E+17	0.018	1	12.78	9108
5.84E+17	0.018	0.8	12.78	9108
2.14E+18	0.018	0.6	12.78	9108
5.81E+18	0.018	0.4	12.78	9108
1.23E+19	0.018	0.2	12.78	9108
2.27E+19	0.018	0	12.78	9108
3.23E+17	0.018	1	12.78	9108
3.19E+17	0.0216	1	12.78	9108
3.19E+17	0.0252	1	12.78	9108
3.23E+17	0.0288	1	12.78	9108
3.33E+17	0.0324	1	12.78	9108
3.47E+17	0.036	1	12.78	9108
0.00E+00	0.0396	1	12.78	9108
3.88E+17	0.0432	1	12.78	9108
4.16E+17	0.0468	1	12.78	9108
4.43E+17	0.0504	1	12.78	9108
4.80E+17	0.054	1	12.78	9108
2.90E+17	0.018	1	12.78	7950
2.62E+17	0.018	1	12.78	6791
2.40E+17	0.018	1	12.78	5633
2.32E+17	0.018	1	12.78	4475
2.43E+17	0.018	1	12.78	3317
2.71E+17	0.018	1	12.78	2158
3.16E+17	0.018	1	12.78	1000
3.31E+17	0.018	1	15.24	9108
7.87E+17	0.018	1	17.7	9108
3.26E+18	0.018	1	20.16	9108
1.05E+19	0.018	1	22.62	9108
2.44E+19	0.018	1	25.08	9108
4.52E+19	0.018	1	27.54	9108
7.27E+19	0.018	1	30	9108

Table 36: Values for error associated with a corresponding potential fault values when running an insufficient outdoor air fault test with a less efficient energy recovery system during summer weather for Old CE

SUM SQUARED ERROR	INFILTRATION	UNOCCUPIED SETBACK COEFFICIENT	PREHEAT TEMPERATURE	MINIMUM OUTDOOR AIR [kg/hr]
1.10E+18	0.018	1	12.78	9108
1.15E+18	0.018	0.8	12.78	9108
1.25E+18	0.018	0.6	12.78	9108
1.50E+18	0.018	0.4	12.78	9108
9.51E+18	0.018	0	12.78	9108
1.10E+18	0.018	1	12.78	9108
1.11E+18	0.0216	1	12.78	9108
1.13E+18	0.0252	1	12.78	9108
1.15E+18	0.0288	1	12.78	9108
1.17E+18	0.0324	1	12.78	9108
1.19E+18	0.036	1	12.78	9108
1.21E+18	0.0396	1	12.78	9108
1.25E+18	0.0468	1	12.78	9108
1.27E+18	0.0504	1	12.78	9108
1.30E+18	0.054	1	12.78	9108
9.73E+17	0.018	1	12.78	7950
8.84E+17	0.018	1	12.78	6791
8.32E+17	0.018	1	12.78	5633
8.16E+17	0.018	1	12.78	4475
8.36E+17	0.018	1	12.78	3317
8.92E+17	0.018	1	12.78	2158
9.84E+17	0.018	1	12.78	1000
1.08E+18	0.018	1	15.24	9108
9.64E+17	0.018	1	17.7	9108
1.05E+18	0.018	1	20.16	9108
2.70E+18	0.018	1	22.62	9108
1.05E+19	0.018	1	25.08	9108
2.52E+19	0.018	1	27.54	9108
4.68E+19	0.018	1	30	9108

Table 37: Values for error associated with a corresponding potential fault values when running an insufficient outdoor air fault test while monitoring changes in CO2 during summer weather for Old CE

SUM SQUARED ERROR	INFILTRATION	UNOCCUPIED SETBACK COEFFICIENT	PREHEAT TEMPERATURE	MINIMUM OUTDOOR AIR [kg/hr]
8.96E+17	0.018	1	12.78	9108
8.21E+17	0.018	0.8	12.78	9108
7.99E+17	0.018	0.6	12.78	9108
8.57E+17	0.018	0.4	12.78	9108
2.65E+18	0.018	0.2	12.78	9108
8.02E+18	0.018	0	12.78	9108
8.96E+17	0.018	1	12.78	9108
8.96E+17	0.0216	1	12.78	9108
8.97E+17	0.0252	1	12.78	9108
9.00E+17	0.0288	1	12.78	9108
9.04E+17	0.0324	1	12.78	9108
9.09E+17	0.036	1	12.78	9108
9.15E+17	0.0396	1	12.78	9108
9.21E+17	0.0432	1	12.78	9108
9.29E+17	0.0468	1	12.78	9108
9.38E+17	0.0504	1	12.78	9108
9.47E+17	0.054	1	12.78	9108
8.73E+17	0.018	1	12.78	7950
8.53E+17	0.018	1	12.78	6791
8.38E+17	0.018	1	12.78	5633
8.26E+17	0.018	1	12.78	4475
8.18E+17	0.018	1	12.78	3317
8.13E+17	0.018	1	12.78	2158
8.11E+17	0.018	1	12.78	1000
8.82E+17	0.018	1	15.24	9108
7.61E+17	0.018	1	17.7	9108
8.43E+17	0.018	1	20.16	9108
2.64E+18	0.018	1	22.62	9108
1.08E+19	0.018	1	25.08	9108
2.58E+19	0.018	1	27.54	9108
4.78E+19	0.018	1	30	9108

REFERENCES

[1] M. Frankel and C. Turner, "How Accurate is Energy Modeling in the Market?," in *ACEEE Summer Study on Efficiency in Buildings*, 2008.

[2] Y. Li and Z. O'Neill, "A Critical Review of Fault Modeling of HVAC Systems in Buildings," *Building Simulation,* vol. 11, pp. 953-975, 2018.

[3] S. J. Christopher Fernandez, *Continuous Monitoring Metering and Evaluation,* Atlanta, 2016.

[4] M. L. Sanke et al, "Continuous Monitoring, Modeling, and Evaluation of Actual Building Energy Systems," in *Proceedings of the ASME 2014 8th International Conference on Energy Sustainability*, Boston, 2014.

[5] P. G. Loutzenhiser, *Empirical Validations of Shading/Daylighting/Load Interactions in Building Energy Simulation Tools*, Retrospective Theses and Dissertations, 2006.

[6] US Department of Energy, "EnergyPlus Version 8.8.0 Documentation Engineering Reference," 26 September 2017. [Online]. Available: https://energyplus.net/sites/all/modules/custom/nrel_custom/pdfs/pdfs_v8.8.0/EngineeringReference.pdf. [Accessed 15 February 2018].

[7] X. Li and J. Wen, "Review of building energy modeling for control and operation," *Renewable and Sustainable Energy Reviews,* vol. 37, pp. 517-537, 2014.

[8] S. Katipamula and M. R. Brambley, "Review Article: Methods for Fault Detection Diagnostics, and Prognostics for Building Systems - A Review, Part I," *HVAC&R Research,* vol. 11, no. 1, pp. 3-25, 2011.

[9] M. Royapoor and T. Roskilly, "Building model calibration using energy and environmental data," *Energy and Buildings*, vol. 94, pp. 109-120, 2015.

[10] American Society of Heating, Refrigerating, and Air-Conditioning Engineers, Inc., "Air-Conditioning Cooling Load," in *ASHRAE Handbook 1985 Fundamentals Inch-Pound Edition*, Atlanta, American Society of Heating, Refrigerating, and Air-Conditioning Engineers, Inc., 1985, pp. 26.1-26.42.

[11] B. Checket-Hanks, "The News," The News, 2002. [Online]. Available: https://www.achrnews.com/articles/90359-hvac-load-calculations-old-and-new. [Accessed 12 February 2018].

[12] T. Kusuda, "NBSLD, computer program for heating and cooling loads in buildings. Final report," National Bureau of Standards, Washington, D.C. (USA). Center for Building Technology, United States, 1974.

[13] D. B. Crawley and et al, "Beyond BLAST and DOE-2: EnergyPlus, a new-generation energy simulation program," in *ACEEE Summer Study*, 1998.

[14] US Department of Energy, "EnergyPlus," US Department of Energy, 2018. [Online]. Available: https://energyplus.net/. [Accessed 1 April 2018].

[15] Integrated Enviromental Solutions Limited, "IES," Integrated Environmental Solutions Limites, 2018. [Online]. Available: https://www.iesve.com/. [Accessed 26 April 2018].

[16] Southface, "High Performance HVAC and Mechanical," in *Greenprints 2018 Conference,* Atlanta, 2018.

[17] L. Han and M. Neumann, "Effect of dimensionality on the Nelder–Mead simplex method," *Optomization Methods and Software,* vol. 21, no. 1, pp. 1-16, 2016.

[18] C. Fernandez and S. Jeter, "COMPARISON AND IMPLEMENTATION OF THERMALLY MASSIVE WALL AND ROOF MODELS FOR USE IN SIMPLIFIED BUILDING ENERGY MODELS," *ASME (in press).*

[19] A. Guillemin and N. Morel, "An innovarive lighting controller integrated in a self-adaptive building control system," *Energy and Buildings,* vol. 33, pp. 477-487, 2001.

[20] A. Dounis and C. Caraisos, "Advanced control system engineering for energy and comfort management in a building environment - A review," *Renewable and Sustainable Energy Reviews,* vol. 13, pp. 1246-1261, 2009.

[21] K. J. McCartney and J. F. Nicol, "Developing an adaptive control algorithm for Europe," *Energy and Buildings,* vol. 34, pp. 623-635, 2002.

[22] S. Wang and X. Jin, "CO2-Based Occupancy Detection for On-Line Outdoor Air Flow Control," *Indoor Built Environment,* vol. 7, pp. 165-181, 1998.

[23] E. Mathews et al, "HVAC control strategies to enhance comfort and minimise energy useage," *Energy and Buildings,* vol. 33, pp. 853-563, 2001.

[24] A. Persily, J. Braun, S. Emmerich, K. Mercer and T. Lawrence, *Recommendations for Application of CO2-Based Demand Controlled Ventilation Including Proposed Guidance for ASHRAE Standard 62 and California's Title 24,* 2003.

[25] H.-x. Zhao and F. Magoules, "A review on the prediction of building energy consumption," *Renewable and Sustainable energy Reviews,* vol. 16, no. 6, pp. 3586-3592, 2012.

[26] H. Salt, "TRANSIENT CONDUCTION IN A TWO-DIMENSIONAL COMPOSITE SLAB-I. THEORETICAL DEVELOPMENT OF TEMPERATURE MODES," *Int. J. Heat Mass Transfer,* vol. 26, no. 11, pp. 1611-1616, 1983.

[27] E. J. Correa and R. M. Cotta, "Enganced lumped-differential formulations of diffusion problems," *Applied Mathematical Modeling,* vol. 22, pp. 137-152, 1998.

[28] M. Royapoor and T. Roskilly, "Building model calibration using energy and environmental data," *Energy and Buildings,* vol. 94, pp. 109-120, 2015.

[29] J. V. Beck, Parameter Estimation in Engineering and Science, New York: John Wiley & Sons, 1977.

[30] S. A. Klein, "Engineering Equation Solver," F-Chart Software, 2017.

[31] The MathWorks, Inc, "MathWorks," The MathWorks, Inc, 2017. [Online]. Available: https://www.mathworks.com/help/optim/ug/fminsearch-algorithm.html. [Accessed 21 November 2017].

[32] The MAthWorks, Inc., "MathWorks," MathWorks, 2017. [Online]. Available: https://www.mathworks.com/help/optim/ug/fminunc.html#but9rn9-5. [Accessed 4 October 2017].

[33] M. M. Gouda, S. Danaher and C. Underwood, "Building thermal model reduction using nonlinear constrained optimization," *Building and Environment,* vol. 37, pp. 1255-1265, 2002.

[34] S. Wang and X. Xu, "Simplified building model for transient thermal performance estimation using GA-based parameter identification," *International Journal of Thermal Sciences,* vol. 45, pp. 419-432, 2006.

[35] J. v. Schijndel, "Inverse Modeling of the Indoor Climate using a 2-State-5-Parameters Model in MatLab," Eindhoven University of Technology, 2011.

[36] J. Su, "Improved Lumped Models for Asymmetric Cooling of a Long Slab by Heat Convection," *Int. Comm. Heat Mass Transfer,* vol. 28, no. 7, pp. 973-983, 2001.

[37] A. P. R. González, M. E. Eames and D. A. Coley, "Lumped Parameter Models for Building Thermal Modelling: An Analytic approach to simplifying complex multi-layered constructions," *Energy and Buildings,* vol. 60, pp. 174-184, 2013.

[38] B. Eisenhower, Z. O'Neill, S. Narayananb, V. A. Fonoberovc and I. Mezic, "A methodology for meta-model based optimization in building energy models," *Energy and Buildings,* vol. 47, pp. 292-301, 2012.

[39] A. El-Leathy, S. Jeter, H. Al-Ansary, S. N. Danish, R. Saeed, S. Abdel-Khalik, M. Golob, E. Djajadiwinata and Z. Al-Suhaibani, "Thermal performance evaluation of lining materials used in thermal energy storage for a falling particle receiver based CSP system," *Solar Energy,* vol. 178, no. 15, pp. 268-277, 2019`.

[40] A. El-Leathy, S. Jeter, H. Al-Ansary, S. N. Danish, R. Saeed, S. Abdel-Khalik, M. Golob, E. Djajadiwinata and Z. Al-Suhaibani, "Experimental measurements of thermal properties of high-temperature refractory materials used for thermal storage," *AIP Conference Proceedings,* vol. 1734, no. 1, pp. 050012-1:7, 2016.

[41] T. Lawrence and D. B. Crawley, "How HVAC sytstems can improve resilience of the build environment," in *49th International HVAC&R Congress*, Belgrade, 2018.

[42] J. E. Braun, T. M. Lawrence and et al, "Demonstration of Load Shifting and Peak Load Reduction with Control of Building Thermal Mass," *Commercial Buildings: Technologies, Design, Performance Analysis, and Building Energy Trends,* vol. 3, pp. 55-68, 2002.

[43] C. Fernandez, "Findings of CULC errors," 2015.

[44] C. Fernandez, "EBB error report," 2016.

[45] C. Fernandez, "CNES Model Report," 2014.

[46] C. Fernandez, "Love Building CO2 Control," 2014.

[47] C. Fernandez, "Biotech Quad Cooling Load Investigation," 2017.

[48] C. Fernandez, ""Evaluation of Old CE building performance for retrofit benifit"," 2019.

[49] C. Fernandez, "Library Model Results," 2017.

[50] C. Fernandez, "Living Building Modeling Results," 2018.

[51] S. McVae, *Johnson Controlls Fault Detection Meeting,* Atlanta, 2018.

[52] D. Rodin and S. K. Yee, "Simultaneous measurement of in-plane and through-plane thermal conductivity using beam-offset frequency domain thermoreflectance," *AIP Publishing,* vol. 014902, no. 88, pp. 1-8, 2017.

[53] P. G. Loutzenhiser and et al, "Empirical validation of models to compute solar irradiance on inclined surfaces for building energy simulation," *Solar Energy,* no. 81, pp. 254-267, 2007.

[54] P. G. Loutzenhiser, G. M. Maxwell and H. Manz, "An empirical validation of the daylighting algorithms and associated interactions in building energy simulation programs using various shading devices and windows," *Energy,* vol. 32, no. 10, pp. 1855-1870, 2017.

[55] H. Manz, P. Loutzenhiser, T. Frank, P. A. Strachan, R. Bundi and G. Maxwell, "Series of experiments for empirical validation of solar gain modeling in building energy simulation codes—Experimental setup, test cell characterization, specifications and uncertainty analysis," *Building and Environment,* vol. 41, no. 12, pp. 1784-1797, 2006.

[56] Z. M. Zhang and G. Machin, "Chapter 3. Theory of Thermal Radiation and Radiative Properties," in *Radiometric Temperature Measurements I. Fundamentals*, Cambridge, Academic Press, 2009.

[57] X. Xu and S. Wang, "A simplified dynamic model for existing buildings using CTF and thermal network models," *International Journal of Thermal Sciences,* vol. 47, no. 9, pp. 1249-1262, 2008.

[58] W. T. Richard, T. M. Lawrence, M.-C. Boudreau and K. Johnsen, "Design of a demand response system: economics and information systems alignment," in *21st European Confrence on Information Systems*, 2013.

[59] M. Avci, A. Rahmani and S. Asfour, "Model predictive HVAC load control in buildings using real-time electricity pricing," *Energy and Buildings*, vol. 60, pp. 199-209, 2013.

[60] Y. Ma and A. Kelman, "Predictive Control for Energy Efficient Buildings with Thermal Storage," *IEEE Control Systems,* vol. 32, pp. 44-64, 2012.

[61] S. Aghniaey, T. M. Lawrence, J. Mohammadpour, W. Song, R. T. Watson and M. C. Boudreau, "Optimizing thermal comfort considerations with electrical demand response program implementation," *Building Services Engineering Research and Technology*, vol. 39, no. 2, pp. 219-231, 2018.

[62] T. M. Lawrence, R. T. Watson, M.-C. Boudreau and J. Mohammadpour, "Data flow requirements for integrating smart buildings and a smart grid through model predictive control," *Procedia Engineering,* vol. 180, pp. 1402-1412, 2017.

[63] G. Yang, Z. Li and G. Augenbroe, "Development of prototypical buildings for urban scale building energy modeling: A reduced order energy model approach," *Science and Technology for the Built Environment,* vol. 24, no. 1, pp. 33-42, 2018.

[64] S. Nagpal, C. Mueller, A. Aijazi and C. F. Reinhart, "A methodology for auto-calibrating urban building energy models using surrogate modeling techniques," 2017. [Online]. Available: https://doi.org/10.1080/19401493.2018.1457722.

[65] G. Yang, Z. Li and G. Augenbroe, "Development of prototypical buildings for urban scale building energy modeling: A reduced order energy model approach," *Science and Technology for the Built Envionment,* pp. 33-42, 2017.

[66] S. Privara, *Building modeling as a crucial part for building predictive control,* Department of Control Engineering, 2013.

[67] A. S. Derakhtenhani, J. A. Candanedo, Y. Chen, V. R. Dehkordi and A. K. Athienitis, "Modeling approaches for the characterization of building thermal dynamics and model-based control: A case study," *Science and Technology for the Built Environment,* pp. 824-836, 2014.

[68] Y. Ma, G. Anderson and F. Borrelli, "A Distributed Predictive Control Approach to Building Temperature Regulation," in *American Control Conference*, San Francisco, 2011.

[69] R. T. Muehleisen and B. Craig, "Integration of the CEN/ISO Monthly Building Energy Model into OpenStudio," in *ACEEE Summer Study on Energy Efficient Buildings*, Pacific Grove, 2014.

[70] S. Nagpal, C. Muller, A. Aijazi and C. F. Reinhart, "A methodology for auto-calibrating urban building energy models using surrogate modeling techniques," *Journal of Building Performance Simulation,* 2017.

[71] T. Hastie, R. Tibshirani and J. Friedman, "11 Neural Networks," in *The Elements of Statistical Learning Data Mining, Inference, and Prediction Second Edition*, Stanford, Springer, 2008, pp. 389-416.

[72] MATLAB, *Neural Time Series App.*

[73] S. Lawrence, L. C. Hiles and A. C. Tsoi, "Lessons in Neural Network Training: Overfitting May be Harder than Expected," in *Fourteenth National Confrence on Artifical Intelligence*, Menlo Park, 1997.

[74] Y. Zhao, T. L. Zuejun Zhang and C. Zhang, "Artifical intelligance-based fault detection and diagnosis methods for building energy systems: Advantages, challenges, and the future," *Renewable and Sustainable Energy Reviews,* vol. 109, pp. 85-101, 2019.

[75] D. Jacob, S. Dietz, S. Komhard, C. Nuemann and S. Herkel, "Black-box models for fault detection and performance monitoring of buildings," *Journal of Building Performance Simulation,* pp. 53-62, 2009.

[76] F. Stephen and et al., "Hybrid Model-based and Data-driven Fault Detection and Diagnostics for Commercial Buildings," in *ACEEE Summer Study on Energy Efficiency in Buildings*, Pacific Grove, 2016.

[77] A. H. Neto and F. A. S. Fiorelli, "Comparison between detailed model simulation and artifical neural network for forecasting building energy consumption," *Energy and Buildings,* vol. 40, no. 12, pp. 2169-2176, 2008.

[78] F. Magoules, H.-x. Zhao and D. Elizondo, "Development of an RDP neural network for building energy consumption fault detection and diagnosis," *Energy and Buildings,* vol. 62, pp. 133-138, 2013.

[79] S. R. Mohandes, X. Zhang and A. Mahdiyar, "A comprehensive review on the application of artifical neural networks in building energy analysis," *Neurocomputing,* vol. 340, pp. 55-75, 2019.

[80] MathWorks, "MathWorks," MathWorks, 2018. [Online]. Available: https://www.mathworks.com/help/nnet/ug/design-time-series-narx-feedback-neural-networks.html. [Accessed 23 August 2018].

[81] MathWorks, "MathWorks," MathWorks, 2018. [Online]. Available: https://www.mathworks.com/help/nnet/gs/neural-network-time-series-prediction-and-modeling.html. [Accessed 23 August 2018].

[82] H. Fawaz and et al, "Deep learning for time series classification: a review," *Data Mining and Knowledge Discovery,* vol. 33, pp. 917-963, 2019.

[83] A. Tealab, "Time series forecasting using artifical neural networks methodologies: A systematic review," *Future Computing and Informatics Journal,* vol. 3, pp. 334-340, 2018.

[84] Y.-y. Song and Y. Lu, "Decision tree methods: applications for classification and prediction," *Shanghai Archives of Psychiatry,* vol. 27, no. 2, pp. 130-135, 2015.

[85] A. J. Myles and et al, "An introduction to decision tree modeling," *Jounral of Chrmometrics,* vol. 18, pp. 275-285, 2004.

[86] A. Priyam, Abhijeet, R. Gupta, A. Rathee and S. Srivastava, "Comparative Analysis of Decision Tree Classification Algorithms," *International Journal of Current Engineering and Technology,* vol. 3, no. 2, pp. 334-337, 2013.

[87] A. Jamehbozorg and S. M. Shahrtash, "A Decision-Tree-Based Method for Fault Classification in Single-Circuit Transmission Lines," *IEEE Transactions on Power Delivery,* vol. 25, no. 4, pp. 2190-2196, 2010.

[88] M. Amarnath, V. Sugumaran and H. Kumar, "Exploiting sound signals for fault diagnosis of bearings using decision tree," *Measurement,* vol. 46, no. 3, pp. 1250-1256, 2013.

[89] V. Sugumaran, V. Muralidharan and K. I. Ramachandran, "Feature selection using decision tree and classification through proximal support vector machine for fault diagnostics of roller bearing," *Mechanical Systems and Signal Processing,* vol. 21, no. 2, pp. 930-942, 2007.

[90] N. Srivastavs, G. Hinton, A. Krizhevsky, I. Sutskever and R. Salakhutdinov, "Dropout: A Simple Way to Prevent Neural Networks from Overfitting," *Journal of Machine Learninig Research,* vol. 15, pp. 1929-1958, 2014.

[91] E. Weinan, C. Ma, S. Wojtowytsch and L. Wu, Towards a Mathematical Understanding of Neural Netowrk-Based Machine Learning: what we know and what we don't, preprint arXiv, 2020, p. 1929.

[92] R. D. Hurrion, "An example of simulation optimisation using a neural network metamodel: finding the optimum number of kanbans in a manufacturing system," *Journal of the Operation Research Society,* vol. 48, no. 11, pp. 1105-1112, 1997.

[93] A. Nagabandi and et al, "Neural Network Dynamics for Model-Based Deel Reinforcement Learning with Model-Free Fine-Tuning".

[94] M. Manfren, N. Aste and R. Moshksar, "Calibration and uncertainty analysis for computer models – A meta-model based approach for integrated building energy simulation," *Applied Energy,* vol. 103, pp. 627-641, 2013.

[95] S. Qiu, Z. Li, Z. Pang, W. Zhang and Z. Li, "A quick auto-calibration approach based on normative energy models(NEM)," *Energy and Buildings,* 2018.

[96] W. Tian, "A review of uncertainty analysis in building energy assessment," *Renewable and Sustainable Energy Reviews,* vol. 20, pp. 411-419, 2012.

[97] Z. Yuna and A. Godfried, "Optimal demand charge reduction for commercial buildings through a combination of efficiency and flexibility measures," *Applied Energy,* vol. 221, pp. 180-194, 2018.

[98] P. Raftery, M. Keane and A. Costa, "Calibrating whole building energy models: An evidence-based methodology," *Energy and Buildings,* vol. 43, no. 12, pp. 3666-3679, 2011.

[99] E. Khanna, A. Bernett and T. Dogan, "Towards Automated Model Generation and Calibration to Facilitate Multi Building Scale Energy Modeling," in *eSim*, Ithaca, 2018.

[100] X. Pang, M. Wetter, P. Bhattacharya and P. Haves, "A framework for simulation-based real-time whole building performance assessment," *Building and Environment,* vol. 54, pp. 100-108, 2012.

[101] J. Schein, S. T. Bushby, N. S. Castro and J. M. House, "A rule-based fault detection method for air handling units," *Energy and Buildings,* vol. 38, no. 12, pp. 1485-1492, 2006.

[102] C. Miller, Z. Nagy and A. Schlueter, "Automated daily pattern filtering of measured building performance data," *Automation in Construction,* vol. 49, pp. 1-17, 2015.

[103] R. Sterling and et al., "Model-based fault detection and diagnosis of air handling units: A comparison of methodologies," *Energy Procedia,* vol. 62, pp. 686-693, 2017.

[104] L. Zhengwei, C. J. Paredis, G. Augenbroe and G. Huang, "A rule augmented statistical method for air-conditioning system fault detection and diagnostics," *Energy and Buildings* , vol. 54, pp. 154-159, 2012.

[105] B. Dong, Z. O'Neill and Z. Li, "A BIM-enabled information infrastructure for building energy Fault Detection and Diagnostics," *Automation in Construction,* vol. 44, pp. 197-211, 2014.

[106] C. G. Mattera, M. Jradi and H. R. Shaker, "Online Energy Simulator for building fault detection and diagnostics using dynamic energy performance model," *Internaltional Journal of Low-Carbon Technologies,* vol. 13, no. 3, pp. 231-239, 2018.

[107] S. Frank and et al., "Hybrid Model-based and Data-driven Fault Detection and Diagnostics for Commercial Buildings," in *ACEEE Summer Study on Energy Efficiency in Buildings*, Pacific Grove, 2016.

[108] L. Wang and et al., "Monitoring-based HVAC Commissioning of an Existing Office Building for Energy Efficiency," *Applied Energy,* vol. 102, pp. 1382-1390, 2013.

[109] W. Kim and S. Katipamula, "A review of fault detection and diagnostics methods for building systems," *Science and Technology for the Built Environment,* vol. 24, pp. 3-21, 2017.

[110] Ridder et al, "HVAC System With Predictive Free Cooling Control Based on the Cost of Transitioning Into a Free Cooling State". US Patent 9982903 B1, 29 May 2018.

[111] Matsuoka et al, "Generating and Implementing Thermodynamic Models of a Structure". US Patent 9910449 B2, 6 March 2018.

[112] Modi et al, "Heating Controls and Methods for an Environmental Control System". US Patent 10012407 B2, 3 July 2018.

[113] Matsuoka et al, "Control Unit With Automatic Setback Capability". US Patent 8950686 B2, 10 February 2015.

[114] Przyblski, "Building Management System with Linked Thermodynamic Models for HVAC Equipment". US Patent 9798336, 24 October 2017.

[115] O'Neill et al, "Model Based System and Method for Estimating Parameters and States in Temperature Controlled Spaces". US Patent 9037302 B2, 19 May 2015.

[116] J. E. Braun, K. W. Montgomery and N. Chaturveid, "Evaluating the Performance of Building Thermal Mass Control Strategies," *HVAC&R Research,* vol. 7, no. 4, pp. 403-428, 2001.

[117] S. P. Kavanaugh, HVAC Simplified, Atlanta: ASHRAE, 2006.

[118] T. Kusuda, "Fundamentals of Building Heat Transfer," *Journal of Research of the National Bureau of Standards,* vol. 82, no. 2, pp. 97-106, 1977.

[119] J. D. Spitler, D. E. Fisher and C. O. Pedersen, "The Radiant Time Series Cooling Load Calculation Procedure," *ASHRAE Transactions,* vol. 103, no. 2, pp. 503-515, 1997.

[120] B. C. Raychaudhuri, "Transient Thermal Response of Enclosures: The Integrated Thermal Time-Constant," *Int. J. Heat Mass Transfer,* vol. 8, no. 1, pp. 1439-1449, 1965.

[121] X. Q. Li, Y. Chen and D. Fisher, "Applicability of Calculation Methods for Conduction Tranfer Function of Building Constructions," *International Journal of Thermal Sciences* , vol. 48, no. 1\, pp. 1441-1451, 2009.

[122] D. Pubeikis, V. Stankevicius and A. Burlingis, "The Effect of the Fourier Number of Calculation of an Unsteady Heat Transfer of Building Walls," *Journal of Civil Engineering and Management,* vol. 16, no. 2, pp. 298-305, 2010.

[123] ASHRAE, ASHRAE Handbook 1981 Fundamentals, Atlanta: American Society of Heating, Refrigerating and Air-Conditioning Engineers, Inc., 1981.

[124] NREL, "RReDC," U.S. Department of Energy, 19 January 2015. [Online]. Available: https://rredc.nrel.gov/solar/old_data/nsrdb/1991-2005/tmy3/. [Accessed 26 March 2020].

[125] T. O. Al Kasabi, S. Abdel-Khalik and et al, "Design of a commercial solar-powered greenhouse," *Desalination ,* vol. 39, pp. 53-62, 1981.

[126] Engineering ToolBox, 2009. [Online]. Available: https://www.engineeringtoolbox.com/solar-radiation-absorbed-materials-d_1568.html. [Accessed 09 February 2021].

[127] Engineering ToolBox, "Emissivity Coefficient Materials," 2003. [Online]. Available: https://www.engineeringtoolbox.com/emissivity-coefficients-d_447.html. [Accessed 09 February 2021].

[128] CONSTRUCTION ENGINEERING RESEARCH LAB (ARMY) , " Building Loads Analysis and System Thermodynamics (BLAST) Program Users Manual," Champaign, 1981.

[129] D. E. Fisher and C. O. Pedersen, "Convective heat transfer in building energy and thermal load calculations," *ASHRAE Transactions,* vol. 103, pp. 137-148, 1997.

[130] T. Defraeye, B. Blocken and J. Carmeliet, "Convective Heat Transfer Coefficients for Exterior Building Surfaces: Existing Corelations and CFD Modelling," *Energy Conversion and Management,* vol. 52, no. 1, pp. 512-522, 2011.

[131] V. Corrado and E. Fabrizio, "Assessment of Building Cooling Energy Need Through a Quasi-Steady State Model: Simplified Correlation for Gain-Loss Mismatch," *Energy and Buildings,* vol. 39, pp. 569-579, 2007.

[132] H. Li, T. Hong, A. Parker and M. Neukomm, "Characterizing patterns and variability of building electric load profiles in time and frequency domains," *Applied Energy,* vol. 291, no. 116721, 2021.

[133] Y.-S. Kim, M. Heidarinejad, M. Dahlhausen and J. Srebric, "Building energy model calibration with schedules derivied from electricity use data," *Applied Energy,* vol. 190, no. 15, pp. 997-1007, 2017.

[134] American Society of Heating, Refrigerating and Air-Conditioning Engineers, Inc., "Nonresidential Air-Conditioning Cooling and Heating Load," in *1993 ASHRAE Handbook Fundamentals,* Atlanta, American Society of Heating, Refrigerating and Air-Conditioning Engineers, Inc., 1993, pp. 26.1 - 26.65.

[135] ISO, *ISO 15099 Thermal performance of windows, doors, and shading devices - Detailed calculations,* Geneva: ISO 2003, 2003.

[136] G. Spiro, Interviewee, [Interview]. 13 July 2018.

[137] T. Nielsen and S. Svendsen, "Simplified hourly calculation of energy performance in accordance with the Energy Performance of Buildings Directive," 2018.

[138] M. Deru, R. Judkoff and J. Neymark, "Whole-Building Energy Simulation with a Three-Dimensional Ground-Coupled Heat Transfer Model," in *American Society of Heating, Refrigerating and Air-Conditioning Engineers, Inc. (ASHRAE) Winter Meeting,* Chicago, 2002.

[139] Big Ladder Software, "Big Ladder Software," Big Ladder Software, 2014. [Online]. Available: https://bigladdersoftware.com/epx/docs/8-0/engineering-reference/page-043.html. [Accessed 12 February 2018].

[140] F. C. Winkelmann et al, "Simulation Reserarch Lab," September 2001. [Online]. Available: https://simulationresearch.lbl.gov/dirpubs/47972.pdf. [Accessed 21 February 2108].

[141] T. M. Lawrence, R. T. Watson, M.-C. Boudreau, K. Johnsen, J. Perry and L. Ding, "A new paradigm for the design and management of building systems," *Energy and Buildings,* vol. 51, pp. 56-63, 2012.

[142] T. Lawrence, S. Aghniaey, R. T. Watson and J. M. Velni, "A case study to automate demand response on a university campus," in *World Sustainable Built Environment Conference*, Hong Kong, 2017.

[143] U.S. Department of Energy, "eia," U.S. Department of Energy, 17 August 2017. [Online]. Available: https://www.eia.gov/energyexplained/index.php?page=us_energy_commercial. [Accessed 27 August 2018].

[144] United States Department of Labor, "osha," United States Department of Labor, 24 February 2003. [Online]. Available: https://www.osha.gov/pls/oshaweb/owadisp.show_document?p_table=interpretations&p_id=24602. [Accessed 13 July 2018].

[145] T. M. Lawrence and J. E. Braun, "Evaluation of simplified models for predicting CO2 concentrations in small commercial buildings," *Building and Environment,* vol. 41, no. 2, pp. 184-194, 2006.

[146] C. Y. Chao, "Development of a dual-mode demand control ventilation strategy for indoor air quality control and energy savings," *Building and Environment,* vol. 39, no. 4, pp. 385-397, 2004.

[147] Kele Digital Platforms, "Kele," Kele, [Online]. Available: https://www.kele.com/gas-and-specialty-sensors/22dc-51/3-series.aspx. [Accessed 8 July 2020].

[148] Nova Instruments , "Degree controls, inc.," Degree controls, Inc/, [Online]. Available: https://degreec.com/pages/s-series-probe. [Accessed 8 July 2020].

[149] D. Eberly, "Geometric Tools," 1 February 2020. [Online]. Available: https://www.geometrictools.com/Documentation/FiniteDifferences.pdf. [Accessed 19 June 2020].

[150] a. beck, "3.3 Confidence Intervals," in *Parameter Estimation in Engineering and Science*, New York, John Wiley & Sons, 1977, pp. 102-108.

[151] N.-Z. Sun and A. Y. Sun, "156: Inverse Methods for Parameter Estimation," in *Encyclopedia of Hydrological Scuences*, New York, Wiley, 2006.

[152] W. W.-G. Yeh, "Review of Parameter Identification Procedures in Groundwater Hydrology: The Inverse Problem," *Water Resources Research,* vol. 22, no. 2 , pp. 95-108, 1986.

[153] K. Mosegaard, "Monte Carlo sampling of solutions to inverse problems," *Journal of Geophysical Research,* vol. 100, no. B7, pp. 12431-12447, 1995.

[154] Y. Shi, *Uncertainty Quantification of Building Energy Models that Assume Ideal Temperature Control,* Georgia Institute of Technology, 2020.

[155] M. P. Anderson, W. W. Woessner and R. J. Hunt, "Chapter 9 - Model CalibrationL Assessing Performance," in *Applied Groundwater Modeling*, London, Elsvier Inc., 2015, pp. 375-441.

[156] Bre, "UK-NCM," [Online]. Available: https://www.uk-ncm.org.uk/. [Accessed 9 July 2020].

[157] F. Del Risco, Interviewee, *Problems with Georgia Tech Buildings.* [Interview]. 05 March 2019.

[158] Newcomb & Boyd, *Student Health Center Georgia Institute of Technology*, Atlanta, 2002.

[159] York, *Air Systems - Energy Series Energy Recovery Wheel*, York: Johnson Controls Ltd, 2001.

[160] Johnson Controls Inc., *GT Old C.E. Building Renovation,* Roswell, 2008.

[161] K. M. Elovitz, "HPAC Engineering," Energy Economics Inc., 1 October 2009. [Online]. Available: https://www.hpac.com/iaq-ventilation/article/20928092/controlling-outside-airflow-in-vav-systems. [Accessed 30 August 2021].

[162] K. Benne and et al, "Assessment of the Energy Impacts of Outside Air in the Commercial Sector," National Renewable Energy Laboratory, Golden, 2009.

[163] P. Charbonneau, "HAO," Department de Physique, 2018. [Online]. Available: http://www.hao.ucar.edu/modeling/pikaia/pikaia.php. [Accessed 14 May 2018].

[164] T. M. Lawrence and J. E. Braun, "Calibrated Sumulation for Retrofit Evaluation of Demand-Controlled Ventilation in Small Commerical Buildings," *ASHRAE Transactions,* vol. 113, no. 2, pp. 227-240, 2007.

[165] K.-H. Chang, "Stochastic Nelder–Mead simplex method – A new globally convergent direct search method for simulation optimization," *European Journal of Operational Research*, vol. 220, no. 3, pp. 684-694, 2012.

[166] S. S. a. J. Nelder, "Scholarpedia," Scholarpedia, 21 October 2011. [Online]. Available: http://www.scholarpedia.org/article/Nelder-Mead_algorithm. [Accessed 29 September 2017].

[167] S. A. Teukolsky, W. T. Vetterling and B. P. Flannery, "10.5. Downhill Simplex Method in Multidimensions," in *Numerical Recipes 3rd Edition: The Art of Scientific Computing*, Hong Kong, Golden Cup, 2007, pp. 502-507.

[168] M. Tabassum and K. Mathew, "A Genetic Algorithm Analysis Towards Optomized Solutions," *International Journal of Digital Information and Wireless Communication*, vol. 4, no. 1, pp. 124-142, 2014.

[169] A. K. Persily and R. A. Grot, "Air Infiltration and Building Tightness MEasurements in Passive SOlar Residences," National Bereau of Standards, Washington, D.C., 1984.

[170] C. Younes, C. A. Shdid and G. Bitsuamlak, "Air infiltration through building envelopes: A review," *Journal of Building Physics,* vol. 35, no. 3, pp. 267-302, 2011.

[171] K. Gowri, D. Winiarski and R. Jarnagin, "Infiltration Modeling Guidelines for Commercial Building Energy Analysis," Pacific Northwest National Laboratory, 2009.

[172] G. Ansanay-Alex, "Estimating Occupancy using indoor carbon dioxide concentrations only in an office building: a method and qualitative assessment," Clima, 2016.

[173] F. Ascione, L. Bellia, A. Capozzoli and F. Minichiello, "Energy saving strategies in air-conditionoing for museums," *Appled Thermal Engineering,* vol. 29, pp. 676-686, 2009.

[174] DesignBuilder Software Ltd., Stroud, 2020.

[175] J. Kim, J. Cai and J. E. Braun, "Common Faults and Their Prioritization in Small Commercial Buildings," Purdue University, December 2017. [Online]. Available: https://www.nrel.gov/docs/fy18osti/70136.pdf. [Accessed 29 June 2020].

[176] ASHRAE, "ASHRAE Epidemic Task Force," 6 January 2021. [Online]. [Accessed 27 April 2021].

[177] J. Su, D. V. Vargas and K. Sakurai, "One Pixel Attack for Fooling Deep Neural Networks," *IEEE Transactions on Evolutionary Computation,* vol. 23, no. 5, pp. 828-841, 2019.

[178] M. J. Mendell and G. A. Heath, "Do Indoor Pollitants and Therman Conditions in Schools Influence Stuent Performance? A Critical Review of the Literature," *Indoor Air Journal,* vol. 15, pp. 27-32, 2005.

[179] D. L. Shrestha and D. P. Solomatine, "Machine learning approaches for estimation of prediction interval for the model output," *Neural Networks,* vol. 19, no. 2, pp. 225-235, 2006.

[180] J. Groß, "1.1 Linear Models," in *Linear Regression*, Heidelberg, Springer-Verlag Berlin, 2003, pp. 3-6.

[181] Department of Energy, "DOE2," Department of Energy, 2018. [Online]. Available: http://www.doe2.com/equest/. [Accessed 1 April 2018].

[182] K. Gown, D. Winiarski and R. Jarnagin, "Infiltration Modeling Guidelines for Commercial Building Energy Analysis," U.S. Department of Energy, 2009.

[183] L. G. Harriman, G. W. Brundrett and R. Kittler, in *humidity control design guide for commercial and institutional buildings*, Atlanta, ASHRAE, 2001.

[184] T. Hong, J. kim and M. Lee, "Integrated Task Performance Score for the Building Occupants Based on the CO2 Concentration and Indoor Climate Factor Changes," *Applied Energy,* vol. 228, pp. 1707-1713, 2018.

[185] J. Swift, E. Avis, B. Millard and T. M. Lawrence, "Air Distribution Strategy Impact on Operating Room Infection Control," in *Clima*, 2007.

[186] S. A. Kalogirou, "Applications of artifical neural-networks for energy systems," *Applied Energy,* vol. 67, pp. 17-35, 2000.

[187] C. A. L. F. C. S. P. S. Khan I., "Building Energy Management Through Fault Detection Analysis Using Pattern Recognition Techniques Applied on Residual Neural Networks," *Pizzuti C., Spezzano G. (eds) Advances in Artificial Life and Evolutionary Computation,* vol. 445, 2014.

[188] M. Schlechtingen and I. F. Santos, "Comparative analysis of neural network and regression based condition monitoring approaches for wind turbine fault detection," *Mechanical Systems and Signal Processing,* vol. 25, no. 5, pp. 1849-1875, 2011.

[189] B. F. Winkler, "Bayesian Regularization of Neural Networks," in *Methods in Molecular Biology*, Livingstone, Humana Press, 2008, pp. 23-42.

[190] H. Rostami, J. Blue and C. Yugma, "Automatic equipment fault fingerprint extraction for the fault diagnostic on the batch process data," *Applied Soft Computing,* vol. 68, pp. 972-989, 2018.

[191] H. Shu-Guang, H. Zhen and G. A. Wang, "Online monitoring and fault identification of mean shifts in bivariate processes using decision tree leaning techniques," *Journal of Intelligent Manufacturing* , vol. 24, no. 1, pp. 25-34, 2013.

[192] M. B. Castellanos and et al, "Fault identification using a chain of decision trees in an electrical sibmersible pump operating in a liquid-gas flow," *Journal of Petroleum Science and Engineering,* vol. 184, 2020: 106490.

[193] Onicon, *FT-3200 Master Specification,* Largo, 2021.

[194] Sierra and M. Olin, *Thermal Energy/BTU Ultrasonic Flow Meters Improve Energy Efficiency HVAC Sytstem,* Monterey: Sierra Instruments, 2019.

[195] Air Monitor Corporation, *VOLU-probe/FI,* Santa Rosa, 1999.

[196] McMaster-Carr, "Threaded Thermocouple Probes with Thermowell for Liquids and Gases," McMaster-Carr, 2021. [Online]. Available: mcmaster.com. [Accessed 24 July 2021].

[197] Onicon, *FSM 3 series flow meter master specs,* Largo, 2021.